THE BRACING REQUIREMENTS OF STEEL BEAMS OF INTERMEDIATE SLENDERNESS

by

John Tubman, B.Sc.

A thesis submitted for the degree of
Doctor of Philosophy

Department of Civil Engineering
University of Glasgow

April 1986

To

my Parents

and

Alison

ACKNOWLEDGEMENTS

The work described in this thesis was carried out in the Department of Civil Engineering at the University of Glasgow under the general direction of Professor A. Coull whose unstinting help and sincere advice were always gratefully received.

I am greatly indebted to my immediate supervisor, Mr. H. M. Nelson, for his valuable guidance, advice and constructive criticism throughout the research work and in the preparation of this thesis.

To the staff of the Structures Laboratory and, in particular Messrs. A.I. Todd, R. Thornton, W. Thompson and the late J. Love, I extend my most sincere thanks. Their good humour, even under the most desperate circumstances, was unflagging.

My grateful thanks are also due:

to Miss A. MacKinnon, Miss E. McArthur and Mrs. A. McVey of the Faculty's computing staff for their unstinting help in trying to resolve many worrying computing problems.

to The Science and Engineering Research Council for funding by far the greater proportion of the work.

to Professor P. J. Dowling of Imperial College, London for permission to use FINAS and to Mr. D. Bates for his guidance in its use.

to Professor H. B. Sutherland, Mr. H. M. Nelson and Dr. P. D. Arthur for their help in securing additional funds when NASTRAN failed to live up to expectations. Also to the Public Works and Municipal Services Congress and Exhibition Council for the award of a research grant which permitted FINAS analytical work to be completed.

to All other members of staff and research students in the Dept. of Civil Engineering for their contributions and the opportunity for discussion.

to Scott Wilson Kirkpatrick & Partners (Scotland) for the use of their word processor.

to My parents, parents-in-law and wife, Alison, for their continual encouragement and indefatigable patience over the last few years and to Alison for her good-humoured perseverance in word-processing a difficult text on a foreign subject.

Finally, I extend my eternal gratitude to my parents for the many opportunities afforded to me by their sacrifices in the interests of my education.

SYNOPSIS

Steel beams, whether rolled or built-up, contain unavoidable initial imperfections and residual stresses and are subject to unintentional eccentricity of applied loading. Such beams which also possess inadequate lateral restraint are prone to failure as a result of lateral-torsional instability, which occurs under elastic or inelastic conditions depending on the slenderness of the member. A review of the literature pertaining to the bracing requirements of steel beams revealed little published work concerned with the restraint of beams of intermediate and low slenderness which fail inelastically. The provision of adequate midspan restraint for the prevention of inelastic instability in centrally loaded, single span I-beams formed the basis of this study.

The non-linear analysis capabilities of the finite element programmes MSC/NASTRAN and FINAS were employed to provide theoretical verification of the results of a series of tests on small-scale, fabricated, steel I-beams. Measured initial geometrical imperfections of the test beams were modelled in the finite element idealisation by suitable adjustment of nodal coordinates and both geometrical and material non-linearites were accounted for in the analysis. Numerical instability and convergence difficulties were encountered in both analyses, although their occurrence was less frequent in FINAS. In FINAS analyses where these difficulties did not arise, collapse loads were determined and post-buckling behaviour followed with relative ease.

A bracing fork device for the provision of a predetermined stiffness of midspan restraint was developed and subsequently employed in all tests. Strain gauges attached to the prongs of this device permitted bracing forces to be measured at any stage in the tests.

In general, satisfactory correlation was achieved between finite element and experimental results, allowing bracing criteria for single span, centrally loaded and restrained beams to be proposed. As anticipated, the bracing requirements of inelastic beams proved more onerous than those demanded by the classical bifurcation analysis employed in problems of elastic beam buckling. A subsequent series of

comparative designs in accordance with the three current (1985) British steelwork codes (BS 449, BS 5950 and BS 5400) revealed that bracing members designed as struts in compliance with the minimum strength and maximum slenderness criteria of these documents provided adequate stiffness and strength of restraint.

CONTENTS

Page No.

ACKNOWLEDGEMENTS iii
SYNOPSIS v
CONTENTS vii
NOTATION xii

CHAPTER 1 - INTRODUCTION, REVIEW OF PREVIOUS RESEARCH AND SCOPE OF THE PRESENT STUDY

1.1 General Introduction 1
1.2 Review of Previous Research 6
1.2.1 Lateral-Torsional Buckling of Unbraced Steel Beams 6
1.2.2 Initial Imperfections in Real Beams 8
1.2.3. Elastic Lateral-Torsional Buckling of Beams either Laterally or Torsionally Restrained on the Span 17
1.2.4 Elastic Lateral-Torsional Buckling of Beams Laterally and Torsionally Restrained on the Span 29
1.2.5 Restraint Systems Associated with Inelastic Lateral-Torsional Buckling of Beams 31
1.3 Summary of Previous Research and Scope of the Present Study 40
1.3.1 Summary of Previous Research 40
1.3.2 Scope of the Present Study 42

CHAPTER 2 - THE APPLICATION OF THE ENERGY METHOD TO PROBLEMS OF ELASTIC INSTABILITY OF RESTRAINED BEAMS

2.1 Introduction 58
2.1.1 Introduction to the Rayleigh-Ritz Method 58
2.1.2 Reasons for the Presentation of Elastic Stability Analyses 59
2.1.3 Assumptions 61

Page No.

2.2 Simply-Supported Beam under Uniform Moment and with Central Elastic Restraint 62
2.3 Simply-Supported Beam under Uniform Moment and with Rigid Central Restraint 72
2.4 Simply-Supported Beam under Central Point Loading and with Central Elastic Restraint 73
2.5 Simply-Supported Beam under Central Point Loading and with Rigid Central Restraint 79
2.6 Re-analysis of the Lateral Restraint Problem of Section 2.4 using an Assumed Displacement Function of Higher Order 82
2.7 Computer Programmes MODBRACE and AUTOBRAC and Description of Numerical Results 85
2.7.1 The Computer Programme MODBRACE 85
2.7.2 The Computer Programme AUTOBRAC 88
2.7.3 Numerical Results Arising from the Analyses presented in Sections 2.2 to 2.6 90

CHAPTER 3 - FINITE ELEMENT ANALYSIS
3.1 Differences Between Classical Buckling and Instability Analyses 108
3.2 Non-Linear Finite Element Solutions 112
3.2.1 Materially Non-Linear Analysis 114
3.2.2 Geometrically Non-Linear Analysis 116
3.2.3 Solution of Problems involving Coupled Non-Linearity 118
3.3 The Search for a Finite Element Programme capable of Combined Non-Linear Analysis 120
3.3.1 The Development of an Elasto-Plastic Analysis Programme 120
3.3.2 MSC/NASTRAN: Description and Limitations 122
3.3.3 FINAS: Description and Advantages over NASTRAN 127
3.4 Finite Element Mesh Generation from Measured Imperfection Data 130

Page No.

CHAPTER 4 - REQUIREMENTS OF THE EXPERIMENTAL PROGRAMME AND CONSTRUCTION OF THE TEST RIG

4.1 General Requirements of the Test Programme 142
4.2 The Suitability of Model Tests for the Prediction of the Lateral-Torsional Buckling Behaviour of Steel Beams 144
4.3 Requirements of and Construction of Test Apparatus for the Model Beam Test Programme 147
4.3.1 The Test Frame 147
4.3.2 End Supports 147
4.3.3 Loading Apparatus 149
4.3.4 Measurement of Beam Displacements 153
4.3.5 The Provision of Finite Lateral Restraint Stiffness at Midspan 157
4.4 Calibration of Instruments and Bracing Forks 164
4.4.1 Calibration of Statham Gold Load Cell 164
4.4.2 Displacement Transducer Calibration 165
4.4.3 Bracing Fork Calibration 165
4.5 Conclusions 169

CHAPTER 5 - PRELIMINARIES TO THE MODEL BEAM TEST PROGRAMME

5.1 Fabrication of Model Beams 188
5.2 Residual Stresses in As-Welded Model Beams 191
5.3 Reasons for and Details of Stress-Relieving of Model Beams 195
5.4 Geometrical Properties of Model Beams 198
5.5 Material Properties of Model Beams 205
5.6 Rate of Plastic Straining Employed in Tests 211
5.7 Experimental Procedure 220
5.7.1 Preparations for a Model Beam Test 220
5.7.2 Test Procedure 222

CHAPTER 6 - EXPERIMENTAL RESULTS AND COMPARISON WITH FINITE ELEMENT ANALYSES

6.1 The Selection of R^2 Values to be Used in Model Beam Tests 235

Page No.

6.2 Experimental and Finite Element Results 240

6.2.1 Set 1: Shear Centre Loading on Beams of $R^2 = 6.5$ 240

6.2.2 Set 2: Shear Centre Loading on Beams of $R^2 = 11.5$ 243

6.2.3 Set 3: Shear Centre Loading on Beams of $R^2 = 18.5$ 246

6.2.4 Set 4: Compression Flange Loading on Beams of $R^2 = 6.5$ 247

6.2.5 Set 5: Compression Flange Loading on Beams of $R^2 = 11.5$ 248

6.2.6 Set 6: Compression Flange Loading on Beams of $R^2 = 18.5$ 249

6.3 Discussion of Experimental and Finite Element Results 251

6.3.1 Discussion of Experimental Results 251

6.3.2 Comparison of Finite Element with Experimental Results 257

CHAPTER 7 - FINAS PARAMETRIC STUDY - SOME FACTORS INFLUENCING THE MAGNITUDE OF BRACING FORCES

7.1 The FINAS Braced Beam Model 285

7.2 Presentation and Discussion of Results 287

7.3 Comparison of Results of the Parametric Study with Those of Chapter 6 290

CHAPTER 8 - COMPARISON OF THE RESULTS OF THIS STUDY WITH PREVIOUS RESEARCH AND THE REQUIREMENTS OF CONTEMPORARY DESIGN CODES

8.1 Comparison of the Elastic Bracing Requirements of Chapter 2 with the Results of Previous Research Employing Elastic Buckling Theory 300

8.2 Comparison of Experimental and Finite Element Results of Chapter 6 with Those of the Elastic Bifurcation Analysis of Chapter 2 303

Page No.

8.3 Comparison of Experimental and Finite Element Results of Chapter 6 with Previously Published Bracing Requirements and those Currently Specified in Codes of Practice 309

CHAPTER 9 - CONCLUSIONS AND RECOMMENDATIONS FOR FURTHER STUDY

9.1 Conclusions 327

9.2 Recommendations for Future Research 331

REFERENCES 333

APPENDIX I - Computer Programmes MODBRACE and AUTOBRAC 341

APPENDIX II - Computer Programme NEWMESH 364

APPENDIX III - Error in Measuring "Midspan" Deflections at a Point 10mm from Midspan of Test Beams 380

APPENDIX IV - Corrections to be Applied to Measured Vertical Deflection of Test Beams 382

APPENDIX V - Strain-Bending Moment Relationships for Bracing Prongs 389

APPENDIX VI - Programme KURVTURE and Rate of Straining Calculations 395

APPENDIX VII - Comparative Design Calculations 401

NOTATION

The following notation is employed in this thesis. In all cases the symbols are defined where they first appear in the text.

a	height of application of point load above shear centre
a_f	distance from root of bracing prong to the point of contact between prong and beam flange
A	coefficient employed in assumed twist function
$A_b{}^*$	required cross-sectional area of lateral restraint
A_b	cross-sectional area of lateral restraint provided
A_f	cross-sectional area of compression flange of beam $= b_f t_f$
A_x	cross-sectional area of beam or bracing prong
b	breadth of rectangular cross-section
b_f	breadth of compression flange
B	coefficient employed in assumed twist function
$[B]$	strain matrix in conventional finite element notation
c	critical stress factor
c_{II}	value of critical stress factor consistent with second mode elastic buckling
C	torsional rigidity of cross-section = GJ
C_1	warping rigidity of cross-section = $E\Gamma$
C_2	coefficient employed in assumed twist function
D	overall depth of beam section
D_1, D_2, D_3	terms employed in bifurcation analysis of Chapter 2
e	non-dimensional stiffness of torsional restraint $= \frac{K_T l}{GJ}$
e_{cr}	critical value of 'e' for fully effective torsional restraint
E	Young's modulus
$[E]$	elasticity matrix employed in finite element analysis

E_{st}	strain hardening modulus
$[E_{ep}]$	elasto-plastic stress-strain matrix employed in materially nonlinear finite element analysis
f_s	form factor for shear
$F_1,\ldots,F_9$	terms employed in bifurcation analysis of Chapter 2
F_L, F_R	lateral forces acting on bracing prongs at the points of contact with beam flanges
F_{OL}, F_{OR}	initial values of F_L, F_R arising from setting up the experimental apparatus
g	distance from neutral axis of beam to nearer edge of yielded zone in cross-section
G	shear modulus
$G_{11},\ldots,G_{33}$	terms employed in bifurcation analysis of Chapter 2
h	level of attachment of translational restraint relative to shear centre
h_G	distance from beam centroid to centroid of steel ball attached to underside of beam at midspan
h_{CF}	distance from web/compression flange junction to centroid of above steel ball
I	2nd moment of area
I_η	2nd moment of area of beam cross-section about its minor axis
I_{maj}	2nd moment of area of beam cross-section about its major axis
J	St. Venant torsion constant for beam cross-section
k	effective length factor
k_H	constant of proportionality relating yield stress σ_y to Vickers hardness number V_H
K	absolute stiffness of translational (lateral) restraint
K_{cr}	critical value of K corresponding to λ_{cr}
K_T	absolute stiffness of rotational (torsional) restraint
$[K]$	elastic structural stiffness matrix
$[K_0]$	initial linear elastic global stiffness matrix
$[K_\sigma]$	geometric stiffness matrix

l	span of beam
l_b	length of lateral restraint member
l_L, l_R	lengths of the two spans adjacent to the braced point
l_{av}	defined by reciprocal average length of adjacent spans: $\frac{1}{l_{av}} = \frac{1}{2}\left(\frac{1}{l_L} + \frac{1}{l_R}\right)$
l_a	length of longer adjacent span ie. greater of l_L and l_R
L	spacing of lateral restraints
M	applied uniform bending moment
M_y	bending moment at first yield in section
M_p	fully plastic moment
M_{ffy}	moment at which flanges fully yielded, web still elastic
M_{cr}	critical (or ultimate) moment
M_E	elastic critical moment of beam/restraint system
M_{lb}	maximum lateral bending moment in compression flange coexistent with moment M_p about major axis of beam
$(M_{cr})_{UM}$	critical moment of unrestrained beam under uniform moment
M_{nok}	moment associated with critical load P_{nok}
M_L, M_R	moments on the left and right bracing prongs at the strain gauged cross-sections arising from forces F_L, F_R
M_{OL}, M_{OR}	initial values of M_L, M_R arising from setting up the experimental apparatus
P	point load applied to beam
P_y	point load producing first yield in cross-section
P_p	theoretical value of central point load producing plastic hinge at midspan
P_{ffy}	point load at which flanges fully yielded, web still elastic
P_{br}	axial force in lateral restraint
P_c	compression flange force
P_{cy}	fully yielded compression flange force = $A_f \sigma_y$

P_{cr}	critical (or ultimate) load
P_{crI}	elastic first mode critical load of unbraced beam with load applied at the appropriate level on the cross-section
P_{crII}	elastic second mode critical load of braced beam
$P_{cr\lambda}$	elastic critical load of braced beam with appropriate load/restraint geometry and restraint stiffness
P_{nok}	critical load of beam under shear centre loading and without lateral restraint
P_{ult}	ultimate load sustained by beam
$Q_o,\ldots,Q_3$	terms employed in rate of straining analysis of Chapter 5
$\{Q\}$	vector of structure nodal forces in finite element analysis
r	radius
r_y	minor axis radius of gyration
R	non-dimensional shape parameter = $\left(\frac{l^2GJ}{E\Gamma}\right)^{\frac{1}{2}}$
t_f	thickness of compression flange
t_w	web thickness
u	lateral deflection of beam
u_o	initial lateral deflection of compression flange at midspan
U	strain energy of beam/restraint system
V	potential energy of load system
V_H	Vickers hardness number
w	uniformly distributed load
X	axis of global cartesian coordinate system
Y	axis of global cartesian coordinate system
z_e	elastic section modulus of beam cross-section
z_p	plastic section modulus of beam cross-section
z_b^*	required elastic section modulus of bracing member about an axis parallel to the longitudinal axis of the restrained member

Z	axis of global cartesian coordinate system
α	vertical deflection of shear centre during virtual disturbance of beam
β	vertical deflection of point of load application relative to shear centre during virtual disturbance of beam
γ	shear strain
γ_1	parameter employed in conversion of bracing fork strains to internal moment
Γ	warping constant for beam cross-section
δ	central lateral deflection of beam
δ_0	amplitude of initial lateral crookedness
Δ	as an independent variable denotes vertical deflection; as prefix to another variable (eg. ΔM_L) denotes finite change in prefixed variable
Δ_{meas}	measured vertical deflection of steel ball attached to underside of beam at midspan
Δ_{inc}	vertical deflection of above ball attributable to beam deformation only
Δ_G	vertical deflection of beam centroid
$\{\Delta\}$	vector of structure nodal displacements
ϵ	direct strain
ϵ_y	yield strain = σ_y/E
ϵ_{st}	strain at onset of strain hardening
$\{\epsilon_0\}$	vector of initial internal strains
ζ	axis of local cartesian coordinate system
η	axis of local cartesian coordinate system
η_P	Perry-Robertson imperfection factor
θ	rotation of beam
θ_p	rotation of beam under applied moment M_p
λ	non-dimensional stiffness of lateral restraint = $\dfrac{Kl^3}{48EI_\eta}$
λ_{cr}	critical value of 'λ' for fully effective lateral restraint

λ_{LT}	slenderness parameter for lateral-torsional buckling employed in BS 5400 and BS 5950
μ	rotation capacity $= \dfrac{\theta}{\theta_p} - 1$
ξ	axis of local cartesian coordinate system
Π	total potential energy of beam/restraint system
ρ	load factor
σ	stress
σ_y	yield stress
σ_{yt}	uniaxial yield stress in tension
σ_{rc}	maximum residual compressive stress in section
$\{\sigma_o\}$	vector of initial, internal stresses
τ, τ_1	twist corrections applied to vertical deflection readings
φ	angle of twist (radians)
φ_c	midspan angle of twist
φ_o	initial angle of twist at midspan (radians)
χ	in-plane curvature of beam
χ_y	in-plane curvature of beam at first yield in section
ψ	shape parameter for rectangular sections (Ref. 12)

CHAPTER 1

INTRODUCTION, REVIEW OF PREVIOUS RESEARCH AND SCOPE OF THE PRESENT STUDY

CHAPTER 1

INTRODUCTION, REVIEW OF PREVIOUS RESEARCH AND SCOPE OF THE PRESENT STUDY

1.1 General Introduction

There are two possible modes of failure of a beam subjected to loading in the plane of its maximum flexural rigidity:

(a) Excessive in-plane deformations following the attainment of full in-plane strength. This strength is determined not only by the cross-sectional geometry of the beam and its yield stress but also by the loading and support geometry. Plastic hinge action is consistent with this type of failure which occurs only in beams of low slenderness ("stocky" beams). Well-proven methods exist for the prediction of ultimate strength.

(b) In the case of more slender beams, failure occurs by flexural-torsional (or lateral-torsional) buckling, a phenomenon in which lateral bending is accompanied by twisting of the member and, in general, warping of the cross-section (Fig. 1.1).

In practice, slender elements such as beams of narrow rectangular section and of narrow-flanged I-section lack both lateral flexural rigidity and torsional rigidity and are consequently susceptible to the latter mode of failure. Other thin-walled open section beams such as channels or zeds also have low torsional rigidity, whereas box girders display high lateral bending and torsional rigidities and hence do not, in general, become laterally unstable.

Although a distinction has been made between in-plane plastic collapse and failure by flexural-torsional instability, the latter need not occur solely under elastic conditions. Inelastic instability occurs in beams of intermediate slenderness, where the rigidity of the member decreases with the spread of plasticity through the section, both the in-plane and out-of-plane deformations of the beam being defined by the behaviour of the elastic core (Fig. 1.2).

In the case of an initially perfect beam subjected to an uniform moment, the same degree of stiffness degradation applies at all sections on the span and consequently this represents the most unfavourable pattern of loading on the beam.

Figure 1.3 shows a typical non-dimensional relationship between ultimate load (M_{cr}/M_p) and beam slenderness (l/r_y), wherein the following notation has been used:

M_{cr}	critical (or ultimate) moment
M_p	fully plastic moment
l	span
r_y	minor axis radius of gyration

Three regions of slenderness have been identified in Fig. 1.3 . The first, covering a small range of slenderness values, is characterised by attainment of the fully plastic moment. Beams in this category are often described as "stocky". The second region contains beams of intermediate slenderness which fail by inelastic buckling at a moment smaller than the fully plastic moment, M_p. The failure load of a beam in this category is significantly lower than that predicted by elastic theory for the same slenderness (broken line in figure). The range of slenderness values over which inelastic buckling occurs is controlled by a number of factors, not least of which is the presence of residual stresses, discussed more fully in Section 1.2.2 . Slender beams which fail at, or close to, the theoretical elastic critical load for their slenderness compose the third category.

A direct analogy can be drawn between the ultimate behaviour of beams and that of columns: the beam which achieves its full in-plane strength can be compared with the column which reaches its squash load in that both attain full plasticity; and the failure of a column of thin-walled open cross-section in a mode of combined twisting and lateral bending is akin to the phenomenon of flexural-torsional buckling of a beam in which attainment of the ultimate load is accompanied by gross lateral and torsional deformations.

Mathematically, the case of a column buckling elastically by bending in a plane of symmetry of its cross-section is more readily analysed (using tabulated values of the stability functions[1], for example) than the problem of column buckling involving twist and hence also torsion. No beam buckling mode analogous to the in-plane buckling behaviour of columns exists due to inevitable twisting of the beam during buckling. Twisting occurs because the lateral bending stiffness of the tension flange increases with increasing flange tension, whereas the tendency towards instability of the compression flange increases with increasing compression. As the buckling load of the beam is reached, twisting of the cross-section is therefore unavoidable. The analogy with column behaviour is thus only of value for member failure attributable either to the attainment of full plasticity or to buckling involving torsional deformation.

The classical solution[2] to the elastic beam stability problem assumes an initially perfect beam under ideal loading conditions and attempts to determine the smallest applied load at which a bifurcation of the equilibrium modes is possible. Being essentially an eigenvalue analysis, this solution predicts no out-of-plane deformations until the critical load is reached when, theoretically, these deflections become infinite (Fig. 1.4). Nevertheless, the mode shape corresponding to the critical load is readily obtained.

In practice, however, all beams possess initial imperfections, are subject to some unintentional eccentricity of applied loading and do not necessarily behave elastically. The most significant imperfections and their effects are described more fully in Section 1.2.2 . Although the inclusion of some of these imperfections in the analysis is possible, the complexity of the solution becomes disproportionately greater with increasing number of imperfections included. In some instances, closed-form solutions of the governing differential equations become no longer practicable. However, in cases where some account can be taken of the imperfections, the analysis shows that lateral deflections commence as soon as load is applied (Fig. 1.4).

Indeed, as the ultimate load is approached, the lateral displacements become large and the initial assumption of small displacements no longer applies.

In the case of non-linear material behaviour, the calculated value of critical load is dependent on the assumed variation in strain across the section during buckling. The tangent modulus theory, in which it is assumed that no strain reversal occurs in the cross-section during buckling, has received considerable support and yields results in close agreement with experimentation.

As an alternative to the closed-form solutions obtained from the differential equations of equilibrium by Timoshenko[2], the energy methods can be used to provide closed-form solutions to the elastic beam buckling problem. However, more complex analyses, often based on assumed displacement functions and the principles of minimum total potential energy, seldom yield closed-form solutions suitable for hand calculation of critical loads. Nevertheless, the resulting equations are generally suitable for computer-based numerical solution using iterative methods such as the determinant search technique. That the accuracy of solutions obtained using assumed displacement functions is dependent of the form of the assumed functions is shown by example in Chapter 2.

More recent solutions to a wide variety of structural stability calculations have been computer-based. Early finite difference and finite integral techniques for the numerical solution of the governing equations have been overshadowed in recent years by finite element analysis. In cases where direct comparison of finite element with exact theoretical solutions is possible, very close correlation can be observed. In addition, it has been found that algorithms for the solution of materially and geometrically non-linear behaviour can be incorporated into the analysis.

Although experimental investigations into both the elastic and inelastic buckling of beams are possible, full-scale inelastic buckling tests are relatively expensive since the beam suffers plastic deformation during the test, thus preventing its re-use in subsequent tests.

Just as the usable strength of a slender column can be increased by the provision of a greater degree of end fixity or by the attachment of intermediate restraints along its length, a beam susceptible to failure by flexural-torsional buckling can be similarly restrained, as shown in Fig. 1.5 . The spacing of such intermediate restraints can also be reduced in order to decrease the slenderness (and also the effective length) of the primary member and hence increase its resistance to buckling. Although both longhand analytical solutions (equilibrium-based and energy-based) and computer-based finite difference, finite integral and finite element solutions of the restraint problem are generally also possible, the complexity of the manual methods even in some cases of relatively simple braced beam systems renders them unmanageable and recourse must be made to the computer-based, specific numerical solutions.

It is generally recognised that there are two criteria to be met by bracing if it is to be considered effective: adequate axial and/or rotational stiffness in order to provide sufficient lateral and/or torsional restraint to the beam at the point of attachment; and adequate strength in order to withstand any forces developed as a result of deformation of the beam.

In general, for a given system of loading, the plastic design method permits the use of lighter, more slender members than would be required by conventional elastic design methods. However, since stability varies inversely as slenderness, the requirements of restraint systems associated with plastically-designed structures will, intuitively, be more exacting. As it is a stated requirement of the method that "adequate" restraint be provided to any member so designed, the designer should give careful consideration to the bracing criteria, no matter how trivial these might appear numerically.

1.2 Review of Previous Research

1.2.1 Lateral-Torsional Buckling of Unbraced Steel Beams

The elastic and inelastic lateral-torsional buckling behaviour of unbraced beams has received considerable attention in the literature. The techniques employed in published work range from the purely experimental[3-7] to closed-form and elementary numerical solutions of the governing differential and energy equations[8-18] and to the more modern, computer-based finite integral[19,20] and finite element techniques[21-23].

As a result of this work, unified approaches allowing the analysis of a wide range of elastic and inelastic buckling problems have been published by Nethercot, Rockey and Trahair[24-27]. These have been observed to be "approximate but accurate" by Allen and Bulson[9].

As noted in Section 1.1, all real beams possess initial geometrical and material imperfections. These are random in nature and have a significant effect on the response of a member to an applied load (Fig. 1.4). Geometrical imperfections reported in the literature are discussed more fully in Section 1.2.2 . Several modifications to the well-established Southwell extrapolation technique[28] for geometrically imperfect struts have been proposed in an attempt to permit the calculation of the elastic critical loads of real beams not loaded to failure. Originally proposed as a method of predicting the elastic critical loads of pin-ended struts with sinusoidal initial crookedness, the "Southwell" technique rectifies the pre-buckling load-deflection hyperbola for the column (similar to that shown in Fig. 1.4 for the "real" beam) to produce a linear relationship from which estimates of the critical load and magnitude of the initial imperfection may be deduced.

Successive modifications to the Southwell procedure by Massey[29], Trahair[30], Meck[31] and Attard[32] have been based on Massey's[29] theoretical observation that the central lateral deflection 'δ' of a beam with sinusoidal initial crookedness of amplitude 'δ_o' when subjected to an uniform bending moment 'M' can be related to the elastic critical moment M_{cr} by the relation

$$\frac{\delta}{M^2} = \frac{\delta}{M_{cr}^2} + \frac{\delta_o}{M_{cr}^2} \qquad \ldots(1.1)$$

from which it can be deduced that the plotting of experimental values of 'δ/M^2' against 'δ' yields a straight line of slope $1/M_{cr}^2$. Contributions by Trahair[30], Meck[31] and Attard[32] have extended the scope of Massey's method to include the effects of concentrated loading, varying levels of load application with respect to the member cross-section and to the case of end-loaded cantilever beams. Collectively, this published work presents useful, non-destructive procedures for the determination of the elastic critical loads of simply-supported beams and cantilevers.

The requirements for the elastic design of beams in both the current British Steelwork Code BS 449[33] and the previous Australian Code[34] were based largely on early work employing the mathematical theory of stability[2,8]. The lateral stability of beams and girders was further investigated by Kerensky, Flint and Brown[35], whose attempts to simplify the procedure for designing beams against failure by lateral-torsional buckling did much to influence the requirements of BS 153: 1958[36] and the previous editions of the British[37] and Australian[34] Codes. Following the introduction of structural sections in Grade 55 steel, Dibley[38] performed a series of lateral-torsional buckling tests on thirty such sections in order to assess the Code requirements[37] which had been based on the work of Kerensky et al.[35] for lower grade steels.

More recently, reflecting the versatility of the finite element method[21-23], theoretical studies have been made of the importance of parameters such as the magnitude and distribution of residual stresses and initial imperfections in as-rolled beams[39-41]. Indeed, many of the limiting cases from these studies have served to verify previous closed-form solutions.

It is evident that the determination of elastic and inelastic critical loads for beams has received considerable attention in the literature. As a result, exact or approximate solutions exist for a large number of combinations of loading and structural geometry and it can be said that, in particular, the buckling behaviour of beams which fail in the elastic range is now well understood. As previously noted however, the majority of studies have assumed rigid translational and rotational intermediate supports in cases of both elastic and inelastic buckling. In part, this has been due to the greater complexity of an analysis in which the supports are considered to have finite rather than infinite stiffness.

1.2.2 Initial Imperfections in Real Beams

As noted in Sections 1.1 and 1.2.1, whereas various random imperfections exist in real beams, these are neglected in the mathematically "well-behaved" beams used in classical buckling solutions such as those of Timoshenko[2,8]. The influence of initial imperfections on the load-deflection behaviour of a beam is shown in Fig. 1.4. The lateral stability of the member is reduced as the magnitude of the initial imperfection increases. Just as such imperfections reduce the beam's stability and hence its critical load, their presence demands more rigorous bracing systems if instability is to be prevented. Initial imperfections are therefore of major importance in the present study.

In general, initial imperfections can be assigned to one of three categories: geometrical, loading or material. Nethercot[39] has identified the most significant imperfections in each category; Table 1.1 abstracted from Ref. 39 and presented here with minor amendments, summarises these imperfections and, where possible, comment is made on their relative importance.

Although Table 1.1 does not provide an exhaustive list of all possible imperfections in a beam or in its loading and support geometry, it does indicate the main factors affecting beam stability. It will be observed that, of the eight imperfections noted for real beams, only that concerned with deflection in the plane of the applied load consistently produces an increase in the calculated critical load. Consequently, for design purposes, this effect is frequently ignored in calculation of critical loads, thereby providing slightly conservative (ie. low) estimates of strength. Although typical

Table 1.1: Beam Imperfections

	Assumptions of classical buckling theory (eg. Timoshenko[2])	Real Beams	Comments
Geometry	1. Initially perfectly straight, undeformed beam	1. Initially deformed, with initial bow and twist	1. Initial deformations have a significant effect on load-deflection behaviour and reduce load-carrying capacity of beam.
	2. Cross-sectional dimensions constant over length of beam	2. Variations in cross-sectional dimensions	2. Generally, variations small for rolled beams as controlled by strict rolling tolerances (eg. BS4, Part 1)[42]. Effects of small variations insignificant compared with those arising from initial bow and twist and residual stresses.
		3. Deflections in plane of applied load	3. Neglect of this errs on the safe side but its inclusion increases theoretical elastic critical loads of beams typically by 1 - 6%[43].
Loading	1. Loading applied in plane of major axis only	1. Applied loads not truly vertical	1. Small Component of applied load in horizontal plane produces minor axis bending.
		2. Applied loads eccentric to shear centre of section	2. Loads not acting through the shear centre induce torsion in the beam.

Table 1.1: Beam Imperfections (contd)

	Assumptions of classical buckling theory (eg. Timoshenko[2])	Real Beams	Comments
Material	1. Initially stress free	1. Residual stresses present	1. Residual stress patterns in as-rolled beams highly variable. Pattern and level of stress is dependent on method of production, distribution of material between flanges and web, rate of cooling and any locked-in stresses due to handling, straightening or bending.
	2. Perfectly elastic	2. Section may yield under increasing load or as a result of large out-of-plane deflections	2. Yielding reduces the stiffness of the section with the elastic core providing most of the residual stiffness. Effect previously described in Section 1.1.
		3. Variations in yield stress throughout cross-section and along beam	3. Nethercot[44] notes lower values generally observed in flanges than in web. Also slight difference between yield stress in tension and that in compression. Net effect is usually to err on the safe side.

increases in critical load of between 1 and 6 per cent have been attributed to this effect in Table 1.1, the increase in any particular case is dependent on the cross-sectional geometry of the beam, its span and the nature of the applied loading. A detailed account of this effect has been published by Trahair and Woolcock[43], who noted increases in excess of 20 per cent for American rolled 8WF31 sections used as beams. (The 8WF31 section corresponds approximately to the British 203 x 203 UC 46 metric section.) As the use of column sections as beams was considered the exception rather than the rule, the lower increases of between 1 and 6 per cent noted for typical beam sections have been given in Table 1.1 .

Published work by Nethercot[39-41], examining the effect of residual stresses on calculated inelastic critical loads of beams, concluded that these loads were less affected by the pattern of residual stress than by peak values of residual flange stress since the latter determine the moment at which flange yielding commences. Fig. 1.6 shows Nethercot's[41] prediction of the effect of residual stress level on the critical load of an 8WF31 section over a large range of slenderness (l/r_y) values. In the derivation of these curves (based on the tangent modulus concept), the beam has been assumed to be simply supported and loaded with equal end moments. In addition, an elastic-perfect plastic material behaviour has been assumed (Fig. 1.7). The notation employed in Fig. 1.6 is as defined in Section 1.1 for Fig. 1.3 except for the following additional parameters:

σ_y yield stress of beam material

σ_{rc} maximum residual compressive stress in section

Fig. 1.6 shows that the presence of residual stresses decreases the critical load of the beam, the actual decrease being a function of the slenderness (l/r_y) and the magnitude of the residual stress (σ_{rc}). The graph also shows that one effect of increasing the residual stress level is to extend the range of slenderness values over which inelastic buckling occurs.

Although the effects of non-vertical and eccentric loading on the load-carrying capacity of beams are likely to be significant, these imperfections are again random in nature. Arguably, the difficulty in obtaining representative values of eccentricity and 'out-of-plumb' exceeds that associated with the determination of representative values of residual stresses. Therefore, although the individual or combined effects of loading imperfections can be examined theoretically, even with relative ease in cases of elastic buckling, few field measurements or experimental data are available to provide the necessary link between theory and practice.

With the exception of initial geometric deformations (ie. initial bow and twist), the relative importance of each of the other imperfections shown in Table 1.1 has been indicated therein.

Of all the imperfections listed, the presence of initial bow and/or initial twist in a length of beam has probably the most detrimental effect on the stability and behaviour of the member in service. As indicated in Fig. 1.4, beams possessing these imperfections deflect laterally and twist from the onset of loading. Consequently, the buckling behaviour of such beams does not conform to the classical mathematical analysis presented by Timoshenko [2]. Although the elastic and inelastic behaviour of beams and columns is generously reported in the literature, there exist very few quantitative assessments of such imperfections in test specimens. This is substantiated by examination of the literature concerned with theoretical and experimental investigations into beam and column stability problems. Table 1.2 summarises relevant data obtained from a total of thirty-one references considered most likely to furnish the necessary information. The following notation has been used in Table 1.2:

u_0	initial lateral deflection of compression flange at midspan
l	span of beam
φ_o	initial angle of twist at midspan (radians)
D	overall depth of beam section
η_P	Perry-Robertson imperfection factor
r_y	minor axis radius of gyration

Sinusoidal distributions of both crookedness and twist were assumed by Trahair[30] and Meck[31] in their derivations of modified Southwell

Table 1.2: Measured Geometrical Imperfections Reported in the Literature

Ref	Author(s) & date	beam or column	measured or assumed values			notes
			u_o/l	φ_o(rad)	$\varphi_o D/l$	
28	Southwell (1932)	pinned col.	-	-	-	proposed Fourier series for initial imperfections
45	Zuk (1956)	beams	1/1000	-	-	assumed sinusoidal forms for initial bow and twist - value only assigned to initial bow
35	Kerensky et al. (1956)	beams & girders	-	-	-	no measured values given but uses Perry-Robertson $\eta_p=0.003(l/r_y)$ for flanges, giving either general curvature in plan or initial twist
46	Winter (1958)	beams	1/250 - 1/500	-	-	proposed values assigned to the independent compression half of the beam
47	Massey (1962)	beams	1/1000	1/3000	-	assumed sinusoidal distributions
48	Massey (1963)	beams	1/1000	1/2500	-	assumed sinusoidal distributions
30	Trahair (1969)	beams	-	-	-	assumed sinusoidal distributions of bow and twist
38	Dibley (1969)	beams	.0029†	-	-	4 measured values from British sections in Grade 55 steel
			.0034†	-	-	† value measured as offset from a chord joining the ends of a simply supported beam overhanging at both ends
			.000996	-	-	
			.001292	-	-	

Table 1.2: Measured Geometrical Imperfections Reported in the Literature (contd)

Ref	Author(s) & date	beam or column	measured or assumed values			notes
			u_0/l	φ_0(rad)	$\varphi_0 D/l$	
39	Nethercot (1974)	beams	-	-	-	results based on Perry-Robertson imperfection factor - no measured values given
24	Nethercot et al. (1976)	beams	-	-	-	no measured imperfections but quotes Perry-Robertson η_p as used in draft code B/20
49	Medland (1977)	columns	1/1000	-	-	assumed sinusoidal distribution for initial bow
31	Meck (1977)	beams	-	-	-	assumed sinusoidal distributions but no values given
50	Fukumoto et al. (1980)	beams	.00008	-	.000138	mean values from 75 Japanese rolled beams
51	Fukumoto et al. (1981)	welded beams	.000296	-	.000504	mean values from 68 Japanese welded beams
4	Dux & Kitipornchai (1981)	continuous beams	.0002 .0004 .0003 .0008 .0005 .0007 .0004 .0005 .0004	.003 .002 .003 .003 .001 .003 .002 .002 .003	.00014 .000114 .000192 .000256 .000205 .00022 .000146 .000128 .000171	values quoted for initial bow & twist at elastic shear centre in 9 Australian rolled beams
32	Attard (1982)	cantil. beam	1/400	.05	-	assumed values at free end
52	Fukumoto et al. (1982)	2 span cont. beams	.00057 .0004	- -	.0004 .00052	mean values for each of 2 spans in 21 Japanese rolled beams
53	Lui et al.(1983)	columns	1/1000	-	-	assumed sinusoidal bow - value conforms to AISC delivery specification

plot procedures for beams. Initial sinusoidal bows of amplitude equal to one-thousandth of the span were assumed by Zuk[45], Massey[47,48], Medland[49] and Lui and Chen[53] in theoretical analyses, Massey's analyses also assuming particular values for sinusoidal distributions of initial twist (Table 1.2).

Sinusoidal distributions of crookedness and twist were relinquished by Kerensky et al[35] in favour of the Perry-Robertson approach which, they demonstrated, could be applied to all cases of elastic or inelastic buckling of beams and girders in order to obtain satisfactory design curves. In consequence, the Perry-Robertson approach was subsequently adopted in both BS 153(1958)[36] and BS 449(1959)[37]. More recently, Nethercot[24,39,54] has highlighted the reliability of the approach and its potential for application in limit-state as well as elastic design methods. Its incorporation in the new limit-state Bridge Code[55] and Steelwork in Buildings Code[56] lends further support to these assertions.

Only five of the published works examined prior to compilation of Table 1.2 presented numerical data obtained from direct measurement of imperfections in test beams. Of these, only that of Dibley[38] reported measurements on British sections, the sections being rolled in Grade 55 steel. Fukumoto et al.[50-52] presented mean imperfections for a total of ninety-six rolled and sixty-eight welded beams manufactured in Japan whilst Dux and Kitipornchai[4] reported test measurements for each span in each of nine tests on continuous beams. The values shown in Table 1.2 for Dux and Kitipornchai's tests indicate the maximum values recorded for each beam.

All values of non-dimensional initial bow (u_0/l) measured by Fukumoto et al.[50-52] and Dux and Kitipornchai[4] on Japanese and Australian rolled sections, respectively, were lower than the "rule of thumb" value of 0.001 noted in the theoretical beam analyses of Zuk[45] and Massey[47,48]. Dibley's[38] results indicated larger initial crookedness in his test beams. The AISC[57] delivery specification for structural steel shapes demands an initial straightness tolerance of $u_0/l = 0.001$ whilst the rolling tolerance specified in BS 4: Part 1[42] is $u_0/l = 0.00104$. A tolerance on non-dimensional initial bow of 0.001 was also demanded by a bridge design memorandum issued by the

Department of the Environment[58] following publication of the report of the Merrison Committee and the so-called "IDWR" document in 1973. Initial twist was also limited by this document, twist being expressed in terms of the relative misalignment of the flanges as shown in Fig. 1.8 . Similar tolerances on initial imperfections are demanded by Part 6 of the new British Bridge Code[55].

As would be expected, reported values of non-dimensional initial twist ($\varphi_o D/l$) displayed a scatter similar to that observed in the u_0/l measurements. On the basis of the results presented in Table 1.2, typical values of non-dimensional twist in beams lie in the range 0.0001 to 0.0006.

In conclusion, several random initial imperfections occur in real beams and have a significant effect on beam behaviour and, consequently, on the adequacy of associated bracing systems. Generally, initial crookedness, twist and residual stresses have the most detrimental effect, although accidental eccentricity and misalignment of nominally vertical applied loading also play an important, though less quantifiable, role. The imperfections listed in Table 1.1 do not occur in isolation. Depending on their distribution, coexistent initial imperfections can have an additive or relieving effect as far as their destabilising influence is concerned.

In practice, as it is not feasible to measure any of the imperfections listed in Table 1.1 either prior to, or during, erection of steelwork, design rules governing the suitability of sections in particular applications must incorporate allowances for the most unfavourable combinations of initial imperfections. The use of an enhanced value of one of the imperfections to make allowance for others which cannot be measured is therefore an attractive solution. Winter[46] was among the first to advocate such an approach for column design when it was proposed that an enhanced crookedness of about double the AISC crookedness tolerance be employed to account for the presence of other imperfections. The current trend towards limit-state design codes[55,56] based on probabilistic concepts should provide a framework into which the probability of occurrence of random initial imperfections can be included. Such an approach would provide a method of allowing for imperfections consistent with limit-state philosophy.

1.2.3 Elastic Lateral-Torsional Buckling of Beams either Laterally or Torsionally Restrained on the Span

In 1951 Flint[59] published the results of theoretical and experimental investigations concerned with the buckling of beams provided with intermediate elastic supports. The results of tests on aluminium alloy model I-section beams gave support to the equilibrium- and energy-based solutions which had formed the basis of the theoretical analysis. Attention was focussed on four main topics: the influence of complete and partial end support; the effect of intermediate torsional restraints; and the influence of intermediate restraints such as filler joists. It was found that in order to enforce the second mode of instability in the primary member, it was generally necessary to attach the stay above the shear centre.

In the case of a simply-supported beam under central point loading applied at its top flange, a single translational restraint to this flange of stiffness greater than the lateral bending stiffness of the primary member by a factor (denoted by 'λ') of about ten was suggested to be adequate for the enforcement of the elastic second mode of buckling. For shear centre restraint, λ was noted to increase to fifteen. Any increase in the axial stiffness of the brace beyond these full-bracing values proved ineffective in increasing the critical load of the primary member.

The non-dimensional translational restraint stiffness 'λ' is defined[59] by

$$\lambda = \frac{K\ell^3}{48EI_\eta} \qquad \ldots(1.2)$$

where K = absolute stiffness of translational restraint

l = span of beam

E = Young's modulus

I_η = 2nd moment of area of beam cross-section about its minor axis

In the case of tension flange restraint, although the second mode could not be achieved even for very large restraint stiffnesses, significant increases in critical load relative to unbraced values were nevertheless observed.

Flint had demonstrated that, although the second mode critical load could not be altered by changing the level of attachment of the bracing, the brace stiffness required to achieve this load was minimised when the brace was attached at the level of the compression flange.

Tests were also conducted[59] on parallel primary members interconnected by a single midspan brace. Although the bracing element possessed both axial and flexural stiffness, Flint's tests revealed that, under identical loading patterns on the beams, it was possible for them to buckle together in such a way that the lateral restraint afforded by their interconnection was zero. In this event, the axial stiffness of the brace was not utilised. However, the flexural stiffness of the brace or filler joist provided a degree of midspan torsional restraint to the primary members (Fig. 1.9), thereby increasing the overall stability of the system. Although the provision of relatively high values of such torsional restraint did not permit second mode buckling loads to be achieved in the tests, theoretical analyses showed that considerable increases in critical load could be realised. The relationship between beam stability and torsional restraint stiffness is shown in non-dimensional form in Fig. 1.10, taken from Ref. 59 where the effects of the beam's warping rigidity have been neglected. Although subsequent work by Taylor and Ojalvo[60] showed neglect of this parameter to have considerable effect on the elastic analysis, Fig. 1.10 nevertheless illustrates the beneficial effect of midspan torsional restraint. In this figure, the following notation has been adopted and is consistent with that employed in Chapter 2:

$$e = \text{non-dimensional torsional restraint stiffness}$$

$$= \frac{\text{flexural stiffness of interconnecting brace}}{\text{torsional stiffness of primary beam}} \quad \text{or}$$

$$= \frac{\text{stiffness of torsional spring restraint (Fig. 1.5)}}{\text{torsional stiffness of primary beam}}$$

$$= \frac{K_T l}{GJ} \qquad \ldots(1.3)$$

where K_T = absolute stiffness of torsional restraint

l = span of beam

G = shear modulus

J = St. Venant torsion constant for beam

Also, c = critical stress factor

$$= \frac{\text{critical moment of system}}{\left\{\begin{array}{l}\text{critical moment of unbraced beam of equal span}\\ \text{under uniform moment}\end{array}\right\}}$$

The possibility of attainment of the second mode elastic critical load by the provision of only torsional restraint is considered later in this Section and again in Chapter 2. An investigation into the effectiveness of elastic cross beams has been presented by Nishida et al[61]. This showed that the degree of torsional restraint provided by the cross beams was often sufficient, theoretically, to induce second mode buckling in the primary beams.

In a study devoted to the examination of the strength and stiffness criteria to be met by translational restraints in order to provide "full" restraint to elastic beams and columns, Winter[46] proposed an analytical model for beams in which the compression flange, isolated from the web and tension flange, was regarded as an independent strut free to buckle in its own plane. It was recognised that the beam was more stable against lateral buckling than its isolated compression portion. Consequently, on the grounds that the total force in the compression portion of the beam at the instant of lateral buckling was known to be larger than the Euler column load of that portion when isolated, but of the same order of magnitude, it was suggested that bracing dimensioned to be adequate for an independent compression flange would prove sufficient and would not be wasteful.

In order to justify the conclusion that the provision of anything less than full bracing to primary members was uneconomical due to the relatively modest section sizes required for such restraint, Winter presented the results of a series of tests on model I-section columns braced by cardboard strips. These results showed that the usable column strength could be increased by a factor approaching fifteen as a result of the attachment of inexpensive, intermittent bracing. In those tests where fracture of the bracing strips accompanied failure of the column, the tensile strength of the individual braces was approximately one per cent of the column strength. Additionally, the test demonstrated an interrelatonship between bracing stiffness and strength: the stiffer braces not only increased the column strengths but also required less strength themselves in order to produce a given column load.

Based on Winter's conservative "independent compression flange" method for proportioning beam bracing systems, a specific example investigating the requirements for fully effective, continuous restraint of an 18WF50 beam showed that the total restraining force did not exceed 5% of the compression flange squash load.

Extending the previous work by Winter[46] on the strength requirement of braces, Zuk[45] presented a theoretical investigation into the bracing forces developed in eight typical cases of braced beams and braced columns. Within the limitations imposed by an assumed initial crookedness of span/1000 in the beam (Table 1.2), elastic material behaviour and small deflection theory, the solutions obtained were either exact (resulting from direct solution of the governing differential equations of equilibrium) or approximate (from the principles of minimum total potential energy). Results of beam analyses indicated a maximum brace force not exceeding 2% of the compression flange force at buckling in braces attached to the compression flange. Higher forces of about 2.4% of the compression flange force were noted in bracing attached at the level of the shear centre of the beam. Zuk also deduced that a beam restrained by more than one brace would induce into each brace a force of about 2% of the compression flange force at buckling.

Acknowledging the possibility of only finite torsional restraint at beam supports, Schmidt[62] studied the interaction between a single, central, elastic translational restraint and incomplete end torsional supports. A differential equation solution was employed, in which the assumptions of small deflections and no cross-sectional deformations were made. The load and restraint points on the beam were also assumed to be at the same height above the shear centre. Formulae were presented for the calculation of the stiffness requirements of each type of support in order to allow the beam to develop its maximum load-carrying capacity.

Defining the torsional restraint parameter, e, in terms of the torsional stiffness of a support and that of the beam, Schmidt showed that provision of $e \geq 40$ at each end of a beam under central point loading would ensure fully effective torsional end restraint. Beams were noted to be incapable of supporting any load when end supports possessed no torsional stiffness ($e=0$).

In extending the work of Flint[59] on intermediate torsional restraints, Taylor and Ojalvo[60] included the effects of warping in elastic bifurcation analyses applied to three types of loading and two types of torsional restraint. Continuous torsional restraint on the span was shown to result in increasing critical load with increasing restraint stiffness "apparently without limit". In the case of a single, central, elastic torsional restraint, the critical load was again limited by the formation of the well-known two half-wave mode (ie. the elastic second mode) of lateral-torsional buckling. Critical loads corresponding to second mode buckling are characterised by the plateaux of constant 'c' in Figs. 1.11 and 1.12, where Flint's[59] torsional restraint curves (Fig. 1.10) have been superimposed on the results of Taylor and Ojalvo[60]. Flint's analyses have previously been noted to have neglected the contribution made by a beam's inherent warping rigidity to its overall resistance to lateral-torsional instability. In these figures, the shape parameter 'R' is used as a measure of the relative importance of warping rigidity in resisting torsional deformations. The shape parameter 'R' is defined[63] by

$$R = \sqrt{\frac{l^2 GJ}{E\Gamma}} \qquad \ldots(1.4)$$

where GJ = St. Venant torsional rigidity of the section and
$E\Gamma$ = warping rigidity of the section.

High values of R are associated with slender beams in which warping rigidity is low relative to torsional rigidity. Theoretically, the value $R = \infty$ is therefore appropriate to Flint's[59] analyses.

It has been noted in Section 1.1 that, as far as stability is concerned, uniform bending moment represents the most unfavourable type of applied loading on a beam. Figures 1.11 and 1.12 show that beams attain consistently higher critical moments (and hence critical stress factors 'c') under central point loading than under uniform bending moment. However, the apparently greater stability of a beam under concentrated load is not reflected in a reduction in the torsional restraint required for attainment of second mode buckling. For example, values of 'e' approaching 900 are required to induce second mode buckling in beams of high warping rigidity (ie. low 'R') under concentrated load at midspan. However, lower values of between 500 and 530 are sufficient to provide fully effective restraint to identical beams under uniform bending moment.

Figs. 1.11 and 1.12 also show that no further increase in critical load can be achieved by providing torsional restraint stiffness in excess of the minimum value required for full bracing, the "critical brace stiffness", e_{cr}. This confirms earlier conclusions of Flint[59] and Winter[46]. Both second mode critical loads and critical brace stiffnesses are dependent on the cross-sectional geometry of the primary member, described by the parameter 'R', and the nature of the applied loading. The limitations of Flint's[59] analyses are highlighted in Figs. 1.11 and 1.12, from which it can be deduced that allowance for warping rigidity must be made if theoretical elastic bracing analyses are to yield useful results.

Following previous studies of single span elastic beams with and without intermediate restraints, Hartmann[16] extended the investigation to continuous elastic beams which previously could only have been analysed by one of the variations on a lower bound approach developed by Salvadori. This approach treated the continuous beam as a series of simply-supported beams, each with its appropriate moment and shear distribution obtained from analysis of the continuous structure. A lower bound estimate of the critical load of the continuous beam was then taken to be the smallest value of critical load calculated for any of the simply-supported beams.

Hartmann questioned the validity of the inherent assumption that lateral displacements and twist were wholly prevented at interior supports. His published work[16] examined the effects of bracing stiffness at interior supports in an attempt to define minimum stiffnesses satisfying this assumption. As the present study is concerned with the restraint of single span beams, much of Hartmann's work is of no direct relevance. However, analyses presented as an introduction to the main body of his work are relevant and directly comparable with results of previous research.

An elastic analysis based on classical small displacement buckling theory, making allowance for the warping rigidity of sections but neglecting cross-sectional deformations, was employed by Hartmann. This gave the results shown in Fig. 1.13 for a simply-supported beam under central point loading, with load applied at and translational restraint attached at the shear centre. The results have again been plotted non-dimensionally in terms of the critical stress factor 'c', shape parameter 'R' and non-dimensional translational restraint stiffness 'λ'. Flint[59] had proposed the following simplified relationship for the critical stress factor 'c' in terms of 'λ' for a beam of $R=\infty$ under central point loading:

$$c = 1.35\sqrt{1 + \lambda} \qquad \ldots(1.5)$$

In the derivation of this relationship, translational restraint attached at the level of the shear centre had been assumed. The curve described by equation (1.5) is also shown in Fig. 1.13. For values of λ less than two, Flint's curve and that of Hartmann for $R^2=\infty$ are indistinguishable. However, for larger values of λ the divergence is appreciable and critical brace stiffnesses (λ_{cr}) predicted by the two methods are markedly different: Flint's predicted value of $\lambda_{cr} \doteqdot 6$ is significantly less than Hartmann's prediction of $\lambda_{cr} \doteqdot 11$.

Flint, recognising that the relationship described by eqn. (1.5) would be "appreciably in error" as the second critical load was approached, advocated the use of a more refined analysis to improve accuracy. In particular, a minimum total potential energy solution employing two or more trigonometric terms in the assumed displacement function was recommended. Such an approach has been adopted in the analyses presented in Chapter 2.

A later series of confirmatory elastic flexural-torsional buckling tests on two-span beams of rectangular cross-section was carried out by Hartmann[6]. The experiments proceeded under load control and consequently it was not possible to determine the critical load by direct measurement. However, Trahair's "modified plot" method[30] was used to evaluate the experimental critical loads. These differed from the theoretical values[16] by 6% on average.

A more recent study of the adequacy of discrete restraints by Nethercot and Rockey[63] was based on the finite element method. Uniform applied bending moment was assumed throughout the work which investigated the separate effects of translational and torsional restraints. In addition to consideration being given to the effects of warping, allowance for cross-sectional deformation was made in the analysis. Fig. 1.14 shows the results of Ref. 63 for the case of a beam laterally restrained at its shear centre, cross-sectional deformations being prevented only at the restrained section. The corresponding curve from Flint's earlier study[59] of the bracing requirements of slender beams is indistinguishable from Nethercot and Rockey's $R^2=\infty$ curve.

Nethercot and Rockey's relationship between the critical stress factor 'c' and non-dimensional torsional restraint stiffness 'e' is shown in Fig. 1.15 where the curves of Taylor and Ojalvo[60] are superimposed. The curves attributed to Nethercot and Rockey[63] in Figs. 1.14 and 1.15 have been derived on the basis of "complete attachment" of the restraint, a condition modelled in the finite element solution by the prevention of cross-sectional deformations of the beam at the braced section only, all other cross-sections on the span being free to deform.

Comparison of the $R^2=12$ curves in Fig. 1.15 shows that the finite element solution of Ref. 63 predicts a higher value of critical torsional restraint stiffness 'e_{cr}' than does the conventional elastic analysis employed by Taylor and Ojalvo[60]. The predicted values are, approximately, $e_{cr}=150$ (Ref. 63) and $e_{cr}=110$ (Ref. 60). The finite element solution also predicts a slightly lower second mode buckling load and hence it can be deduced that the inclusion of cross-sectional deformations at sections other than the restrained section tends to decrease the predicted second mode critical load whilst also increasing the torsional restraint stiffness required for full bracing.

Classical elastic buckling analysis[2] makes no allowance for cross-sectional deformations. Therefore, the level of attachment of torsional restraint has no effect on calculated critical loads. However, Nethercot and Rockey's[63] finite element analysis, capable of modelling cross-sectional deformations at the braced section in addition to all other locations on the span, was used to assess the effect of deformations of the restrained cross-section on the adequacy of the restraint. Fig. 1.16 shows the results obtained for a beam having $R^2=32$.

Fig. 1.16 shows that, if allowance is made for deformations of the cross-section at all points on the span, shear centre attachment of torsional restraint is slightly more efficient than attachment to either flange, although neither permits the second mode critical load to be attained. This is contrary to the results obtained for translational restraints. Of greater efficiency, but still insufficient for complete restraint, is the provision of half of the total stiffness K_T at each flange. Full bracing could only be achieved by "complete attachment" of the restraint. In this case, the critical value of $e_{cr}=72$ corresponds to that shown in Fig. 1.15 on the $R^2=32$ curve.

Whereas Nethercot and Rockey[63] had examined the bracing requirements of beams with loading restricted to uniform bending moment on the span and translational restraint attached only at the shear centre, a study by Mutton and Trahair[64] extended the investigation to cover a wider range of loading and restraint geometries. The finite integral method was employed for solution of the governing differential equations of equilibrium and deformations of the cross-section were neglected.

Fig. 1.17, presented in terms of the shape parameter R, shows the values of critical non-dimensional torsional restraint stiffness e_{cr} required for full midspan bracing of a beam under central point loading. Although the variation of e_{cr} with R is significant, e_{cr} is independent of the level of application of applied load for slender beams having values of R greater than 30. For beams of lower slenderness, greater values of e_{cr} are noted for compression flange loading than for load applied at points lower on the cross-section. This agrees well with an earlier observation by Flint[59] that loads applied above the shear centre had a greater destabilising effect on the system. Fig. 1.17

predicts that beams loaded with central concentrated loads can always be rigidly braced by a torsional restraint of sufficient stiffness.

A comparison of the predicted values of e_{cr} from Fig. 1.17 with those of Taylor and Ojalvo from Fig. 1.11 and from Ref. 60 is shown in Table 1.3.

Table 1.3: Comparison of e_{cr} Values from Refs. 60 and 64

R^2	Predicted values of e_{cr} for beam under central point loading applied at the shear centre	
	Mutton and Trahair[64]	Taylor and Ojalvo[60]
2	810	881
4	425	456
6	300	326
8	236	253
12	175	179
16	142	147
32	95	95
96	66	57

Allowing for the difficulty in determining accurate values of e_{cr} from the small graphs presented in the published papers[60,64], correlation between the results in Table 1.3 is excellent.

The relationship between critical translational brace stiffness λ_{cr} and shape parameter R for a beam under central point loading is shown in Fig. 1.18. Like Fig. 1.17, Fig. 1.18 has been based on numerical results presented in Ref. 64 but is expressed in terms of the variables employed in the present study. From the nine combinations of load/restraint geometry shown, it is evident that a value of λ=15 is sufficient for the complete midspan restraint of all beams having values of R between 1 and 300 provided that the restraint is to the top (compression) flange. Fig. 1.18 shows that as R increases the effects of loading and restraint geometry on the required translational stiffness λ_{cr} become less significant, until, for values of R close to 300, a narrow range of λ_{cr} values ($8 \leq \lambda_{cr} \leq 15$) encompasses all combinations. This conclusion agrees well with Flint's[59] earlier recommendation of $\lambda_{cr} \leqslant 15$ for compression flange or shear centre restraint. Fig. 1.18 also predicts that beams having $R < 15$ cannot be fully restrained by tension flange bracing alone. Similarly, it is predicted that shear centre restraint is insufficient for beams of $R < 25$ loaded at the compression flange.

Although the results of previous research had supported the use of compression flange bracing, Roeder and Assadi[65] devoted a study to the effectiveness of tension flange restraint. A finite difference solution provided the basis for the theoretical analysis and a short experimental programme was conducted. The results indicated that, although tension flange restraint was incapable of increasing the elastic critical load of a beam under uniform bending moment to a level compatible with failure in the second mode, such restraint nevertheless produced significant increases in the buckling loads of beams of inherently high St. Venant torsional stiffness. In terms of the notation employed in the present study, Roeder and Assadi suggested that torsional stiffness dominated the buckling analysis for beams possessing $R > \pi$. Although increases of less than 8% in the critical loads of beams with $R < \pi$ and with tension flange restraint were observed, an increase in excess of 50% was obtained experimentally for a more slender beam continuously restrained on the tension flange by a thin steel membrane.

In conclusion, since the pioneering work on the subject by Flint[59] and Winter[46], a considerable research effort has been invested in the problem of the elastic lateral-torsional buckling of simply-supported beams restrained either laterally or torsionally on the span. Of primary concern in the majority of the studies reported in this Section has been the need to provide fully effective restraint to the beam in order that the second mode of buckling could be achieved. Winter[46] and Zuk[45] demonstrated the adequacy of modest bracing in providing full restraint to initially straight or crooked beams and concluded that the provision of anything less than fully effective bracing was uneconomical. The minimum stiffness of lateral or torsional restraint required to achieve full bracing is called the critical brace stiffness.

Several factors are important in determining the adequacy of restraint systems possessing only one restraining action: the level of attachment of translational restraint relative to the position of the shear centre of the section; the nature of the applied loading; and the prerequisite of adequate lateral and torsional restraint at the supports.

The work of Hartmann[16], Taylor and Ojalvo[60] and Mutton and Trahair[64] highlighted the need for warping effects to be taken into account in elastic buckling analyses. Both critical brace stiffnesses and second mode critical loads were shown to be dependent on the warping rigidity of the primary member. However, warping plays a less significant role in very slender beams where the greater part of the resistance to torsional deformation is derived from the St. Venant torsional stiffness rather than from warping rigidity. Consequently, slender beams conform most closely to the behaviour predicted by Flint[59].

Predicted critical loads were noted to decrease and critical brace stiffnesses to increase when allowance was made for cross-sectional deformations in a finite element analysis presented by Nethercot and Rockey[63]. The exact nature of the deformations was dependent on the method of attachment of the torsional brace but in all cases their presence was seen to reduce the effectiveness of the restraint. The optimum locations for attachment of bracing on the cross-section were found to be different for torsional than for translational restraint. It was suggested[63] that, to obtain fully effective restraint from a central torsional brace, the brace should be capable of preventing the occurrence of cross-sectional distortion.

This Section has demonstrated that, in the majority of cases, fully effective restraint can be provided by either translational or torsional restraint on the span. In only a few cases where the level of attachment of restraint is "low" relative to the compression flange and shear centre is this impossible. In practice, most bracing members provide both translational and torsional restraint and hence utilisation of both types would appear advantageous. Some of the benefits of combined restraint reported in the literature are described in the next Section.

1.2.4 Elastic Lateral-Torsional Buckling of Beams Laterally and Torsionally Restrained on the Span

In their finite element study of Ref. 63, Nethercot and Rockey also examined the effect of combined translational and torsional restraint on the stability of simply-supported beams under uniform moment. As in the previous Section, warping rigidity was found to play an important role in determining the buckling behaviour of the system.

Fig. 1.19 illustrates the increase in stability of an R^2=32 beam (that of Fig 1.16) achieved by the provision of combined lateral and torsional restraint at midspan. Without torsional restraint (e=0), translational restraint of non-dimensional stiffness λ=10 is required for full bracing; however, even the provision of a very modest torsional restraint of e=10 reduces the translational bracing requirement to λ=3.5. On the other hand, infinite torsional restraint at midspan is itself insufficient to brace the beam adequately. Coexistent shear centre translational restraint having $\lambda \geqslant 2$ is therefore required for attainment of second mode buckling. Tabulated values of 'c' for other combinations of λ, e and R^2 values are given in Ref. 63. In all cases, allowance for combined bracing action considerably enhances beam stability.

Another recent investigation into the combined axial and flexural rigidity requirements of single, midspan, elastic restraints was made by O'Connor[66]. The only type of applied loading considered was uniform bending moment. A simplified analytical model was employed in which the beam was modelled by its flanges, the web playing a minor role and serving only to couple flange displacements and twists. Winter[46] had previously used a similar but rather more simplified approach in modelling a beam by its isolated compression flange. No experimental or more refined theoretical studies were cited by O'Connor in support of the closed-form solutions presented. In addition, the extremely unwieldy presentaton of equations, the lack of precise definition of symbols and the presence of several errors both in the equations and accompanying text render O'Connor's paper[66] almost unusable.

In addition to the many investigations concerned with discrete intermediate restraints, several have dealt with continuous or diaphragm bracing of beams and columns. That of Trahair[67] dealing with the continuous restraint of elastic beam-columns has noted the increasing effectiveness of continuous translational and torsional restraint with distance above the shear centre, a conclusion seen to be in agreement with the findings of earlier studies into discrete restraint.

A recent appraisal of various forms of bracing for elastic systems has been published by Trahair and Nethercot[68]. Reflecting the paucity of information on the subject, this review cited few previous studies concerned with combined translational and torsional restraint. However, one of the previous investigations of particular importance was noted to be that of Mutton and Trahair[64].

Following their examination of isolated translational and torsional restraint systems in Ref. 64, Mutton and Trahair in the same published work showed that, where sufficiently high torsional restraint was provided to beams under central point loading, it was possible in all cases to dispense with the need for bracing possessing axial rigidity. Although the study by Nethercot and Rockey[63] had considered a different and more onerous type of applied loading, namely uniform bending moment, a discrepancy is apparent between Refs. 63 and 64. Contrary to the findings of Mutton and Trahair, Nethercot and Rockey predicted that torsional restraint in isolation would be unable to provide complete restraint. A possible explanation is that, in addition to the more severe loading assumed in Ref. 63, allowance for deformations of the cross-section was also made therein. It has previously been noted (Section 1.2.3) that the effect of these deformations was to increase predicted critical brace stiffnesses.

Conversely, torsional restraint was not required where a sufficient degree of translational restraint to the compression flange was provided. In cases where translational restraint was attached lower on the cross-section, rotational restraint was often additionally required. Fig. 1.20 shows combined torsional and translational restraint stiffnesses required[64] for full bracing with tension flange or shear centre attachment of translational restraint. In agreement with the trend observed in Figs. 1.11 to 1.15, 1.17 and 1.18, Fig. 1.20 predicts that more substantial bracing systems are required for the complete restraint of beams of low R.

However, it must be noted that beams in this category are generally of low to intermediate slenderness (Fig. 1.3) and are consequently more susceptible to inelastic than to elastic instability. The current requirements of effective restraint systems for the prevention of first mode inelastic buckling of beams are presented in Section 1.2.5.

1.2.5 Restraint Systems Associated with Inelastic Lateral-Torsional Buckling of Beams

Unlike the bracing of beams for the prevention of failure by elastic flexural-torsional buckling, the requirements of bracing associated with beams of intermediate and low slenderness which fail under inelastic conditions (Fig. 1.3) have received relatively scant attention in the literature. The pioneering work on this topic was reported by Massey[47] who, on the basis of an assumed linear elastic-perfect plastic material characteristic (Fig. 1.7) proposed an equilibrium-based solution for the force developed in a single translational restraint. Other major assumptions were those of a single span, simply-supported beam of doubly-symmetric I-section under uniform bending moment, restrained at its midspan by a rigid horizontal support. Sinusoidal distributions both of initial crookedness and twist were incorporated, permitting solution for the restraint forces. A doubly-symmetric distribution of plasticity over the cross-section (Fig. 1.2) was assumed for varying degrees of plasticity from the onset of yield to full flange plasticity. This pattern of yielding was considered by Lay and Galambos[69] to be unacceptable in an initial deflection problem as presented by Massey. Its use in a classical buckling analysis was justified as no out-of-plane deflections occurred until the buckling condition was reached. However, in the initial deflection problem, lateral deflections and twist commenced from the onset of loading and consequently longitudinal stresses due to lateral bending and twist would destroy the symmetry of Massey's assumed distribution. Six tests on steel model I-beams were performed in an attempt to verify the theoretical predictions.

The main conclusion arising from both the theoretical and experimental results was that, for short inter-brace distances, there was a possibility of brace forces exceeding the contemporary American design recommendations[70]. Subsequent criticism both of the theoretical analysis and the experimental procedure by Lay, Galambos and Schmidt[69] questioned the interpretation of the results in relation to the American Code. The supposedly correct interpretation invalidated Massey's expressed concern.

Massey had assumed that the bracing force developed in a central lateral restraint would be the force developed in an infinitely rigid restraint at the same point. As noted by Lay and Galambos[69], "there is no reason why [the latter] force should be synonymous with the bracing condition required to ensure the adequate structural performance" of the beam. Prior to Massey's paper[47] in 1962, Flint[59], Winter[46] and Zuk[45] had demonstrated the adequacy of central translational bracing of finite rather than infinite stiffness in providing complete restraint to beams and columns. On the basis of Winter's conclusion that stiffer braces required less strength, Massey's[47] assumption of infinite translational restraint would have resulted in a lower bound estimate of the bracing force. Massey noted that the contemporary American practice of designing bracing members to resist a force equal to 2% of the ultimate compression flange force appeared satisfactory for beams of span greater than $130r_y$; for more stocky beams, it was possible for brace forces to exceed the 2% design value by a considerable margin. However, Lay and Galambos[69] showed the basis of Massey's calculations to be in error and that, on correct interpretation, the results presented in Ref. 47 predicted brace forces significantly less than those permitted by the 2% design rule.

A later method of predicting the bracing requirements of inelastic steel beams under uniform moment was developed by Lay and Galambos[71]. Earlier work by the same authors had provided an expression for the transverse bending moment at which local buckling of the compression flange would occur. Lay[72,73] employed the discontinuous theory of yielding in the derivation of critical compression flange breadth to thickness ratios for the attainment of local buckling. The occurrence of local buckling was also dependent on the moment gradient on the beam, the length of the yielded region and the strain hardening properties of the steel. These parameters were then incorporated into a theoretical derivation[73] of an expression for the local buckling moment M_{lb}, defined as the maximum lateral bending moment that could develop in the compression flange under a coexistent moment of M_p in the plane of the web.

The major effect of inelastic buckling in a beam is to reduce the ability of the member to carry its plastic moment M_p through a range of inelastic deformations. A measure of this ability is the rotation capacity μ, defined in equation (1.6):

$$\mu = \frac{\theta}{\theta_p} - 1 \qquad \ldots(1.6)$$

where θ and θ_p are as shown in Fig. 1.21. Adequate rotation capacity is therefore an essential requirement of beams used in plastic design.

In the subsequent derivation of bracing requirements in Ref. 71, the beam model shown in Fig. 1.22 was employed to allow the applied moment on an initially crooked beam to be expressed in terms of the critical moment of an equivalent idealised model. The Southwell approximation for columns allowed the two moments to be related by the initial crookedness and lateral deflections of the compression flange. Lateral buckling of the idealised beam occurred when the T-shaped compression element buckled laterally. The two longitudinal pins assumed in the model transformed the cross-section into a lateral mechanism and the torsional rigidity of the section was neglected.

Lay[72] had shown that the combination of compressive in-plane bending strains and the strain distribution arising from lateral deformations of the imperfect beam would generally result in local buckling of the compression flange. As this determined the upper limit of the load-carrying capacity of the member, the criteria for the spacing of restraints developed by Lay and Galambos[73] were based on attainment of that value of μ corresponding to local buckling of the compression flange. For a required rotation capacity μ, the restraint spacing L was given by

$$\frac{kL}{r_y} = \frac{\pi}{\sqrt{\epsilon_y}} \sqrt{\frac{\frac{\epsilon_{st}}{\epsilon_y} - 1}{1 + 0.7\mu \frac{E}{E_{st}}}} \qquad \ldots(1.7)$$

where k = effective length factor (0.54 for predominantly elastic side spans, 0.8 for fully-yielded side spans)

r_y = radius of gyration of beam section about its minor axis

ϵ_y = yield strain of steel forming beam = σ_y/E

ϵ_{st} = strain at onset of strain hardening (Fig. 1.23)

E = Young's Modulus

E_{st} = strain hardening modulus (Fig. 1.23)

As the rotation capacity at the onset of local buckling was not always readily calculable, Lay and Galambos suggested an optimum value for American rolled sections of

$$\mu = 0.8 \left(\frac{\epsilon_{st}}{\epsilon_y} - 1\right) \qquad \ldots(1.8)$$

On the assumption of braces fully yielded at the termination of the beam's rotation capacity, the required cross-sectional area of a single brace A_b^* was shown[71] to be

$$A_b^* = \frac{2}{3}\left[\frac{\frac{\epsilon_{st}}{\epsilon_y} - 1}{\frac{E}{E_{st}} - \sqrt{\frac{E}{E_{st}}}}\right]\frac{A_f b_f}{\ell_{av}} \qquad \ldots(1.9)$$

in which A_f = area of compression flange of beam = $b_f t_f$

b_f = compression flange breadth

t_f = compression flange thickness

$1/l_{av}$ = reciprocal average length of adjacent spans

$$= \frac{1}{2}\left(\frac{1}{\ell_R} + \frac{1}{\ell_L}\right)$$

l_L, l_R = lengths of the two spans adjacent to the braced point.

The corresponding ultimate force in the brace $(P_{br})_{max}$ was expressed non-dimensionally in terms of the ultimate compression flange force, P_{cy}:

$$\frac{(P_{br})_{max}}{P_{cy}} = \frac{2}{3}\left[\frac{\frac{\epsilon_{st}}{\epsilon_y} - 1}{\frac{E}{E_{st}} - \sqrt{\frac{E}{E_{st}}}}\right]\frac{b_f}{\ell_{av}} \qquad \ldots(1.10)$$

In keeping with the results of earlier theoretical investigations[45,46] into the forces developed in column bracing, equation (1.10) predicts increasing brace force with decreasing span. A numerical example by Lay and Galambos showed that for a 10WF25 beam in A36 steel, restrained at intervals of $35r_y$ in accordance with AISC recommendations[70], the bracing design force $(P_{br})_{max}$ reached a value of 3.2% of the ultimate compression flange force. Although this exceeded the '2% rule', Lay and Galambos noted that the assumptions made in the derivation of equations (1.9) and (1.10) would result in conservative (ie. safe) bracing design.

Recognising that the adequacy of translational bracing systems was also dependent on an axial stiffness criterion, the authors proposed an inequality relating the actual cross-sectional area of the brace supplied, A_b, to its length, l_b:

$$\frac{\ell_b}{\ell_{av}} < 0.86 \left(\frac{A_b}{A_f}\right)\left(\frac{\ell_a}{b_f}\right)^2 \qquad \ldots(1.11)$$

where $A_b \geqslant A_b^*$ from equation (1.9)
l_a = length of longer adjacent span ie. greater of l_L and l_R.

This brace stiffness criterion was based on limiting the lateral deflection of the primary member at the point of restraint. Any lateral relaxation of intermediate supports increased the effective length of the primary member and hence reduced its resistance to inelastic lateral buckling: the axial stiffness requirement was deemed to be valid for an increase in effective length not exceeding 8%. In this context, the brace-to-beam and brace anchorage connections were required to be almost completely slip-free. As demonstrated in Ref. 71, the requirements of equations (1.9) and (1.11) are easily met in practice and consequently the provision of slip-free connections will frequently prove critical in bracing system design. Either welded or friction grip bolted connections should satisfy this requirement.

In cases where tension flange restraint was not provided in addition to compression flange restraint of the above proportions, the following flexural strength and stiffness requirements were to be met by each compression flange bracing member:

$$z_b^* = \frac{0.75\, \ell_{av}\, t_w}{1 - \frac{A_b^*}{A_b}} \qquad \ldots(1.12)$$

where z_b^* = required brace section modulus about an axis parallel to the longitudinal axis of the beam.

t_w = web thickness of beam

For a beam of cross-sectional area 'A_x' and depth 'D', the corresponding flexural stiffness requirement was

$$\left(\frac{\ell}{D}\right)_{brace} \leqslant \frac{0.38\, b_f A_f}{\epsilon_y D A_x} \qquad \ldots(1.13)$$

The requirements of equations (1.12) and (1.13) were again shown to be easily met in most practical situations. Nevertheless, this flexural stiffness requirement has been criticised by Salmon and Johnson[74] as being too onerous. However, in order that any assumed torsional restraint afforded to the beam by the flexural stiffness of the brace was actually made available, a moment connection of prescribed strength was also required. Morris[75] later showed that typical purlin-to-beam connections were generally not markedly moment resistant and advocated that the small torsional stiffness such bolt groups might possess should be ignored.

In an extension of his previous work on elastic flexural-torsional buckling, Hartmann[12] examined the effect of lateral and torsional restraint stiffnesses on the inelastic buckling behaviour of simply-supported beams of rectangular cross-section. A tangent modulus solution was employed and the cases of central point loading and third point loading were examined in order to determine minimum restraint stiffness criteria. In the case of central point loading, both the transverse load and lateral bracing actions were assumed to apply at the shear centre, whereas two combinations of load/restraint geometry were examined for third point loading: shear centre loading with either shear centre or compression flange restraint. Under third point loading little increase in critical load was achieved by changing from shear centre to compression flange restraint. The main reason for this was thought to be the stabilising influence of adjacent, non-critical segments in the continuous beam.

Hartmann's results from Ref. 12 are shown non-dimensionally in terms of the critical stress factor 'c' and non-dimensional translational restraint stiffness 'λ' in Fig. 1.24 . Whereas the shape parameter R played an important role in the graphical presentation of results in previous Sections, the negligible warping rigidity of rectangular sections has necessitated the use of an alternative shape parameter. In Fig. 1.24 the slenderness parameter ψ has been employed:

$$\psi = \frac{\sigma_y D \ell}{E b^2} \qquad \ldots(1.14)$$

where D = depth of rectangular cross-section of beam

b = breadth of rectangular cross-section

l = span

Hartmann noted that the upper ($\psi > 6.8$) curve corresponded to elastic failure of a braced beam with zero warping rigidity. Examination of the $R^2 = \infty$ curve in Fig. 1.13 shows the two curves to be identical, both predicting a critical brace stiffness of $\lambda_{cr} \doteq 11$. For values of ψ between 4.3 and 6.8, failure was by second mode inelastic buckling, whilst beams of ψ less than 4.3 were noted to fail by in-plane collapse resulting from the formation of a plastic hinge at midspan.

A critical brace stiffness of $\lambda_{cr} \doteq 12$ was required for attainment of second mode inelastic lateral-torsional buckling of the $\psi = 4.8$ beam. This was slightly greater than the value of $\lambda_{cr} \doteq 11$ required for 2nd mode elastic buckling in the case of $\psi \geqslant 6.8$. As values of λ_{cr} necessary for the attainment of in-plane collapse on the $\psi = 4$ and $\psi = 2.9$ curves were lower than that required for second mode elastic buckling, Hartmann concluded that the elastic value ($\lambda_{cr} = 11$) would provide a conservative estimate of inelastic bracing requirements. Although the value of $\lambda_{cr} = 12$ is only slightly greater than $\lambda_{cr} = 11$ predicted by the elastic curve, Hartmann's conclusion is dependent on all such differences being small. As the $\psi = 4.8$ curve in Fig. 1.24 is the only curve which relates to second mode inelastic instability, more inelastic curves would be required to verify the validity of this recommendation.

In addition, the effects of warping would have to be indicated before such a recommendation could be applied to sections other than the rectangular section employed in this study.

Fukumoto and Kubo[76] later presented the results of an investigation into the optimum bracing stiffnesses for the prevention of inelastic flexural-torsional buckling in parallel, inter-braced steel girders containing residual stresses and subjected to an uniform bending moment. An energy approach similar to that employed by Flint[59] formed the basis of the theoretical analysis, although the method of allowing for the spread of plasticity through the section was not described. A series of eleven tests was performed in order to verify the theoretical solutions.

No basis for the comparison of measured restraint forces was provided due to the assumption of an initially perfect beam in the analysis. However, the bracing forces measured in the tests did not exceed 2% of the compression flange force.

In a recent paper concerned with the provisions of the new British Code[56] in relation to the design of beams, Nethercot[77] has noted that little guidance is given in present codes as to what constitutes "effective lateral restraint". The current Australian Code[78] demands, in addition to the "2½%" strength rule, a minimum axial brace stiffness of $10(P_c)_{max}/L$ where $(P_c)_{max}$ is the maximum compression flange force and 'L' the spacing of restraints. Combining these two requirements, the maximum permissible lateral deflection at the braced point is 0.0025L. Lay and Galambos[71] previously showed that the maximum permissible lateral deflection of the braced point consistent with the brace fully yielded was 0.098 inches for a 10WF25 beam restrained at intervals of $35r_y$. The value of r_y for this section was 1.31 inches, giving a restraint spacing of 45.85 inches and a permissible ratio of lateral deflection (u) to restraint spacing (L) of

$$\frac{u}{L} = \frac{0.098}{45.85} = 0.0021$$

which is seen to be more onerous than the Australian Code requirement of 0.0025. In support of the above conclusion, Nethercot[77] has indicated that the stiffness requirement of the Australian Code has been considered to be inadequate.

In a guide to plastic design methods, Morris and Randall[79] quoted a required brace cross-sectional area of 4% of the area of the compression flange with no indication of a stiffness requirement. However, in a later paper[75], Morris conceded that the stiffness requirement might in fact be critical and consequently would control the design of restraints. This conclusion had arisen from the observed premature failure of restraints during ultimate load tests on portal frames. Morris also stated that compression flange restraint should be provided at a point not further than D/2 from a theoretical plastic hinge location, 'D' being the overall depth of the primary member.

In conclusion, it can be said that there have been very few previous investigations into the requirements of bracing systems associated with the prevention of first mode inelastic instability in beams of medium to low slenderness. Of greatest importance has been the study of Lay and Galambos[71] in which design criteria for the proportioning of bracing members were proposed. All of these criteria were considered to be relatively easy to satisfy in practice, although the provision of rigid brace anchors and slip-free brace-to-beam connections was suggested to be a more onerous requirement.

Reflecting the need for considerably more research work on the subject, current design recommendations[33,57,78,79] for the proportioning of bracing display considerable disagreement. Although previous research has shown that, in general, bracing requirements are not difficult to meet in practice, it is imperative that the designer has access to precise and unambiguous minimum values of bracing stiffness and strength.

1.3 Summary of Previous Research and Scope of the Present Study

1.3.1 Summary of Previous Research

The foregoing review of previous research presented in Sections 1.2.1 to 1.2.5 has revealed that by far the greater proportion of research effort to date has been concerned with the elastic buckling of beams and methods of restraint for its prevention. Various types of analysis have been employed in these studies, ranging from relatively simple equilibrium-based and energy-based manual solutions[59] to complex computer-based finite integral[64], finite difference[65] and finite element[63] techniques.

Major limitations of the classical elastic buckling analysis[2] have been identified. These include its inability to predict out-of-plane deflections arising from initial imperfections in the beam or loading geometry. Consequently, its use in assessing the adequacy of restraint systems is limited to its ability to predict critical brace stiffnesses but not brace forces. Allowance for initial geometrical and loading imperfections can be made using an "initial deflection" analysis[47] which predicts lateral deflections from the commencement of loading and is therefore also capable of predicting bracing forces. Imperfect beams have been shown[46] to demand more substantial systems of bracing than similar initially perfect beams. The interrelationship between bracing stiffness and bracing strength was also demonstrated; stiffer braces not only increased beam strengths but also required less strength themselves. In the formulation of design rules for the proportioning of bracing systems it is necessary to use enhanced values of certain imperfections to make allowance for those imperfections which cannot be measured or which cannot be included in the analysis.

The complexity of lateral-torsional buckling analysis is further increased by the inclusion of non-linear material behaviour and plasticity. In all but the simplest of cases, recourse must be made to computer-based solutions for inelastic instability analyses. Nethercot[39] has noted that "the region of medium slenderness in which the effects of plasticity and instability interact is the most difficult to deal with. It is also the category which includes most beams used in practical situations".

Sections 1.2.3 to 1.2.5 have demonstrated the ability of translational or torsional restraints working in isolation or in combination to provide fully effective restraint to beams under different types of applied loading. The adequacy of bracing was seen to be dependent not only on its stiffness and strength but also on the span of the beam and the relative importance of the beam's warping rigidity in resisting torsional deformations, the nature of the applied loading, the magnitude and distribution of initial imperfections and the level of attachment of restraint. On the basis of elastic buckling theory, compared with slender beams, those of low to intermediate slenderness were shown[16,60,63] to require greater bracing stiffnesses for full restraint and hence attainment of second mode buckling. However, these more stocky beams were also those more prone to failure by inelastic than by elastic buckling. The paucity of information on the subject of restraint systems required for the attainment of second mode inelastic critical loads is reflected in the small number of references cited in Section 1.2.5 compared with the numbers dealt with in Sections 1.2.3 and 1.2.4 . The only comprehensive theoretical study on this subject[71] has indicated the adequacy of even modest systems of bracing in providing complete restraint to beams prone to first mode inelastic instability. This work forms the basis of the contemporary AISC bracing design recommendations[57].

Recently, the increasing popularity of the plastic design method and the trend towards the applicaion of limit state philosophy to structural steelwork design have prompted a few commentators[75,77,79-81] to summarise the criteria for the provision of adequate restraint. Briggs[80] has highlighted the divergence of opinion on the subject. In a recent review of bracing requirements, Nethercot[77] has indicated the adequacy of the "2½% rule" used as the strength requirement in current British[33] and Australian[78] Standards but in addition has advocated for general use a minimum axial brace stiffness greater than the lateral bending stiffness of the primary member by a factor of approximately twenty-five (ie. $\lambda \geqslant 25$).

Although theoretically the criterion for adequate restraint should be one of stiffness rather than of strength, advocates of the latter have argued that, in practice, the strength requirement is easier to apply and that bracing proportioned in accordance with current strength requirements generally possesses adequate stiffness. In support of this, Horne[80] has noted that contemporary strength and stiffness requirements give results of the same order. Nevertheless, recent discussion by Swindells[81] of a paper by Morris[75] revealed a lack of appreciation of the importance of adequate brace stiffness in design.

1.3.2 Scope of the Present Study

In view of the relatively scant attention paid to the bracing requirements of beams of low to intermediate slenderness in the literature, the present study was undertaken in order to investigate both the stiffness and strength criteria to be met by braces providing complete midspan restraint to simply-supported, single span beams in this range of slenderness. Throughout the remainder of the present study the following assumptions have been made:

(i) Complete lateral and torsional restraint is provided at the end supports of the beam. However, the beam is free to rotate in plan and in elevation at these points.

(ii) Warping of the cross-section at the supports is not prevented and

(iii) Other deformations of the beam cross-section have been neglected on the assumption that these will be prevented either by local stiffening at points of restraint or by the method of restraint attachment adopted.

The critical loads and bracing requirements of beams under uniform bending moment have received a considerable amount of attention in the literature, probably due to the simpler analysis required for this type of loading. However, the occurrence of this loading condition in practice is rare and the case of moment gradient along the span is much more common. Into this latter category falls the case of central point loading. As seen in Section 1.2, bracing requirements for central point loading are commonly more demanding than for uniform moment due to the necessity of reaching higher in-plane loads before attainment of the second mode buckling load. Consequently, the case of central point loading is extensively examined in the present study.

Based on a classical elastic buckling analysis, Chapter 2 examines the stiffness requirements of translational and torsional bracing for fully effective midspan restraint of a single span beam under uniform bending moment and central point loading. The effects of varying levels of load application and restraint attachment are considered and a series of graphs showing critical combinations of translational and torsional restraint stiffnesses is presented.

In Chapter 3, details of finite element procedures employed in subsequent chapters for the solution of the inelastic instability problem are presented. The methods adopted for incorporating initial imperfections and non-linear material and geometrical behaviour are also described. As typical brace-to-beam connections are not markedly moment resistant[75], attention has been restricted to midspan restraints possessing only axial stiffness in the experimental and finite element study reported in the third and subsequent chapters.

Chapter 4 describes the requirements of the experimental programme, reasons for the use of model steel beams in the test programme and construction of the test rig and its associated instrumentation.

The model beam test programme is further described in Chapter 5 where fabrication of the model beams is discussed together with the determination of material and geometrical properties of the beams and the experimental procedure adopted.

Examination of the literature has shown that few previous investigators have attempted to measure actual bracing forces associated with the restraint of initially imperfect beams. These forces have been measured in the series of tests forming part of the present study; Chapter 6 presents finite element and experimental results obtained from the computer analyses and test programme. Comparison of these results is also made in this Chapter. In addition, the relationship between bracing stiffness and strength is investigated.

Chapter 7 presents a short parametric study based on the finite element programme FINAS. For beams containing initial geometrical imperfections of sinusoidal form, the influence of several variables (including beam span, load/restraint geometry and lateral restraint stiffness) on theoretical bracing forces is indicated. Comparison is then made between the results of this parametric study and those of Chapter 6.

Chapter 8 presents a comparison of the results of Chapters 2 and 6 with those of previous investigators and with contemporary bracing design recommendations.

Conclusions arising from the present work and its relationship to previous research are given in Chapter 9, which also contains suggestions for future work.

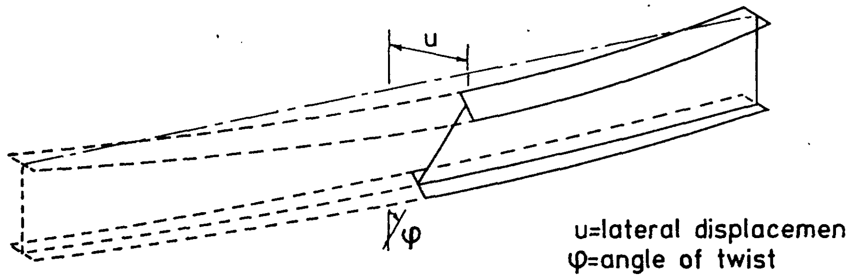

Fig. 1.1 : Lateral-torsional buckling failure

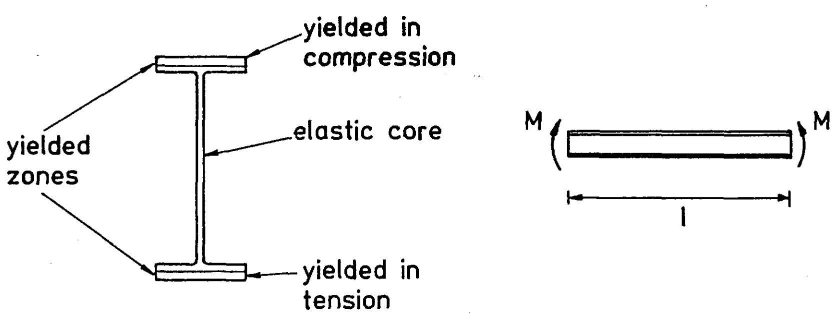

Fig. 1.2 : Elastic core and yielded zones of a beam under uniform bending moment

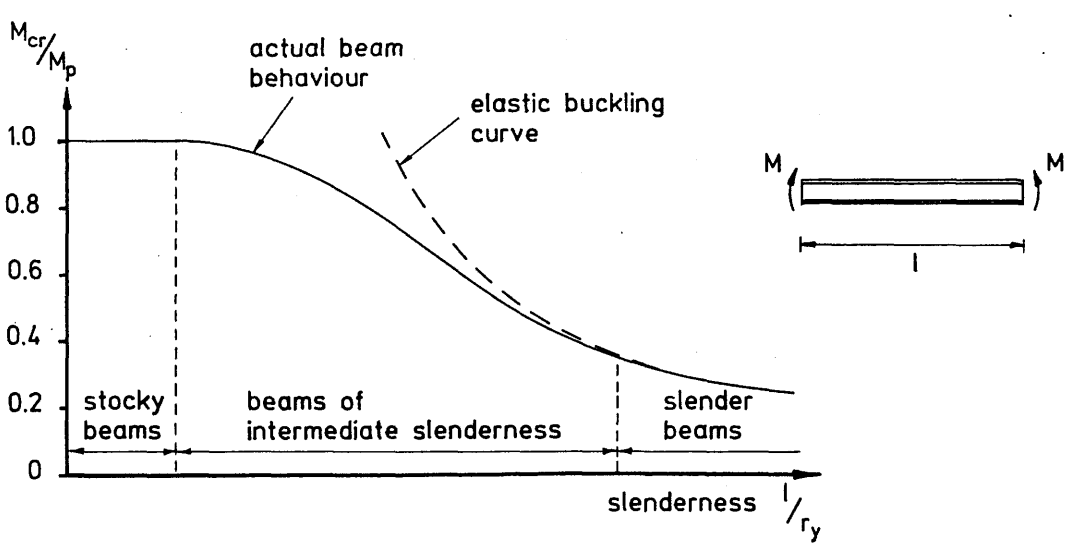

Fig. 1.3 : Typical relationship between ultimate load and beam slenderness

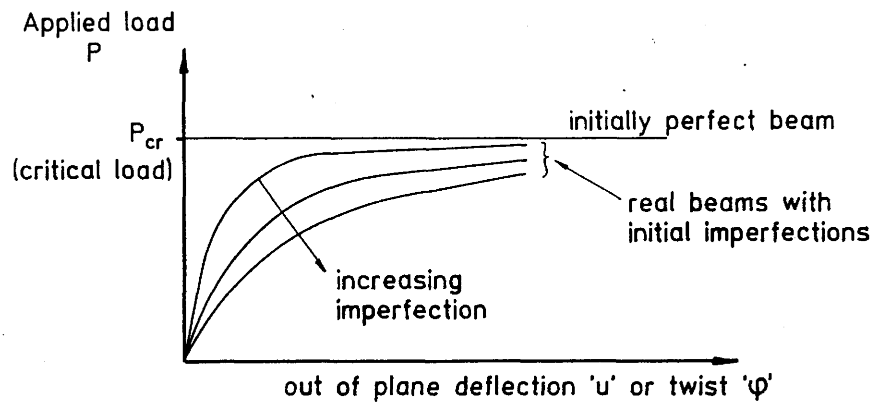

Fig. 1.4 : Out of plane displacements arising from the loading of initially perfect and imperfect beams

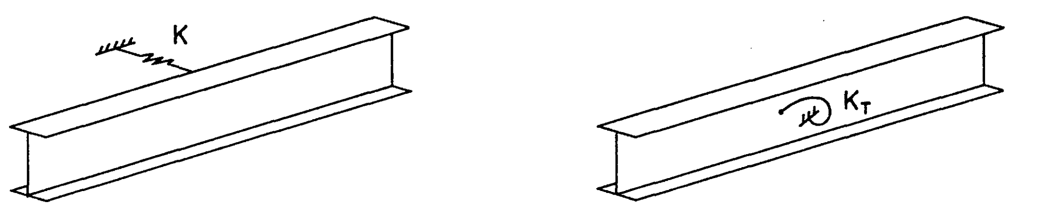

(a) lateral (translational) restraint provided by bracing member

(b) torsional (rotational) restraint provided by brace attached at an intermediate point on the span

Fig. 1.5 : Intermediate restraints on the span of a beam (restraints conventionally represented by elastic springs as shown)

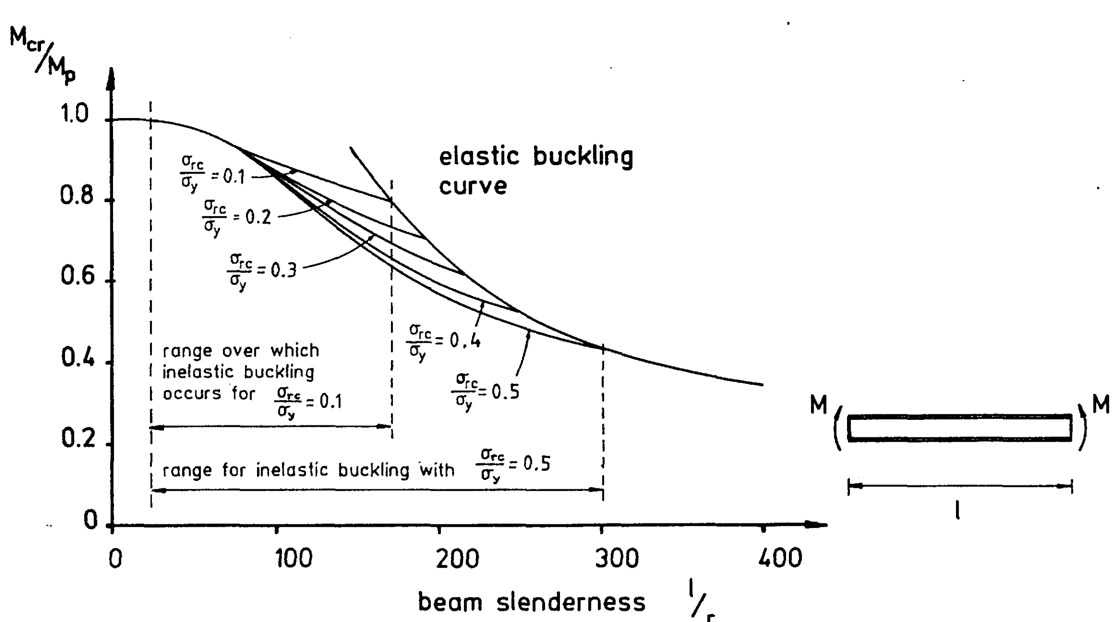

Fig. 1.6 : Effect of residual stress level on the critical load of an 8WF31 (203x203x46 UC) section for various spans

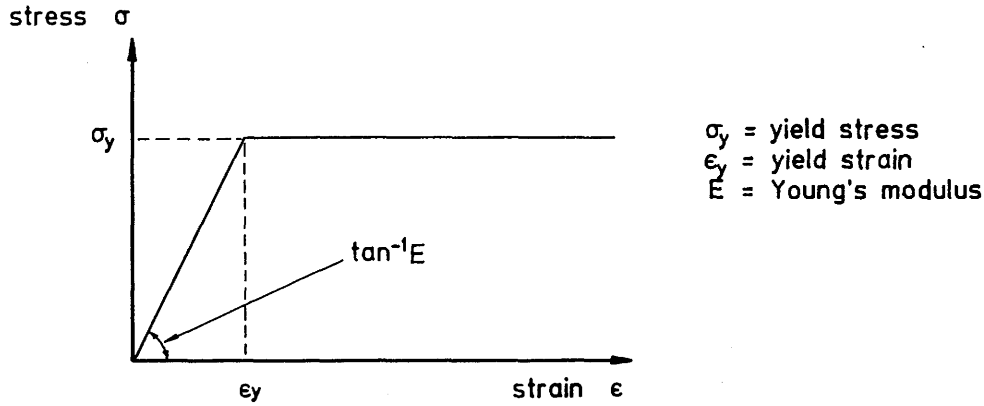

Fig. 1.7 : Idealised elastic - perfect plastic stress - strain relationship for structural steel

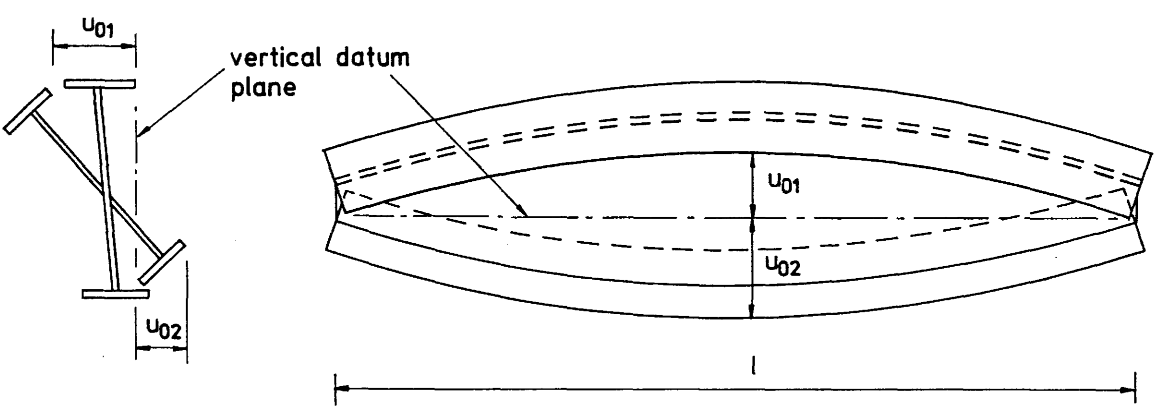

$$u_{01} + u_{02} \not> \frac{l}{1000} \quad \text{and} \quad \not> \frac{D}{100}$$

where D = overall depth of beam

Fig. 1.8 : Relative misalignment of one flange with respect to the other. Tolerances shown are those demanded by Ref. 58.

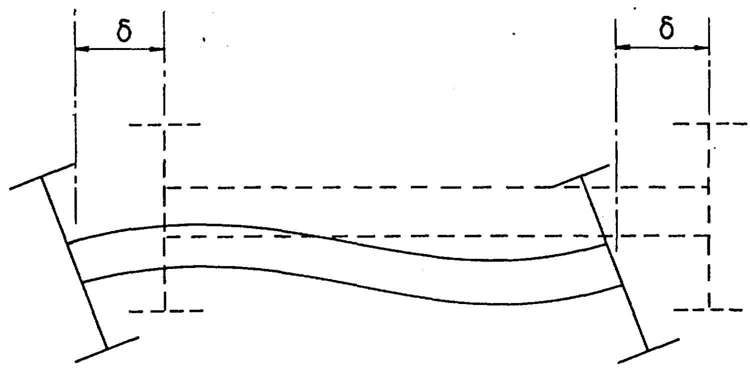

Fig. 1.9 : Lateral-torsional buckling of parallel, interbraced beams

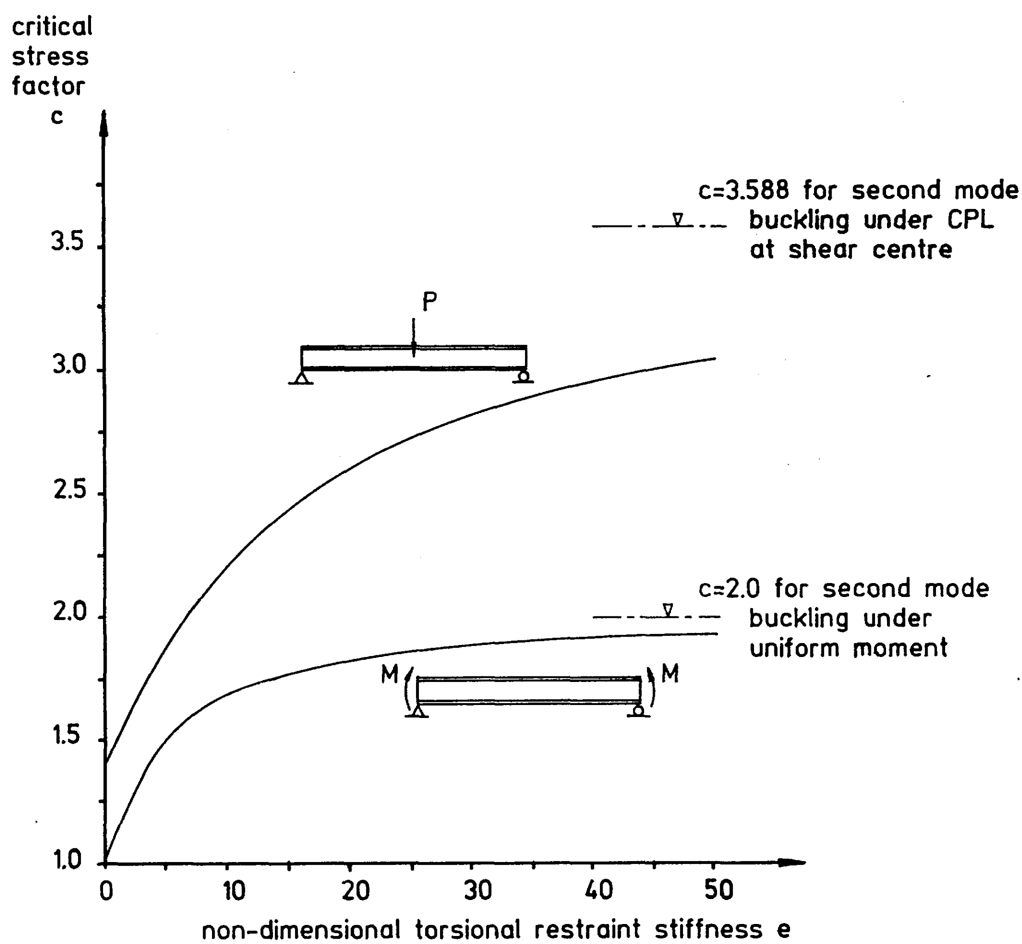

Fig. 1.10 : The influence of midspan torsional restraint on the elastic stability of simply-supported beams under uniform bending moment and central point loading (Ref. 59). (Warping effects neglected ie. $R^2=\infty$)

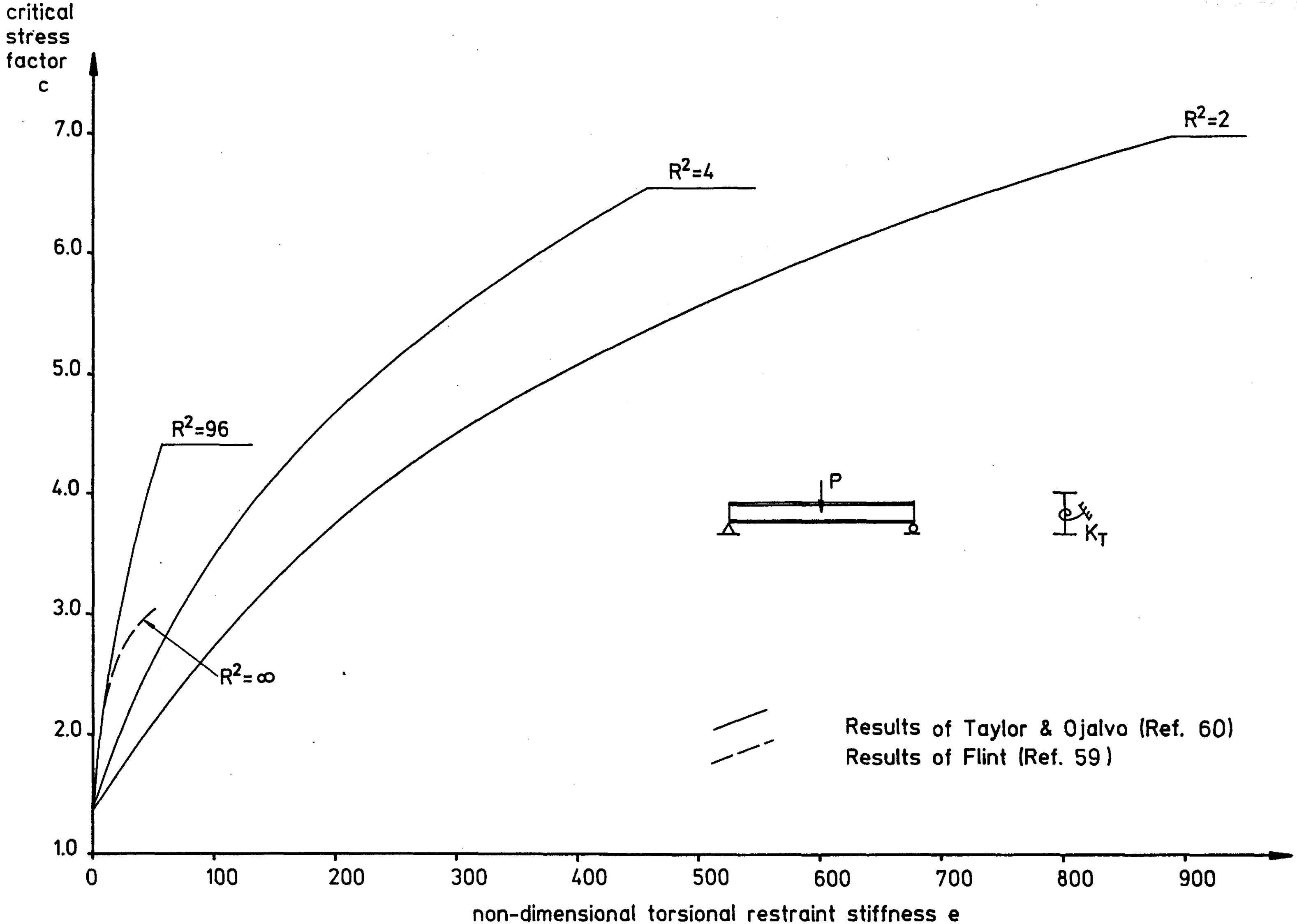

Fig. 1.11 : Comparison of results of Ref. 59 with those of Ref. 60 showing relationship between critical stress factor 'c' and torsional restraint parameter 'e' for beam under central point loading.

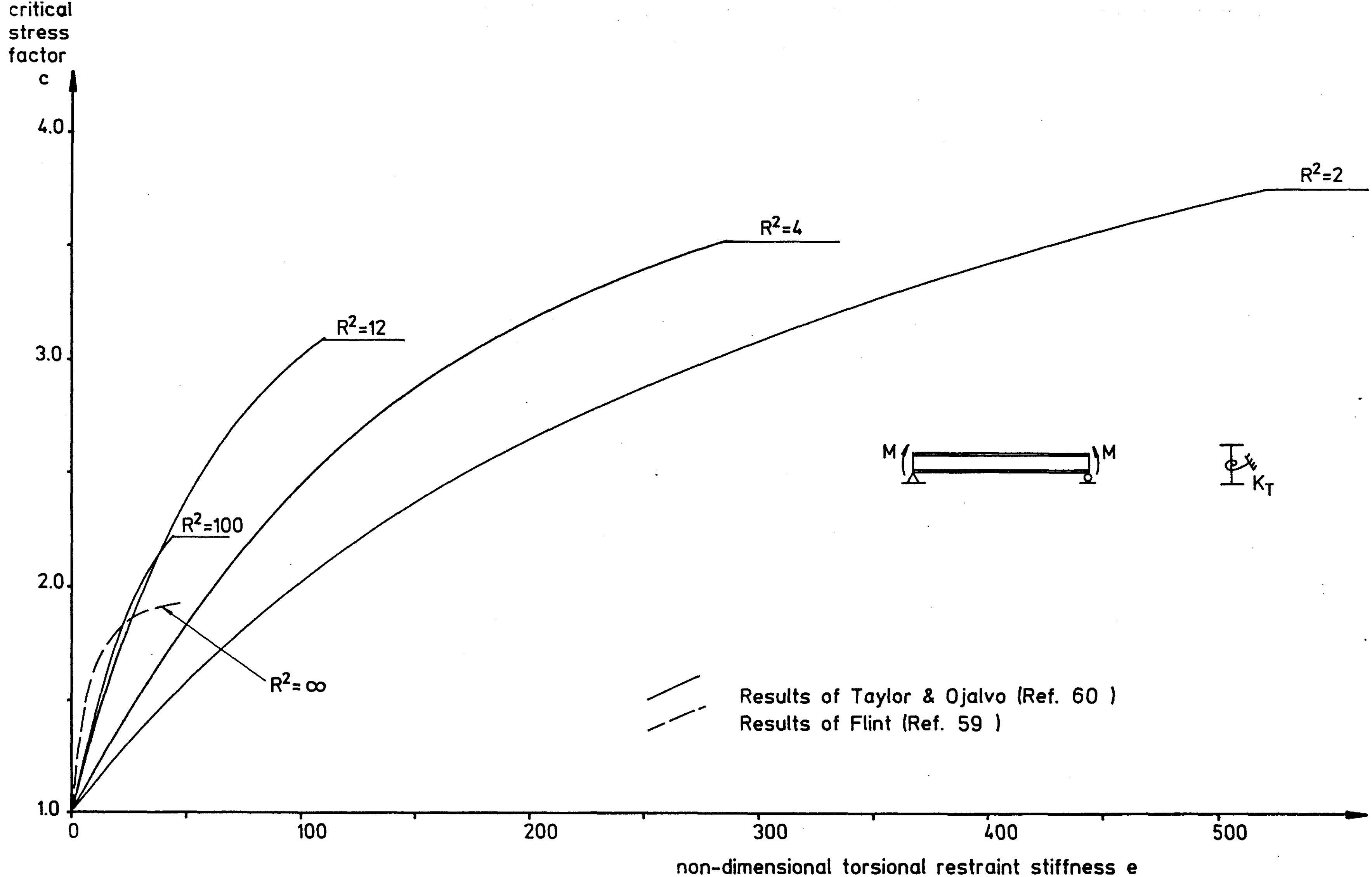

Fig. 1.12 : Comparison of results of Ref. 59 with those of Ref. 60 showing relationship between critical stress factor 'c' and torsional restraint parameter 'e' for beam under equal end moments.

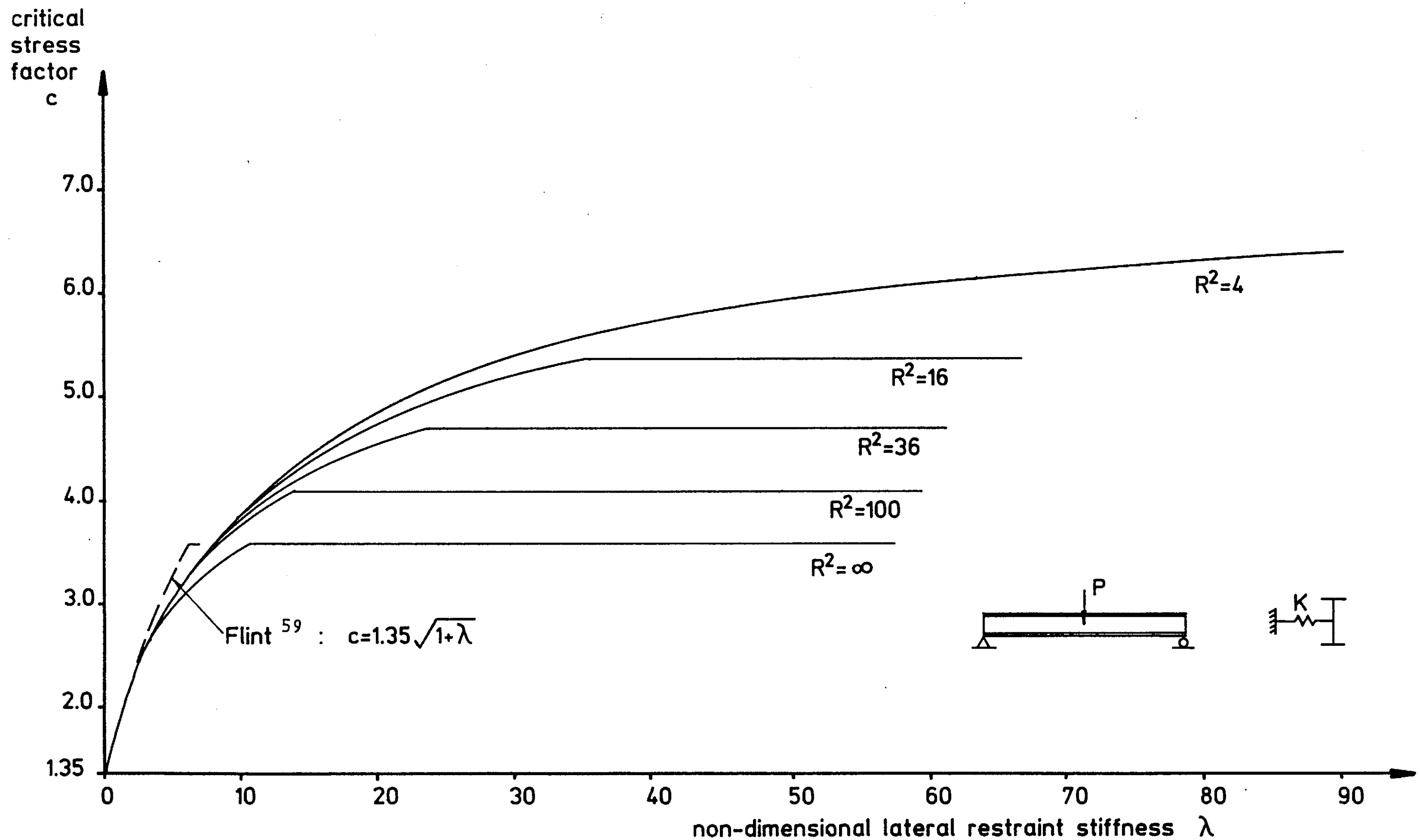

Fig. 1.13 : Hartmann's [16] elastic c-λ curves for beams under central point loading, restrained at shear centre level at midspan.

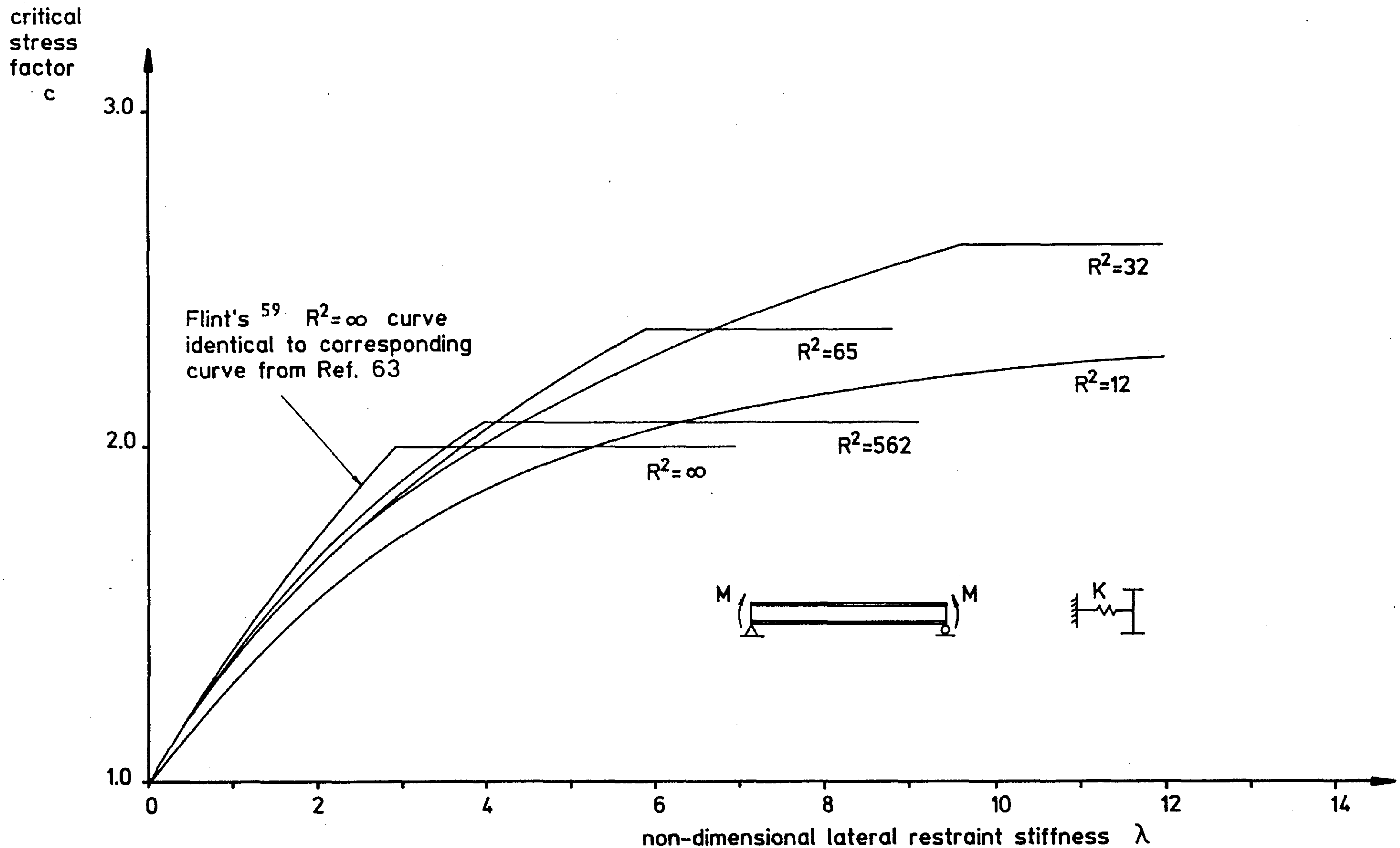

Fig. 1.14 : Comparison of Flint's[59] $R^2=\infty$ curve with those of Nethercot & Rockey[63], showing c-λ relationships for beams under uniform moment, restrained at shear centre level at midspan.

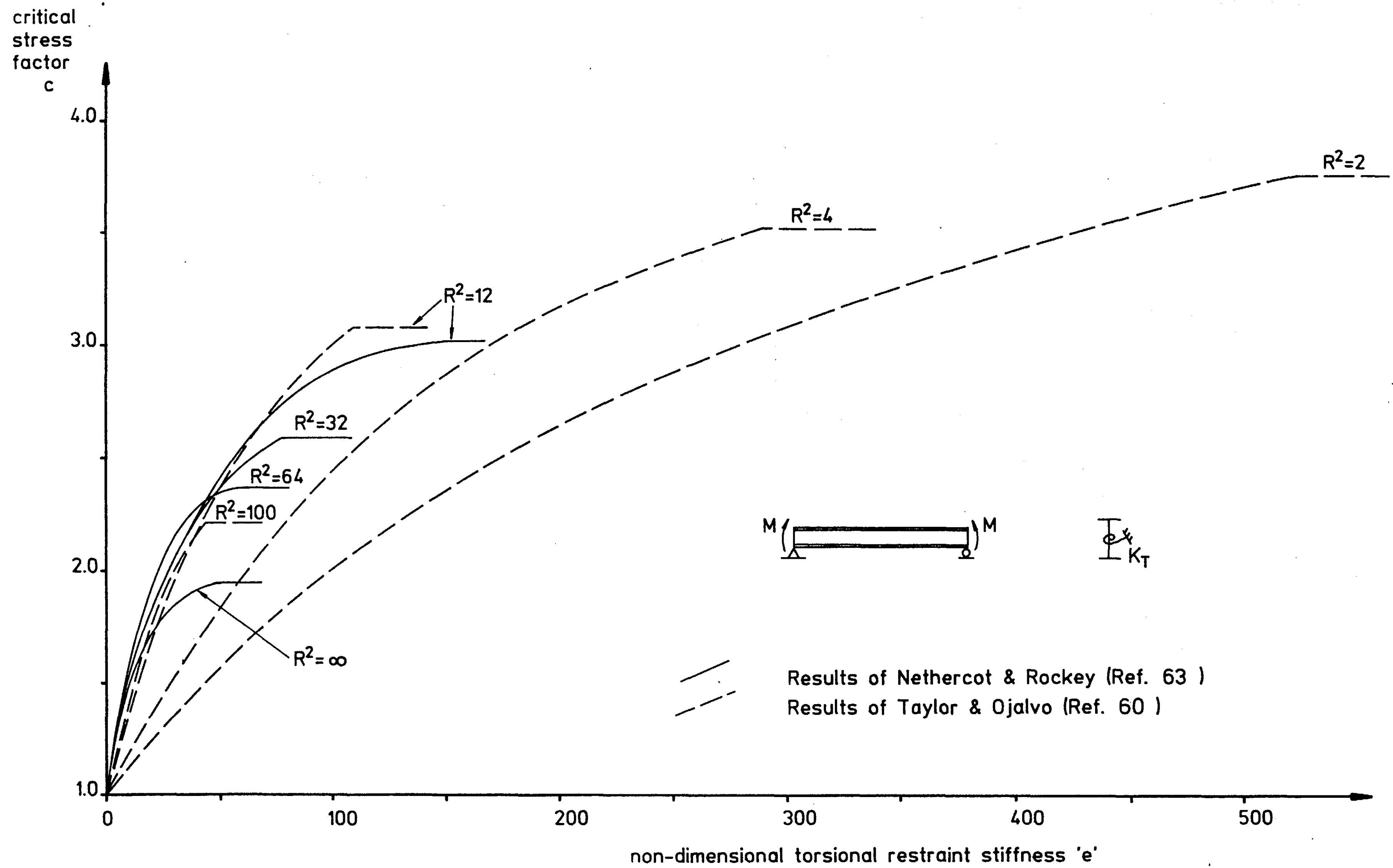

Fig. 1.15 : Comparison of results of Ref. 63 with those of Ref. 60 showing relationship between critical stress factor 'c' and torsional restraint parameter 'e' for beam under equal end moments.

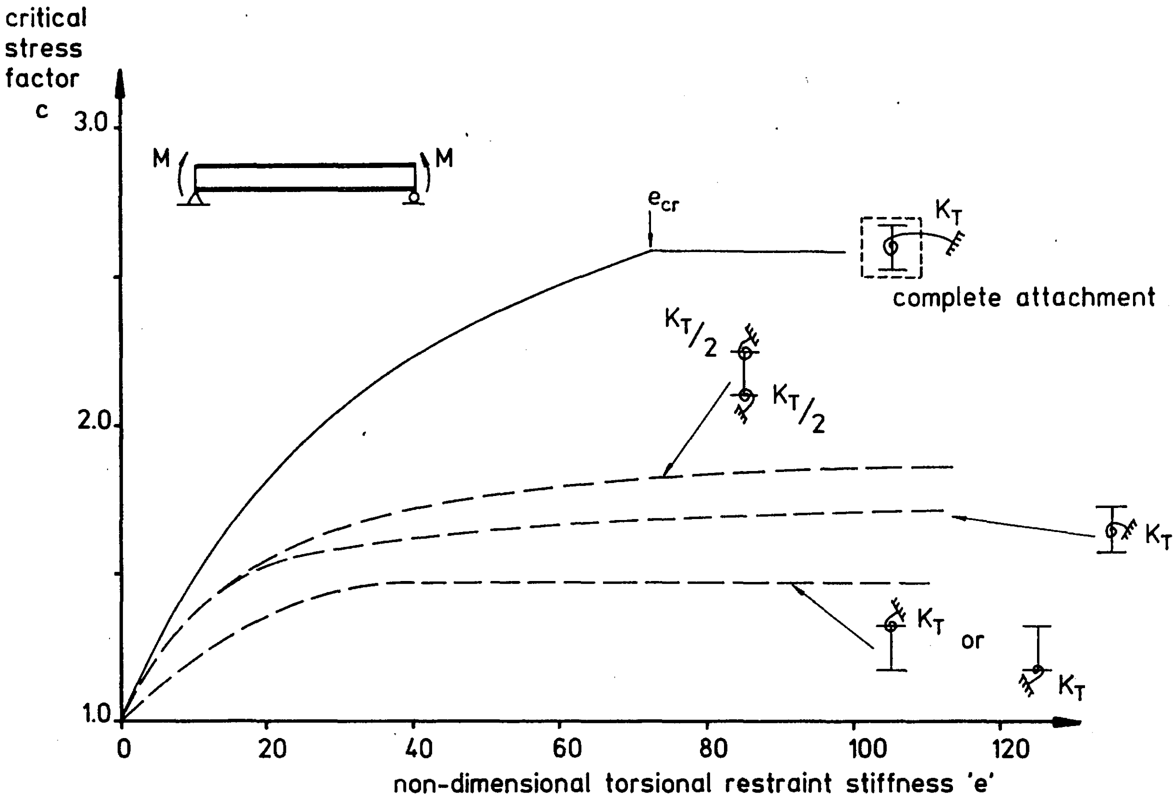

Fig. 1.16 : Relationship between critical stress factor 'c' and torsional restraint parameter 'e' for beam of R^2=32 and varying levels of attachment of torsional restraint at midspan. Based on finite element analysis of Nethercot & Rockey[63] allowing for cross-sectional deformations.

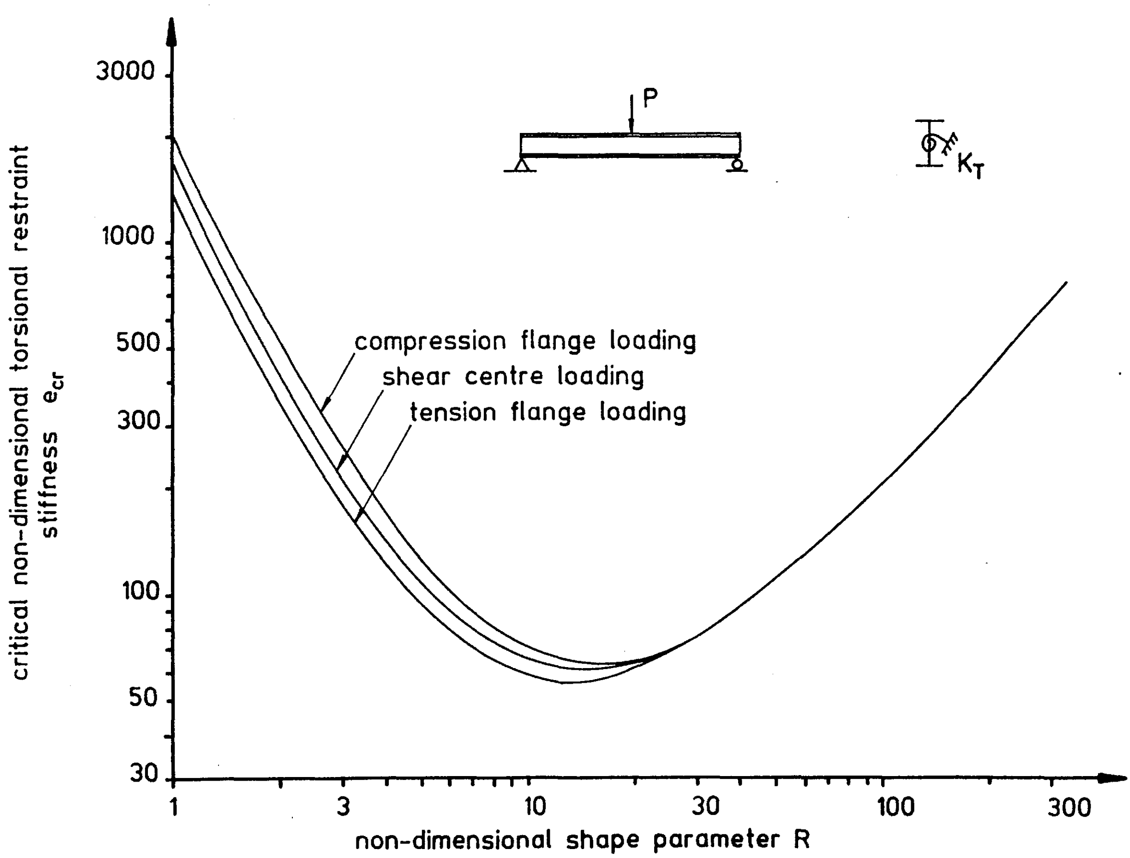

Fig. 1.17 : The effect of level of load application on critical torsional restraint stiffness 'e_{cr}' for beams under central point loading (Mutton & Trahair[64])

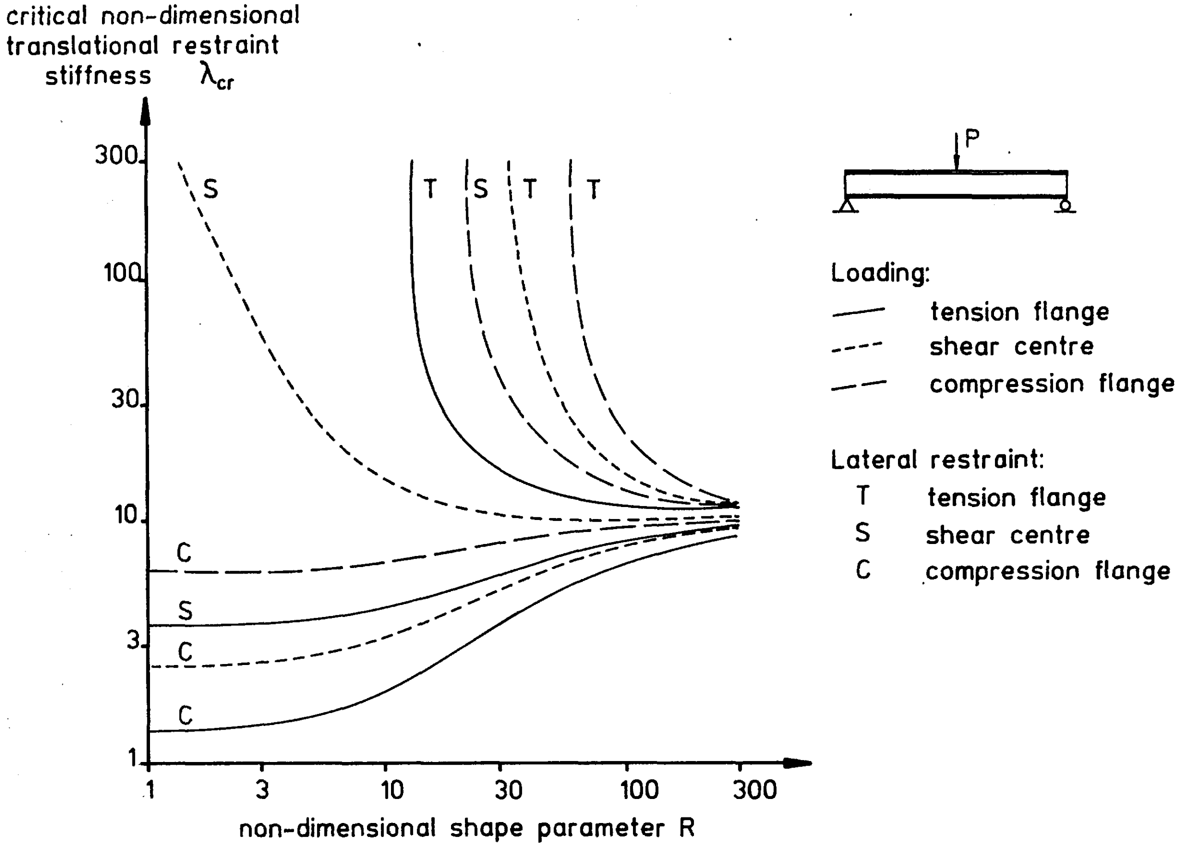

Fig. 1.18 : The effect of level of load application and restraint attachment on critical translational restraint stiffness λ_{cr} for beams under central point loading (Ref. 64).

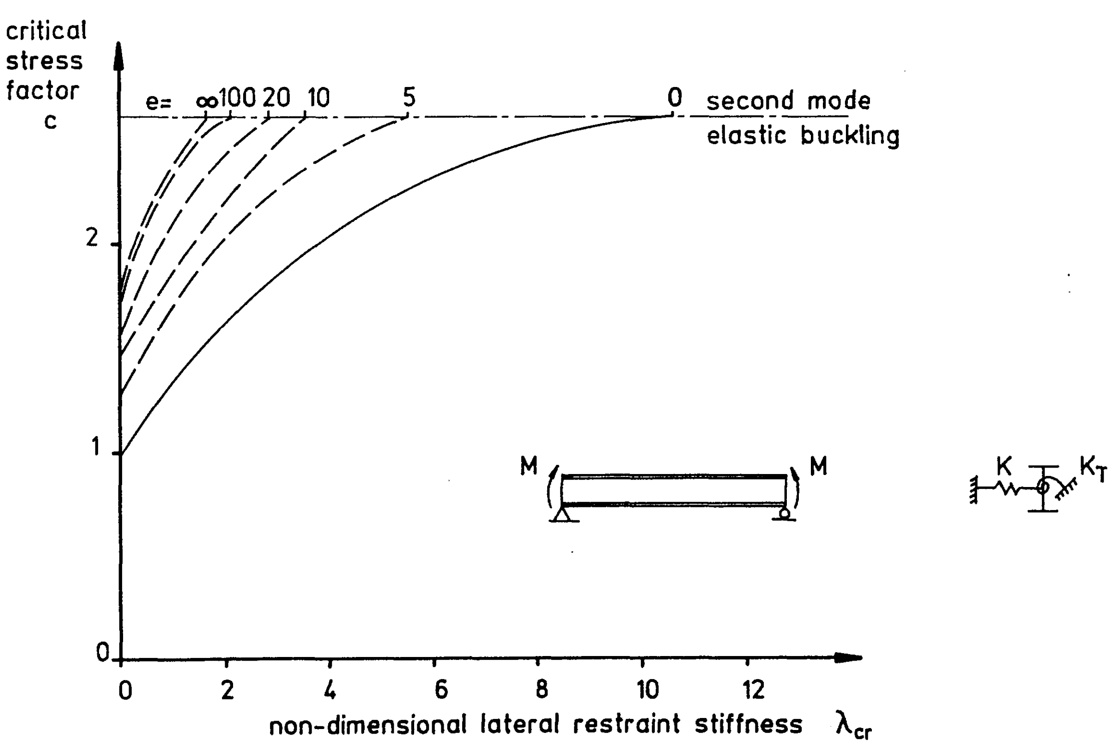

Fig. 1.19 : The influence of combined lateral and torsional midspan restraint on an R^2=32 beam under uniform moment loading (Ref. 63)

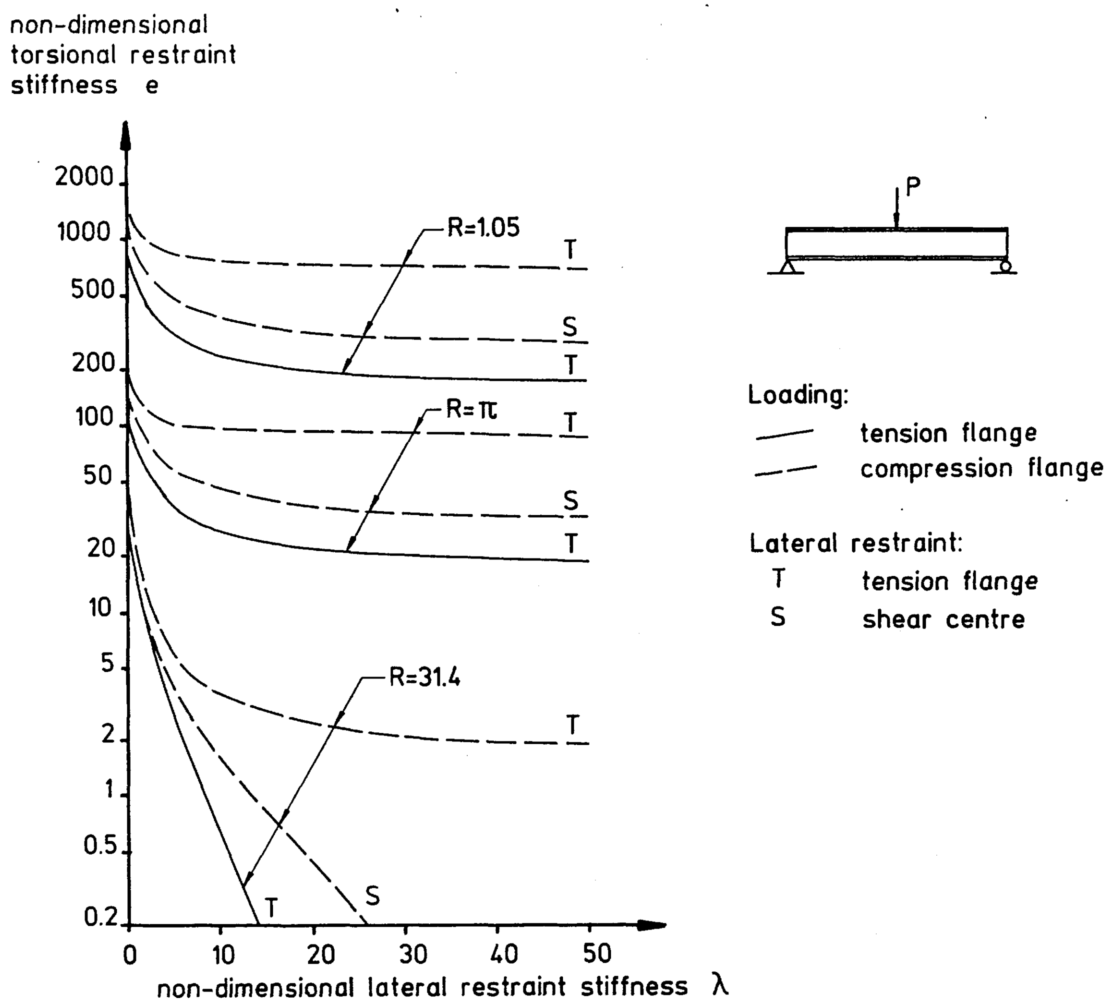

Fig. 1.20 : The influence of combined lateral and torsional midspan restraint on beams under central point loading (Ref. 64)

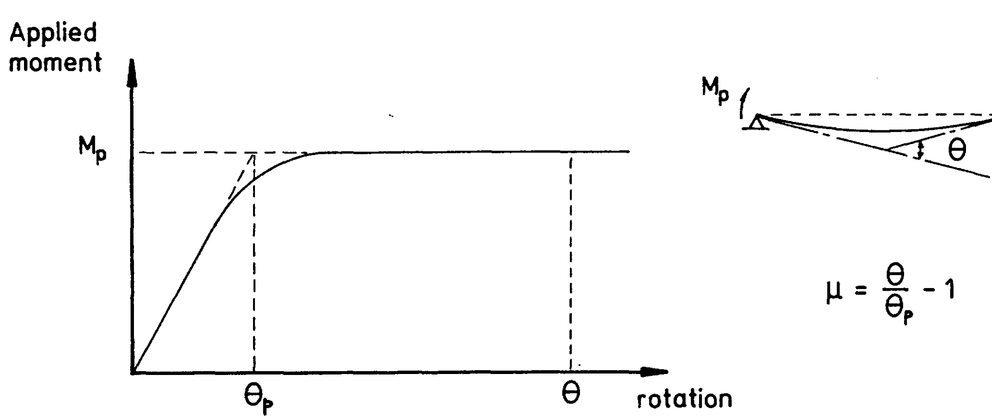

Fig. 1.21 : Typical moment vs. rotation relationship for a simply-supported beam under uniform moment. Rotation capacity is denoted by μ

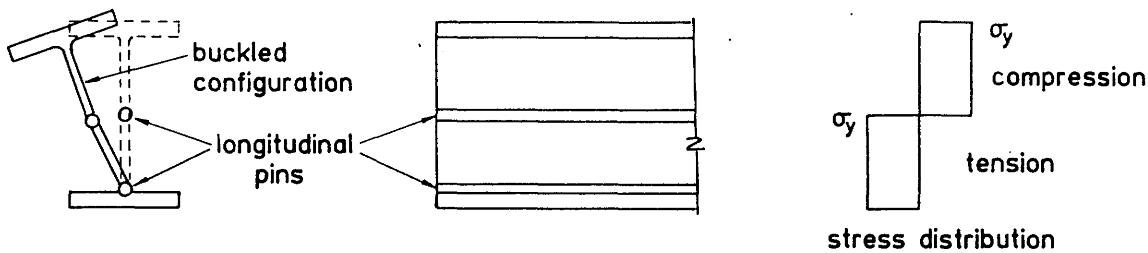

Fig. 1.22 : Strut behaviour of compression tee employed in the lateral buckling analysis of Lay & Galambos [71, 73]

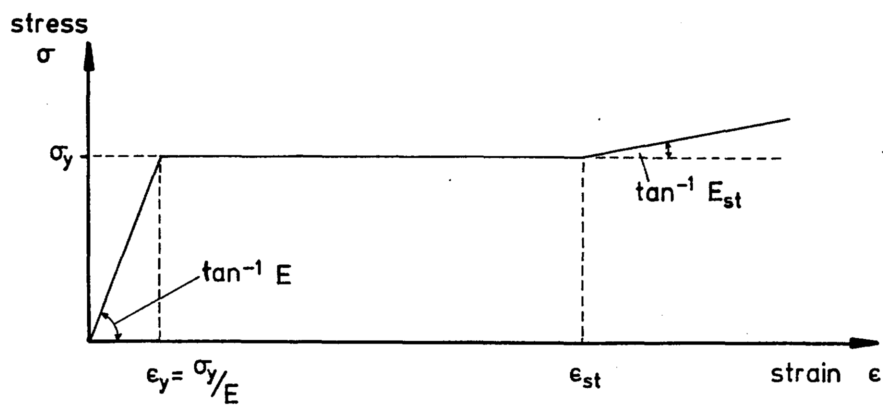

Fig. 1.23 : Strain hardening material characteristic of steel employed by Lay & Galambos [71]

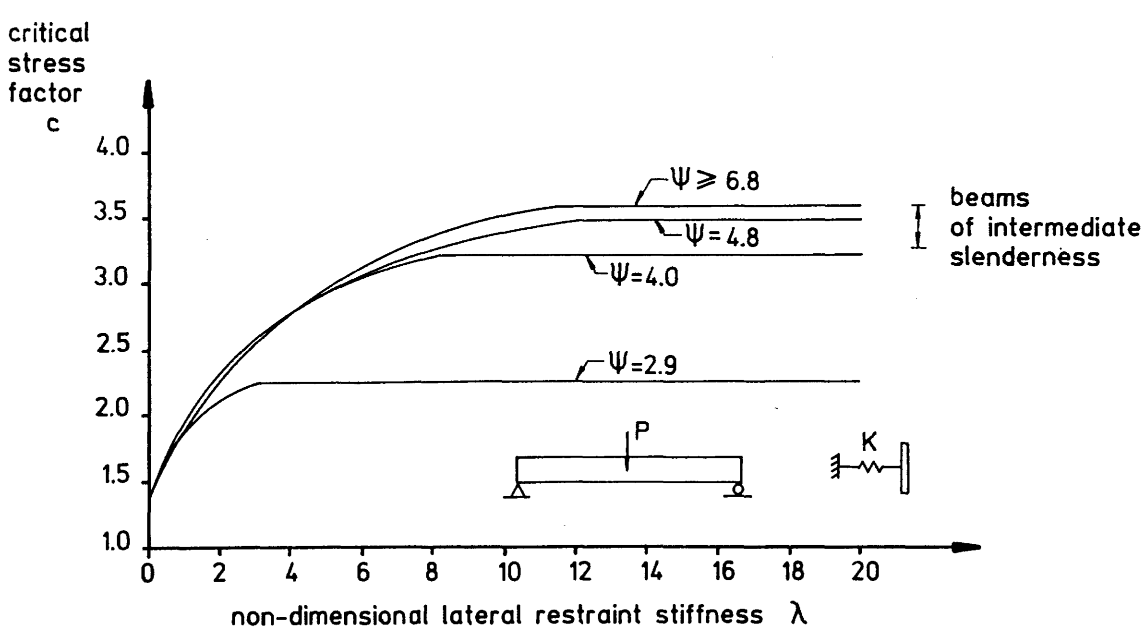

Fig. 1.24 : Relationship between critical stress factor c and translational restraint parameter λ for rectangular section beams prone to elastic or inelastic lateral-torsional buckling (Ref. 12)

CHAPTER 2

THE APPLICATION OF THE ENERGY METHOD TO PROBLEMS OF ELASTIC INSTABILITY OF RESTRAINED BEAMS

CHAPTER 2

THE APPLICATION OF THE ENERGY METHOD TO PROBLEMS OF ELASTIC INSTABILITY OF RESTRAINED BEAMS.

2.1 Introduction

2.1.1 Introduction to the Rayleigh-Ritz Method

As noted in the previous chapter, several methods have been employed for the solution of the problem of elastic buckling of beams with and without systems of restraint. Although there has been a recent trend towards the application of the finite element method to problems of structural stability, the classical elastic analyses based on the differential equations of equilibrium and on the energy methods still prove superior in certain cases where their inherent assumptions can reasonably be expected to be realised in practice. Unlike the computer-based analyses, the latter provide general solutions which allow the effects of variations in individual parameters to be assessed directly and which, in addition, do not require recourse to complex and often expensive computer programmes. However, in cases where beams are subjected to a series of discrete loads or where the loading and restraint geometry is more complex, solution of the governing differential equations of equilibrium becomes intractable and the energy-based Rayleigh-Ritz method[82] can be used to provide approximate solutions to the problem of elastic buckling.

In practice, few structures can adequately be described by a single or even a small number of degrees of freedom assigned to predetermined locations such as joints or support positions. The approximation of the Rayleigh-Ritz method lies in the definition of a displacement field by a small number of displacement functions, each containing a small number of independent coefficients. In general, the assumed functions are chosen to satisfy the kinematic boundary conditions (ie. those involving translations and rotations) but they need not satisfy the static boundary conditions (involving forces and moments). The total potential energy of the system, denoted by Π, can then be expressed in terms of these assumed functions.

The applied load corresponding to attainment of the neutral equilibrium condition is defined to be the critical, buckling or bifurcation load. Attainment of this condition is characterised by a zero change in Π when the system undergoes an infinitely small virtual displacement and so the bifurcation state lies between the conditions of stable and unstable equilibrium. Buckling loads calculated by this method are "exact" only if the assumed functions are identical to the actual ones. However, the solution is not over-sensitive to the exact form of the assumed displacement function (for example, half sine wave compared with a parabola) provided that the shape of the function corresponds to the general shape of the deformed structure. Nevertheless, the predicted behaviour becomes increasingly better as the assumed displacement function approaches the actual mode of deformation.

The use of only a few coefficients in each of the assumed displacement functions is equivalent to the introduction of additional geometric constraints so that the idealised system is stiffer than the real one and buckling loads are generally greater.

In the five analyses presented in Sections 2.2 to 2.6, the Rayleigh-Ritz method has been employed in order to determine the critical loads of beams with varying degrees of lateral and torsional restraint. In addition, the analyses permit critical combinations of λ (equation 1.2) and e (equation 1.3) for full bracing to be obtained for beams under uniform moment or concentrated midspan loading.

2.1.2 Reasons for the Presentation of Elastic Stability Analyses

A few previous studies concerned with the elastic instability of braced beams were noted in the previous chapter. Although both strain energy and the equilibrium equations formed the basis of many of these analyses, several limiting assumptions regarding the nature of the applied loading and the level of application of both loading and restraint (the "load/restraint geometry") were made by Flint[59], Schmidt[62], Taylor and Ojalvo[60], Hartmann[16] and Nethercot and Rockey[63]. The major limitations of these studies are summarised in Table 2.1 .

Table 2.1: Major Limitations of Previous Elastic Buckling Studies

Study	Main Limitations
Flint[59]	warping rigidity neglected (ie. $R^2 = \infty$ in all cases)
Schmidt[62]	midspan restraint possessed only translational stiffness; load and restraint applied at same level above shear centre
Taylor and Ojalvo[60]	only torsional restraints considered
Hartmann[16]	load and restraint applied at shear centre
Nethercot and Rockey[63]	translational restraint applied only at shear centre; uniform bending moment assumed throughout

The results presented by Mutton and Trahair[64] provide the most complete published account of the classical elastic buckling behaviour of simply-supported beams with midspan restraint, subjected to both uniform moment and central point loading. However, there is some difficulty in obtaining numerical results for cases other than those presented graphically due to the dependence of the solution on the method of finite integrals. In particular, the graphical results presented for the case of a beam under central point loading and with only partial translational restraint are limited to only three values of Nethercot and Rockey's[63] shape parameter R, defined in eqn. (1.4).

In order to obtain more information concerning the effectiveness of partial restraint and the requirements for complete restraint over a wider range of values of R and load/restraint geometries, five analyses based on the Rayleigh-Ritz method were carried out and are presented in Sections 2.2 to 2.6. Comparison of the results of these elastic buckling analyses with inelastic instability results obtained experimentally and by finite element analysis is presented in Chapter 8.

2.1.3 Assumptions

The following assumptions are common to the analyses presented in Sections 2.2 to 2.6 . The more important consequencies of these assumptions are indicated.

(i) The beam is initially perfect and behaves elastically. As a result, the forces developed in the translational and torsional restraints during buckling are indeterminate.

(ii) No initial eccentricity of load occurs.

(iii) Small deflection theory is valid.

(iv) In-plane deflections are negligible. In practice this is valid in the majority of cases as the in-plane flexural rigidity is generally considerably greater than the minor axis rigidity. In addition, the tendency for in-plane deflections to enhance the buckling resistance of the beam is neglected. Consequently, in isolation this assumption would lead to slightly conservative (ie. low) values of critical load being obtained.

(v) No distortion of the cross-section under load or during buckling occurs. The possibility of local or secondary buckling occurring prior to failure in the primary mode of instability is therefore also neglected.

(vi) Loads do not change in magnitude or direction during buckling.

(vii) The beam is of doubly-symmetric I-section. Hence the shear centre and centroid coincide.

(viii) The beam has "simply-supported" end conditions. Thus, lateral deflection and twist are prevented whilst warping and rotation about the minor axis are wholly unrestrained at the supports (Fig. 2.1).

(ix) The strain energy associated with shear is negligible in comparison with that due to bending. This is valid for beams of high span-to-depth ratio: such slender beams are the most susceptible to failure by elastic flexural-torsional buckling in any case.

2.2 Simply-Supported Beam under Uniform Moment and with Central Elastic Restraint

The case of a simply-supported beam of span 'l', restrained at midspan and subjected to an uniform moment is shown in Fig. 2.2 . The right-handed global (X,Y,Z) coordinate system has its origin at midspan and at the centroid of the beam in its undisturbed position. The Z-axis is coincident with the undisturbed longitudinal axis of the beam and the X-axis lies normal to the plane of the web: 'u' represents a translational displacement in the X-direction. In addition, a local right-handed coordinate system (ξ,η,ζ) is defined relative to the m-n plane and is shown in the plan view of Fig. 2.3 . The m-n plane lies normal to the longitudinal axis of the beam in its laterally deflected position.

The location of the elastic midspan translational restraint of stiffness 'K' is shown in plan in Fig. 2.3; both the translational and torsional restraints are shown in sectional elevation in Fig. 2.4 . The translational restraint is attached at level 'h' above the shear centre, whilst the torsional restraint is attached at the shear centre in such a way as to conform to Nethercot and Rockey's[63] "complete attachment" condition. Fig. 2.4 also shows the orientation of the midspan cross-section of the beam following a small virtual displacement involving both lateral deflection and twist. At midspan (z=0), the lateral deflection of the centroid is denoted by 'δ' and 'φ_c' is the rotation of the cross-section. The angle of twist, 'φ', at any section on the beam is assumed to increase according to the sense of rotation indicated by the right-hand screw rule relative to the positive direction of the global Z-axis.

As shown in Fig. 2.5, M_X and M_η are defined as positive in sense when they produce positive curvature of the element in the Y-Z and ζ-ξ planes, respectively.

The total extension of the translational spring resulting from the virtual disturbance (Fig. 2.4) is $\delta+\varphi_c h$ and consequently the force developed in the brace is $K(\delta+\varphi_c h)$. Equilibrium demands that two lateral reactions, each of magnitude $\frac{1}{2}K(\delta+\varphi_c h)$, be developed at the supports as shown in Fig. 2.6 .

The bending moment M_X about the X-axis is equal to the applied uniform moment M at all sections along the beam. In the following derivation, the bending moments at a section distant 'z' from the origin will be considered, as shown in Fig. 2.6(a). The in-plane moment vector M_X lies in the m'-n' plane and can be resolved into its components M_1 and M_2 (Fig. 2.6(b)), which also lie in the m'-n' plane. In Fig. 2.6(b) the vectorial representation of moments has been employed and is based on the right-hand screw rule. M_X is positive as shown, in accordance with the sign convention of Fig. 2.5 .

The bending moment applied to the beam about its weak axis in the disturbed position is M_η. Assumption (iii) of Section 2.1.3 allows the component of M_η arising from the in-plane moment M_X to be approximated by M_1 with negligible error. The other contribution to M_η arises from the force $\frac{1}{2}K(\delta+\varphi_c h)$ applied to the beam at z=1/2 . This contribution is consequently $\frac{1}{2}K(\delta+\varphi_c h)(\frac{\ell}{2}-z)$. Although M_1 has the same vectorial sense as the positive sense of M_η, the contribution from the lateral reaction acts in the opposite sense. M_η can therefore be expressed as:

$$M_\eta = M_1 - \frac{K}{2}(\delta + \varphi_c h)\left(\frac{\ell}{2} - z\right)$$

Substituting $M_1 = M_X\varphi = M\varphi$ into the above gives

$$M_\eta = M\varphi - \frac{K}{2}(\delta + \varphi_c h)\left(\frac{\ell}{2} - z\right)$$

According to the bending moment convention, the lateral bending produced by M_η can be approximately described by

$$M_\eta = EI_\eta u''$$

where EI_η = the flexural rigidity of the beam about its weak axis

and u'' = the curvature of the beam in the X-Z plane according to small deflection theory. (The standard superscript notation denotes differentiation with respect to z).

Hence the differential equation of lateral bending becomes

$$EI_\eta u'' = M\varphi - \frac{K}{2}(\delta + \varphi_c h)\left(\frac{\ell}{2} - z\right) \qquad \ldots(2.1)$$

Denoting the strain energy of the beam/restraint system by 'U', the increase in strain energy, ΔU, of the system during the virtual disturbance of Fig. 2.4 is

$$\Delta U = \frac{EI_\eta}{2}\int_{-\ell/2}^{\ell/2} (u'')^2\,dz + \frac{C}{2}\int_{-\ell/2}^{\ell/2} (\varphi')^2\,dz + \frac{C_1}{2}\int_{-\ell/2}^{\ell/2} (\varphi'')^2\,dz$$

$$+ \frac{K}{2}(\delta + \varphi_c h)^2 + \frac{K_T}{2}\varphi_c^2$$

in which $C=GJ$, the product of the shear modulus G and the St. Venant torsional constant J for the cross-section. C is defined as the torsional rigidity of the section.

and $C_1=E\Gamma$, the warping rigidity of the section. E is Young's modulus and Γ the warping constant.

The symmetric first mode of buckling in a single half-wave is assumed. Symmetry allows the increase in strain energy to be written as

$$\Delta U = EI_\eta\int_0^{\ell/2} (u'')^2\,dz + C\int_0^{\frac{\ell}{2}} (\varphi')^2\,dz + C_1\int_0^{\frac{\ell}{2}} (\varphi'')^2\,dz$$

$$+ \frac{K}{2}(\delta + \varphi_c h)^2 + \frac{K_T}{2}\varphi_c^2 \qquad \ldots(2.2)$$

The change in potential of an applied force is equal to the product of the magnitude of the force and the corresponding displacement, due attention being paid to the sense of the displacement. In the case of the applied lateral bending moment $M\varphi$, the change in potential of the moment with respect to a small element dz of the beam (Fig. 2.7) is equal to the product of the moment ($M\varphi$) and the angle subtended by the element ($d\theta$) at its centre of curvature. The curvature of the element is approximately $u''=1/r$, where 'r' is the instantaneous radius of curvature. Assuming the properties of a circular arc,

$$d\theta = \frac{dz}{r} = u''\,dz \qquad \ldots(2.3)$$

Denoting the potential energy of the load system by 'V', the change in potential of the applied moment over the element is

$$dV = -(M\varphi)\,d\theta = -M\varphi u''\,dz$$

and over the full length of the beam is

$$\Delta V = -\int_{-\ell/2}^{\ell/2} M\varphi u'' dz$$

or

$$\Delta V = -2M\int_{0}^{\ell/2} \varphi u'' dz \qquad \ldots(2.4)$$

Taking the total potential energy of the system in the undisturbed position to be zero, the total potential of the system in the displaced position is obtained from eqns. (2.2) and (2.4) and is

$$\Pi = EI_\eta\int_0^{\ell/2}(u'')^2 dz + C\int_0^{\ell/2}(\varphi')^2 dz + C_1\int_0^{\ell/2}(\varphi'')^2 dz$$

$$- 2M\int_0^{\ell/2}\varphi u'' dz + \frac{K}{2}(\delta + \varphi_c h)^2 + \frac{K_T}{2}\varphi_c^2 \qquad \ldots(2.5)$$

The total potential is therefore a function of the two displacement degrees of freedom 'u' and 'φ'. Instead of assuming displacement functions for each, eqn. (2.1) can be used to substitute for u", making Π dependent only on the displacement function assumed for φ. Rearranging eqn. (2.1) gives

$$u'' = \frac{M}{EI_\eta}\varphi - \frac{K}{2EI_\eta}(\delta + \varphi_c h)\left(\frac{\ell}{2} - z\right) \qquad \ldots(2.6)$$

and substituting for u" in eqn. (2.5) gives

$$\Pi = EI_\eta\int_0^{\ell/2}\left\{\frac{M\varphi}{EI_\eta} - \frac{K(\delta+\varphi_c h)}{2EI_\eta}\left(\frac{\ell}{2} - z\right)\right\}^2 dz + C\int_0^{\ell/2}(\varphi')^2 dz$$

$$+ C_1\int_0^{\ell/2}(\varphi'')^2 dz - 2M\int_0^{\ell/2}\left\{\frac{M\varphi}{EI_\eta} - \frac{K(\delta+\varphi_c h)}{2EI_\eta}\left(\frac{\ell}{2} - z\right)\right\}\varphi dz$$

$$+ \frac{K}{2}(\delta + \varphi_c h)^2 + \frac{K_T}{2}\varphi_c^2$$

Expanding and grouping terms with a common integral leads to

$$\Pi = \frac{-M^2}{EI_\eta}\int_0^{\ell/2}\varphi^2 dz + \frac{K^2(\delta+\varphi_c h)^2}{4EI_\eta}\int_0^{\ell/2}\left(\frac{\ell}{2} - z\right)^2 dz$$

$$+ C\int_0^{\ell/2}(\varphi')^2 dz + C_1\int_0^{\ell/2}(\varphi'')^2 dz$$

$$+ \frac{K}{2}(\delta + \varphi_c h)^2 \quad + \quad \frac{K_T}{2}\varphi_c^2 \qquad \ldots(2.7)$$

where it should be noted that integration of δ and φ_c does not need to be performed as these are constant with respect to integration in z.

A twisted mode $\varphi(z)$ is assumed and contains two trigonometric terms involving the cosine function. This function reflects the symmetrical nature of the deflected shape associated with first mode buckling. The assumed function is

$$\varphi = A\cos\frac{\pi z}{\ell} + B\cos\frac{3\pi z}{\ell} \qquad \ldots(2.8)$$

where A and B are independent coefficients. This function satisfies the kinematic boundary condition $\varphi=0$ at $z=\pm 1/2$. The derivatives φ' and φ'' are therefore

$$\varphi' = -\frac{\pi}{\ell}A\sin\frac{\pi z}{\ell} - \frac{3\pi}{\ell}B\sin\frac{3\pi z}{\ell}$$

and

$$\varphi'' = -\frac{\pi^2}{\ell^2}A\cos\frac{\pi z}{\ell} - \frac{9\pi^2}{\ell^2}B\cos\frac{3\pi z}{\ell}$$

Thus the assumed function also satisfies what is effectively a static boundary condition: $\varphi''=0$ at $z=\pm 1/2$.

Substituting for φ and its derivatives in eqn. (2.7) allows the integrations to be performed. Hence,

$$\int_0^{\ell/2} \varphi^2\, dz = \frac{\ell}{4}(A^2 + B^2)$$

$$\int_0^{\ell/2} \left(\frac{\ell}{2} - z\right)^2 dz = \frac{\ell^3}{24}$$

$$\int_0^{\ell/2} (\varphi')^2\, dz = \frac{\pi^2}{4\ell}(A^2 + 9B^2)$$

and $\displaystyle\int_0^{\ell/2} (\varphi'')^2 dz \quad = \quad \frac{\pi^4}{4\ell^3}\left(A^2 + 81B^2\right)$

Eqn. (2.7) then yields

$$\Pi = \frac{-M^2\ell}{4EI_\eta}\left(A^2 + B^2\right) + \frac{K^2\ell^3(\delta+\varphi_c h)^2}{96EI_\eta} + \frac{\pi^2 C}{4\ell}\left(A^2 + 9B^2\right)$$

$$+ \frac{\pi^4 C_1}{4\ell^3}\left(A^2 + 81B^2\right) + \frac{K}{2}(\delta+\varphi_c h)^2 + \frac{K_T}{2}\varphi_c^2$$

$$= \frac{-M^2\ell}{4EI_\eta}\left(A^2 + B^2\right) + \frac{K}{2}(\delta+\varphi_c h)^2\left(1 + \frac{K\ell^3}{48EI_\eta}\right)$$

$$+ \frac{\pi^2 C}{4\ell}\left(A^2 + 9B^2\right) + \frac{\pi^4 C_1}{4\ell^3}\left(A^2 + 81B^2\right) + \frac{K_T}{2}\varphi_c^2 \qquad \ldots(2.9)$$

Introducing the non-dimensional restraint parameter λ, previously defined in eqn. (1.2), eqn. (2.9) becomes

$$\Pi = \frac{-M^2\ell}{4EI_\eta}\left(A^2 + B^2\right) + \frac{K}{2}(\delta+\varphi_c h)^2(1+\lambda) + \frac{\pi^2 C}{4\ell}\left(A^2 + 9B^2\right)$$

$$+ \frac{\pi^4 C_1}{4\ell^3}\left(A^2 + 81B^2\right) + \frac{K_T}{2}\varphi_c^2 \qquad \ldots(2.10)$$

At this stage, it is necessary to express δ and φ_c in terms of the unknowns A and B . In Fig. 2.8, the element curvature is

$$u'' = \frac{d\theta}{dz}$$

and so the length of arc $z_3 z_3'$ is

$$|\text{arc } z_3 z_3'| = \left(\frac{\ell}{2} - z\right) d\theta$$

$$= \left(\frac{\ell}{2} - z\right) u'' dz$$

Integrating over all such elements on the half-span to obtain the total lateral deflection at midspan yields

$$\delta = \int_0^{\ell/2} \left(\frac{\ell}{2} - z\right) u'' \, dz \qquad \ldots(2.11)$$

Using eqn. (2.6) to remove u" gives

$$\delta = \int_0^{\ell/2} \left(\frac{\ell}{2} - z\right)\left(\frac{M\varphi}{EI_\eta} - \frac{K}{2EI_\eta}(\delta + \varphi_c h)\left(\frac{\ell}{2} - z\right)\right) dz$$

Substituting for φ from eqn. (2.8) and expanding gives

$$\delta = \frac{M}{EI_\eta}\int_0^{\ell/2} \left(\frac{\ell}{2} - z\right)\left(A \cos\frac{\pi z}{\ell} + B\cos\frac{3\pi z}{\ell}\right) dz$$

$$- \frac{K(\delta + \varphi_c h)}{2EI_\eta}\int_0^{\ell/2} \left(\frac{\ell}{2} - z\right)^2 dz$$

$$= \frac{MA}{EI_\eta}\int_0^{\frac{\ell}{2}} \left(\frac{\ell}{2} - z\right)\cos\frac{\pi z}{\ell} dz + \frac{MB}{EI_\eta}\int_0^{\frac{\ell}{2}} \left(\frac{\ell}{2} - z\right)\cos\frac{3\pi z}{\ell} dz - \frac{K(\delta + \varphi_c h)}{2EI_\eta}\int_0^{\frac{\ell}{2}} \left(\frac{\ell}{2} - z\right)^2 dz$$

which, on evaluation of the integrals, reduces to

$$\delta = \frac{M\ell^2}{\pi^2 EI_\eta}\left(A + \frac{B}{9}\right) - \frac{K\ell^3(\delta + \varphi_c h)}{48EI_\eta}$$

Adding $\varphi_c h$ to each side gives

$$\delta + \varphi_c h = \frac{M\ell^2}{\pi^2 EI_\eta}\left(A + \frac{B}{9}\right) - \frac{K\ell^3(\delta + \varphi_c h)}{48EI_\eta} + \varphi_c h$$

or

$$(\delta + \varphi_c h)\left(1 + \frac{K\ell^3}{48EI_\eta}\right) = \frac{M\ell^2}{\pi^2 EI_\eta}\left(A + \frac{B}{9}\right) + \varphi_c h$$

Substituting eqn. (1.2) and noting that $\varphi_c = A+B$ gives

$$(\delta + \varphi_c h) = \frac{1}{1+\lambda}\left\{\frac{M\ell^2}{\pi^2 EI_\eta}\left(A + \frac{B}{9}\right) + h(A + B)\right\} \qquad \ldots(2.12)$$

Therefore,

$$(\delta + \varphi_c h)^2 = \frac{1}{(1+\lambda)^2}\left\{\frac{M^2\ell^4}{\pi^4 E^2 I_\eta^2}\left(A + \frac{B}{9}\right)^2 + h^2(A+B)^2\right.$$

$$\left. + \frac{2M\ell^2 h}{\pi^2 EI_\eta}(A+B)\left(A + \frac{B}{9}\right)\right\} \qquad \ldots(2.13)$$

Substituting eqn. (2.13) into the expression for Π in eqn. (2.10) leads to

$$\Pi = \frac{-M^2\ell}{4EI_\eta}(A^2+B^2) + \frac{\pi^2 C}{4\ell}(A^2+9B^2) + \frac{\pi^4 C_1}{4\ell^3}(A^2+81B^2)$$

$$+ \frac{K}{2(1+\lambda)}\left\{\frac{M^2\ell^4}{\pi^4E^2I_\eta^2}\left(A+\frac{B}{9}\right)^2 + h^2(A+B)^2 + \frac{2M\ell^2h}{\pi^2EI_\eta}(A+B)\left(A+\frac{B}{9}\right)\right\} + \frac{K_T}{2}\varphi_c^2$$

$$= \frac{-M^2\ell}{4EI_\eta}(A^2+B^2) + \frac{KM^2\ell^4}{2\pi^4E^2I_\eta^2(1+\lambda)}\left(A+\frac{B}{9}\right)^2 + \frac{Kh^2(A+B)^2}{2(1+\lambda)}$$

$$+ \frac{KM\ell^2h}{\pi^2EI_\eta(1+\lambda)}(A+B)\left(A+\frac{B}{9}\right) + \frac{\pi^2C}{4\ell}(A^2+9B^2)$$

$$+ \frac{\pi^4C_1}{4\ell^3}(A^2+81B^2) + \frac{K_T}{2}(A+B)^2$$

Adopting the non-dimensional form of torsional stiffness 'e' defined in eqn. (1.3) and substituting for K in terms of λ from eqn. (1.2) gives

$$\Pi = \frac{-M^2\ell}{4EI_\eta}(A^2+B^2) + \frac{24M^2\ell\lambda}{\pi^4EI_\eta(1+\lambda)}\left(A+\frac{B}{9}\right)^2$$

$$+ \frac{24EI_\eta h^2\lambda}{\ell^3(1+\lambda)}(A+B)^2 + \frac{48Mh\lambda}{\pi^2\ell(1+\lambda)}(A+B)\left(A+\frac{B}{9}\right)$$

$$+ \frac{\pi^4C_1}{4\ell^3}(A^2+81B^2) + \frac{\pi^2C}{4\ell}(A^2+9B^2) + \frac{eC}{2\ell}(A+B)^2$$

$$= F_1(A^2+B^2) + F_2\left(A+\frac{B}{9}\right)^2 + F_3(A+B)^2 + F_4(A+B)\left(A+\frac{B}{9}\right)$$

$$+ F_5(A^2+9B^2) + F_6(A^2+81B^2) \qquad \ldots(2.14)$$

in which

$$C = GJ$$

$$C_1 = E\Gamma$$

and

$$F_1 = \frac{-M^2\ell}{4EI_\eta}, \qquad F_2 = \frac{24M^2\ell\lambda}{\pi^4 EI_\eta(1+\lambda)},$$

$$F_3 = \frac{24EI_\eta h^2\lambda}{\ell^3(1+\lambda)} + \frac{eC}{2\ell}, \qquad F_4 = \frac{48Mh\lambda}{\pi^2\ell(1+\lambda)},$$

$$F_5 = \frac{\pi^2 C}{4\ell}, \qquad F_6 = \frac{\pi^4 C_1}{4\ell^3} \qquad \ldots(2.15)$$

An equilibrium configuration of the system is characterised by a stationary value of the total potential energy Π. Mathematically, this is expressed in the Rayleigh-Ritz method as the pair of simultaneous equations

$$\frac{\partial\Pi}{\partial A} = 0 \qquad \text{and} \qquad \frac{\partial\Pi}{\partial B} = 0$$

in terms of the current notation.

Differentiating eqn. (2.14) with respect to A and B in turn gives

$$\frac{\partial\Pi}{\partial A} = A\left\{2(F_1+F_2+F_3+F_4+F_5+F_6)\right\} + B\left(\frac{2F_2}{9} + 2F_3 + \frac{10F_4}{9}\right) \qquad \ldots(2.16)$$

$$\frac{\partial\Pi}{\partial B} = A\left(\frac{2F_2}{9} + 2F_3 + \frac{10F_4}{9}\right) + B\left\{2\left(F_1 + \frac{F_2}{81} + F_3 + \frac{F_4}{9} + 9F_5 + 81F_6\right)\right\} \qquad \ldots(2.17)$$

Thus, in matrix notation:

$$\begin{bmatrix} \partial\Pi/\partial A \\ \partial\Pi/\partial B \end{bmatrix} = \begin{bmatrix} G_{11} & G_{12} \\ G_{21} & G_{22} \end{bmatrix} \begin{bmatrix} A \\ B \end{bmatrix} = \underset{\sim}{0} \qquad \ldots(2.18)$$

in which

$$G_{11} = 2(F_1 + F_2 + F_3 + F_4 + F_5 + F_6)$$

$$G_{12} = \frac{2F_2}{9} + 2F_3 + \frac{10F_4}{9}$$

$$G_{21} = G_{12}$$

$$G_{22} = 2\left(F_1 + \frac{F_2}{81} + F_3 + \frac{F_4}{9} + 9F_5 + 81F_6\right) \qquad \ldots(2.19)$$

It has been observed by Tauchert[82] that the condition of neutral equilibrium is identically satisfied by assuming that A,B are indeterminate but non-zero and solving the system of equations

$$\frac{\partial \Pi}{\partial A} = \frac{\partial \Pi}{\partial B} = 0$$

as an eigenvalue problem. Therefore, for any combination of beam and restraint geometry, the critical applied moment is that value which makes the determinant

$$\det\left[G\right] = G_{11}G_{22} - G_{12}G_{21}$$

vanish. Due to the complexity of the expressions G_{ij}, a closed-form solution for the critical moment is not feasible and consequently a numerical solution is required.

In order to evaluate the elastic critical loads of restrained beams, a simple computer programme "MODBRACE", which automatically locates the zero determinant using a "search and bisect" strategy was written. A description of the programme is given in Section 2.7 and a programme listing together with details of a typical run are given in Appendices I(a) and (b). An associated programme "AUTOBRAC" for the determination of critical combinations of non-dimensional restraint stiffnesses $\{\lambda, e\}_{cr}$ for the enforcement of second mode buckling in single span beams was also developed. Appendix I also contains details of this programme.

Numerical solutions for several combinations of the variables included in the above analysis have been performed using programmes MODBRACE and AUTOBRAC. The combinations considered are shown diagrammatically in Fig. 2.9 and are described more fully in Section 2.7 .

2.3 Simply-Supported Beam under Uniform Moment and with Rigid Central Restraint

In the case of a beam with rigid restraint at midspan, failure occurs in the antisymmetric two half-wave mode in which a "node" or point of contraflexure occurs at midspan in the plan view. The boundary conditions u=0 and $\varphi=0$ are now seen to apply not only at the ends of the beam but also at this central node. In addition, the development of an antisymmetric mode does not preclude warping deformations at the node. Consequently, if free warping at this point is assumed then the following boundary conditions are seen to apply:

$$u = 0 \text{ and } \varphi = \varphi'' = 0 \quad \text{at} \quad z = 0, \pm l/2$$

The conditions u=0 and $\varphi = \varphi''=0$ are noted to be those assumed at the supports in the previous analysis and hence the expressions developed therein are appropriate in this case, subject to the following:

(i) for the purposes of calculation, the length of the beam should be taken as one-half of the actual span and

(ii) the relative brace rigidities λ and e should be set equal to zero. Otherwise, restraint at the quarter point would be applied.

Agreement between the boundary conditions in this and in the previous section (as noted above) is a necessary but insufficient criterion for the direct application of the previous analysis to this case of second mode buckling. Uniformity of the applied loading is also a requirement. In this respect, Fig. 2.10 indicates the reasons for the applicability of first mode analysis to the second mode problem in the case of uniform moment loading but not in the case of central point loading.

The second mode of buckling is the highest which can be attained by a beam restrained at midspan, irrespective of the stiffness of the restraints. Consequently, the critical load of a system in which there is rigid (ie. infinite) central restraint is identical to that of a system possessing only a finite degree of restraint, providing the latter falls within the "fully effective" category as defined by Flint[59] and Winter[46]. The numerical results derived from this Section therefore provide plateaux of constant c on the curves of Fig. 2.19, described more fully in Section 2.7 .

2.4 Simply-Supported Beam under Central Point Loading and with Central Elastic Restraint

In the following analysis, both the level of load application and the level of attachment of lateral restraint relative to the shear centre are variable. The load 'P' acts at a height 'a' above the shear centre, the restraint at height 'h' as described in Section 2.2 . The geometry of the arrangement relative to the cross-section of the beam is shown in Fig. 2.11 .

There are many similarities between the present analysis and that of Section 2.2 . In this Section, the differences between the two analyses are noted and, although the steps in this analysis are presented in sufficient detail to permit an understanding of the method, many of the intermediate steps involving only algebraic manipulation have been omitted to avoid repetition.

The in-plane bending moment distribution on the beam is as shown in Fig. 2.12, where it is noted that the in-plane bending moment M_X at any section z is given by

$$M_x = \frac{P}{2}\left(\frac{\ell}{2} - z\right) \qquad \ldots(2.20)$$

The lateral bending equation corresponding to eqn. (2.1) of Section 2.2 is therefore

$$EI_\eta u'' = \varphi \frac{P}{2}\left(\frac{\ell}{2} - z\right) - \frac{K}{2}(\delta + \varphi_c h)\left(\frac{\ell}{2} - z\right) \qquad \ldots(2.21)$$

It should be noted that the application of the load at a height 'a' above the shear centre does not affect the equation of lateral bending as it produces no additional component of the load in this direction. This can be verified by replacing the applied load by its statically-equivalent actions at the shear centre (Fig. 2.13). The additional destabilising torque indicated in Fig. 2.13(b) has no effect on the equation of lateral bending.

The change in strain energy of the beam/restraint system is similarly unaffected by the level of load application and is given by eqn. (2.2). However, the change in potential of the applied load during the virtual disturbance is dependent not only on the type of loading but also on the level at which load is applied relative to the shear centre. For a load applied above the shear centre, the point of load application falls more than the shear centre by an amount 'β' dependent on 'a' and 'φ_c' (Fig. 2.14). Conversely, for a load applied below the shear centre, the load point falls less than the shear centre. The vertical deflection (α) of the shear centre during the virtual disturbance is a function of 'δ' as defined in eqn. (2.11). Employing a small angle approximation consistent with assumption (iii) in Section 2.1.3, α can be defined as the summation (over the half-span) of all the small vertical displacements of the elements of length dz (Fig. 2.8) arising from their curvature u" and instantaneous twist φ. Hence, in the limit,

$$\alpha = \int_0^{\ell/2} \varphi\left(\frac{\ell}{2} - z\right) u''\, dz \qquad \ldots(2.22)$$

The additional component of vertical deflection, β, is obtained by noting that, in Fig. 2.14,

$$\beta = a - a\cos\varphi_c$$

$$= a(1 - \cos\varphi_c)$$

Expanding $\cos\varphi_c$ as a Taylor series and neglecting terms of greater than quadratic degree gives

$$\cos\varphi_c \simeq 1 - \frac{\varphi_c^2}{2}$$

which, on substitution, yields

$$\beta = \frac{a\varphi_c^2}{2} \qquad \ldots(2.23)$$

Hence the change in potential of the applied load during the disturbance is given by

$$\Delta V = \frac{-Pa\varphi_c^2}{2} - P\int_0^{\ell/2} \varphi\left(\frac{\ell}{2} - z\right) u''\, dz \qquad \ldots(2.24)$$

The total potential of the system following the disturbance is then given by eqns. (2.2) and (2.24) and is

$$\Pi = EI_\eta \int_0^{\ell/2} (u'')^2 dz + C\int_0^{\ell/2} (\varphi')^2 dz + C_1 \int_0^{\ell/2} (\varphi'')^2 dz$$

$$+ \frac{K}{2}(\delta + \varphi_c h)^2 + \frac{K_T}{2}\varphi_c^2 - \frac{Pa\varphi_c^2}{2}$$

$$- P\int_0^{\ell/2} \varphi\left(\frac{\ell}{2} - z\right) u'' dz \qquad \ldots(2.25)$$

Rearranging eqn. (2.21) gives

$$u'' = \frac{P}{2EI_\eta}\left(\frac{\ell}{2} - z\right)\varphi - \frac{K(\delta + \varphi_c h)}{2EI_\eta}\left(\frac{\ell}{2} - z\right) \qquad \ldots(2.26)$$

which is substituted into eqn. (2.25) for all occurrences of u". The twist function φ as given in eqn. (2.8) is again valid as the deflected shape of the beam is similar to that assumed in Section 2.2 . Likewise, the same boundary conditions are valid. The expressions for φ and its first and second derivatives are also substituted into eqn. (2.25) and the integrations performed to give

$$\int_0^{\ell/2} (u'')^2 dz = \frac{A^2P^2\ell^3}{192E^2I_\eta^2}\left(1 + \frac{6}{\pi^2}\right) + \frac{5ABP^2\ell^3}{64\pi^2E^2I_\eta^2}$$

$$+ \frac{B^2P^2\ell^3}{576E^2I_\eta^2}\left(3 + \frac{2}{\pi^2}\right) - \frac{APK\ell^3(\delta+\varphi_c h)}{2\pi^2E^2I_\eta^2}\left(1 - \frac{2}{\pi}\right)$$

$$- \frac{BPK\ell^3(\delta+\varphi_c h)}{54\pi^2E^2I_\eta^2}\left(3 + \frac{2}{\pi}\right) + \frac{K^2\ell^3(\delta+\varphi_c h)^2}{96E^2I_\eta^2}$$

$$\int_0^{\ell/2} (\varphi')^2 dz = \frac{\pi^2}{4\ell}(A^2 + 9B^2)$$

$$\int_0^{\ell/2} (\varphi'')^2 dz = \frac{\pi^4}{4\ell^3}(A^2 + 81B^2)$$

$$\int_0^{\ell/2} \varphi\left(\frac{\ell}{2} - z\right)u'' dz = \frac{A^2P\ell^3}{96EI_\eta}\left(1 + \frac{6}{\pi^2}\right) + \frac{5ABP\ell^3}{32\pi^2EI_\eta} + \frac{B^2P\ell^3}{288EI_\eta}\left(3 + \frac{2}{\pi^2}\right)$$

$$- \frac{AK\ell^3(\delta+\varphi_c h)}{2\pi^2 EI_\eta}\left(1-\frac{2}{\pi}\right) - \frac{BK\ell^3(\delta+\varphi_c h)}{54\pi^2 EI_\eta}\left(3+\frac{2}{\pi}\right)$$

Substitution of the above expressions in eqn. (2.25) gives, after grouping and cancellation of terms:

$$\Pi = \frac{-A^2P^2\ell^3}{192EI_\eta}\left(1+\frac{6}{\pi^2}\right) - \frac{5ABP^2\ell^3}{64\pi^2EI_\eta} - \frac{B^2P^2\ell^3}{576EI_\eta}\left(3+\frac{2}{\pi^2}\right)$$

$$+\frac{\pi^2C}{4\ell}(A^2+9B^2) + \frac{\pi^4C_1}{4\ell^3}(A^2+81B^2) + (\delta+\varphi_c h)^2\left(\frac{K^2\ell^3}{96EI_\eta}+\frac{K}{2}\right)$$

$$-\frac{Pa\varphi_c^2}{2} + \frac{K_T\varphi_c^2}{2} \qquad \ldots(2.27)$$

Based on eqns. (2.11) and (2.26), a similar expression to that of eqn. (2.12) can be obtained for $(\delta+\varphi_c h)$. Hence,

$$(\delta+\varphi_c h)^2 = \frac{64}{(48EI_\eta+K\ell^3)^2}\left(9A^2D_1 + B^2D_2 + 6ABD_3\right) \qquad \ldots(2.28)$$

in which

$$D_1 = \frac{P^2\ell^6}{\pi^4}\left(1+\frac{4}{\pi^2}-\frac{4}{\pi}\right) + \frac{4P\ell^3EI_\eta h}{\pi^2}\left(1-\frac{2}{\pi}\right) + 4E^2I_\eta^2h^2$$

$$D_2 = \frac{P^2\ell^6}{9\pi^4}\left(1+\frac{4}{9\pi^2}+\frac{4}{3\pi}\right) + \frac{4P\ell^3EI_\eta h}{\pi^2}\left(1+\frac{2}{3\pi}\right) + 36E^2I_\eta^2h^2$$

and

$$D_3 = \frac{P^2\ell^6}{3\pi^4}\left(1-\frac{4}{3\pi}-\frac{4}{3\pi^2}\right) + \frac{6P\ell^3EI_\eta h}{\pi^2}\left(1-\frac{2}{\pi}\right)$$

On subsititution of eqn. (2.28), eqn. (2.27) becomes

$$\Pi = \frac{-Pa}{2}(A^2+B^2+2AB) - \frac{A^2P^2\ell^3}{192EI_\eta}\left(1+\frac{6}{\pi^2}\right) - \frac{5ABP^2\ell^3}{64\pi^2EI_\eta}$$

$$-\frac{B^2P^2\ell^3}{576EI_\eta}\left(3+\frac{2}{\pi^2}\right) + \frac{\pi^2C}{4\ell}(A^2+9B^2) + \frac{\pi^4C_1}{4\ell^3}(A^2+81B^2)$$

$$+\frac{2K(9A^2D_1 + B^2D_2 + 6ABD_3)}{3EI_\eta(48EI_\eta + K\ell^3)} + \frac{K_T}{2}(A+B)^2$$

$$= \left(\frac{eC}{2\ell} - \frac{Pa}{2}\right)(A^2+B^2+2AB) - \frac{A^2P^2\ell^3}{192EI_\eta}\left(1+\frac{6}{\pi^2}\right) - \frac{5ABP^2\ell^3}{64\pi^2EI_\eta}$$

$$- \frac{B^2P^2\ell^3}{576EI_\eta}\left(3+\frac{2}{\pi^2}\right) + \frac{\pi^2C}{4\ell}(A^2+9B^2) + \frac{\pi^4C_1}{4\ell^3}(A^2+81B^2)$$

$$+ \frac{2\lambda}{3EI_\eta\ell^3(1+\lambda)}(9A^2D_1 + B^2D_2 + 6ABD_3) \qquad \ldots(2.29)$$

$$= F_1(A^2+B^2+2AB) + F_2(A^2) + F_3(AB) + F_4(B^2) + F_5(A^2+9B^2)$$

$$+ F_6(A^2+81B^2) + F_7(A^2) + F_8(B^2) + F_9(AB) \qquad \ldots(2.30)$$

in which

$$F_1 = \frac{1}{2}\left(\frac{eC}{\ell} - Pa\right), \qquad F_2 = \frac{-P^2\ell^3}{192EI_\eta}\left(1+\frac{6}{\pi^2}\right),$$

$$F_3 = \frac{-5P^2\ell^3}{64\pi^2EI_\eta}, \qquad F_4 = \frac{-P^2\ell^3}{576EI_\eta}\left(3+\frac{2}{\pi^2}\right),$$

$$F_5 = \frac{\pi^2C}{4\ell}, \qquad F_6 = \frac{\pi^4C_1}{4\ell^3},$$

$$F_7 = \frac{6D_1\lambda}{EI_\eta\ell^3(1+\lambda)}, \qquad F_8 = \frac{2D_2\lambda}{3EI_\eta\ell^3(1+\lambda)},$$

$$F_9 = \frac{4D_3\lambda}{EI_\eta\ell^3(1+\lambda)} \qquad \ldots(2.31)$$

Differentiating eqn. (2.30) with respect to A and B gives

$$\frac{\partial \Pi}{\partial A} = A\left\{2(F_1+F_2+F_5+F_6+F_7)\right\} + B(2F_1+F_3+F_9)$$

$$\frac{\partial \Pi}{\partial B} = A(2F_1+F_3+F_9) + B\left\{2(F_1+F_4+9F_5+81F_6+F_8)\right\}$$

and expressing

$$\frac{\partial \Pi}{\partial A} = \frac{\partial \Pi}{\partial B} = 0$$

in matrix notation gives

$$\begin{bmatrix} \partial\Pi/\partial A \\ \partial\Pi/\partial B \end{bmatrix} = \begin{bmatrix} G_{11} & G_{12} \\ G_{21} & G_{22} \end{bmatrix} \begin{bmatrix} A \\ B \end{bmatrix} = \underset{\sim}{0}$$

where

$$G_{11} = 2(F_1+F_2+F_5+F_6+F_7)$$

$$G_{12} = 2F_1+F_3+F_9$$

$$G_{21} = G_{12}$$

$$G_{22} = 2(F_1+F_4+9F_5+81F_6+F_8) \qquad \ldots(2.32)$$

Numerical solution is again performed using the programmes MODBRACE and AUTOBRAC, in which the above eqns. (2.32) have been incorporated. The number of possible combinations of the parameters l, λ, e, h, a is much greater than for the case of uniform moment loading in Fig. 2.9 . A similar tree-diagram for the central point loading case is shown in Fig. 2.15. Numerical results are described in Section 2.7 .

2.5 Simply-Supported Beam under Central Point Loading and with Rigid Central Restraint

As noted in Section 2.3 and illustrated in Fig. 2.10, the direct application of the first mode buckling analysis presented in Section 2.4 to the case of second mode failure of a beam with rigid, central restraint under the action of a central point load is not possible due to an incompatibility between the in-plane bending moment distributions.

In order to evaluate the critical loads of systems possessing "fully effective" or rigid midspan restraint and subjected to central point loading, it is only necessary to consider one half of the beam with its associated in-plane bending moment distribution as shown in Fig. 2.10 . The origin of the (X, Y, Z) coordinate system is located at the left-hand end of the half-span ie. at midspan on the actual beam.

The boundary conditions u=0 and $\varphi=\varphi''=0$ apply at z=0 and z=1/2, but in this case the antisymmetric nature of the buckled shape necessitates the use of an assumed twisted mode $\varphi(z)$ based on the sine rather than on the cosine function. The simplest function satisfying the φ and φ'' boundary conditions is

$$\varphi = A\sin\frac{2\pi z}{\ell} + B\sin\frac{4\pi z}{\ell} \qquad ...(2.33)$$

The presence of rigid restraint at z=0 simplifies the analysis as there is consequently no elastic restraint applied at any point on the half-span. The analysis is further simplified by noting that the requirement φ =0 at z=0 (ie. at midspan) demands that the change in potential of the applied load (P) during the virtual deformation is independent of its level of application (a) on the cross-section and consequently no term involving 'a' appears in the expression for ΔV.

The differential equation of lateral bending may be stated as

$$u'' = \frac{P}{2EI_\eta}\left(\frac{\ell}{2}-z\right)\varphi \qquad ...(2.34)$$

The change in potential of the applied load must be derived by the method of Section 2.2 in which the change in potential is expressed as the product of a lateral bending moment and the corresponding subtended angle. Hence

$$\Delta V = -\frac{P}{2}\int_0^{\ell/2}\left(\frac{\ell}{2}-z\right)\varphi u'' dz \qquad \ldots(2.35)$$

As no elastic restraint is present, the terms involving K and K_T in the strain energy expression, eqn. (2.2), are omitted and thus the total potential is written as

$$\Pi = \frac{EI_\eta}{2}\int_0^{\ell/2}(u'')^2 dz + \frac{C}{2}\int_0^{\ell/2}(\varphi')^2 dz + \frac{C_1}{2}\int_0^{\ell/2}(\varphi'')^2 dz$$

$$- \frac{P}{2}\int_0^{\ell/2}\left(\frac{\ell}{2}-z\right)\varphi u'' dz \qquad \ldots(2.36)$$

Performing the substitution indicated by eqn. (2.34) and substituting for φ and its derivatives from eqn. (2.33), integration of the four terms in eqn. (2.36) leads to an expression for Π involving the two independent coefficients A and B:

$$\Pi = \frac{-P^2}{8EI_\eta}\left\{\frac{A^2\ell^3}{16}\left(\frac{1}{3}-\frac{1}{2\pi^2}\right) + \frac{B^2\ell^3}{16}\left(\frac{1}{3}-\frac{1}{8\pi^2}\right) + \frac{2\ell^3 AB}{9\pi^2}\right\}$$

$$+ \frac{\pi^2 C}{2\ell}\left(A^2+4B^2\right) + \frac{2\pi^4 C_1}{\ell^3}\left(A^2+16B^2\right) \qquad \ldots(2.37)$$

Differentiating with respect to A and B yields

$$\begin{bmatrix}\partial\Pi/\partial A\\ \partial\Pi/\partial B\end{bmatrix} = \begin{bmatrix}G_{11} & G_{12}\\ G_{21} & G_{22}\end{bmatrix}\begin{bmatrix}A\\ B\end{bmatrix} = \underset{\sim}{0}$$

in which

$$G_{11} = \frac{-P^2\ell^3}{64EI_\eta}\left(\frac{1}{3}-\frac{1}{2\pi^2}\right) + \frac{\pi^2 C}{\ell} + \frac{4\pi^4 C_1}{\ell^3}$$

$$G_{12} = \frac{-P^2\ell^3}{36\pi^2 EI_\eta}$$

$$G_{21} = G_{12}$$

$$G_{22} = \frac{-P^2\ell^3}{64EI_\eta}\left(\frac{1}{3} - \frac{1}{8\pi^2}\right) + \frac{4\pi^2 C}{\ell} + \frac{64\pi^4 C_1}{\ell^3} \qquad \ldots(2.38)$$

Solution of the simultaneous equations

$$\frac{\partial \Pi}{\partial A} = \frac{\partial \Pi}{\partial B} = 0$$

as an eigenvalue problem is again performed with the aid of programmes MODBRACE and AUTOBRAC as described in Section 2.7 .

2.6 Re-analysis of the Lateral Restraint Problem of Section 2.4 using an Assumed Displacement Function of Higher Order

An analysis by Flint[59] for the case of a simply-supported beam with midspan restraint and under the action of a central point load showed that the energy analysis provided results which were subject to considerable error when the assumed displacement function lacked terms of sufficiently high order. Flint's initial analysis employed only one trigonometric term in the assumed twist function:

$$\varphi = A\cos\frac{\pi z}{\ell}$$

and the numerical results were noted to be appreciably in error (Section 1.2.3 and Fig. 1.13) for values of the restraint stiffness parameter λ greater than about 1.5 . Both Flint's subsequent results and those presented in Figs. 2.19 to 2.27 of this present work indicate the unacceptable limitation imposed by this latter condition, on the grounds that relative brace stiffnesses (ie. values of λ) greater than 1.5 are frequently required in order to provide full restraint to the primary member. A subsequent analysis by Flint involving a two-term displacement function (as employed in Sections 2.2 and 2.4) provided a satisfactory solution which was later verified by the results of a series of tests on model beams.

Because the analyses presented in Sections 2.4 and 2.5 are more general than that presented by Flint[59], it was considered necessary to examine the effect of incorporating a yet more refined displacement function within the framework of the analysis of Section 2.4. As this re-analysis was perceived solely as a verification of the previous analysis, the effects of variations in the level of load application (a) and torsional restraint stiffness (K_T) were omitted in order to simplify the solution. The assumed twist function $\varphi(z)$ was:

$$\varphi = A\cos\frac{\pi z}{\ell} + B\cos\frac{3\pi z}{\ell} + C_2\cos\frac{5\pi z}{\ell}$$

in which A, B, C_2 are independent coefficients: the subscript notation was employed for the third coefficient to avoid confusion with the rigidities C and C_1 already in use.

Details of the analysis are not presented, as the algebra was found to be substantially more tedious than that of Section 2.4 . However, the final condition

$$\frac{\partial \Pi}{\partial A} = \frac{\partial \Pi}{\partial B} = \frac{\partial \Pi}{\partial C_2} = 0$$

can be expressed by the matrix equation

$$\begin{bmatrix} \partial\Pi/\partial A \\ \partial\Pi/\partial B \\ \partial\Pi/\partial C_2 \end{bmatrix} = \begin{bmatrix} G_{11} & G_{12} & G_{13} \\ G_{21} & G_{22} & G_{23} \\ G_{31} & G_{32} & G_{33} \end{bmatrix} \begin{bmatrix} A \\ B \\ C_2 \end{bmatrix} = \underset{\sim}{0}$$

in which

$$G_{11} = \frac{-P^2\ell^3}{96EI_\eta}\left(1+\frac{6}{\pi^2}\right) + \frac{\pi^2 C}{2\ell} + \frac{\pi^4 C_1}{2\ell^3} + 36K\frac{F_1^2}{F_4}$$

$$G_{12} = G_{21} = \frac{-5P^2\ell^3}{64\pi^2 EI_\eta} + 12K\frac{F_1F_2}{F_4}$$

$$G_{13} = G_{31} = \frac{-13P^2\ell^3}{576\pi^2 EI_\eta} + 36K\frac{F_1F_3}{F_4}$$

$$G_{22} = \frac{-P^2\ell^3}{288EI_\eta}\left(3+\frac{2}{\pi^2}\right) + \frac{9\pi^2 C}{2\ell} + \frac{81\pi^4 C_1}{2\ell^3} + 4K\frac{F_2^2}{F_4}$$

$$G_{23} = G_{32} = \frac{-17P^2\ell^3}{256\pi^2 EI_\eta} + 12K\frac{F_2F_3}{F_4}$$

$$G_{33} = \frac{-P^2\ell^3}{EI_\eta}\left(\frac{1}{96}+\frac{1}{400\pi^2}\right) + \frac{25\pi^2 C}{2\ell} + \frac{625\pi^4 C_1}{2\ell^3}$$

$$+ 36K\frac{F_3^2}{F_4} \qquad \ldots(2.39)$$

and K = absolute brace stiffness, as distinct from the relative brace stiffness λ.

$$F_1 = \frac{P\ell^3}{\pi^2}\left(1 - \frac{2}{\pi}\right) + 2EI_\eta h$$

$$F_2 = \frac{P\ell^3}{3\pi^2}\left(1 + \frac{2}{3\pi}\right) + 6EI_\eta h$$

$$F_3 = \frac{P\ell^3}{25\pi^2}\left(1 - \frac{2}{5\pi}\right) + 2EI_\eta h$$

$$F_4 = 3EI_\eta\left(48EI_\eta + K\ell^3\right)$$

The matrix [G] was again noted to be symmetric about the leading diagonal and therefore,

$$G_{21} = G_{12} \quad ; \quad G_{31} = G_{13} \quad ; \quad G_{32} = G_{23}$$

A numerical solution was employed in obtaining the results shown in Table 2.2. Agreement between the numerical results is excellent and consequently it can be deduced that the very small increase in the accuracy of critical loads predicted by the more refined analysis does not justify the considerably more complex algebra involved in the derivation of eqns. (2.39).

Table 2.2: Comparison of Results Obtained from Analyses Employing Two and Three-Term Trigonometric Displacement Functions.

λ	critical stress factor 'c' for beam under centroidal loading, top flange restraint, R^2=4.608	
	Section 2.4 analysis	Section 2.6 analysis
0	1.363	1.363
0.569	2.606	2.611
1.139	3.802	3.813
1.822	5.175	5.202
2.619	6.686	6.795

2.7 Computer Programmes "MODBRACE" and "AUTOBRAC" and Description of Numerical Results

This Section describes the computer programmes "MODBRACE" and "AUTOBRAC" referred to in previous Sections 2.2 to 2.6, and their application to the numerical solution of a large number of combinations of load/restraint geometry for single span beams under uniform bending moment and central point loading.

2.7.1 The Computer Programme "MODBRACE"

As noted in the previous Sections, owing to the complexity of the final homogeneous equations derived from the Rayleigh-Ritz analyses, closed-form solutions for the critical loads were not possible. Consequently, a numerical method for the solution of the eigenvalue problem (as described in Section 2.2) was developed in the form of the interactive computer programme MODBRACE, written in FORTRAN and run on a GEC 4070 computer.

For a given arrangement of loading and restraint, the programme reads in the geometric and material properties of the system. Then, for successively better estimates of the critical applied load, the determinant of the matrix [G] (as defined in previous Sections) is calculated and displayed. The user defines the level of convergence deemed to satisfy the requirement

$$\det [G] = 0,$$

and halts the programme when the required convergence has been achieved. A table of final results is then displayed.

The user starts the search for the zero determinant by entering an initial estimate of the critical load or moment of the system. Although this estimate may be appreciably in error, it is automatically refined by a "search and bisect" strategy:

(i) the user's initial estimate is modified until at least one positive and at least one negative value of the determinant have been found;

(ii) the greatest value of applied load causing a positive determinant is then stored, as is the least value of applied load causing a negative determinant;

(iii) these two values of applied load are then averaged and det[G] calculated on the basis of this improved estimate;

(iv) steps (ii) and (iii) are repeated until the user-defined convergence criteria are satisfied, when the table of final results is displayed.

The above strategy is illustrated in Fig. 2.16 in which P_1 represents the initial critical load estimate provided by the user. As the corresponding determinant, det_1, is positive, the programme increases P to obtain a better estimate P_2, for which the determinant is calculated. As det_2 is also positive, P_3 becomes the next estimate and this gives a negative determinant. P_2 and P_3 are then stored in accordance with step (ii) as these represent the current lower and upper bounds on the actual critical load, P_{cr}. P_4 is the mean of P_2 and P_3 and the corresponding determinant, det_4, is noted to be positive. P_4 then replaces P_2 as the lower bound estimate. The process is repeated for successively better estimates $P_5,\ldots,P_n$ until the determinant is considered to be sufficiently small, at which stage P_n is a very good approximation to the actual critical load.

A listing of the programme is given in Appendix I(a) together with the output from a typical run (Appendix I(b)) showing data input, the selection of the type of analysis, the results of successive evaluations of the determinant and the format of the final results. Commands and values entered by the user are underlined.

In the example shown, an I-section beam is subjected to central point loading and has a single translational restraint at midspan. Load is applied at the top flange (a=24.4255mm) and the restraint is attached at the shear centre of the section (h=0). The axial stiffness of the brace exceeds the lateral bending stiffness of the beam by a factor of 13.664 (ie. λ=13.664). It can be seen that estimates of critical load P_{cr} settle at 1417.257 Newtons after only twenty iterations. However, the determinant corresponding to this twentieth iteration is still unacceptably high and the programme is instructed to continue until the magnitude of the determinant becomes less than 0.01. Consequently, it is noted that refinement of the estimates in the fourth and subsequent decimal places accounts for a change in magnitude of the determinant by a factor of 10^6 in this example. The need for a high degree of precision in evaluating the terms of the matrix [G] is obvious. Therefore, double precision storage of variables is employed throughout the computer programme.

In order to check that the lowest critical load of the system is obtained, the well-known Sturm sequence check is performed. The sequence is formed from the leading diagonal terms of the reduced G matrix after Gaussian elimination, and the number of sign agreements between consecutive terms of the sequence is counted. According to the properties of the sequence, the number of sign agreements is equal to the number of eigenvalues (and hence, in this case, critical loads) smaller than the current estimated value.

The table of final results displayed by the programme shows not only the critical load and critical moment of the system, but also the ratio of the critical load P_{cr} to the critical load P_{nok} of an identical beam with load applied at the shear centre and without lateral restraint. P_{nok} is calculated from the closed-form solution presented by Allen and Bulson[9]:

$$P_{nok} = \frac{16.94}{\ell^2}\sqrt{EI_\eta C\left(1+\frac{\pi^2 C_1}{C\ell^2}\right)} \qquad \ldots(2.40)$$

In addition, the ratio of the critical moment M_{cr} to that of an identical unrestrained beam under uniform moment $(M_{cr})_{UM}$ is shown, $(M_{cr})_{UM}$ being calculated from

$$(M_{cr})_{UM} = \frac{\pi}{\ell}\sqrt{EI_\eta C\left(1+\frac{\pi^2 C_1}{C\ell^2}\right)} \qquad \ldots(2.41)$$

The ratio M_{cr}: $(M_{cr})_{UM}$ is the critical stress factor 'c' introduced in Section 1.2.3 . In view of the fact that uniform moment generally represents the most severe condition of loading on a beam, the critical stress factor is probably the most useful non-dimensional parameter in the comparison of critical loads of dissimilar systems.

The critical moment corresponding to eqn.(2.40) is

$$M_{nok} = \frac{P_{nok}\,\ell}{4}$$

$$\simeq \frac{4.235}{\ell}\sqrt{EI_\eta C\left(1 + \frac{\pi^2 C_1}{C\ell^2}\right)}$$

and hence the theoretical critical stress factor for an unrestrained beam subjected to a central point load applied at its shear centre is

$$c = \frac{M_{nok}}{(M_{cr})_{UM}} = \frac{4.235}{\pi} \simeq 1.35 \qquad \ldots(2.42)$$

2.7.2 The Computer Programme "AUTOBRAC"

The programme AUTOBRAC permits the rapid evaluation of critical combinations of non-dimensional restraint parameters 'λ' and 'e' required for complete midspan restraint of single span beams under uniform bending moment and central point loading. Previous research by Nethercot and Rockey[63] and Mutton and Trahair[64] indicated the benefits accruing from the provision of combined translational and torsional restraint. In order to assess these benefits in the case of simply-supported beams of low to intermediate slenderness, AUTOBRAC was developed from the programme MODBRACE described in the previous Section.

A flow chart for AUTOBRAC is shown in Appendix I(c) and is followed by a listing of the programme. That part of the flow chart bounded by the broken line indicates the logic for the programme MODBRACE. Although the flow chart describes AUTOBRAC in reasonable detail, the latter section dealing with the determination of the critical $\{\lambda, e\}$ combination for complete restraint requires further explanation. In the following, it has been assumed that the value of 'e' is constant throughout the analysis (ie. $\delta e=0$) and that the corresponding value of λ required for a critical $\{\lambda, e\}$ combination is to be determined.

On exit from loop 1 on the flow chart, a series of critical stress factors 'c' and their associated $\{\lambda, e\}$ pairs are stored. These reflect the following relationships:

$\{\lambda_1, e_1\}$	is consistent with first mode buckling at a critical stress factor of	c_1
$\{\lambda_1 + \delta\lambda, e_1\}$	- do. -	c_2
$\{\lambda_1 + 2\delta\lambda, e_1\}$	- do. -	c_3
...		...
$\{\lambda_1 + (n-1)\delta\lambda, e_1\}$	- do. -	c_n

where both c_n and c_{n-1} are greater than the known critical stress factor c_{II} for second mode buckling (determined from a previous MODBRACE run). A least squares polynomial is then fitted through the points $(\lambda_i, c_i)_{i=1,n}$ as shown in Fig. 2.18 . The point of intersection of the polynomial with the line $c=c_{II}$ corresponds to attainment of second mode buckling and the value of λ required for the critical combination can be deduced. The point of intersection is calculated by AUTOBRAC which subsequently displays the calculated values of λ and e.

Appendices I(d) and I(e) show examples of the use of AUTOBRAC. In the former, 'e' is set equal to zero for the duration of the analysis whilst $\lambda_1=0.1$ and $\delta\lambda=1.5$. A previous analysis by MODBRACE had shown that the critical stress factor for second mode buckling of the beam was $c_{II}=1.329$. AUTOBRAC continues to increment λ until the values c=1.3347 and c=1.3486, both greater than the required c=1.329, have been obtained. The search for two values of c above the second mode critical value ensures that the behaviour of the approximating polynomial for $c > c_{II}$ remains accurate and therefore that the point of intersection can be determined with accuracy. In this case, AUTOBRAC predicts a critical combination of $\{\lambda, e\}_{cr} = \{13.593, 0\}$.

The same problem is analysed in Appendix I(e) except that e=0.5 is used throughout the analysis. As before, $c_{II}=1.329$ and a critical restraint combination $\{\lambda, e\}_{cr} = \{8.579, 0.5\}$ is predicted. The inclusion of the small torsional restraint e=0.5 reduces the translational stiffness requirement from $\lambda=13.593$ to $\lambda=8.579$. The provision of torsional restraint therefore proves beneficial, as previously noted by Nethercot and Rockey[63] and Mutton and Trahair[64].

2.7.3 Numerical Results Arising from the Analyses Presented in Sections 2.2 to 2.6

As demonstrated in Figs. 2.9 and 2.15, the number of possible combinations of the variables employed in the previous analyses is very large. Therefore, in reporting the results of such an investigation, it is essential that a non-dimensional form of presentation be employed in order to make the results more generally applicable. Here, Nethercot and Rockey's[63] shape parameter 'R' (eqn. (1.4)) and the critical stress factor 'c' (Sections 1.2.3 and 2.7.2) are employed.

In order to verify that the calculated critical loads obtained from the previous analyses were dependent solely on the value of R^2 and not on other cross-sectional properties, the critical loads of two beams of grossly different size (Fig. 2.17), but with the same value of R^2, were obtained for a series of values of λ. The non-dimensional results shown in Table 2.3 display only very slight differences and consequently the graphical presentation of numerical results based on the parameter 'R' is justified.

Table 2.3: Variation of the Ratio P_{cr}/P_{nok} with λ for the Beams of Fig. 2.17 (R constant).

λ	P_{cr}/P_{nok} for R^2 = 25.342, h = 0	
	Beam 1 (Fig. 2.17)	Beam 2
0	1.0094	1.0097
2.8895	1.9015	1.9033
6.5014	2.4994	2.5042
11.558	3.0096	3.0198
18.059	3.4110	3.4288
24.560	3.6668	3.6934

The results of several analyses of beams subjected to uniform moment and laterally restrained at midspan are shown in Fig. 2.19 .

Figs. 2.20 to 2.23 show corresponding graphs for beams under central point loading. Six values of the R^2 parameter have been considered throughout. In Figs. 2.19 to 2.23 only the effects of translational restraint stiffness have been considered as this is generally the sole criterion in the design of bracing systems. Consequently, e=0 in each of these figures.

As can be seen from the graphs, the analyses of Sections 2.3 and 2.5 provide plateaux which indicate the maximum load-carrying capacity of the beams as governed by second mode elastic buckling. It can also be observed that, in some cases, the elastic critical load corresponding to second mode buckling cannot be attained, irrespective of the degree of lateral restraint supplied at midspan. This is particularly true in cases where the level of attachment of the restraint is below the level of load application (Figs. 2.21 and 2.22). In each of the figures, the criteria for adequate compression flange restraint are seen to be less onerous than for shear centre restraint. In no case could complete restraint be achieved by tension flange bracing, although this produced significant increases in the first mode critical loads of beams under central point loading with load applied at the tension flange (Fig. 2.23).

Numerical results based on the more refined analysis of Section 2.6 are indistinguishable from those used to produce the middle curve in Fig. 2.20 . Table 2.2 shows results obtained by the analyses of Sections 2.4 and 2.6 for the case of a beam under central point loading and with R^2=4.608. The differences between the results are seen to be negligible. Indeed, on the basis that the energy solution generally overestimates the critical load, the results obtained from the simpler analysis of Section 2.4 are to be preferred. Certainly, the slight differences between the results do not justify the greatly increased complexity of the more refined analysis.

In Fig. 2.20, the curve representing the case of a central point load applied at the shear centre of the beam is seen to indicate a critical stress factor of approximately 1.36, which agrees well with the value of 1.35 in eqn. (2.42) obtained from closed-form solutions.

Figs. 2.24 to 2.27 show the critical combinations of λ and e values required for the enforcement of second mode elastic buckling in single span beams. The case of uniform applied bending moment is dealt with in Fig. 2.24 and central point loading cases in Figs. 2.25 to 2.27. In Fig. 2.24, curves are shown for the six values of R^2 considered in Figs. 2.19 to 2.23 and for compression flange, shear centre and tension flange restraint. Allowance for the level of load application is made in Figs. 2.25 to 2.27.

The figures confirm the greater efficiency of bracing attached to the compression flange than to the shear centre or tension flange. In addition, tension flange bracing must possess high rotational and translational stiffness in order to provide complete restraint to the primary member. In agreement with the trend observed by Hartmann[16], Nethercot and Rockey[63], Taylor and Ojalvo[60] and Mutton and Trahair[64], stocky beams (ie, those of low R) require more substantial systems of bracing than slender beams for attainment of second mode critical loads. However, as illustrated in Figs. 2.19 to 2.23, the second mode critical loads are not the same for beams of unequal R. Hence, the curves shown in Figs. 2.24 to 2.27 do not relate to a single value of 'c' but rather to a different value for each value of R. Thus, although stocky beams require greater restraint, their second mode critical loads are correspondingly greater than those of slender beams.

Discussion of these results in relation to those of previous research and to finite element and experimental results obtained in the present study is presented in Chapter 8.

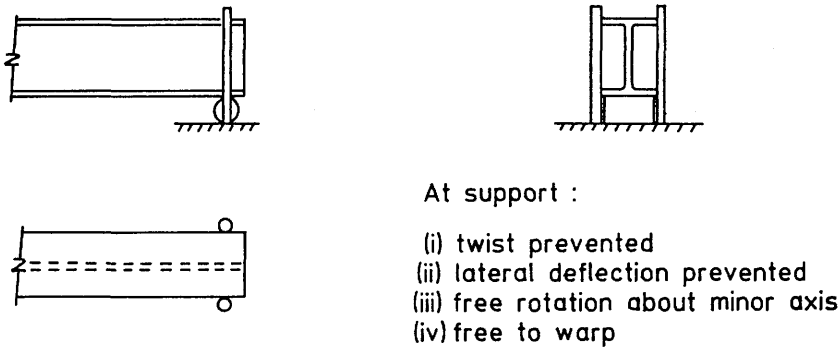

Fig. 2.1 : "Simply-supported" end conditions with respect to lateral bending, warping and twist.

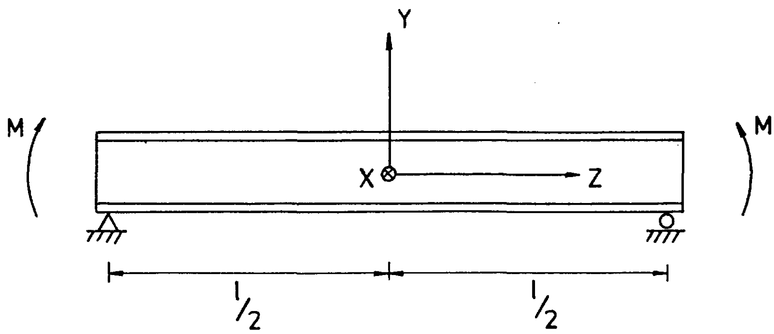

Fig. 2.2 : Beam under uniform moment showing origin and orientation of the X, Y, Z axes

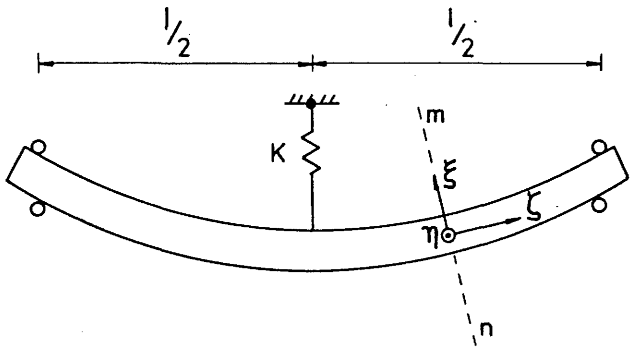

Fig. 2.3 : Plan view of beam showing orientation of local coordinate system and location of the lateral restraint of stiffness K. (The torsional restraint at midspan is not shown in this view.)

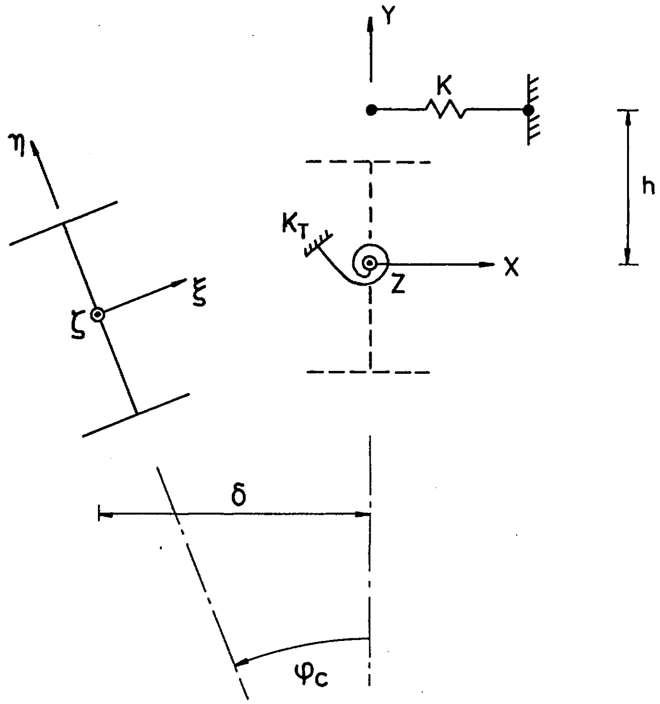

Fig. 2.4 : The undisturbed and disturbed locations of the midspan cross-section of the beam showing the torsional restraint (K_T) and the level of attachment of the translational brace (K) relative to the shear centre of the section.

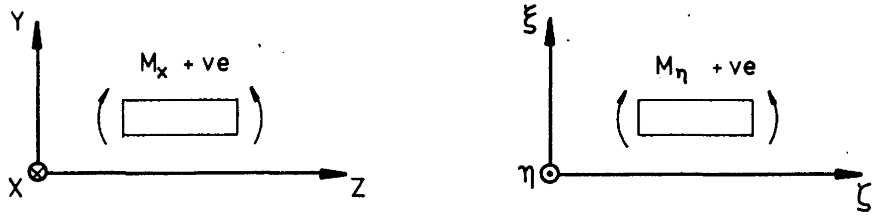

Fig. 2.5 : Sign conventions for bending moments in the Y-Z and ζ-ξ planes

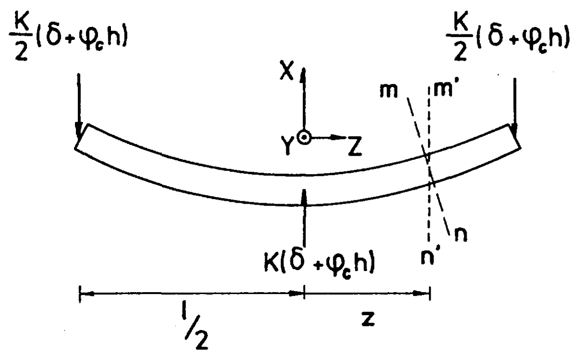

(a) Brace force and reactions in the disturbed position in plan view

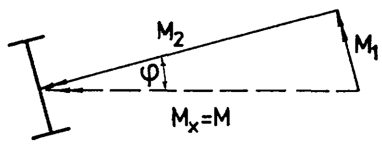

(b) In-plane moment M_x resolved into components M_1 and M_2 in the m'-n' plane (view in the -ve Z direction)

Fig. 2.6 : Plan view of disturbed configuration of beam and the resolution of in-plane moment M_x

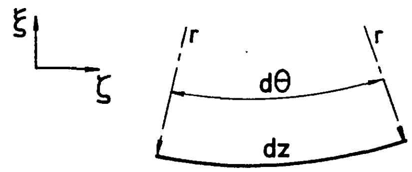

Fig. 2.7 : The angle dθ subtended by an element dz in the ζ-ξ plane. The radius of curvature is 'r'.

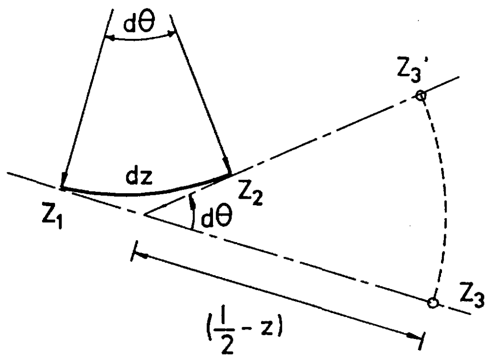

Fig. 2.8 : Displacement of the end of a beam attributable to the curvature (u") of infinitesimal element dz

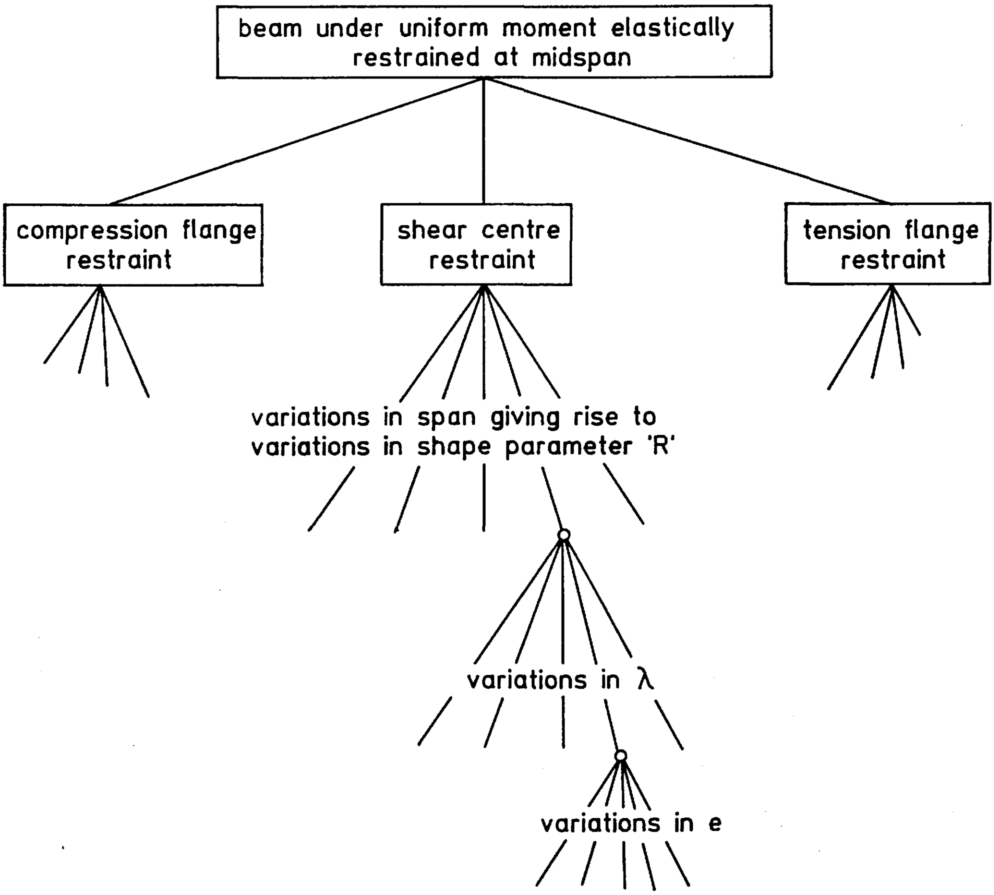

Fig. 2.9 : Combinations of variables for analysis considered in Section 2.2

		uniform moment	central point load
1^{st} mode	B.M.D. buckling mode	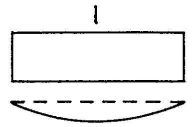	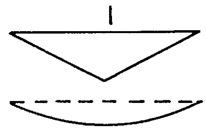
2^{nd} mode	B.M.D. buckling mode	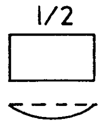	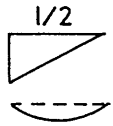
	notes	2^{nd} mode (BMD + buckling mode) pair for the half span corresponds to 1^{st} mode pair for the whole span	mismatch between the 2^{nd} mode BMD for the half span and the 1^{st} mode BMD for the whole span

Fig. 2.10 : Differences between 1^{st} and 2^{nd} mode buckling analyses in the cases of uniform moment and central point loading

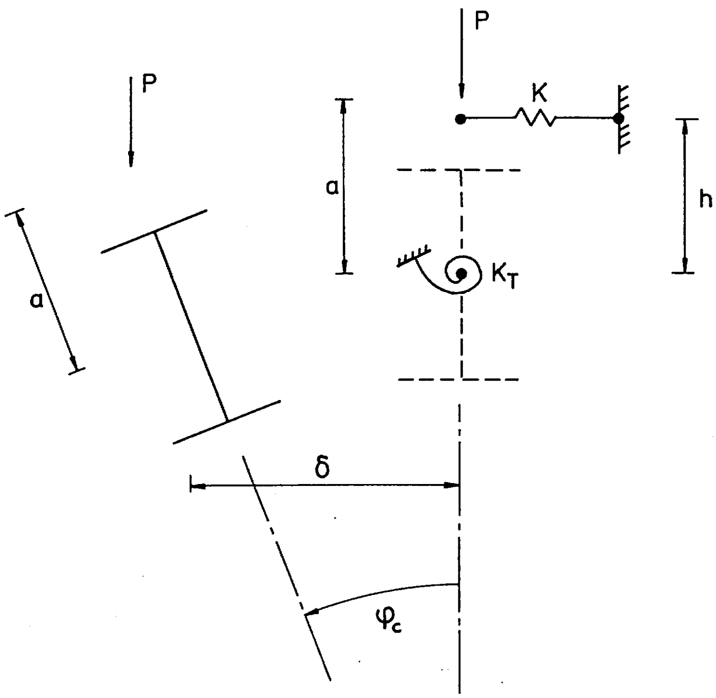

Fig. 2.11 : Variable levels of load application and translational restraint attachment in the case of a beam under central point loading

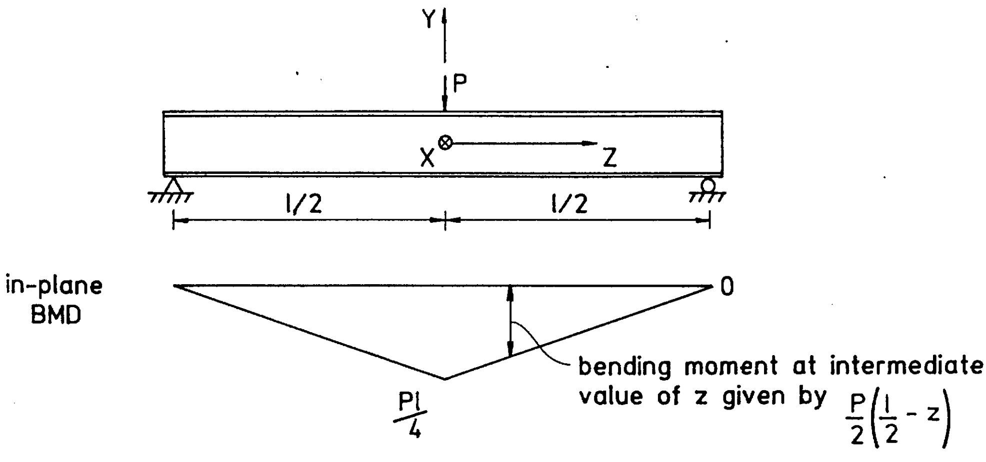

Fig. 2.12 : Beam under central point loading and the associated distribution of in-plane bending moment

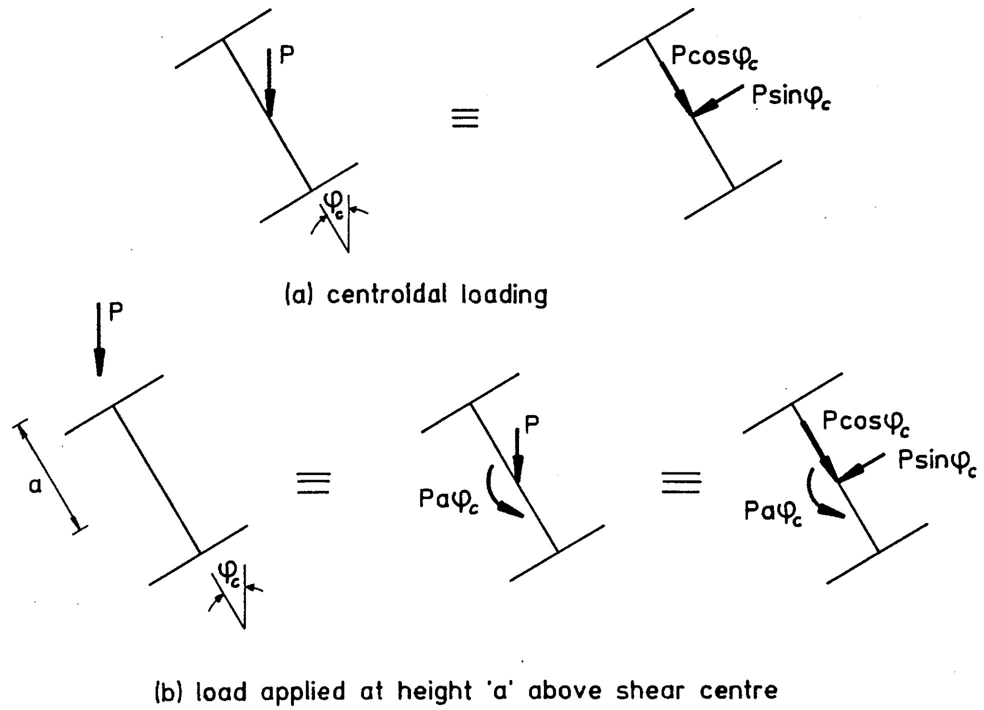

Fig. 2.13 : Comparison between the actions of a point load applied at the shear centre and at height 'a'

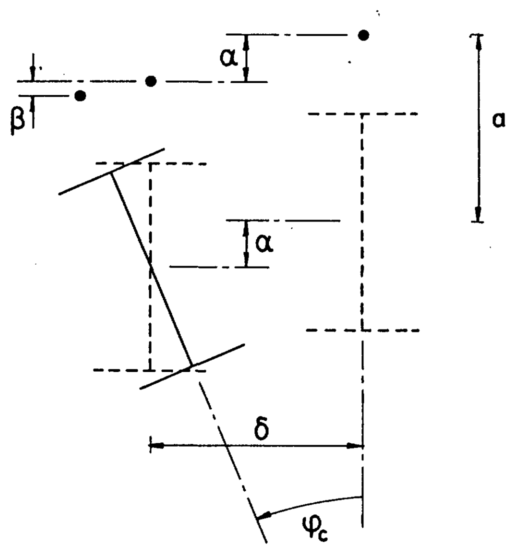

Fig. 2.14 : The vertical deflection $(\alpha+\beta)$ of the point of load application when load is applied above the shear centre

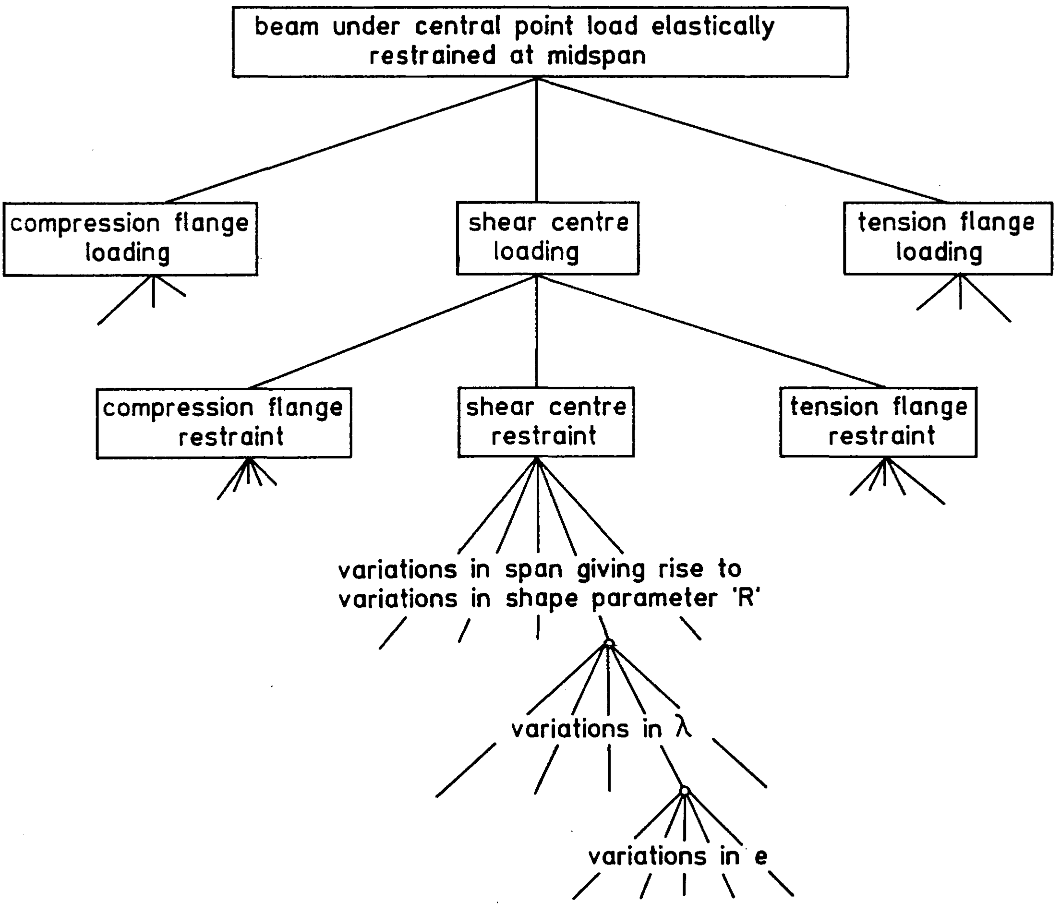

Fig. 2.15 : Combinations of variables for the analysis considered in Section 2.4.

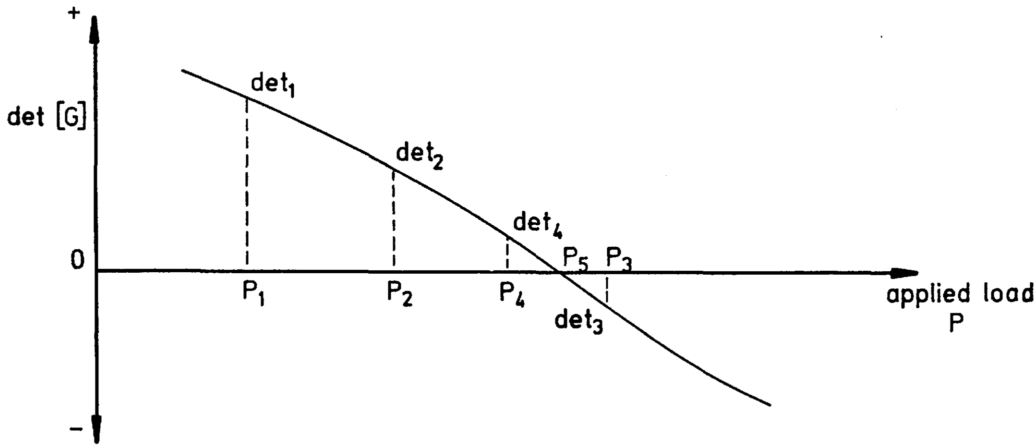

Fig. 2.16 : The "search and bisect" strategy adopted in programmes MODBRACE and AUTOBRAC

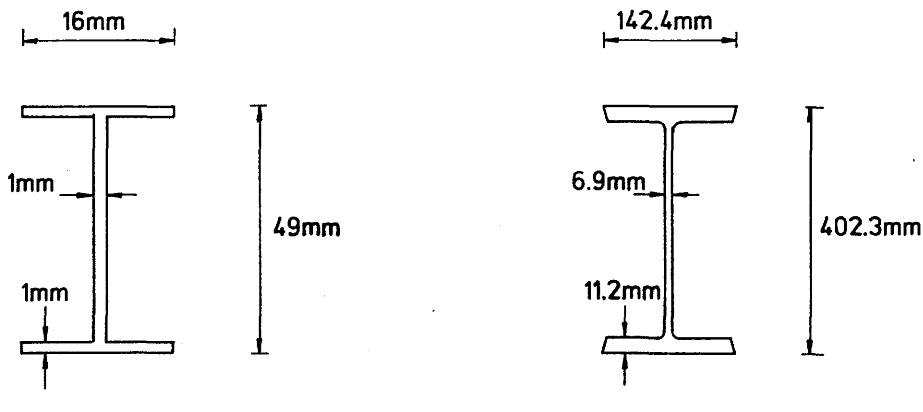

beam 1

beam 2
(406x140x46 UB)

Fig. 2.17 : Beams used to verify the sole dependence of elastic critical load on the shape parameter R

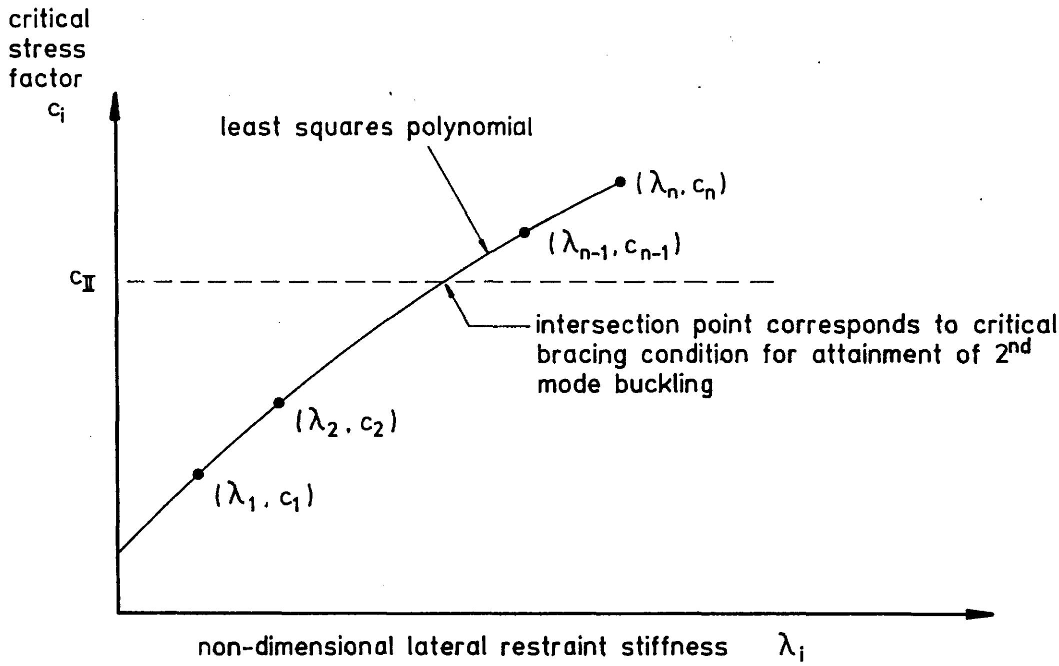

Fig. 2.18 : Determination of critical value of λ for second mode buckling by calculation of point of intersection of $c=c_{II}$ line and (λ, c) curve

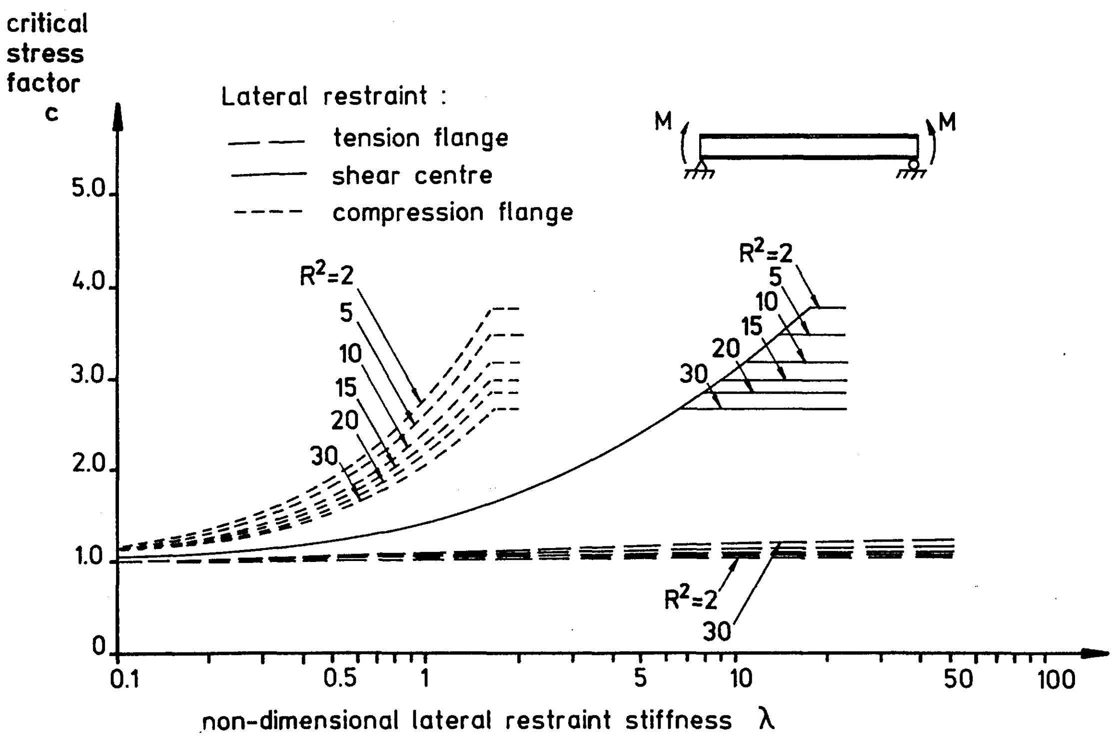

Fig. 2.19 : c-λ curves for beams under uniform moment loading and with varying R values and levels of lateral restraint

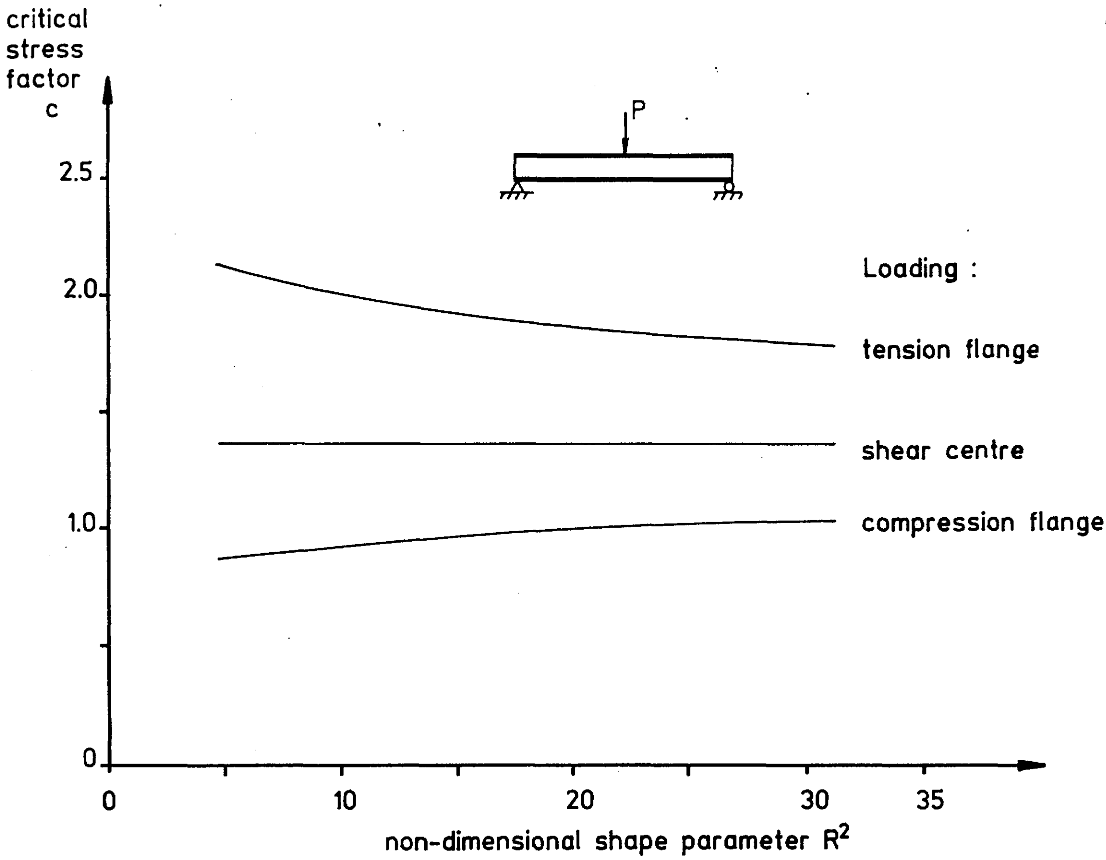

Fig. 2.20 : Elastic critical loads of beams under central point loading and without intermediate restraint

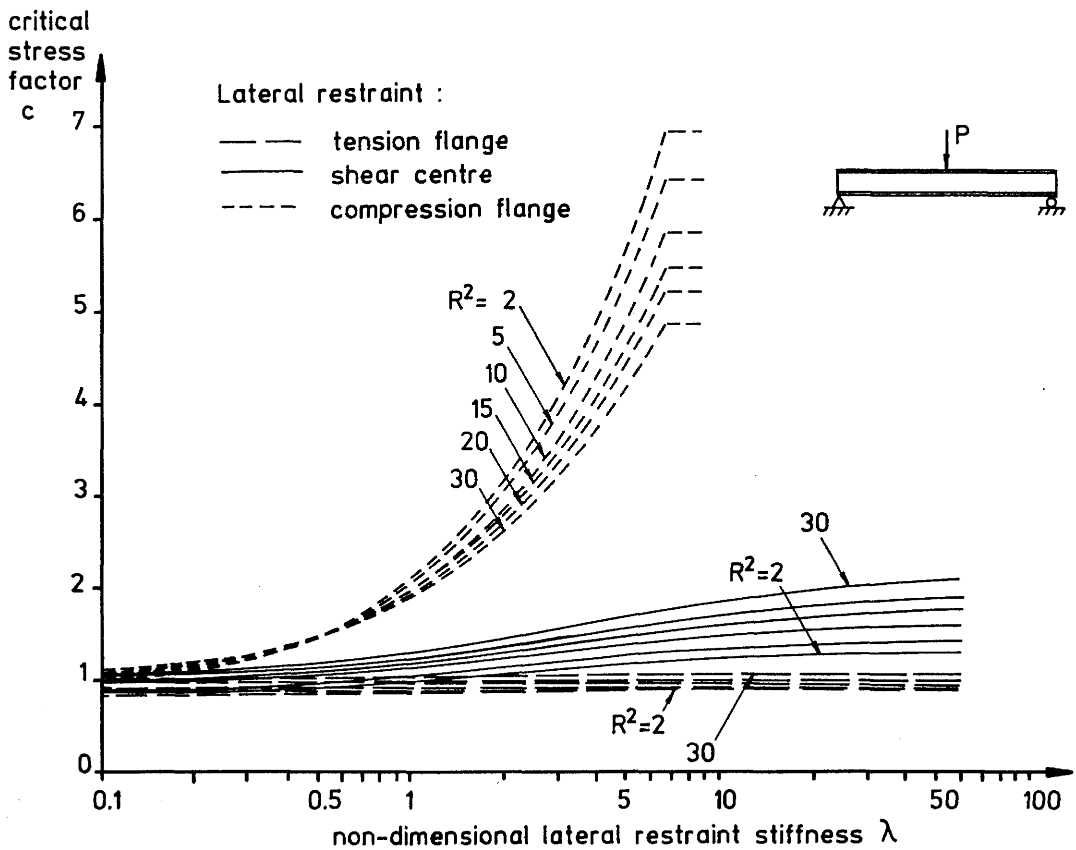

Fig. 2.21 : c-λ curves for beams under central point loading at compression flange level

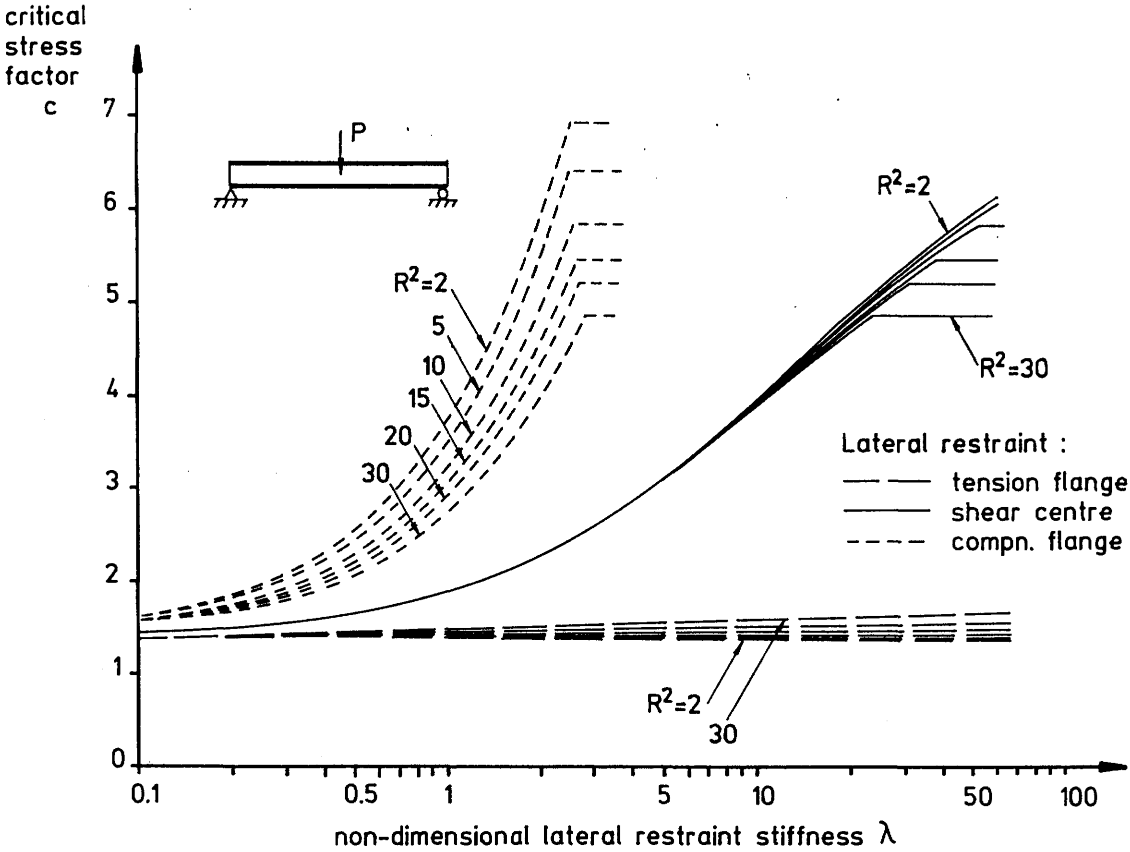

Fig. 2.22 : c-λ curves for beams under central point loading at shear centre level

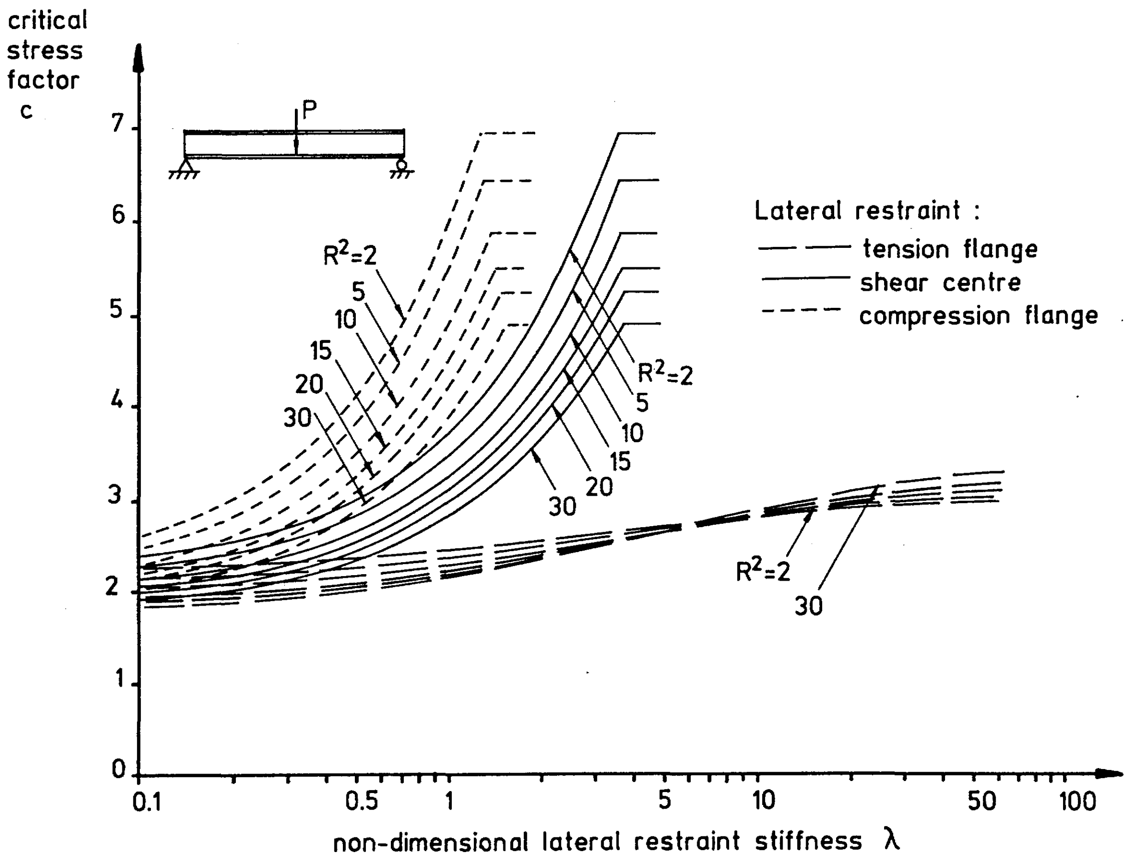

Fig. 2.23 : c-λ curves for beams under central point loading at tension flange level

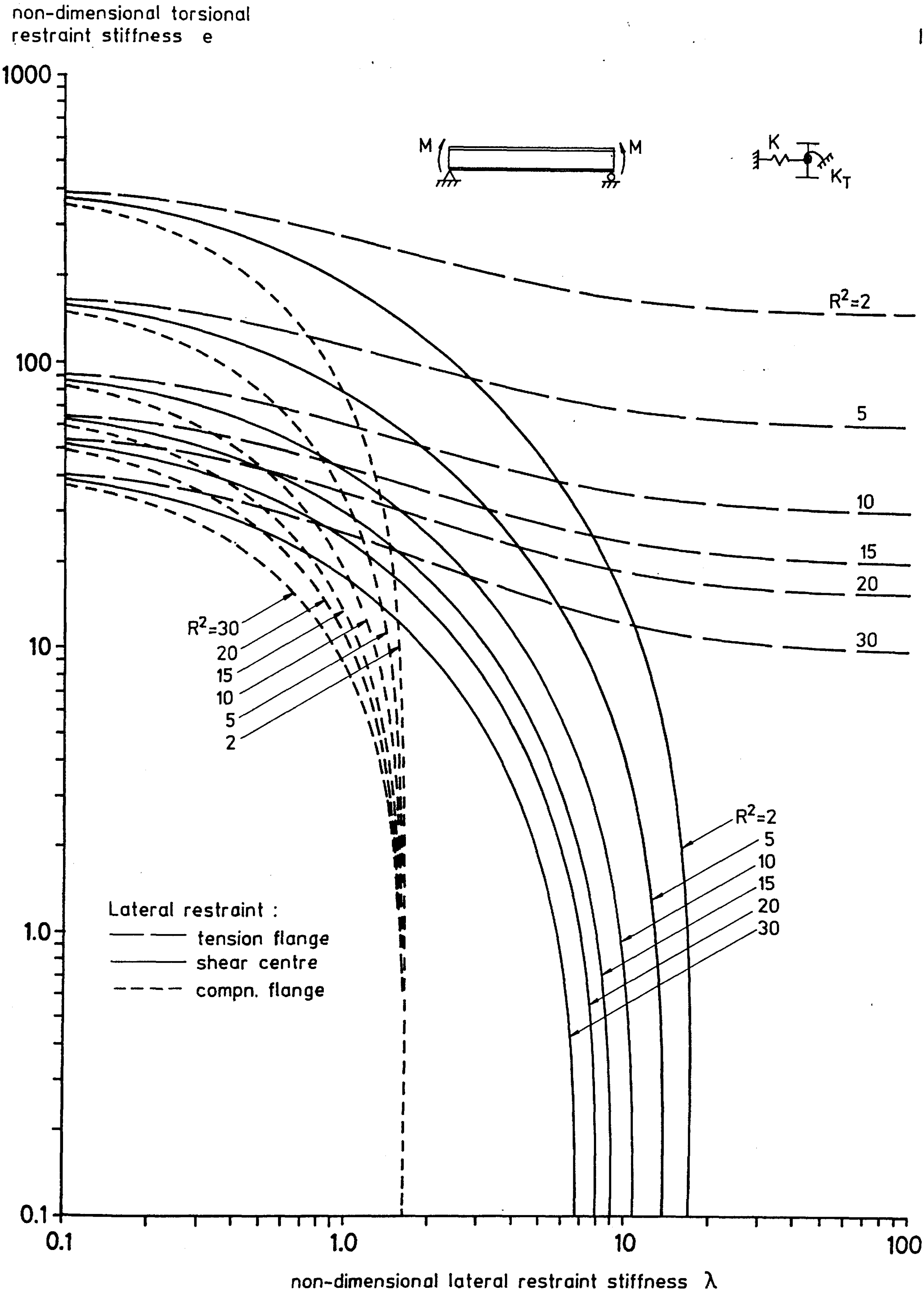

Fig. 2.24 : e-λ interaction curves for fully effective restraint of beams under uniform moment loading

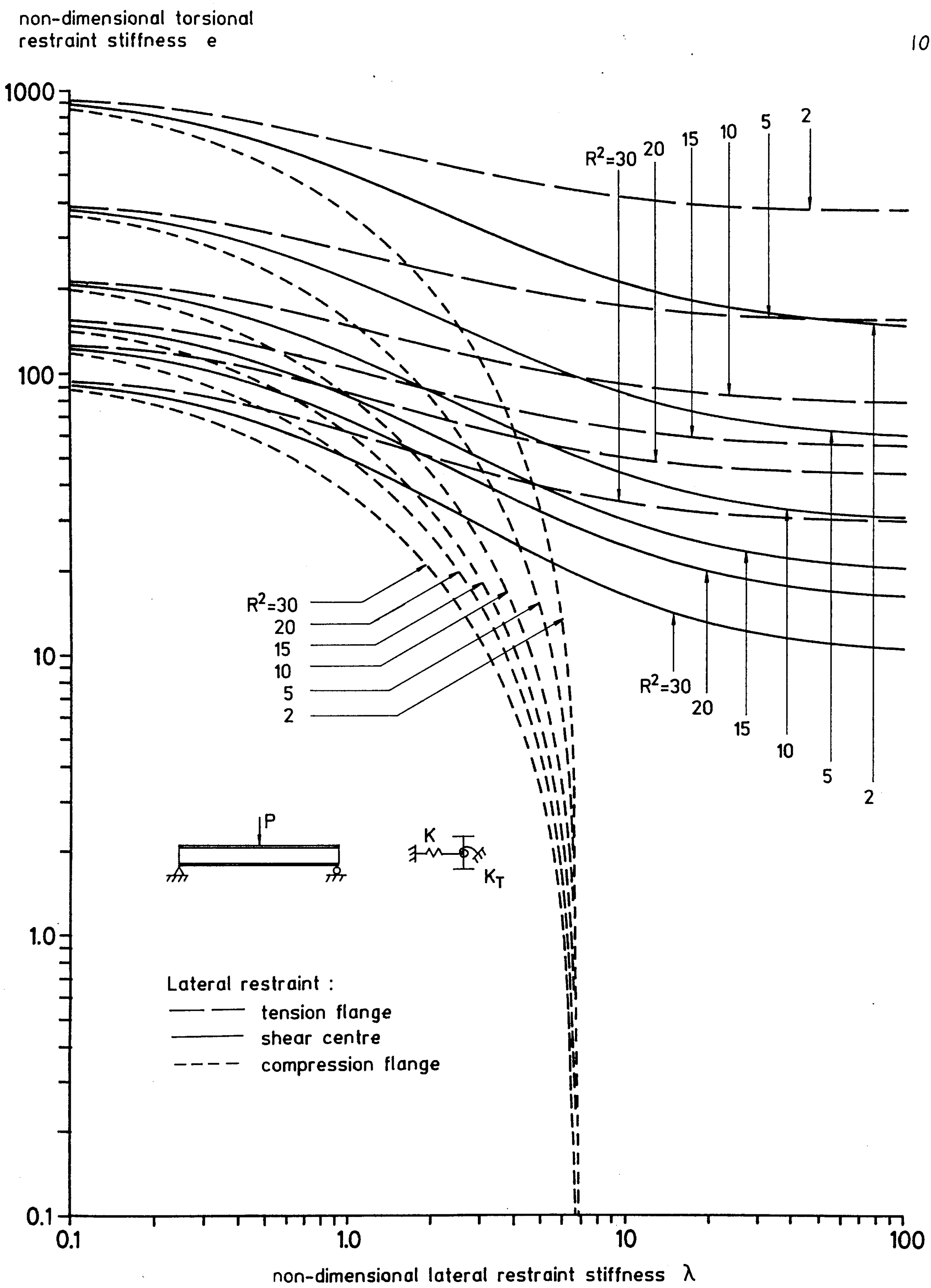

Fig. 2.25 : e-λ interaction curves for fully effective restraint of beams under central point loading at compression flange level

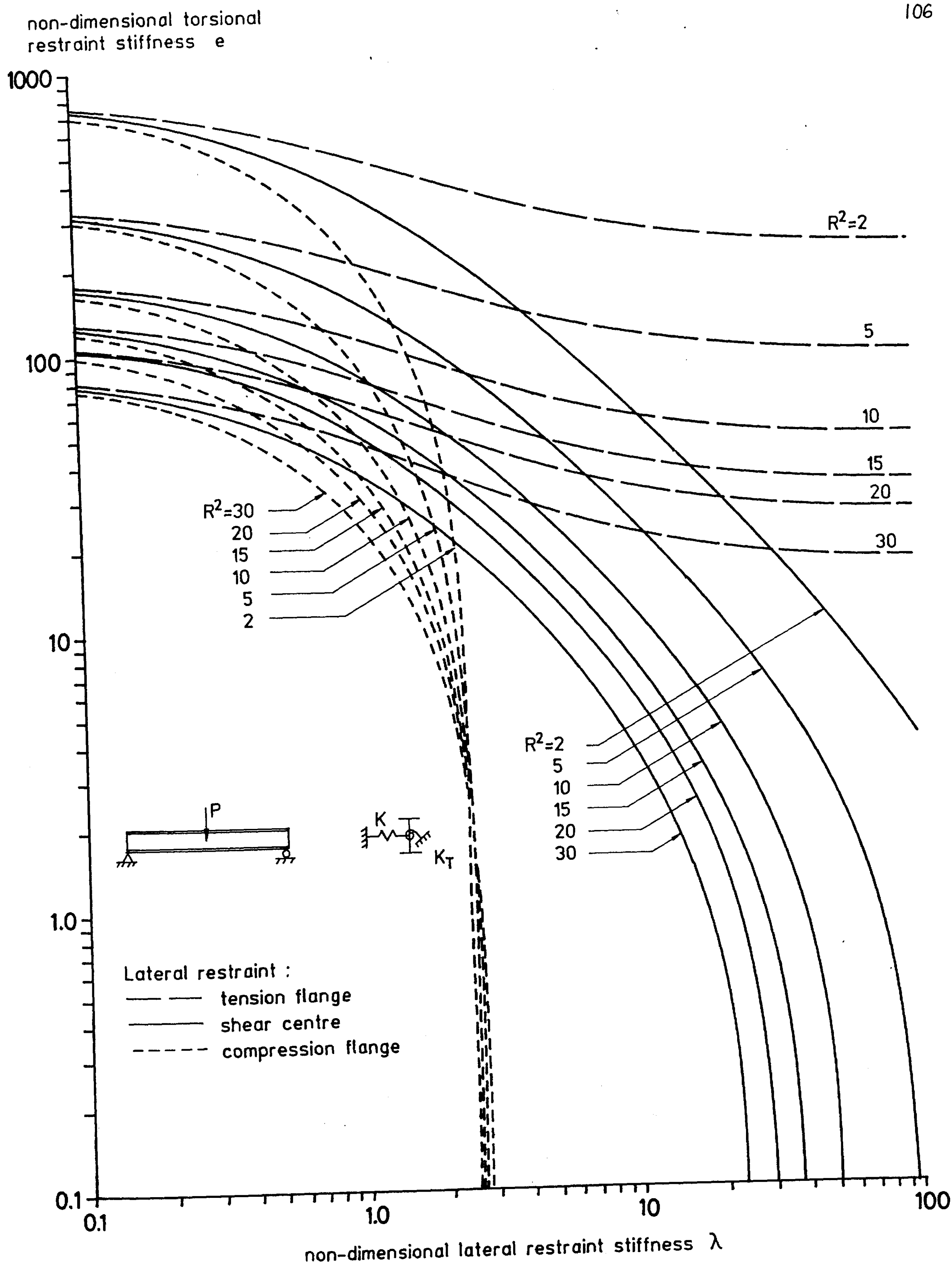

Fig. 2.26 : e-λ interaction curves for fully effective restraint of beams under central point loading at shear centre level

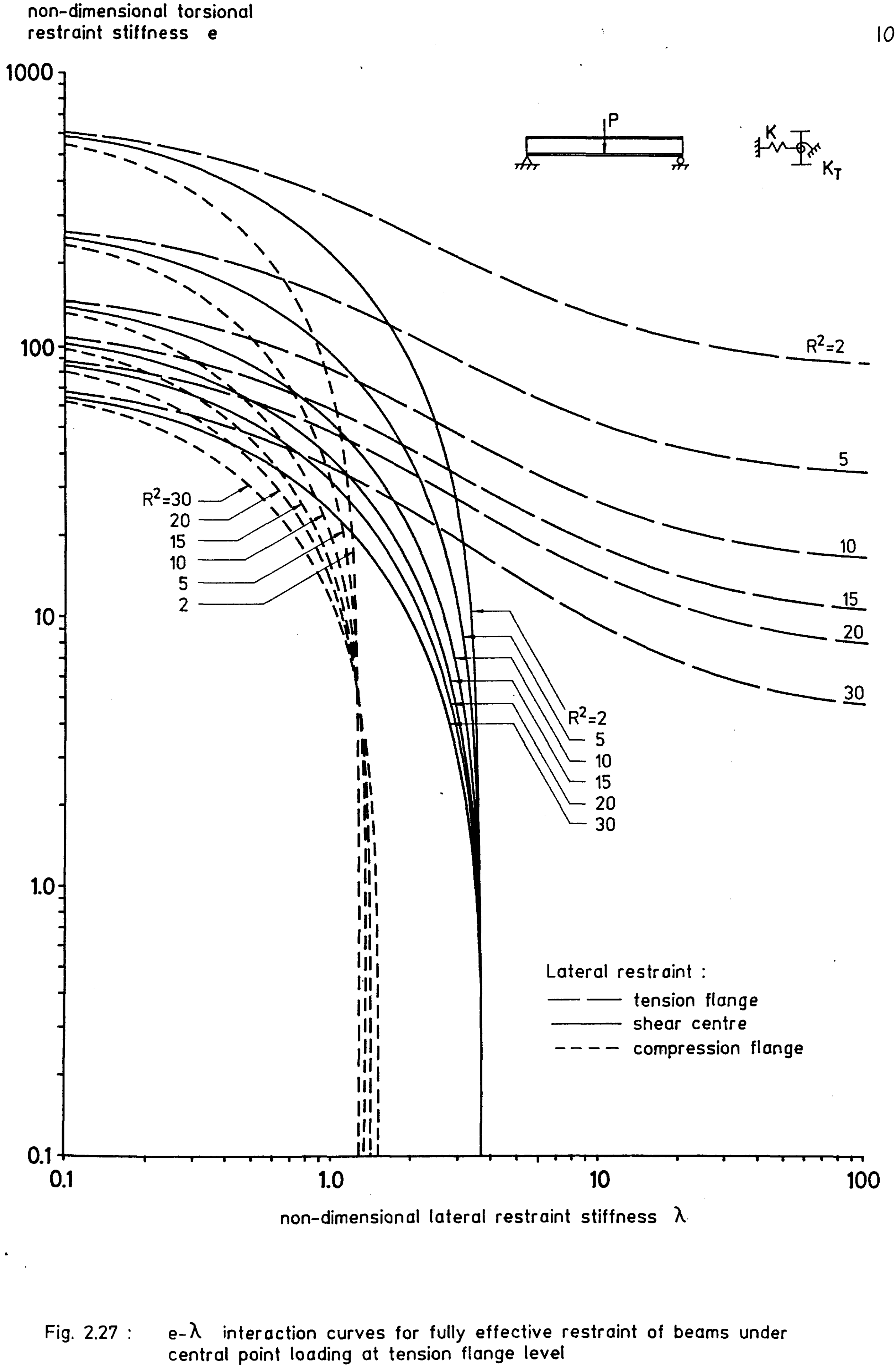

Fig. 2.27 : e-λ interaction curves for fully effective restraint of beams under central point loading at tension flange level

CHAPTER 3

FINITE ELEMENT ANALYSIS

CHAPTER 3

FINITE ELEMENT ANALYSIS

In this Chapter, reasons for the adoption of a coupled non-linear (ie. simultaneously geometrically and materially non-linear) analysis in the present study are presented; the selection of a finite element programme capable of performing the coupled non-linear analysis is then discussed; and finally, details of the computer programme written to perform finite element mesh generation for the initially imperfect test beams are then presented.

3.1 Differences Between Classical Buckling and Instability Analyses

Notwithstanding the recent adoption of limit state philosophy for the design of structural steelwork[55,56], small deflection, linear elastic theory still provides the analytical techniques by which internal forces in the vast majority of building and bridge structures are determined. The validity of this approach is dependent on the magnitude of displacements being small in relation to the overall structural dimensions. This circumstance justifies the use of equilibrium equations which are strictly only applicable to the geometry of the undeformed structure. Moreover, the principle of superposition applied to the results of such analyses offers considerable analytical benefits. In the past, sufficiently numerous and attractive have been the advantages of this elastic, small deflection approach to merit consideration of the application of its fundamental principles to problems of buckling.

Roberts and Jhita[83] have identified three elastic buckling modes for I-section beams:

(a) local buckling, in which changes in cross-sectional geometry occur in the absence of overall lateral displacement and twisting of the beam,

(b) lateral-torsional buckling, in which lateral deflections and twist occur without local changes in cross-sectional geometry, and

(c) distortional buckling, which combines lateral displacement, twist and cross-sectional deformations.

In terms of the above classification, the analyses of Chapter 2 fall into the lateral-torsional buckling category whilst the finite element study of Nethercot and Rockey[63], which makes allowance for cross-sectional deformations, is classified as distortional buckling. Throughout the present study, only lateral-torsional buckling is considered as it is assumed that local buckling can be prevented by adherence to relevant flange outstand, web slenderness and web stiffening requirements specified in the appropriate design documents[33,55,56,70].

First order buckling analysis may correctly be used to predict the load at which a structure becomes unstable if pre-buckling displacements and the resulting second order effects are negligible. Its use as a basis for the design of slender, laterally unsupported beams has been justified experimentally[30].

Mathematically, buckling occurs when two infinitesimally close equilibrium configurations are both possible. As noted in Chapter 2, the buckling analysis of initially perfect beams under simple conditions of loading may be performed longhand by solutions based either on the differential equations of equilibrium or on the energy theorems employed in that Chapter. However, recourse must be made to numerical solutions of the eigenvalue problem in more complex cases. Finite element formulation of this eigenvalue problem can be expressed by the equation

$$\left([K] + \rho\,[K_\sigma]\right)\{\Delta\} = \{0\} \qquad \ldots(3.1)$$

in which $[K]$ = conventional structural stiffness matrix based on elastic small deflection theory.

ρ = load factor.

$[K_\sigma]$ = structural stability (or geometric stiffness) matrix which accounts for the stiffening or weakening effect of the forces determined by an initial elastic analysis.

$\{\Delta\}$ = vector of structure nodal displacements corresponding to the difference between two equilibrium configurations.

The smallest value of ρ which provides a zero determinant of the total global stiffness ($[K] + \rho [K_\sigma]$) and hence a non-trivial solution of eqn. (3.1) defines the first critical load of the system. The eigenvector $\{\Delta\}$ describes the corresponding mode shape of buckling.

Although of use in the calculation of critical loads of unrestrained and restrained beams, this bifurcation approach has disadvantages arising from non-uniqueness of the load-displacement behaviour at attainment of the buckling or critical load. As only mode shapes of buckling (in the form of eigenvectors) rather than absolute buckling displacements are available, beam deflections at points of restraint attachment are indeterminate. Consequently, as bracing forces are also indeterminate, a more refined analysis capable of predicting absolute buckling deformations must be employed in studies concerned with the strength requirements of bracing.

The introducton of an initial imperfection into the geometry of the braced member affords the opportunity to calculate both lateral deflections and bracing forces based on small deflection theory. The nature of such a solution has been indicated by Trahair and Nethercot[68].

While the field of applicability of the linear elastic, small deflection theory is extensive, use of this method in the case of beams in bending is only valid where in-plane and lateral displacements represent a small fraction of the overall cross-sectional dimensions. For larger displacements, non-linear effects become more pronounced and accuracy of the infinitesimal theory progressively worsens. Whereas small deflection theory permits equilibrium equations to be written for the geometry of the undeformed structure, consideration of the effects of geometrical non-linearity demands that the equations are written with respect to the deformed geometry, which is not known in advance.

Although some degree of non-linearity occurs in most practical structures due to the presence of some or all of the imperfections described in Section 1.2.2, the severity of non-linear behaviour varies widely. In the case of the lateral-torsional stability of real, imperfect beams, non-linearity is frequently aggravated by the occurrence of yielding as, in practice, few beams are of sufficiently large span to confine their loading response to the wholly elastic behaviour exhibited by beams of very high slenderness.

It is necessary to differentiate between the mathematically idealised phenomenon of buckling and the collapse condition attained by real beams. The former represents the bifurcation analysis previously described whereas collapse, in the presence of non-linear behaviour, is similarly attributable to vanishing structural stiffness, but without bifurcation of the equilibrium paths. In cases of beam instability, progressive softening of the structure leads to development of a neutral equilibrium or collapse condition at a load considerably lower than the first order buckling prediction of the infinitesimal theory.

In the present study, the non-linear analysis capabilities of the two finite element programmes NASTRAN and FINAS were employed to compute the ultimate rather than the buckling loads of beam/restraint systems used in the experimental investigation.

3.2 Non-Linear Finite Element Solutions

The well-proven linear elastic analysis techniques of the finite element method[84-86] can be used as the basis for analyses involving both material and geometrical non-linearities. A review of two typical methods employed in non-linear analysis is presented for completeness in this Section; no attempt has been made to describe the solution strategies developed and commonly adopted to minimise computing time. Moreover, detailed derivations of the fundamental equations employed in these solutions are not incorporated in such a brief review.

In Sections 3.2.1 and 3.2.2 which follow, it is assumed that linear or first order elastic strain-displacement equations are valid viz. for a three-dimensional state of strain[86]:

$$\begin{Bmatrix} \epsilon_x \\ \epsilon_y \\ \epsilon_z \\ \gamma_{xy} \\ \gamma_{yz} \\ \gamma_{zx} \end{Bmatrix} = \begin{Bmatrix} \partial u/\partial x \\ \partial v/\partial y \\ \partial w/\partial z \\ \partial v/\partial x + \partial u/\partial y \\ \partial w/\partial y + \partial v/\partial z \\ \partial u/\partial z + \partial w/\partial x \end{Bmatrix} \qquad \ldots(3.2)$$

Eqn. (3.2) relates direct strains ϵ_x, ϵ_y, ϵ_z and shear strains γ_{xy}, γ_{yz}, γ_{zx} to the translational degrees of freedom u, v, w in coordinate directions x, y, z. In conventional finite element notation[84], eqn. (3.2) is expressed in terms of the strain matrix [B] in the vector equation

$$\{\epsilon^e\} = [B]\,\{\Delta^e\} \qquad \ldots(3.3)$$

where $\{\epsilon^e\}$ is the element strain vector and $\{\Delta^e\}$ the vector of element nodal displacements.

In addition, the constitutive law

$$\{\sigma^e\} = [E]\left(\{\epsilon^e\} - \{\epsilon_o^e\}\right) + \{\sigma_o^e\} \qquad \ldots(3.4)$$

in which $\{\sigma^e\}$ = vector of element stresses
$[E]$ = elasticity matrix
$\{\epsilon_o^e\}$ = vector of initial element strains and
$\{\sigma_o^e\}$ = vector of initial element stesses
is used to relate element stress to strain under linear elastic conditions.

Considering inelastic effects in an assumed isotropic, non-strain hardening material, the von Mises yield criterion

$$(\sigma_x - \sigma_y)^2 + (\sigma_y - \sigma_z)^2 + (\sigma_z - \sigma_x)^2$$

$$+ 6\left(\tau_{xy}^2 + \tau_{yz}^2 + \tau_{zx}^2\right) - \frac{2}{3}\sigma_{yt}^2 = 0 \qquad \ldots(3.5)$$

is frequently employed, in which direct stresses σ_x, σ_y, σ_z and shear stresses τ_{xy}, τ_{yz}, τ_{zx} are related to the uniaxial tensile yield stress σ_{yt}. The von Mises criterion has been shown to be of particular value in predicting the onset of plasticity in steels[86,87].

An associated flow rule (ie. based on the von Mises criterion) is used to derive the Prandtl-Reuss equations[85] which subsequently permit small but finite inelastic stress changes $d\{\sigma\}$ to be related to small increments of strain $d\{\epsilon\}$ via an instantaneous elastic-plastic stress-strain matrix $[E_{ep}]$[85,86]:

$$d\{\sigma\} = [E_{ep}]\, d\{\epsilon\} \qquad \ldots(3.6)$$

Reference to foregoing eqns. (3.2) to (3.6) will be made in Sections 3.2.1 and 3.2.2 when considering common solution techniques employed in materially and geometrically non-linear analysis.

3.2.1 Materially Non-Linear Analysis

In small strain, linear elastic problems the well-known stiffness relationship

$$[K]\{\Delta\} = \{Q\} \qquad \ldots(3.7)$$

is generally employed in finite element analysis. In this equation [K] is as defined in eqn. (3.1) whilst $\{Q\}$ represents a vector of structure nodal forces and $\{\Delta\}$ the vector of corresponding nodal displacements. As well as including all externally applied loads on the structure, vector $\{Q\}$ accounts for nodal forces arising from internal, initial stresses $\{\sigma_o\}$ and strains $\{\epsilon_o\}$.

In linear elastic analysis, the constitutive law of eqn. (3.4) and the strain-displacement relationship of (3.3) are employed and, in addition, displacement continuity and equilibrium requirements must be satisfied. It has been found[84,85] that the small strain-displacement relationship often proves satisfactory even in cases where a non-linear constitutive law applies. In these circumstances, there is still a need for continuity of displacements and statical equilibrium. Consequently, only the linear constitutive law of eqn. (3.4) need be altered to make allowance for material non-linearity. Zienkiewicz[84] proposes that, as the non-linear constitutive relation will be some linear function 'f' linking $\{\sigma^e\}$ and $\{\epsilon^e\}$ eg.

$$\{\sigma^e\} = f\left(\{\epsilon^e\}\right) \qquad \ldots(3.8)$$

then a solution of the materially non-linear problem can be found by suitable adjustment of one of [E], $\{\epsilon_o^e\}$ or $\{\sigma_o^e\}$ in eqn. (3.4).

An "initial stress" approach, in which modifications are made to the initial stress vector $\{\sigma_o^e\}$, is advocated for materials which soften under increasing strain: structural steels conform to this description. For a given strain, the corresponding stress in structural steel can be uniquely determined. This is evident from examination of the commonly assumed elastic-perfect plastic characteristic shown in Fig. 1.7 . The "initial strain" approach, based on $\{\epsilon_o^e\}$ is suitable for materials which exhibit considerable hardening whilst the "variable stiffness" approach, in which matrix [E] is modified on each iterative step in the numerical solution, is extremely expensive in computing time.

In both materially and geometrically non-linear analysis, a combined incremental-iterative procedure is generally adopted in which loads (or prescribed displacements) are applied in increments until the desired load, total displacement or collapse condition is attained. Within each increment an iterative procedure is employed until equilibrium requirements are satisfied within the bounds of a previously defined convergence criterion. The strategy is best described by the following steps:

(a) The first increment of applied load $\{Q_1\}$ is applied and corresponding elastic displacements $\{\Delta_1\}$ calculated using the initial linear elastic stiffness matrix $[K_0]$:

$$\{\Delta_1\} = [K_o]^{-1}\{Q_1\} \qquad \ldots(3.9)$$

(b) Eqn. (3.3) is then employed to calculate element strains from element nodal displacements.

(c) True or actual stresses corresponding to these strains are calculated using the yield criterion and, in particular, eqn. (3.6).

(d) Setting $\{\sigma^e\}$ in eqn. (3.4) equal to the vector of true stresses from (c), that value of $\{\sigma_o^e\}$ satisfying the equation represents the new initial stress vector. $\{\sigma_o^e\}$ can therefore be regarded as the level of initial stress required to bring the predictions of the elastic constitutive law of eqn. (3.4) into agreement with the actual stresses.

(e) As the vector of applied loads is dependent on the level of initial stress, a change of $\{d\sigma_o^e\}_1$ results in a vector of "corrective" or "residual" loads $\{dQ_1\}_1$. This residual force vector represents the difference between the externally applied loads on the structure and the nodal forces arising from internal stresses.

(f) A vector of additional displacements $\{d\Delta_1\}_1$ corresponding to the residual load $\{dQ_1\}_1$ is calculated from

$$\{d\Delta_1\}_1 = [K_o]^{-1}\{dQ_1\}_1 \qquad \ldots(3.10)$$

(g) The total strains for the new displaced configuration $\{\Delta_1\} + \{d\Delta_1\}_1$ are calculated and steps (b) to (f) repeated as an iterative process until an acceptable level of convergence is achieved. On the n^{th} iteration of the first load increment, the criterion for convergence may be based on the relative magnitude of either the residual load vector $\{dQ_1\}_n$ or incremental displacement vector $\{d\Delta_1\}_n$. The vector of cumulative nodal displacements after convergence on the r^{th} iteration of the first increment is

$$\{\Delta\} = \{\Delta_1\} + \sum_{i=1}^{r} \{d\Delta_1\}_i \qquad \ldots(3.11)$$

(h) When convergence is achieved for the first increment of applied load $\{Q_1\}$, the second and subsequent increments $\{Q_2\}$, $\{Q_3\},\ldots,\{Q_m\}$ are applied and the iterative procedure of steps (a) to (g) employed until convergence is achieved in each increment.

In practice, the initial stress method in materially non-linear analysis has the combined benefits of a relatively simple theoretical basis and satisfactory computational efficiency. More efficient procedures have been developed[88] but at the expense of increased theoretical and programming complexity.

Perhaps the main advantage of the initial stress method is that the stiffness matrix remains unchanged during each load increment. In the procedure outlined above, matrix $[K_0]$ is used throughout the first load increment: reduction of the matrix is therefore only performed once, at the start of the increment. However, efficiency of the numerical solution is increased if the structural stiffness matrix is updated at the start of each load increment. This approach then corresponds to the modified Newton-Raphson iterative procedure illustrated with reference to steps (a) to (g) in Fig. 3.1 .

3.2.2 Geometrically Non-Linear Analysis

A geometrically non-linear problem is one in which a non-linear relationship exists between global displacements and strains. In the analysis of this type of problem, one commonly adopted approach is to define element local coordinate systems which follow the elements as the structure deforms under load. The displaced element local coordinate system may have large translational and/or rotational motion relative to the structure global coordinate system; however, deformation of each element with respect to its own displaced local system is assumed to be small so that, at the element level, the small strain-displacement relationship of eqn. (3.3) remains valid. Consequently, a requirement of this method is that elements should be sufficiently small to ensure "small" displacements with respect to each local coordinate system. In terms of the global or overall pattern of displacements, this type of analysis is generally known as the large displacement-small strain approach. Like the procedure adopted for materially non-linear analysis in Section 3.2.1, the strategy employed is both incremental and iterative in nature.

Details of the solution strategy are well presented by Cook[85] and are presented below in a slightly modified form to emphasise similarity with the procedure described in Section 3.2.1 .

(a) The first increment of load $\{Q_1\}$ is applied and global nodal displacements $\{\Delta_1\}$ calculated from eqn. (3.9).

(b) The global displacements of the element nodes result from combined rigid body motion and local distortion of the elements. The rigid body motion component can be subtracted out once the displaced position and orientation of the local coordinate system are established. Nodal displacements with respect to the local system, $\{\Delta_1{}^e\}$, are then calculated.

(c) In the case of small strains, element stiffness matrices $[K_1{}^e]$ are linear with respect to the local coordinate systems; that is, they are not dependent on displacements. Consequently they remain constant for all states of deformation.

(d) Forces at element nodes arising from element distortions are determined using the element stiffness matrices:

$$\{Q_1^e\} = -[K_1^e]\{\Delta_1^e\} \qquad \ldots(3.12)$$

(e) Vectors $\{Q_1{}^e\}$ and matrices $[K_1{}^e]$ are then referred to the global coordinate system by means of coordinate transformations. The resulting "global" element matrices are $\{Q_1{}^e\}_g$ and $[K_1{}^e]_g$. The overall global stiffness matrix $[K_1]$ for the current configuration is obtained from

$$[K_1] = \Sigma\, [K_1{}^e]_g$$

and a global vector of nodal loads $\Sigma\{Q_1{}^e\}_g$ formed.

(f) A residual force vector $\{dQ_1\}_1 = \{Q_1\} + \Sigma\{Q_1{}^e\}_g$ is determined and a vector of corresponding displacements calculated from $\{d\Delta_1\}_1 = [K_1]^{-1}\{dQ_1\}_1$. The total displacement $\{\Delta_1\} + \{d\Delta_1\}_1$ then gives the updated prediction of the equilibrium configuration.

(g) A convergence check is performed on either $\{dQ_1\}_1$ or $\{d\Delta_1\}_1$ and the iterative process continued if required.

In this method of solution, all essential non-linear behaviour is accounted for by coordinate transformations.

3.2.3 Solution of Problems Involving Coupled Non-Linearity

Similarity between the incremental-iterative procedures for material and geometrical non-linearity described in Sections 3.2.1 and 3.2.2 suggests the possibility of merging the two procedures to produce a programme capable of performing combined or coupled non-linear analysis. This has been successfully achieved, much of the work being reported in the literature[88] and, to a lesser extent, in documentation accompanying the more versatile, commercially available finite element programmes (eg. NASTRAN, LUSAS). Details of the strategy adopted for a combined analysis are omitted herein but follow immediately from the steps given in the two preceding Sections.

Such coupled analyses are computationally lengthy, demanding in terms of their frequent access to a computer's central processor and hence considerably more expensive than corresponding linear elastic analyses. Nevertheless, with judicious choice of increment size and the specification of adequate but not unduly severe convergence criteria, effective solutions of the coupled non-linear problem are possible. In addition, much more refined solution strategies than those described above and highly efficient matrix manipulation and reduction techniques are employed in commercial programmes. Two such programmes capable of combined non-linear analysis, NASTRAN and FINAS, were employed in the present study and are described more fully in Section 3.4 .

3.3 The Search for a Finite Element Programme Capable of Combined Non-Linear Analysis

In the literature, guidance is available[88-90] on the transition from the theory of non-linear solutions, outlined in Section 3.2, to the computer implementation of the method. Nevertheless, this transition is extremely time-consuming both in terms of programming and subsequent programme testing and debugging. In this Section, the initial stages in the development of a non-linear finite element programme are briefly described and reasons given for the subsequent adoption of two "off-the-shelf" programmes, MSC/NASTRAN and FINAS. The capabilities of these programmes are then described and consideration given to their application to the problem of inelastic lateral-torsional instability of restrained beams.

3.3.1 The Development of an Elasto-Plastic Analysis Programme

As the first stage in the development of a finite element programme capable of combined materially and geometrically non-linear analysis, attention was focussed on the development of a materially non-linear programme. In this, the model adopted for non-linear material behaviour was that described by Owen and Hinton[89]. The geometrically non-linear analysis capability was later to be included.

Initially, routines from three sources[84,91,92] were assembled to form an elastic analysis programme employing eight-noded isoparametric plane stress elements. The parabolic isoparametric formulation was chosen both for ease of programming and for its proven versatility and numerical "good behaviour"[92]. Although two translational degrees of freedom in the plane of the element at each node were sufficient to describe the in-plane behaviour of the flange and web panels, compatibility of displacements between flanges and web could only be achieved in the longitudinal direction (Fig. 3.2). Moreover, no out-of-plane stiffness was ascribed to the flange and web panels. Nevertheless, at the outset it was decided that the plane stress element should form the basis of the non-linear programme as the subsequent substitution, if required, of a more versatile element into the framework of an operational programme would be relatively straightforward.

The frontal solution advocated by Hinton and Owen[92] was not implemented in the elastic plane stress programme. Instead, a simpler, though less efficient, half band solver was adopted. This proved adequate during testing of the elastic programme. Compatibility of longitudinal displacements at coincident flange and web nodes, such as A and A' in Fig. 3.2 was achieved by means of a contragredient transformation described by Cook[85].

In extending the capabilities of the elastic programme to include a non-linear constitutive law, an initial stiffness approach was employed in the incremental-iterative process. The solution strategy of the initial stiffness method is represented graphically in Fig. 3.3 and it is evident that close similarities exist with the initial stress strategy depicted in Fig. 3.1 . The fundamental difference lies in the continued use of the initial stiffness matrix $[K_0]$ beyond the first increment of load. This allows reduction of the half band global stiffness matrix by Gaussian elimination before entry into the incremental and iterative cycles shown in Fig. 3.4 . The reduced matrix and Gaussian elimination factors are then stored: the elimination factors are subsequently used to reduce applied load vectors $\{Q_1\}$, $\{dQ_1\}_1$,..., etc. and relationships of the form of eqn. (3.7) solved using the reduced forms of the load vector and stiffness matrix to give displacements $\{\Delta_1\}$, $\{d\,\Delta_1\}_1$,..., etc.

The apparent advantage of the "once and for all" reduction of the stiffness matrix in minimising computational effort is partly offset by the need for a greater number of iterations before convergence on each load increment. In highly non-linear problems, recalculation of global stiffness on each increment is to be preferred as a net saving in computing time is likely; by definition, the initial stiffness method can be expected to provide an efficient solution where non-linear behaviour is less pronounced.

Unfortunately, in terms of both computing time and core storage requirements, the contragredient transformation used to enforce compatibility of longitudinal displacements in the elastic programme was found to be unacceptably inefficient in the context of the elasto-plastic analysis programme, where minimisation of both of these quantities was important. An alternative method of ensuring displacement compatibility by means of an array of nodal freedoms was introduced. This proved considerably more efficient.

The elasto-plastic programme was written in FORTRAN for use on the University's ICL 2976 mainframe computer. On completion of this programme a review of the project timetable revealed that an insufficient amount of time allocated to computer analysis remained for implementation of the geometrical non-linearity capability. Moreover, the development of a combined non-linear programme was not the primary aim of the project and it was feared that a considerable amount of time would be required to implement the more efficient solution routines and data storage schemes needed for coupled non-linear analysis.

A more determined search for a suitable, commercially available and accessible programme eventually revealed that the large MSC/NASTRAN suite was mounted at the Science and Engineering Research Council's (S.E.R.C) Rutherford Appleton Laboratory at Chilton. An allocation of computing time was subsequently granted by S.E.R.C. and remote access to the system was via a local GEC 4070 computer linked to the S.E.R.C. network. The capabilities and limitations of NASTRAN are briefly described in the following Section.

3.3.2 MSC/NASTRAN: Description and Limitations

The programme MSC/NASTRAN is a very large, general purpose finite element analysis suite. The original version of NASTRAN was developed by the National Aeronautics and Space Administration (NASA) in the United States but in 1969 the MacNeal Schwendler Corporation assumed responsibility for maintaining, updating, documenting and marketing the commercial version of the programme, which then became known as MSC/NASTRAN. Currently the largest, most comprehensive finite element package available, the programme is being continuously developed and currently (1985) offers a wide range of static, dynamic, eigenvalue, aeroelastic and heat transfer solutions.

The combined materially and geometrically non-linear analysis capability of MSC/NASTRAN was used in the present study. Of the large selection of elements available in the element library, a considerably smaller subset was available for use in non-linear solutions. Of these, the quadrilateral isoparametric shell element QUAD4[93] and subsequently the BEAM element were selected for use in predicting the non-linear response of restrained beam systems.

Initially, the four-noded QUAD4 shell element was adopted for modelling the entire beam cross-section. With five degrees of freedom per node (three translational, two rotational), these elements allowed warping and cross-sectional deformations of the beam to be included in the analysis in addition to bending, axial, torsional and shear effects. As a first step in assessing the suitability of the QUAD4 element in this application, the linear elastic behaviour of a simply-supported I-beam of span 200mm, overall depth 50mm, flange breadth 16mm and general metal thickness 1mm was examined under central point loading. The low span-to-depth ratio of four selected for this test problem was chosen to check the accuracy of the programme in calculating both bending and shear deflections.

Of the total theoretical vertical midspan deflection 'Δ' given by

$$\Delta = \frac{P\ell^3}{48EI_{maj}}\left(1 + \frac{12 f_s EI_{maj}}{GA_x \ell^2}\right) \qquad \ldots(3.13)$$

in which l = beam span

EI_{maj} = major axis flexural rigidity

f_s = form factor for shear in the plane of the web (f_s = 1.656 for the above beam dimensions)

G = shear modulus

A_x = cross-sectional area of beam

the contribution from shear (second term in parenthesis) was found to be about 46% of the bending deflection and was therefore of considerable importance. Finite element idealisations of the above beam employing twenty QUAD4 elements (4 in web, 16 in flanges) and forty-eight QUAD4 elements (16 in web, 32 in flanges) as shown in Figs. 3.5(a) and (b) were subjected to central point loading. For all preliminary work in NASTRAN, mesh grading from the relatively coarse mesh employed in elastic regions to the central, finer inelastic mesh was "sudden" and not achieved by use of transition regions consisting of triangular elements or constraint equations. The latter were to be employed during "production" runs if the QUAD4 analysis proved economical.

The results of these linear elastic analyses are shown in Fig. 3.5(c) where the total elastic deflection predicted by eqn. (3.13) is also shown. Agreement between the load-deflection responses is observed to be excellent, the 48 element analysis having been performed using the non-linear facility in MSC/NASTRAN. The 48 element mesh was preferred as it provided aspect ratios for the flange elements of approximately three, half the value attainable using the 20 element mesh.

Although the 48 element mesh had been shown to be adequate for use in elastic regions, further mesh refinement was required to enable plasticity and large deflections to be dealt with. As an alternative to QUAD4 mesh refinement in these zones, the introduction of higher-order shell elements such as the parabolic isoparametric QUAD8 would probably have been more efficient. Unfortunately, use of this eight-noded shell element was restricted to linear elastic analysis. In accounting for non-linear material behaviour a von Mises yield criterion was used in conjunction with an elastic-perfect plastic material response in the form of Fig. 1.7 .

Although suitable for testing convergence under linear elastic conditions, the initially perfect beam model did not afford the opportunity to test the large displacement capability. Consequently, in the preliminary series of combined non-linear analyses an initial lateral bow of sinusoidal form and of amplitude one-thousandth of the span (viz. 0.2mm) was incorporated into the analysis by suitable adjustment of nodal coordinates. The greatest extent of the theoretical yielded zone was known for $P=P_p$ and therefore mesh refinements were confined to this region. Solutions employing 64, 80 and 132 elements (Fig. 3.6) were performed and the results of these NASTRAN analyses are shown in Fig. 3.7 . The greater vertical displacement of the initially imperfect beam is immediately obvious. Increments of enforced vertical displacement at midspan rather than of applied load were used in these and in all subsequent finite element analyses to facilitate attainment of collapse loads.

The graphs of Fig. 3.7 indicate satisfactory convergence for the 132 element model, for which the fully plastic load, P_p, falls within 2.5% of the theoretical value. A considerably refined mesh in the central, inelastic region of this model produced flange and web element aspect ratios of approximately 1.5 and 2.0, respectively. In "numerically integrated" elements, such as the QUAD4, where strains and subsequently stresses are evaluated at a limited number of integration or Gauss points within the element, there is inevitably a lag between the onset of yield at an element boundary and the detection of yield at the Gauss points. Mesh refinement in probable areas of first yielding increases the likelihood of early detection and hence provides a more accurate prediction of non-linear response. The degree of mesh refinement in inelastic zones of the 132 element model was therefore considered satisfactory.

It was then considered necessary to examine the sensitivity of NASTRAN to the magnitude of initial imperfections on the test span. The measured, initially imperfect shape of model beam P1 (see Table 5.3) was translated into a mesh of QUAD4 elements using the programme NEWMESH described in Section 3.4 . The resulting mesh for the 600mm span beam consisted of 732 elements. Analysis of beam P1 was followed by a further two analyses in which sinusoidal distributions of initial imperfections were assumed: amplitudes of the sinusoidal crookedness were respectively double and half the maximum recorded value for beam P1. Comparison of the results of the three analyses revealed considerable discrepancies arising from these differences in initial imperfections, particularly in relation to predicted lateral deflections of the flanges. Consequently, as bracing force, one of the main subjects of study, was linearly related to flange lateral displacement, there was a need for accurate measurement and subsequent numerical modelling of initial imperfections.

In addition to a substantial increase in data preparation time for the longer beam P1, both computing time and storage requirements were greatly increased. Central processor times well in excess of one hour per analysis were recorded; although a considerable drain on the total computing time allocated by S.E.R.C., infrequent runs of this duration were nevertheless possible. However, the amount of direct access storage required for updating and manipulating global stiffness matrices within the NASTRAN data base proved excessive and eventually, even with a considerably enhanced storage allocation on S.E.R.C.'s large IBM 3081 computer, allocated space was insufficient to perform the QUAD4 shell analysis. Implementation of the NASTRAN restart facility in an attempt to condense much of the stored data from previous load increments proved only partially successful, in that although this permitted the analysis of a few additional load increments in each analysis, premature termination of analyses recurred due to the excessive, cumulative storage demand created by successive restart runs.

Approaches to other large users of NASTRAN revealed that none had attempted a combined non-linear analysis of comparable magnitude. However, it was felt that the problem was exacerbated by the need to perform such a large analysis on a multi- rather than a single-user system: commercial organisations running NASTRAN on in-house systems had the ability to dedicate very large areas of direct access storage to single NASTRAN analyses; this was not the case on the S.E.R.C. system.

As the 600mm span beam represented the shortest to be employed in the experimental programme, it was evident that problems were likely to worsen as analyses of longer spans were attempted. Consequently, analysis based on the QUAD4 shell element was not considered thereafter; instead, attention turned to the NASTRAN BEAM element.

The BEAM element in NASTRAN is a straight, two-noded element having, in addition to three translational and three rotational degrees of freedom at each end node, an additional, seventh freedom at each of these locations allowing warping deformations to be included in the analysis. In materially non-linear applications, the BEAM element is capable of developing inelastic behaviour only at its ends, plastic hinges being possible in these locations with elastic response elsewhere. Although primarily intended for use in collapse analysis of frames, this type of element was considered suitable for use in the restrained beam analysis provided that several short elements were employed in regions of potentially inelastic behaviour.

Simple analyses employing only a few BEAM elements were sufficient to demonstrate the satisfactory performance of the element under linear elastic conditions. The effect on predicted bracing forces of omitting the geometrically non-linear analysis option was then examined using the recorded imperfection data for test beam M2 (Table 5.4). Differences in bracing force of about 100% are evident in Fig. 3.8 for applied loads in excess of $0.9P_p$. This result confirmed the need for inclusion of the large displacement option in all analyses.

Use of the BEAM element meant that cross-sectional deformations were no longer modelled in the NASTRAN analysis; however, this was considered to be of minor significance. Of considerably greater importance were the substantially reduced computing time and storage demands compared with the QUAD4 analysis. Consequently, NASTRAN analyses were no longer constrained by the amount of available storage space and it was possible to employ BEAM element solutions in attempting to provide theoretical verification of experimental results.

In this latter application, it became evident that the numerical procedures employed in NASTRAN for the solution of highly non-linear problems were inadequate, and divergence of the solution occurred in every analysis before attainment of the collapse condition. The problem of divergence had rarely been encountered in previous NASTRAN analyses, probably due to the premature failure of earlier QUAD4 analyses on other grounds. Considerable refinement of the beam element mesh in midspan regions of the centrally loaded, centrally braced beam models was carried out but, although only very small increments of enforced displacement were applied at each stage in the analyses, numerical instability inevitably frustrated all attempts to attain peak loads. Indeed, results of NASTRAN BEAM analyses presented for comparison with experimental results in Chapter 6 display little sensitivity to the softening and destabilising effects of yielding and the occurrence of large deflections.

Access to the FINAS programme, currently (1985) being developed in Imperial College, London, by Bates[94] et al., was subsequently arranged.

3.3.3 FINAS: Description and Advantages over NASTRAN

The FINAS beam element was used to good effect, as demonstrated by the degree of correlation achieved between finite element and experimental results presented in Chapter 6. The element used was a 3-noded space beam suitable for modelling thin-walled members of open cross-section. As in NASTRAN, geometrical non-linearity was accounted for by means of a co-rotational or "updated Lagrangian" formulation corresponding to the large displacement-small strain approach described in Section 3.2.2 . Additional similarities with the preceding NASTRAN analyses were the adoption of a von Mises yield criterion and the facility to include warping deformations as a seventh degree of freedom at each of the element's three nodes.

Idealisation of the initially imperfect, restrained beams tested in the experimental programme was satisfactorily achieved using only twelve beam elements to model the physical beam and an additional element to represent the midspan translational restraint. Gradation of the beam mesh from longer elements at the end supports to shorter at midspan was again employed and, as access to the FORTRAN source code of FINAS was not possible, physical modelling of the brace was required instead of simply augmenting the appropriate diagonal term in the global stiffness matrix of the unrestrained beam.

Consideration of the sense of initial beam crookedness allowed the bracing element to be attached on the side of the idealised beam appropriate to the development of axial tension in the brace. The possibility of mobilisation of axial compression was avoided due to the decrease in axial stiffness accompanying increasing compressive load and the conflicting requirement for constant restraint stiffness.

The greater versatility of FINAS numerical solutions over those implemented in NASTRAN is demonstrated in Fig. 3.9 which shows the effect of increasing initial bow in unrestrained beams of 600mm span containing sinusoidal imperfections of amplitude 1/500, 1/1000 and 1/4000. The theoretical elastic critical load of the corresponding initially perfect beam, derived from the programme MODBRACE, is also indicated in that figure. The collapse load attained by the 1/4000 beam is noted to be a close approximation to the theoretical elastic critical load. In performing finite element analyses corresponding to the twenty model beam tests, the ability of FINAS to deal with non-positive definite matrices was important. This capability, used in conjunction with displacement rather than load control, frequently allowed attainment of true collapse loads and in some cases subsequent prediction of post-collapse behaviour.

FINAS was previously used as the basis of a theoretical study of box girder collapse by Dowling et al[95]. In that application, several solutions were curtailed by the occurrence of numerical instability in shell element analyses. In such cases, non-convergence of the solution was assumed to be indicative of collapse. Although problems of non-convergence had been encountered in the use of NASTRAN in the present study, it was considered inadvisable to adopt a similar collapse criterion as the NASTRAN BEAM elements were not as capable of modelling inelastic or large displacement effects.

Divergence of FINAS analyses was also occasionally encountered in the present study although to a much lesser extent than with NASTRAN. In general, however, FINAS analyses were considerably more fruitful and numerically stable and were frequently capable of modelling highly non-linear behaviour as displayed, for example, by model beam M10 (Fig. 6.11). Nevertheless, both NASTRAN and FINAS proved incapable of solving the problem of an initially imperfect beam under uniform moment loading. Attempted analyses of this problem produced almost immediate divergence and consequential failure in both programmes.

The acceptability of both FINAS and NASTRAN results when compared with experimental findings is discussed in Chapters 6, 7 and 8.

3.4 Finite Element Mesh Generation from Measured Imperfection Data

A prerequisite for finite element analysis of the beams employed in the experimental programme reported in Chapters 4 to 6 was a facility for the generation of a finite element model incorporating those geometrical imperfections measured by the procedure described in Chapter 5. A computer programme, "NEWMESH", was written to perform this task and a listing of the programme is given in Appendix II. The most important features of the programme are discussed in this Section.

The FINAS beam and both the NASTRAN BEAM and QUAD4 elements were employed at different stages in the study and so the results given by NEWMESH were in a form broadly compatible with the input data to these programmes.

In Appendix II, the major segments of the programme are indicated by the letter codes A to L. In the remainder of this Section, the most important of these segments are described. Section A contains a brief description of the programme, the variables used and array dimensions. This is followed in Section B by a routine which accepts measured initial imperfection data and calculates geometrical properties for the "average" cross-section. As described in Chapter 5, prior to model beam tests several lines of initial imperfection readings (each line containing sixteen readings) were taken on the web surface (lines W1 to W3) and flange tips (lines T1, C1) over the full length of the test span. The locations of these sixteen readings were as shown in Table 3.1 for the 600, 800 and 1000mm spans employed in tests.

Inspection of Table 3.1 shows that the readings were not equally spaced; rather, their spacing was determined by the normalised coordinate

$$\bar{x} = -\cos\left(\frac{\pi(j-1)}{N}\right) \qquad \ldots(3.14)$$

in which j = reading number

N = total number of readings = 16

The spacing of points was greatest at the centre of the test span and decreased towards the ends, reflecting the need for greater definition near the ends of the range to counteract the tendency of approximating polynomials to develop fluctuations in these regions. Sixteen points on the test span (ie. N=16) proved sufficient for specification of the imperfection data and, as described later, the interpolation of a smooth polynomial curve through this data.

Table 3.1: Location of Sampling Points for Initial Geometrical Imperfections

Reading No. j	Normalised Coordinate $\bar{x}$	Location of Sampling Point on Test Span of		
		600mm	800mm	1000mm
1	-1.0000	0	0	0
2	-0.9781	6.56	8.74	10.93
3	-0.9135	25.94	34.58	43.23
4	-0.8090	57.29	76.39	95.49
5	-0.6691	99.26	132.35	165.44
6	-0.5000	150.00	200.00	250.00
7	-0.3090	207.30	276.39	345.49
8	-0.1045	268.64	358.19	447.74
9	0.1045	331.36	441.81	552.26
10	0.3090	392.70	523.61	654.51
11	0.5000	450.00	600.00	750.00
12	0.6691	500.74	667.65	834.56
13	0.8090	542.70	723.61	904.51
14	0.9135	574.06	765.42	956.77
15	0.9781	593.44	791.26	989.07
16	1.0000	600.00	800.00	1000.00

Allowance for the effect of self weight deflections on the measured imperfections was necessary as the beam was supported on the tips of its flanges during imperfection measurement and consequently minor axis bending under self weight affected the readings. Under self weight, the deflected form shown in Fig. 3.10(b) is predicted by the Macauley equation

$$\Delta = \frac{w}{24EI_\eta}\left\{(x^4-g^4) - 2L\langle x-g\rangle^3 + 6L\langle x-g\rangle\left[\left(\frac{L}{2}-g\right)^2 - \frac{L^2}{12}\right]\right\} \qquad ...(3.15)$$

for the beam shown in Fig. 3.10(a). The self weight correction was performed in Section Ⓒ of the programme.

The "slant" correction applied in D was based on the assumption that the four vertices of the web panel of the test beam were coplanar in the vertical plane. In the experimental investigation, this condition was achieved by use of the web-plumbing device described in Chapter 4. All corrected initial crookedness and twist data could then be referred to known conditions at the supports. Compatibility of support conditions and the distribution of initial imperfections relative to the direction of applied loading was therefore achieved between the finite element model and actual test beam.

Imperfection readings corrected for both self weight and slant by the above methods were then used as the basis of routine F, which fitted Chebyshev polynomial approximations to the distribution of imperfections in the flanges and web. Subsequently, in G, these polynomials were used to calculate a set of nodal coordinates defining the initial deformed geometry of the whole beam.

A facility for plotting the initially deformed surface of the web was included at H in the programme. This allowed a rapid qualitative asssessment of the distribution of web imperfections prior to tests and, of greater significance, indicated the sense of compression flange initial crookedness relative to the test rig and hence the probable direction of flange lateral movement during lateral-torsional instability. As an example, the web surface plot shown in Fig. 3.11 shows increasing twist on the section towards midspan and initial convexity of the compression flange in the -ve Y direction. Under test, this beam failed in a lateral-torsional mode in which the lateral deflection of the compression flange increased in the direction of initial compression flange bow.

In sections J and K, data for the FINAS beam and NASTRAN BEAM and QUAD4 elements was generated. Reflecting the need for a different data format for each of these elements the NEWMESH output file contained three distinct groups of data. Deletion of the two unwanted groups and insertion of appropriate load case data and job control statements, etc. then provided a data file suitable for use in either the FINAS or NASTRAN analyses.

NEWMESH was used successfully as a mesh generator for both NASTRAN and FINAS in all finite element work undertaken in the present study.

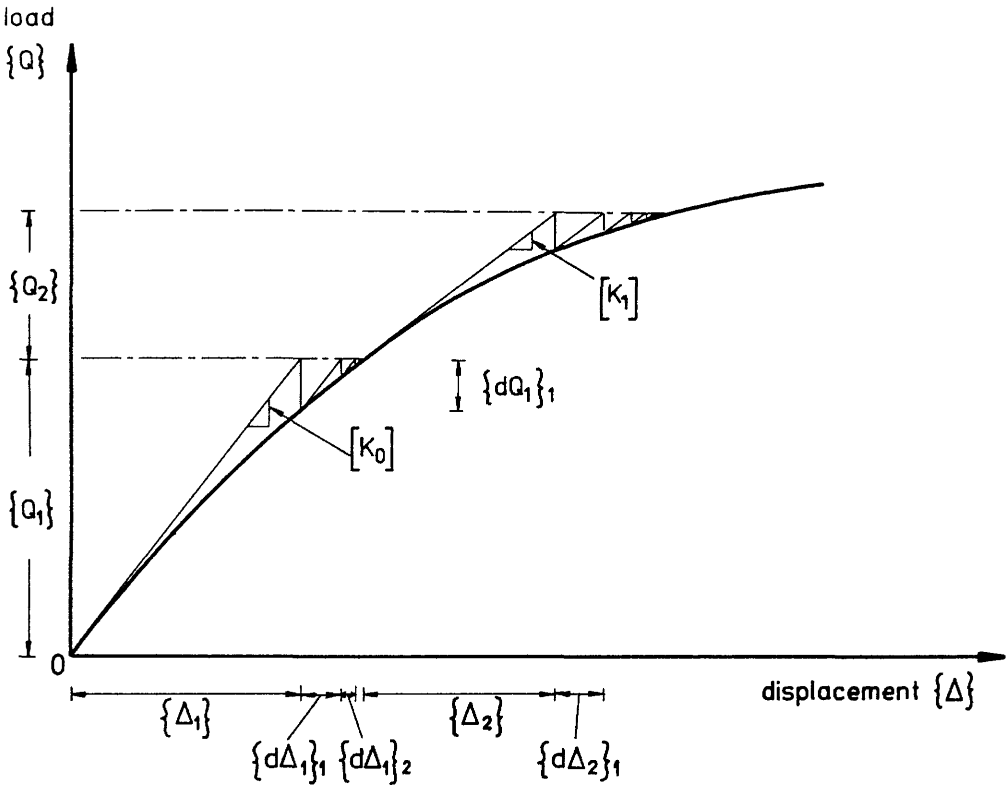

Fig. 3.1 : Modified Newton-Raphson incremental-iterative procedure employed in non-linear analysis

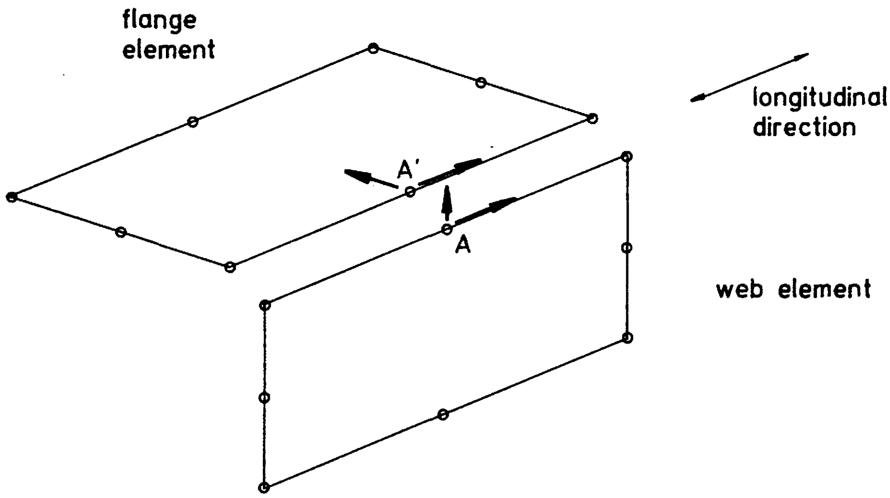

Fig. 3.2 : Incompatibility between web and flange element freedoms using the parabolic isoparametric plane stress element

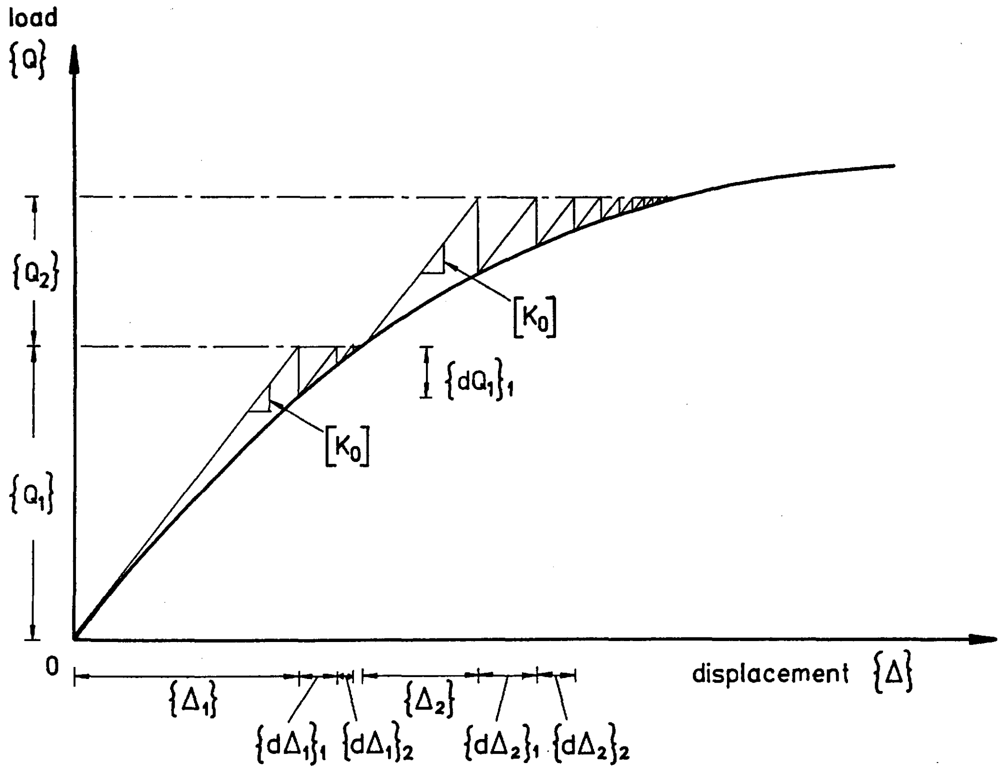

Fig. 3.3 : Solution strategy of Initial Stiffness Method

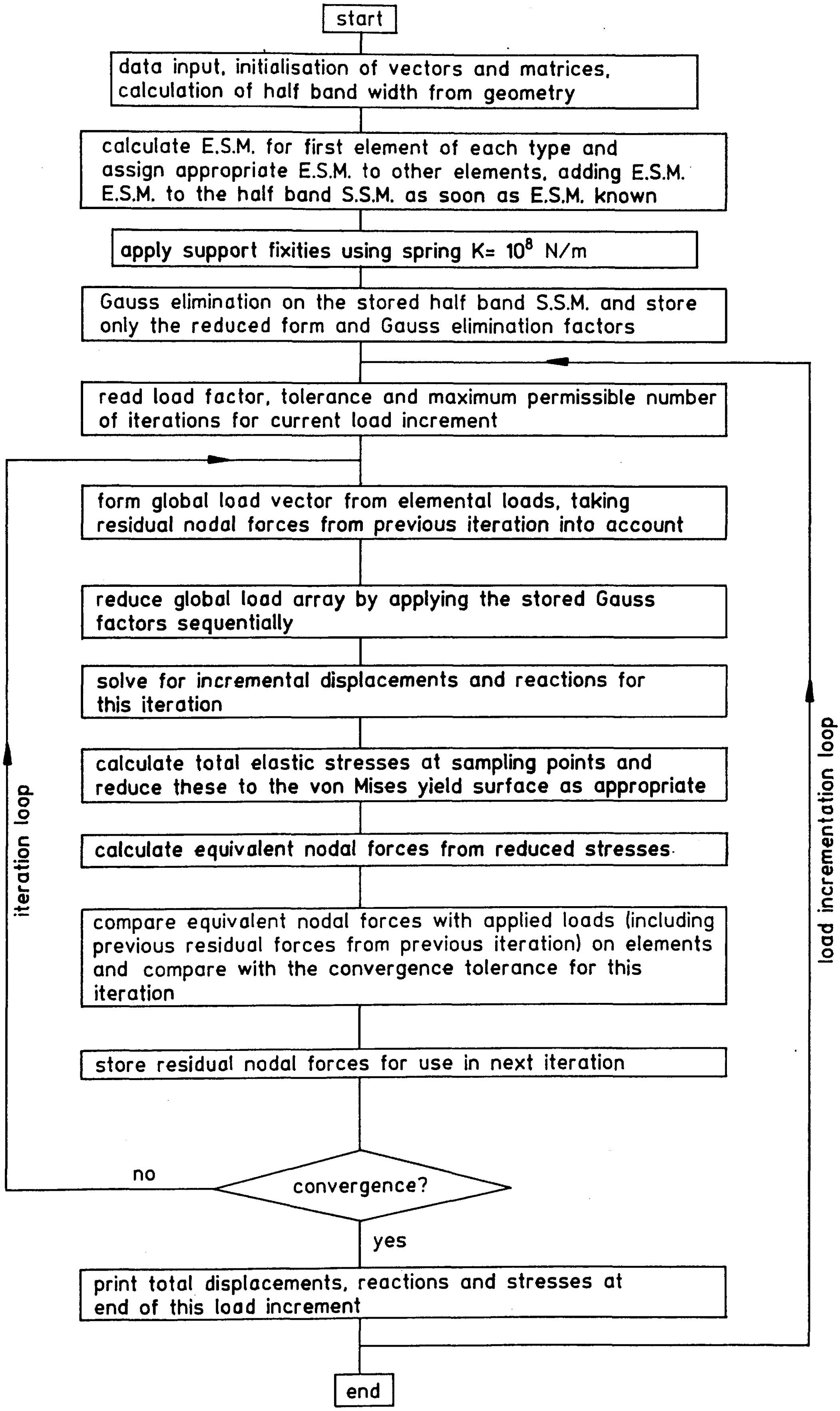

Fig. 3.4 : Descriptive flow chart for elasto-plastic programme

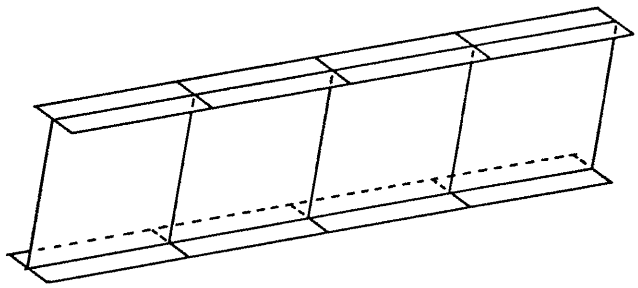

(a) 20 No. QUAD4 element mesh

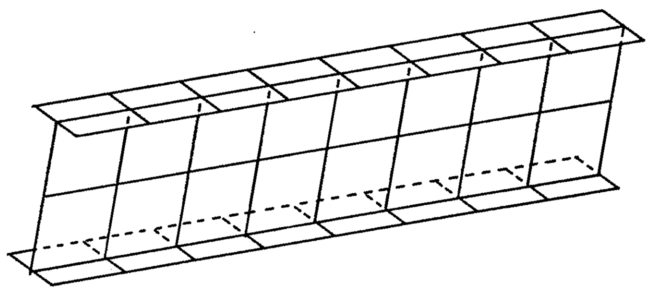

(b) 48 No. QUAD4 element mesh

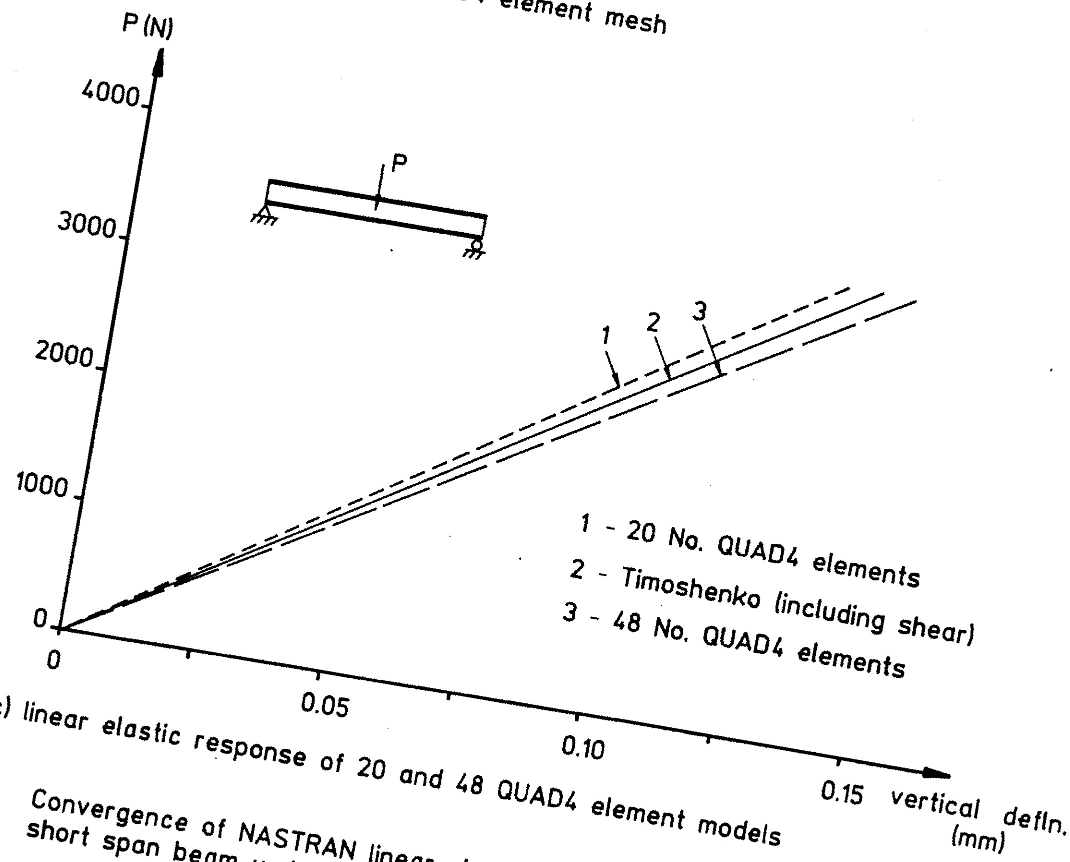

(c) linear elastic response of 20 and 48 QUAD4 element models

Fig. 3.5 : Convergence of NASTRAN linear elastic solutions for an initially perfect, short span beam under central point loading

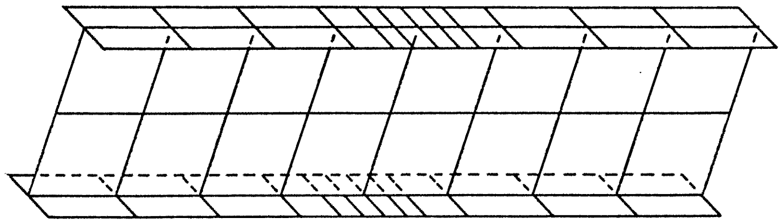

64 elements

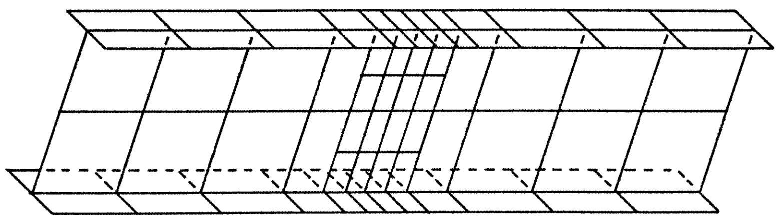

80 elements

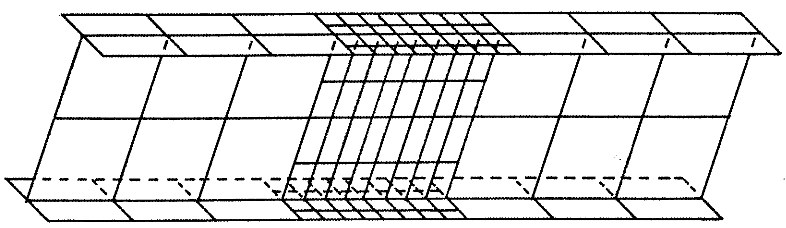

132 elements

Fig. 3.6 : Successive refinements of QUAD4 element mesh for NASTRAN non-linear analysis

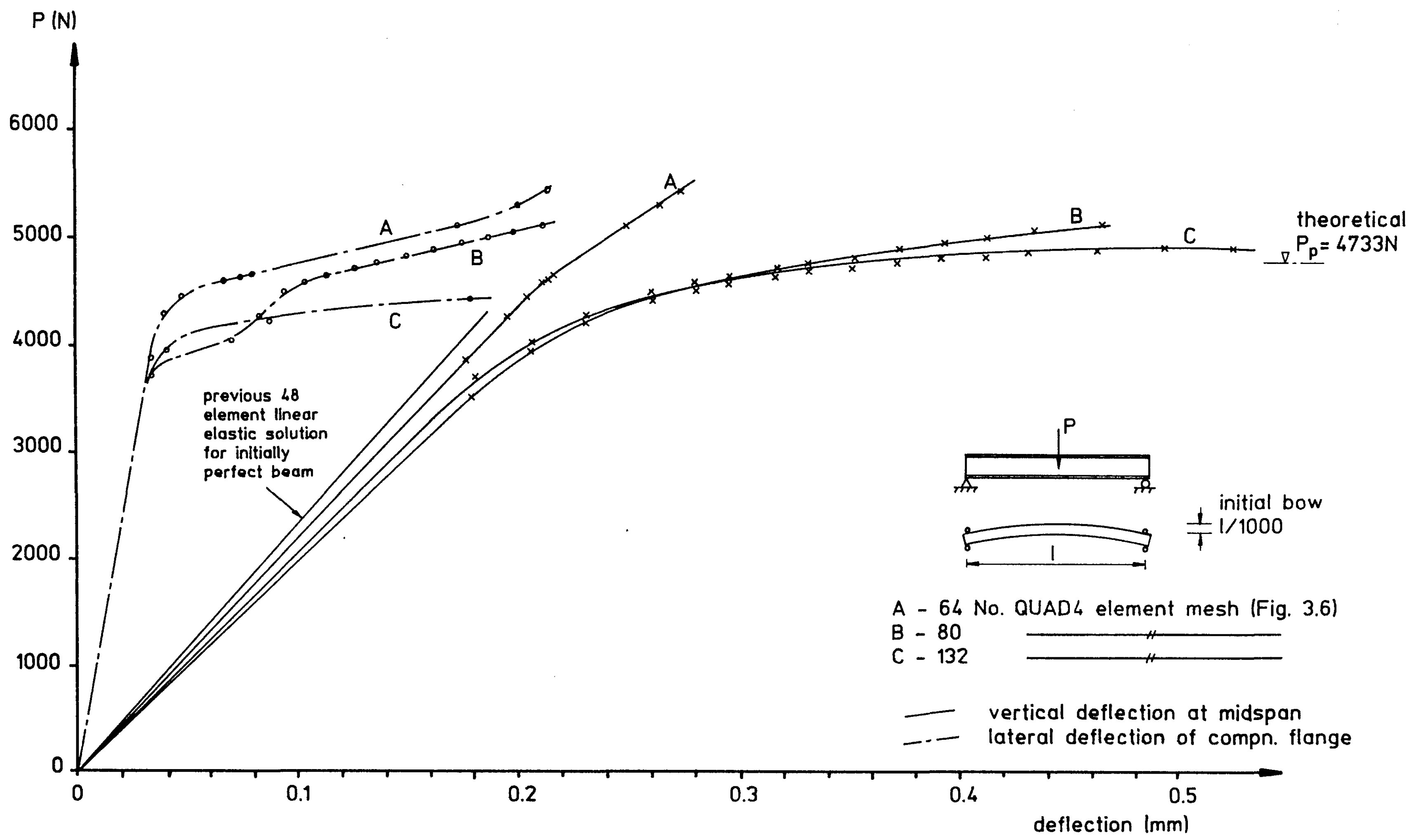

Fig. 3.7 : Convergence of NASTRAN non-linear solutions for an initially imperfect, short span beam under central point loading

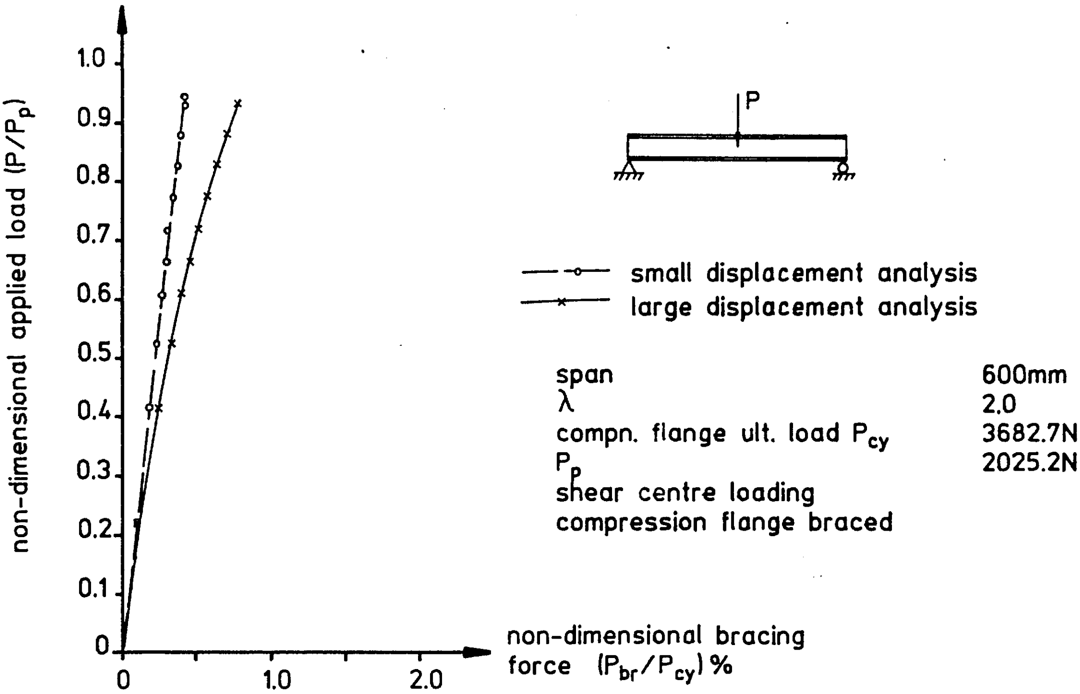

Fig. 3.8 : Applied load vs. bracing force for test beam M2, showing the effect of the large displacement analysis option

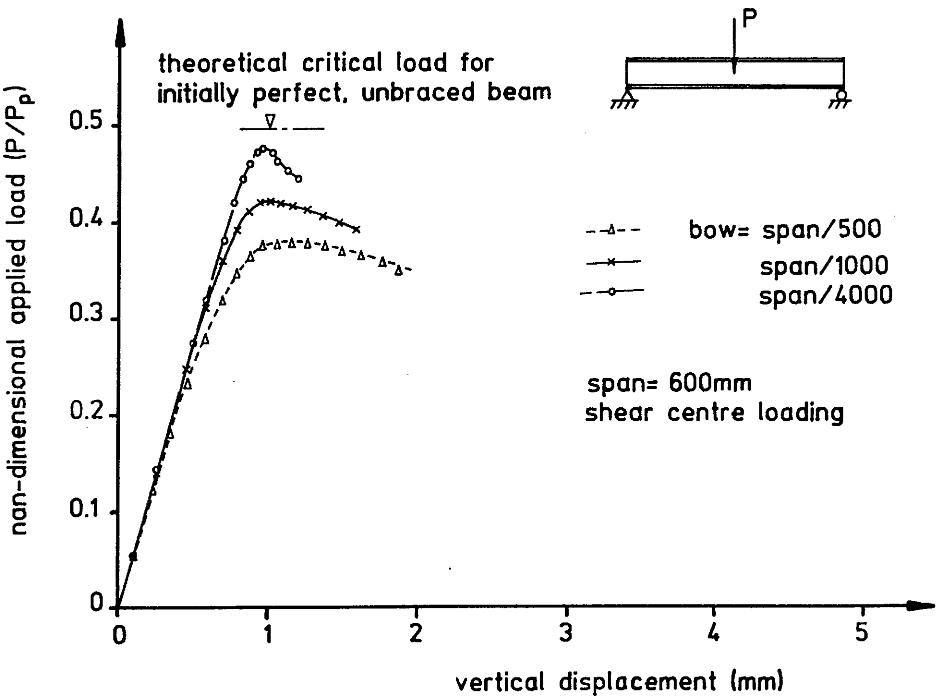

Fig. 3.9 : The effect of increasing initial crookedness in unrestrained beams in FINAS analyses

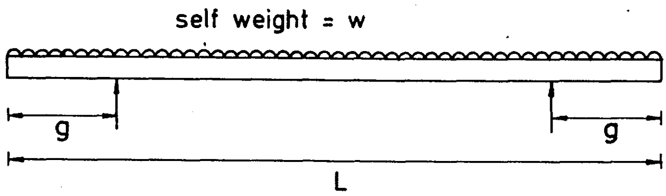

(a) beam under self weight U.D.L.

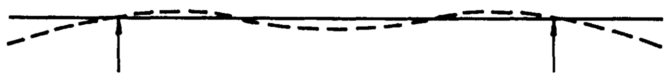

(b) corresponding deflected form

Fig. 3.10 : Beam subjected to minor axis bending during imperfection measurement

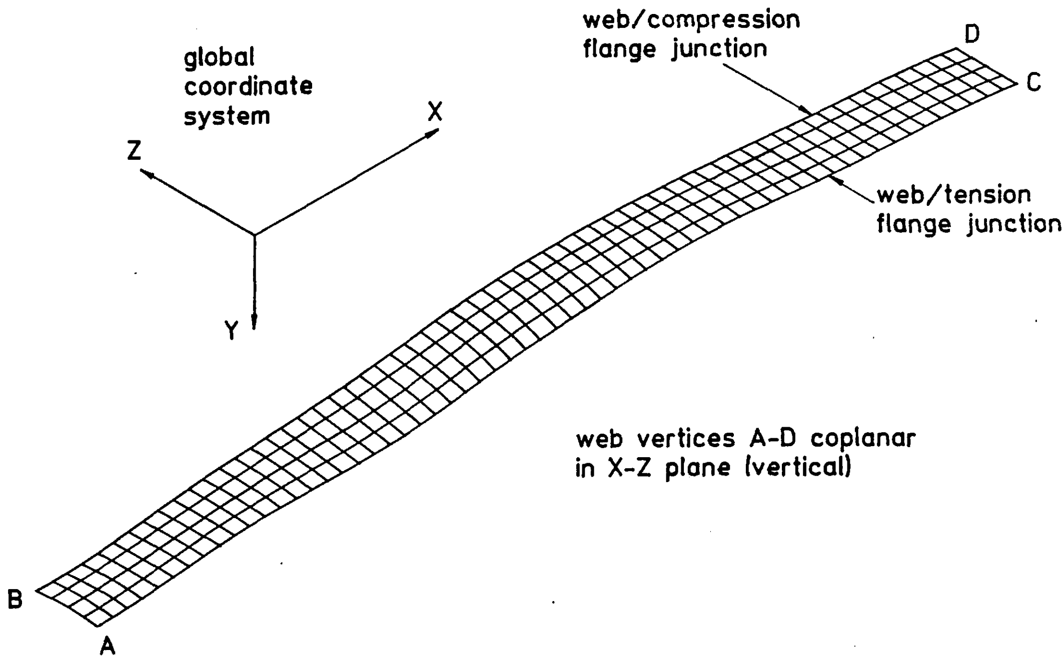

Fig. 3.11 : NEWMESH plot showing initial deformed shape of web and crookedness of web/flange junctions

CHAPTER 4

REQUIREMENTS OF THE EXPERIMENTAL PROGRAMME AND CONSTRUCTION OF THE TEST RIG

CHAPTER 4

REQUIREMENTS OF THE EXPERIMENTAL PROGRAMME AND CONSTRUCTION OF THE TEST RIG

This Chapter describes the general requirements and objectives of the experimental programme and provides details of the test rig developed to achieve these objectives.

4.1 General Requirements of the Test Programme

The primary aim of the experimental work was to provide information on the minimum translational bracing stiffnesses necessary to afford fully effective midspan lateral restraint to simply-supported steel beams. The forces developed in the bracing during testing were also required. Initially, both central point loading and uniform moment loading conditions on the beams had been envisaged but the large amount of time spent on the design, construction and alteration of the test rig resulted in a curtailed experimental programme concerned only with central point loading.

As demonstrated by the classical buckling analyses for these two loading conditions in Chapter 2, the maximum efficiency of a single translational restraint is achieved when the compression flange of the primary element is braced. It was decided that this level of bracing attachment should be employed throughout the experimental programme.

Although compression flange bracing was to be employed in each test, the degree of restraint afforded by the bracing (as denoted by λ) was to change from one test to the next. Consequently, some means of providing variable restraint stiffness had to be devised. Likewise, test spans had to be variable in order that beams of different slenderness could be tested. Finally, load was to be applied at either the shear centre or compression flange level of the test beam.

All tests were to be carried out under displacement rather than load control as the ability to attain and pass a test beam's experimental critical load before entering the post-buckling phase was required. Displacement control was achieved using the "loading" apparatus described later in this Chapter; hence any subsequent reference to beam "loading" should be interpreted as meaning the application of an increment of enforced displacement at a point on the beam and in the stated or implied sense of the applied "loading".

In order that the limits of applicability of the test results could be assessed at the conclusion of the experimental programme, it was imperative that details be recorded of actual support conditions, the effect of secondary restraint exerted on the beam by loading devices and other instrumentation and the maximum rate of straining employed in the tests. The detrimental effect of initial material and geometric imperfections on the load-carrying capacity of beams was emphasised in Section 1.2.2 . Consequently, measurement of geometrical imperfections and the magnitude and distribution of residual stresses in the beam was also required. Where stress-relieving was considered necessary in order to reduce the high levels of locked-in stresses, details of the process were to be obtained. Kitipornchai and Trahair[5] noted that the results of several earlier full-scale tests were difficult to interpret because some or all of these details had either not been measured or not been reported.

In addition to these physical requirements of the test programme, it was imperative that the cost of the programme be minimised. Model beams had been successfully used in previous lateral-torsional buckling studies conducted by Massey[47], Hartmann[6], Flint[59], Trahair[3] and Litle et al[96]. As in the present study, cost and ease of testing had consistently been noted to be important considerations. For these reasons and because of the considerably reduced floor area required for a model beam test programme, this type of study was preferred to a series of full-scale tests. However, prior to the planning of the experimental work, a review of the effectiveness of previous small-scale model studies was considered necessary.

4.2 The Suitability of Model Tests for the Prediction of the Lateral-Torsional Buckling Behaviour of Steel Beams

As noted in previous Chapters, the present study involves both geometrical and material non-linearity as attention is focussed on beams of short to intermediate slenderness. Hence failure is not confined to lateral-torsional buckling within the elastic range; inelastic failure is possible for more stocky beams. Harris[97] has noted that the presence of material non-linearity causes particular problems as this must be correctly modelled for the small-scale structure to be useful in predicting the behaviour of the prototype.

Dux and Kitipornchai[4] have argued that all inelastic lateral-torsional buckling tests should be performed on full-scale beams because inelastic behaviour is influenced by material and geometrical imperfections, whilst Nethercot[40,41] has shown that residual stresses cause significant reductions in the inelastic failure loads predicted by classical buckling analysis. Inevitable differences between the residual stress distributions present in model and full-scale beams were stated by Kitipornchai and Trahair[5] as one of their main objections to the use of small-scale models under inelastic conditions. However, their conclusions following a series of full-scale tests on four as-rolled and two annealed beams indicated that the effect of the residual stresses was much less significant than that due to geometrical imperfections. Reference was also made[5] to the discontinuous nature of the yielding process and hence to the physical impossibility of allowing for scale effects in the formation of yield planes in the model and prototype.

Reiterating doubts expressed in Ref. 5, Mills[98] has stated that buckling and initial yielding phenomena, which are a function of the initial state of stress, cannot be investigated using small-scale models. However, various measurements of residual stresses in as-rolled and welded beams have served only to illustrate the randomness both of patterns and magnitudes of residual stresses in these beams. Any subsequent handling of the beams causes a degree of stress-relieving and therefore the final distribution of residual stresses within an erected steel member is so unpredictable that the philosophy of neglecting residual stresses and making some allowance for this omission by using enhanced values of other initial imperfections has obvious attractions.

Similarity problems are made more acute by the unique yielding and strain hardening properties of structural steel. Machined sections of the more readily worked phosphor bronze have been used in the past in an attempt to model the plastic behaviour of steel; however, the relatively short yield plateau and high strain-hardening rate exhibited by this material result in an unacceptable incompatibility between prototype and model. Plastics too, though easily machined, are unsuitable due to the large strains which accompany first yield and to their frequent brittleness at high strains. They are also susceptible to creep at room temperature.

Trahair[3,30], reporting the results of a series of tests on slender aluminium I-section model beams has noted that the die-quenched material used was chosen specifically for its high limit of proportional stress and its low modulus of elasticity. This combination allowed tests to be carried out over a wide range of beam slendernesses, yet permitting all to be completed within the elastic range. Hartmann[6] and Flint[59] employed stainless steel and aluminium alloy model beams respectively in studies again concerned only with elastic behaviour.

The use of steel for both the model and prototype clearly fulfils the similitude requirements, although it must be conceded that fabrication of the models is both labour-intensive and time-consuming. Details of the fabrication of the model steel beams used in the present study are given in Chapter 5, where several alternative methods of fabrication are discussed.

Only a few studies concerned with the inelastic behaviour of model steel beams exist[47,96,98-101], and of these, only that of Massey[47] has been concerned with the inelastic lateral-torsional behaviour of I-beams. Although Massey's experimental programme has been severely criticised by Lay, Galambos and Schmidt[69], it should be noted that the use of model steel beams was not being questioned; rather, they questioned the validity of Massey's fundamental assumption that the force required to hold the midspan section of an I-beam completely fixed against out-of-plane movement was synonymous with the force developed in effective elastic bracing.

A recent programme of research into the effects of buckling in shell elements of offshore structures concluded[102] that "research using small-scale models has shown that this technique, with its intrinsic low cost, could be used to provide a wider base of information from which to develop an understanding of, and simple methods of analysis for, offshore welded steel structures". The problems of inelastic material behaviour and large deflections previously noted (Chapter 3) to exist in the present study were also experienced in that research, thereby increasing the importance of the above conclusion in relation to the present study and, in particular, to the model beam test programme. Owens and Dowling[100], in a short discussion of the benefits of model steel structures, have noted that "with care, model tests on steel structures can be a valuable aid in understanding elasto-plastic behaviour".

4.3 Requirements of and Construction of Test Apparatus for the Model Beam Test Programme

Following the decision to adopt a model beam test programme as the basis of the experimental investigation into the adequacy of restraint systems, a test apparatus capable of providing the necessary support, loading and restraint conditions noted in Section 4.1 was required. Details of the development of the apparatus and its associated instrumentation are presented in this Section. Fabrication of the model beams, the determination of their material properties and initial geometric imperfections and the experimental procedure employed in the tests are described in Chapter 5.

4.3.1 The Test Frame

The fundamental requirements of the test rig were that it should provide both a rigid reference frame from which to measure displacements and a reaction frame from which load could be applied to the test beam. Tests were to be conducted on model beams of low to intermediate slenderness in the range $6 < R^2 < 20$ under central concentrated loading. For the predicted typical material and geometric properties of the model beams, this was to be achieved by testing beams of span 600mm to 1000mm.

An U-frame from a previous experimental model bridge investigation was adopted as the basic structural frame. Several modifications to the frame were made during a series of fifteen preliminary tests. The frame, incorporating some of these modifications, is shown in Fig. 4.1 . Additional refinements are described in the remainder of this Chapter.

4.3.2 End Supports

The end supports were to be capable of providing simply-supported end conditions with respect to both in-plane and lateral bending actions, warping and twist. Fig. 2.1 illustrates these requirements for lateral bending, warping and twist.

The in-plane requirements were met (Fig. 4.2) by supporting the beam on hardened steel rollers; one roller was positioned in a V-groove, thereby effectively providing knife-edge support at one end of the beam; the other end of the beam was supported on an identical roller, itself placed on a ground, horizontal surface. Hence, the support conditions for in-plane bending closely approximated the theoretical simply-supported condition by allowing shortening of the span accompanying in-plane curvature.

The requirements of Fig. 2.1 were fulfilled by the adjustable knife-edged plates shown in Fig. 4.2 . These plates allowed the flanges of the beams to rotate independently in their own planes so that the beam was free to warp. Lateral displacement and twist were prevented, although a small gap of 0.05mm was left between the flanges and knife-edge at one side of the beam to ensure that the knife-edges did not "bite" into the flanges, thereby providing unwanted rotational restraint to the flanges in plan. To further reduce this tendency, a small quantity of grease was applied at each of the four points of contact between the flanges and knife-edges on each support frame.

In addition to providing simply-supported end conditions in plan and elevation as described above, it was necessary to ensure that the four corners of the mid-surface of the web at the supports were coplanar in the vertical plane. This configuration was employed throughout the experimental and theoretical work to provide compatibility of support conditions between the mathematical and physical models, thereby justifying direct comparison of numerical results provided that other similitude requirements were met. In a series of nine experimental tests, Dux and Kitipornchai[4] demanded verticality of the web at both support and load points. This requirement imposed constraints on the beam which would not occur in practice; twist and initial crookedness at load points should be determined solely by the known end conditions and measured distributions of initial twist and bow on the span. In general, a vertically applied load will not act in the instantaneous plane of the web at the loaded cross-section.

Due to small variations in flange breadths, it was not possible to enforce verticality of the web at supports merely by ensuring that the knife-edges were vertical and that the tips of the flanges touched these edges. Instead, it was necessary to use the web plumbing bracket shown in Fig. 4.3 . A lightweight two-vial spirit level was mounted on an aluminium bracket and accurate machining of the upper surface and nibs ensured that the bubble on the transverse vial was central when the nibs were placed against a vertical surface. The bracket was clamped to the web by means of a set screw passing through a small (4mm diameter) hole in the web and bearing on a similar backing bracket on the opposite side of the web. The finite size of the bracket and spirit level block meant that verticality of the web was checked at a point approximately 35mm from the support and within the test span. This error was considered to be acceptable because measured imperfections in the webs of the test beams were small and also because 35mm was a relatively small proportion of the test spans which ranged from 600mm to 1000mm.

Fig. 4.4 shows the web plumbing bracket in use. The bracket has been left in position after initial plumbing of the web and the photograph shows the beam at a later stage in the test when lateral deflection of the compression flange and twist had reached noticeable levels. The transverse vial bubble is not central, indicating that the web was no longer vertical at this cross-section; however, the bubble in the longitudinal vial has remained central, indicating little in-plane deflection at midspan. The end support frame of Fig. 4.2 is also shown in Fig. 4.4 .

4.3.3 Loading Apparatus

As noted in Section 4.1, only the case of central point loading was considered in the experimental programme. However, the ability to apply load at either shear centre or compression flange level of the cross-section was desired. Additionally, it was imperative that the transverse concentrated load should always act in a vertical direction. This had been observed by Lindner[103] to be a critical requirement in lateral-torsional buckling tests as a theoretical analysis had revealed that apparent critical loads for beams not consistently loaded in the vertical plane could exceed the "true" elastic critical loads by as much as 150%. Unfortunately, details of the theoretical analysis were not given.

As a corollary to the requirement for vertical loading throughout, there was a need to minimise the lateral restraint afforded to the test beam by the loading apparatus. All lateral restraint was to be provided by the bracing device described in Section 4.3.5 so that both the bracing force and bracing stiffness could be measured. Conversely, the stability of the beam was not to be adversely affected by any unintentional lateral force or torsional moment arising from application of nominally vertical loading.

The slotted pulley arrangement shown in Figs. 4.6 and 4.7 was employed. A slot in the upper pulley of Fig. 4.7 was cut to the shape of the cross-section of the test beam, allowing load to be applied either through the shear centre (Fig. 4.6(a)) or through the junction between the web and compression flange (Fig. 4.6(b)) depending on the position of the slot relative to the centre of the pulley. Regardless of the amount of lateral deflection or twist undergone by the beam, load was always applied through the centre of the pulley. Frictional effects in the lower pulley of Fig. 4.7 were reduced by the introduction of a high quality ball bearing between the shaft and pulley. This helped to minimise torsional restraint on the beam by allowing the upper pulley to rotate as the angle of twist on the beam tended to increase.

In preliminary tests performed during development of the experimental apparatus, a proving ring with a maximum rated load of 400 lbf (1780 N) was used to measure applied loads. The arrangement is shown in Fig. 4.8 . Load was applied to the beam by tightening the nut below the reaction plate as indicated in the figure. Deformation of the ring under load was measured by a linear variable differential transformer (LVDT) linked to a PDP-8/L data logging system. The LVDT had replaced a dial gauge (reading to 0.002mm) because it had been found to be both more sensitive and more convenient as lateral deflections of the beam were also being logged by the PDP-8/L. A major advantage of electrical sensing of both lateral displacements and load was that the readings could be taken almost simultaneously by a pulse from the logger. This was important in the present study due to the rapid changes in some or all of these quantities at loads close to the critical load and in the post-buckling range.

The LVDT used had been chosen to suit the proving ring's maximum diametric extension of approximately 2.9mm at its rated load. The full travel of the LVDT was about 5mm and consequently only the middle 60% of its range was utilised, thereby ensuring excellent linearity of displacement versus output signal response in use. The ring was calibrated in a Tinius Olsen 200,000 lbf "Electomatic" Universal Testing Machine and excellent repeatability of readings was achieved. Moreover, the calibration showed an almost perfectly linear relationship between applied load and data logger reading.

The need to maintain verticality of applied load and to minimise any lateral restraining or destabilising forces associated with load application has been stressed. Although use of the pulley system (Figs. 4.6 and 4.7) ensured that load was consistently applied through the centre of the pulley and that torsional restraining or destabilising moments were minimised, it did not guarantee that loads would be applied vertically. For this reason, controlled transverse movement of the proving ring had to be permitted. This was achieved by means of four hardened steel balls running in two V-grooves as shown in Fig. 4.8 . After each increment of load, the system was allowed to settle and the lateral displacement of the beam due to the increment was recorded. The base of the proving ring was then moved by this amount in the same direction so that the proving ring was positioned directly below the point of loading on the beam at the start of the next increment. In practice, this positioning became more difficult with increasing applied load and at high loads it was frequently impossible to move the base without disturbing the beam, thereby upsetting lateral and vertical deflection readings.

Another serious disadvantage of the proving ring system was that the self weight of the ring and base plate (totalling about 27 N) acted as a preload on the beam. Although this force was generally negligible in relation to the failure loads of the test beams (see Chapter 6), its presence demanded that all loads recorded by the data logger be increased by 27 N. For these reasons and because the proving ring was cumbersome to set up, an alternative load transducer was selected.

A Statham "Gold Load Cell" with a maximum rated load of 500 lbf (2224 N) was substituted for the proving ring. As before, automatic recording of load was possible via the PDP-8/L data logger as operation of the cell was again based on an LVDT within the cell. During tests, applied load was continuously displayed by a digital volt meter (DVM) connected to the data logger. This facility was required in order that load increments of known magnitude could be applied. It was also very useful at the onset of instability and during post-buckling deformations when small increments of enforced displacement produced sudden reductions in the load sustained by the beam.

The cell had previously been used in compression and so adjustment of the LVDT within the casing was necessary until a linear load versus output signal response was obtained for the cell acting in tension. Several calibrations were performed during the series of preliminary tests with a further two calibration checks being performed during the main series of tests reported in Chapter 6. Details of the initial cell calibrations are presented in Section 4.4 . However, it is sufficient to note here that the cell was found to be highly reliable and gave excellent repeatability.

In order that the transverse position of the load cell could be altered to maintain verticality of applied load, a "follower" carriage for the cell was devised and constructed. This is shown in Fig. 4.5 . The small load cell was able to be bolted to the carriage, thus providing a much less cumbersome arrangement than had been possible with the proving ring. An additional benefit was that the weight of the cell was carried by the carriage and consequently the only preload applied to the beam was the negligible self weight of the wire strand loop and lower pulley. Details of the carriage are given in Fig. 4.9 . The same two pulley system of Fig. 4.7 was employed but in this case load was applied to the beam by tightening the nut under the top cross member as shown in Fig. 4.9 . The lower pulley of Fig. 4.7 appears at the top of Fig. 4.5 and again in Fig. 4.9 . Adjustment of the transverse position of the carriage in sympathy with the recorded lateral deflection of the beam was made possible by the screw drive shown in Figs. 4.5 and 4.9 . Transverse movement of the carriage was detected by a Mercer dial gauge reading to 0.01mm (Fig. 4.5). This guage has been omitted from Fig. 4.9 for clarity.

A recurrent fault in one of the DVM printed circuits in the PDP-8/L data logger caused several delays in the test programme and eventually the DVM became so unreliable that a Solartron 3530 "Orion" data logging system was employed instead. Both the scanning and printing speeds of this system were superior to those of the PDP-8/L and the electronics appeared subject to less temperature drift during long tests. Up to four channels could be monitored simultaneously and continuously, allowing, for example, the effect of load application on lateral displacement to be examined. A cassette tape facility in the data logger allowed calibration factors, scanning intervals and gauge factors for foil resistance strain gauges to be stored for use in subsequent tests. Use of the Statham load cell in conjunction with the Orion data logger proved completely satisfactory during the experimental programme.

4.3.4 Measurement of Beam Displacements

Measurement of both lateral and vertical displacements at certain points on the test beams was required. Two methods of measuring deflections were available: Mercer mechanical dial gauges reading to 0.01mm and with a plunger travel of about 50mm; and Novatech type RR102 electrical displacement transducers with the same travel and a resolution of approximately 0.001 inch (0.025mm). Both of these types were used, the former being preferred for measurements where the rate of change of displacement, both during load application and in the post-buckling condition, was small. Dial gauges allowed direct readings to be taken without the need for a data logger; displacement transducers were to be preferred when simultaneous readings of rapidly changing loads, displacements and strains were required. In general, there was a greater need for rapid sensing of lateral than of vertical displacements and the use of dial gauges was restricted to measurement of the latter quantity.

Measurement of vertical deflection of the beam at midspan was carried out by a dial gauge suspended by means of a magnetic base from one of two angle-section side rails connected to the frame as shown in Fig. 4.10 . Due to the presence of the upper loading pulley at midspan, it was not possible to measure vertical deflection at exactly the same point. In practice, "central" vertical deflection was measured approximately 10mm from the midspan cross-section. However, elastic theory predicts negligible differences between the true midspan deflection and the deflection at a point 10mm from midspan. The slight error increases with decreasing span as shown in Table 4.1, but in all cases the differences are negligible.

Table 4.1: Error in Measuring Vertical Deflection 10mm from Midspan

Model beam test span (mm)	Ratio of measured to midspan vertical deflection (based on Engineer's Theory of Bending and vertical deflection measured 10mm from midspan)
600	0.9984
800	0.9991
1000	0.9994

The values shown in Table 4.1 were derived using the moment-area theorem. Details of the calculation are shown in Appendix III.

Section 1-1 in Fig. 4.10 shows the method of transmitting vertical deflection of the beam to the plunger of a dial gauge. Use of the rigid arm was necessary due to the size of the dial gauge in relation to the gap in the loop formed by the wire strand. A ball embedded in an aluminium block, itself glued to the underside of the tension flange, made point contact with a horizontal milled surface at the end of the arm remote from the dial gauge. As shown in Fig. 4.10, the vertical position of the ball does not uniquely determine the vertical position of the section centroid (coincident with the shear centre in this case) and consequently lateral deflections of the flanges relative to their initial positions were recorded in order that centroidal deflections could be deduced from dial gauge readings. The geometrical relationship between deflection and rotation of the beam and the measured vertical deflection of the ball is derived in Appendix IV(a). The correction indicated by this relationship was applied to all measured vertical deflections. The resulting vertical deflections were then consistent with centroidal deflections obtained from FINAS and NASTRAN finite element analyses.

Further preliminary tests indicated that "corrected" experimental values of centroidal vertical deflection were consistently about twice as great as theoretical predictions. Fig. 4.11 shows the observed elastic load-deflection behaviour of four 600mm span test beams. Their load-deflection characteristics differ unacceptably from the predictions of elastic beam theory for a beam with the average geometrical properties of the four test beams. Allowance for the effect of shear deformations contributed less than an additional 5% to the bending deflections on the 600mm span and consequently this was not the major source of error.

Several other possible reasons for the discrepancy were investigated and eventually the problem was traced to deflection of the test rig under load: the overall rigidity of the test frame had been increased by attachment of the two side rails (Fig. 4.10) and therefore appreciable deformation of the outer frame was considered unlikely. However, when inverted dial gauges clamped to the side rails were used to measure vertical deflection of the support plates, significant deflections were observed during beam loading. A strategy of measurement rather than attempted prevention of these deflections was adopted and in all subsequent tests the vertical deflection of the web/compression flange junction of the test beam was recorded at each end support.

In the determination of actual centroidal vertical deflections of a beam at midspan, two corrections to measured midspan vertical deflections were required: first, the average support deflection was calculated and subtracted from the measured deflection of the ball at midspan to give the actual midspan movement of the ball due to deformations of the beam; the centroidal deflection of the beam was then calculable from the measured midspan angle of twist and the twist correction 'τ' derived in Appendix IV(a). Corrections 1 and 2 in Appendix IV(c) illustrate the application of these support and twist corrections to actual test data.

Fig. 4.12 shows support and midspan deflections measured during a preliminary test on a 600mm span beam. Corrected midspan deflections are seen to be approximately 18% larger than those predicted by beam theory. Although still large, this error was assumed to be cumulative from small errors in measured E and I values, measured deflections and the inherent conservativeness of deflections predicted by simple elastic beam theory. Subsequent comparison of finite element and experimental deflections in the main series of model tests showed excellent agreement (Chapter 6).

At the commencement of the series of preliminary model tests, a system of measurement of lateral deflections similar to that employed by Massey[11] was envisaged. This permitted lateral deflections of the flanges to be measured using dial gauges, and corresponding angles of twist calculated. A free-standing frame was constructed to straddle the test frame and to support the pulley and dial gauge system shown schematically in Fig. 4.13 . Wire strands soldered to the flanges were tensioned by counterbalance weights and a dial gauge was connected "in series" with each strand to measure lateral deflection of the flange. Frictional effects at the pulleys were reduced by running each on a ball bearing.

In setting up this system prior to each of the few preliminary tests in which it was employed, a small spirit level was suspended from the taut cross wire on each side of each flange and the level of the pulleys adjusted until the wires were horizontal. This operation could only be carried out when the beam and its end support frames had been set up according to the web plumbing procedure described in Section 4.3.2 . Unfortunately, the process of levelling the cross wires of Fig. 4.13 demanded vertical adjustment of the four pulleys and caused unavoidable disturbance of the test beam. Consequently, the need for the beam's initial midspan crookedness and twist at the start of a test to be determined solely by its initial geometrical imperfections and support conditions was violated.

Moreover, at the outset it had been anticipated that the system of Fig. 4.13 would later be modified to provide midspan restraint of predetermined stiffness to the test beam. An arrangement similar to that employed by Massey in Ref. 47 had been envisaged in which the strands would fulfil a dual purpose by providing both the required restraint stiffness and the mechanical link to the appropriate dial gauge. The pitfalls of Massey's bracing system, described in Chapter 1, were to be avoided by providing restraint of finite rather than infinite stiffness. Further examination revealed the apparent impossibility of reconciling the need for wires of low axial stiffness anchored to an immovable point on the test frame with that for accurate measurement of lateral deflections, requiring freedom of movement of the beam and counterbalance weights. Furthermore, preliminary calculations based on values of λ_{cr} for elastic systems from Chapter 2 suggested that typical axial stiffnesses of wire strand were far in excess of the restraint stiffnesses to be investigated in the main series of tests (see Section 4.3.5).

For all these reasons, and because anticipated frictional effects in the dial gauges and at the pulleys would have imposed unquantifiable midspan restraint to test beams, all lateral deflections at midspan and at one quarter point were subsequently measured by 50mm travel Novatech displacement transducers clamped to the side rails as shown in Fig. 4.14 .

To accommodate vertical movement of the flanges relative to the transducers, a vertical cross piece was attached to the tip of the stainless steel shaft and, to prevent rotation of the central shaft, a second shaft was attached to the cross piece and guided in a slotted block affixed to the body of the transducer. In this way, the cross piece remained vertical as shown in Fig. 4.14 . A lead provided the electrical connection initially to the PDP-8/L and subsequently to the Orion data logger, enabling simultaneous readings of load and lateral deflection to be taken.

In order to minimise the lateral restraint or destabilising force imposed on the flanges by the transducers, the compression return springs within the transducers were cut and the remaining piece of spring stretched to the length of the original spring. The spring stiffness was consequently reduced to 0.06 N/mm, representing only 0.23% of the smallest restraint stiffness employed in the main series of tests. Nevertheless, further precautions were taken to ensure that the restraining or destabilising influence of the transducers was minimised during tests. These precautions are described in Section 5.7 .

4.3.5 The Provision of Finite Lateral Restraint Stiffness at Midspan

As noted in Section 4.1, the experimental programme was to be concerned with the minimum requirements of compression flange lateral bracing necessary for the complete midspan restraint of simply-supported beams under central point loading. Stiffness of the single midspan restraint was to remain constant during each test but was to vary from test to test to allow the effectiveness of different restraint stiffnesses to be assessed for beams of constant span. A direct method of measuring forces induced in the bracing was also required. Criticism[69] of Massey's experimental method[47] of measuring lateral bracing forces was discussed in Section 1.2.5, where the importance of measuring bracing forces associated with restraints of finite rather than of infinite stiffness was emphasised.

Adoption of a modified form of Massey's bracing system, combining measurement of lateral deflections with the provision of midspan lateral restraint was discussed in the preceding Section. Development of such a system was halted for the reasons stated there. Separate systems to perform these functions were then developed.

On the preliminary assumption that restraint stiffnesses of the same order of magnitude as those required for the enforcement of second mode buckling in Chapter 2 would be used in the test programme, it was estimated that the system of bracing would be required to provide minimum values of λ of about two or three (Fig. 2.22). The definition of λ in eqn. (1.2) and the predicted typical geometrical properties of the model beams were used to deduce that the minimum restraint stiffness required of the bracing system would be approximately

$$K_{min} = \frac{48 E I_\eta \lambda_{min}}{\ell^3_{max}}$$

$$= \frac{48 \times 205000 \times 583 \times 2}{(1000)^3} = 11.5 \text{ N/mm}$$

Axial stiffnesses of different lengths of wire strand were calculated to examine the possibility of compression flange restraint of this stiffness being provided by the strand. Taking Young's Modulus of the strand to be that of mild steel (typically 205kN/mm^2), the axial stiffness of a strand of 0.5mm effective diameter and of length L=0.5m was

$$K = \frac{A_x E}{L} = \frac{\pi \times 0.5^2 \times 205000}{4 \times 500}$$

$$= 80.5 \text{ N/mm}$$

which is seen to be considerably greater than the minimum estimated stiffness of 11.5 N/mm. The use of wire strand or fine piano wire was therefore ruled out on the grounds that an excessive length of small diameter wire would have been required in order to provide the required minimum stiffness.

As considerably smaller lateral stiffnesses were evidently attainable by utilising the flexural rather than axial properties of potential bracing elements, a system based on the flexural stiffness of a cantilever was devised in which a two-pronged "bracing fork" provided a predetermined lateral restraint stiffness to the compression flange of the test beam. The principle of operation of the system is shown in Figs. 4.15 and 4.16 .

Each tip of the compression flange made contact with the side of a length of 3/16 inch (4.762mm) diameter Stubbs steel rod Ⓐ, the upper, threaded portion of each rod being screwed into an 18mm diameter rigid cylinder Ⓑ. The cylinders Ⓑ were secured to a close tolerance block Ⓒ by nuts Ⓓ to form the bracing fork assembly. Ground vertical faces on block Ⓒ permitted only vertical sliding relative to the ground, close tolerance inside faces of the side walls Ⓔ, rear plate Ⓕ and front cover plate (not shown). Vertical movement of the bracing fork assembly (Ⓐ-Ⓓ) was controlled by four threaded rods Ⓖ which penetrated the box through tapped holes in the top plate and bottom returns of the side plates. These allowed clamping of the bracing fork assembly at any desired level relative to the beam, a necessary requirement as the lateral restraint stiffness of the bracing was determined by dimension 'a_f' (Fig. 4.16), the distance from the root of the cantilever to the point of contact between flange and fork.

Neglecting the effect of shear deformations, beam theory predicted the lateral stiffness of restraint provided by the fork to be

$$K = \frac{3(EI)_{fork}}{a_f^3}$$

Eqn. (1.2) could then be used to calculate the required active leg length 'a_f' for a given value of λ:

$$a_f = \ell \left(\frac{(EI)_{fork}}{16\lambda\,(EI_\eta)_{beam}} \right)^{1/3} \qquad \text{...(4.1)}$$

The bracing "box" containing the sliding bracing fork assembly was supported by two brackets clamped to the side rails as shown in Fig. 4.16, thereby preventing movement of the box relative to the test frame. Constant lateral restraint could only be provided if the bracing forks moved in sympathy with the vertical movement of the beam's compression flange in order that dimension 'a_f' remained constant during the test. At the end of each increment of applied load, the required vertical movement of the forks was calculated by the methods described in Appendices IV(b) and IV(c). The forks were then repositioned according to this calculated movement so that the correct restraint stiffness was achieved at the start of each load increment. Vertical movement of the forks was measured by the dial gauge shown in Fig. 4.16 . The specimen calculation labelled "Correction 3" in Appendix IV(c) shows that the effect of the twist correction τ_1, is insignificant for small angles of twist at midspan. Only in the proximity of the buckling load and in the post-buckling range does the τ_1 term play a significant role.

Although the dial gauge shown in Fig. 4.16 allowed the vertical position of the fork to be set, it did not eliminate the possibility of a slight rotation of the bracing fork in the plane of the beam cross-section. The accurately machined and ground deep vertical faces of block Ⓒ (Fig. 4.5) and those of the enclosing four plates of the box, coupled with the close tolerance fit-up achieved between these parts ensured that rotations of this nature would be minimised. Nevertheless, any such rotation would have allowed apparently free lateral deflection of the beam flange, as the flange movement would not have been opposed by the flexural stiffness of the prong. Consequently, small movements of the flange giving rise to no change in bracing force would have been possible. A spirit level was attached to header block Ⓒ by means of the bracket shown in Fig. 4.17 . Use of the spirit level during enforced "vertical" movement of the bracing fork ensured that the prongs remained truly vertical; therefore all lateral flange movement was accompanied by bending of one of the prongs. The completed bracing fork system is shown in use in the photographs of Figs. 4.18 to 4.21 .

Forces induced in the bracing forks as a result of their restraining action on the beam were deduced from recorded strains in small electrical resistance foil strain gauges, Ⓗ in Fig. 4.15 . These gauges had an active length of 3mm, their longitudinal axes running parallel to the length of the prongs. Four gauges were stuck to the two prongs of the bracing fork using the recommended cyanoacrylate adhesive and no peeling of gauges was observed during the tests. The gauges were so arranged (Fig. 4.16) as to record the maximum strains in the prongs at a level 6mm below their fixed ends, these strains arising from lateral loading applied by the beam flange. The centres of the four gauges lay on a line perpendicular to the longitudinal axis of the test beam in plan view.

Initially a Vishay P-350A Digital Strain Indicator was used to read each of the four strain gauges in turn. An identical dummy gauge common to the four active gauges was used in a half-bridge arrangement to compensate for changes in ambient temperature. Following replacement of the PDP-8/L data logger by the Orion system, the Vishay Strain Indicator was no longer used and strains were recorded by the Orion system. This permitted strain readings to be taken simultaneously with load cell and displacement transducer readings.

Excessive bending of the prongs occurred in several tests and consequently yielded prongs had to be replaced after each test. The mechanical properties of the Stubbs steel of which the prongs were made (Section 4.4) dictated that replacement be carried out when the strain at the fixed end of the prong exceeded 2600 $\mu\epsilon$. Replacement was facilitated by the ability to unscrew the prongs Ⓐ in Fig. 4.15 from the upper cylinders Ⓑ. A die was used to thread the upper section of the replacement rod which was then screwed tightly into the tapped hole in the upper cylinder. Two strain gauges were then fixed to the new prong and the prong calibrated as described in Section 4.4 .

Bracing forces were calculated from strain readings on the basis of calibration factors derived as described in Section 4.4 . The calibration factor for a prong allowed measured elastic strains in the prong to be converted into equivalent bending moments. Strains in excess of the yield strain of the prong material (approximately 2600 $\mu\epsilon$) were also converted to equivalent moments on the basis of a theoretical expression for inelastic bending discussed in Section 4.4 .

Determination of brace forces from the elastic or inelastic moments derived from strain readings was based on the following analysis. During a test, the compression flange of a test beam was laterally restrained by the bracing fork as shown in Fig. 4.22(a). The restraint stiffness was determined by the active leg length 'a_f' whilst the distance between the centre of the strain gauge and the midplane of the compression flange was (a_f-6)mm. M_{0L} and M_{0R} were used to denote any small initial moments which might exist at the gauge cross-sections in the left and right prongs as a result of setting up the fork; F_{0L} and F_{0R} were the corresponding forces on the prongs at the points of contact with the flange. The initial net lateral force acting to the right on the beam was then $(F_{0L}-F_{0R})$ (Fig. 4.22(b)). At the end of a load increment the strain gauge readings indicated moment changes of ΔM_L and ΔM_R in the left and right prongs, respectively (Fig. 4.22(c)). These were accompanied by changes ΔF_L and ΔF_R in the lateral forces on the beam. The strain gauge readings were dependent only on these incremental values and not on the initial values. That is to say, the initial net lateral force on the beam could not be determined from initial or subsequent strain measurements.

The net lateral force on the beam towards the right was then equal to the initial net force plus $(\Delta F_L - \Delta F_R)$. For either elastic or inelastic bending in the prongs,

$$\Delta M_L = \Delta F_L (a_f - 6)$$

and

$$\Delta M_R = \Delta F_R (a_f - 6)$$

from which

$$\Delta F_L = \frac{\Delta M_L}{(a_f - 6)}$$

and

$$\Delta F_R = \frac{\Delta M_R}{(a_f - 6)}$$

Thus, net lateral force (acting to the right) on beam

$$= \left(F_{OL} - F_{OR}\right) + \frac{\Delta M_L - \Delta M_R}{(a_f - 6)}$$

If it is assumed that the initial net lateral force $(F_{OL}-F_{OR})$ is negligible in comparison with bracing forces arising during the test, then

net lateral force (acting to the right) on beam

$$= \frac{\Delta M_L - \Delta M_R}{(a_f - 6)} \qquad \ldots(4.2)$$

As ΔM_L and ΔM_R at any stage in a test represented the changes in bending moment from initial values M_{OL}, M_{OR}, the net bracing force on the beam at any stage could be determined from strain gauge readings. In performing this conversion, firstly either the calibration factors for elastic bending of the prongs or the theoretical expression of Section 4.4 for inelastic bending was applied; secondly, eqn. (4.2) was used to determine the net lateral bracing force.

4.4 Calibration of Instruments and Bracing Forks

In this Section, calibrations of the Statham load cell, Novatech displacement transducers and bracing forks with the Orion data logging system are described.

4.4.1 Calibration of Statham Gold Load Cell

As noted in Section 4.3.3, the 500 lbf capacity load cell was adjusted to permit its use in tension. Prior to its use in the model beam test programme, calibration of the cell was performed in a 200,000 lbf capacity Tinius Olsen "Electomatic" Universal Testing Machine operating in its 0-2000 lbf range. The output signal from the load cell was fed into the Orion data logger and three load/unload cycles up to the full rated load of the cell performed. Increments of 50 lbf (222.4 N) and 40 lbf (177.9 N) were employed and the scatter of recorded data about the best fitting line was negligible as shown in Fig. 4.23 . Electrical connections from the load cell were compatible with a full-bridge measurement of strain on the Orion logger and consequently the ordinate of Fig. 4.23 is presented in terms of measured strain. Applied load (N) is shown on the abscissa.

The best fitting line in Fig. 4.23 gives a calibration factor of

$$\frac{2200\,\mathrm{N}}{10400\,\mu\epsilon} = 0.21154\ \mathrm{N}/\mu\epsilon$$

which was stored on the cassette tape used by the Orion logger and subsequently used by the logger to convert the input signal to an equivalent load which was then displayed on the logger screen.

Two single load-unload check calibrations were performed during the main series of model beam tests. These served to verify the long-term consistency of load cell readings and justified the continued use of the above calibration factor.

4.4.2 Displacement Transducer Calibration

Linked to the Orion data logger, the four 50mm travel Novatech displacement transducers were calibrated in a purpose-made vernier calibration device in which the transducer barrel was clamped and displacements of the shaft tip could be enforced to the nearest 0.002mm. Calibration of the transducers was performed in increments of 1mm over the central 45mm of their 50mm travel and observed linearity of response was excellent. The following table lists the calibration factors for the four transducers when used with the Orion data logging system.

Table 4.2: Calibration Factors for Novatech Displacement Transducers

Transducer	Transducer location during test	Calibration factor ($mm/k\Omega$)
A	compression flange, 1/4 point of span	6.896
B	tension flange, 1/4 point of span	6.795
C	compression flange, midspan	6.886
D	tension flange, midspan	6.781

4.4.3 Bracing Fork Calibration

Prior to the calibration of any bracing forks, tensile tests were performed on two 100mm lengths of 3/16 inch (4.76mm) diameter Stubbs steel rod cut at random from the delivered batch of ten 13-inch lengths. Tensile tests were performed in the Tinius Olsen testing machine previously described and a Tinius Olsen type S-2 extensometer was linked to a drum plotter which produced a load-strain curve as the test proceeded. Based on the average cross-sectional dimensions of the specimens, stress-strain curves for the material were derived and the following material characteristics deduced from the "average" stress-strain curve shown in Fig. 4.24:

$$E = 196.9 \text{ kN/mm}^2$$
$$\epsilon_y \doteq 0.0026$$

The maximum strain rate employed in the plastic range of tensile tests was less than the recommended maximum value of 300 microstrain per minute quoted in Ref. 104. It was assumed that the compressive and tensile stress-strain characteristics of the prong material were identical.

The elastic behaviour of each bracing prong in bending was investigated prior to the use of the prong in a model test. The bracing fork assembly was clamped horizontally in the rubber jaws of a vice to prevent damage to the ground surfaces of the clamped block Ⓒ (Fig. 4.15). A shallow circumferential groove had been machined close to the end of each prong and at a known distance from the centre line of the strain gauges as shown in Fig. 4.25 . A single strand wire loop was then located in the groove and used to support a lightweight (0.448 N) aluminium load hanger. Dead weights were then added to the load hanger in 2N increments. Strain gauge readings corresponding to known applied bending moments at the gauge section were taken for the two gauges on the prong. The absolute values of the two gauge readings were then averaged to give an average gauge strain for each value of applied bending moment at the gauge cross-section. Loading was continued until the measured strains approached the known yield strain ϵ_y and then the prong was unloaded in decrements of 2N.

A value of (applied moment)/(corresponding average absolute gauge strain) was calculated for each increment of load during loading and unloading. These values were then averaged to give the prong calibration factor relating measured strains to applied bending moment. Using the calibration factor in conjunction with eqn. (4.2), bracing forces could then be derived from measured fork strains. Values of the prong calibration factor used in tests ranged from 2.068 Nmm/$\mu\epsilon$ to 2.248 Nmm/$\mu\epsilon$, reflecting slight differences in the flexural rigidities (EI) of the prongs and also small positional errors in the fixing of strain gauges.

As noted in Section 4.3.5, the calibration factor was only applicable to the case of elastic bending of the prongs and consequently a theoretical expression for inelastic bending of the prongs was derived. This was based on a tri-linear approximation to the stress-strain curve for the material shown in Fig. 4.24 . Appendix V contains the derivation of this moment-strain relationship which was used in place of the calibration factor for the conversion of all measured strains in excess of $2600\mu\epsilon$. Table 4.3 summarises the formulae applied to strain readings to obtain corresponding bending moments at the gauge cross-section. In this table, the notation of Appendix V has been adopted:

ϵ_{max} = mean value of absolute bending strains

(eg. if $\epsilon_1 = -16\mu\epsilon$ and $\epsilon_2 = 14\mu\epsilon$,

$\epsilon_{max} = 0.000015$)

r = radius of bracing prong in mm (= 2.381mm)

$$y_1 = \frac{\epsilon_y r}{\epsilon_{max}} = \frac{0.0026r}{\epsilon_{max}} \quad \text{(mm)}$$

$$\theta_1 = \sin^{-1}(y_1/r) \quad \text{(rad)}$$

$$y_2 = \frac{0.0044r}{\epsilon_{max}} \quad \text{(mm)}$$

$$\theta_2 = \sin^{-1}(y_2/r) \quad \text{(rad)}$$

$$\gamma_1 = r^4/y_1 \quad (\text{mm}^3)$$

Table 4.3: Moment-Strain Relationships used in Deriving Brace Forces from Measured Bracing Fork Strains

Mean absolute bending strain ϵ_{max}	Factor or formulae to be applied to ϵ_{max} to derive corresponding bending moment M (Nmm)
$\epsilon_{max} \leqslant 0.0026$	use prong calibration factor ie. M = (calibration factor)$\cdot\epsilon_{max}$
$0.0026 < \epsilon_{max} \leqslant 0.0044$	$M = 154657r^3\epsilon_{max} - 72.96\gamma_1(\pi - 2\theta_1 + \sin 2\theta_1) - 97.3y_1{}^3\cot\theta_1 + 389.13r^3\cos\theta_1$
$\epsilon_{max} > 0.0044$	$M = 154657r^3\epsilon_{max} + 145.92\theta_1\gamma_1 - 72.96\gamma_1\sin 2\theta_1 + 389.13r^3\cos\theta_1 - 97.3y_1{}^3\cot\theta_1 + 87.82\theta_2\gamma_1 - 43.91\gamma_1\sin 2\theta_2 + 396.31r^3\cos\theta_2 - 99.07y_2{}^3\cot\theta_2 - 116.87\pi\gamma_1$

4.5 Conclusions

An experimental programme concerned with the determination of minimum translational stiffness criteria to be met by bracing systems in order to provide full midspan restraint to beams of low to intermediate slenderness was required. In addition, bracing forces arising from the restraint of such beams were to be measured.

A study of the literature concerned with previous structural investigations using steel models revealed that, with care, tests on both elastic and inelastic model steel structural elements could provide useful results. The presence of different residual stress patterns in model and prototype beam sections and an inability to make allowance for scale effects in the formation of yield planes were noted to be the main objections to the use of model beams in an experimental programme. Nevertheless, a model test programme offered the additional advantages of low cost and a requirement for a much reduced area of test floor. The cost factor was of considerable importance as the beams were to be tested under inelastic conditions and consequently their re-use in subsequent tests was not possible.

A series of fifteen preliminary tests on model beams was performed during development of the test rig and its associated instrumentation. These tests also allowed an experimental procedure to be devised for later use in the main series of tests. Problems encountered during the development of systems for the end support of beams, load application, displacement measurement and midspan bracing have been described. Reference has also been made to the associated data logging and strain measurement systems. Finally, the calibration of load and displacement transducers was described and a method proposed for the calculation of bracing forces from measured bracing fork strains.

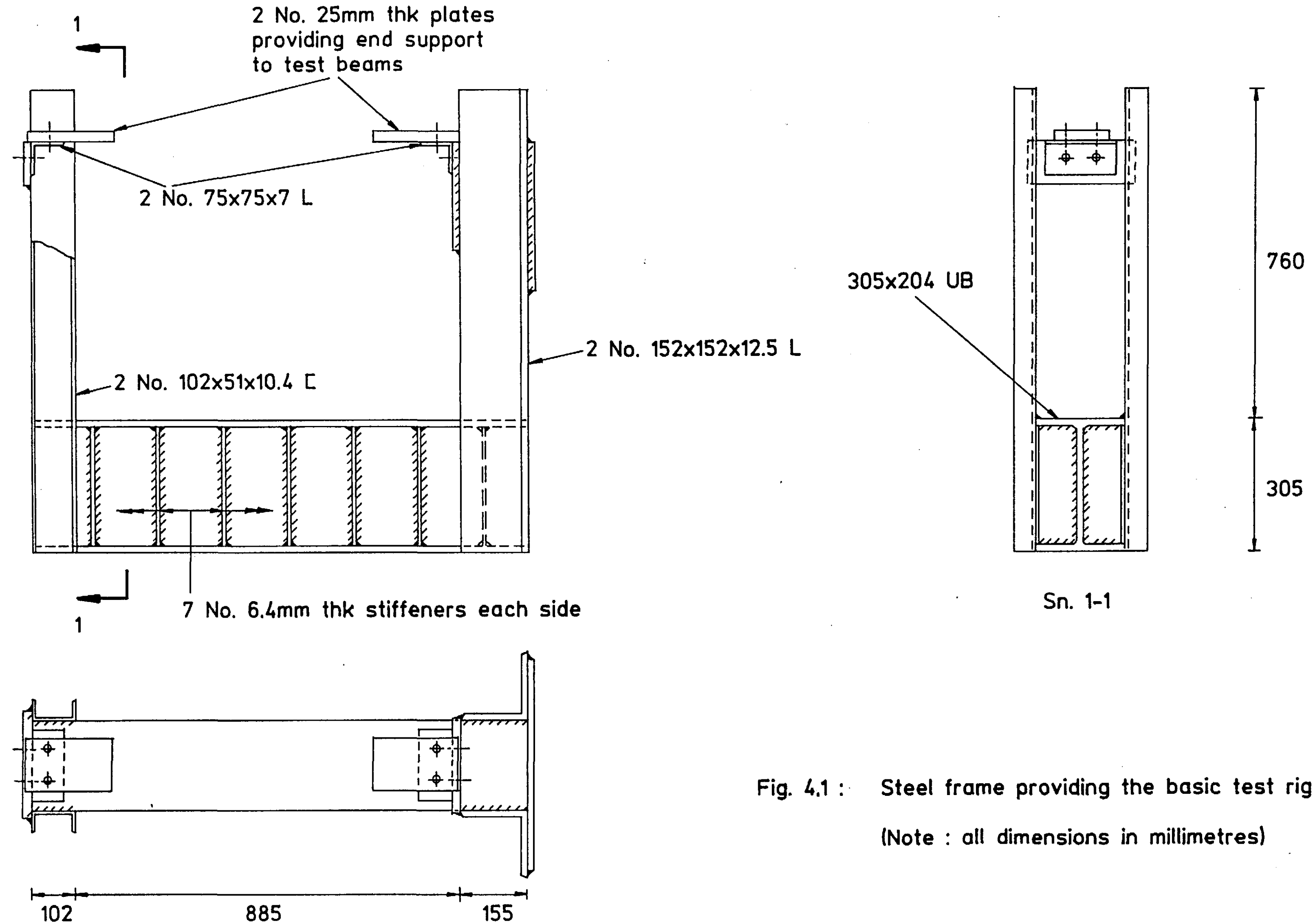

Fig. 4.1 : Steel frame providing the basic test rig

(Note : all dimensions in millimetres)

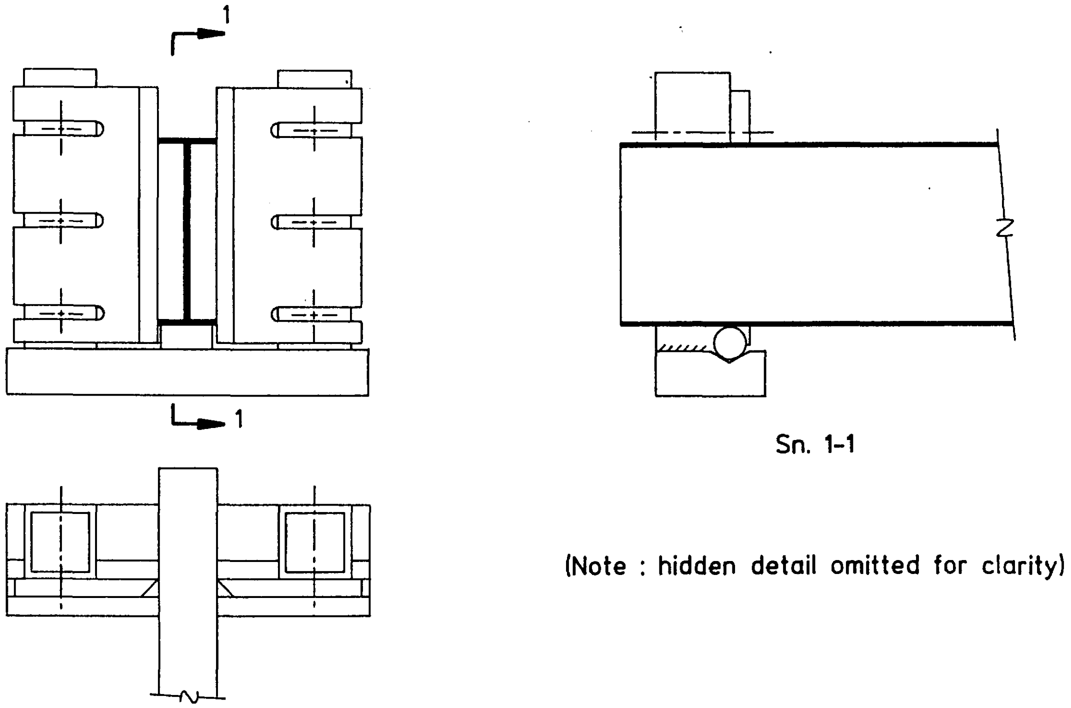

Fig. 4.2 : Details of one end support frame for model beams. Similar frame (incorporating roller to permit longitudinal movement) at other end

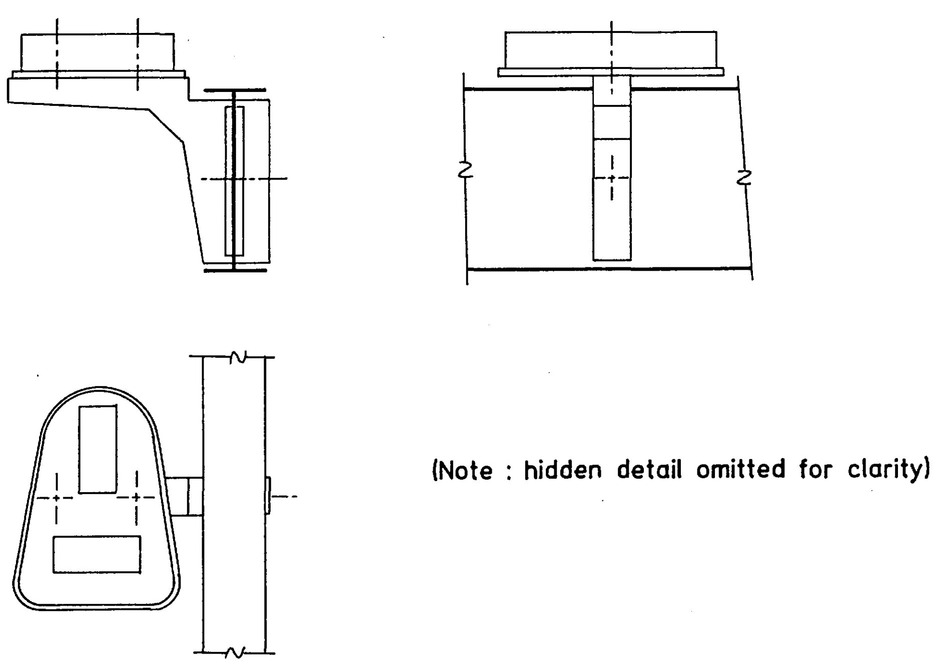

Fig. 4.3 : Web plumbing device

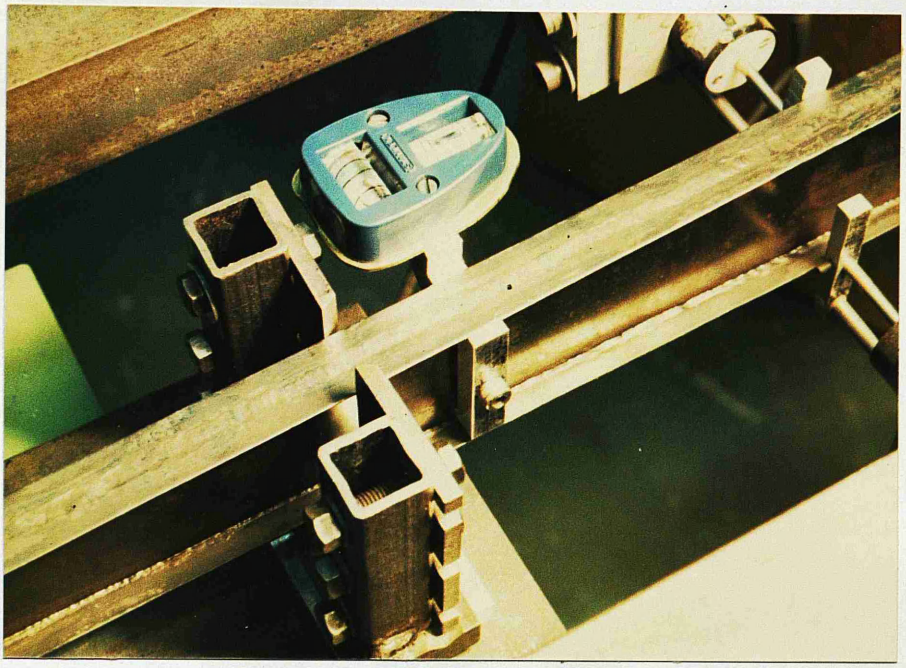

Fig. 4.4 : Support frame of Fig. 4.2 and web plumbing bracket of Fig. 4.3 attached to beam during test

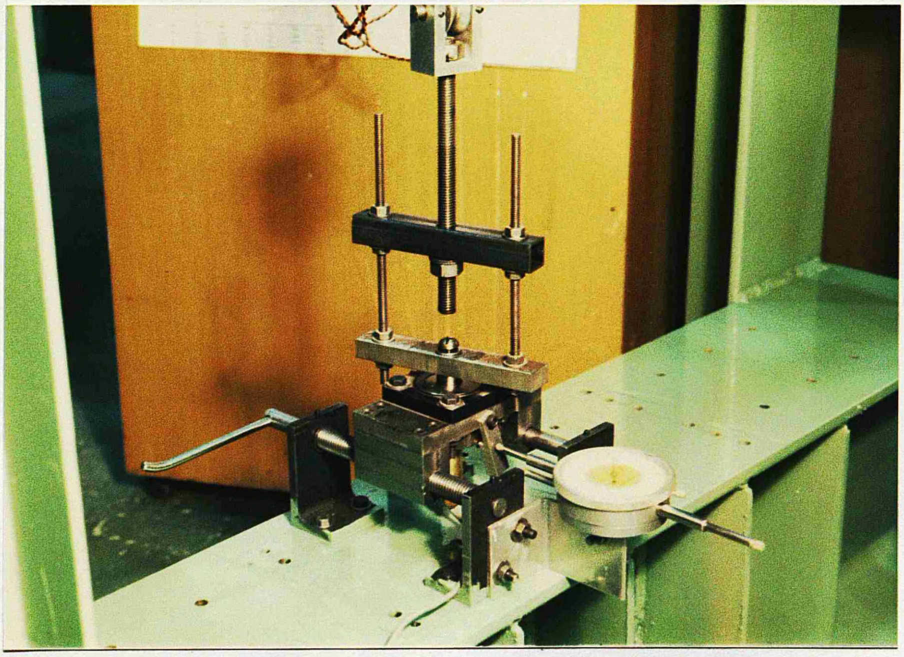

Fig. 4.5 : Load cell carriage and lower linkage of pulley system for applying central point load to model beams

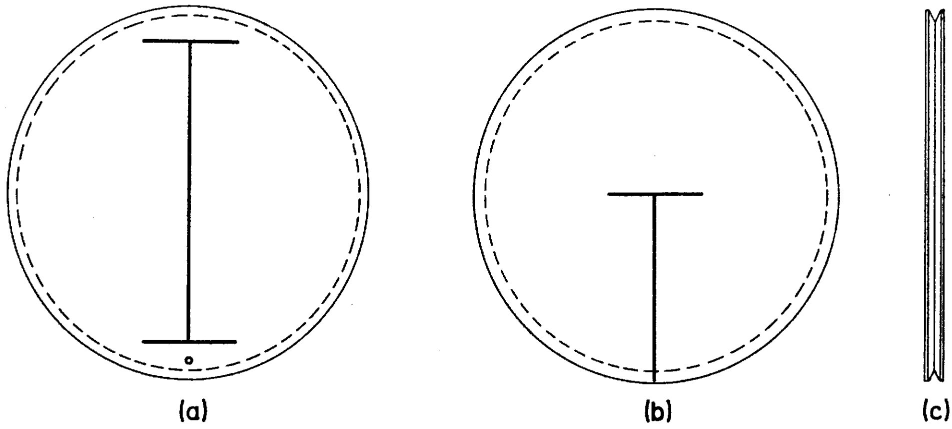

Fig. 4.6 : Slotted pulleys for applying load through the shear centre (a) and web/compression flange junction (b) of the model beam

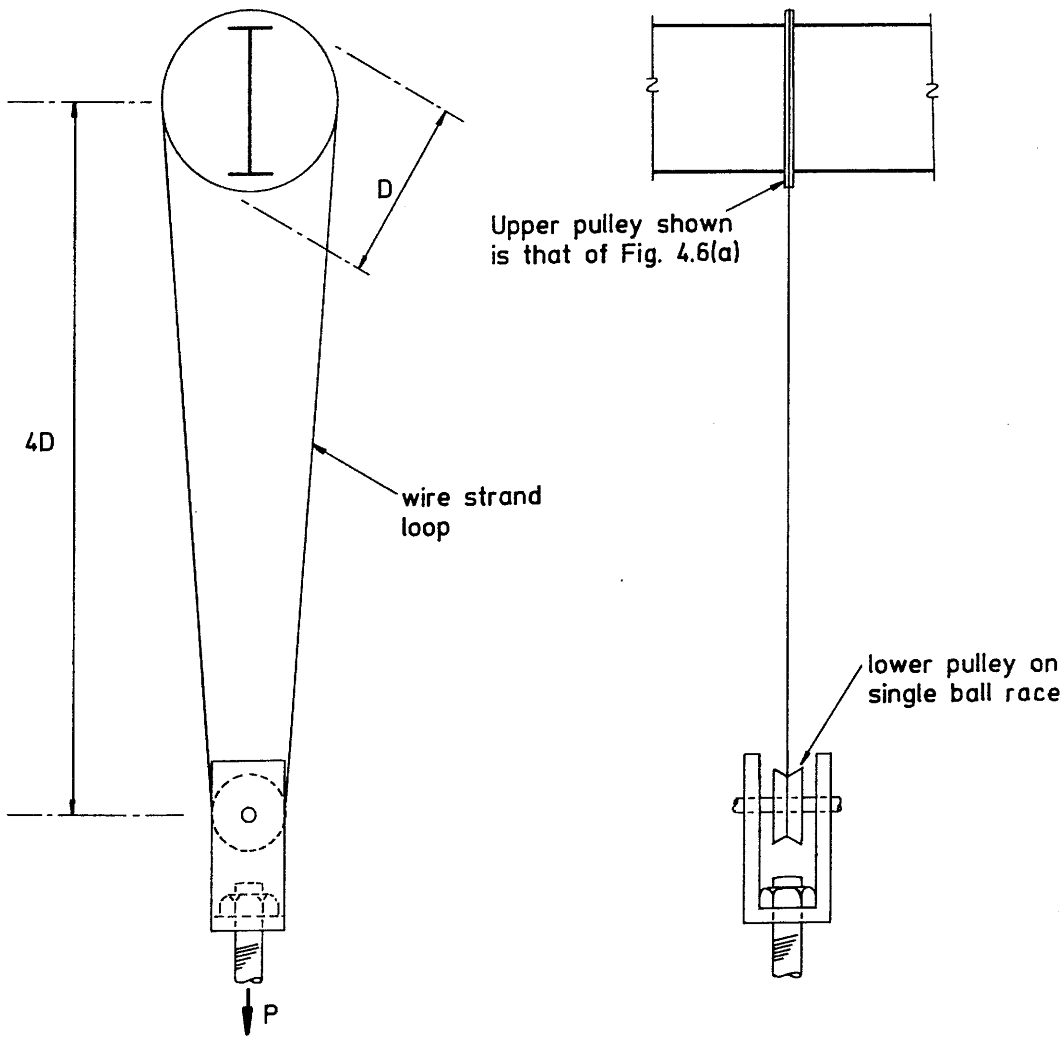

Fig. 4.7 : Pulley arrangement for loading beam. Load 'P' applied through lower linkage shown in Fig. 4.5

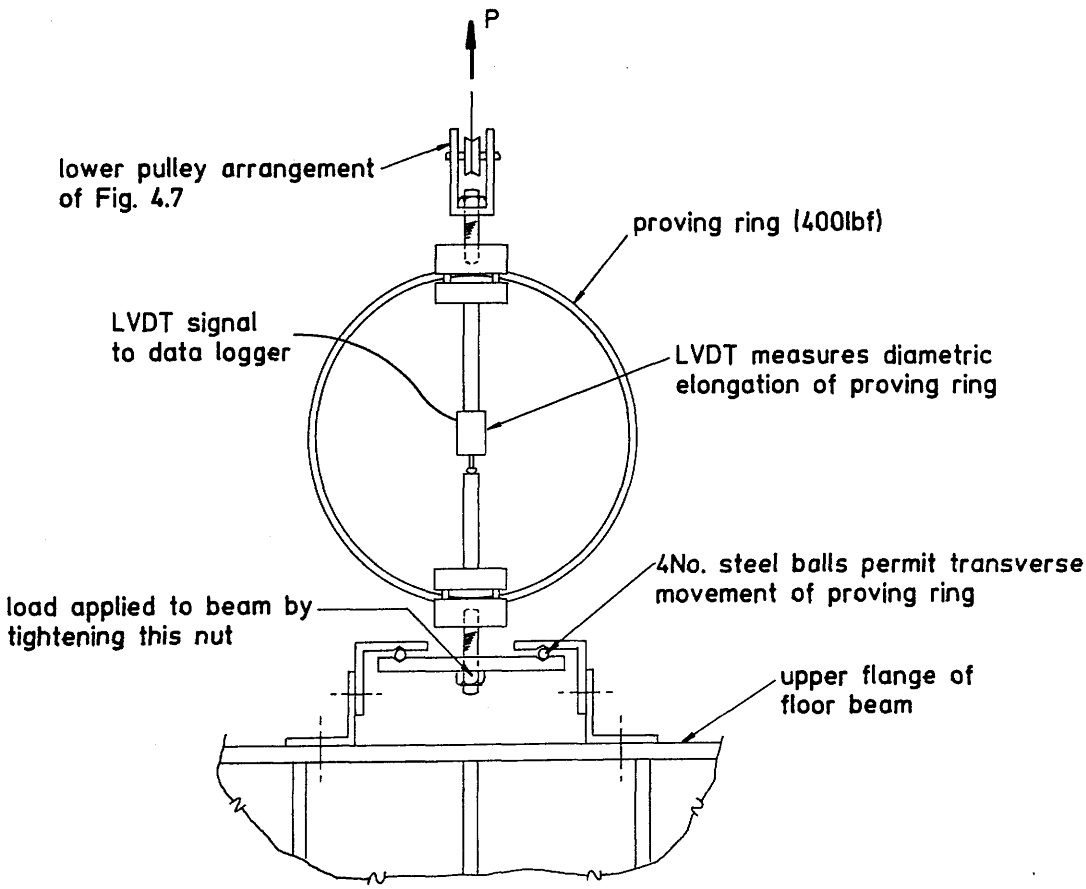

Fig. 4.8 : Proving ring and LVDT used to measure load applied to model beam

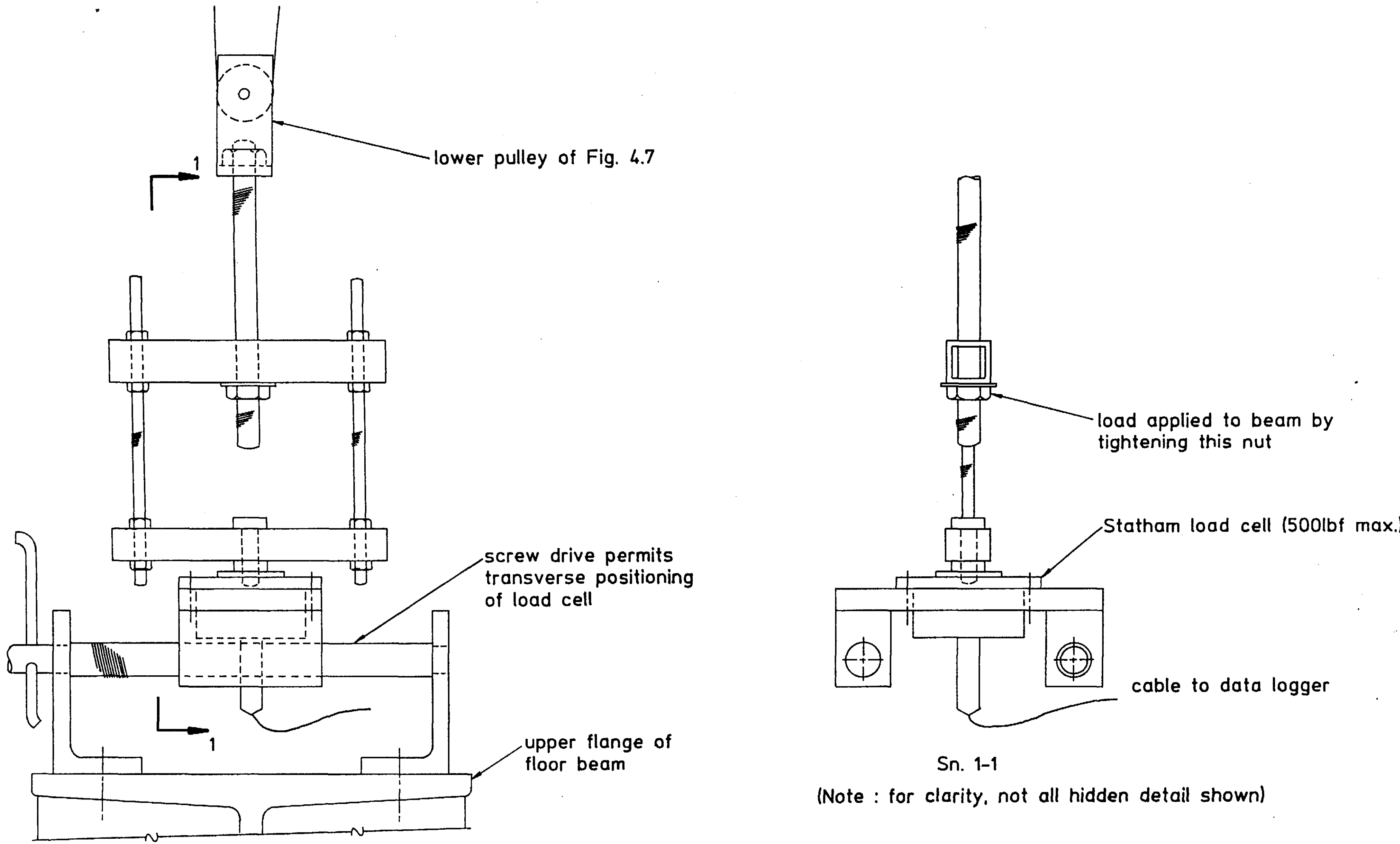

Fig. 4.9 : Follower carriage for Statham load cell. Dial gauge measuring transverse displacement of carriage (shown in Fig. 4.5) omitted for clarity

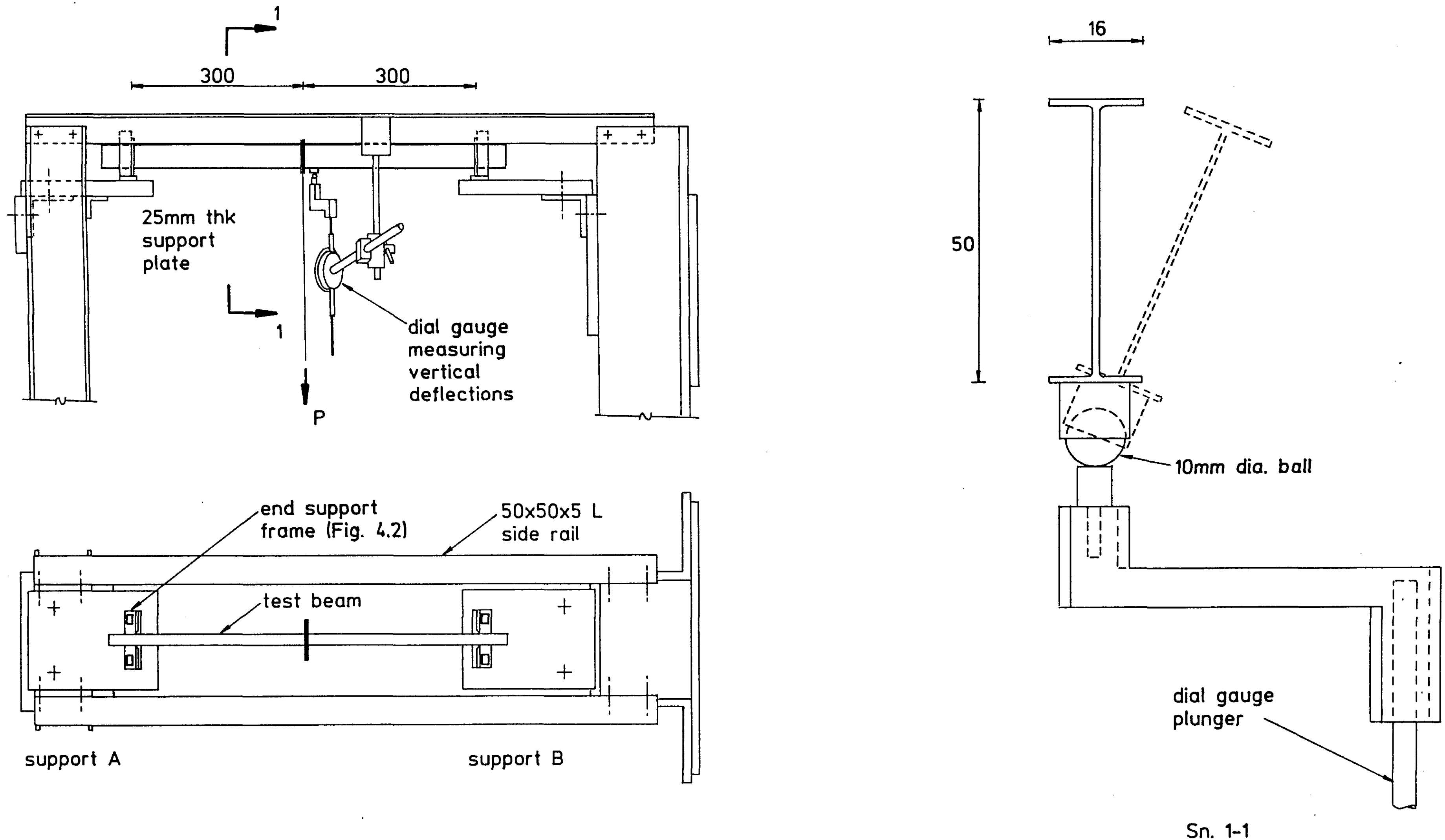

Fig. 4.10 : Upper part of test rig showing method of measuring vertical deflection adjacent to midspan during 600mm span beam test (see also Fig. 4.20)

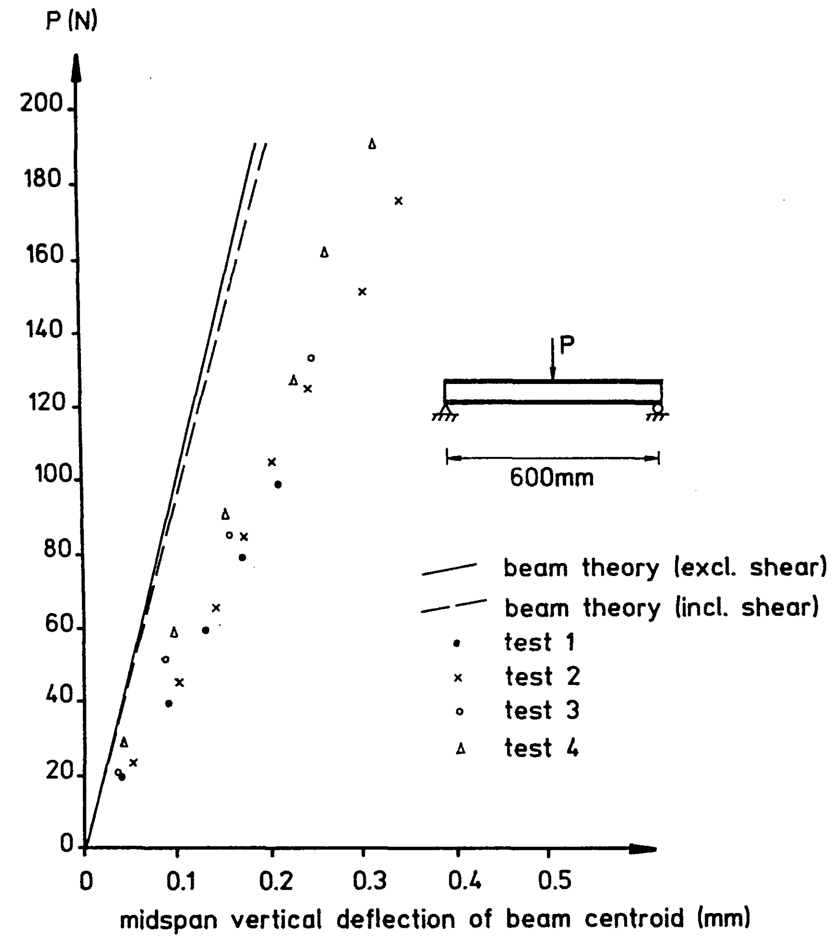

Fig. 4.11 : Discrepancy between experimental and theoretical vertical deflections observed during preliminary tests

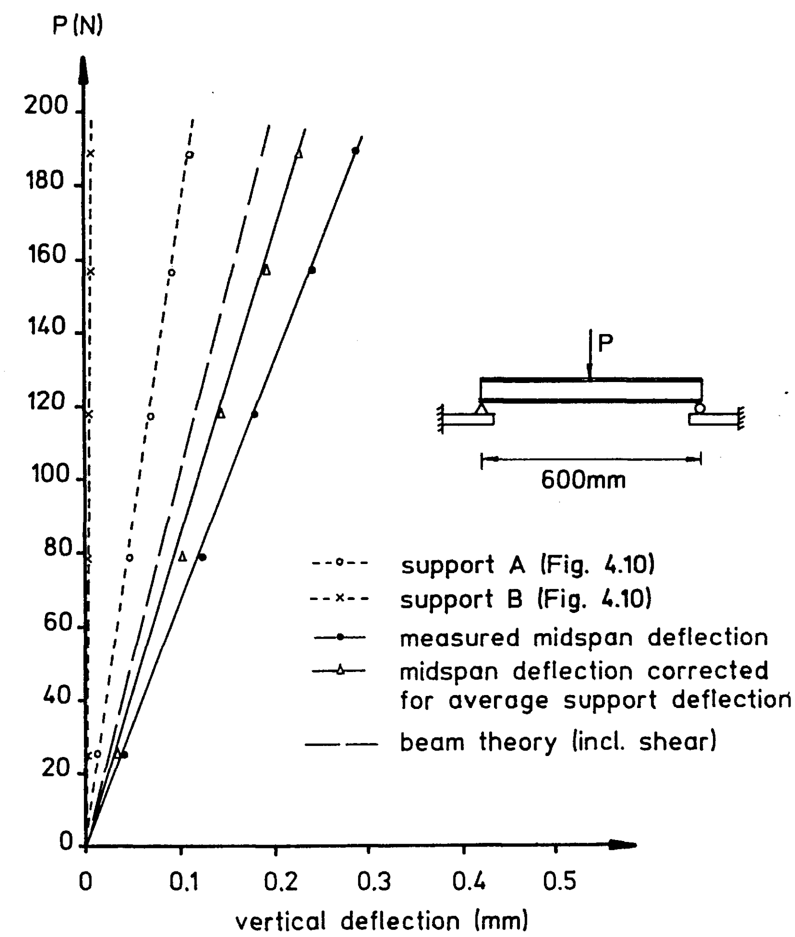

Fig. 4.12 : Measured support deflections and corrected midspan vertical deflection of test beam

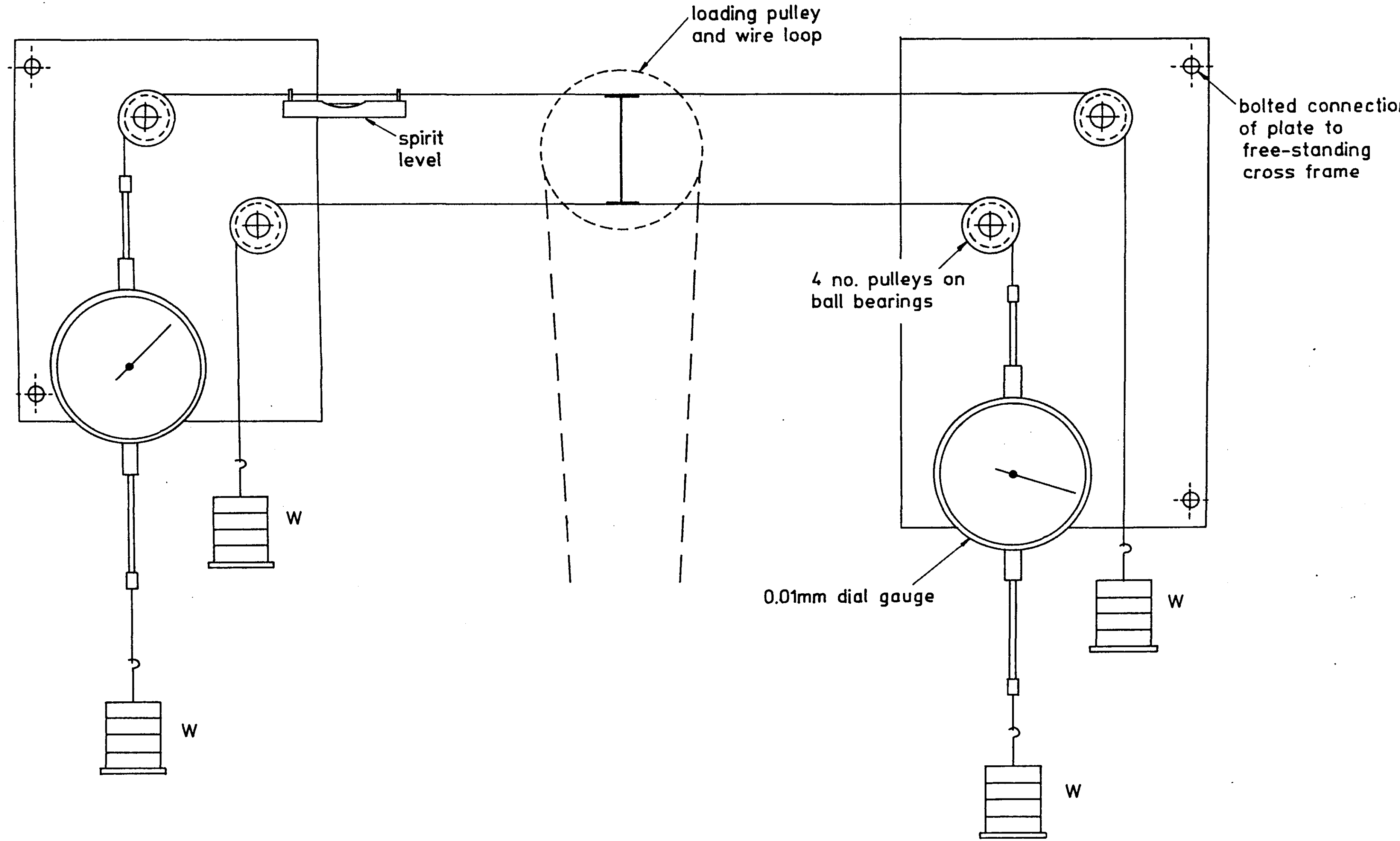

Fig. 4.13 : Initial system used for the measurement of lateral deflections

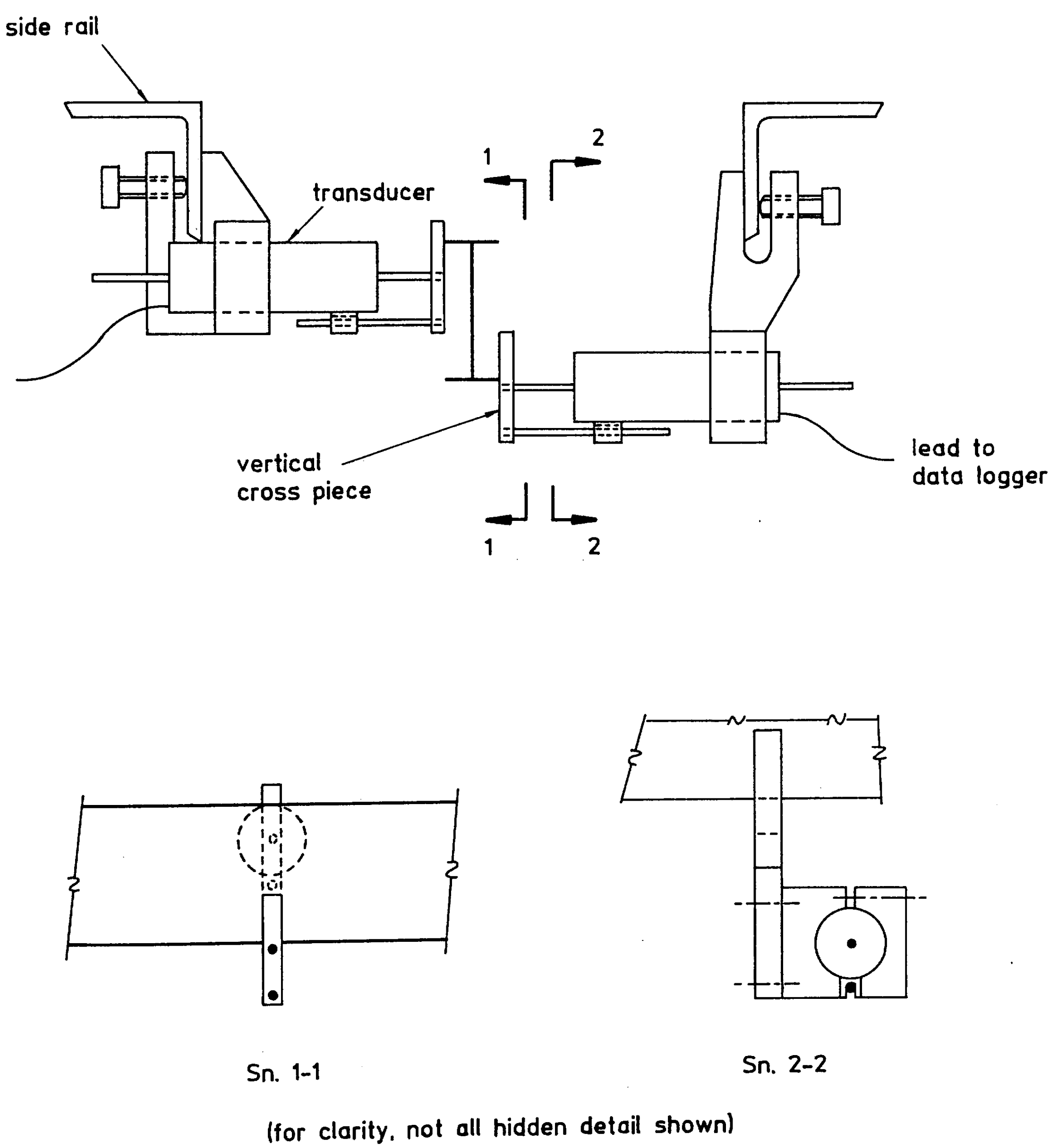

Fig. 4.14 : Displacement transducers used to measure lateral deflections of the flanges

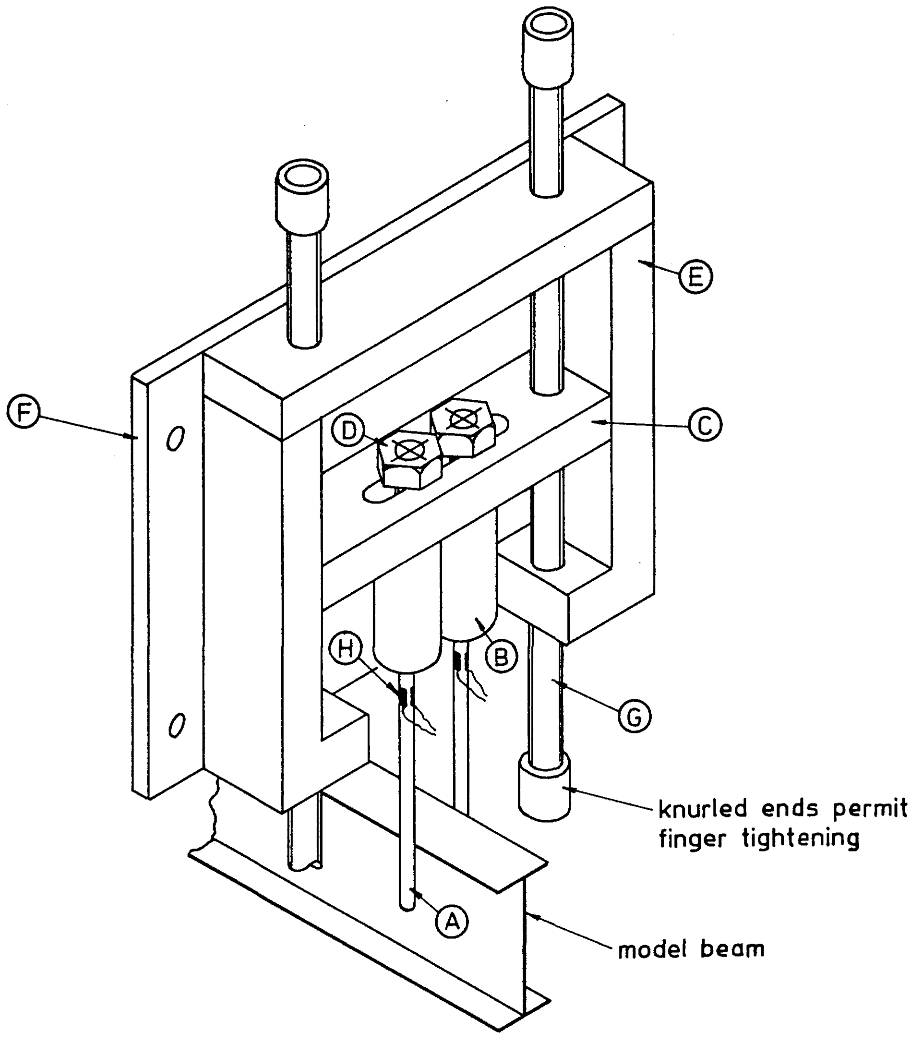

Note : components Ⓐ to Ⓗ described in text of Section 4.3.5.

Fig. 4.15 : Layout of bracing forks relative to model beam. (Note : dial gauge of Fig. 4.16 not shown here for clarity)

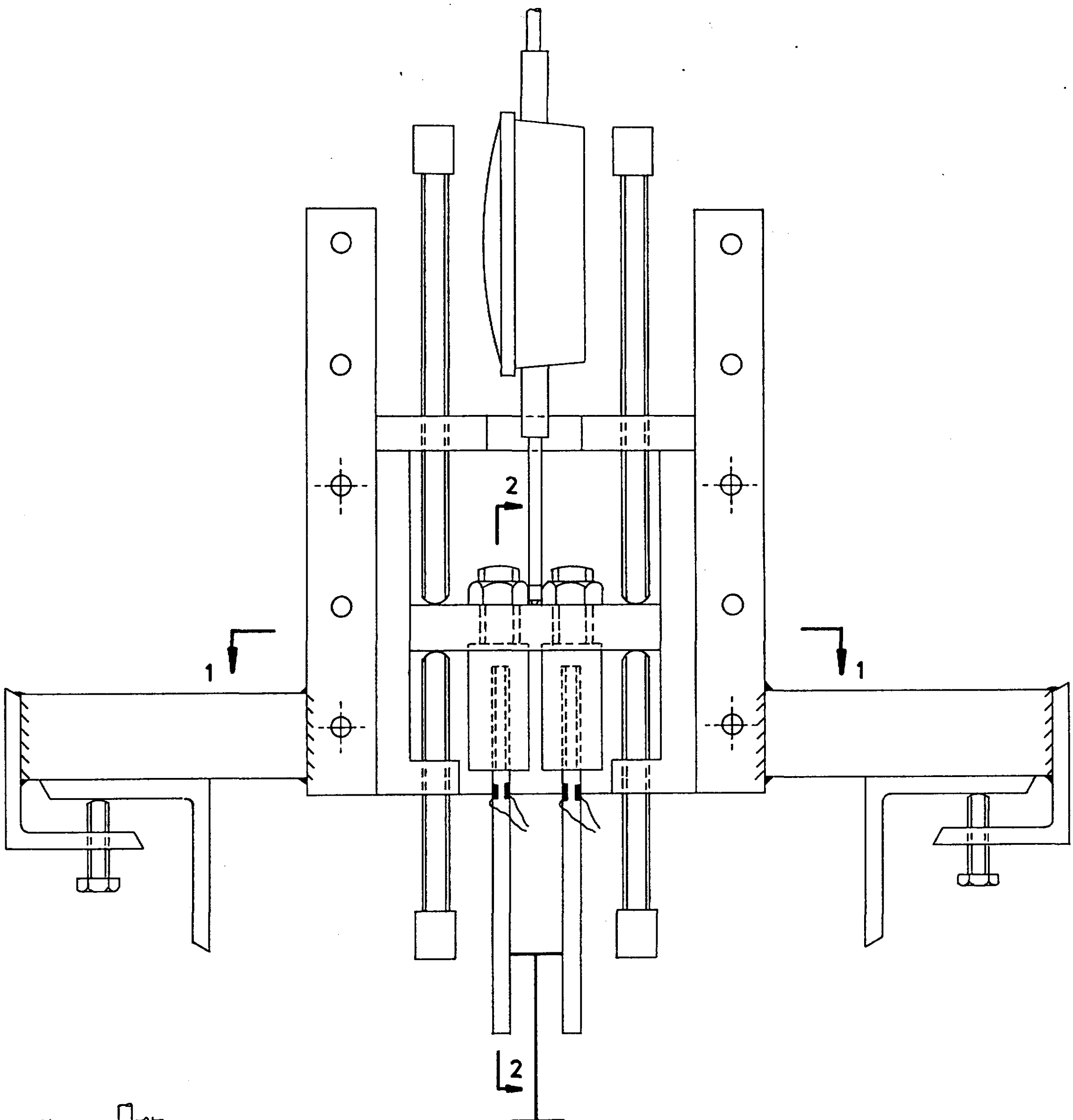

Elevation - front cover plate and dial gauge support from front cover not shown

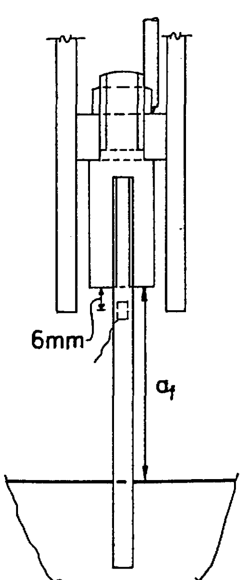

Sn. 2-2
(front cover plate shown)

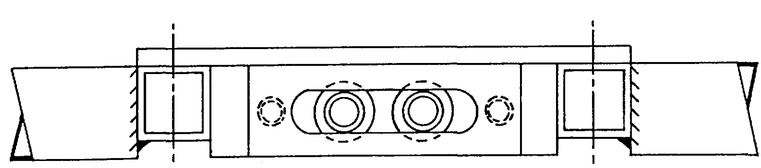

Sn. 1-1
(front cover not shown)

Fig. 4.16 : The bracing fork system

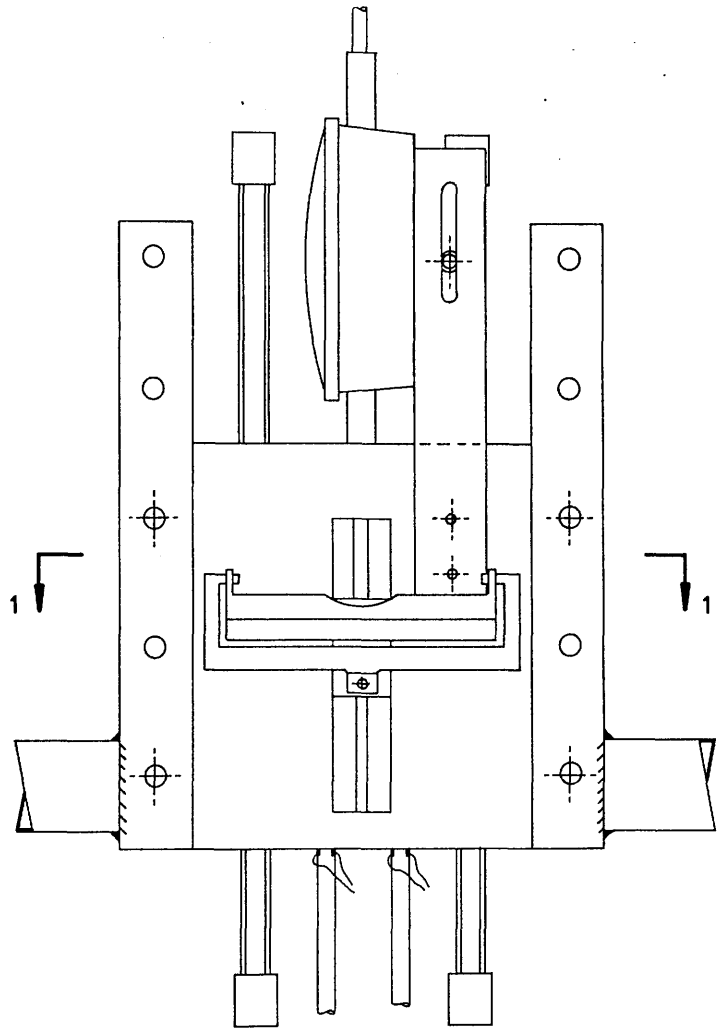

Front elevation showing spirit level, front cover plate and dial gauge mounting

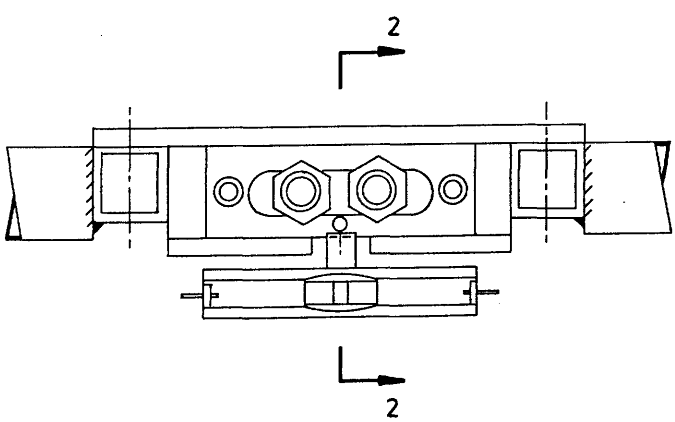

Sn. 1-1

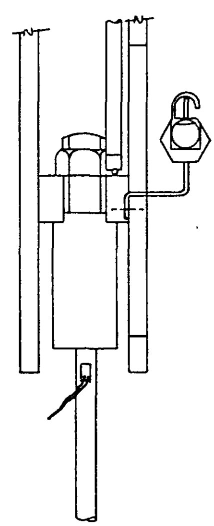

Sn. 2-2

Fig. 4.17 : Spirit level mounted on bracing fork assembly to ensure plate Ⓒ of Fig. 4.15 remains horizontal. (Note : most hidden detail omitted)

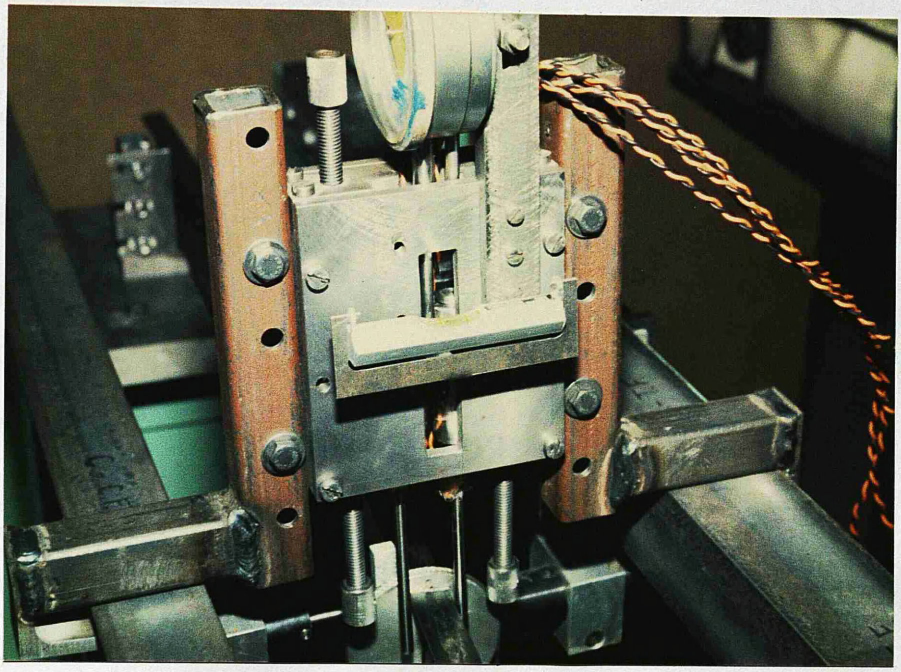

Fig. 4.18 : The bracing fork system with dial gauge and spirit level in position.

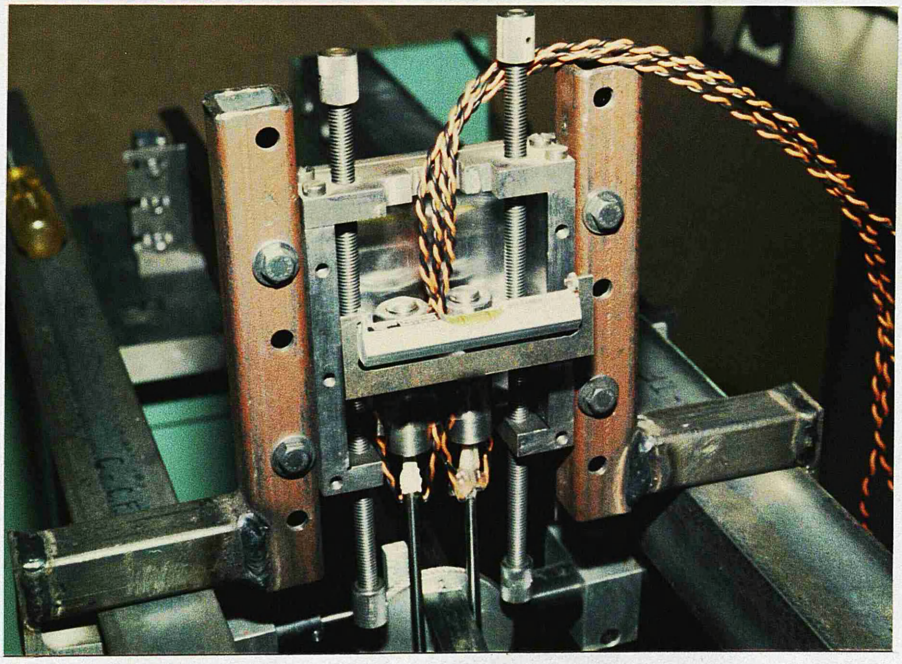

Fig. 4.19 : Bracing fork system with front cover plate and dial gauge removed.

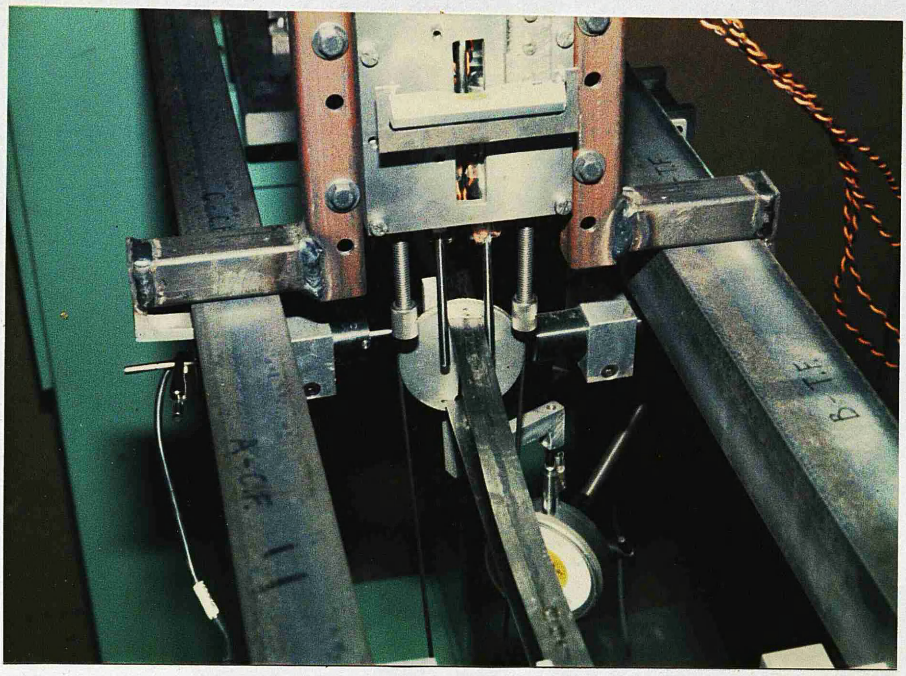

Fig. 4.20 : Bracing forks and upper loading pulley in use. Note second mode buckling configuration with minimal twist at point of loading and twist increasing towards quarter point of span in foreground

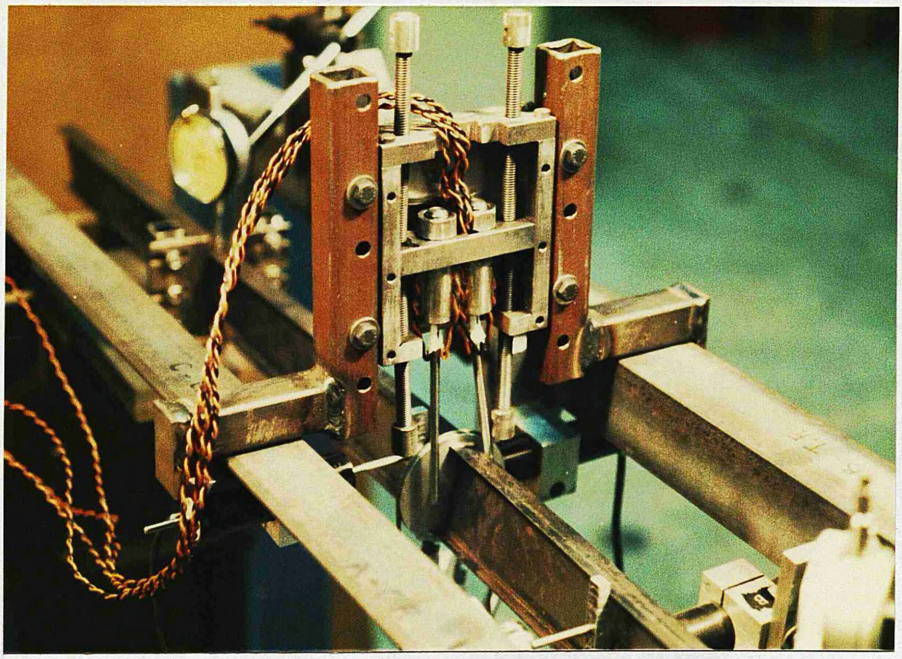

Fig. 4.21 : Bracing forks with front cover plate, dial gauge and spirit level removed. Note first mode buckling configuration with large angle of twist at point of restraint

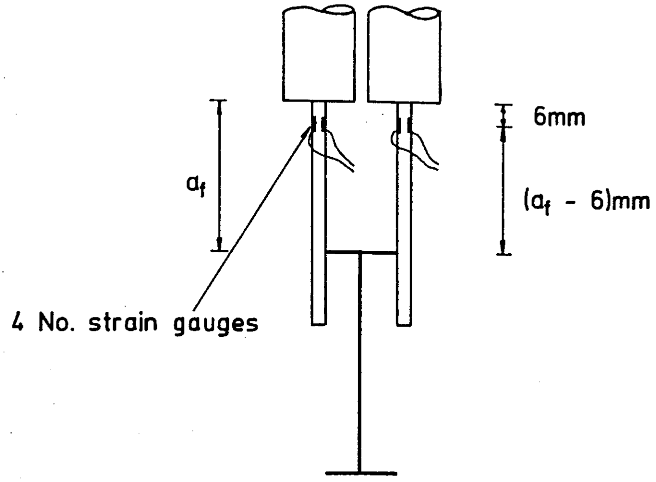

(a) position of bracing fork relative to beam

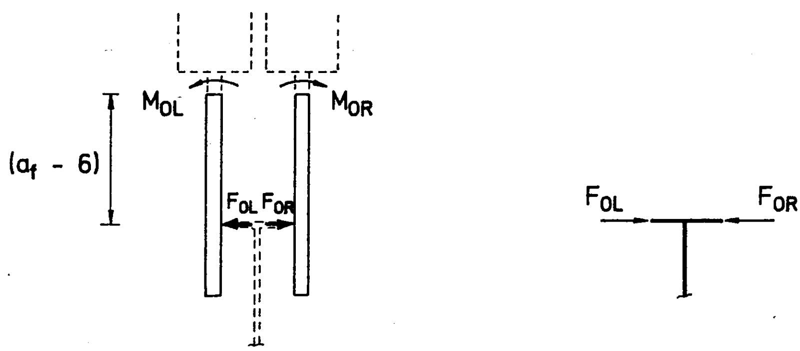

(b) initial bracing fork forces and corresponding lateral forces on beam

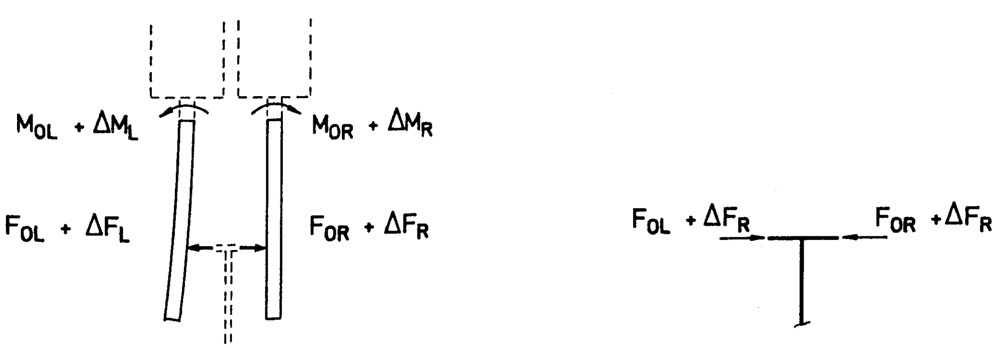

(c) bracing fork and beam forces after lateral deflection of beam flange

Fig. 4.22 : Forces on bracing fork and corresponding lateral forces acting on beam flange.

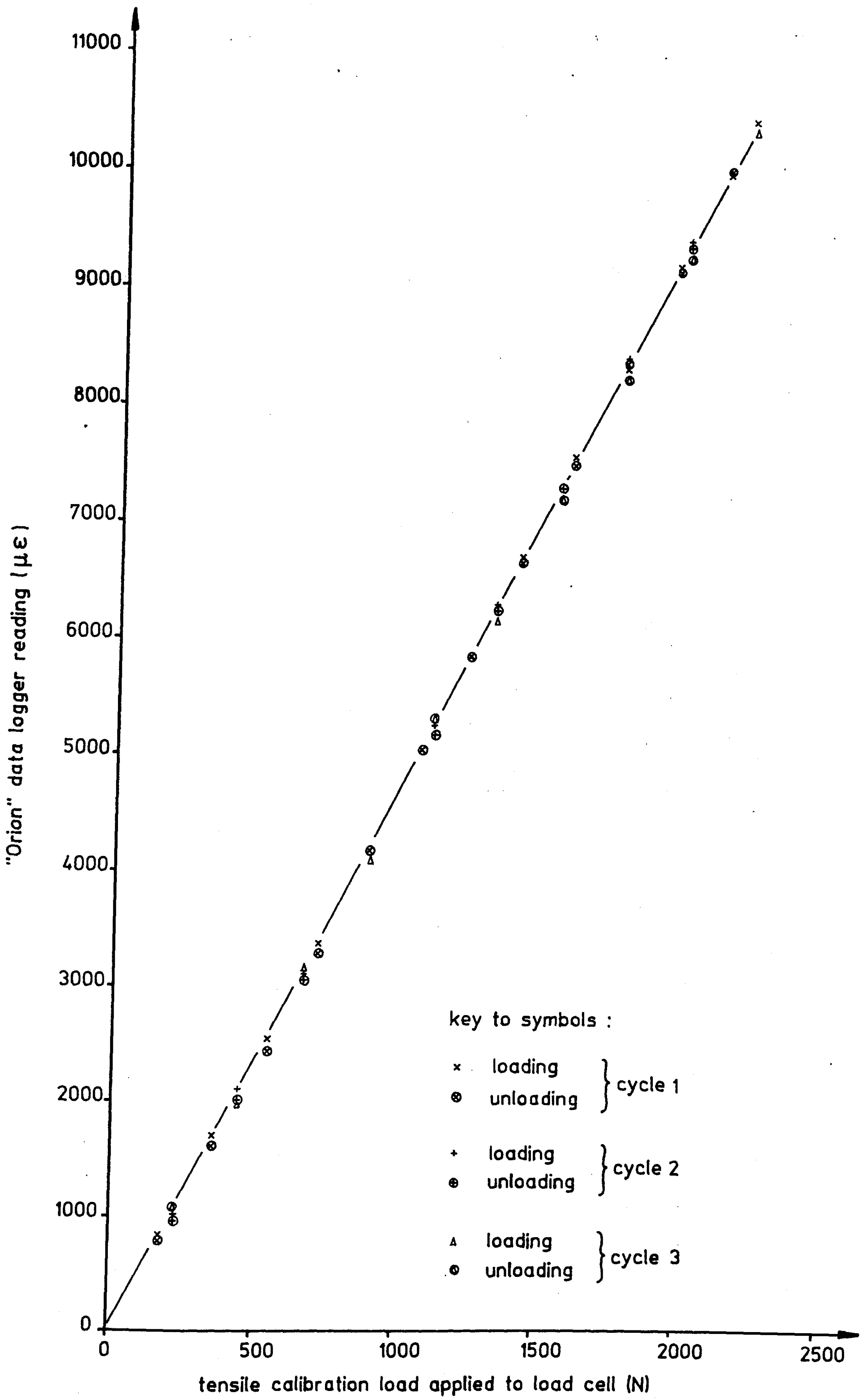

Fig. 4.23 : Statham load cell calibration

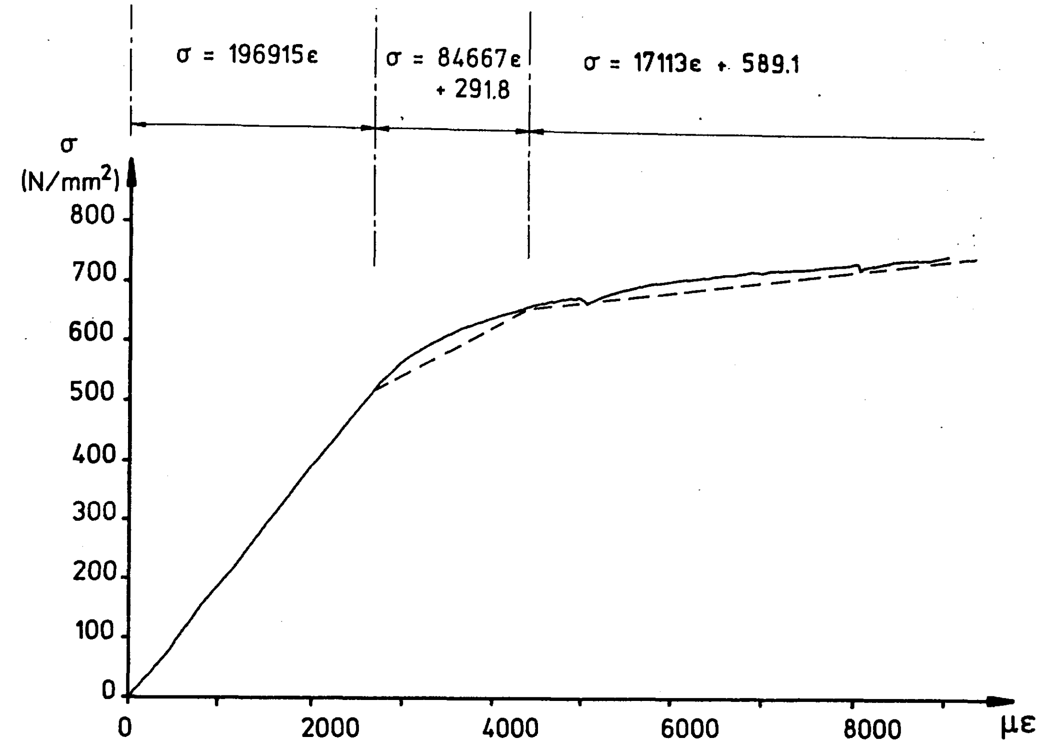

Fig. 4.24 : Typical stress-strain curve for 3/16 inch diameter stubbs steel rod. A tri-linear approximation to the curve is also shown.

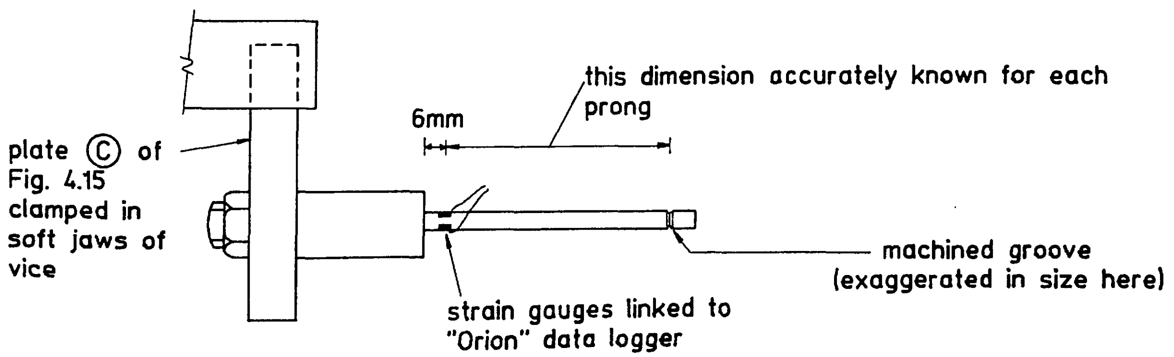

(a) machined groove adjacent to tip of prong

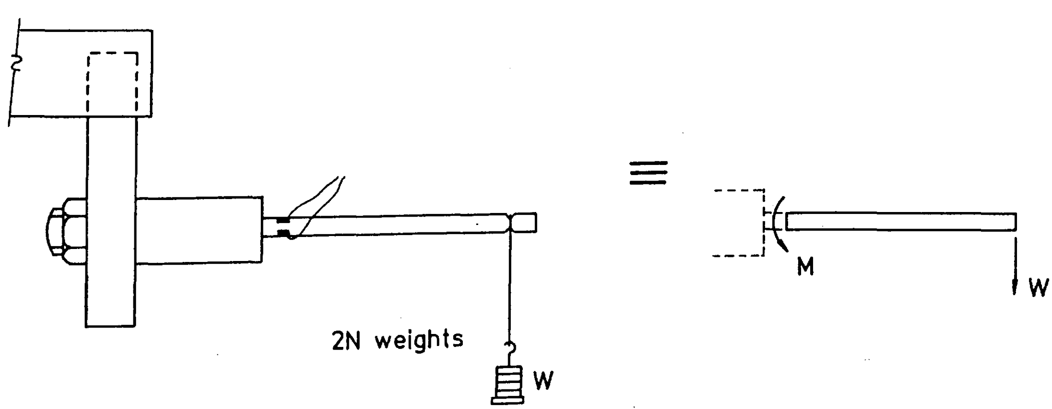

(b) dead weights suspended from prong during calibration

Fig. 4.25 : Calibration of bracing prong using dead weights

CHAPTER 5

PRELIMINARIES TO THE MODEL BEAM TEST PROGRAMME

CHAPTER 5

PRELIMINARIES TO THE MODEL BEAM TEST PROGRAMME

In this Chapter, the fabrication and stress-relieving of model beams and the determination of their material and geometrical properties are described. Details of the experimental procedure adopted during the main series of model beam tests are also given.

5.1 Fabrication of Model Beams

As the experimental programme was concerned primarily with the restraint of inelastic beams, the use of steel as the modelling material provided the only solution to the similarity requirements.

The model beams used in the tests had nominal overall depth and flange breadth dimensions of 50mm and 16mm, respectively. Although exact scaling of a particular prototype section was not intended, the overall depth to flange breadth ratio of about three used in the model beams was considered typical of the ratios common in British rolled Universal Beam sections. The model beams were also nominally doubly symmetric in cross-section so that the centroid and shear centre of the section were coincident.

The beams were fabricated from 20 s.w.g (0.914mm) cold reduced sheet steel to BS 1449, giving a web depth to thickness ratio of about fifty-three, again fairly typical of the values found in Universal Beam sections. However, use of the same thickness of material for the flanges and web meant that flange breadth to thickness ratios in the models were generally higher than for typical Universal Beam sections. Nevertheless, model beam flange outstands were considerably less than the maximum values permitted by BS 449[33] and consequently the probability of occurrence of local flange buckling prior to overall or "primary" instability of the member was minimal.

Several alternative methods of fabricating the beams from the sheet steel were considered. The use of adhesives, employed successfully by Massey in Ref. 11, was rejected on the grounds that the material was too thin to provide an adequately large bonding area at the tee junction between web and flange. Various types of welding were then considered. A welding process was required which would provide neat welds whilst at the same time minimising heat input to the model beam. The latter requirement was desired in order to minimise distortion of the fabricated beam and also to minimise residual stresses in the as-welded section.

Silver solder, used with success in the fabrication of brass and bronze sections, was noted by Litle et al.[96] to lack sufficient plastic strength to join main steel elements or components of a single element. The characteristics of the metal-arc inert gas (MIG) process were examined and it was found that although clean welds were obtained using this process, weld metal deposition was high under large welding currents, with an attendant danger of burnthrough and spatter on the thin material.

The tungsten inert gas (TIG) process was eventually adopted. The benefits of this process were that it allowed greater control over the weld than the MIG process, it provided a cleaner and neater weld, and the chance of burnthrough with thin material was reduced due to the lower arc voltage employed. A mixture of argon and CO_2 was used as the inert shielding gas, giving a smooth arc with a reduced tendency towards spattering of molten weld metal. In welding the model beams, no filler material was used in the TIG process and a "fusion-fillet" weld was obtained. This was preferable to the use of a filler wire which would have resulted in fillet welds grossly disproportionate in size to the overall dimensions of the beam section. TIG welding had been successfully employed by Litle et al.[96], Owen and Dowling[100] and Mills[98].

A substantial welding jig comprising two 1300mm lengths of machined 50x50mm steel bar was used during the welding process. Rebates 20mm wide and 1mm deep were milled in the upper and lower faces of each bar as shown in Fig. 5.1 . Each beam was fabricated from five 1200mm long strips guillotined from the sheet steel: two strips of nominal width 7.55mm formed each flange and the width of the strip forming the web panel was 49mm, allowing the edge of the web plate to stand proud of the flats of the top and bottom rebates by 0.5mm. The web plate was clamped in the jig by means of several G-clamps tightened against the outside faces of the jig and the flange strips were held in position by small clamps at approximately 50mm centres as shown in Fig. 5.1 . Effective clamping served not only to restrain the strips against distortion during the welding process but also to enhance the efficiency of the jig as an heat sink, an essential function due to the small size of the section being fabricated.

After tack welding of the individual strips, final weld runs were continuous along the top and then bottom flange/web junctions. Although contrary to the common requirement for "balancing" welds on opposite sides of a section to minimise camber due to weld shrinkage, continuous runs ensured maximum uniformity of weld along the test specimen. Fig. 4.4 illustrates the degree of uniformity achieved.

Grinding of the welds to remove minor surface irregularities was not permitted in order to avoid unintentional grinding and consequential thinning of the flanges. However, careful local grinding of the weld on the underside of the tension (ie. lower) flange was carried out at the support positions so that uniform bearing of the flange across the cylindrical steel rollers of Fig. 4.2 was achieved.

5.2 Residual Stresses in As-Welded Model Beams

It was shown in Section 1.2.2 and in Fig. 1.6 that the presence of residual stresses in rolled beam sections had a markedly detrimental effect on inelastic buckling loads. It is possible to deduce, therefore, that bracing requirements of steel beams will also be affected by the presence and level of residual stresses in the elements being braced. As the TIG welding process employed in the fabrication of the beams had produced significant heating of the model beams, measurement of the residual stresses in the as-welded sections was considered necessary.

Either Demec mechanical strain gauging or electrical resistance strain gauging techniques were to be employed. Use of an 8 inch Demec gauge was considered. This had been successfully used by Dux and Kitipornchai[4] and by Dibley[38] during residual stress measurements on rolled sections. Its use had also been recommended[104] by a joint DoE/TRRL working group established to investigate practices for the structural testing of steel models. However, the use of Demec gauging with such thin sheet material was thought to be inadvisable due to the probability of excessive bowing and twisting distortions occurring in the coupons after removal from the beam. Consequently, accurate assessment of residual strains by this method was not considered to be feasible.

The longitudinal sectioning technique for the removal of coupons used in Demec gauge measurement of residual strains is also commonly used in conjunction with electrical resistance strain gauging. An alternative approach was, however, adopted by Kitipornchai and Trahair[5]: previous research by Nishino et al had shown that residual stresses in a rolled beam could be sufficiently released by the removal of an intact cross-sectional slice approximately 25mm long; this method was adopted in Ref. 5.

The more traditional longitudinal sectioning method, in conjunction with electrical strain gauging was employed in the present study. A total of eighteen small electrical resistance foil gauges with an active length of 1.6mm and of width 2mm were used in the strain gauge pattern shown in Fig. 5.2 . Measurements were confined to the upper half of the beam section on the assumption of a residual strain distribution symmetric about the neutral axis. As bending of the coupons on removal from the beam was considered probable, gauges were used in pairs, in corresponding positions on opposite surfaces of flange outstands and web. The numbering sequence adopted for gauges is shown in Fig. 5.2, where gauge reference numbers in parenthesis denote gauges used in corresponding locations on the far face. The use of gauges in pairs allowed bending strains in the coupons to be isolated from the desired mean direct strains: measured strains from the gauge pairs were averaged to eradicate the effects of curvature.

Temperature compensation in the active gauges was achieved by means of an identical dummy gauge fixed to the beam at a point clear of the sectioning zone. The dummy and active gauges were linked in a half-bridge configuration and strains were read from a Vishay P-350A Digital Strain Indicator. One set of strain readings from the eighteen gauges was taken prior to removal of the coupons. In order to remove heat generated by sawing, small coupons just larger than the gauges were hand-sawn from the section. After removal of all the coupons and an additional delay to allow the coupons to return to the ambient temperature, a second set of strain readings was taken.

The residual strain at each pair of gauges was then calculated as the difference between the average strains in the pair before and after coupon removal. Measured residual strains obtained by this method were not solely attributable to the welding process. Rather, sectioning of the beam released the aggregate residual strains resulting from cold rolling, handling and welding. Possible errors in the measured residual strains due to strains in the beam arising from bending under self weight were negligible as the beam had been continuously supported during the initial set of strain readings.

Conversion of residual strains to equivalent residual stresses was carried out by multiplying the measured strains by the experimentally determined E value for the as-welded material (see Section 5.5). The value $E=183750$ N/mm^2 was employed and the results of this calculation are shown in Table 5.1 and in Fig. 5.3 . None of the residual stress values of Table 5.1 exceeds the measured tensile yield stress of

174 N/mm^2 (Section 5.5) for the as-welded material.

The most probable pattern of self-equilibrating residual stresses consistent with Table 5.1 stress values is shown in Fig. 5.3, where a longitudinal tensile flange force of approximately 1450N is balanced by a compressive force of the same magnitude in the upper half of the web. Truncation of the flange residual stress pattern adjacent to the web-flange junction was required in order to limit maximum values of residual stress to the yield stress of the material (174 N/mm^2).

Table 5.1: Measured Residual Strains and Conversion to Equivalent Stresses

Strain gauge pair	measured residual strain (tensile +ve) $\mu\epsilon$	equivalent residual stress (N/mm^2) based on E=183750 N/mm^2
1,2	+252	+46.3
3,4	+330	+60.6
5,6	+710	+130.5
7,8	+357	+65.6
9,10	+410	+75.3
11,12	+828	+152.1
13,14	-396	-72.8
15,16	-401	-73.7
17,18	-386	-70.9

In performing the conversion from strain to stress in Table 5.1, no account has been taken of the Poisson effect. In addition, the finite width of gauges (about 2mm) resulted in measured strains being average values over this width. Consequently, the proposed residual stress distribution of Fig. 5.3 could only provide a simple estimate of the level of residual stress likely to be encountered in as-welded model beams. Although encouraging, comparison of this residual stress pattern with typical distributions observed in rolled sections[4,5,38-41] was not justified due to the different methods of manufacture involved. However, typical residual stress patterns for welded members published in Refs. 76,105,106 gave some support to the general form of the proposed distribution. Support for the magnitude of the measured stresses was found in Volume 2 of "The Steel Skeleton"[99] where it was noted that "the use of welding [might] result in the yield stress being reached in the neighbourhood of every weld even under no-load conditions."

5.3 Reasons for and Details of Stress-Relieving of Model Beams

In view of the high levels of residual stress inferred by the measured residual strains in the model beam section, and because the flexural stiffness of the beams would be affected by the presence of zones of yielded material along the flange/web junctions, consideration was given to the possibility of stress-relieving all test beams. Harris[97], reporting a series of tests on TIG-welded model steel frames at the Massachusetts Institute of Technology, noted that, after fabrication, the frames were stress-relieved to restore the necessary strength and ductility. Litle et al.[96] have noted that stress-relieving is necessary when critical portions of a structure are heat affected by the method of fabrication. Such was the case in the present study.

However, concern over the use of stress-relieving in steel model structures has been expressed by Mills[98]. His objection was that use of this technique made it impossible "to duplicate the initial stress state of the prototype [and consequently] phenomena that are a function of initial stress, such as buckling and initial yielding, could not be duplicated by the model." Although Nethercot's findings in Ref. 41 tend to support this view, the theoretical analyses therein have been solely concerned with the residual stress imperfection to the exclusion of the effects of initial geometrical imperfections. A series of prototype tests on as-rolled and annealed beams by Kitipornchai and Trahair[5] revealed that the effect of residual stresses on the buckling behaviour of real beams was slight: of much greater consequence was the presence of initial geometric imperfections. From these findings it is possible to infer that, to a great extent the adverse effects of residual stresses on beam stability are masked by the more detrimental effects of initial geometric imperfections. On these grounds, there existed the option of tolerating the presence of the measured residual stress distribution.

Methods of making allowance for the measured residual stress distribution in finite element analyses were also considered. As noted in Chapter 3, the residual stress option in FINAS had not been implemented at the time the finite element analyses were performed, and no similar facility was available in NASTRAN. Owing to its simplicity, perhaps the most attractive method was that adopted in a study of box girder stiffened webs by Dowling et al[95]. Their reduction of the measured yield stress of plate material by the average value of measured compressive residual stress was judged to be conservative and was employed in finite element analyses to provide lower bound estimates of collapse loads. However, this method was considered inappropriate in the present study as all residual stresses in the most critical portion of the beam, its compression flange, were apparently tensile.

Finally, having considered the available options, it was decided that all model beams would be stress-relieved due to the presence of very high residual stresses over much of the flange breadth. It was of interest to note that Massey[47] had employed stress-relieving even in the case of milled components which were subsequently to be glued to form model steel I-beams. Table 5.2 gives details of stress-relieving and annealing processes employed in previous investigations involving steel beams.

Table 5.2: Details of Stress-Relieving Processes used in Previous Studies

Investigator	Ref.	Beam size & type	Soaking Temp. (°C)	Soak Duration (mins)	Cooling
Kitipornchai, Trahair	5	Aus. 10UB29	600	unspecified	200C°/hr
Massey	47	1"x½" I-sectn.	650	30	"slow"
Mills	98	1"x2/3" I-sectn.	595	60	in furnace
Baker, Horne, Heyman	99	7/8"x7/8" square	930	60	in slaked lime box, in air
Neal	101	1"x1/8" rect.	910	unspecified	390C°/hr

Complete annealing or normalising of the beams was thought to be inadvisable due to the softening of the material produced by these processes and consequently stress-relieving, carried out at a temperature considered to be less than the critical point for the sheet steel, was carried out. Details of the stress-relieving cycle used are shown in Fig. 5.4 .

The length of the model beams (1200mm) meant that a temporary furnace had to be constructed: readily accessible furnaces of the required length were of the cylindrical open-ended type and had only been used for maximum temperatures of between 450°C and 500°C. Steep temperature gradients were known to develop near the ends of these furnaces and the increased risk of beam distortion during heat treatment was unacceptable.

Heat input to the temporary furnace was by means of ceramic heating elements and five thermocouples were placed in different locations in the furnace to record the surface temperatures of the beams. Uniformity of temperature was sensibly achieved throughout the volume of the furnace and the thermocouples were read at intervals of six minutes during the process. Fig. 5.4 has been plotted from the average thermocouple readings over the twenty-hour duration of the stress-relieving cycle. The beams were cooled in still air in the furnace.

On removal of the beams from the furnace when cool, a thin layer of mill-scale which had formed on each was easily removed by light rubbing with steel wool. A thin coating of light oil was then applied to each beam to prevent superficial corrosion. No noticeable distortion of the beams was attributable to the stress-relieving process. In large measure this was thought to be due to the homogeneity of the beams in which no filler material had been employed during welding.

5.4 Geometrical Properties of Model Beams

The importance of initial geometric imperfections in determining the stability and hence the load-carrying capacity of real beams has been emphasised in Chapters 1 and 3 and in Section 5.3 of this Chapter. Some measured values of initial crookedness and twist reported in the literature were presented in Table 1.2 . A few of the contemporary tolerances imposed by national design codes were also indicated in Chapter 1.

Few methods of measuring the initial geometric imperfections of beams have been reported in the literature. Indeed, Table 1.2 indicates that, in the majority of previous investigations in which reference to geometric imperfections has been made, idealised distributions of initial imperfections have been assumed; only in a small number of studies has an attempt been made to quantify geometric imperfections prior to tests.

In Ref. 104 it is recommended that a "continuous scanning instrument" be used to produce line contours of the surfaces of panels forming structural units. No reference to the use of this method in beam buckling investigations could be found although it has become a well-established technique in offshore research for determining the initial imperfect shape of stiffened cylindrical shells. It has also been used in box girder research[95]. Both Dibley[38] and Dux and Kitipornchai[4] employed a fine wire stretched taut between the ends of the test beam. Offsets from the wire to the tips of flanges and shear centre were measured, permitting the initial bowed shape of test beams to be determined. In neither paper is any indication given of the apparatus employed in measuring these offsets.

In the determination of cross-sectional dimensions of test beams, Dibley[38] reported that average values of flange thickness, flange breadth and overall section depth were calculated from only four readings of each of these quantities over the beam length. Average values of web thickness were based on six readings from each beam. Flange widths and thicknesses and section depths were read at metre intervals by Dux and Kitipornchai[4] whilst, like Dibley, measurements of web thickness were only possible near sawn or flame cut ends. Spans in tests reported in Ref. 4 varied from five to eleven metres, giving a minimum of six readings of each cross-sectional dimension on the test span.

In the present study, the method employed for measuring initial crookedness and twist over the span length was that illustrated in Fig. 5.5 . In this, the table of a milling machine was used to support two parallel rollers spaced at a distance equal to the test span of the beam. The beam was supported such that its longitudinal axis was normal to those of the rollers and the overhangs were equal. The length of beam between the supporting rollers would form the test span. Identification marks on the compression flange and at the ends of the span meant that, subsequently, the distribution of imperfections relative to the beam in the test frame could be determined.

An aluminium rod firmly held in the jaws of the mill was used to support a Mercer dial gauge reading to 0.01mm. Dial gauge readings were taken at a total of 16 points on each of the five lines marked ①-⑤ in Fig. 5.5 . The sampling points on each line were not equally spaced; rather, their locations were dictated by the degree of the Chebyshev polynomial used to fit a curve through the line of imperfection readings in the computer programme NEWMESH described in Chapter 3. Although the locations of the readings were symmetrically disposed about midspan, the spacing of readings decreased towards the supports, reflecting the need for greater definition of the curve at its ends.

The forty-eight readings taken on lines ② , ③ and ④ defined the three-dimensional shape of the web. The thirty-two flange tip readings from lines ① and ⑤ were supplemented by the same number of flange breadth measurements taken at the same locations. Flange breadths were measured by a micrometer capable of reading to 0.001mm. This micrometer was also used to take twenty random readings of metal thickness and a further twenty measurements of the overall depth of the section, from which average values of metal thickness and overall beam depth were calculated.

Only when the forty-eight web readings, sixty-four flange readings, average metal thickness, average overall depth, beam span and self weight had been determined was it possible to employ the computer programme NEWMESH (Chapter 3) for finite element mesh generation and the determination of cross-sectional geometric properties and initial imperfections on the test span. Beam self weight was required in order to correct the initial dial gauge readings on lines ① to ⑤ for the effect of minor axis self weight deflection of the beam between supporting rollers in Fig. 5.5 . A plotting option within NEWMESH allowed an initial surface plot of the web panel to be obtained. This allowed a rapid qualitative appraisal of the magnitude and distribution of web imperfections prior to the start of a test. A typical web plot has been shown in Fig. 3.11 .

In the course of the present study, two distinct groups of geometrical measurements were taken: the first on twelve beams from manufacturing batches one and two, used in the preliminary tests carried out during development of the test rig; and the second series on the twenty-three beams from manufacturing batch three used in the three final preliminary tests and in the main test programme. Eight beams of span 600mm were selected from manufacturing batches one and two (ie. preliminary test beams) and their geometrical properties calculated by the methods previously described. The results are shown in Table 5.3 .

The consistency of cross-sectional geometric properties demonstrated in Table 5.3 was good, although these beams had been manufactured from a slightly thinner material than the prescribed 20 s.w.g . Nevertheless, the beams in these two preliminary batches from the fabricator were considered to be satisfactory and were used in the preliminary model tests.

With regard to the maximum values of initial crookedness and twist recorded on the P-series beams, all values of non-dimensional compression flange bow (u_0/l) were less than the maximum values permitted by AISC[57], BS 4[42], DoE Technical Memorandum BE 3/76[58] and BS 5400[55] requirements, although the value of 0.00095 for beam P1 just satisfied these criteria. Values of the regularised twist parameter ($\varphi_0 D/l$) from Table 5.3 were checked against the limitations on twist imposed by Ref. 58 (previously shown in Fig. 1.8)

Table 5.3: Geometrical Properties of Eight 600mm span beams during Preliminary Tests

Beam Mark	Self Weight (N/m)	Average Material Thickness (mm)	Mean Overall Depth 'D' (mm)	I_{major} (mm^4)	I_{minor} (mm^4)	Max. Comp^n. Flange Bow u_o (mm)	Max. Angle of twist φ_o (rad)	u_o/l	$\varphi_o D/l$
P1	5.041	0.856	49.640	24160	588.0	0.569	0.01150*	0.00095	0.000951
P2	5.082	0.853	49.700	24190	590.2	0.337	0.00272	0.00056	0.000225
P3	5.175	0.841	49.630	23800	582.5	0.132	0.00464	0.00022	0.000384
P4	5.126	0.855	49.611	24130	590.3	0.120	0.00434	0.00020	0.000359
P5	5.240	0.845	49.644	24010	595.3	0.189	0.00431	0.00032	0.000357
P6	5.224	0.857	49.692	24300	593.9	0.248	0.00359	0.00041	0.000297
P7	5.248	0.853	49.611	24150	597.3	0.232	0.00457	0.00039	0.000378
P8	5.281	0.849	49.608	24160	607.0	0.265	0.00421	0.00044	0.000348

* denotes outwith the imperfection tolerances of Ref. 58

by noting that, on the simplifying assumption of equal flange outstands,

$$u_{o1} + u_{o2} = \varphi_o D$$

and so the Ref. 58 requirements:

$$u_{o1} + u_{o2} \ngtr 1/1000$$

and

$$u_{o1} + u_{o2} \ngtr D/100$$

reduced to

$$\varphi_o D/1 \ngtr 0.001 \qquad \text{...(5.1)}$$

and

$$\varphi_o \ngtr 0.01 \qquad \text{...(5.2)}$$

in which the angle of twist φ_o is expressed in radians. All $\varphi_o D/1$ values in Table 5.3 satisfied eqn. (5.1) although the restriction imposed by eqn. (5.2) was violated by the φ_o=0.0115 value for beam P1.

Corresponding results for all beams used in the main series of tests (beams M1 to M20) are shown in Table 5.4, although midspan values have been shown for quantities u_o and φ_o. In addition, the sign of these quantities has been shown relative to the sign convention for finite element and experimental results shown in Fig. 3.11 . The greatest tendency towards instability of a beam occurs when initial crookedness of the compression flange is affine with the sense of the initial angle of twist. Under the convention of Fig. 3.11, this occurs when u_o and φ_o are of opposite sign.

Values in the last three columns of Tables 5.3 and 5.4 not satisfying the Ref. 58 1/1000 crookedness tolerance or the twist tolerances of eqns. (5.1) and (5.2) have been flagged with asterisks. It is clear that the requirement of eqn. (5.2) is more onerous than that of eqn. (5.1).

Although all beams shown in Table 5.4 were required to be fabricated from s.w.g. 20 sheet steel, s.w.g. 19 material (thickness 1.016mm) had been used for beams M17 to M20, giving rise to slightly greater values of self weight, material thickness and mean overall depth for these beams. However, a corresponding small reduction in

Table 5.4: Geometrical Properties of Beams used in the Main Series of Tests

Beam Mark	Span l (mm)	Self Weight (N/m)	Average Material Thickness (mm)	Mean Overall Depth 'D' (mm)	I_{major} (mm^4)	I_{minor} (mm^4)	Midsp. Compn. Flange Bow u_o (mm)	Midsp. Angle of Twist φ_o (rad)	$\lvert u_o \rvert / l$	$\lvert \varphi_o \rvert D / l$
M1	600	5.694	0.912	49.813	26735	725.4	-0.234	-0.00046	0.00039	0.000038
M2	600	5.706	0.917	49.842	27223	767.8	-0.719	+0.00534	0.00120*	0.000444
M3	600	5.692	0.918	49.810	26881	729.0	-0.393	+0.00038	0.00066	0.000032
M4	800	5.652	0.910	49.848	27079	766.5	+1.186	+0.00359	0.00148*	0.000224
M5	800	5.702	0.903	49.838	26441	709.1	+0.057	-0.00888	0.00007	0.000553
M6	800	5.675	0.915	49.862	26855	723.8	+0.721	-0.00004	0.00090	0.000002
M7	800	5.630	0.917	49.853	27287	772.0	-0.705	-0.00434	0.00088	0.000270
M8	1000	5.656	0.908	49.793	26442	704.2	+0.554	+0.01074*	0.00055	0.000535
M9	1000	5.688	0.907	49.774	26535	719.6	-0.720	-0.02690*	0.00072	0.001339*
M10	1000	5.619	0.910	49.846	26525	701.0	+1.007	+0.00247	0.00101*	0.000123
M11	600	5.682	0.916	49.892	27329	774.7	-0.370	-0.00385	0.00062	0.000320
M12	600	5.627	0.912	49.861	26760	722.0	-0.526	+0.00584	0.00088	0.000485
M13	600	5.698	0.917	49.856	26932	731.0	+0.555	-0.00270	0.00092	0.000224
M14	600	5.575	0.913	49.848	26627	706.4	-0.427	+0.00069	0.00071	0.000059
M15	800	5.644	0.911	49.841	27082	766.0	+1.450	-0.00699	0.00181*	0.000435
M16	800	5.643	0.909	49.846	26773	732.6	-0.061	-0.02050*	0.00008	0.001277*
M17	800	6.008	1.004	50.100	27746	596.5	+0.068	+0.00629	0.00008	0.000394
M18	800	6.006	1.019	50.231	28254	600.4	+0.216	+0.00172	0.00027	0.000108
M19	800	5.967	1.004	50.152	27958	609.1	+0.184	-0.01113*	0.00023	0.000698
M20	800	5.956	1.005	50.074	27559	580.0	+0.585	+0.00114	0.00073	0.000071

* denotes outwith the imperfection tolerances of Ref. 58

flange breadth meant that I_{major} values were little affected whilst I_{minor} values were slightly lower than those for beams M1 to M16. As explained in Chapter 6, these unexpected variations in cross-sectional properties caused little interruption to the test programme as the beams were being tested on the basis of approximately equal values of the shape parameter R (eqn. (1.4)). Minor changes in cross-sectional properties could therefore be accommodated by altering the length of the test span 'l'.

5.5 Material Properties of Model Beams

For the purposes of data input to finite element and other theoretical analyses, values of Young's Modulus (E) and yield stress (σ_y) were required for the test beams.

Initially, an assessment of the change in stress-strain behaviour of the material from the as-welded to the stress-relieved conditions was required. Prior to stress-relieving, three tensile specimens of full section thickness were cut from the webs of beams P1 and P3 outwith their test spans. The dimensions of these specimens were in accordance with the guidelines set down in BS 18: Part 3[107] and the rate of plastic straining employed in tensile tests was less than the value of 300 $\mu\epsilon$/minute recommended in Ref. 104. All tensile tests except those later performed on very small flange specimens were carried out in the Tinius Olsen Universal Testing Machine previously described. A Tinius Olsen type S-2 tension extensometer was connected to a drum plotter on the testing machine, allowing the load-extension behaviour of tensile specimens to be plotted automatically during tests.

Stress-strain curves for the three specimens from the as-welded beams exhibited no definite yield plateaux, as typified by the curve for the beam P3 specimen shown in Fig. 5.6 . An estimate of the yield stress of the material in this condition was obtained from the 0.2% proof stress and was approximately 169N/mm^2 as shown in the Figure. A corresponding value of E=180000N/mm^2 was deduced for this specimen. The two other specimens were similarly tested and average values of E=183750N/mm^2 and σ_y=174N/mm^2 calculated from the three sets of results.

After stress-relieving, a single tensile specimen of standard[107] proportions was cut from the remaining available web area of beam P3 and tested. This displayed a stress-strain behaviour corresponding well to the elastic-perfect plastic description with a well-defined upper yield point as shown in Fig. 5.6 . The measured value of Young's Modulus for this specimen was E=195800N/mm^2, only about 6% greater than the average value of 183750 N/mm^2 for the as-welded specimens.

In accordance with the procedures recommended for the determination of yield stress in Ref. 104, the maximum rate of plastic straining was again less than 300 $\mu\epsilon$/min and the static yield stress of σ_y=182N/mm^2 was calculated as the average of the "trough" values following enforced two-minute stoppages of the cross-head at strains of 5000$\mu\epsilon$ and 8000$\mu\epsilon$ as shown in Fig. 5.6 . The difference between the measured yield stresses of the stress-relieved and as-welded materials was therefore approximately 7.5%.

As the strain control facility on the Tinius Olsen testing machine would not deal with the very low cross-head speeds required, manual control over the speed of cross-head separation was necessary to achieve the desired low rate of straining. This proved difficult as unintentional momentary stoppages of the cross-head were unavoidable, giving rise to unsightly but harmless troughs on the recorded stress-strain curves. The distinction between these unintentional stoppages and the stoppages enforced for static yield stress determination must be emphasised.

Prior to commencement of the main series of beam tests reported in Chapter 6, the testing of at least two stress-relieved beams taken from the batch to be used in those tests was judged to be prudent in order that the material properties of the thicker sheet metal (0.914mm rather than 0.851mm) could be used to provide a theoretical value of fully plastic moment M_p against which would be checked an experimentally determined in-plane ultimate moment. This also provided an ideal opportunity to test the bracing fork device, which was used here to provide a high degree of midspan lateral restraint to the beam: on account of the short span of 600mm used in the tests, there was little doubt that in-plane collapse would be the mode of failure.

Determination of the properties of the stress-relieved thicker material was based on a series of four tensile tests on specimens cut from the webs of beams subsequently marked P13 and P14. The specimens were again shaped to BS 18[107] and tested in accordance with Ref. 104. The stress-strain curve for one web specimen cut from beam P13 is shown in Fig. 5.7 and is typical of the curves obtained for the other three specimens. Table 5.5 shows values of Young's Modulus and yield stress obtained from these tests. Average values are also shown.

Table 5.5: Measured and Average Web Values of E and σ_y for Use in Main Tests

Tensile specimen cut from web of beam	Measured value of E (N/mm^2)	Measured value of σ_y (N/mm^2)
P13	195300	190.2
P13	204100	198.3
P14	185700	187.8
P14	198700	209.5
Average	196000	196.4

Although the elastic load-deflection behaviour of beam P13 agreed well with beam theory, the measured in-plane ultimate load compared considerably less favourably with the theoretical value based on the average value of σ_y from Table 5.5 . The 15% difference was considered to be unacceptably large and several possible reasons for the discrepancy were examined. As the rate of straining employed in tests did not exceed the recommended[104] limit of 300 microstrain per minute (Section 5.6) and because the stress concentration effects due to central point loading observed by Baker, Horne and Heyman[99] produced only a 5% discrepancy between theoretical and experimental results, the only other major source of error was considered to lie in the measured yield stress value. Variation of yield stress within the heat-affected zone was considered probable.

As the yield stress of the web had been determined with a reasonable degree of certainty (Table 5.5), only the yield stress of the flange material was to be investigated. Determination of flange yield stress by the method of direct tensile testing was evidently considerably more difficult than the determination of web yield stress by the same method due to the much smaller size of the flange and its non-uniform thickness adjacent to the welded junction with the web. A method allowing a qualitative assessment of flange yield stress relative to web yield stress was therefore sought.

On the basis of an empirical relationship between yield stress and hardness proposed by McClintock and Argon[108], in which the two quantities were predicted to be approximately linearly related, a series of Vickers hardness tests was undertaken. A number of rectangular web and flange specimens were cut from regions of beam P13 not plastically deformed during the test. The surfaces of these specimens were ground to allow accurate measurement of the size of indentations produced by the diamond pyramidal indenter used in the Vickers test. An Eseway Vickers Type SPV-2 Hardness Tester was used and a constant indenter load of 10kgf maintained by a pneumatic pressure of 5.0 ± 0.2kgf/cm^2.

The constant of proportionality linking hardness (V_H) and yield stress (σ_y) values was established by means of tests on two web specimens of known yield stress (196.4N/mm^2). The location of indentations on these specimens was as shown in Fig. 5.8(a) where measured and average hardness values are also shown. The constant of proportionality (k_H) in the relation

$$\sigma_y = k_H V_H \qquad \ldots(5.3)$$

was therefore

$$k_H = \frac{\sigma_y}{\text{mean } V_H}$$

$$= \frac{196.4 \ \text{N/mm}^2}{104.3 \ \text{kgf/mm}^2} = 1.883 \ \frac{\text{N/mm}^2}{\text{kgf/mm}^2} \qquad \ldots(5.4)$$

The V_H readings on the web indicated an almost constant yield stress over the depth of the web panel. This had been anticipated.

Four ground flange specimens were tested, each with fifteen equally spaced indentations across the breadth as shown in Fig. 5.8(b). Average V_H values from the four specimens exhibited a pronounced peak at mid-breadth of the flange, coincident with the location of the flange/web weld. Values at the tips of the flanges corresponded approximately to the average recorded value for the web, indicating a similar yield stress. On the basis of the conversion indicated by eqns. (5.3) and (5.4) above, the variation in yield stress across the flange (Fig. 5.8(b)) was calculated, giving rise to a mean flange yield stress of 235.4N/mm^2.

The empirical nature of the relationship in eqn. (5.3) meant that the calculated mean flange yield stress could only be considered indicative of a higher value in the flanges than in the web. A more refined approach was necessary.

A series of tensile tests on small, paralled-sided flange specimens was carried out. These specimens were cut from the flanges, milled to uniform breadth over their length and ground to a thickness corresponding to the disappearance of all surface irregularities due to welding. Two sets of such specimens were manufactured: the first of width approximately 4.5mm cut from the flange outstands and as close as possible to the flange tips (Fig. 5.9(a)); the second, of width 14mm, cut from the centre of the flange (Fig. 5.9(b)). The need for considerably more grinding of the specimens cut from central locations resulted in typical thicknesses of about 0.53mm in these specimens.

The specimens were tested in the 0-5kN range of an Instron 1190 Materials Testing Machine, which was preferred to the Tinius Olsen machine for these tests due to its greater accuracy in measuring small loads. A strain control facility allowed the rate of plastic straining used in tests to be held constant at approximately 250 $\mu\epsilon$/min. The recommended method of determining static yield stress from Ref. 104 was followed: the four flange tip specimens displayed an average yield stress of 202.4N/mm^2 whilst an average value of 271.2N/mm^2 was noted for the 14mm broad specimens. On the assumption that measured yield stress over the flange could reasonably be approximated by the distribution shown in Fig. 5.10, a weighted mean calculation showed the mean flange stress to be 262.6N/mm^2. This value was significantly higher than 235.4N/mm^2 predicted by the Vickers test.

Earlier in this Section it was noted that only one value of yield stress could be specified for the beam elements in the NASTRAN and FINAS programmes. In order to fulfil this requirement, the method advocated by Lindner[103] for the determination of an effective yield stress value from unequal flange and web values was adopted. This method produced an effective yield stress giving the same fully plastic moment M_p as would be obtained by using the different yield stresses of the flange and web. The following were the most probable cross-sectional dimensions of a beam fabricated in the jig of Fig. 5.1 from 0.914mm thick sheet material:

flange and web thickness	=	0.914mm
depth of web	=	48.0mm
overall depth of section	=	49.828mm
flange breadth	=	16.0mm

Therefore,

force in one fully yielded flange $= 16 \times 0.914 \times 262.6$
$= 3839.2\text{N}$

force in one fully yielded half of web $= 24 \times 0.914 \times 196.4$
$= 4308.2\text{N}$

fully plastic moment in section, M_p $= 2(3839.2 \times 24.457 + 4308.2 \times 12)$
$= 291187.4\text{Nmm}$

Now, plastic section modulus, z_p $= 2(14.62 \times 24.457 + 21.936 \times 12)$
$= 1241.59\text{mm}^3$

and so effective yield stress $= M_p/z_p$
$= 234.5\text{N/mm}^2$

The material properties $E = 196000\text{N/mm}^2$ and $\sigma_y = 234.5\text{N/mm}^2$ were subsequently used in all calculations relating to the main series of tests. Correlation between theoretical and experimental collapse loads was excellent, as demonstrated by the test results presented in Chapter 6.

5.6 Rate of Plastic Straining Employed in Tests

In the testing of steel structures, the rate of straining has been noted[104] to have a small but significant effect on the yield stress of the material. Ref. 104 recommends that "the rate of application of load should be such that in the most highly stressed part of the [model], the rate of change of strain should not exceed 300 microstrain per minute." This is consistent with the rate of straining recommended therein for the conduct of tensile tests. In the literature, the significance of the rate of straining used in tests has been realised in a few studies such as those of Kitipornchai and Trahair[5] and Dux and Kitipornchai[4]. Although the rate of straining adopted by Sawyer in Ref. 7 was very high, though not quantified, his experimental results showed good correlation with a semi-graphical analytical method for predicting the moment-deflection characteristics of beams: this correlation gave support to the belief that straining rates played a minor role in determining the response of beams under load.

Nevertheless, as the recommendations of Ref. 104 had been employed in carrying out the tensile tests reported in Section 5.5, the use of a rate of straining in the beam tests similar to that used in determining material properties was considered advisable. A theoretical analysis of the permissible rate of load application was undertaken in order that the maximum rate of straining due to in-plane bending in tests would not exceed 300 $\mu\epsilon$/min. Details of this analysis are presented here, although many of the purely algebraic intermediate steps in the analysis have been omitted. An elastic-perfect plastic material has been assumed (Fig. 1.7).

In the following analysis, the notation of Fig. 5.11(a) for an I-beam is employed and the following additional notation is used:

χ	in-plane curvature of beam
χ_y	in-plane curvature at first yield in section
M	in-plane bending moment (ie. about ξ-axis)
M_y	in-plane bending moment at first yield in section
z_e	elastic section modulus for in-plane bending

g	distance from neutral axis to nearer edge of yielded zone in cross-section
I	second moment of area
ϵ	strain
ϵ_y	yield strain

Consider the beam of Fig. 5.11 in major axis bending. The curvature χ_y consistent with attainment of an in-plane bending moment of M_y is given by

$$\chi_y = \frac{M_y}{EI} \qquad \text{...(5.5)}$$

Since

$$M_y = \sigma_y \frac{I}{D/2}$$

eqn. (5.5) can be expressed as

$$\chi_y = \frac{2\sigma_y}{DE} \qquad \text{...(5.6)}$$

When the applied moment M exceeds M_y, two situations are possible:

(i) plasticity wholly contained within the flanges and

(ii) plasticity extending throughout the depths of the flanges and into the web, leaving only a core of elastic material in the web.

These two cases will be examined separately.

<u>Case (i)</u> Yielded zone confined to the flanges: $\left(\frac{D}{2} - t_f\right) < g \leqslant \frac{D}{2}$

This situation is illustrated in Fig. 5.11(b) where Ⓔ and Ⓟ represent the elastic and plastic regions of the beam cross-section, respectively. These regions are symmetrically disposed about the neutral axis. The total bending moment M in the section is the sum of the moment contributions from the elastic and plastic zones.

For the elastic zone Ⓔ ,

remaining elastic depth of flange $= g - \left(\frac{D}{2} - t_f\right)$

and the moment of inertia of two such elastic zones about the neutral axis

$$= \frac{b_f}{6}\left(g - \frac{D}{2} + t_f\right)^3 + \frac{b_f}{2}\left(g - \frac{D}{2} + t_f\right)\left(g + \frac{D}{2} - t_f\right)^2$$

Also, I of elastic web

$$= \frac{t_w}{12}\left(D - 2t_f\right)^3$$

and consequently the total inertia of the elastic zones is

$$I_{Ⓔ} = \frac{b_f}{6}\left(g - \frac{D}{2} + t_f\right)^3 + \frac{b_f}{2}\left(g - \frac{D}{2} + t_f\right)\left(g + \frac{D}{2} - t_f\right)^2$$

$$+ \frac{t_w}{12}\left(D - 2t_f\right)^3$$

The corresponding elastic section modulus of these zones is then

$$z_{Ⓔ} = z_e = \frac{I_{Ⓔ}}{g}$$

from which the moment contribution from the elastic zone ($M_{Ⓔ}$) is

$$M_{Ⓔ} = z_e\,\sigma_y$$

or

$$M_{Ⓔ} = \sigma_y \left\{ \frac{b_f}{6g}\left(g + t_f - \frac{D}{2}\right)^3 + \frac{b_f}{2g}\left(g + t_f - \frac{D}{2}\right)\left(g - t_f + \frac{D}{2}\right)^2 \right.$$

$$\left. + \frac{t_w}{12g}\left(D - 2t_f\right)^3 \right\} \qquad \ldots(5.7)$$

For the plastic zone Ⓟ ,

force in zone Ⓟ $= \sigma_y\, b_f \left(\frac{D}{2} - g\right)$

and the lever arm of the couple is $\left(\frac{D}{2}+g\right)$, giving a moment contribution from the plastic zones of

$$M_{Ⓟ} = \sigma_y b_f \left(\frac{D^2}{4} - g^2\right) \qquad \text{...(5.8)}$$

The total moment in the section (M) is then obtained from eqns.(5.7) and (5.8), giving

$$M = M_{Ⓔ} + M_{Ⓟ}$$

or

$$M = \sigma_y \left\{ \frac{b_f}{6g}\left(g + t_f - \frac{D}{2}\right)^3 + \frac{b_f}{2g}\left(g + t_f - \frac{D}{2}\right)\left(g - t_f + \frac{D}{2}\right)^2 \right.$$

$$\left. + \frac{t_w}{12g}\left(D - 2t_f\right)^3 + b_f\left(\frac{D^2}{4} - g^2\right) \right\} \qquad \text{...(5.9)}$$

The moment at first yield in the section (M_y) is most readily obtained by setting g = D/2 in eqn. (5.9) to give

$$M_y = \frac{\sigma_y}{D}\left\{ b_f t_f \left[\frac{t_f^2}{3} + (D - t_f)^2\right] + \frac{t_w}{6}(D - 2t_f)^3 \right\} \qquad \text{...(5.10)}$$

A relationship between strain (ϵ) and curvature (χ) is obtained from the Engineer's Bending Theory on the basis that shear deformations are neglected:

$$\chi = \frac{\epsilon}{\eta} \qquad \text{...(5.11)}$$

in which η represents the distance from the neutral axis to the level at which strain ϵ occurs.

At the edge of the elastic zone Ⓔ, η = g and the strain is the yield strain, given by

$$\epsilon_y = \frac{\sigma_y}{E}$$

The curvature is then

$$\chi = \frac{\sigma_y}{Eg} \qquad \text{...(5.12)}$$

The relationship between the curvature of the beam in Fig. 5.11(b) and the curvature at first yield (from eqn. (5.6)) is then

$$\frac{\chi}{\chi_y} = \frac{D}{2g} \qquad \text{...(5.13)}$$

which holds for all values of $\chi > \chi_y$

The corresponding relationship between applied bending moment M and M_y is obtained from eqns. (5.9) and (5.10), giving

$$\frac{M}{M_y} = \frac{D\left\{\frac{b_f}{6g}\left(g+t_f-\frac{D}{2}\right)^3 + \frac{b_f}{2g}\left(g+t_f-\frac{D}{2}\right)\left(g-t_f+\frac{D}{2}\right)^2 + \frac{t_w}{12g}\left(D-2t_f\right)^3 + b_f\left(\frac{D^2}{4}-g^2\right)\right\}}{\left\{b_f t_f\left[\frac{t_f^2}{3}+\left(D-t_f\right)^2\right] + \frac{t_w}{6}\left(D-2t_f\right)^3\right\}}$$

which, on simplification, reduces to

$$\frac{M}{M_y} = \frac{3gb_fD^3 - 4g^3b_fD + Q_0}{2gQ_1} \qquad \text{...(5.14)}$$

in which Q_0 and Q_1 are only dependent on cross-sectional properties:

$$Q_0 = Db_f\left(8t_f^3 - 12Dt_f^2 + 6D^2t_f - D^3\right) + Dt_w\left(D-2t_f\right)^3$$

and $$Q_1 = 6b_ft_f\left[\frac{t_f^2}{3} + \left(D-t_f\right)^2\right] + t_w\left(D-2t_f\right)^3 \qquad \text{...(5.15)}$$

Rearranging eqn. (5.13)gives

$$g = \frac{D\chi_y}{2\chi} \qquad \text{...(5.16)}$$

which, when substituted into eqn. (5.14), yields

$$\frac{M}{M_y} = \frac{3D^3 b_f(\chi_y/\chi) - D^3 b_f(\chi_y/\chi)^3 + 2Q_o/D}{2Q_1(\chi_y/\chi)}$$

or $$\left(\frac{\chi_y}{\chi}\right)^3 + \left[Q_2\left(\frac{M}{M_y}\right) - 3\right]\left(\frac{\chi_y}{\chi}\right) - Q_3 = 0 \qquad \text{...(5.17)}$$

where $$Q_2 = \frac{12t_f}{D^3}\left[\frac{t_f^2}{3} + (D - t_f)^2\right] + \frac{2t_w}{D^3 b_f}(D - 2t_f)^3 \qquad \text{...(5.18)}$$

and $$Q_3 = \frac{2}{D^3}(8t_f^3 - 12Dt_f^2 + 6D^2 t_f - D^3) + \frac{2t_w}{D^3 b_f}(D - 2t_f)^3 \qquad \text{...(5.19)}$$

in which Q_2 and Q_3 are again only dependent on cross-sectional properties.

Eqn. (5.17) allows the term (χ_y/χ) to be calculated for bending moments M greater than M_y. Eqns. (5.6) and (5.11) then permit the strain at any level in the cross-section to be calculated. Solution of the cubic equation (5.17) was carried out by the short computer programme KURVTURE, listed in Appendix VI.

Use of the above equations is best illustrated by the qualitative example which follows. A beam in bending is subjected to a central point load P_n which is slightly greater than the load causing first yield, P_y. The midspan bending moment under load P_n is M_n; hence

$$\frac{P_n}{P_y} = \frac{M_n}{M_y} \qquad \text{...(5.20)}$$

Eqns. (5.18) and (5.19) are evaluated for the beam's cross-sectional geometry and eqn. (5.17) is solved for (χ_y/χ_n). χ_y is known from eqn. (5.6) and consequently χ_n, the beam curvature under load P_n, is calculable. The strain ϵ_n in the extreme fibre of the flange (ie. $\eta = D/2$) is calculated from eqn. (5.11).

The load is to be increased to a value P_{n+1} and the same procedure is followed in calculating the corresponding outer fibre strain ϵ_{n+1}. The change in strain resulting from the load increment $(P_{n+1} - P_n)$ is then $(\epsilon_{n+1} - \epsilon_n)$. For the rate of straining during the increment not to exceed 300 $\mu\epsilon$/min (ie. 0.0003 ϵ/min), the load increment should be applied uniformly over a time interval of not less than

$$\frac{\epsilon_{n+1} - \epsilon_n}{0.0003} \quad \text{minutes} \qquad \ldots(5.21)$$

<u>Case (ii)</u> Elastic zone confined to web: $0 \leq g \leq \left(\frac{D}{2} - t_f\right)$

The extent of the elastic (Ⓔ) and plastic (Ⓟ) zones for this case are shown in Fig. 5.11(c). A derivation similar to that of Case (i) is employed.

For the elastic zone,

$$M_{Ⓔ} = z_e \sigma_y = \frac{2 t_w g^2 \sigma_y}{3} \qquad \ldots(5.22)$$

and for the plastic zone, two component forces can be identified (Fig. 5.11(c)):

$$F_1 = (b_f - t_w)\, t_f\, \sigma_y$$

and $F_2 = \left(\frac{D}{2} - g\right) t_w \sigma_y$

The respective lever arms for these forces are $(D-t_f)$ and $(D/2 + g)$, giving

$$M_{Ⓟ} = F_1 (D - t_f) + F_2 \left(\frac{D}{2} + g\right)$$

$$= (D - t_f)(b_f - t_w)\, t_f \sigma_y + \left(\frac{D^2}{4} - g^2\right) t_w \sigma_y \qquad \ldots(5.23)$$

The total moment from elastic and plastic zones is

$$M = \sigma_y \left[(D-t_f)(b_f-t_w)t_f + \left(\frac{D^2}{4}-g^2\right)t_w + \frac{2t_w g^2}{3} \right] \qquad \ldots(5.24)$$

and M_y is unchanged from eqn. (5.10), giving

$$\frac{M}{M_y} = \frac{D\left[(D-t_f)(b_f-t_w)t_f + \frac{D^2 t_w}{4} - \frac{t_w g^2}{3}\right]}{b_f t_f\left[\frac{t_f^2}{3} + (D-t_f)^2\right] + \frac{t_w}{6}(D-2t_f)^3}$$

Substitution for g from eqn. (5.16) readily yields

$$\left(\frac{\chi_y}{\chi}\right)^2 = Q_4 - Q_5\left(\frac{M}{M_y}\right) \qquad \ldots(5.25)$$

where $$Q_4 = \frac{12t_f(D-t_f)(b_f-t_w)}{D^2 t_w} + 3 \qquad \ldots(5.26)$$

and

$$Q_5 = \frac{12}{D^3 t_w}\left\{b_f t_f\left[\frac{t_f^2}{3} + (D-t_f)^2\right] + \frac{t_w}{6}(D-2t_f)^3\right\} \qquad \ldots(5.27)$$

Following the method previously described in Case (i), eqns. (5.25) to (5.27), (5.6) and (5.11) are used to calculate the maximum bending strains in the cross-section due to applied loads P. An advantage in this case is that the quadratic eqn. (5.25) can be directly solved by hand calculation.

The equations derived in this Section were used to derive several curves relating loading rate to exising applied load for three spans of beam. These are shown in Figs. 5.12 to 5.14 . The assumed cross-sectional dimensions of beam were those shown in Section 5.5 . The numerical results on which these graphs were based are presented in Appendix VI.

Figs. 5.12 to 5.14 were used in all tests reported in Chapter 6 to ensure that the rate of straining in model beam tests did not exceed the value used in tensile tests. Although the graphs permitted some degree of control over the rate of straining due to in-plane flexure of the beam, it was not possible to extend the analysis to include the effect of lateral bending on the rate of straining. This was due to the high degree of dependence of lateral bending moments on initial imperfections.

5.7 Experimental Procedure

In this Section, the steps involved in preparation for a model beam test are described and then the sequence of readings and calculations associated with the running of a test are described.

As previously noted, all tests were conducted under displacement control and consequently it was possible to "load" beams into their post-buckling states. However, in order to obtain useful results for the beams in that condition, great care was required in determining the size of "load" increments to be applied; as the most readily identifiable warning of imminent buckling failure of a test beam was a reduction in its lateral bending stiffness under increasing vertical load, careful scrutiny of displacement transducer readings was required throughout each test. The following procedures allowed both lateral deflections and corrected vertical midspan deflections of the beam to be plotted as tests proceeded. The combined effects of yielding and instability could then be assessed at any stage in a test and the size of subsequent load increments adjusted accordingly.

5.7.1 Preparations for a Model Beam Test

The following preparations were carried out before each test:

(i) The test span 'l' was determined: this was usually dictated by the type of failure observed in the preceding test and the need to determine an approximate value of the critical translational restraint parameter λ_{cr} (see Chapter 6). The support points and midspan were then marked on the beam.

(ii) Two small holes were drilled in the web of the beam, within the test span and about thirty-five millimetres from the proposed support positions. These were subsequently used to allow the web plumbing device (Section 4.3.2 and Figs. 4.3 and 4.4) to be employed.

(iii) Beam geometric properties and initial imperfections were then determined by the methods decribed in Section 5.4 . Readings were then analysed by the computer programme NEWMESH (Chapter 3) to give cross-sectional properties of the beams and initial imperfections on the test span.

(iv) The adequacy of restraint in the preceding test generally dictated the value of non-dimensional bracing stiffness λ to be used. The active leg length (a_f) of bracing prong required to achieve this value of λ was then calculated from eqn. (4.1), in which all terms on the right hand side of the equation were known.

(v) Any new bracing prongs required were made and a superficial reference groove machined near the tip of the prong and at a known distance from the proposed centre-line of strain gauges. The strain gauges were then accurately fixed at a level of 6mm below the base of the retaining cylinder (B in Fig. 4.15). The location and orientation of gauges was as described in Section 4.3.5 and illustrated in Figs. 4.16 and 4.22 .

(vi) New prongs were calibrated using the method of Section 4.4.3 to arrive at an elastic calibration factor (Nmm/$\mu\epsilon$).

(vii) The bracing fork assembly (A to D in Fig. 4.15) was then loaded into its housing, having first made certain that nuts D were slack.

(viii) The upper loading pulley of Fig. 4.6 was then slotted over the beam and moved into its final location at midspan (this position previously marked in step (i)).

(ix) The test beam was loaded into the test frame and a plumb bob suspended from a small hole in the upper pulley (Fig. 4.6(a)) was used to locate the beam centroid centrally over the centre of the Statham load cell. In this way, it was possible to ensure that the initial load on the beam would be applied truly vertically.

(x) The end support frames were then positioned and the web plumbing device (Figs. 4.3 and 4.4) used to ensure verticality of the web at supports. The knife edge plates were locked in position and the knife edges greased. Laterally, slight freedom (0.05mm) of flange movement was allowed as described in Section 4.3.2 .

(xi) The tension linkage between the Statham load cell and upper loading pulley was introduced as shown in Figs. 4.5, 4.7 and 4.9 .

(xii) The dial gauges used to measure midspan deflection of the beam

(Figs. 4.10 and 4.20) and support deflections (Section 4.3.4) were then positioned.

(xiii) The front plate and dial gauge of the bracing fork arrangement were attached and the front spirit level (Fig. 4.17) secured in place.

(xiv) Four displacement transducers were then located at midspan and at one quarter point of span. The tee pieces attached to the plungers of the transducers were set to bear on the tips of the upper and lower flanges of the test beam as shown in Figs. 4.4 and 4.14 .

(xv) The bracing prongs were slid together until contact was made with the tips of the compression flange. Plumbing of the prongs was carried out using the front spirit level shown in Fig. 4.17 .

(xvi) The required active leg length 'a_f' was set using the machined groove close to the tip of the prong as a reference mark.

(xvii) All electrical connections were then made and a dummy strain gauge used in a half-bridge arrangement with the bracing fork gauges.

5.7.2 Test Procedure

The following procedure was found to be satisfactory for use during model beam tests:

(i) An initial set of readings from the following gauges and transducers was taken: the load cell and four electrical displacement transducers; the dial gauges used for the measurement of vertical deflection of the beam at midspan, vertical movement of the bracing fork assembly, vertical deflection of the two supports and transverse movement of the load cell carriage; finally, the four strain gauges fixed to the bracing prongs.

(ii) The initial angle of twist on the test beam at midspan was noted from NEWMESH computer output.

(iii) The plungers of the displacement transducers were retracted in order to minimise lateral forces acting on the beam during application of increments of vertical "load". The plungers were held in this retracted position by crocodile clips.

(iv) (This step was not required before application of the first increment of load). The transverse position of the load cell carriage was adjusted in order to keep applied load truly vertical. In the case of centroidal loading on the beam, the carriage was moved in sympathy with the observed lateral deflection of the beam centroid. Alternatively, when compression flange loading was being applied, the lateral deflection of this flange dictated the required movement of the carriage.

(v) The next increment of "load" in the form of enforced vertical displacement was applied. The size of this increment was dependent on the degree of yielding in the section and the beam's proximity to buckling, characterised by the magnitude of lateral deflections of the flanges measured after the previous increment of applied load.

The rate of loading was dictated by a maximum permissible strain rate of 300 $\mu\epsilon$/min: Figs. 5.12 to 5.14 were employed to help achieve this.

(vi) The system was allowed to attain a stable state. Under elastic conditions this was attained almost immediately after load was applied. However, under inelastic conditions and just before buckling, delays in excess of thirty minutes were not uncommon. This agreed well with the observations of Neal[101] and those of Ref. 104.

(vii) Next, dial gauges at the supports and that measuring vertical deflection of the beam at midspan were read.

(viii) The crocodile retaining clips were removed and the displacement transducer plungers allowed to return gently until contact was made between the end tee pieces and the flanges of the beam.

(ix) A set of readings of flange lateral deflections was then taken. This was read from the data logger display.

(x) The corrections shown in Appendices IV(a) - IV(c) were applied to the vertical and lateral deflection readings in order to obtain the true midspan vertical deflection of the beam and the required vertical movement of the bracing forks.

(xi) The bracing forks were then moved vertically by the amount calculated in (x). The finger screws were used to control vertical movement and the forks were kept vertical throughout by use of the front spirit level as described in Section 4.3.5 .

(xii) All channels connected to the data logger were read to give the applied load, lateral deflections and bracing fork strains.

(xiii) Load versus vertical deflection and load versus lateral deflection plots were then updated and bracing forces calculated from bracing fork strains by the methods described in Section 4.3.5 .

(xiv) Steps (iii) to (xiii) were repeated until the end of the test.

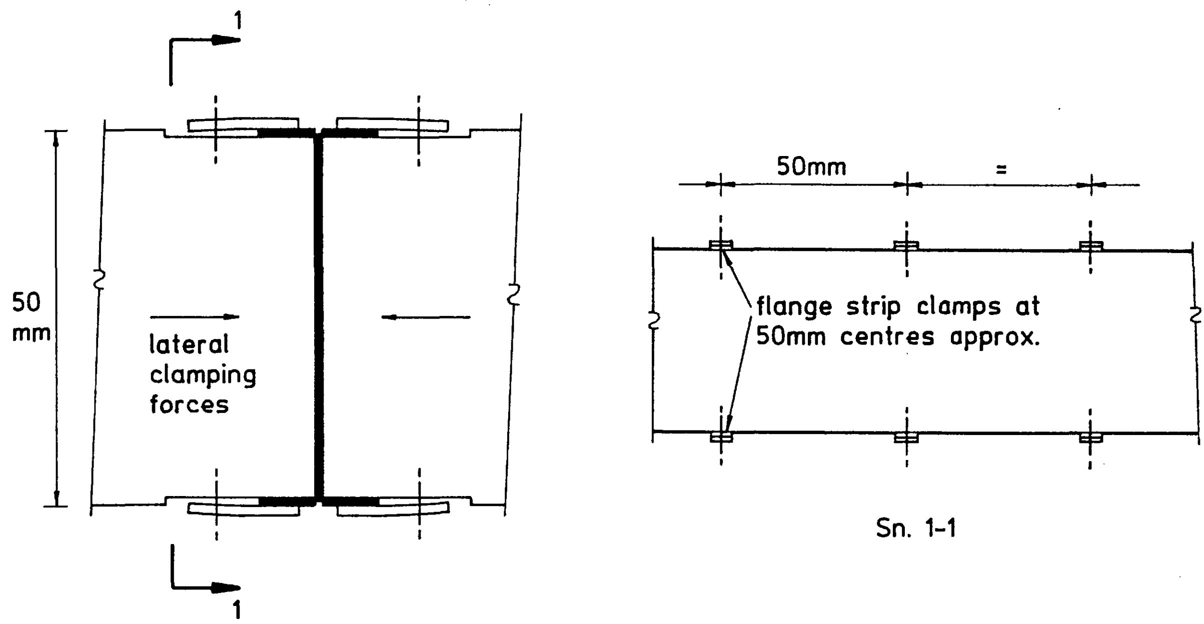

Fig. 5.1 : Clamped web and flange strips prior to TIG welding to form I -beam section. (Flange and web strips of beam shaded)

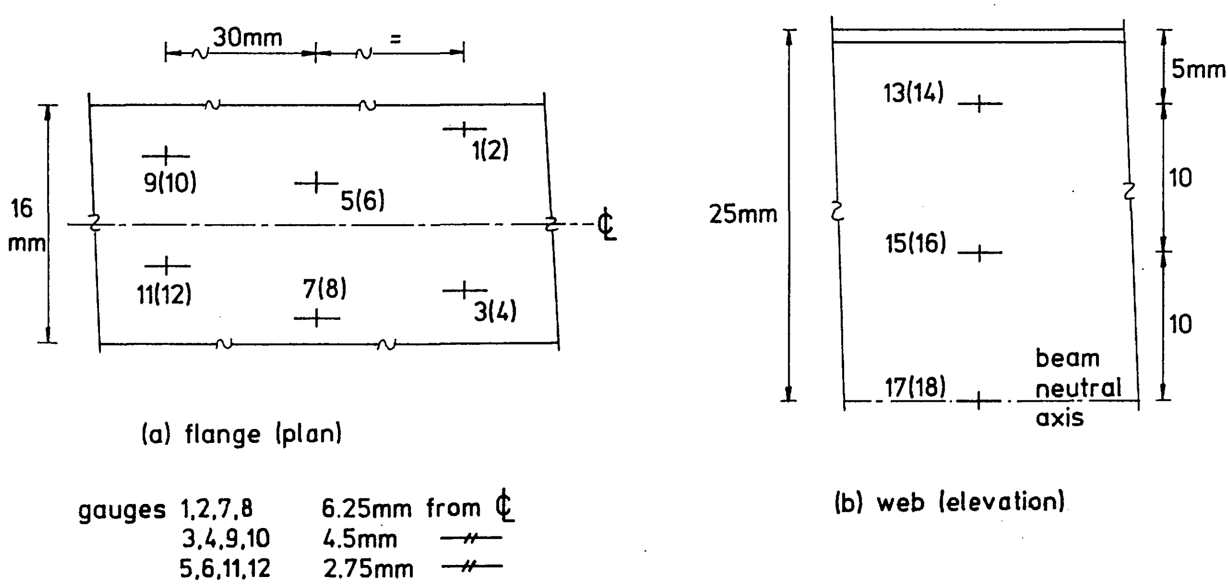

Fig. 5.2 : Strain gauge locations for residual strain measurement

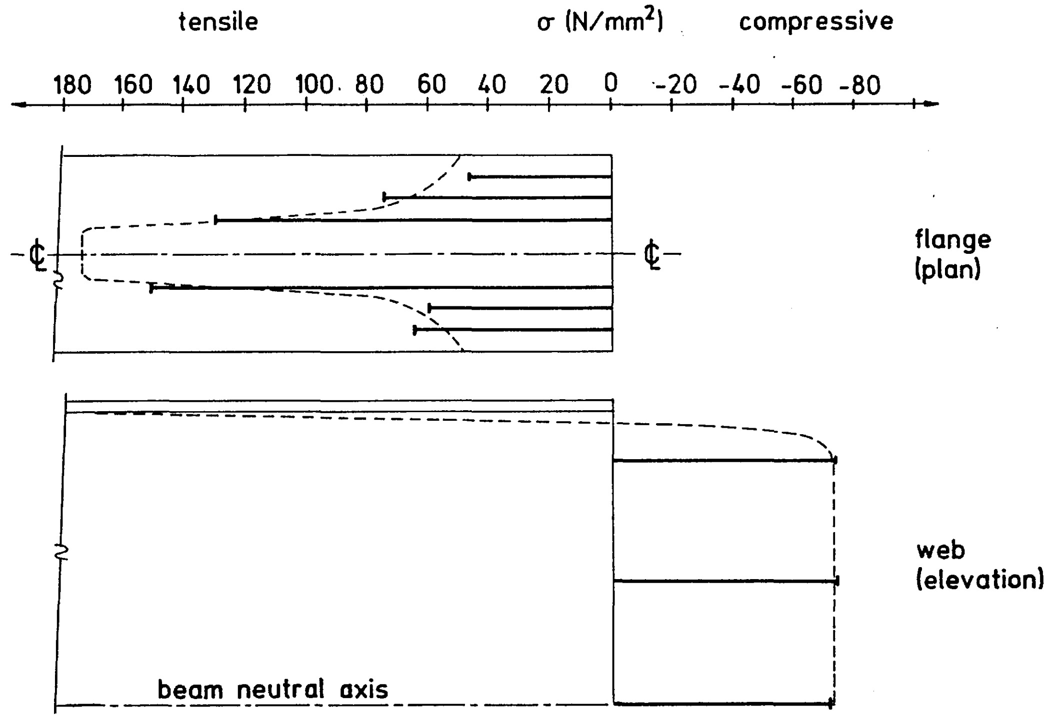

Fig. 5.3 : Measured residual stresses and proposed self-equilibrating residual stress distribution

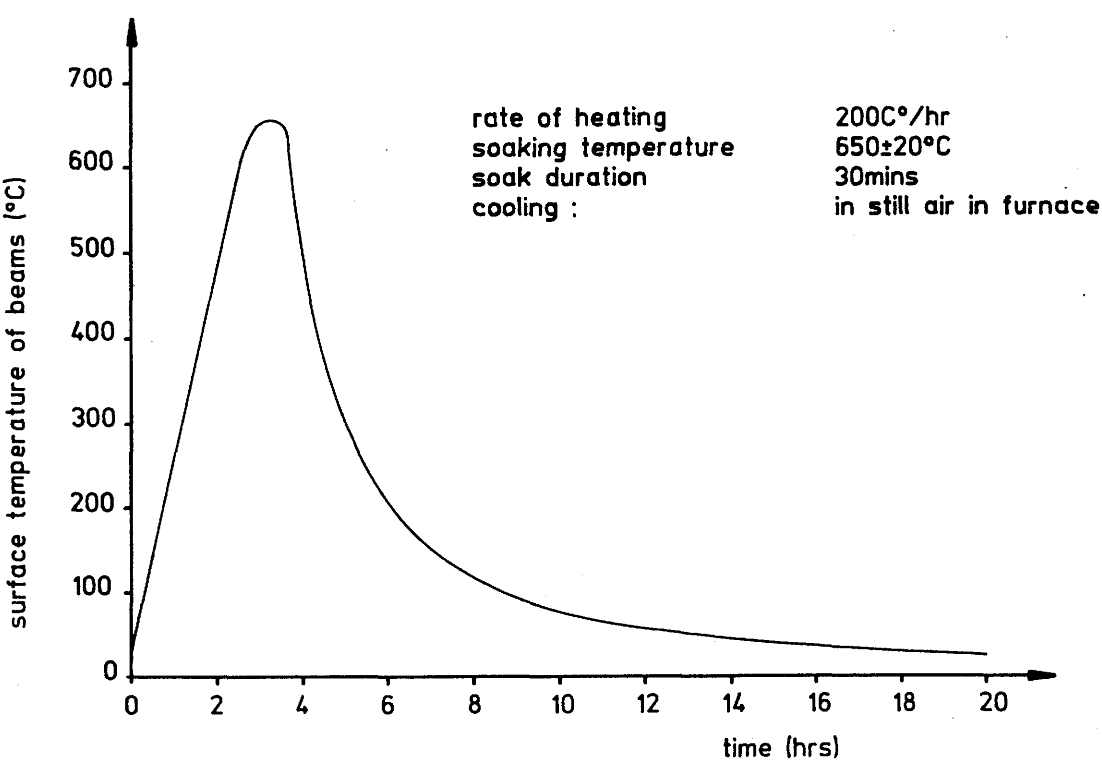

Fig. 5.4 : Temperature cycle used for stress-relieving of model beams

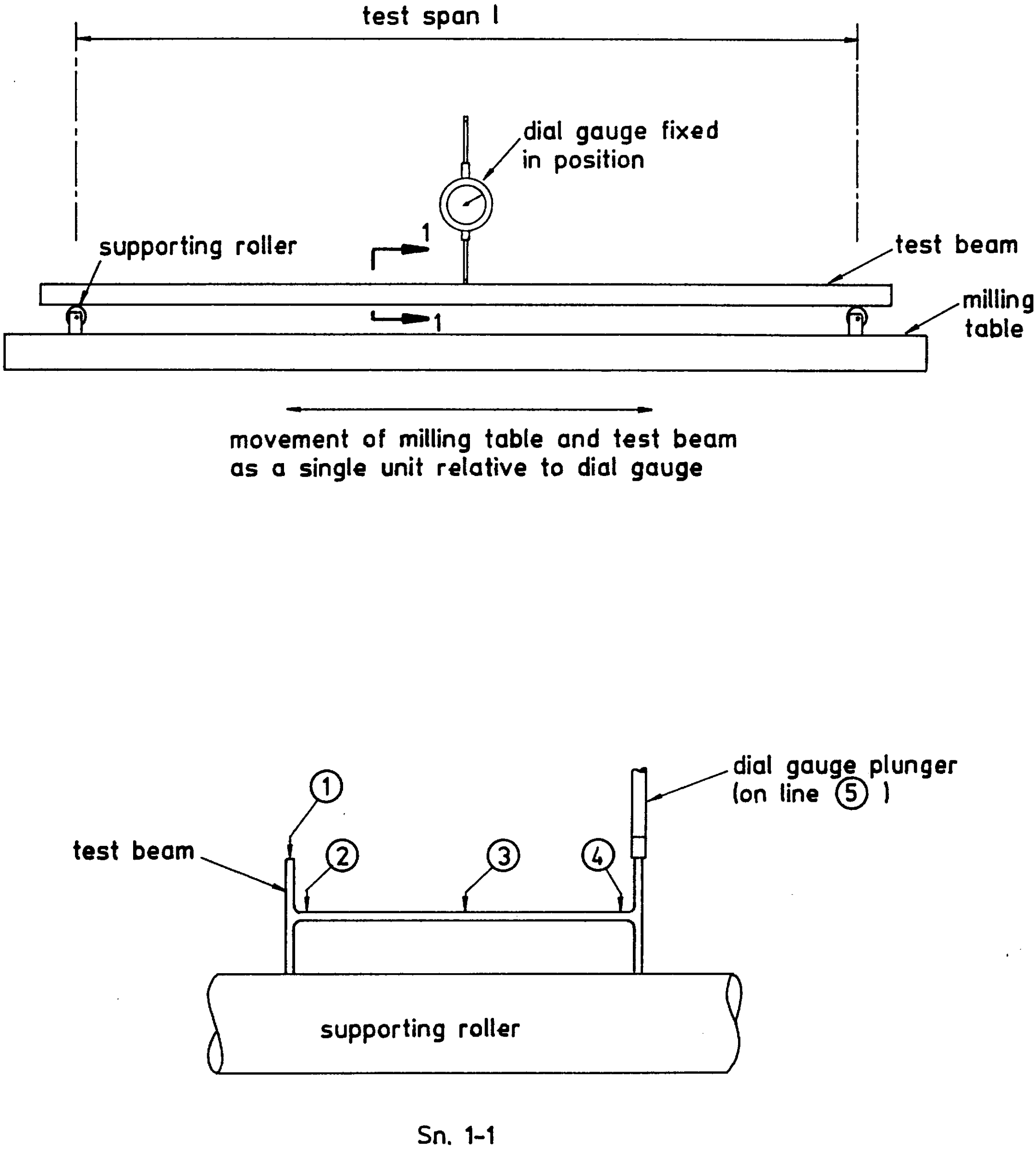

Fig. 5.5 : Arrangement for measuring model beam imperfections

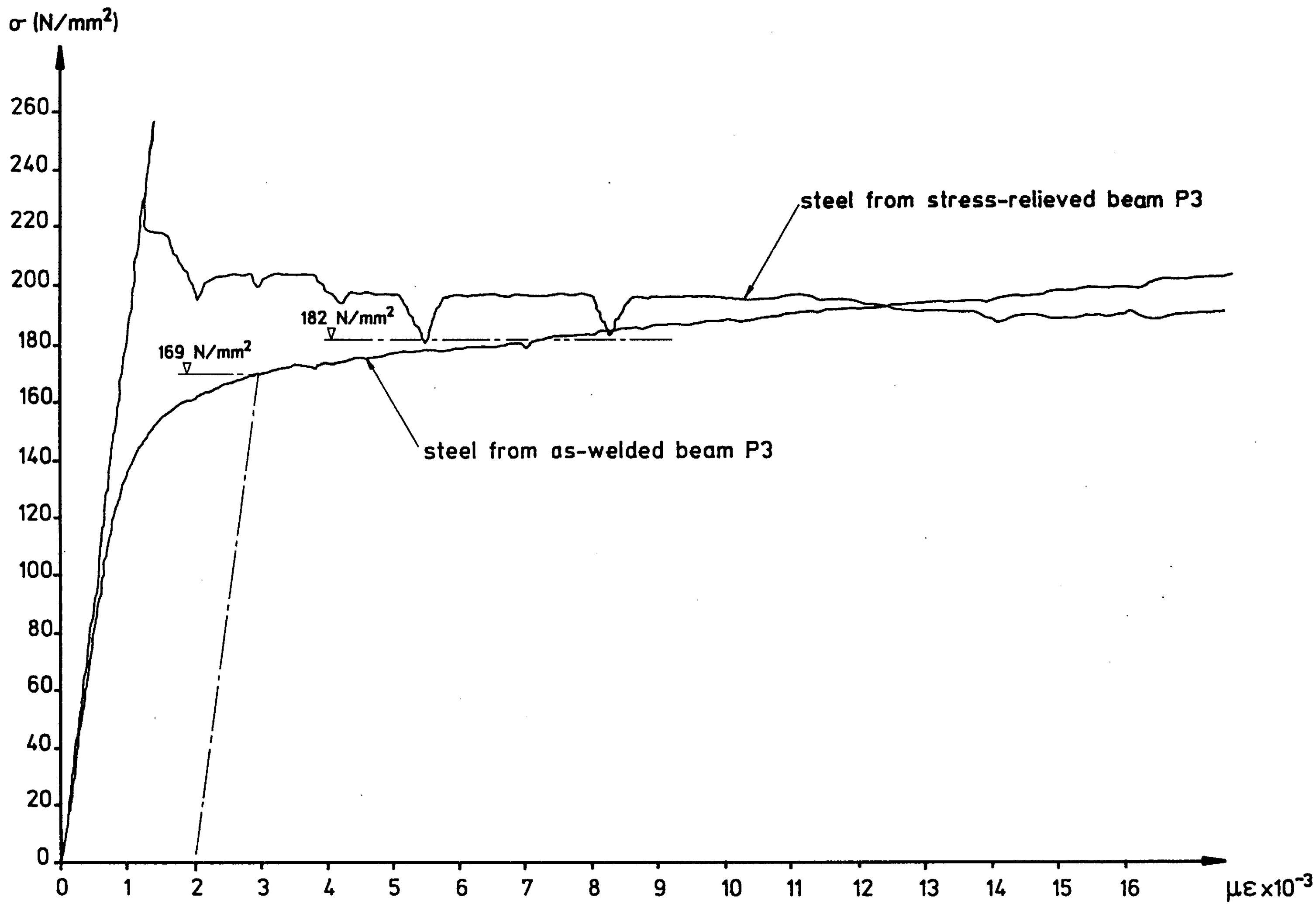

Fig. 5.6 : Stress-strain curves for as-welded and stress-relieved material cut from preliminary test beam

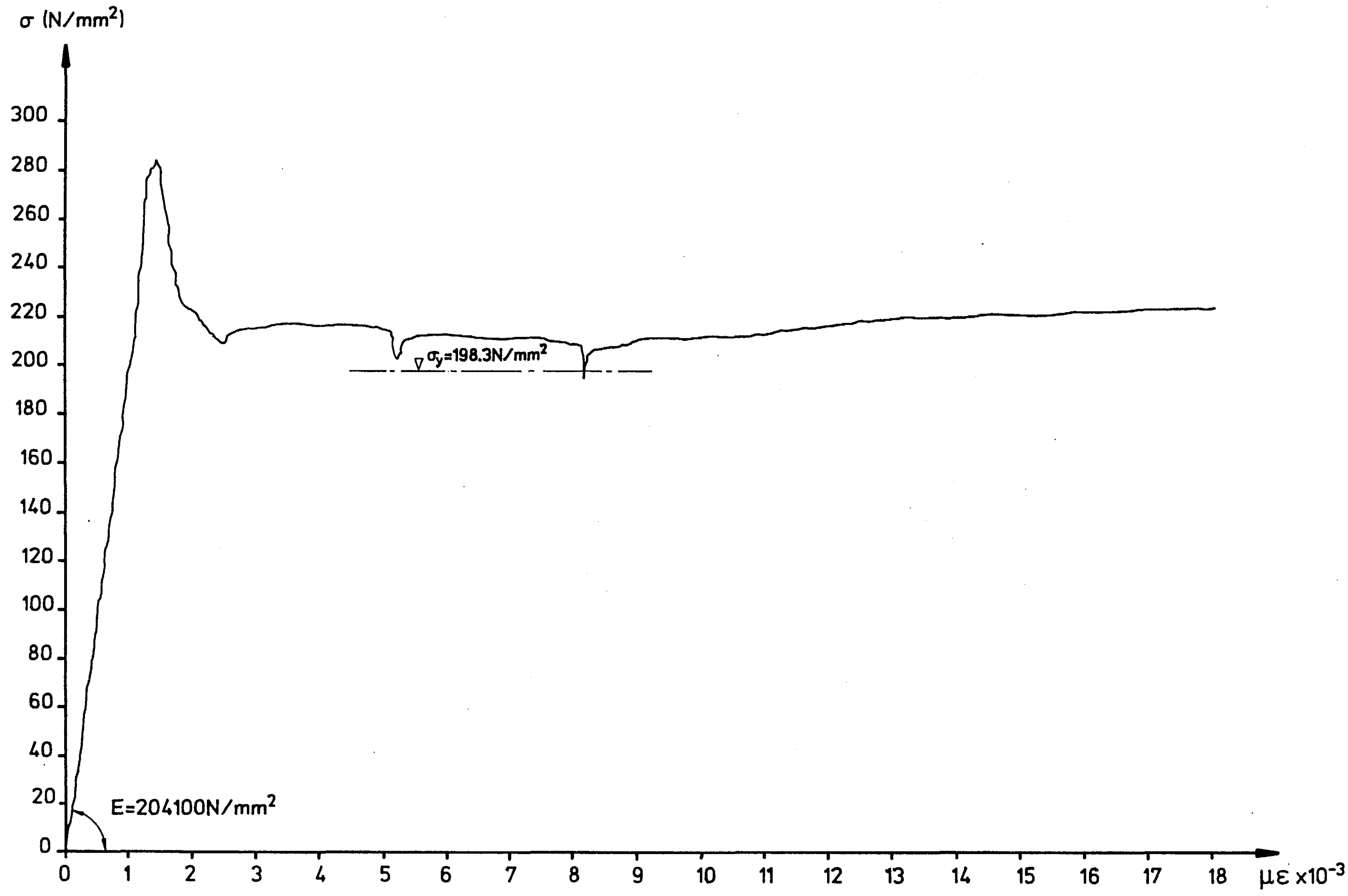

Fig. 5.7 : Stress-strain curve for stress-relieved web specimen from beam P13 to determine material properties for use in the main series of tests

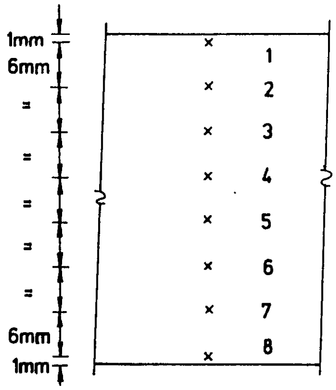

Rdg.	Vickers Hardness values V_H (kgf/mm^2) specimen 1	specimen 2	average
1	105.1	101.2	103.15
2	106.1	102.7	104.40
3	107.2	101.7	104.45
4	103.1	106.1	104.60
5	106.6	106.1	106.35
6	104.1	105.1	104.60
7	105.6	103.6	104.60
8	103.1	103.6	102.35

mean=104.3

(a) Vickers Hardness results for web specimens

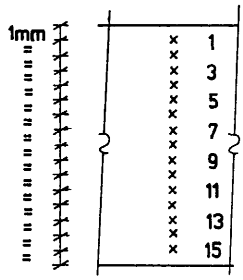

Rdg.	Vickers Hardness V_H (kgf/mm^2) spec. 1	spec. 2	spec. 3	spec. 4	ave.	corresponding σ_y
1	98.9	98.9	92.4	99.8	97.5	183.6
2	96.7	95.8	95.3	95.8	95.9	180.6
3	93.2	100.3	98.5	100.3	98.1	184.7
4	111.4	105.6	95.3	97.1	102.4	192.8
5	125.8	121.9	96.7	113.6	114.5	215.6
6	159.5	182.0	108.2	140.7	147.6	277.9
7	177.0	183.0	160.4	183.0	175.8	331.0
8	176.0	190.0	189.0	190.0	186.2	350.6
9	174.0	180.0	197.0	176.0	181.8	342.3
10	176.0	139.2	177.0	142.3	158.6	298.6
11	164.0	103.6	124.5	106.6	124.7	234.8
12	121.9	102.2	104.1	103.1	107.8	203.0
13	107.7	107.2	103.1	101.7	104.9	197.5
14	110.3	105.1	101.2	102.2	104.7	197.1
15	95.8	105.6	100.3	100.3	100.5	189.2

(b) Vickers Hardness results for flange specimens

Fig. 5.8 : Vickers Hardness results for flange and web specimens

(a) flange tip specimens (b) central specimen

Fig. 5.9 : Flange tensile specimens

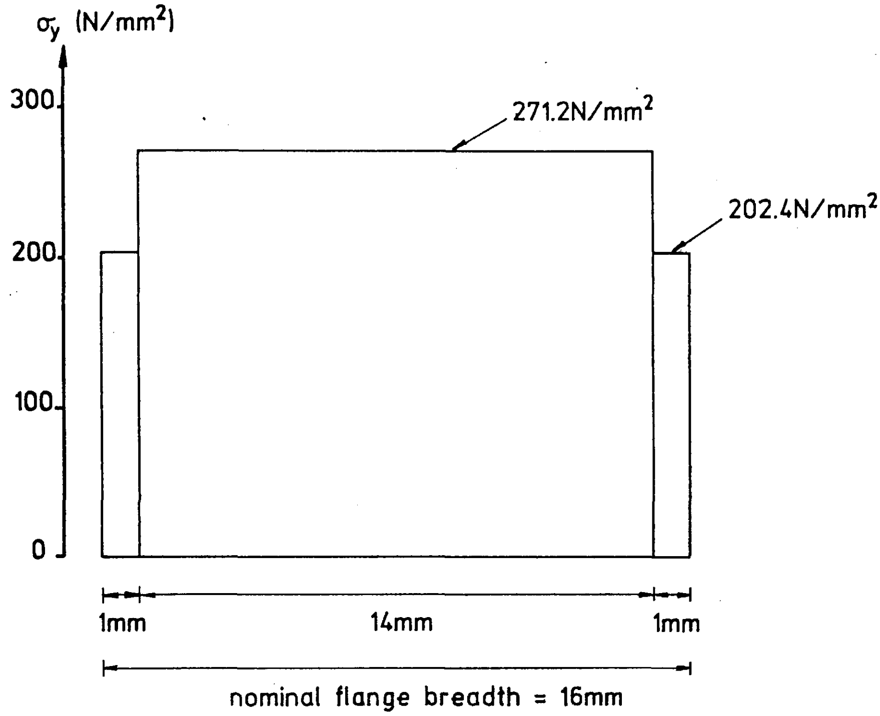

flange : weighted mean $\sigma_y = \dfrac{14 \times 271.2 + 2 \times 202.4}{16} = 262.6\text{N/mm}^2$

Fig. 5.10 : Assumed flange yield stress distribution and calculation of mean flange yield stress

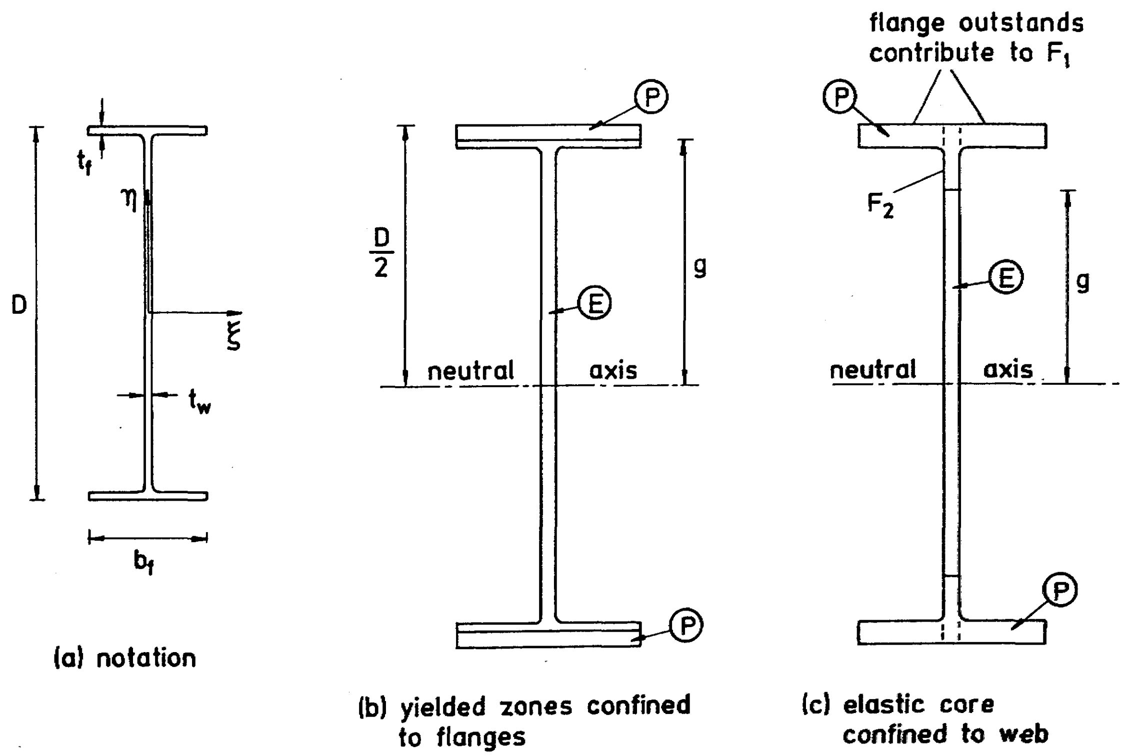

Fig. 5.11 : Notation employed in Section 5.6 and distribution of elastic and plastic zones in the cross-section

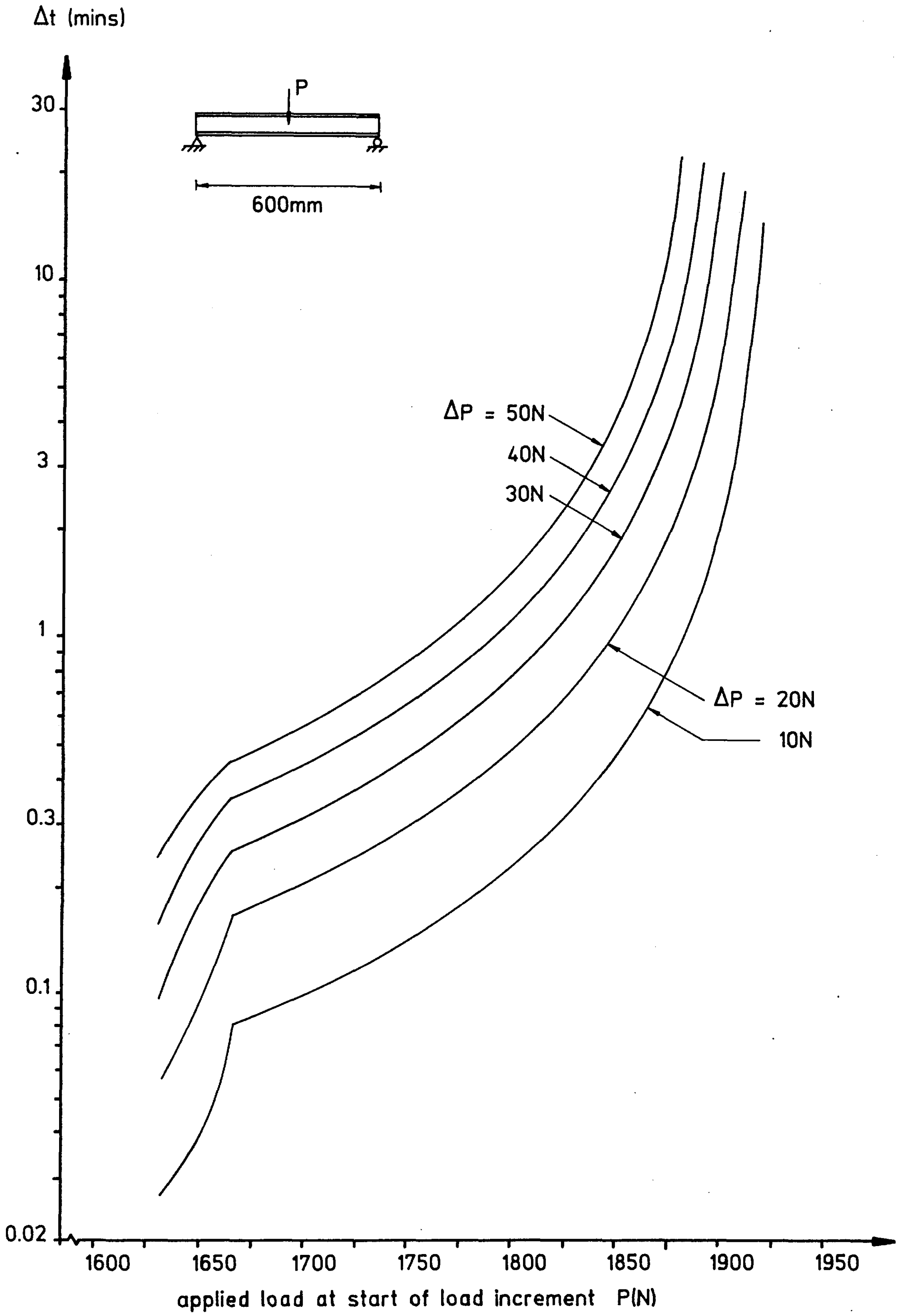

Fig. 5.12 : Minimum time intervals Δt(minutes) for the application of load increments ΔP as shown. Beam span=600mm.

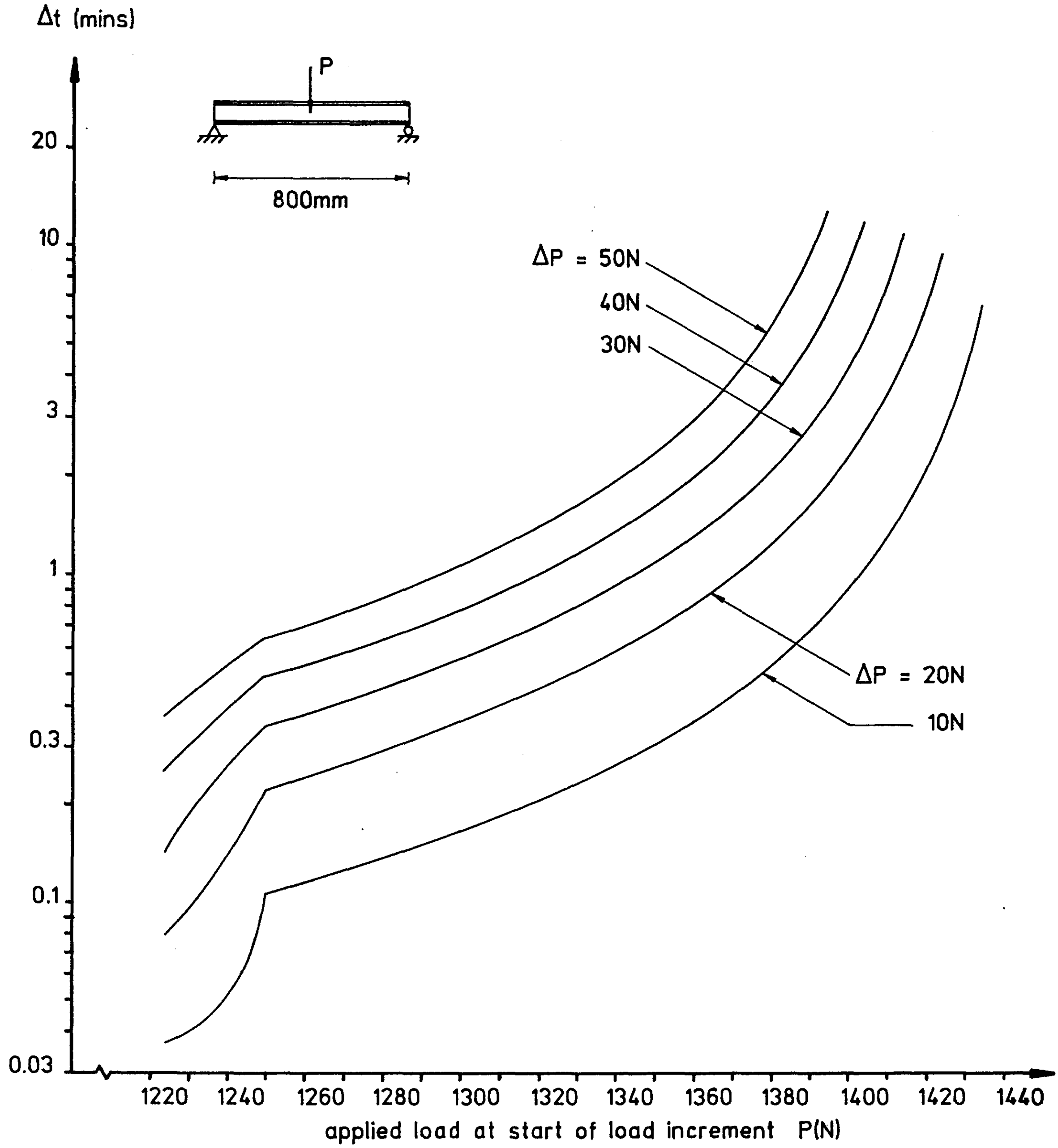

Fig. 5.13 : Minimum time intervals Δt(minutes) for the application of load increments ΔP as shown. Beam span=800mm.

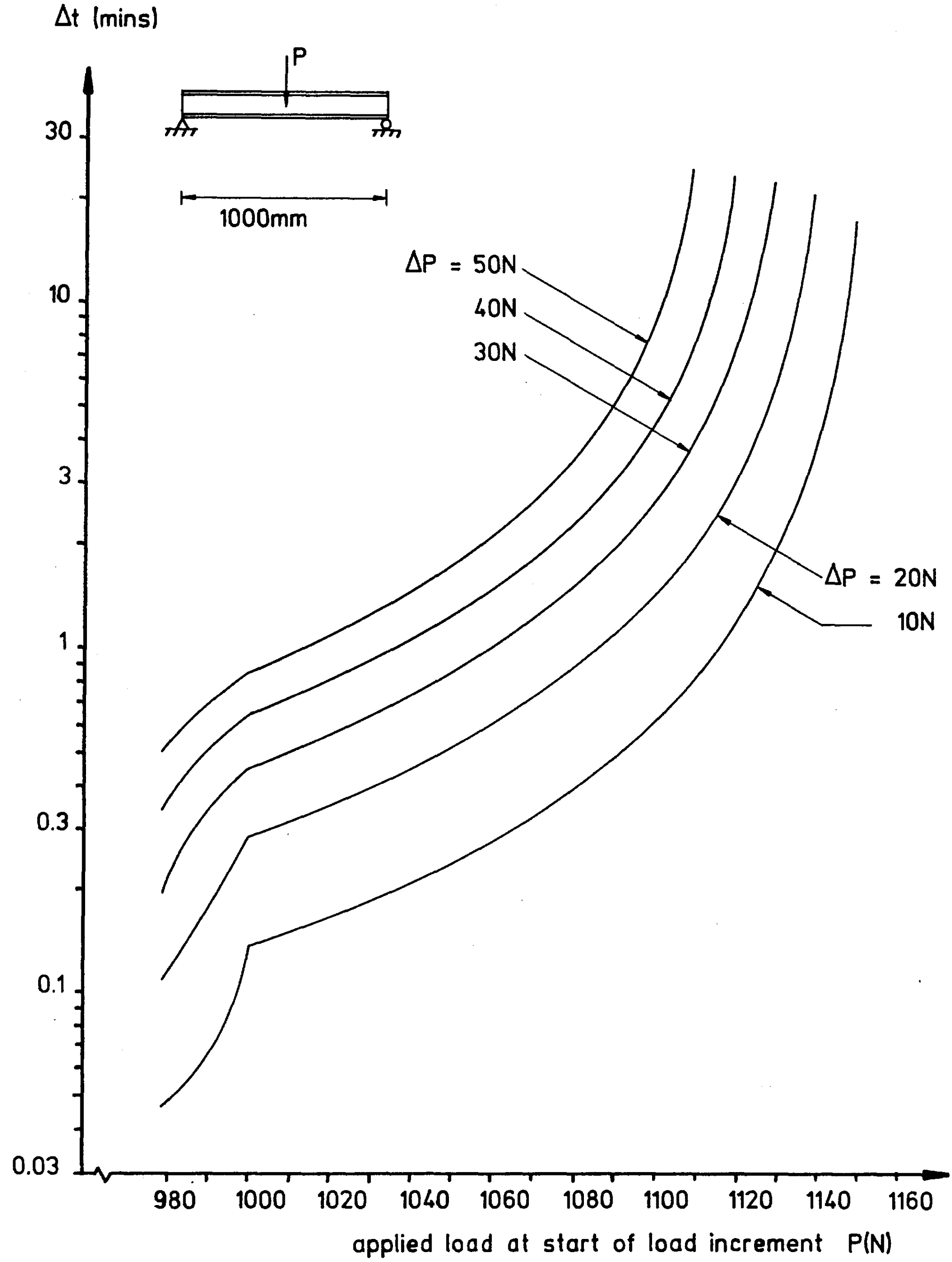

Fig. 5.14 : Minimum time intervals Δt(minutes) for the application of load increments ΔP as shown. Beam span=1000mm.

CHAPTER 6

EXPERIMENTAL RESULTS AND COMPARISON WITH FINITE ELEMENT ANALYSES

CHAPTER 6

EXPERIMENTAL RESULTS AND COMPARISON WITH FINITE ELEMENT ANALYSES

In this Chapter, the results of a series of twenty tests on model steel beams are presented and comparison is made with the results of a smaller number of FINAS and NASTRAN finite element analyses.

6.1 The Selection of R^2 Values to be Used in Model Beam Tests

The nominal cross-sectional dimensions of test beams shown in Section 5.5 were used to produce the series of elastic and inelastic load capacity curves shown in Fig. 6.1 . The inelastic buckling curve (4) was derived from an analysis of the inelastic buckling behaviour of determinate beams by Nethercot and Trahair[24]. This curve provided an inelastic transition from the in-plane collapse condition $P=P_p$ of line 1 to the elastic second mode buckling failure of curve 3. Values of the shape parameter R^2 corresponding to the beam spans (l) are also shown on the abscissa.

Examination of Fig. 6.1 revealed that the use of R^2 values of approximately 6.5, 11.5 and 18.5 in tests would permit the bracing requirements of beams in the plastic and inelastic regions to be assessed.

Two broad groups of central point loading tests were performed: the first to examine the lateral bracing requirements of beams loaded through the shear centre and with compression flange restraint; the second also with compression flange restraint but accompanied by compression flange loading. The bracing requirements investigated were those of minimum translational restraint stiffness and required bracing element strength, the latter examined on the basis of measured bracing forces.

Within each of these two groups, three sets of tests were conducted: one set for each of the R^2 values previously listed.

Within each set of tests, the number of beams tested was the minimum necessary to establish an approximate critical lateral restraint (λ_{cr}) for the value of R^2 appropriate to the set. Consequently, the number of tests in each set was not constant. A total of twenty model beams was tested.

Some of the cross-sectional dimensions of test beams M1 to M20 were presented in Table 5.4 in Chapter 5. Table 6.1 repeats much of the information contained in that Table and shows, in addition, mean tension and compression flange breadths, R^2, λ and a_f values and the midspan restraint and loading geometries employed in the tests. A considerable scatter of flange breadths is evident from Table 6.1 . However, this had little effect on the test series as R^2 had been chosen as the governing parameter. As the tests were primarily concerned with beams under inelastic and plastic conditions, use of the elastic R^2 parameter as the basis of comparison of experimental results could only be justified by its use in the determination of approximate inelastic buckling loads by the method of Nethercot and Trahair[24]. Comparison of experimental results with both first and second mode elastic critical loads and the minimum restraint criteria of Chapter 2 was facilitated by use of the R^2 parameter. The presentation of results in terms of the currently popular modified slenderness parameter $\sqrt{M_p/M_E}$ (in which M_E is the elastic critical moment) is discussed in Chapter 8. This parameter makes some allowance for the plastic capacity of the section.

The presence of initial imperfections in the beams resulted in slight variations in the actual R^2 values from the average values. These variations are shown in Table 6.2 and were not excessive.

Table 6.1: Dimensions of Test Beams and Characteristics of Restraint and Loading Systems

Test Set	Beam Mark	Beam Geometrical Properties								Restraint				Loading
		Span l (mm)	Average Material Thick-ness (mm)	Mean Compn. Flange Breadth (mm)	Mean Tension Flange Breadth (mm)	Mean Overall Depth D (mm)	I_{major} (mm^4)	I_{minor} (mm^4)	R^2	λ	Active leg length of bracing fork a_f (mm)	Absolute stiffness of lateral restraint K (N/mm)	Level of applic. on beam cross-section	Level of applic. on beam cross-section
1	M1 M2 M3	600 600 600	0.912 0.917 0.918	16.829 17.131 16.829	16.797 17.081 16.779	49.813 49.842 49.810	26735 27223 26881	725.4 767.8 729.0	6.69 6.46 6.79	1 2 3	79.11 61.62 54.77	31.60 66.87 95.25	compn. flange	shear centre
2	M4 M5 M6 M7	800 800 800 800	0.910 0.903 0.915 0.917	17.145 16.736 16.825 17.113	17.132 16.748 16.731 17.151	49.848 49.838 49.862 49.853	27079 26441 26855 27287	766.5 709.1 723.8 772.0	11.26 11.78 12.03 11.45	2 3 4 5	82.20 73.70 66.50 60.42	28.17 39.09 53.20 70.93	compn. flange	shear centre
3	M8 M9 M10	1000 1000 1000	0.908 0.907 0.910	16.683 16.789 16.522	16.663 16.808 16.743	49.793 49.774 49.846	26442 26535 26525	704.2 719.6 701.0	18.83 18.44 19.01	4 6 5	83.89 72.76 78.00	26.50 40.62 32.97	compn. flange	shear centre

Table 6.1: Dimensions of Test Beams and Characteristics of Restraint and Loading Systems (contd)

Test Set	Beam Mark	Beam Geometrical Properties								Restraint				Loading
		Span l (mm)	Average Material Thick- ness (mm)	Mean Compn. Flange Breadth (mm)	Mean Tension Flange Breadth (mm)	Mean Overall Depth D (mm)	I_{major} (mm^4)	I_{minor} (mm^4)	R^2	λ	Active leg length of bracing fork a_f (mm)	Absolute stiffness of lateral restraint K (N/mm)	Level of applic. on beam cross-section	Level of applic. on beam cross-section
4	M11	600	0.916	17.145	17.178	49.892	27329	774.7	6.39	3	53.66	101.26	compn. flange	compn. flange
	M12	600	0.912	16.888	16.687	49.861	26760	722.0	6.70	4	49.92	125.77		
	M13	600	0.917	16.893	16.761	49.856	26932	731.0	6.74	5	46.15	159.18		
	M14	600	0.913	16.544	16.775	49.848	26627	706.4	6.85	6	43.93	184.55		
5	M15	800	0.911	17.122	17.137	49.841	27082	766.0	11.29	6	57.01	84.44	compn. flange	compn. flange
	M16	800	0.909	16.904	16.872	49.846	26773	732.6	11.66	8	52.57	107.69		
6	M17	800	1.004	15.452	15.026	50.100	27746	596.5	18.52	7	58.86	76.72	compn. flange	compn. flange
	M18	800	1.019	15.176	15.222	50.231	28254	600.4	19.13	9	54.01	99.31		
	M19	800	1.004	15.293	15.399	50.152	27958	609.1	18.17	10	51.90	111.92		
	M20	800	1.005	15.067	15.122	50.074	27559	580.0	19.03	12	49.64	127.91		

Table 6.2: Variation of Beam R^2 Values from the Mean

Test Sets	1 and 4		2 and 5		3 and 6	
Mean R^2 value for sets	6.660		11.578		18.733	
Beam Mark and variation from mean R^2 as a percentage of mean R^2	M1	+0.45%	M4	-2.75%	M8	+0.52%
	M2	-3.01%	M5	+1.74%	M9	-1.60%
	M3	+1.95%	M6	+3.90%	M10	+1.48%
	M11	-4.06%	M7	-1.11%	M17	-1.14%
	M12	+0.60%	M15	-2.49%	M18	+2.12%
	M13	+1.20%	M16	+0.71%	M19	-3.01%
	M14	+2.85%			M20	+1.58%

6.2 Experimental and Finite Element Results

In the presentation of test and finite element results the following notation has been adopted:

P = applied load on beam
P_{cy} = fully yielded compression flange force = $b_f t_f \sigma_y$
P_{br} = measured bracing force

K and λ are as previously defined (Chapter 1) whilst P_p is the theoretical fully-plastic load calculated from the measured cross-sectional geometry, beam span and yield stress.

A limited number of finite element analyses were performed for comparison with experimental results. The programmes FINAS and NASTRAN were used and only two finite element analyses were performed for each of the six sets of tests within the experimental programme; in each set, the two analyses were performed on the tests providing the upper and lower bounds to the critical restraint λ_{cr}. In both the FINAS and NASTRAN analyses beam elements were used to model the braced beam, twelve elements being employed in FINAS compared with twenty-four in NASTRAN.

6.2.1 Set 1: Shear Centre Loading on Beams of $R^2 \doteqdot 6.5$

Examination of Fig. 2.22 for the combination $R^2 \doteqdot 6.5$, shear centre loading and compression flange restraint showed that elastic bifurcation theory predicted a critical restraint stiffness of $\lambda_{cr} \doteqdot$ 2.5 for attainment of second mode elastic buckling in the primary member. Although the short span of 600mm employed in this set of tests precluded the possibility of elastic failure, very low values of λ were nevertheless considered appropriate.

A bracing stiffness of 31.60 N/mm was used in the first test, giving a non-dimensional stiffness of λ=1.0 . Preparations for this test and the test procedure adopted were as described in the preceding two Chapters. Fig. 5.12 was used to ensure that the rate of plastic straining in the section due to in-plane flexure did not exceed 300 $\mu\epsilon$/minute. The behaviour of the model beam under test is illustrated by the load-deflection and load-brace force curves of Fig. 6.2 . Failure of model beam M1 was in a partially restrained first mode inelastic buckling configuration; the midspan bracing (λ=1) proved insufficient to provide full lateral restraint to the compression flange of the beam.

The ultimate load (P_{ult}) attained by beam M1 was approximately 91% of its fully plastic load P_p. As the load at first yield (P_y) in the section was approximately $0.842P_p$, a considerable amount of yielding had occurred in the section at failure.

Fig. 6.2 indicates the possibility of examining the post-buckling behaviour of test beams using displacement rather than load control. The tendency for brace forces (Fig. 6.2(b)) to continue to increase under post-buckling conditions was noted. The maximum recorded brace force in this test was approximatly 4.5% of the fully yielded compression flange force P_{cy}, although even higher values would have been observed had the test been continued further into the post-buckling phase. A brace force of $0.017P_{cy}$ accompanied attainment of the beam's ultimate load of $0.91P_p$.

As the restraint stiffness λ=1 had been inadequate in Test 1, λ =2 (equivalent to an absolute bracing stiffness of K=66.9 N/mm) was employed in Test 2. The results of this test are shown in Fig. 6.3 . An ultimate load of $0.98P_p$ was achieved though not sustained and failure, as in Test 1, was in the partially braced inelastic first mode. Testing was again continued well into the post-buckling state, observed brace forces reaching a maximum value of $0.062P_{cy}$ at the conclusion of the test and approximately $0.025P_{cy}$ at attainment of the ultimate load. Lateral deflections of the compression flange at midspan were of the same order as those in Test 1; in both cases maximum recorded values were approximately five times larger than those accompanying the ultimate load.

Both NASTRAN and FINAS finite element comparisons were performed for Test 2. Under elastic conditions, agreement between both sets of finite element results and test results was generally good. The

NASTRAN analysis proved incapable of providing a solution for applied loads P in excess of about $0.93P_p$. In addition, no appreciable reduction in the major or minor axis flexural stiffness of the beam under increasing spread of plasticity through the section was apparent from the NASTRAN results. Although FINAS was better able to predict this stiffness degradation, it was unable to predict inelastic lateral-torsional collapse of beam M2 and, instead, in-plane collapse following the formation of a plastic hinge at midspan was forecast. Even the use of enforced displacement increments of greatly decreasing magnitude with increasing plasticity in the section did not permit the analysis to proceed beyond the final FINAS results shown on the graphs of Fig. 6.3 . Nevertheless, the FINAS ultimate load of $0.99P_p$, determined by the graphical construction shown in Fig. 6.3(a), gave support to the measured yield stress σ_y=234.5 N/mm^2.

Correlation between lateral deflection of the compression flange and measured brace force was observed to be poor in Tests 1 and 2; the apparent bracing stiffness linking these two quantities differed considerably from the intended values in the two tests. This was due to very small rotations of the top plate of the bracing fork assembly (© in Fig. 4.15) as described in Section 4.3.5 . In Test 3 and in all subsequent tests the front spirit level of Fig. 4.17 was used to prevent relaxation of the bracing fork. This was successful.

In both Tests 1 and 2, lateral deflections of the tension flange at midspan were significantly less than, but in the same sense as those of the compression flange. The algebraic difference between corresponding readings was a measure of the angle of twist at midspan.

A non-dimensional bracing stiffness of λ=3 was employed in Test 3 as the λ=1 and λ=2 braces of the first two tests had provided only partial restraint. Formation of a plastic hinge in beam M3 demonstrated the adequacy of the λ=3 restraint. The graphical construction of Fig. 6.3(a) was used in Fig. 6.4(a) to estimate the ultimate load-carrying capacity of the beam as no definite plateau had been obtained on the load-vertical deflection curves. This construction had been employed by Dux and Kitipornchai in Ref. 4 to make allowance for the stress concentration phenomenon observed by Baker, Horne and Heyman in Ref. 99. This effect was noted in Section 5.5 and is discussed more fully later in this Chapter.

The experimental ultimate load was only 3.7% greater than the fully plastic load P_p whilst a FINAS analysis predicted an ultimate load of $1.006P_p$.

A NASTRAN analysis again provided results for loads smaller than $0.94P_p$. Thereafter, no solution was possible due to non-convergence of the iterative process employed in the coupled non-linear analysis.

Correlation between experimental and FINAS brace forces was good; both gave small values of approximately $0.014P_{cy}$ at the ultimate load. In the elastic range, NASTRAN predicted brace forces significantly smaller than either FINAS or measured values. Although measured midspan lateral deflections of the compression flange were very small (typically less than 0.6mm), and therefore consistent with fully effective bracing, correlation with measured brace forces via the brace stiffness K=95.25 N/mm (Table 6.1) was excellent. Recorded tension flange lateral deflections were almost negligible whereas FINAS predicted deflections of equal magnitude but opposite sign in the two flanges.

From the results of the three tests in this first set, it was possible to deduce that the critical restraint stiffness λ_{cr} lay in the range $\lambda=2$ to $\lambda=3$. A summary of experimental results is shown in Table 6.3 .

6.2.2 Set 2: Shear Centre Loading on Beams of $R^2 \doteqdot 11.5$

The starting value of λ used in this set was $\lambda=2$ in Test 4 (Table 6.1). This value was slightly lower than the predicted value of $\lambda_{cr} \doteqdot 2.6$ for second mode elastic buckling from Fig. 2.22 . Beam spans of 800mm were used in four tests (4 to 7) giving R^2 values close to the mean value of 11.578 shown in Table 6.2 .

First mode inelastic instability occurred in Test 4 at a load of approximately $0.98P_p$, indicating the inadequacy of the $\lambda=2$ restraint. The same mode of failure was evident in Tests 5 and 6 where restraint stiffnesses of $\lambda=3$ and $\lambda=4$ had been provided. Failure in Test 5 occurred at a load of approximately $1.06P_p$ and at $1.04P_p$ in

Table 6.3: Experimental Results

Test Set	Beam Mark	R^2	λ	absolute brace stiffness K (N/mm)	level of applicn. of restraint on x-sectn.	level of applicn. of load on x-sectn.	failure mode	theoretical P_y/P_p	P_{ult}/P_p	$\frac{P_{br}}{P_{cy}}$ x100% at ultimate load	finite element analyses performed		Suggested value of λ_{cr} for set	approx. K_{cr} corres-ponding to suggested λ_{cr} (N/mm)
											FINAS	NASTRAN		
1	M1 M2 M3	6.69 6.46 6.79	1 2 3	31.60 66.87 95.25	comp. flange	shear centre	1st mode 1st mode Pl. hinge	.842 .843 .842	0.91 0.98 1.04	1.7 2.5 0.9	NO YES YES	NO YES YES	2.5	81.1
2	M4 M5 M6 M7	11.26 11.78 12.03 11.45	2 3 4 5	28.17 39.09 53.20 70.93	comp. flange	shear centre	1st mode 1st mode 1st mode Pl. hinge	.844 .842 .841 .844	0.98 1.06 1.04 1.04	1.0 3.1 1.0 0.25	NO NO YES YES	NO NO YES YES	4.5	62.1
3	M8 M9 M10	18.83 18.44 19.01	4 6 5	26.50 40.62 32.97	comp. flange	shear centre	1st mode 2nd mode 2nd mode	.841 .842 .841	0.99 1.02 0.97	1.0 0.8 0.3	YES NO YES	YES NO YES	4.5	29.7

Table 6.3: Experimental Results (contd)

Test Set	Beam Mark	R^2	λ	absolute brace stiffness K (N/mm)	level of applicn. of restraint on x-sectn.	level of applicn. of load on x-sectn.	failure mode	theoretical P_y/P_P	P_{ult}/P_P	$\frac{P_{br}}{P_{cy}}$ x100% at ultimate load	finite element analyses performed: FINAS	finite element analyses performed: NASTRAN	Suggested value of λ_{cr} for set	approx. K_{cr} corres-ponding to suggested λ_{cr} (N/mm)
4	M11	6.39	3	101.26	comp. flange	comp. flange	1st mode	.843	0.99	1.8	NO	NO	5.5	171.9
	M12	6.70	4	125.77			1st mode	.842	1.04	0.8	NO	NO		
	M13	6.74	5	159.18			1st mode	.842	0.96	2.9	YES	FAILED		
	M14	6.85	6	184.55			Pl. hinge	.841	0.97	0.7	YES	NO		
5	M15	11.29	6	84.44	comp. flange	comp. flange	1st mode	.843	0.75	3.8	YES	NO	7.0	96.1
	M16	11.66	8	107.69			Pl. hinge	.843	1.02	0.4	YES	NO		
6	M17	18.52	7	76.72	comp. flange	comp. flange	1st mode	.832	0.84	2.4	NO	NO	11.0	119.9
	M18	19.13	9	99.31			1st mode	.831	0.94	1.9	NO	NO		
	M19	18.17	10	111.92			1st mode	.832	0.80	4.4	YES	NO		
	M20	19.03	12	127.91			2nd mode	.831	0.91	0.8	YES	NO		

Test 6. The results of Tests 4, 5 and 6 are shown in Figs. 6.5 to 6.7 . Both FINAS and NASTRAN analyses were carried out for Test 6 and the maximum load attained by the FINAS model on its last convergent iteration was $1.01P_p$.

Although an ultimate load of $1.04P_p$ was attained in both Tests 6 and 7, only the λ=5 restraint provided in Test 7 was adequate to provide fully effective midspan restraint to the beam and in-plane failure was observed. Fig. 6.8 shows experimental and finite element results for Test 7. A more definite plateau in test data is evident in Fig. 6.8(a) than in the case of Test 3 results in Fig. 6.4(a), allowing a more accurate assessment of ultimate load in Test 7.

As in Set 1, the smallest recorded brace force corresponding to attainment of a beam's ultimate load occurred in the fully effective bracing in Test 7. A brace force of only $0.0025P_{cy}$ was noted at the ultimate load condition; corresponding lateral flange deflections were small; and the maximum midspan lateral movement of the compression flange was less than 0.5mm. Considerably larger values had been recorded in the three preceding tests.

Examination of the results summarised in Table 6.3 revealed that an estimated critical restraint stiffness of $\lambda_{cr} \doteqdot 4.5$ for Set 2 was appropriate.

6.2.3 Set 3: Shear Centre Loading on Beams of $R^2 \doteqdot 18.5$

Following the trend in estimated λ_{cr} values in the previous two sets, a starting value of λ=4, higher than that adopted at the start of Set 2, was employed in Test 8. Although a load of $0.99P_p$ was attained, first mode inelastic instability was the mode of failure and a brace force of $0.01P_{cy}$ accompanied the onset of instability (Fig. 6.9). In both Tests 9 and 10, second mode inelastic buckling constituted the failure mode and the respective restraint stiffnesses of λ=6 and λ=5 were fully effective. Small brace forces of less than $0.01P_{cy}$ were recorded at the ultimate load condition (Table 6.3 and Figs. 6.9(b) and 6.10(b)).

FINAS and NASTRAN finite element analyses were performed in Tests 8 and 10 as these Tests had provided the lower and upper bounds on the critical restraint stiffness λ_{cr}. Agreement between finite element and experimental results was acceptable although in Test 8 neither analysis provided results for applied loads greater than $0.94P_p$. However, in Test 10 FINAS predicted the failure load exactly and, in addition, accurately predicted the load-vertical deflection behaviour well into the post-buckling range as shown in Fig. 6.11(a). Brace forces (Fig. 6.11(b)) were less accurately predicted, although the predicted maximum was only $0.011P_{cy}$.

As flange lateral deflections at midspan were negligible, deflections at the quarter point have been shown in Fig. 6.11(c); considerable deflections in the post-buckling range indicated inelastic second mode failure.

The critical restraint stiffness for this Set was estimated to be $\lambda_{cr} \doteqdot 4.5$, as in Set 2.

6.2.4 Set 4: Compression Flange Loading on Beams of $R^2 \doteqdot 6.5$

Based on the elastic buckling theory of Chapter 2, Fig. 2.21 indicated that critical restraint stiffnesses corresponding to $\lambda_{cr} \doteqdot 6.5$ would be necessary for fully effective restraint of beams loaded and braced at compression flange level. In the three sets of tests reported in this and the following two Sections, the slotted pulley of Fig. 4.6(b) was employed to provide compression flange loading on the test beam. All other details of the test frame and its associated instrumentation remained unaltered from previous tests.

A starting value of $\lambda=3$ was employed in Test 11 with a test span of 600mm. Failure of the beam at a load of $0.99P_p$ was due to first mode inelastic instability. Lateral deflections of the compression flange at midspan were large under post-buckling conditions (Fig. 6.12(c)) although almost negligible deflections had been evident during initial elastic loading and in the inelastic range up to $0.95P_p$. A brace force of $0.018P_{cy}$ accompanied the ultimate load-carrying capacity of the beam.

Restraints of $\lambda=4$ and $\lambda=5$ in Tests 12 and 13 also proved inadequate for the prevention of first mode failure although failure loads of $1.04P_p$ amd $0.96P_p$ were recorded in these tests (Figs. 6.13 and 6.14). Corresponding bracing forces of $0.008P_{cy}$ and $0.029P_{cy}$ were noted. The curves of Fig. 6.13(b) and (c) indicate insignificant midspan lateral deflection of the flanges before attainment of the ultimate load in Test 12. Thereafter, in the post-buckling phase, brace forces increased rapidly as the shedding of vertical load progressed. In Test 13 however, brace forces increased from the commencement of loading and continued to increase during post-buckling deformations.

Although both NASTRAN and FINAS analyses were attempted in order to verify the experimental results of Test 13, divergence of the NASTRAN solution at an early stage of loading meant that only FINAS results were available for comparison. As shown in Fig. 6.14(a), convergence problems were also encountered in the Finas solution and no definite mode of failure could be deduced from the finite element results. Nevertheless, the limited comparison of results which was possible (Fig. 6.14) revealed fair correlation.

The $\lambda=6$ restraint provided in Test 14 proved adequate and the ultimate load of $0.97P_p$ was accompanied by a brace force of $0.007P_{cy}$ (Fig. 6.15). A well defined plateau was displayed on the vertical deflection curve based on experimental results in Fig. 6.15(a). As illustrated in Fig. 6.15(c), both theoretical and experimental lateral movements of the compression flange were very small; FINAS predicted much greater, though still small, lateral deflections of the unbraced tension flange.

A critical restraint stiffness of $\lambda_{cr} \doteqdot 5.5$ was estimated for Set 4.

6.2.5 Set 5: Compression Flange Loading on Beams of $R^2 \doteqdot 11.5$

As only two beams were tested in this Set, FINAS analyses were performed for each. The $\lambda=6$ restraint adopted in Test 15 was inadequate and first mode failure of the braced beam at an applied load of $0.75P_p$ (Fig. 6.16) was noted to constitute nominal elastic failure as first yield in the section due to vertical loading was not theoretically predicted until an applied load of $0.843P_p$ had been reached (Table 6.3). In practice, wholly elastic buckling of the beam was unlikely due to increased strains in the cross-section arising from the superimposition of lateral bending on in-plane flexure.

Comparison of experimental and FINAS results in Fig. 6.16 showed that the FINAS ultimate load of approximately $0.87P_p$ was substantially higher than the experimental failure load. Non-convergence of the FINAS solution was encountered in several attempted analyses employing successively smaller increments of enforced vertical displacement.

Fully effective restraint was provided by the $\lambda=8$ bracing employed in Test 16. A marked plateau on the experimental load-vertical deflection curve of Fig. 6.17(a) meant that the ultimate load of $1.02P_p$ was well defined. The same ultimate load was predicted by the FINAS analysis.

The observed tendency for small bracing forces to occur in conjunction with fully effective bracing was perpetuated in this Set of tests. Respective measured bracing forces of $0.038P_{cy}$ and $0.004P_{cy}$ corresponded to ultimate load conditions in the two tests. Although compression flange lateral deflections in Test 16 were almost negligible (Fig. 6.17(c)), tension flange movement was considerable, reflecting the high degree of initial twist in this beam (Table 5.4) and the tendency for the tension flange to straighten under increasing load.

As a result of these two tests, it was concluded that a value of $\lambda_{cr} \doteqdot 7.0$ was appropriate to the Set.

6.2.6 Set 6: Compression Flange Loading on Beams of $R^2 \doteqdot 18.5$

Due to slight changes in cross-sectional dimensions of test beams from those of Sets 1 to 5, the desired R^2 value was achieved in Set 6 by the use of a test span of 800mm.

A restraint stiffness equivalent to $\lambda=7$ was employed in the first test of the set, Test 17. The results of this test (Fig. 6.18) indicate inelastic first mode failure of the beam/restraint system. A force of $0.024P_{cy}$ was developed in the bracing at attainment of the ultimate load of $0.84P_p$ and Fig. 6.18(c) indicates that failure of the beam was largely due to torsional instability.

First mode inelastic instability was also observed in tests on beams M18 and M19, these beams restrained by braces of stiffness $\lambda=9$ and $\lambda=10$, respectively. In Test 18 a brace force of $0.019P_{cy}$ occurred at the ultimate load condition ($P_{ult}=0.94P_p$) whilst a force of $0.044P_{cy}$ was developed in Test 19 at a failure load of $0.8P_p$. Figs. 6.19 and 6.20 show the results of these two tests.

Measured lateral deflections of the flanges in Tests 18 and 19 (Figs. 6.19(c) and 6.20(c)) again indicated a tendency for large angles of twist to be developed at midspan with little lateral movement of the shear centre of the section. This was particularly evident in Test 18.

Inelastic second mode failure of the beam in Test 20 (Fig. 6.21) indicated the adequacy of the $\lambda=12$ restraint provided in that test. As lateral deflections of the flanges at midspan were small, lateral deflection curves for one of the quarter points have been shown in Fig. 6.21(c). A maximum brace force of $0.008P_{cy}$ corresponded to attainment of the ultimate load of $0.91P_p$.

FINAS finite element analyses were performed for Tests 19 and 20. An ultimate load of approximately $0.89P_p$ was predicted in Test 19 and $0.91P_p$ in Test 20. Correlation between finite element and experimental results was therefore excellent in Test 20 and less satisfactory in Test 19. Although the FINAS model was able to predict the actual mode of failure in Test 20, this was not the case in Test 19 where curtailment of the analysis was caused by non-convergence of the solution. Hence the mode of failure in Test 19 was not able to be predicted.

The results shown in Table 6.3 indicate that a critical restraint stiffness of $\lambda_{cr} \doteqdot 11$ was appropriate in the case of Set 6.

6.3 Discussion of Experimental and Finite Element Results

A total of twenty model beam tests was conducted in the main experimental programme forming part of this study. The results of these tests are summarised in Table 6.3. The experimental apparatus and test procedure employed in tests had been developed during a set of fifteen preliminary tests on similar model beams and were as described in Chapters 4 and 5.

6.3.1 Discussion of Experimental Results

With the aid of theoretical curves presented in Figs. 5.12 to 5.14, the rate of straining due to in-plane flexure in tests was maintained below 300 $\mu\epsilon$/minute as recommended in Ref. 104. However, due to the random nature of initial imperfections, it was not possible to make allowance for the effects of additional strains due to lateral bending of the test beams and consequently a guarantee that the maximum rate of straining at any point in the beam did not exceed 300 $\mu\epsilon$/minute during tests could not be given.

Use of this low rate of straining meant that yielding of the cross-section was allowed to develop fully before application of the next load increment. The general "feel" of the experiments was that higher loads could have been attained had a faster loading rate been adopted. Final comparison of experimental and theoretical results indicated that satisfactory agreement could generally be achieved if due care was exercised during tests and the rate of straining kept low.

The load-deflection curves obtained from the twenty tests (Figs. 6.2 to 6.21) illustrate the nature of observed failure modes: in-plane collapse is characterised by a plateau on the vertical deflection curve (Figs. 6.4, 6.8, 6.15 and 6.17) whilst instability in either the first or second mode is indicated by a peak in this curve (all other figures in the series 6.2 to 6.21). However, examination of the vertical deflection curve in isolation does not reveal the specific mode of instability; recourse to the lateral deflection curves for the tension and compression flanges is then necessary. First and second mode buckling failures are characterised by large lateral deflections of the compression flange at midspan and at the quarter points, respectively. The lateral deflection curves also indicate the growth of torsional deformations. A simple qualitative assessment of the angle of twist in a beam at the cross-section under consideration can be made as shown in Fig. 6.22 .

Local or "secondary" buckling failures were not witnessed in any of the tests. In all cases of failure in an unstable mode, primary or overall failure of the member was observed.

The destabilising influence of initial geometrical imperfections was particularly evident in Tests 1, 2 and 15 where significant lateral deflections of the flanges were apparent from the outset of loading. Consistent with these observations, the initial compression flange crookedness of beams M2 and M15 had previously been noted (Table 5.4) to exceed the imperfection tolerances of Ref. 58.

In contrast, the lateral deflection behaviour of beams in Tests 6, 11, 12, 13 and 17 was more akin to the classical buckling prediction: observed deflections were very small prior to attainment of the critical load P_{ult}; immediately thereafter, very large lateral deflections occurred. Initial geometrical imperfections in each of these beams had been noted (Table 5.4) to be small: beam M6 displayed the lowest non-dimensional twist ($\varphi_o D/l$) of any of the test beams whilst the smallest initial compression flange crookedness (u_0/l) was attributed to beam M17.

Table 6.3 indicates that second mode inelastic instability occurred only in the fully restrained beams tested in Sets 3 and 6. These sets were concerned with the bracing requirements of the most slender (R^2=18.5) beams considered in the experimental programme. Less slender beams (Sets 1, 2, 4 and 5)provided with effective intermediate restraint failed due to the formation of a plastic hinge at midspan. Consistently lower non-dimensional ultimate loads (P_{ult}/P_p) were obtained in Set 6 than in Set 3 although the R^2 values of the beams tested in these sets differed little (Table 6.2) from the mean value of 18.73 . The main reason for this discrepancy was considered to be the reduced inherent stability of a beam subjected to compression flange rather than shear centre loading. However, the effect of slight changes in cross-sectional dimensions of the test beams of Set 6 from those of Set 3 could not be assessed in view of the inelastic nature of the failure mode. The elastic analysis of Chapter 2 was therefore not applicable.

As noted in Sections 4.3.5 and 4.4.3, yielding of one or other of the bracing prongs occurred in several tests. This resulted in a reduction in the restraint stiffness provided by the prong and was therefore undesirable. Replacement of a yielded prong and calibration of the new prong were carried out between tests. Close scrutiny of bracing fork strains and the residual stiffnesses of compression flanges at the onset of yield in the prongs revealed that, in the majority of tests in which first mode instability was the mode of failure, buckling did not result from the premature yielding of the prongs. The point at which first yield was detected in the bracing forks in each test is indicated in the appropriate lateral deflection curve by a circle centred on and enclosing the normal symbol used for points on the curve.

Lack of a definite yield plateau on the vertical deflection curve of Fig. 6.4(a) indicated an apparent hardening of the beam during in-plane rotation. A similar phenomenon had been observed in plastic moment tests conducted by Dux and Kitipornchai[4]. Although the central deflection curves presented in Ref. 4 displayed two distinct segments, no yield plateau was obtained. As reported in Chapter 5, tensile tests on specimens cut from the stress-relieved beams had shown the material to conform closely to the ideal elastic-perfect plastic description; strain-hardening behaviour was not displayed by the tensile specimens.

In Volume II of "The Steel Skeleton"[99], the features and disadvantages of single point loading tests were discussed. A series of central concentrated loading and two-point loading tests had been conducted on normalised model beams by Roderick and Phillipps in Cambridge during the post-War extension of the research into the plastic behaviour of structures. The results of these tests were reported by Baker, Horne and Heyman[99]. It was concluded that two-point loading tests were more likely to produce results in agreement with simple plastic theory. An examination of the stress concentrations developed under both types of loading in photo-elastic models revealed significantly different fringe patterns. Under central point loading, the greatest stresses were found to lie on either side of the concentrated load and it was postulated that, under inelastic conditions, the degree of plasticity in the cross-section would be greatest at these points adjacent to but not directly beneath the point of load application. As this behaviour was not consistent with that assumed in the development of simple plastic theory, greater emphasis was placed on the two-point loading tests to provide results in agreement with theoretical predictions. Indeed, fringe patterns observed in photo-elastic models under two-point loading tended to substantiate these hypotheses.

The graphical construction illustrated in Fig. 6.4(a) was employed in order to estimate the plastic loads of beams displaying this apparent strain hardening behaviour. This method had been successfully used by Dux and Kitipornchai[4]. Use of this construction was not required in determining the plastic loads of beams M7, M14 and M16. The reason for the occurrence of apparent hardening only in Test 3 was not known. In no case of in-plane "failure" of test beams did actual collapse take place; most beams displayed considerable ductility and rotation capacity after hinge formation.

Measured plastic loads tended to confirm the average yield stress value of 234.5 N/mm^2 deduced as described in Chapter 5. In addition, all beams which failed in unstable modes in Sets 1 to 4 did so at loads very close to their theoretical plastic loads P_p, indicating the catastrophic effect of full plasticity on the lateral-torsional stability of these beams. The ultimate loads of the five beams which failed due to instability in Sets 5 and 6 ranged from $0.75P_p$ to $0.94P_p$, reflecting the reduced stability of these beams due to their greater slenderness and the destabilising effect of compression flange loading.

In those tests in which fully effective restraint was provided and failure occurred either in the second mode of instability or by plastic hinge formation at midspan (Tests 3, 7, 9, 10, 14, 16 and 20), lateral deflections of the braced compression flange at midspan were very small and measured bracing forces were correspondingly small. In none of these tests did the measured bracing force corresponding to attainment of the ultimate load exceed 1% of the fully yielded compression flange force P_{cy}. On the basis of these test results it is therefore possible to conclude that, for bracing stiffnesses satisfying the fully effective restraint criterion $\lambda \geqslant \lambda_{cr}$, forces developed in the bracing member are unlikely to exceed $0.01P_{cy}$ for applied loads up to and including the ultimate load.

In tests where fully effective midspan restraint was not achieved, much larger bracing forces of up to 4.4% of P_{cy} (in Test 19) accompanied the ultimate load. Still higher bracing forces were observed during post-buckling deformations, the maximum brace force recorded during the experimental programme being approximately 8.1% of P_{cy} in Test 12.

The bracing force curves presented in Figs. 6.23 to 6.28 are the experimental curves of Figs. 6.2 to 6.21 grouped by set and plotted to a common bracing force scale. This form of presentation highlights the much smaller forces developed in fully effective bracing (full lines in figures) than in partially effective bracing (broken lines). Labels on the curves indicate the tests to which the curves refer.

On average, brace forces consistent with the ultimate load condition were observed to be higher in Sets 4 to 6 than in Sets 1 to 3. Although this would tend to re-emphasise the destabilising influence of compression flange loading, restraint stiffnesses employed in Sets 4 to 6 were generally higher than in Sets 1 to 3 and initial imperfections were not the same, making direct comparison of the two sets of results impossible. Only in the case of Tests 3 and 11 is some form of direct comparison justified: in addition to λ values being equal in these tests, R^2 values were nominally the same. At the ultimate condition in the two tests bracing forces of 0.9% and 1.8% of the respective P_{cy} values were recorded, lending support to the above observation.

Although agreement between measured bracing forces and the product (restraint stiffness x lateral deflection of braced point) was generally good, especially under elastic conditions when lateral deflections tended to be small, correlation was less satisfactory for larger lateral deflections as the desired stiffness provided by the bracing prongs was reduced by the combined effects of yielding and the true or "large displacement" behaviour of the prong rather than the small displacement behaviour assumed in calculating the required active leg length 'a_f'. Although allowance for the effects of prong yielding was made in the conversion of measured strains to bracing forces (Section 4.4.3 and Appendix V), no allowance was made for the effects of large displacements or shear deformations of the bracing prong.

An analysis based on elastic small deflection theory and the notation of Chapter 4 showed the lateral deflection 'δ' of a prong at the brace point under a load P_{br} to be

$$\delta = \text{bending deflection} + \text{shear deflection}$$

$$= \frac{P_{br}\, a_f^3}{3(EI)_{prong}} + \frac{10 P_{br}\, a_f}{9(A_x G)_{prong}}$$

and, taking $G \doteqdot E/2.6$:

$$\delta = \frac{P_{br}\, a_f^3}{3(EI)_{prong}} \left(1 + \frac{26 I}{3 A_x a_f^2}\right)$$

For a solid circular section of radius r, $I = \pi r^4/4$ and $A_x = \pi r^2$, giving

$$\delta = \frac{P_{br}\, a_f^3}{3(EI)_{prong}} \left(1 + \frac{26 r^2}{12 a_f^2}\right)$$

and a stiffness $K = P_{br}/\delta$ of

$$K = \frac{3(EI)_{prong}}{a_f^3 \left(1 + \frac{26 r^2}{12 a_f^2}\right)}$$

Examining the significance of the second term in parenthesis in the denominator in relation to unity for the actual radius of the prong (r=2.3812mm) and the smallest active leg length (a_f=43.93mm) used in the tests gave

$$\frac{26 r^2}{12 a_f^2} = 0.0064$$

Consequently, the reduction in stiffness of the bracing prong due to shear deformations was negligible.

Two trends were observed in the estimated λ_{cr} values in Table 6.3: increasing λ_{cr} with increasing shape parameter R^2 and greater values of λ_{cr} required for compression flange than for shear centre loading. For shear centre loading, the largest value of λ_{cr} suggested was 4.5, whilst for compression flange loading $\lambda_{cr} \doteqdot 11$ was suggested. Comparison of these results with currently (1985) proposed bracing requirements is presented in Chapter 8.

Approximate values of critical absolute restraint stiffness K_{cr} corresponding to the suggested values of λ_{cr} are shown in the last column of Table 6.3. A decreasing trend in K_{cr} values with increasing R^2 is observed for the shear centre loading condition in Sets 1 to 3 whilst no corresponding trend can be inferred from the K_{cr} values for Sets 4 to 6. However, K_{cr} values are consistently higher for compression flange than for shear centre loading.

6.3.2 Comparison of Finite Element with Experimental Results

As noted in Chapter 3, the nature of the study demanded the use of a finite element system capable of coupled materially and geometrically non-linear analysis. Initial test runs of the NASTRAN system had revealed the need for considerable refinement of the 'QUAD4' shell element mesh in potentially inelastic zones of the structure. Although this did not pose any difficulties in mesh generation, solution times using the non-linear analysis facility in NASTRAN were excessive and the data storage requirements could not be met by the disk space allocated by staff at the Rutherford Appleton Laboratory. For these reasons, recourse was made to the NASTRAN 'BEAM' element and all NASTRAN results shown in Figs. 6.3 to 6.21 were obtained using this type of element. In all FINAS analyses the considerably more advanced FINAS beam element was employed.

Table 6.3 indicates the tests for which comparative finite element analyses were performed. Both FINAS and NASTRAN analyses were performed in Sets 1 to 3. Although FINAS analyses were also performed in Sets 4 to 6, failure of the NASTRAN analysis after only the first few load increments in Test 13 illustrated the inadequacy of this solution in cases of compression flange loading. Several NASTRAN analyses of the Test 13 data employing successively smaller load increments were attempted but proved unsuccessful. Although FINAS analyses of beams loaded at compression flange level were also more difficult due to greater numerical instability, the use of smaller increments of enforced displacement in the FINAS analyses generally allowed the analysis to proceed well into the inelastic condition.

Examination of the curves presented in Figs. 6.3 to 6.21 reveals a generally acceptable level of correlation between FINAS and experimental results. NASTRAN results were less satisfactory in comparison with FINAS and test results. Under elastic conditions, excellent correlation between observed in-plane bending behaviour and that predicted by both the NASTRAN and FINAS analyses was obtained in all tests. However, finite element predictions of lateral deflections and bracing forces were less accurate, as demonstrated by the curves of Figs. 6.7, 6.8, 6.11, 6.15, 6.17 and 6.21 . With the exception of the graphs presented in Fig. 6.7, each of these figures pertained to tests in which fully effective restraint was provided by the midspan bracing member: lateral deflections and bracing forces in these tests were consequently very small. Thus, although differences between finite element and experimental results were large in some of the cases shown, they represented only very small physical quantities and correlation between finite element and experimental results was therefore regarded as being acceptable.

Very little deviation from the initial in-plane and lateral bending tangent stiffnesses was observed in NASTRAN results, even under applied loads sufficiently large to cause significant yielding in the beam cross-section together with gross lateral deflections and twists. For this reason, the NASTRAN results were of limited usefulness and in no case could they be used to predict the ultimate loads of test beams.

In constrast, the FINAS analysis was generally capable of predicting very large stiffness changes, to the extent that even the post-buckling vertical deflection behaviour of beam M10 was accurately predicted. In Tests 2, 3, 10, 14, 16 and 20 FINAS provided accurate estimates of actual failure loads and correctly predicted the observed modes of failure in Tests 3, 10, 14 and 20. In Test 2, however, the plastic hinge type failure indicated by FINAS was not witnessed in the test; rather, first mode inelastic instability of the partially restrained beam occurred. Similarly, in Test 16 the observed in-plane failure of the test beam was not matched by the tendency towards inelastic second mode failure of the finite element model.

No definite ultimate loads could be deduced from the finite element results for Tests 6, 7, 8, 13, 15 and 19 as non-convergence of the numerical solutions caused termination of the analyses before definite failure of the mathematical models in one of the unstable modes. Nevertheless, examination of the relevant vertical deflection curves showed that the ultimate loads sustained by the idealised beams prior to non-convergence were frequently very good approximations to measured ultimate loads. Although this is not the most satisfactory method of predicting theoretical ultimate loads, non-convergence of a FINAS shell element analysis had previously been used as a failure criterion by Dowling et al.[95] in a study of web buckling in steel box girders. Resulting theoretical ultimate loads agreed well with those measured experimentally.

In conclusion, close study of the finite element results shown in Figs. 6.3 to 6.21 revealed that the FINAS programme had correctly predicted both the failure loads and modes of failure of test beams in one half of the cases in which it had been employed. It had also provided accurate critical load predictions in several other cases where definite modes of failure had not been obtained. FINAS bracing force and lateral deflection predictions were generally acceptable although correlation proved better under elastic than under inelastic conditions. Results obtained from NASTRAN were of only limited usefulness as non-convergence of the numerical solution occurred in all cases, causing analyses to be terminated well before the development of full plasticity. Therefore, it was evident that FINAS was to be preferred for the analysis of such highly non-linear problems.

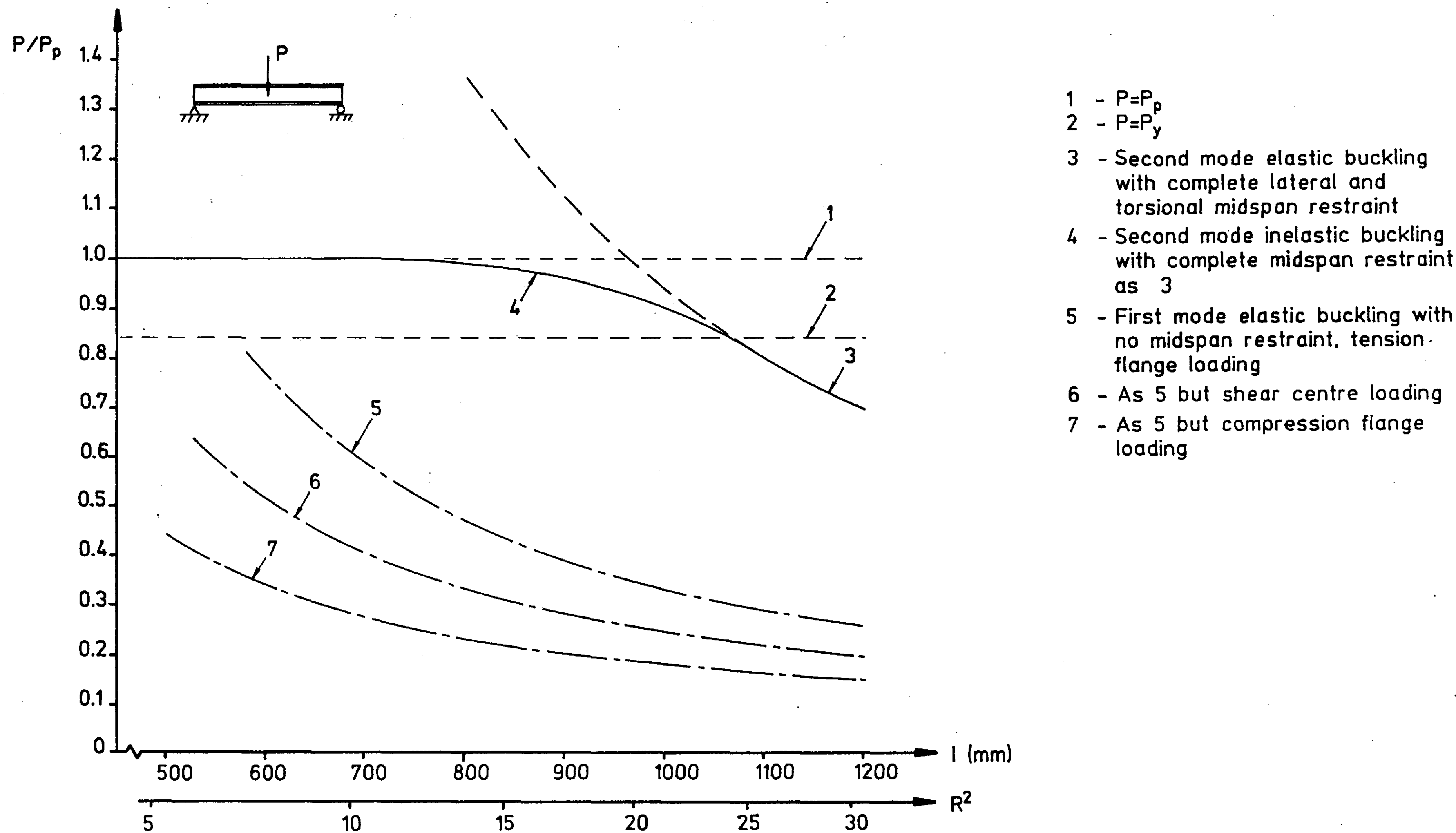

Fig. 6.1 : Theoretical elastic and inelastic behaviour of model beams with cross-sectional geometry as described in Section 5.5.

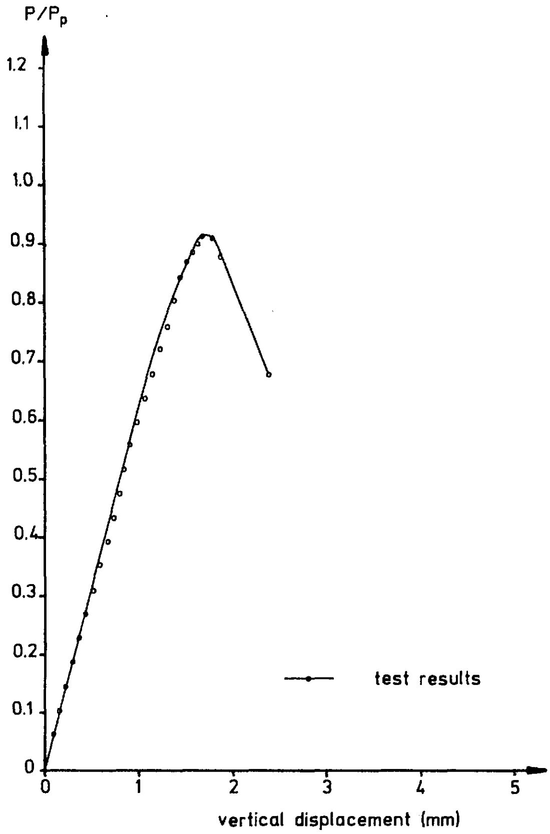

(a) load vs. midspan vertical deflection

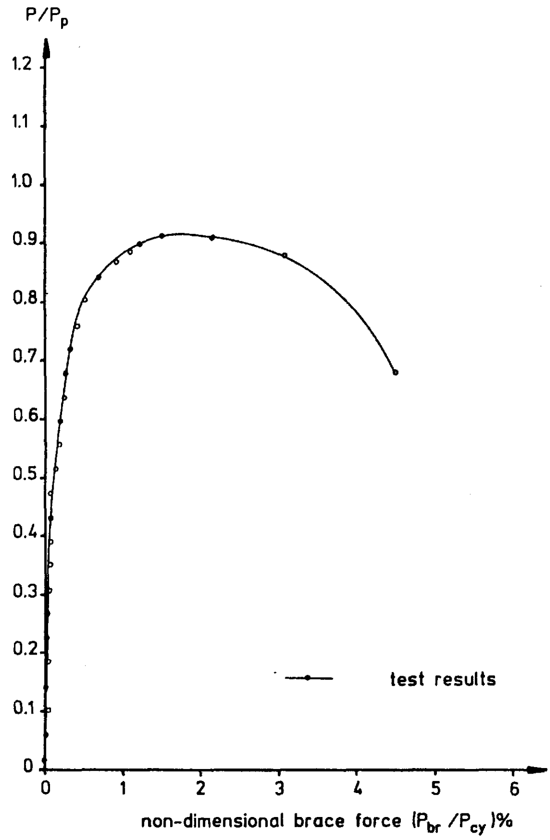

(b) load vs. brace force

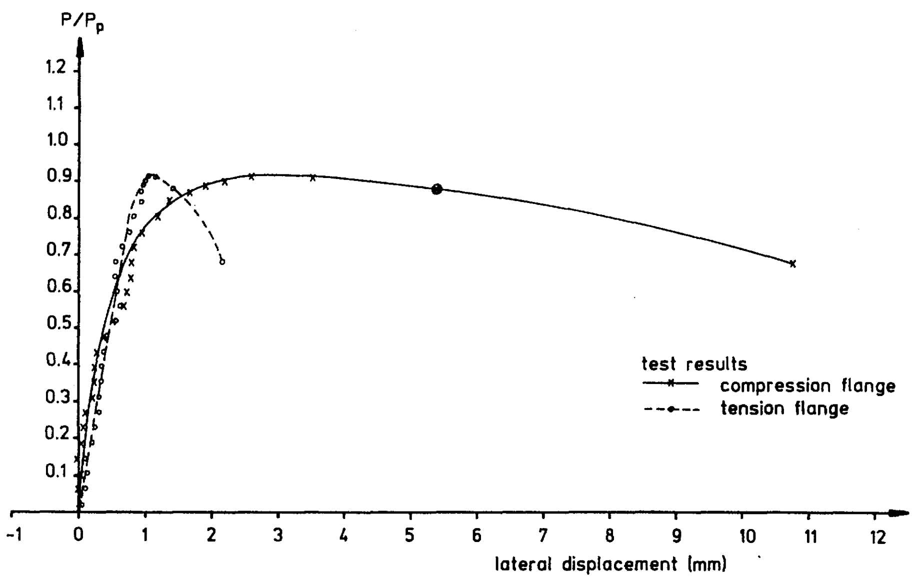

(c) load vs. lateral deflection of flanges at midspan

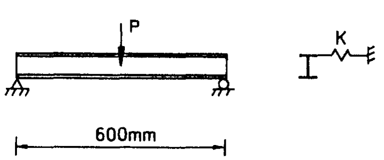

span	600mm
λ	1.0
brace K	31.6N/mm
compn. flange ult. load P_{cy}	3599.3N
P_p	1993.2N
shear centre loading	
compression flange braced	

Fig. 6.2 : Experimental results for Test 1

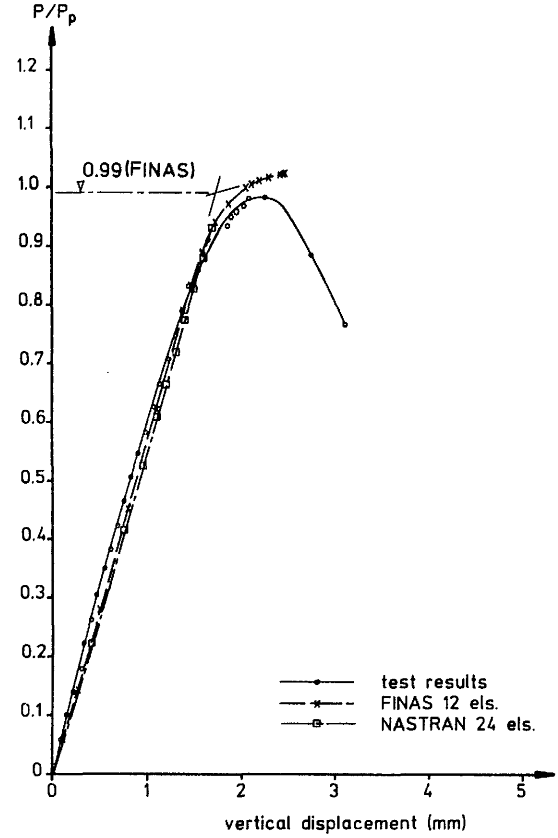

(a) load vs. midspan vertical deflection

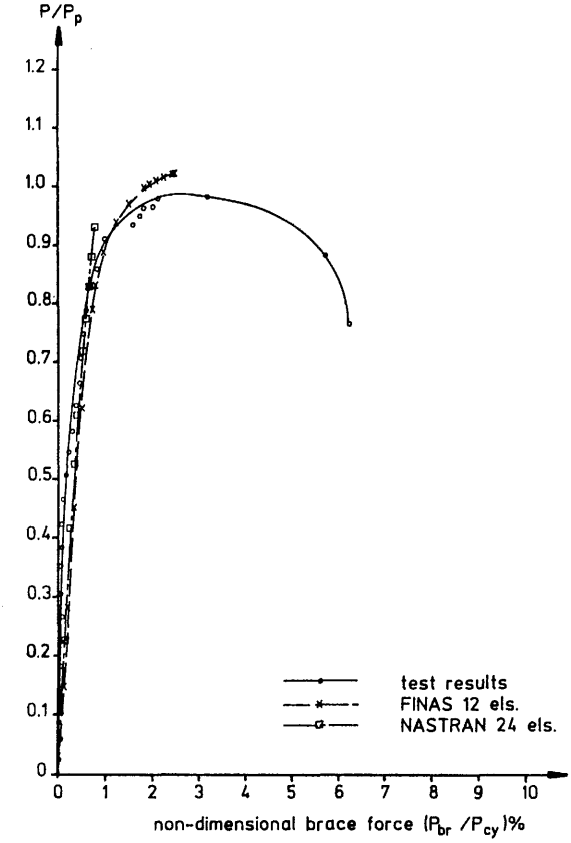

(b) load vs. brace force

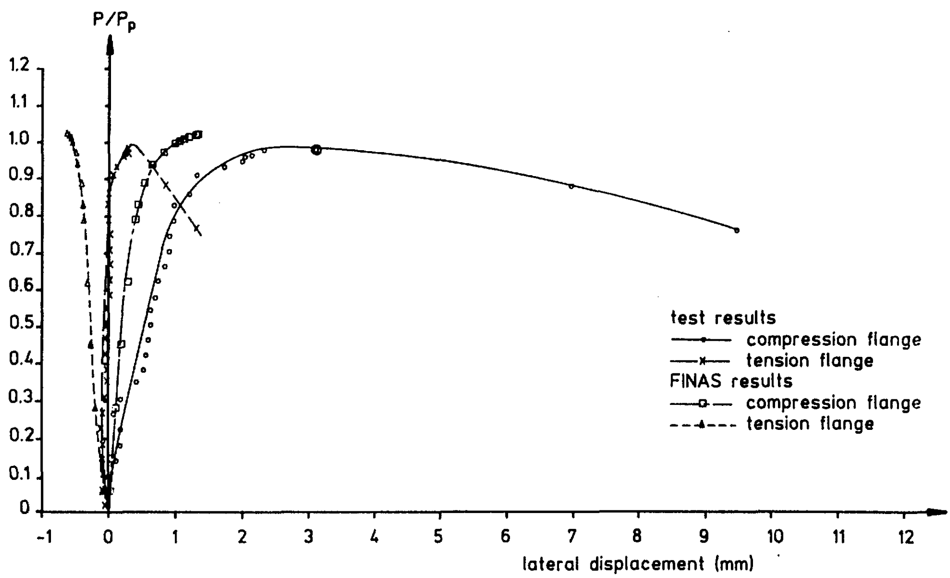

(c) load vs. lateral deflection of flanges at midspan

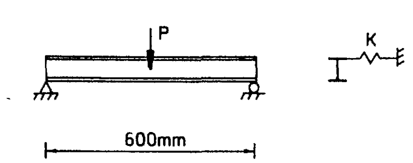

span	600mm
λ	2.0
brace K	66.9N/mm
compn. flange ult. load P_{cy}	3682.7N
P_p	2025.2N
shear centre loading	
compression flange braced	

Fig. 6.3 : Experimental and finite element results for Test 2

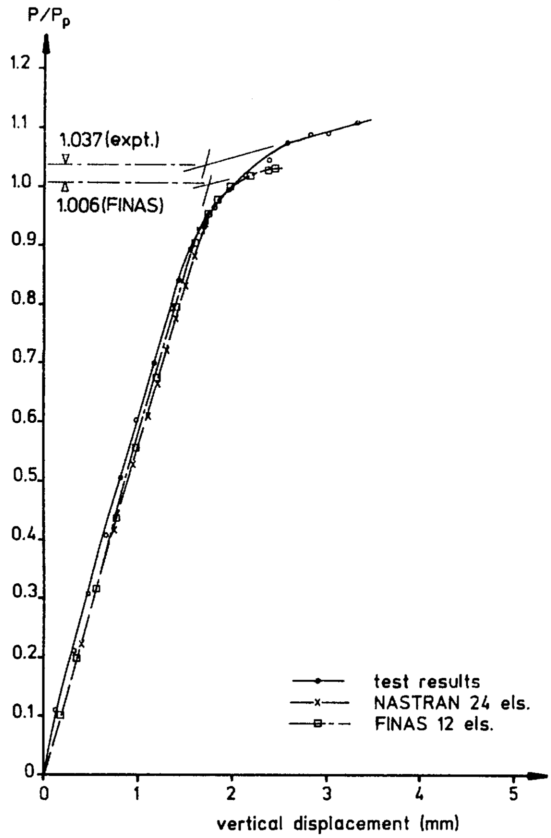

(a) load vs. midspan vertical deflection

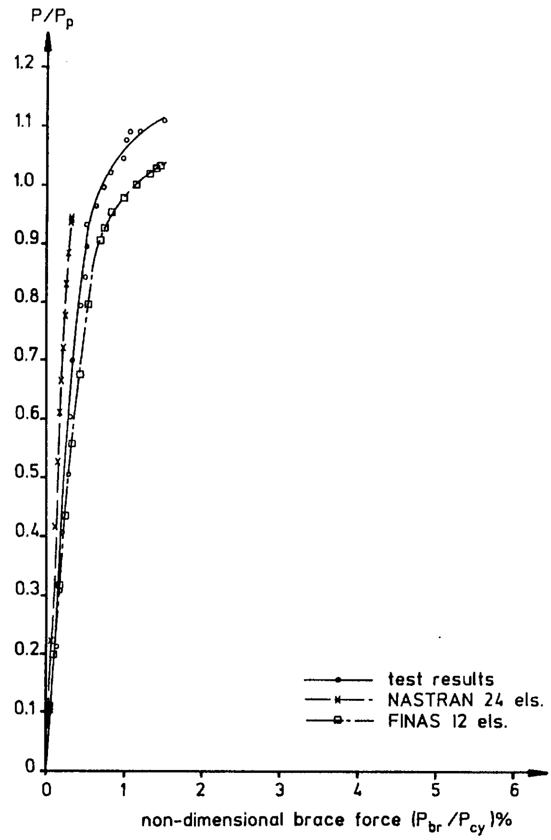

(b) load vs. brace force

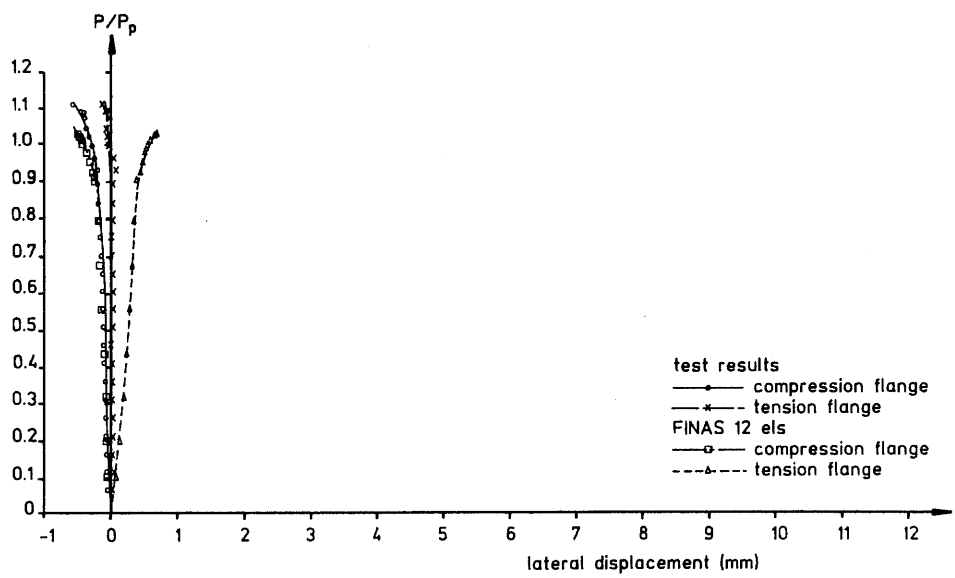

(c) load vs. lateral deflection of flanges at midspan

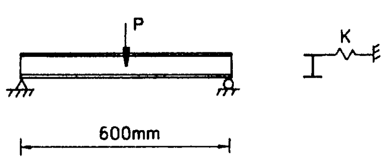

span	600mm
λ	3.0
brace K	95.2N/mm
compn. flange ult. load P_{cy}	3622.2N
P_p	2004.5N
shear centre loading	
compression flange braced	

Fig. 6.4 : Experimental and finite element results for Test 3

(a) load vs. midspan vertical deflection

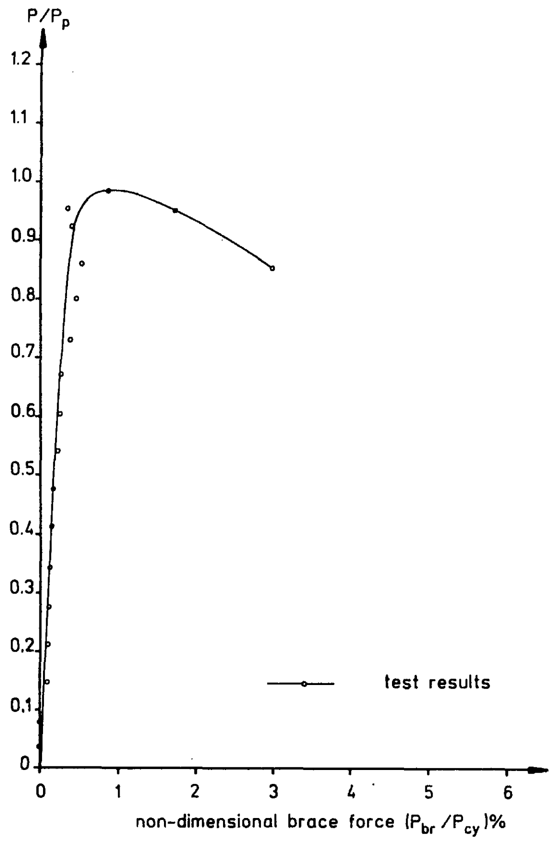

(b) load vs. brace force

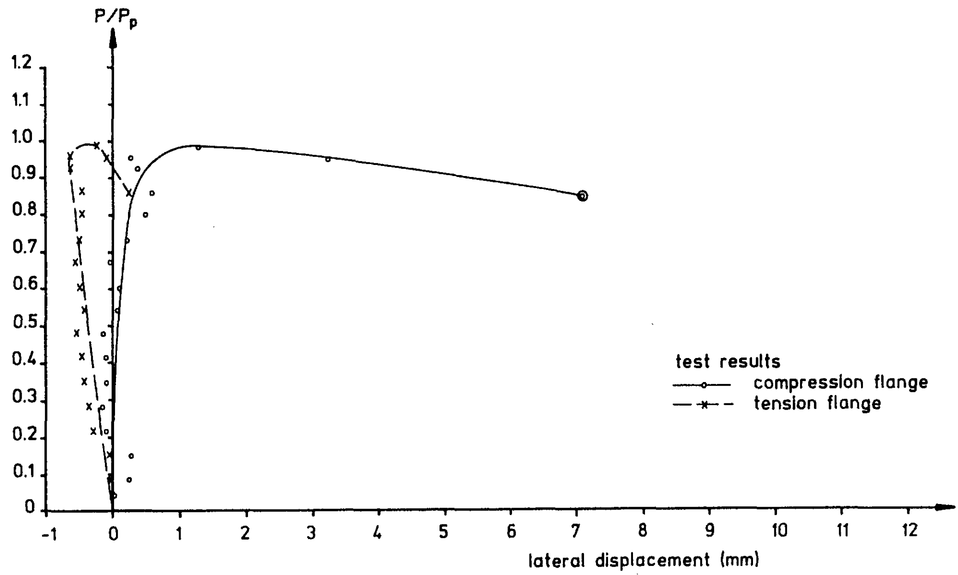

(c) load vs. lateral deflection of flanges at midspan

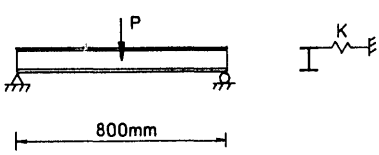

span	800mm
λ	2.0
brace K	28.2N/mm
compn. flange ult. load P_{cy}	3658.8N
P_p	1510.2N
shear centre loading	
compression flange braced	

Fig. 6.5 : Experimental results for Test 4

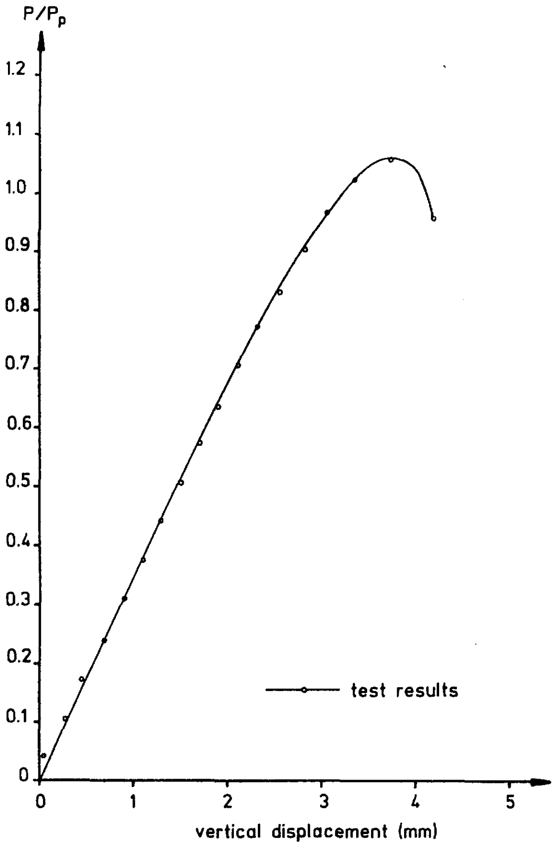

(a) load vs. midspan vertical deflection

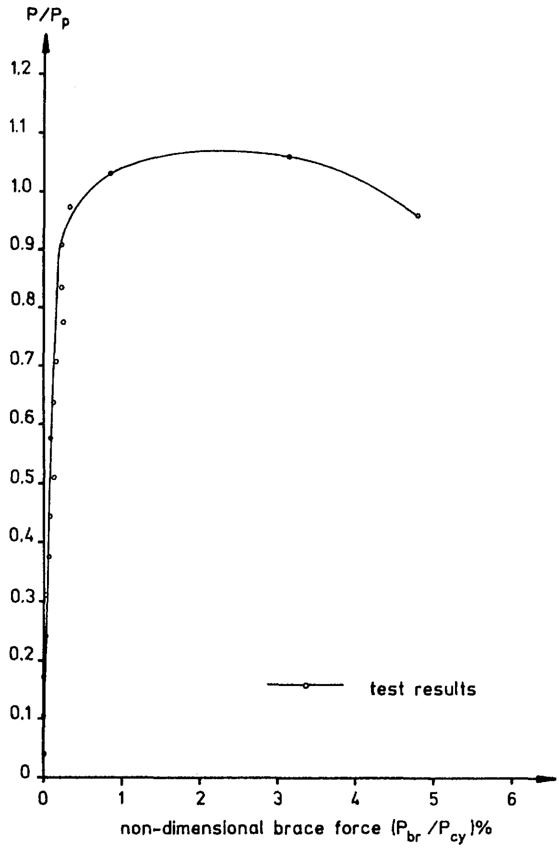

(b) load vs. brace force

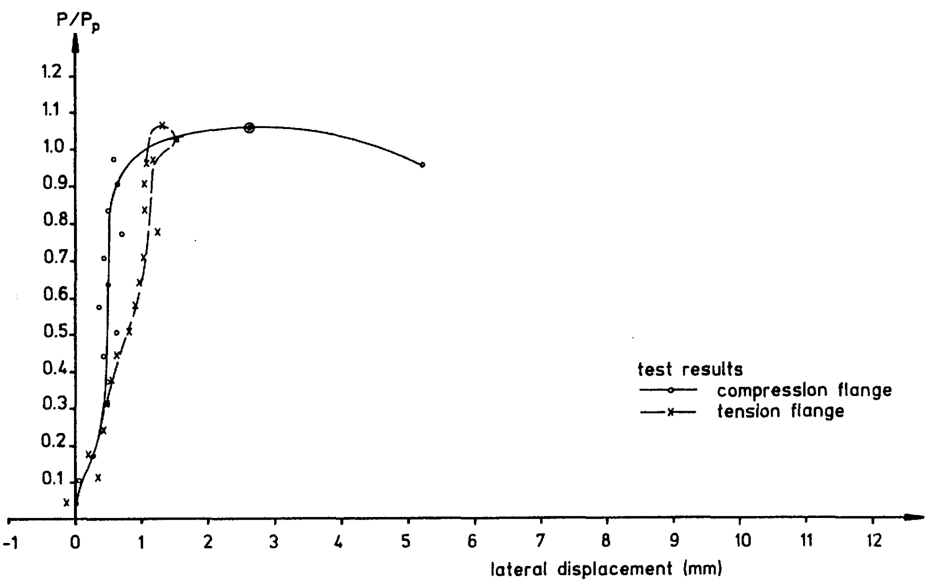

(c) load vs. lateral deflection of flanges at midspan

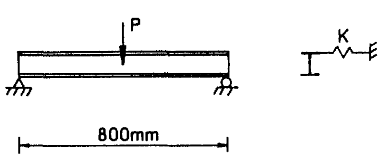

span	800mm
λ	3.0
brace K	39.1N/mm
compn. flange ult. load P_{cy}	3544.1N
P_p	1478.1N
shear centre loading	
compression flange braced	

Fig. 6.6 : Experimental results for Test 5

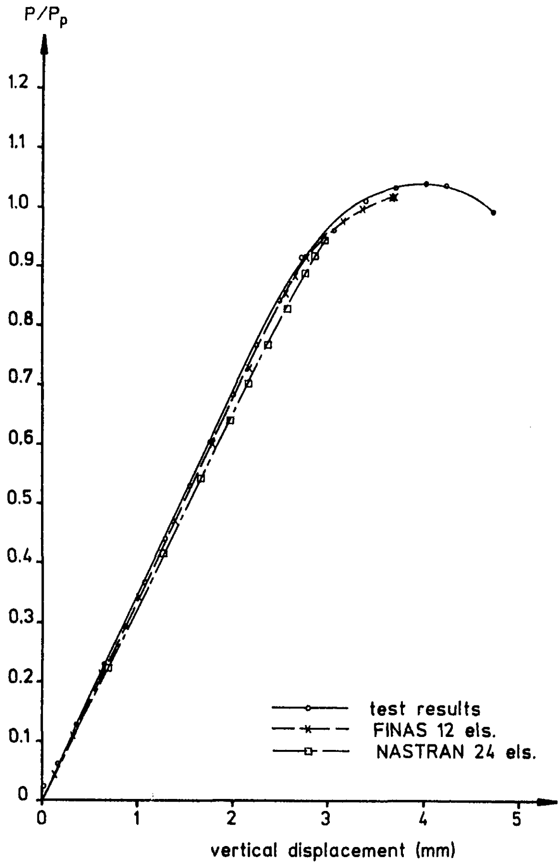

(a) load vs. midspan vertical deflection

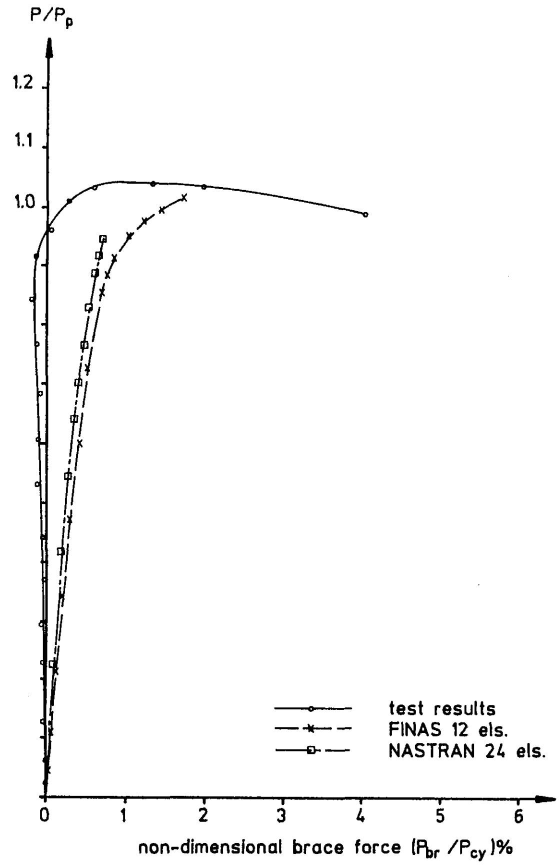

(b) load vs. brace force

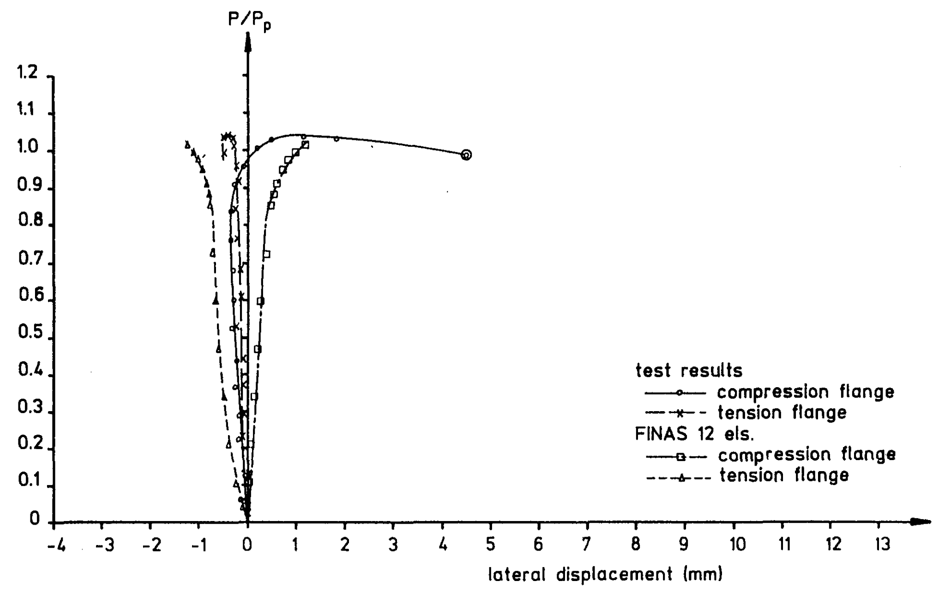

(c) load vs. lateral deflection of flanges at midspan

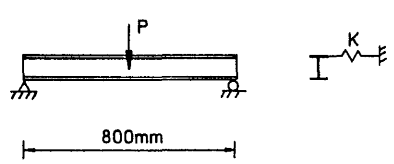

span	800mm
λ	4.0
brace K	53.2N/mm
compn. flange ult. load P_{cy}	3612.2N
P_p	1500.7N
shear centre loading	
compression flange braced	

Fig. 6.7 : Experimental and finite element results for Test 6

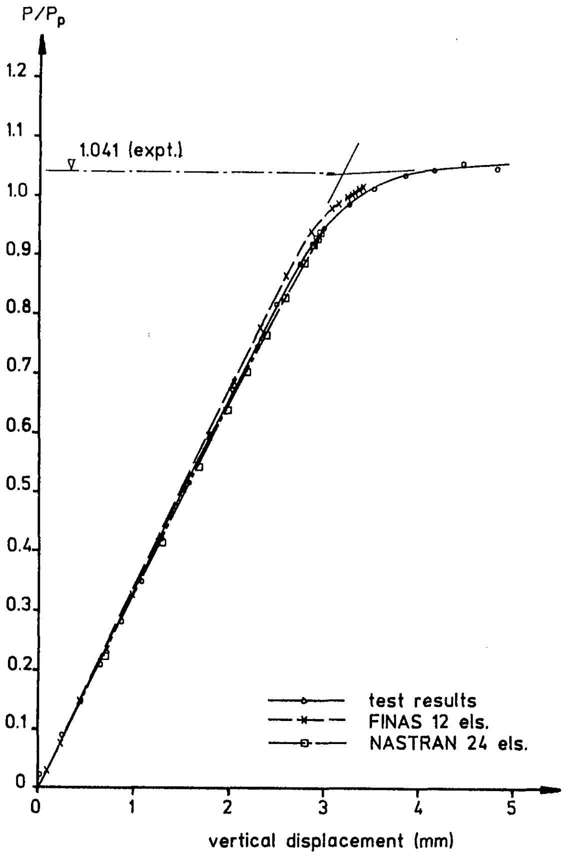

(a) load vs. midspan vertical deflection

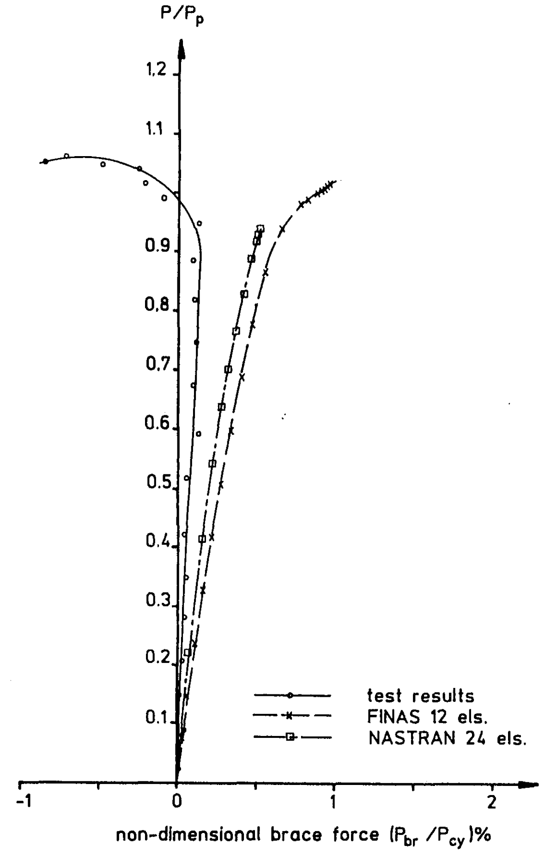

(b) load vs. brace force

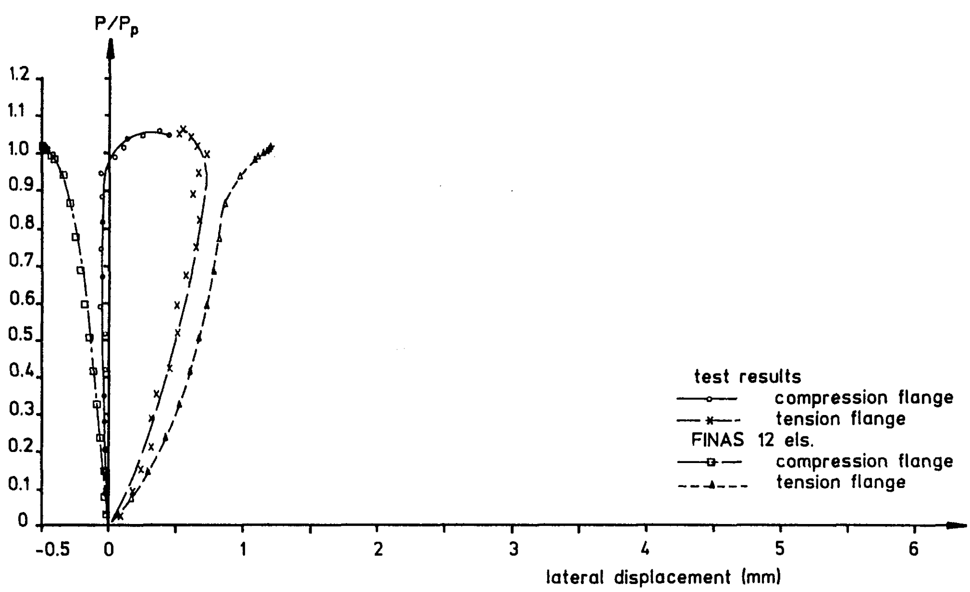

(c) load vs. lateral deflection of flanges at midspan

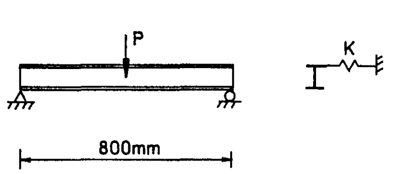

span	800mm
λ	5.0
brace K	70.9N/mm
compn. flange ult. load P_{cy}	3682.1N
P_p	1522.0N
shear centre loading	
compression flange braced	

Fig. 6.8 : Experimental and finite element results for Test 7

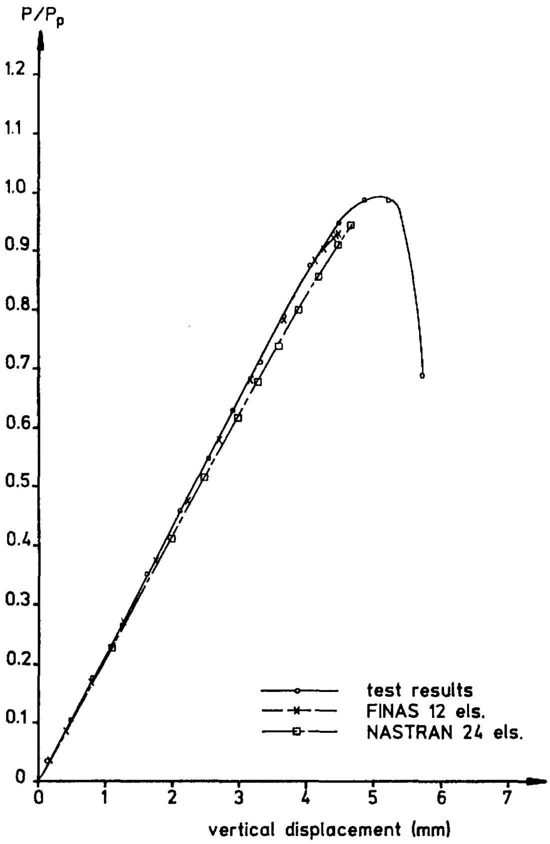

(a) load vs. midspan vertical deflection

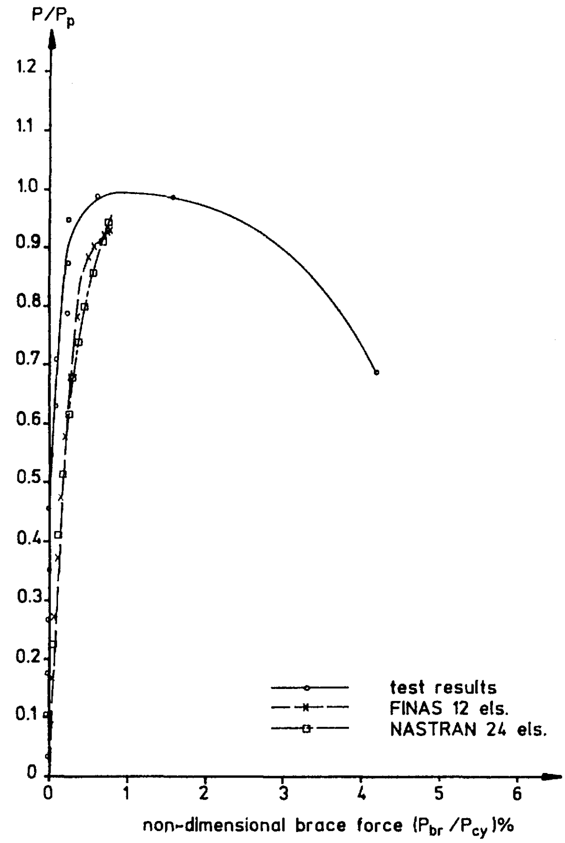

(b) load vs. brace force

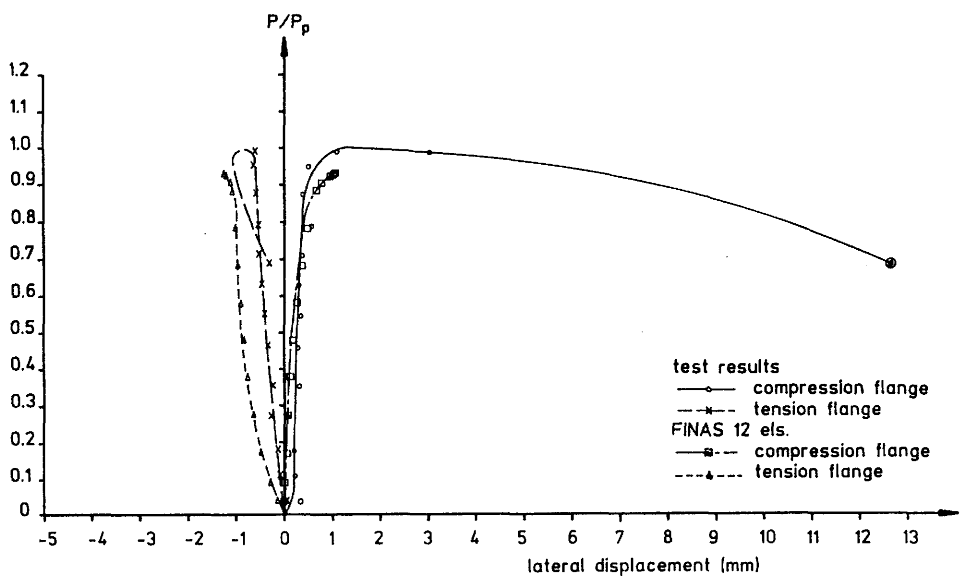

(c) load vs. lateral deflection of flanges at midspan

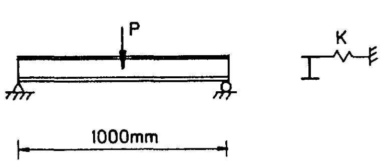

span	1000mm
λ	4.0
brace K	26.5N/mm
compn. flange ult. load P_{cy}	3551.6N
P_p	1184.1N
shear centre loading	
compression flange braced	

Fig. 6.9 : Experimental and finite element results for Test 8

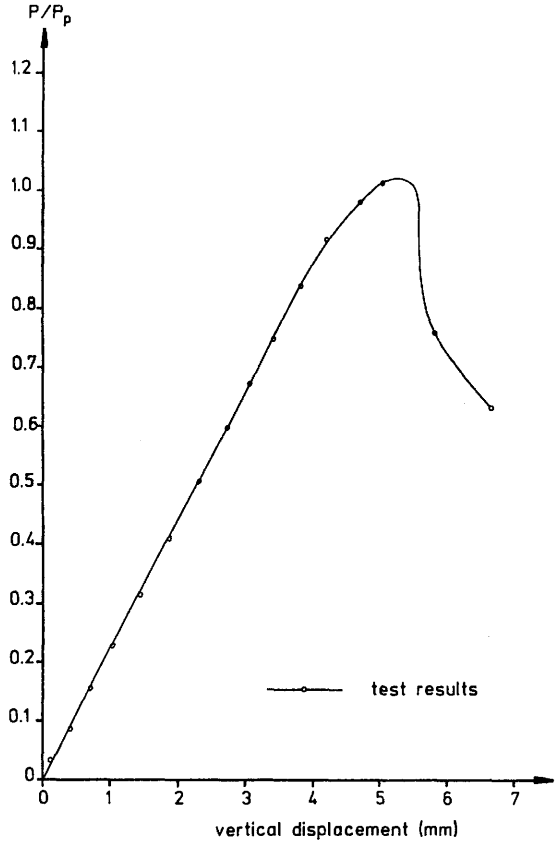

(a) load vs. midspan vertical deflection

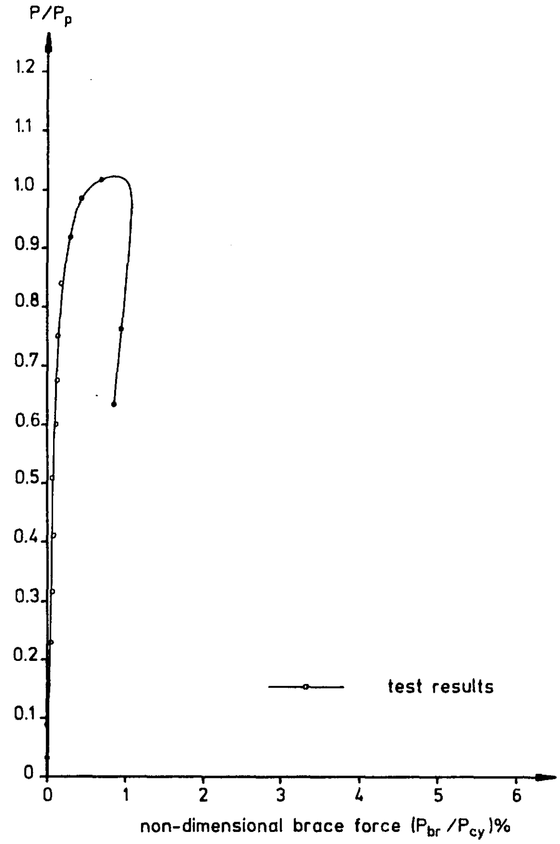

(b) load vs. brace force

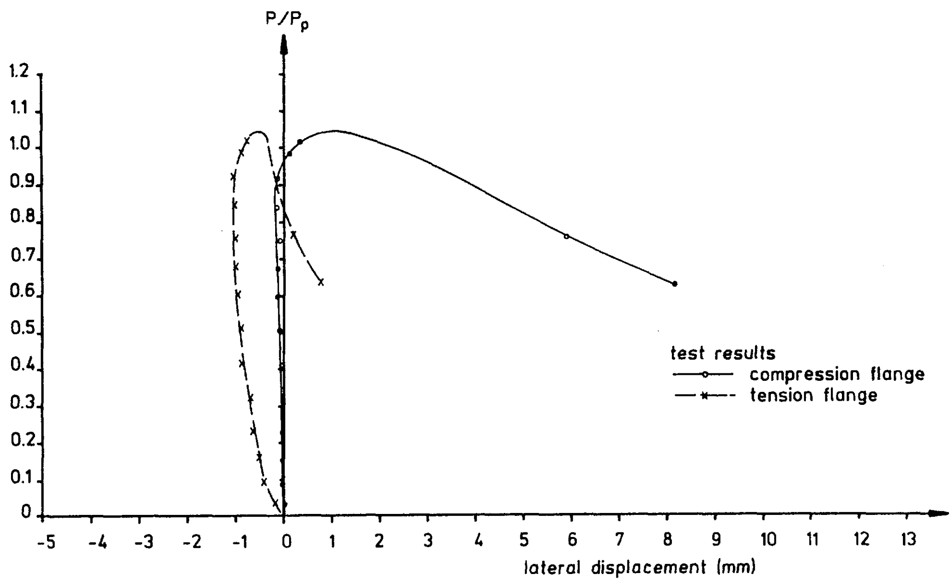

(c) load vs. lateral deflection of flanges at quarter point

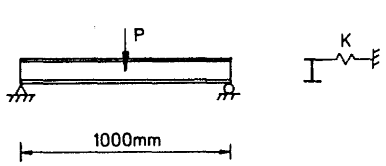

span	1000mm
λ	6.0
brace K	40.6N/mm
compn. flange ult. load P_{cy}	3571.4N
P_p	1187.8N
shear centre loading	
compression flange braced	

Fig. 6.10 : Experimental results for Test 9

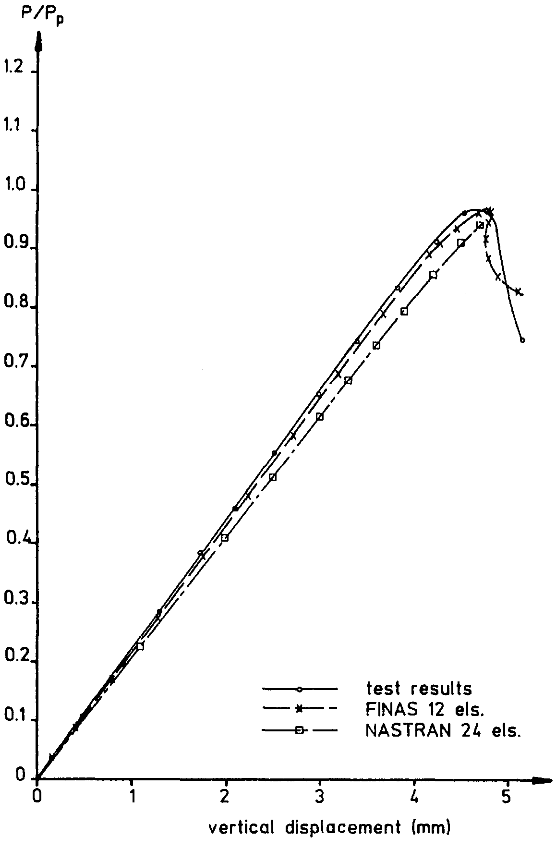

(a) load vs. midspan vertical deflection

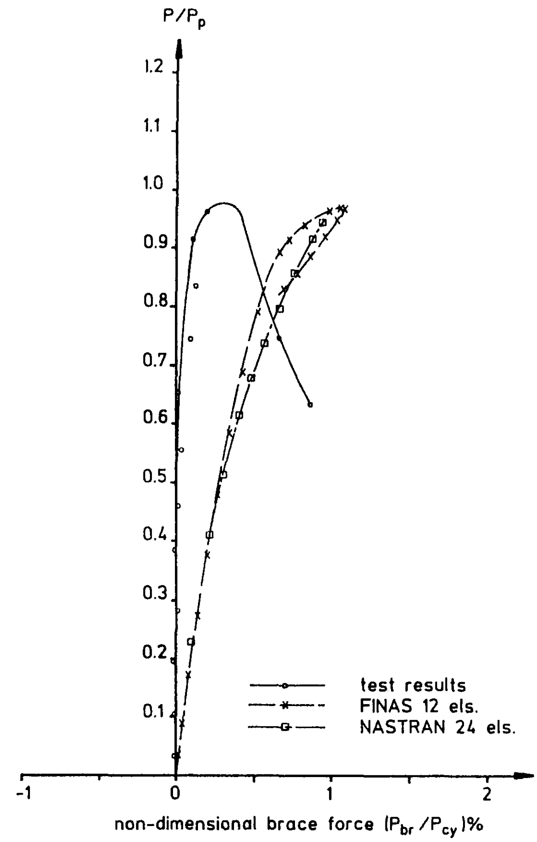

(b) load vs. brace force

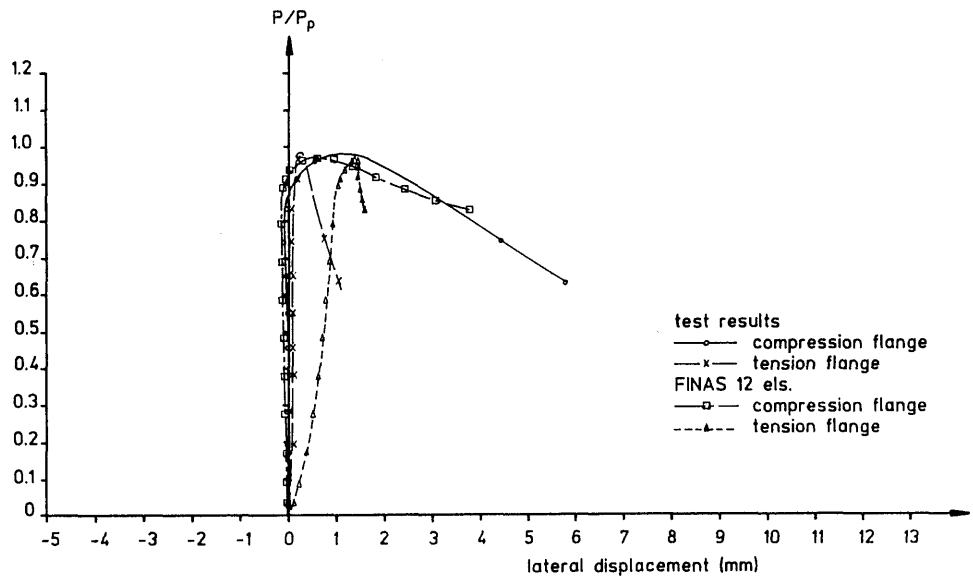

(c) load vs. lateral deflection of flanges at quarter point

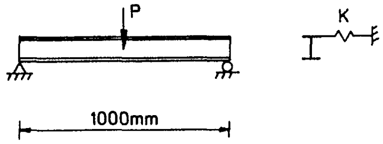

span	1000mm
λ	5.0
brace K	41.9N/mm
compn. flange ult. load P_{cy}	3525.8N
P_p	1187.0N
shear centre lodding	
compression flange braced	

Fig. 6.11 : Experimental and finite element results for Test 10

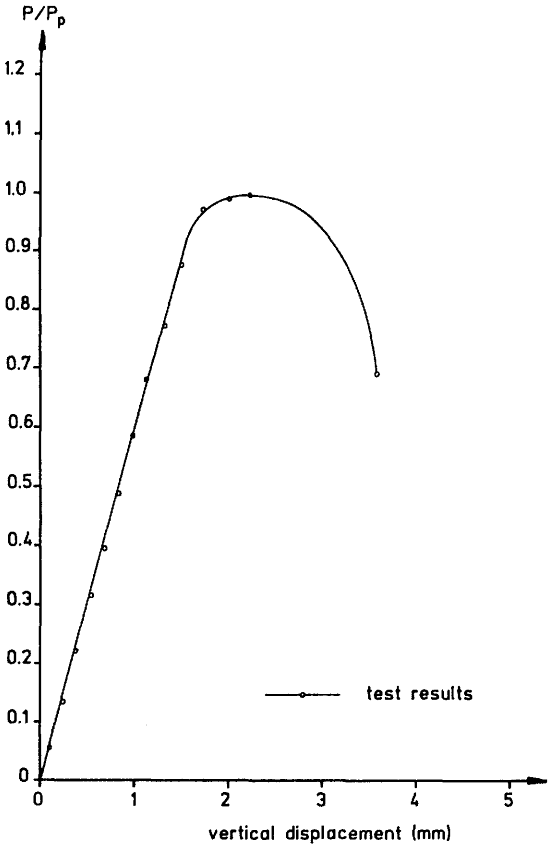

(a) load vs. midspan vertical deflection

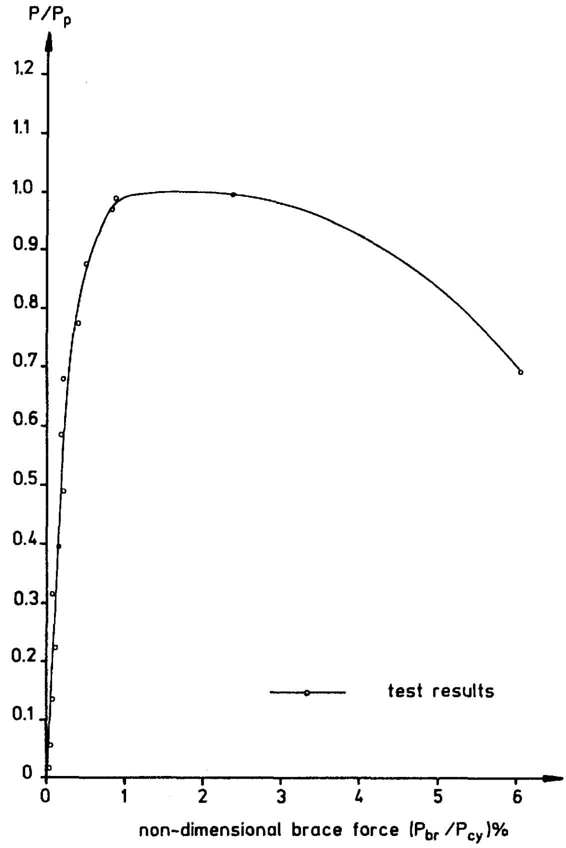

(b) load vs. brace force

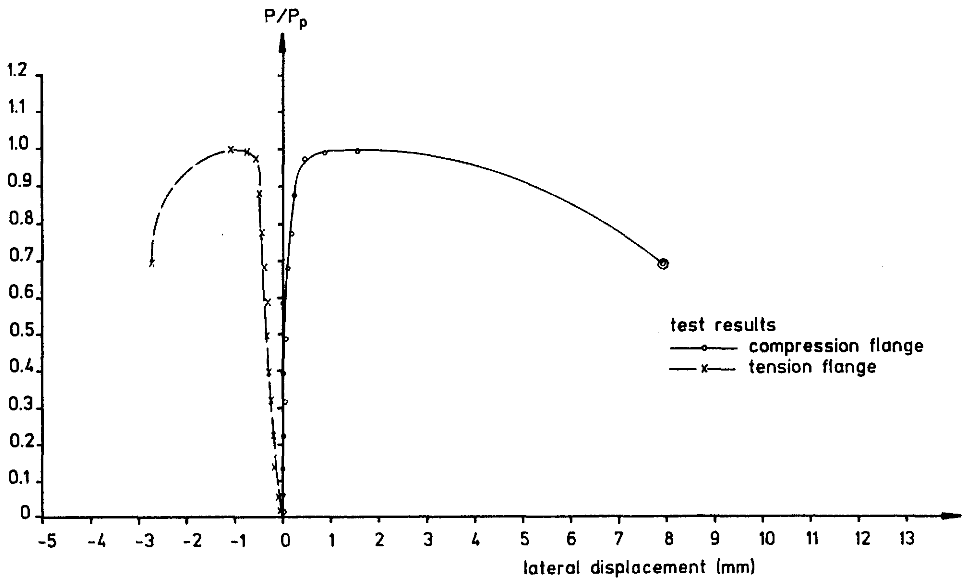

(c) load vs. lateral deflection of flanges at midspan

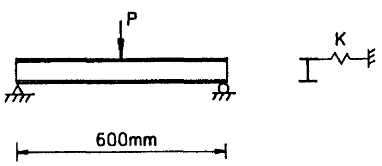

span	600mm
λ	3.0
brace K	101.2N/mm
compn. flange ult. load P_{cy}	3682.9N
P_p	2030.6N
compression flange loading	
compression flange braced	

Fig. 6.12 : Experimental results for Test 11

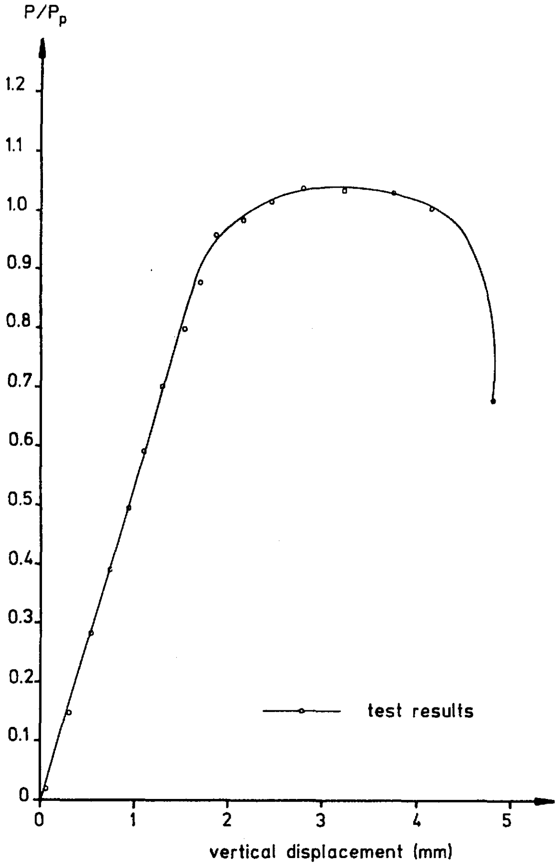

(a) load vs. midspan vertical deflection

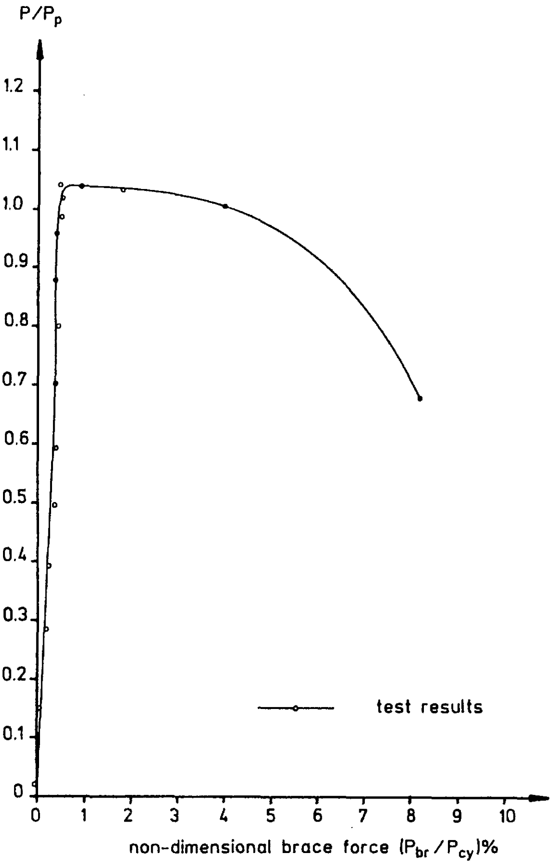

(b) load vs. brace force

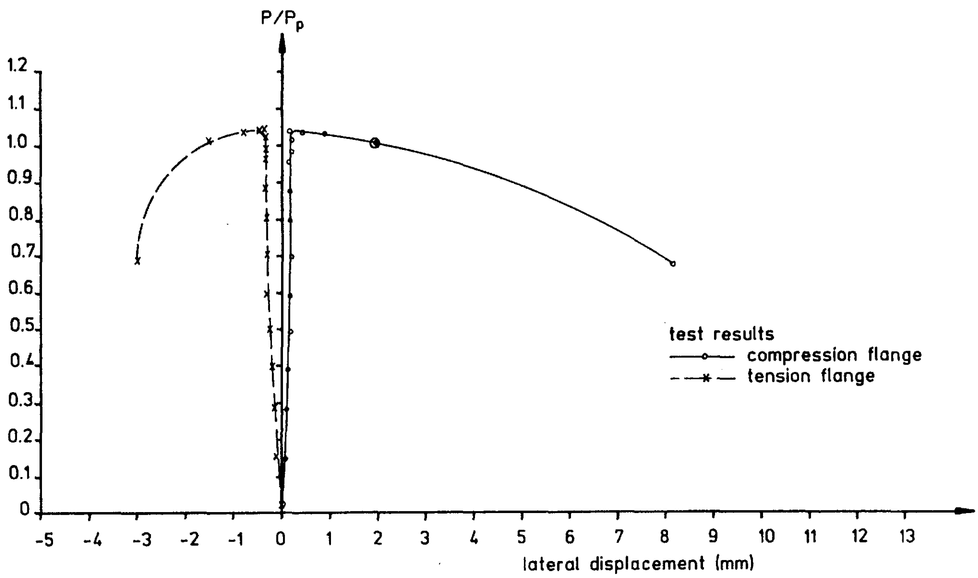

(c) load vs. lateral deflection of flanges at midspan

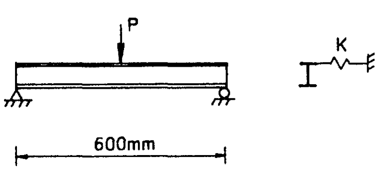

span	600mm
λ	4.0
brace K	125.8N/mm
compn. flange ult. load P_{cy}	3610.7N
P_p	1993.5N
compression flange loading	
compression flange braced	

Fig. 6.13 : Experimental results for Test 12

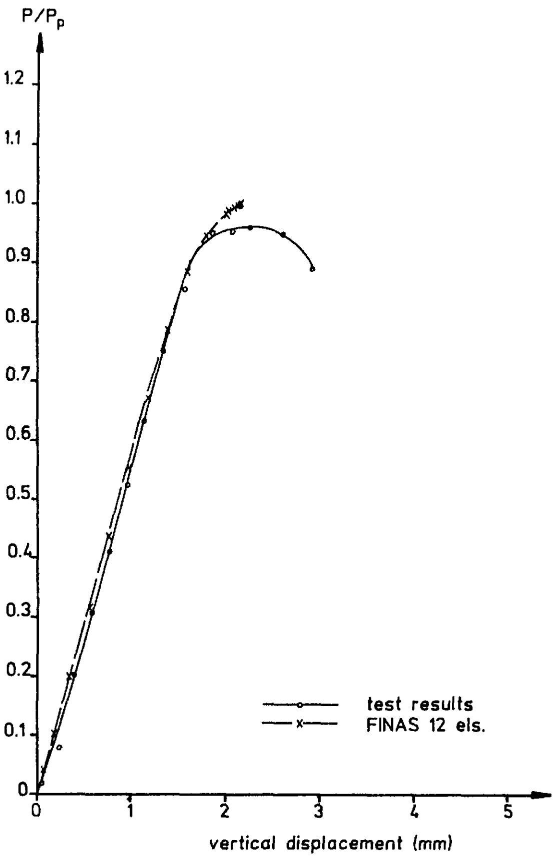

(a) load vs. midspan vertical deflection

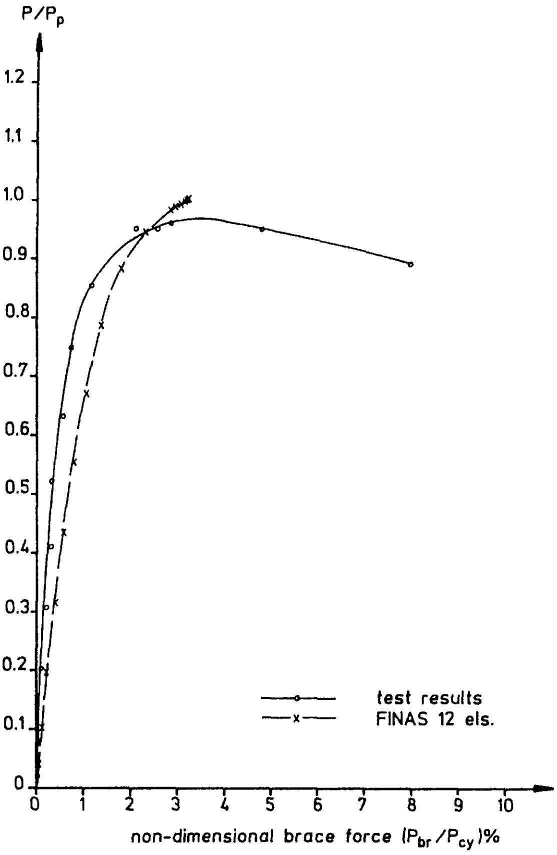

(b) load vs. brace force

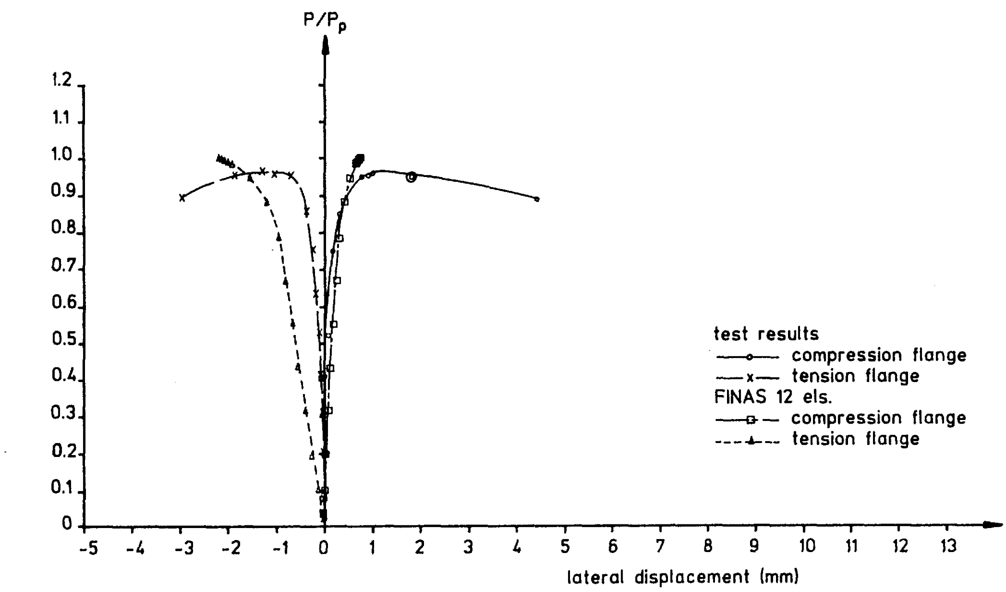

(c) load vs. lateral deflection of flanges at midspan

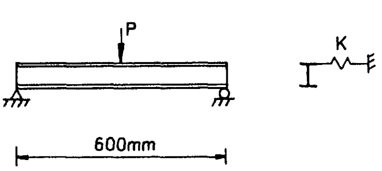

span	600mm
λ	5.0
brace K	159.2N/mm
compn. flange ult. load P_{cy}	3631.2N
P_p	2006.3N
compression flange loading	
compression flange braced	

Fig. 6.14 : Experimental and finite element results for Test 13

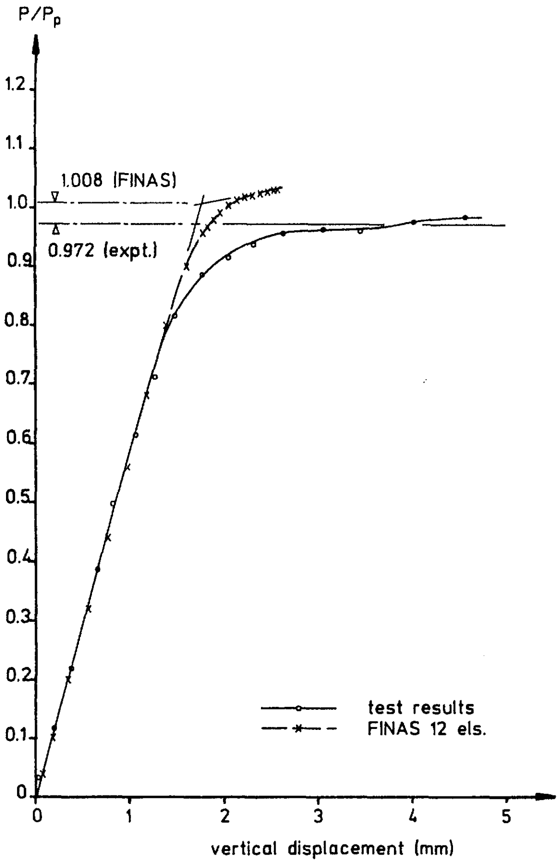

(a) load vs. midspan vertical deflection

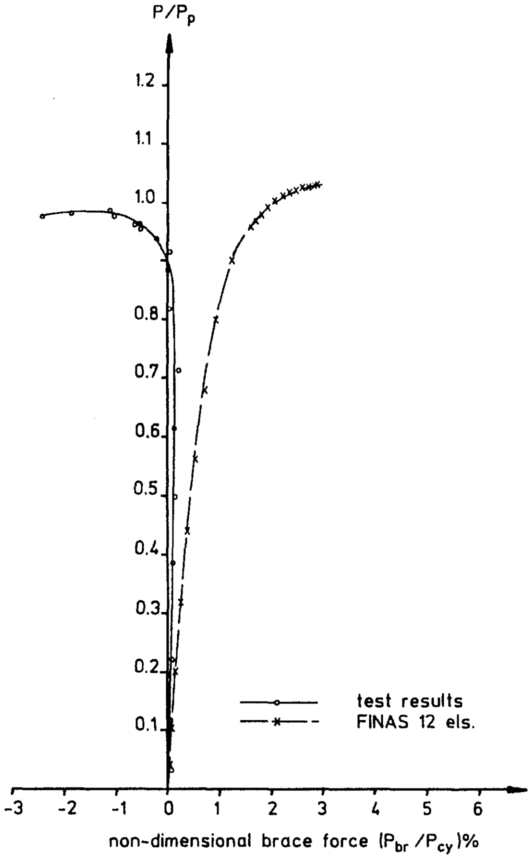

(b) load vs. brace force

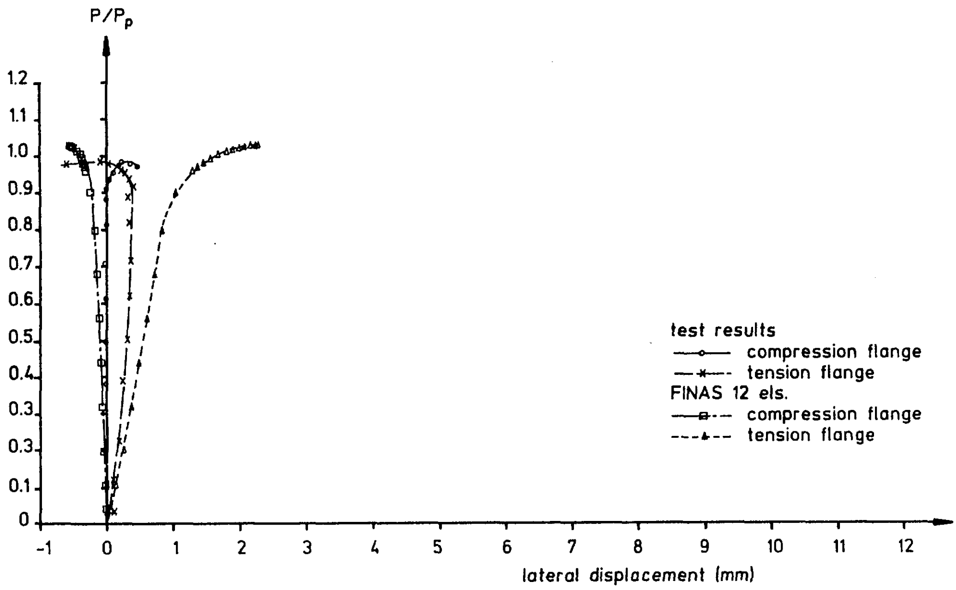

(c) load vs. lateral deflection of flanges at midspan

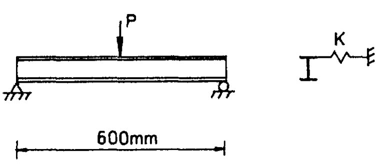

span	600mm
λ	6.0
brace K	184.6N/mm
compn. flange ult. load P_{cy}	3540.6N
P_p	1985.7N
compression flange loading	
compression flange braced	

Fig. 6.15 : Experimental and finite element results for Test 14.

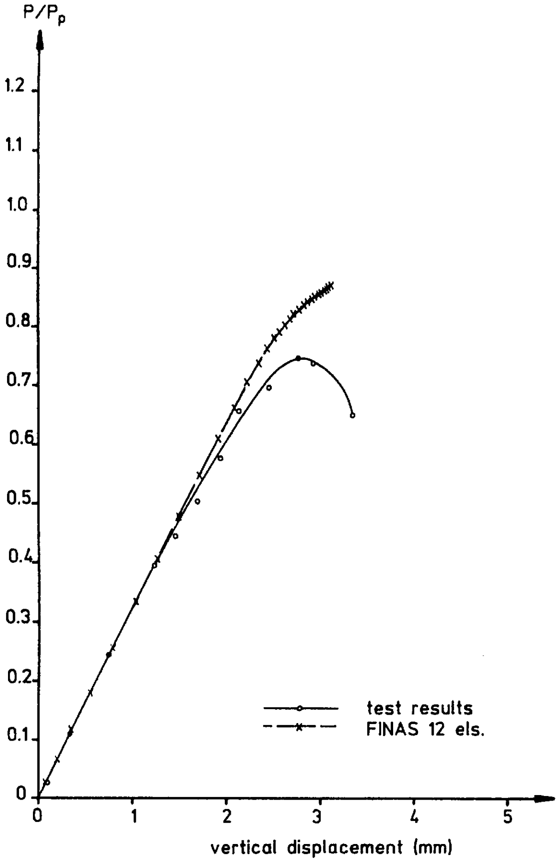

(a) load vs. midspan vertical deflection

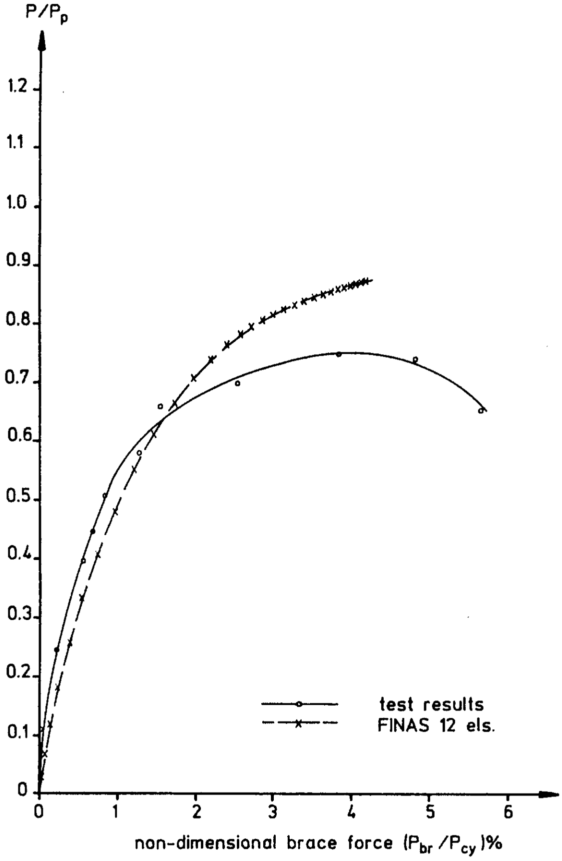

(b) load vs. brace force

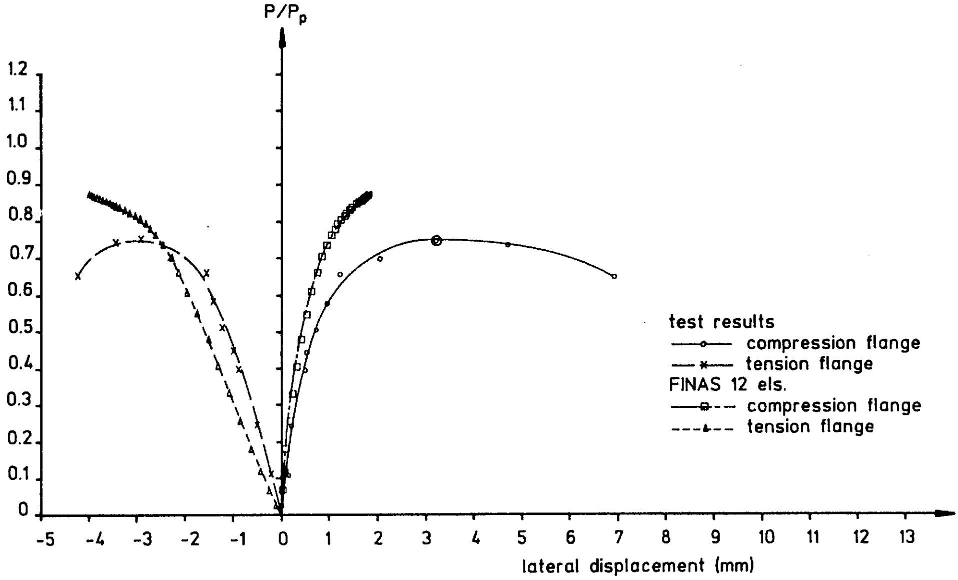

(c) load vs. lateral deflection of flanges at midspan

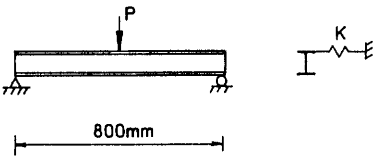

span	800mm
λ	6.0
brace K	84.4N/mm
compn. flange ult. load P_{cy}	3657.1N
P_p	1510.8N
compression flange loading	
compression flange braced	

Fig. 6.16 : Experimental and finite element results for Test 15

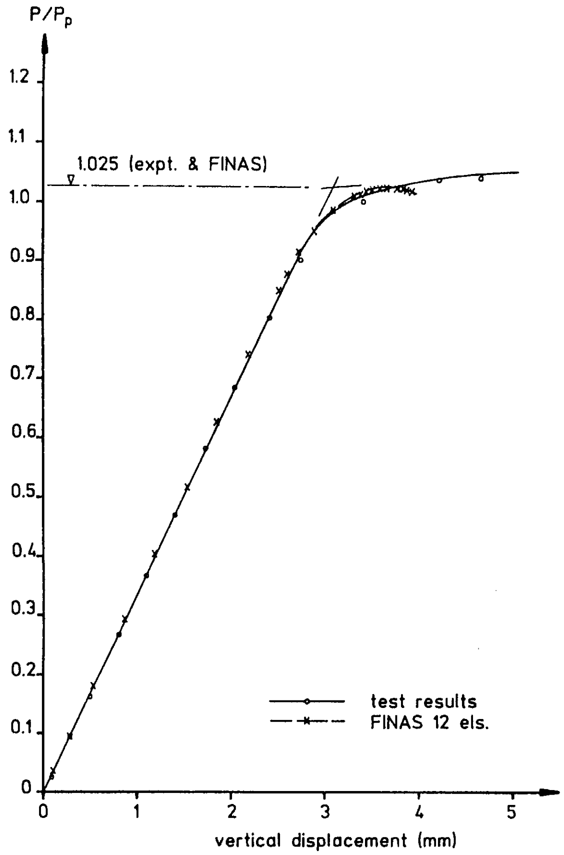

(a) load vs. midspan vertical deflection

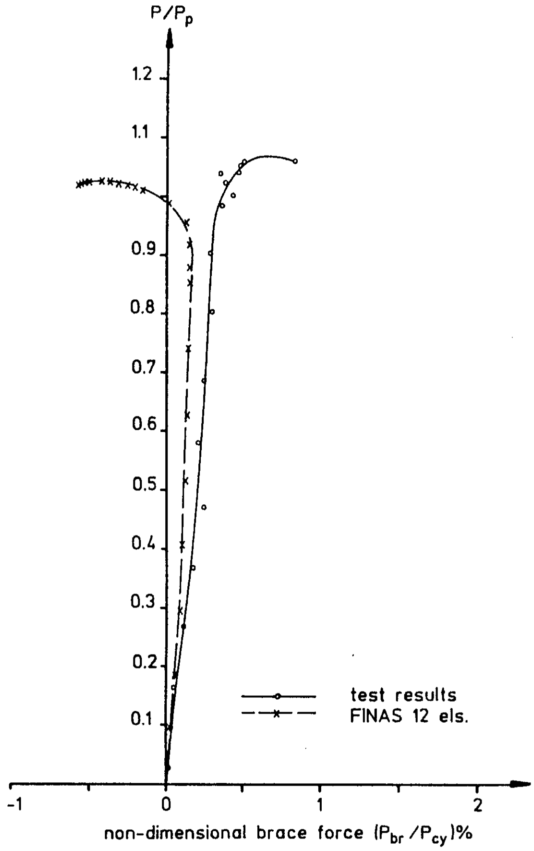

(b) load vs. brace force

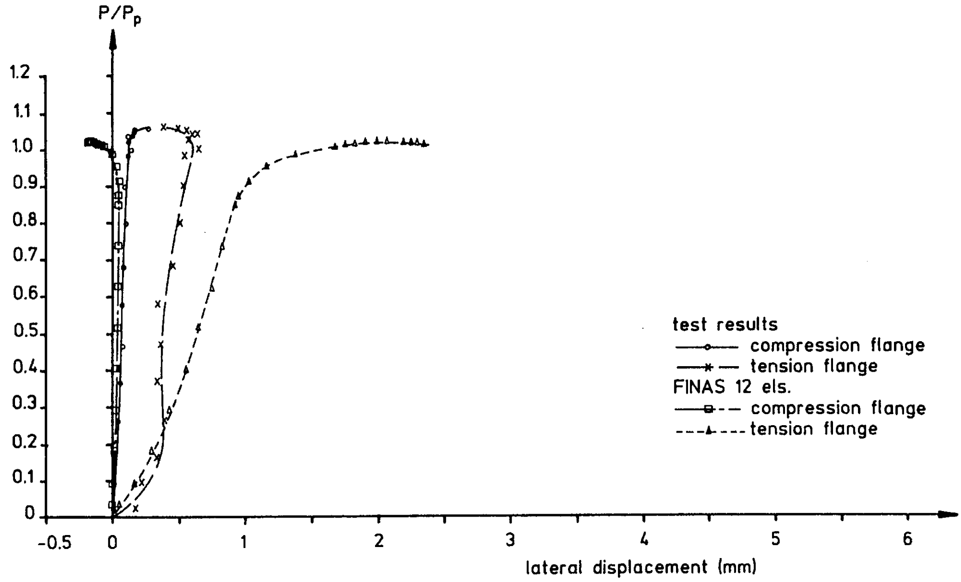

(c) load vs. lateral deflection of flanges at midspan

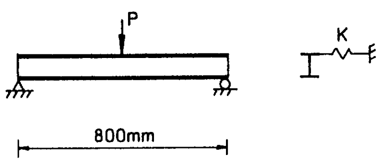

span	800mm
λ	8.0
brace K	107.7N/mm
compn. flange ult. load P_{cy}	3603.0N
P_p	1495.3N
compression flange loading	
compression flange braced	

Fig. 6.17 : Experimental and finite element results for Test 16

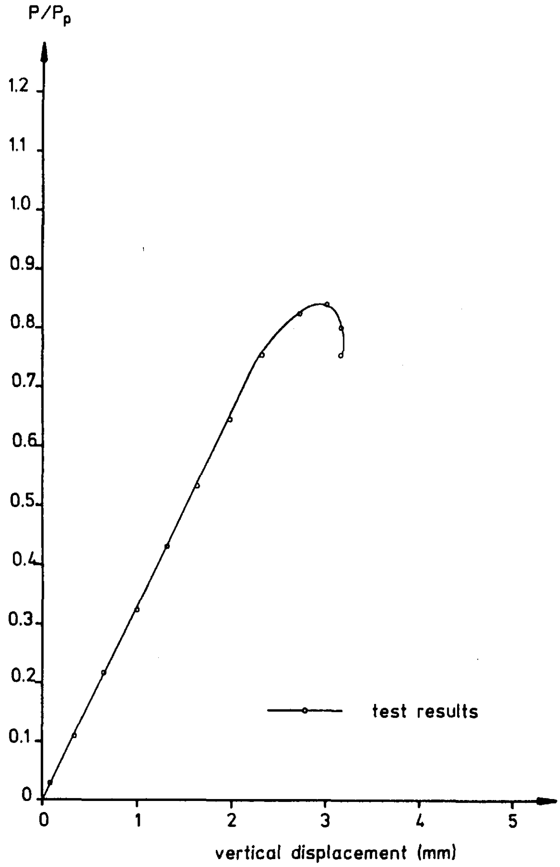

(a) load vs. midspan vertical deflection

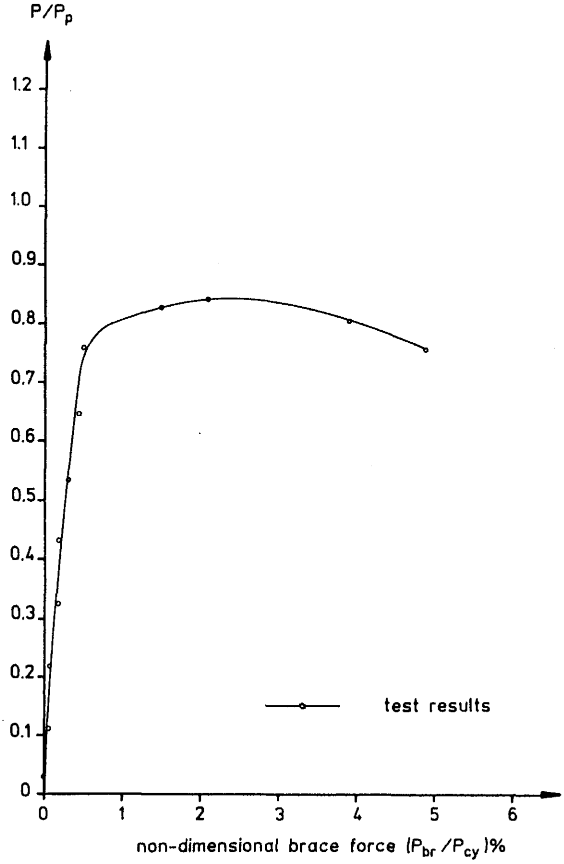

(b) load vs. brace force

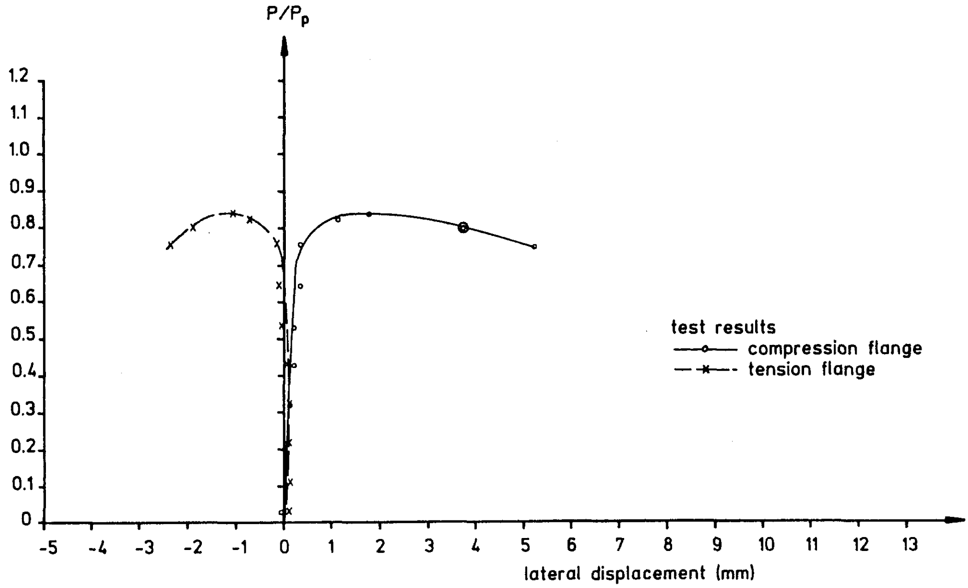

(c) load vs. lateral deflection of flanges at midspan

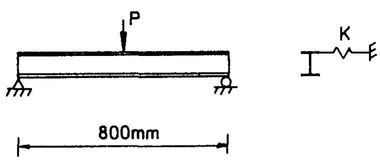

span 800mm
λ 7.0
brace K 76.7N/mm
compn. flange ult. load P_{cy} 3638.1N
P_p 1561.4N
compression flange loading
compression flange braced

Fig. 6.18 : Experimental results for Test 17

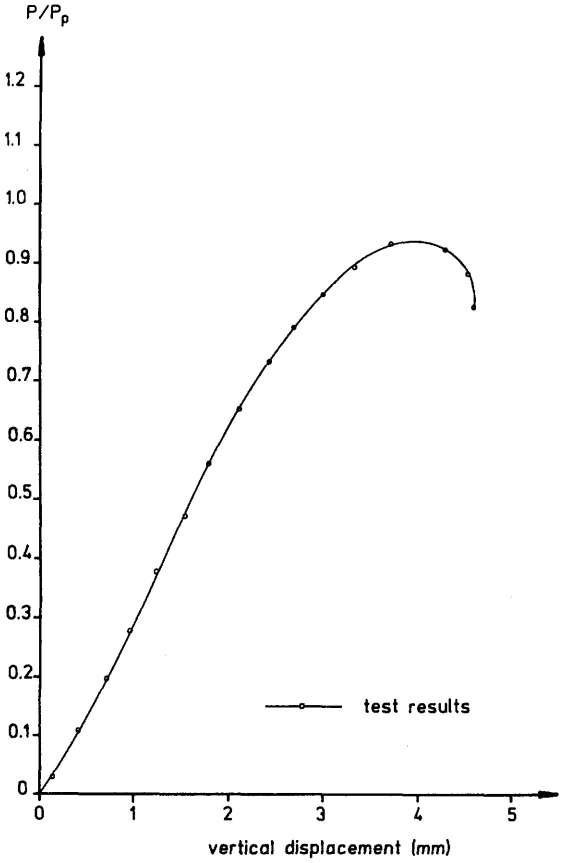

(a) load vs. midspan vertical deflection

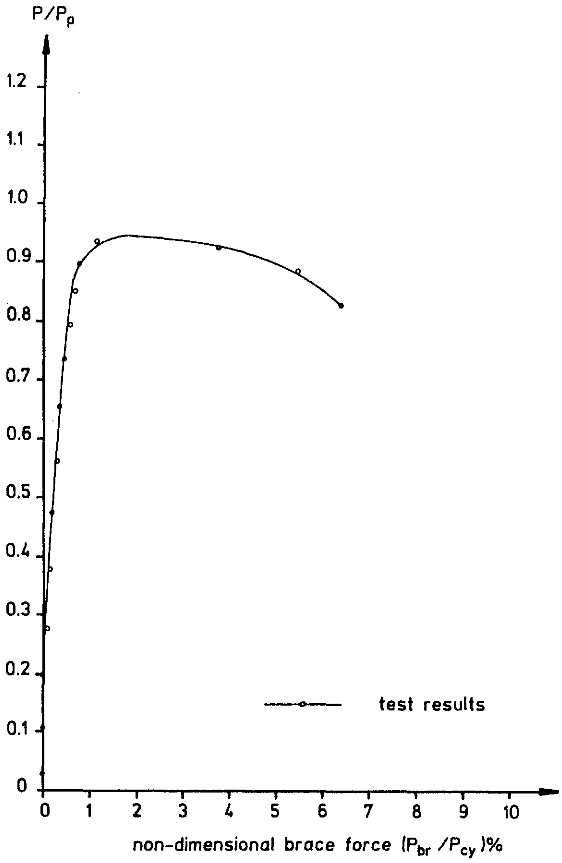

(b) load vs. brace force

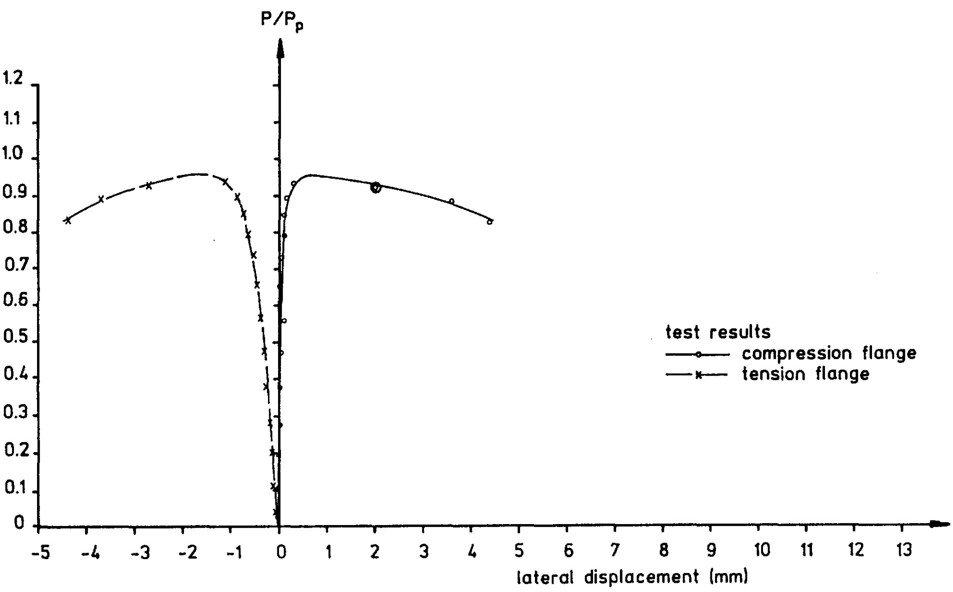

(c) load vs. lateral deflection of flanges at midspan

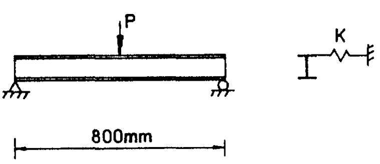

span	800mm
λ	9.0
brace K	99.3N/mm
compn. flange ult. load P_{cy}	3625.4N
P_p	1587.0N
compression flange loading	
compression flange braced	

Fig. 6.19 : Experimental results for Test 18

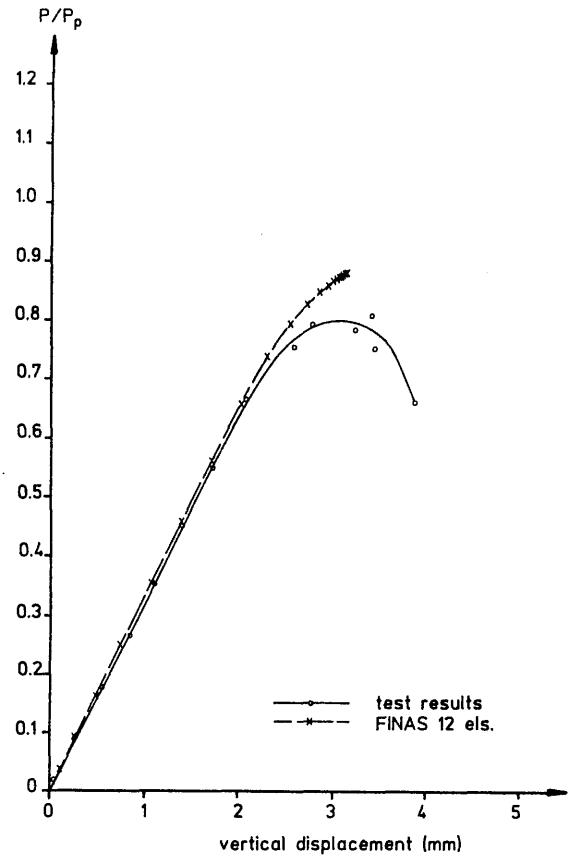

(a) load vs. midspan vertical deflection

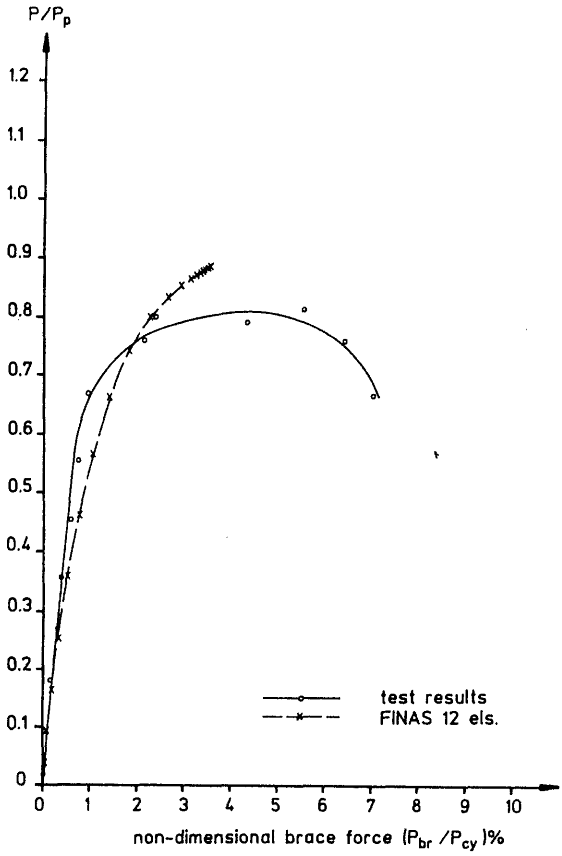

(b) load vs. brace force

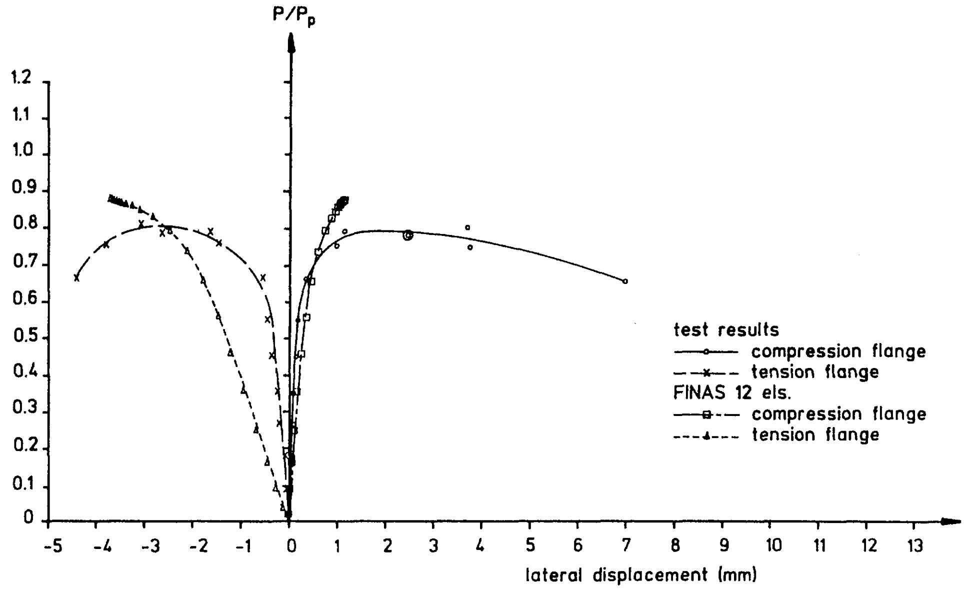

(c) load vs. lateral deflection of flanges at midspan

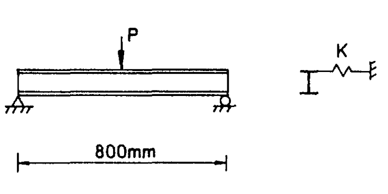

span	800mm
λ	10.0
brace K	111.9N/mm
compn. flange ult. load P_{cy}	3602.2N
P_p	1570.7N
compression flange loading	
compression flange braced	

Fig. 6.20 : Experimental and finite element results for Test 19

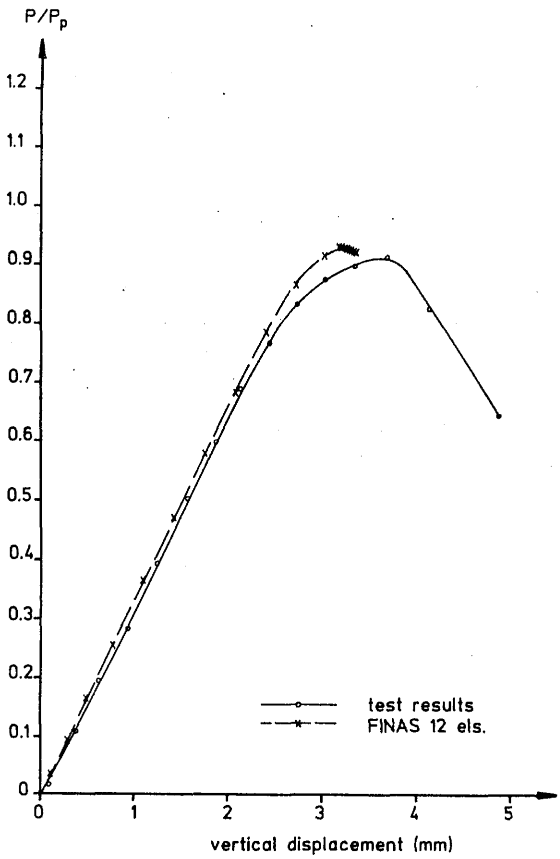

(a) load vs. midspan vertical deflection

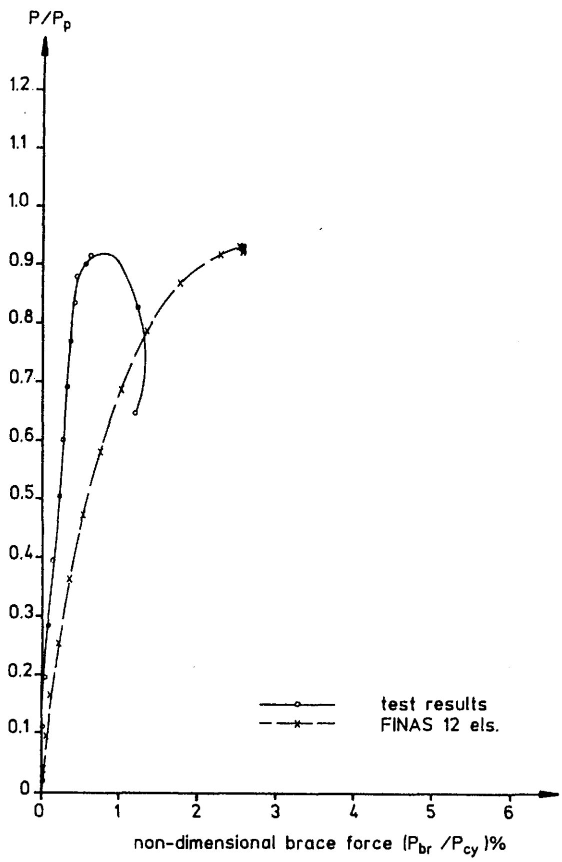

(b) load vs. brace force

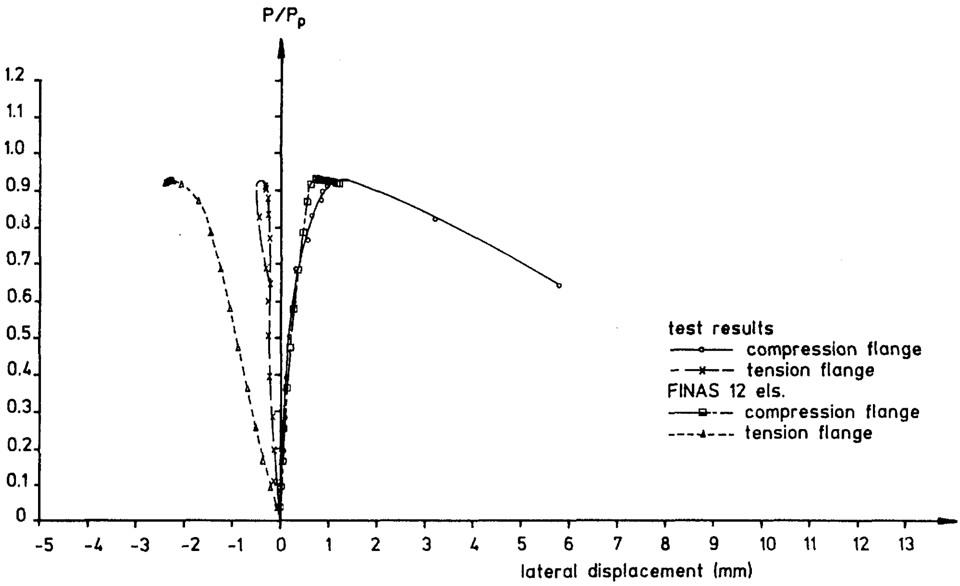

(c) load vs. lateral deflection of flanges at quarter point

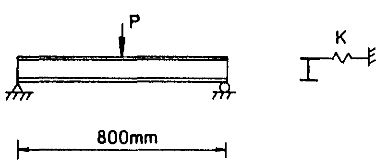

span	800mm
λ	12.0
brace K	127.9N/mm
compn. flange ult. load P_{cy}	3550.2N
P_p	1553.1N
compression flange loading	
compression flange braced	

Fig. 6.21 : Experimental and finite element results for Test 20

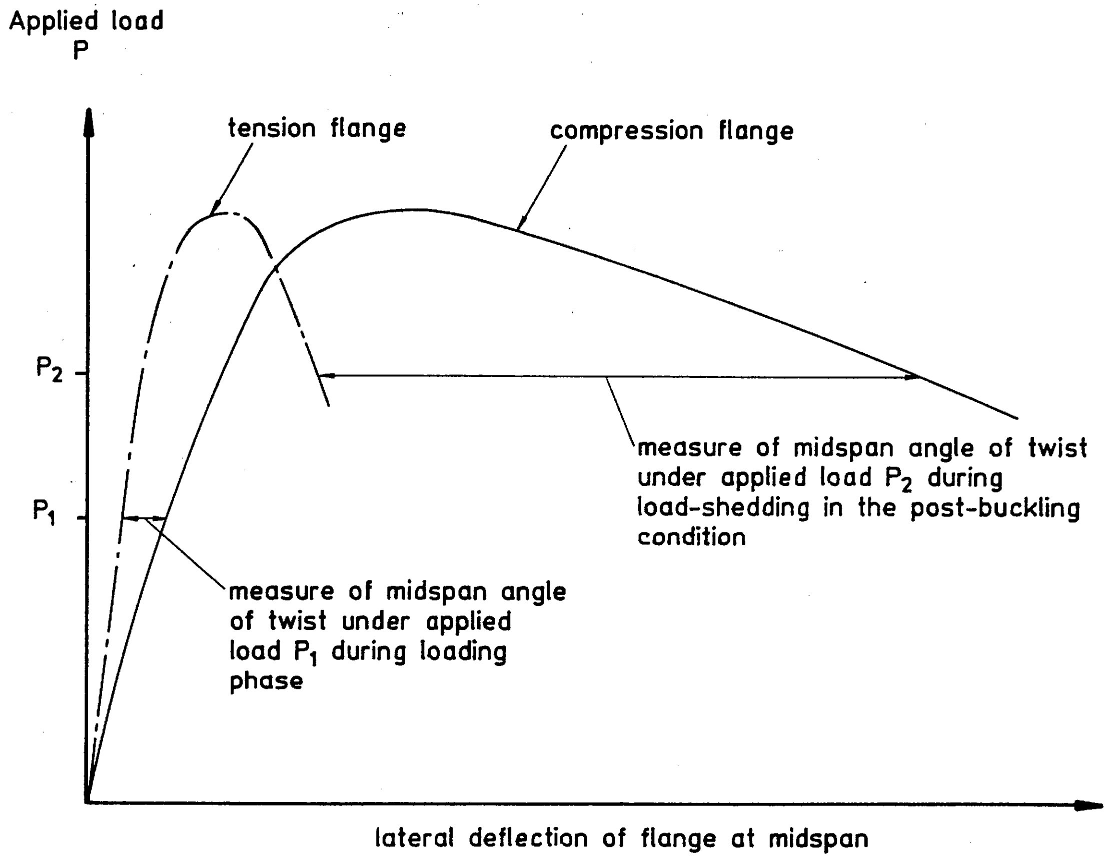

Fig. 6.22 : Qualitative assessment of torsional deformations from lateral deflection measurements

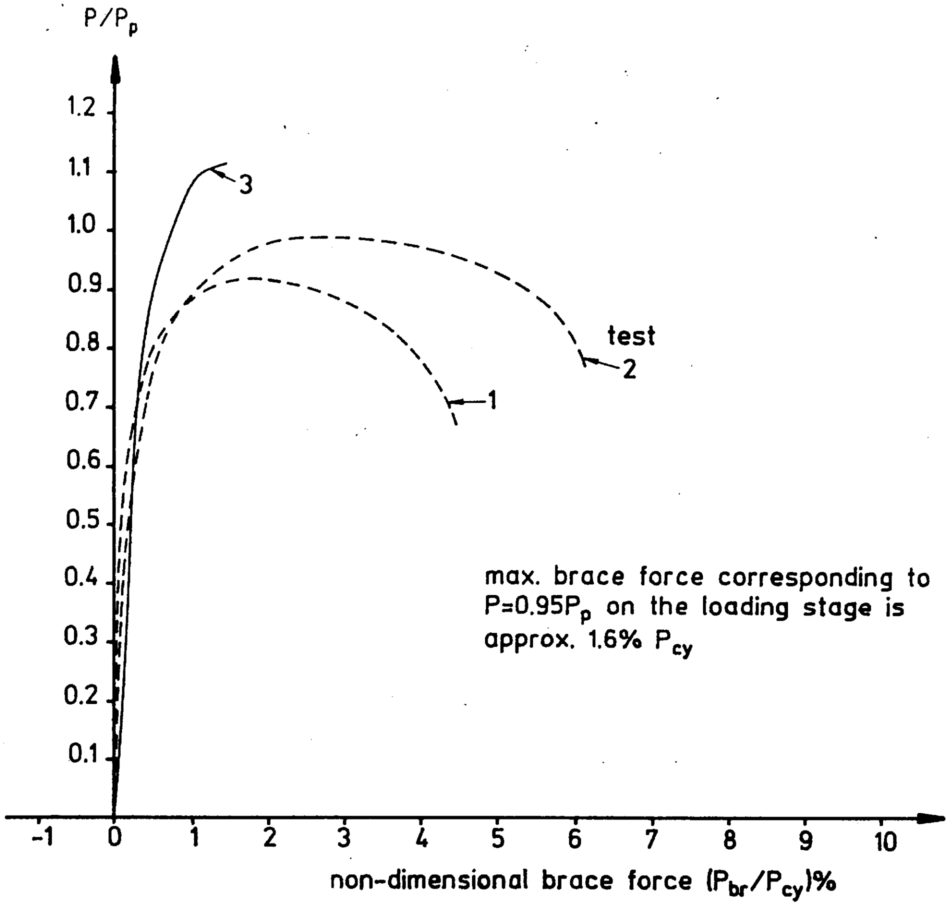

Fig. 6.23 : Experimental bracing force curves for Set 1

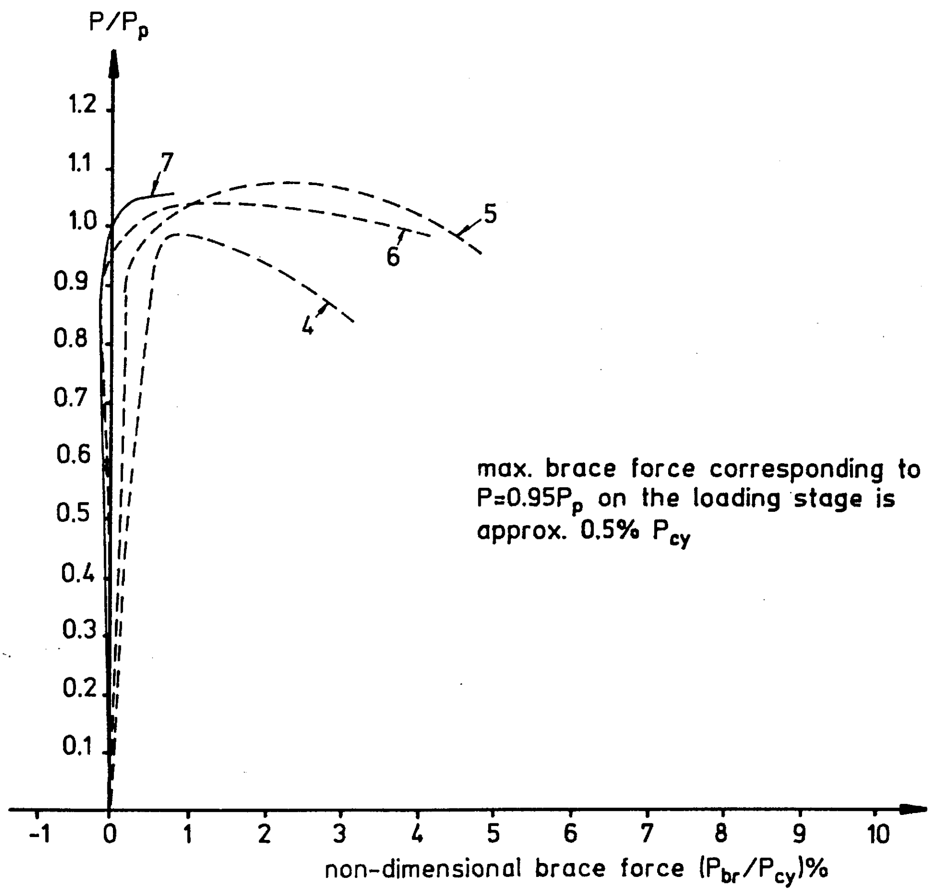

Fig. 6.24 : Experimental bracing force curves for Set 2

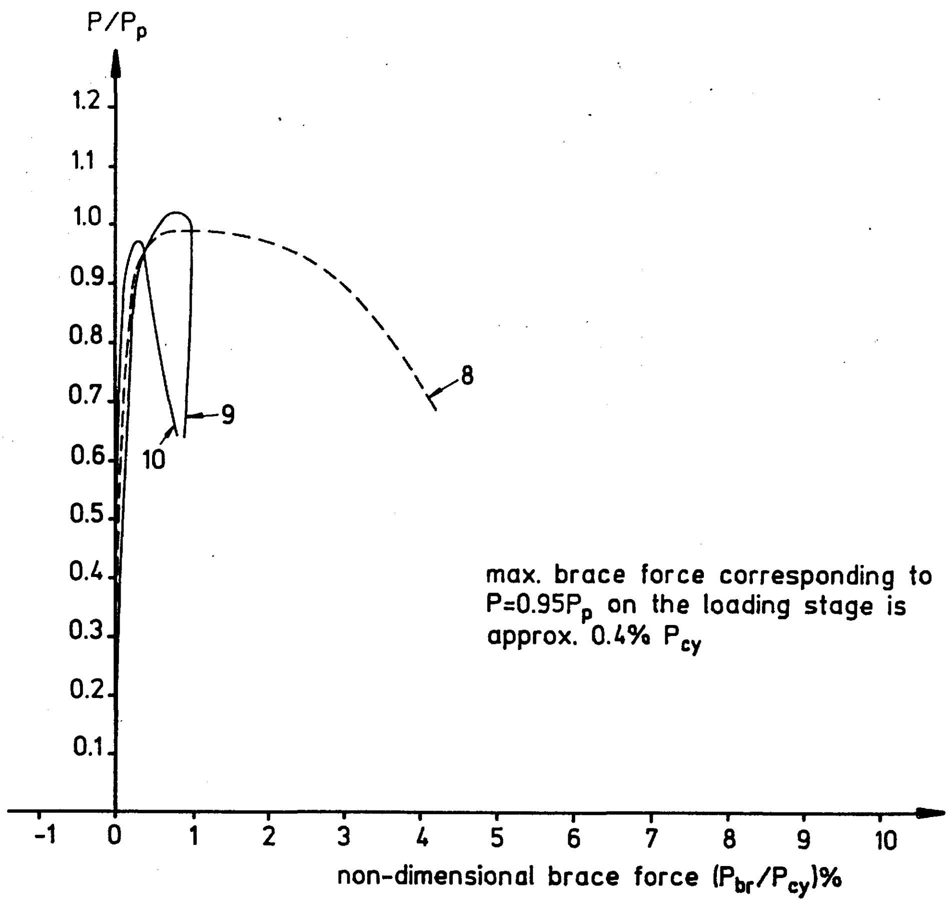

Fig. 6.25 : Experimental bracing force curves for Set 3

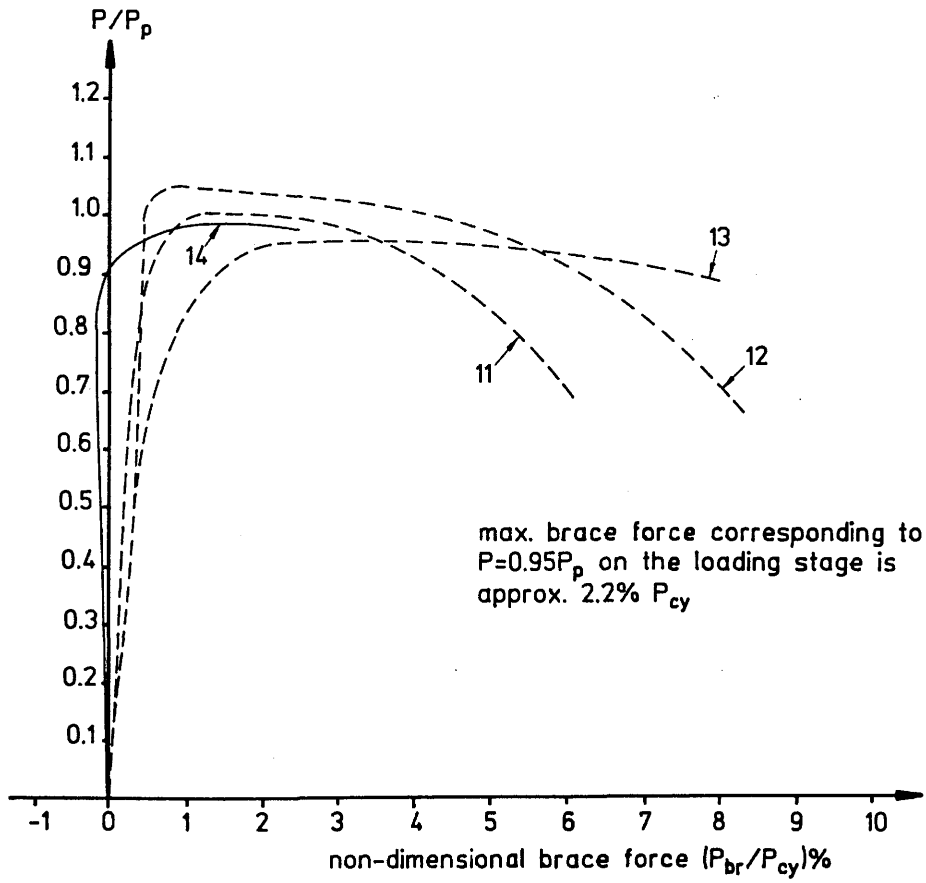

Fig. 6.26 : Experimental bracing force curves for Set 4

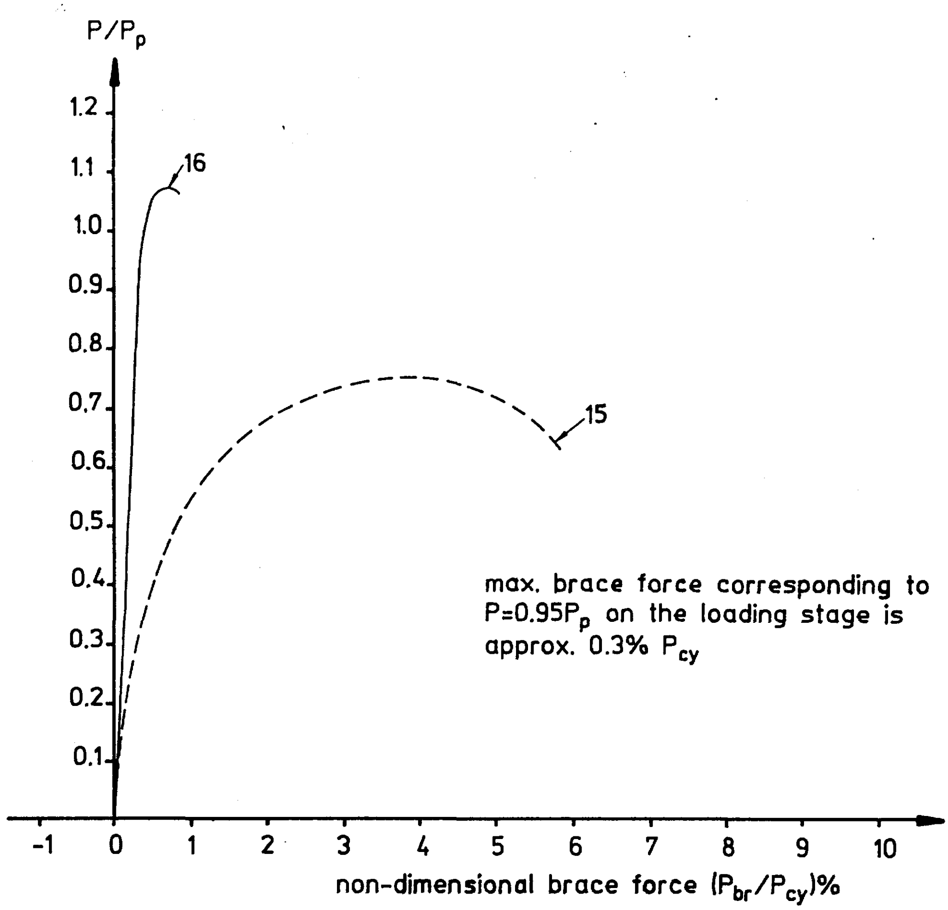

Fig. 6.27 : Experimental bracing force curves for Set 5

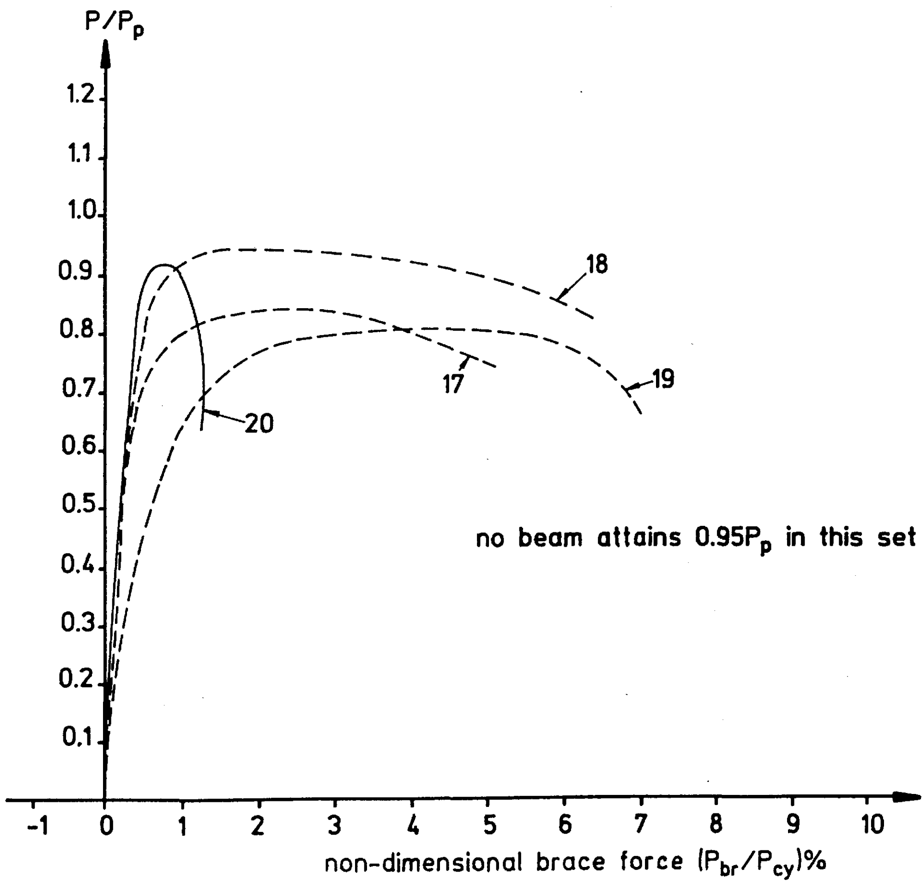

Fig. 6.28 : Experimental bracing force curves for Set 6

CHAPTER 7

FINAS PARAMETRIC STUDY - SOME FACTORS INFLUENCING THE MAGNITUDE OF BRACING FORCES

CHAPTER 7

FINAS PARAMETRIC STUDY - SOME FACTORS INFLUENCING THE MAGNITUDE OF BRACING FORCES

In view of the generally acceptable level of correlation between experimental and FINAS finite element results demonstrated in Chapter 6, a short parametric study based on FINAS was carried out to investigate the influence of three important variables on the magnitude of restraining forces developed in single midspan translational bracing members. The effects of variations in R^2 values, restraint stiffnesses and the relative positions of restraint attachment and load application (the "load/restraint geometry") were examined.

7.1 The FINAS Braced Beam Model

As in Chapter 6 FINAS analyses, the primary member was modelled by twelve beam elements and the lateral restraint member by an additional beam element attached at the appropriate level on the cross-section of the primary member. The coupled materially and geometrically non-linear solution strategy used in previous analyses was again employed.

The cross-sectional dimensions of the FINAS beam were as shown in Fig. 7.1, the general metal thickness of 0.851mm being the average of the measured values for the eight preliminary beams shown in Table 5.3 . A yield stress of 234.5 N/mm^2 and Young's Modulus of 196,000 N/mm^2 were used in conjunction with these geometrical properties. Beam spans of 600mm, 800mm, and 1000mm were employed, giving R^2 values of 6.56, 11.67 and 18.24, very close to the average values for the model beam tests shown in Table 6.2 . Such close agreement facilitated comparison with experimental bracing forces although the inability of the mathematical model to describe the random distributions of initial imperfections present in test beams meant that comparisons had to be of a more qualitative than of a strictly quantitative nature.

Only one pattern of initial geometrical imperfections was employed in the parametric study. The widely accepted non-dimensional initial midspan compression flange crookedness (u_0/l) of 0.001 was incorporated into all FINAS beams; this was accompanied by an initial non-dimensional midspan twist ($\varphi_0 D/l$) of 0.00095, the largest value from Table 5.3 . Sinusoidal distributions of these quantities on the span were assumed. The resulting cumulative imperfection was considered to be relatively large but not unrealistically so.

7.2 Presentation and Discussion of Results

The principal results of the parametric study are shown in Figs. 7.3 to 7.13 . Not all of the bracing force curves obtained from the finite element analyses are presented in these figures; rather, a sufficient number of curves to illustrate the influence of the three parameters R^2, restraint stiffness and load/restraint geometry are shown.

In presenting the curves, no indication of the adequacy of the bracing in providing fully effective restraint has been given. This is due to the fact that convergence problems were experienced in the majority of FINAS analyses undertaken. In all cases in which this problem occurred, applied loads of at least $0.9P_p$ were attained before termination of the analyses. Consequently, as first yield in the beams due to in-plane bending was predicted at an applied load of $0.84P_p$, all beams were loaded well into the inelastic range before convergence problems were encountered. Nevertheless, the prediction of actual failure modes from curtailed analyses was not always possible and therefore this information has been omitted from all graphs for consistency in presentation.

The occurrence of non-convergence in the majority of analyses was considered to be largely the result of the use of a distribution of initial imperfections geometrically similar to the fundamental mode of failure of the beam. Consequently, from the outset the analyses were highly geometrically non-linear and, with the spread of plasticity through the section, subsequently became numerically unstable and non-convergent.

The graphs of Figs. 7.3 to 7.12 have been presented in the same non-dimensional form as the bracing force curves of Chapter 6. The notation used to define the load/restraint geometry of a beam is explained in Fig. 7.2: the two letter prefix describes the levels of load application and restraint attachment on the beam cross-section; the R^2 value is shown after the prefix. In this notation the model beams of Sets 1 to 3 in Chapter 6 would be assigned the prefix SC whilst the prefix CC would describe all beams in Sets 4 to 6.

Figs. 7.3 to 7.8 demonstrate the effect of variations in brace stiffness (λ) on the forces developed in a midspan restraint for beams of varying R^2 and load/restraint geometry. Three load/restraint configurations have been considered: CC, CS and SC. Cases involving either tension flange restraint or tension flange loading have not been considered as the former has been shown (Chapter 2) to be ineffective and the latter to be both relatively uncommon and seldom critical (Fig. 2.23).

Only curves for R^2 values of 6.56 and 11.67 have been shown in Figs. 7.3 to 7.8 as similar trends were displayed by the corresponding R^2=18.24 curves. Bracing forces (P_{br}) are small in all cases, never exceeding 1% of the fully yielded compression flange force P_{cy}. Nevertheless, in keeping with the large initial imperfections present in the beams, bracing forces grow rapidly from the onset of loading. Each of these graphs indicates that, for constant applied load in the elastic range, the bracing force increases with increasing brace stiffness. However, the less stiff braces were less capable of providing fully effective restraint and consequently it is likely that, had the analyses been able to be continued into the post-buckling and post-hinge formation phases, greater forces would have been developed in the lighter than in the more substantial braces.

Figs. 7.3 and 7.7 indicate that, for constant applied load, bracing forces increase non-linearly with bracing stiffness, the rate of increase being greatest for low values of λ. In Fig. 7.3, the difference between the λ=20 and λ=10 curves is negligible; a much more significant discrepancy exists between the λ=2.5 and λ=1 curves.

It is evident from Figs. 7.3 to 7.8 that the onset of yield in the primary member, accompanied by a corresponding local reduction in flexural stiffness, results in a rapid increase in bracing force. The sudden increase is characterised by a knee in the curve. This phenomenon is to be expected as the restraint is positioned at the weakening section and hence its axial stiffness compensates for the reduction in stiffness of the primary member. Whether the brace does or does not fully compensate for the stiffness deficiency in the main member is a measure of its adequacy. Knees on the curves are most pronounced for low values of λ, higher values tending to produce a more linear relationship between applied load and bracing force (Figs. 7.3 and 7.7).

The variation of bracing force with restraint stiffness and load/restraint geometry is illustrated in Figs. 7.9 to 7.11 . For constant λ, the change in brace force arising from a change in the load/restraint geometry is small, this being particularly noticeable in the cases of the R^2=11.7 and R^2=18.2 beams. Indeed, it was not possible to differentiate between the compression flange restraint (SC and CC) curves in Figs. 7.10 and 7.11 . From the close grouping of the curves shown in Figs. 7.9 to 7.11 it can be deduced that although restraint stiffness has a significant effect on brace force, the influence of load/restraint geometry is negligible.

The variation of brace force with R^2 for constant λ is investigated in Figs. 7.12 and 7.13 . These curves demonstrate that brace force is almost independent of R^2 for low values of applied load, the difference being greatest for applied loads in excess of $0.5P_p$. For these higher applied loads, larger forces were developed in braces restraining beams of high R^2.

7.3 Comparison of Results of the Parametric Study with Those of Chapter 6

This Section presents a short comparison of the findings of the FINAS parametric study with the main trends observed in the experimental results presented in Chapter 6. However, such comparison is hindered by inevitable differences between the measured initial imperfections of Chapter 6 and those assumed in the parametric study. Moreover, non-convergence of the FINAS solution in most of the analyses contained in the parametric study limits comparison to the elastic and initial inelastic loading stages of testing. Comparison of bracing forces developed during post-buckling deformations or in-plane rotation at a plastic hinge is therefore not possible.

Results of the parametric study presented in Figs. 7.3 to 7.13 indicate that midspan bracing forces are unlikely to exceed 1% of the fully yielded compression flange force P_{cy} for applied loads smaller than about $0.95P_p$. Table 7.1 shows maximum measured bracing forces corresponding to $P=0.95P_p$ during loading in tests. Where larger bracing forces were developed in tests with failure loads smaller than $0.95P_p$, these larger P_{br} values are shown in the final column of the Table. Bracing forces well in excess of 1% of P_{cy} are shown in four of the six sets of tests. It can be concluded that measured bracing forces generally exceed those derived from the idealised beam/restraint model employed in the parametric study.

Notwithstanding the foregoing conclusion, several beam/restraint systems tested during the experimental programme produced negligible bracing forces prior to attainment of their critical loads. Such behaviour was not witnessed in the parametric study where bracing forces increased steadily from the onset of loading.

The adverse effect of yielding in the primary member on the magnitude of bracing forces is verified both by experimental results (Figs. 6.23 to 6.28) and by those of the parametric study (Figs. 7.3 to 7.13). Only in the case of fully effective restraints in Figs. 6.23 to 6.28 do observed bracing forces appear to be relatively unaffected by the onset of yielding at an applied load of approximately

Table 7.1: Measured Bracing Forces Corresponding to $P = 0.95P_p$ in Tests

Test Beam Set	Maximum non-dimensional bracing force (P_{br}/P_{cy}) corresponding to $P = 0.95P_p$ on the loading stage	Remarks
1 (Fig. 6.23)	(0.016)	$P_{br} = 0.017P_{cy}$ recorded at the ultimate load condition $P_{ult} = 0.91P_p$ in Test 1
2 (Fig. 6.24)	0.005	---
3 (Fig. 6.25)	0.004	---
4 (Fig. 6.26)	0.022	---
5 (Fig. 6.27)	(0.003)	$P_{br} = 0.038P_{cy}$ recorded at the ultimate load condition $P_{ult} = 0.75P_p$ in Test 15
6 (Fig. 6.28)	$P = 0.95P_p$ not attained in tests	$P_{br} = 0.044P_{cy}$ recorded at the ultimate load condition $P_{ult} = 0.80P_p$ in Test 19

$0.84P_p$.

In the parametric study it has been noted that, although restraint stiffness has a significant effect on bracing forces, load/restraint geometry is of negligible importance. Comparison of the results of Tests 3 and 11 in Section 6.3.1 showed that although this was true for applied loads smaller than about $0.95P_p$, thereafter compression flange loading produced higher bracing forces than shear centre loading. Therefore, within the domain of comparison permitted by the results of the parametric study, fair agreement with experimental results was noted in this respect also.

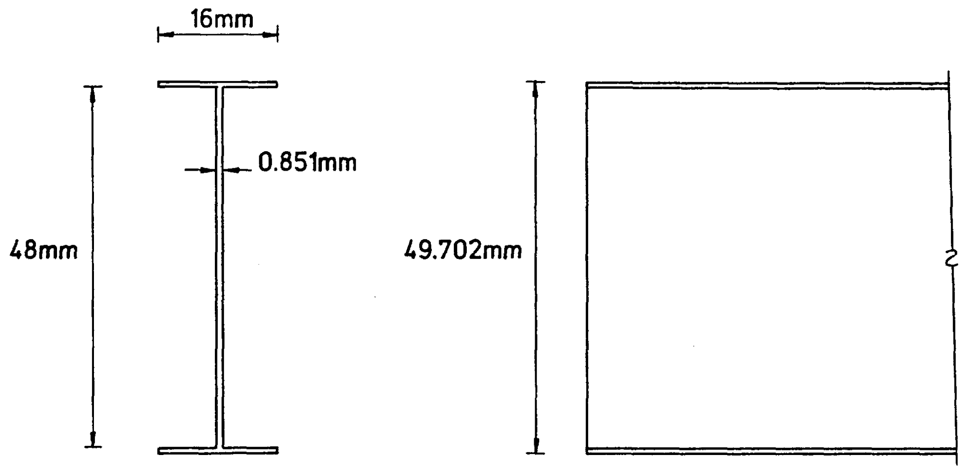

Fig. 7.1 : Cross-sectional dimensions of the beam employed in the FINAS parametric study

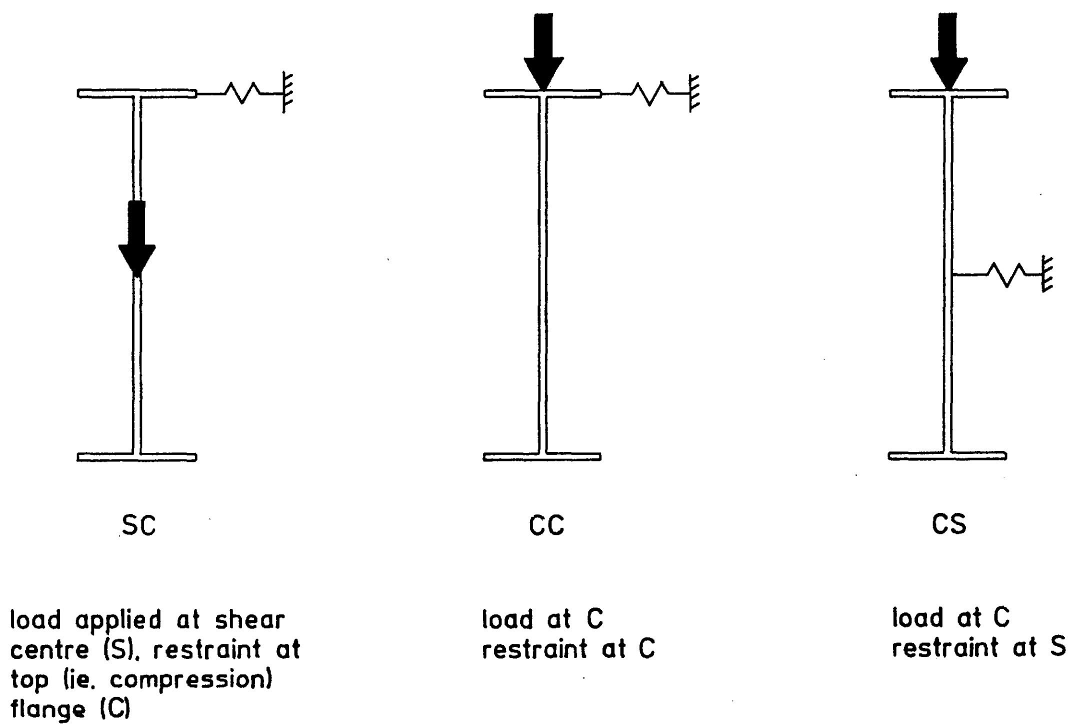

Fig. 7.2 : Load/restraint geometries considered in the FINAS parametric study

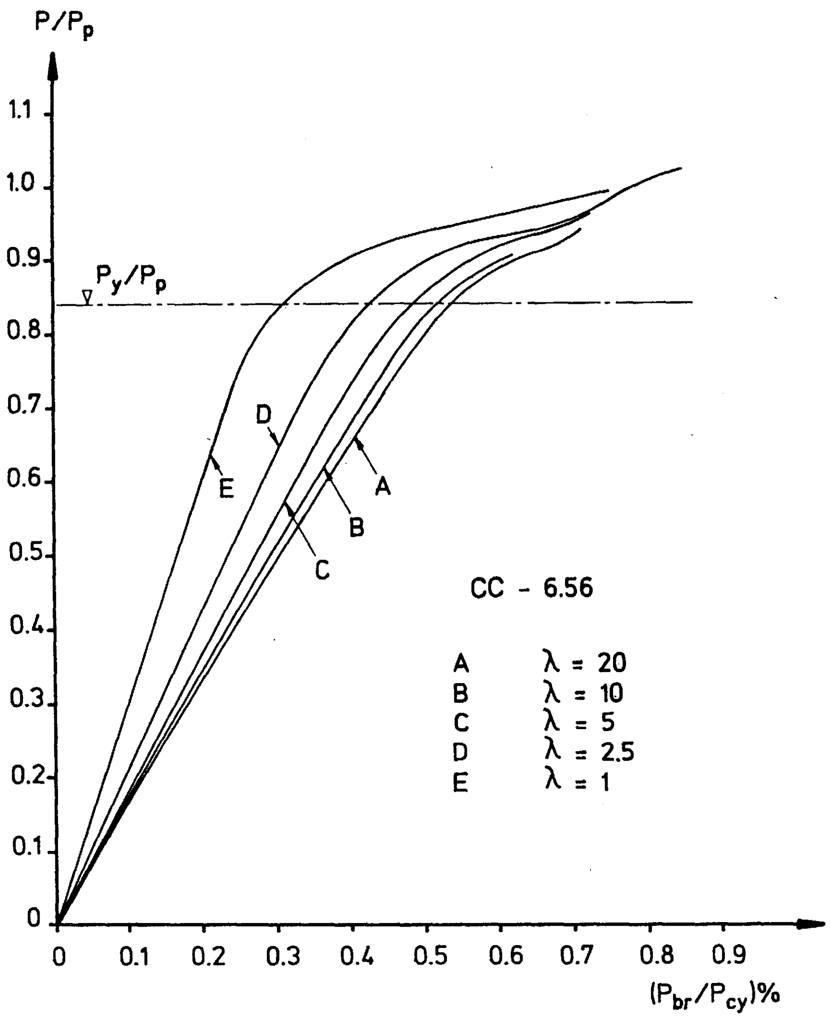

Fig. 7.3 : Relationship between applied load, bracing force and λ for CC load/restraint geometry and R^2=6.56

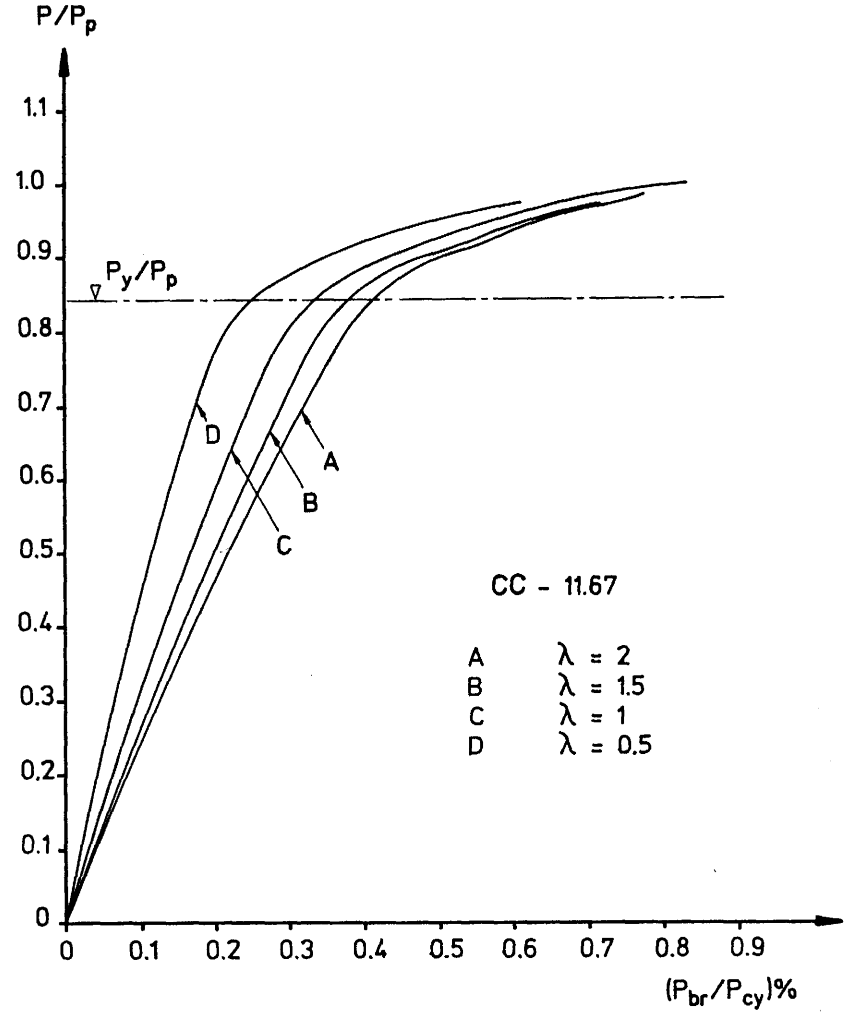

Fig. 7.4 : Relationship between applied load, bracing force and λ for CC load/restraint geometry and R^2=11.67

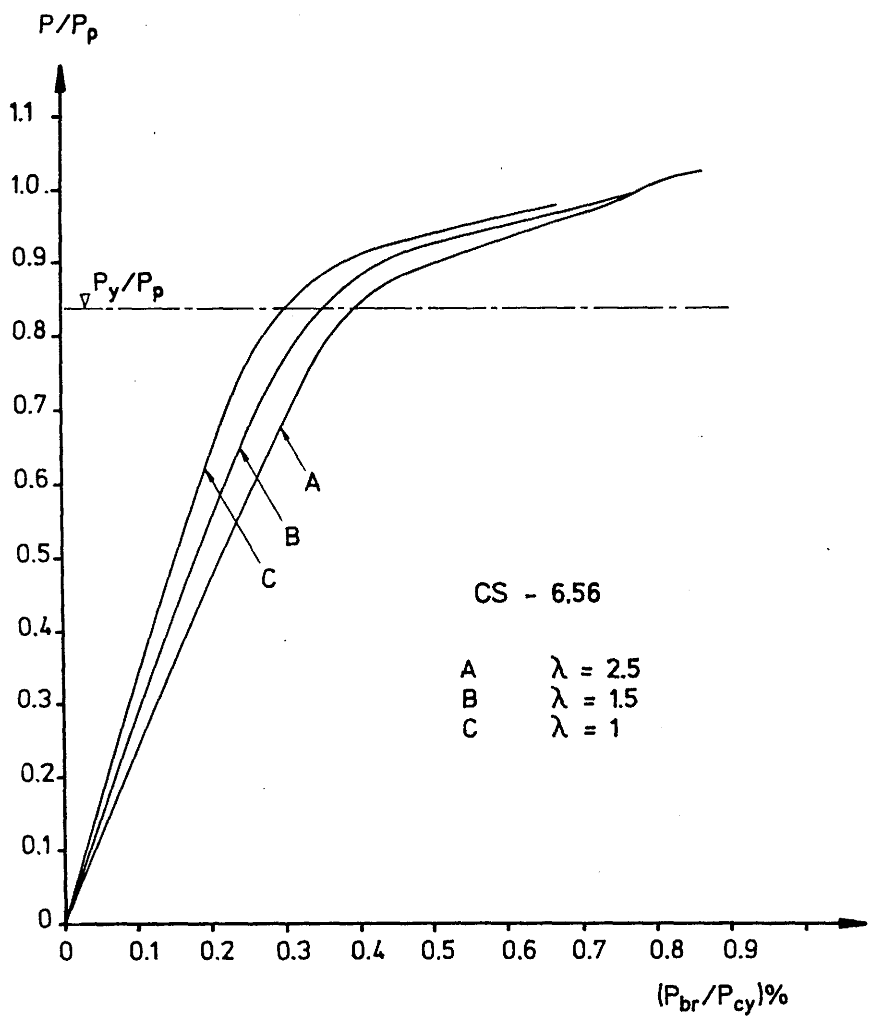

Fig. 7.5 : Relationship between applied load, bracing force and λ for CS load/restraint geometry and R^2=6.56

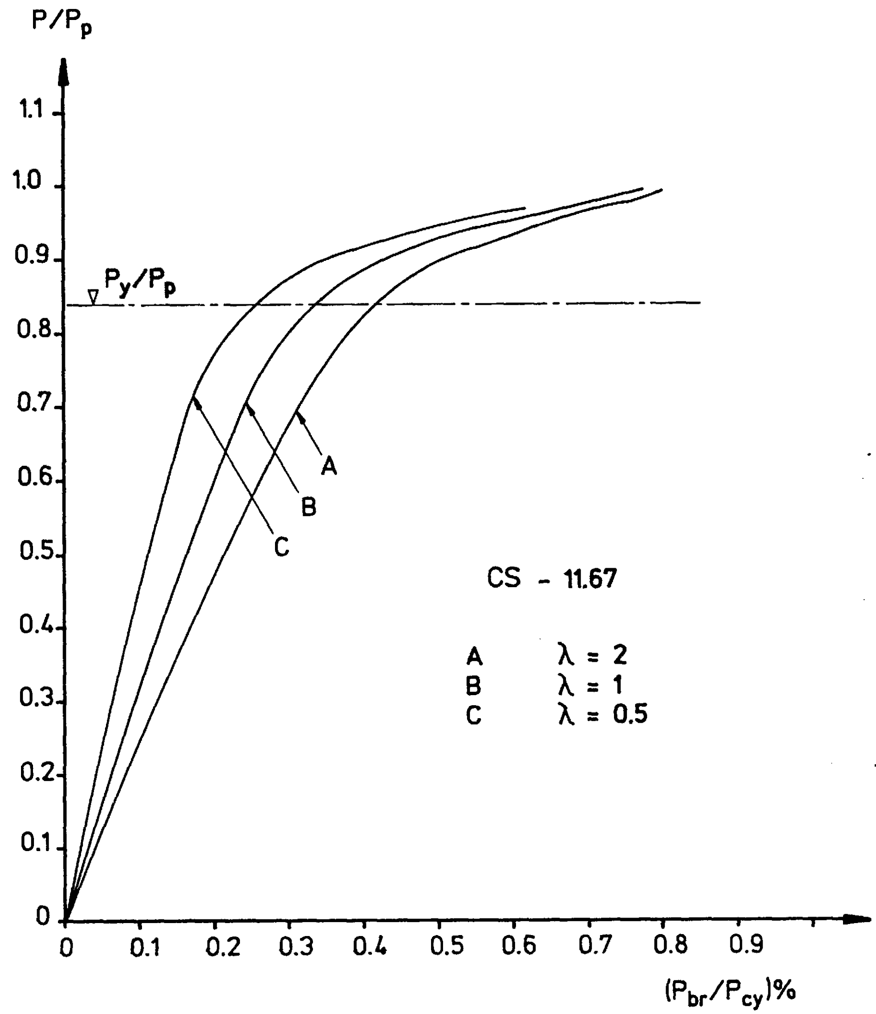

Fig. 7.6 : Relationship between applied load, bracing force and λ for CS load/restraint geometry and R^2=11.67

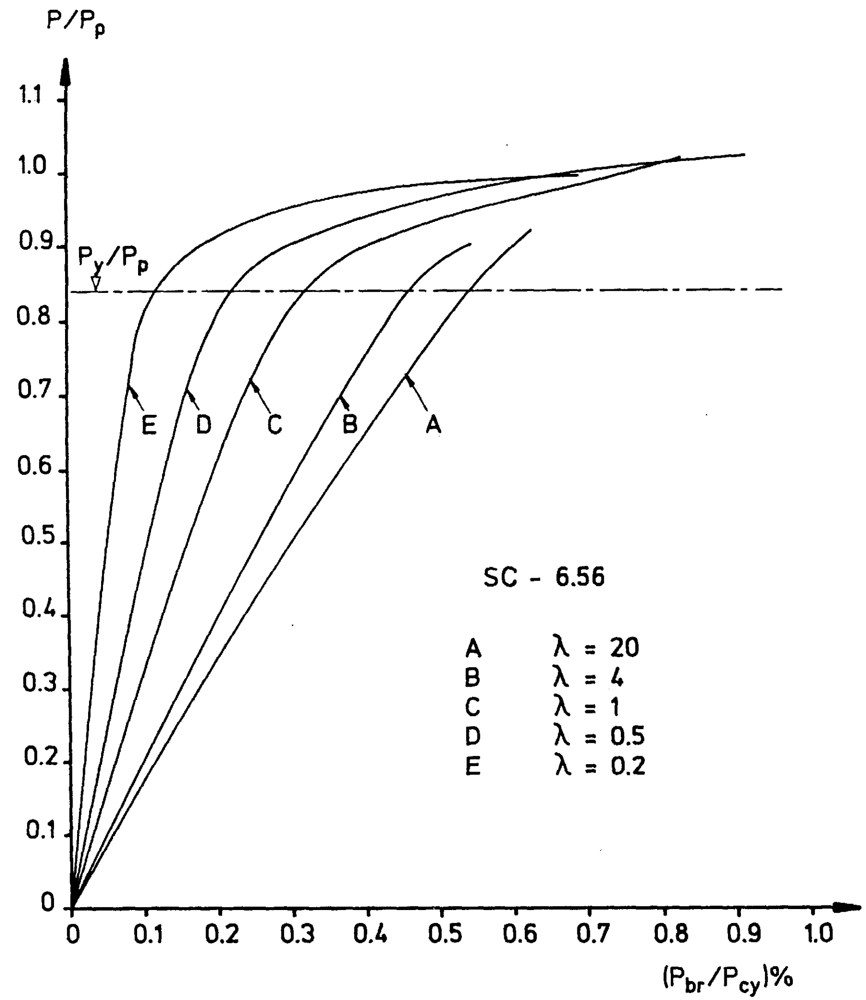

Fig. 7.7 : Relationship between applied load, bracing force and λ for SC load/restraint geometry and R^2=6.56

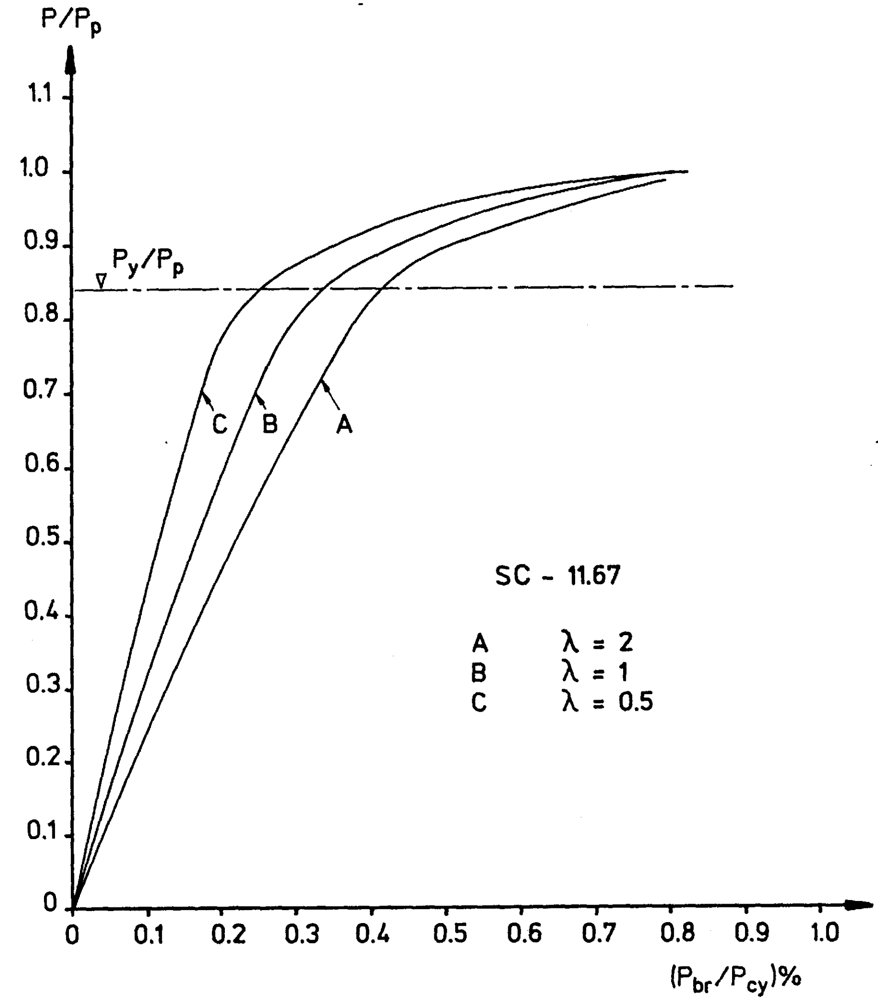

Fig. 7.8 : Relationship between applied load, bracing force and λ for SC load/restraint geometry and R^2=11.67

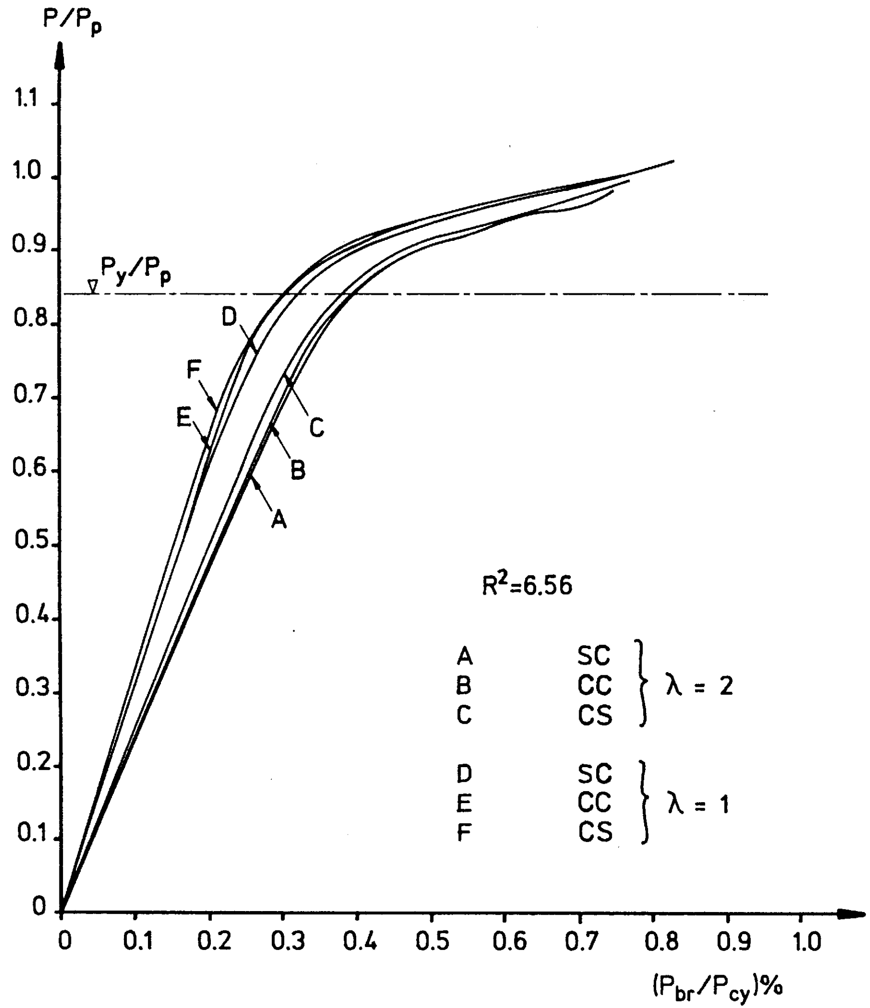

Fig. 7.9 : Relationship between applied load, bracing force, load/restraint geometry and λ for R^2=6.56

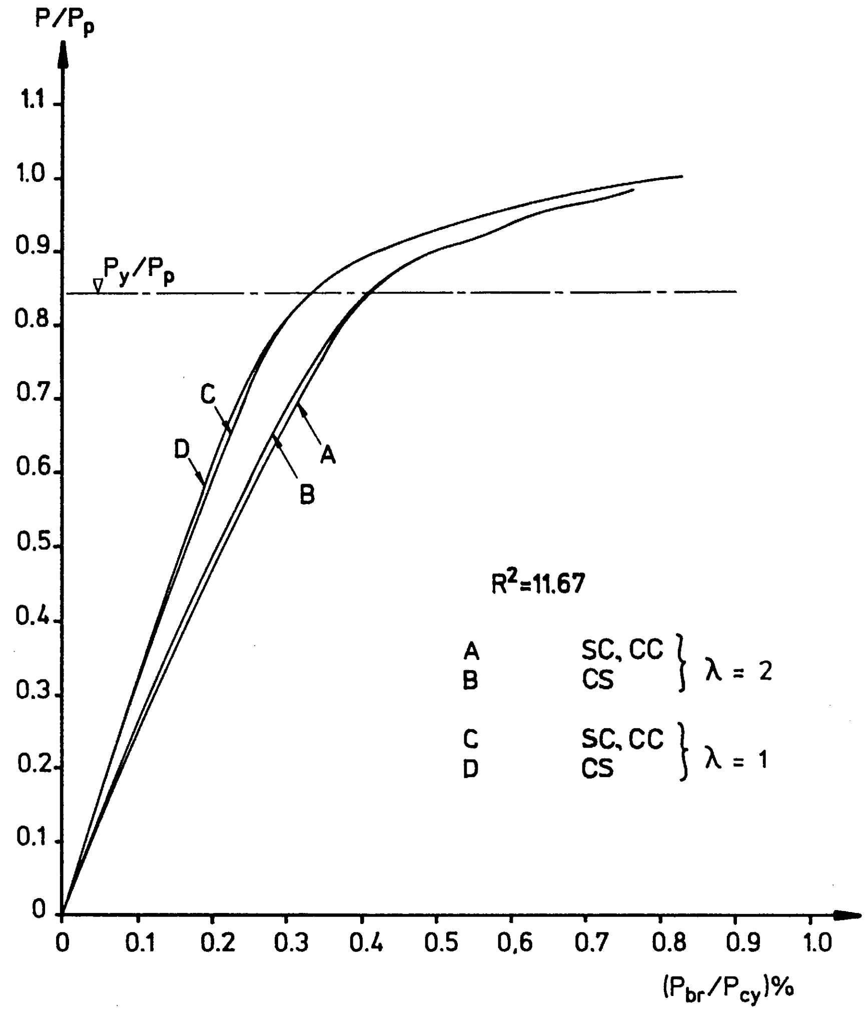

Fig. 7.10 : Relationship between applied load, bracing force, load/restraint geometry and λ for R^2=11.67

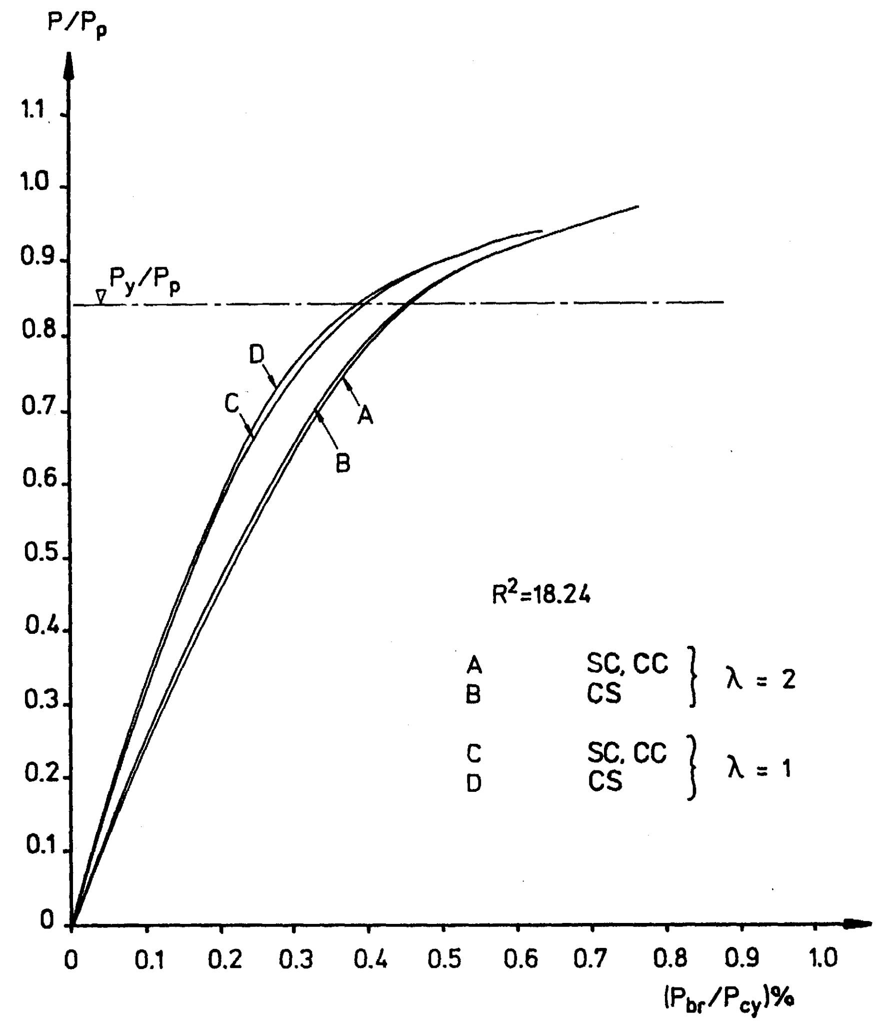

Fig. 7.11 : Relationship between applied load, bracing force, load restraint geometry and λ for R^2=18.24

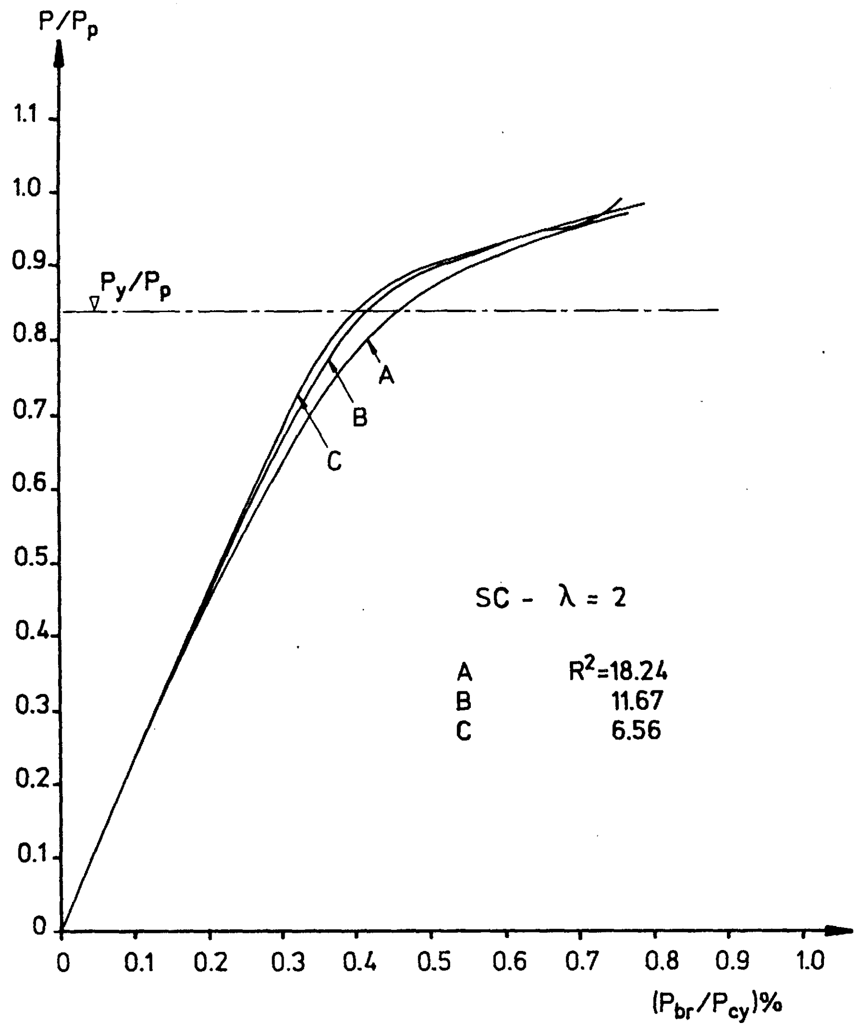

Fig. 7.12 : Relationship between applied load, bracing force and R^2 for SC load/restraint geometry and $\lambda = 2$

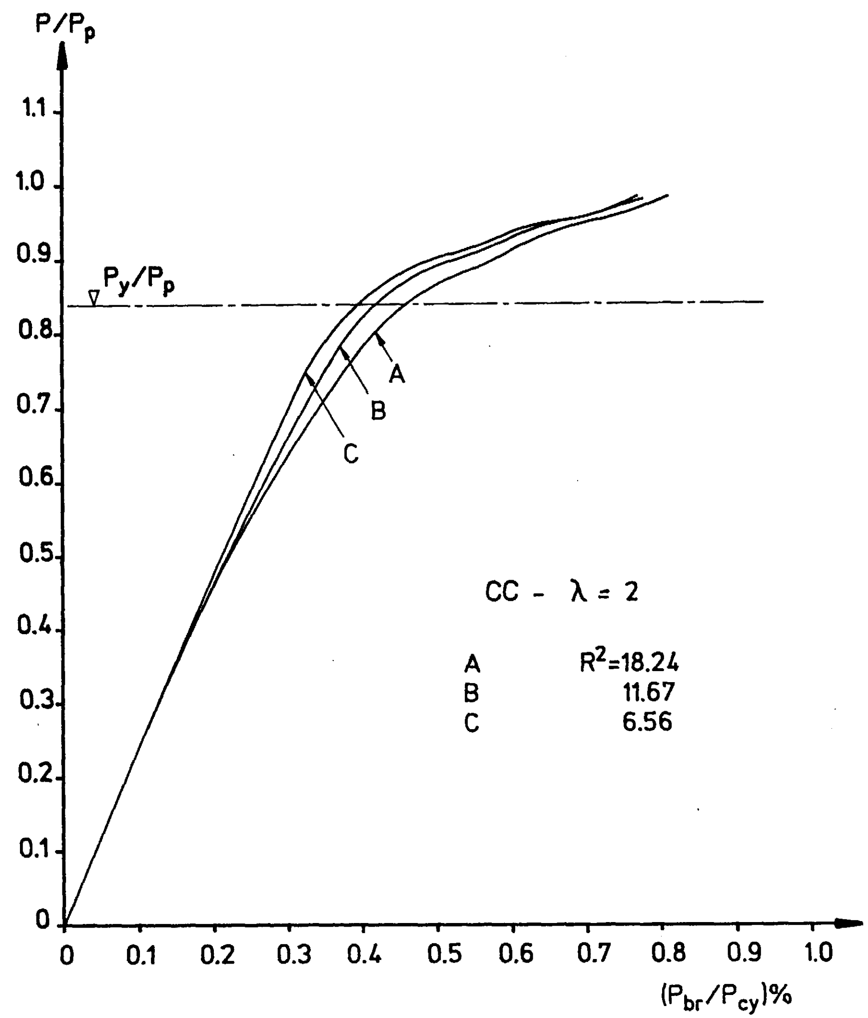

Fig. 7.13 : Relationship between applied load, bracing force and R^2 for CC load/restraint geometry and $\lambda = 2$

CHAPTER 8

COMPARISON OF THE RESULTS OF THIS STUDY WITH PREVIOUS RESEARCH AND THE REQUIREMENTS OF CONTEMPORARY DESIGN CODES

CHAPTER 8

COMPARISON OF THE RESULTS OF THIS STUDY WITH PREVIOUS RESEARCH AND THE REQUIREMENTS OF CONTEMPORARY DESIGN CODES

The results of several previous investigations concerned with the bracing requirements of steel beams were discussed in Chapter 1. Several comparisons of these results were also presented (Figs. 1.11 to 1.15) and it was observed that by far the greater proportion of research effort had been focussed on the bracing requirements of beams susceptible to elastic lateral-torsional instability. In contrast, few studies concerned with the bracing requirements of inelastic steel beams have been published. That of Hartmann[12] was of limited applicability whilst the more generally applicable criteria derived by Lay and Galambos[71] formed the basis of the current AISC[57] bracing requirements. Several other semi-empirical restraint criteria for both elastic and inelastic beams have been suggested in design guides such as those by Morris and Randall[79] and Briggs[80].

It is the purpose of the present Chapter to compare the elastic and inelastic bracing criteria proposed in the present study with those reported in the literature and the requirements of contemporary design codes.

8.1 Comparison of the Elastic Bracing Requirements of Chapter 2 with the Results of Previous Research Employing Elastic Buckling Theory

The bracing requirements of short span, elastic beams were presented in Chapter 2 (Figs. 2.19 to 2.27) in terms of the non-dimensional translational and torsional restraint parameters λ and e. As in the literature, attention was confined to cases of central point loading and uniform applied moment; however, Figs. 2.19 to 2.27 present a more comprehensive account of the influence of load/restraint geometry on λ_{cr} and e_{cr} values for short span beams than is presented elsewhere in the literature (Chapter 1).

Figures 8.1 to 8.5 show comparisons between the results of the elastic buckling analyses presented in Chapter 2 and those of previous investigations. Numerical solutions based on Chapter 2 analyses have been obtained using the computer programmes MODBRACE and AUTOBRAC previously described. In Fig. 8.1, excellent correlation is observed between Hartmann's[16] results and those of the present study for the case of a simply-supported beam under central point loading. The curve representing Flint's[59] simple relationship of eqn. (1.5) for very slender ($R^2=\infty$) beams is also shown. As observed in Chapter 1, correlation between this equation and Hartmann's $R^2=\infty$ results is satisfactory for λ values less than about five. Thereafter, correlation becomes poorer. Hartmann's $R^2=100$ and $R^2=\infty$ curves of Fig. 8.1 are indistinguishable from those of the present study.

The elastic buckling behaviour of beams under uniform bending moment either laterally or torsionally restrained at midspan is examined in Figs. 8.2 and 8.3 . The effect of lateral restraint at shear centre level is illustrated in Fig. 8.2 where a comparison between the results of the present study and those of Nethercot and Rockey in Ref. 63 shows the effect of their allowing for deformations of the cross-section in the buckling analysis. Critical bracing stiffnesses calculated in Ref. 63 were higher than those predicted by AUTOBRAC, the discrepancy being greatest for the lower values of R^2. In keeping with this trend, AUTOBRAC predicted $\lambda_{cr} \doteqdot 10.2$ for the $R^2=12$ beam whereas Nethercot and Rockey's $R^2=12$ curve suggests that shear centre lateral restraint is itself incapable of providing fully effective restraint. Such comparison would apparently indicate the need for theoretical buckling analyses concerned with beams of low slenderness to make allowance for the effect of cross-sectional deformations. However, apart from its use in providing approximate values of critical restraint stiffness, elastic buckling theory applied to braced beams of low R^2 is of little practical value as inelastic instability in these more stocky beams generally occurs at loads considerably smaller than corresponding elastic critical values.

Corresponding results for the case of a beam torsionally restrained at midspan are presented in Fig. 8.3, where the results of Taylor and Ojalvo[60] provide the basis for comparison. In this case, correlation between the two sets of results is more satisfactory than in

Fig. 8.2 . Although a finite difference solution was employed in Ref. 60, all other major assumptions, such as the neglect of cross-sectional deformations, were the same in the two analyses.

The ability of the programme AUTOBRAC to provide results consistent with those of previous investigations for the case of combined midspan lateral and torsional restraint is illustrated in Figs. 8.4 and 8.5 . In Fig. 8.4, comparison between the results of the present study and those of Nethercot and Rockey[63] for combined restraint of an R^2=32 beam under uniform moment is considered. As in Fig. 8.2, the inclusion of deformations of the beam cross-section leads to critical $\{\lambda,e\}$ combinations for second mode buckling slightly more onerous in Ref. 63 than in the present study. Nevertheless, the same trends are evident in the two sets of results.

Corresponding results for the case of central point loading are shown in Fig. 8.5 where critical $\{\lambda,e\}$ restraint combinations are shown for two values of R^2 and several load/restraint configurations. The two-letter codes of Chapter 7 defining load/restraint geometry are employed in Fig. 8.5 . AUTOBRAC was used to produce results for six values of λ; these results are observed to be in excellent agreement with the curves of Mutton and Trahair[64] which were derived using the finite integral method, neglecting the effects of deformation of the beam cross-section.

In conclusion, the numerical results derived from the elastic buckling analyses presented in Chapter 2 are generally in good agreement with published results of previous investigations, although the inclusion of cross-sectional deformations in an analysis by Nethercot and Rockey[63] reduces the calculated stability of members and increases required critical lateral and torsional restraint stiffnesses.

8.2 Comparison of Experimental and Finite Element Results of Chapter 6 with those of the Elastic Bifurcation Analysis of Chapter 2

Although comparison of the results of Chapter 6 with those of Chapter 2 is strictly not justified due to fundamental differences between the behaviour of initially imperfect beams and that of their ideal, mathematical equivalents, such comparison nevertheless serves to emphasise the need for the bracing requirements of short span beams to be derived by a method, either experimental or theoretical, more refined than the elastic bifurcation analysis presented in Chapter 2. The inability of classical bifurcation or eigenvalue analyses to predict lateral deflections and consequently the forces developed in lateral restraints has previously been noted; at best, approximate critical restraint stiffnesses can be predicted by these methods.

Table 8.1 relates the observed ultimate loads of the twenty beams tested in the experimental programme reported in Chapter 6 to the elastic critical loads of both restrained and unrestrained beams of the same span. In this table, the following notation has been adopted:

P_p	concentrated load causing formation of a plastic hinge
P_{ult}	observed ultimate load of initially imperfect test beam
P_{crI}	elastic first mode critical load of unbraced beam with load applied at same level as in test
$P_{cr\lambda}$	elastic critical load of braced beam with load/restraint geometry and restraint stiffness as in test
P_{crII}	elastic second mode critical load of braced beam

In Table 8.1 the elastic critical loads P_{crI}, $P_{cr\lambda}$ and P_{crII} are expressed non-dimensionally in terms of P_p to facilitate comparison with the P_{ult}/P_p values obtained in tests. Also shown in Table 8.1 are the proposed values of λ_{cr} based on test results presented in Table 6.3 and the average λ_{cr} value for each set of tests predicted by elastic bifurcation analysis.

Experimental ultimate loads consistently lie between the P_{crI} and $P_{cr\lambda}$ values, indicating that all inelastic critical loads, for

Table 8.1: Experimental Ultimate Loads in Relation to Elastic Critical Loads

Test Set	Test	P_p (N)	Experimental Ultimate Load P_{ult}/P_p	Results based on elastic analyses of Chapter 2				Proposed λ_{cr} based on test results (from Table 6.3)
				Unbraced Elastic 1st Mode critical load P_{crI}/P_p	Elastic Critical load for λ used in test $P_{cr\lambda}/P_p$	Fully Braced elastic 2nd mode critical load P_{crII}/P_p	Ave. theoretical λ_{cr} value for test set	
1	1	1993	0.91	0.562	1.394	2.551	2.526	2.5
	2	2025	0.98	0.582	2.256	2.653		
	3	2004	1.04	0.563	2.551	2.551		
2	4	1510	0.98	0.374	1.326	1.572	2.580	4.5
	5	1478	1.06	0.357	1.494	1.494		
	6	1501	1.04	0.361	1.504	1.504		
	7	1522	1.04	0.375	1.573	1.573		
3	8	1184	0.99	0.261	1.009	1.009	2.655	4.5
	9	1188	1.02	0.264	1.023	1.023		
	10	1187	0.97	0.260	1.004	1.004		

Table 8.1: Experimental Ultimate Loads in Relation to Elastic Critical Loads (contd)

Test Set	Test	P_p (N)	Experimental Ultimate Load P_{ult}/P_p	Results based on elastic analyses of Chapter 2: Unbraced Elastic 1st Mode critical load P_{crI}/P_p	Elastic Critical load for λ used in test $P_{cr\lambda}/P_p$	Fully Braced elastic 2nd mode critical load P_{crII}/P_p	Ave. theoretical λ_{cr} value for test set	Proposed λ_{cr} based on test results (from Table 6.3)
4	11	2031	0.99	0.382	1.634	2.669	6.742	5.5
	12	1993	1.04	0.367	1.866	2.542		
	13	2006	0.96	0.370	2.152	2.558		
	14	1986	0.97	0.363	2.341	2.499		
5	15	1511	0.75	0.256	1.477	1.572	6.728	7.0
	16	1495	1.02	0.250	1.524	1.524		
6	17	1561	0.84	0.235	1.266	1.266	6.722	11.0
	18	1587	0.94	0.236	1.263	1.263		
	19	1571	0.80	0.236	1.281	1.281		
	20	1553	0.91	0.232	1.242	1.242		

both first and second modes, were smaller than the theoretical elastic second mode critical loads. This observation supports the relationship between the second mode elastic and inelastic curves of Fig. 6.1: for beams of R^2 less than about 24, second mode inelastic buckling occurs, thereby precluding attainment of elastic second mode buckling. Divergence between the inelastic and elastic second mode curves becomes more pronounced as R^2 decreases. This trend is reflected in the P_{ult} and P_{crII} values in Table 8.1 where the discrepancy is greatest in Sets 1 and 4 ($R^2 \doteqdot 6.7$) and least in Sets 3 and 6 ($R^2 \doteqdot 18.7$).

In several cases in Table 8.1, $P_{cr\lambda}/P_p$ is equal to P_{crII}/P_p as the restraint stiffness λ employed in many of the tests was greater than the λ_{cr} value predicted by elastic buckling analysis.

With respect to the required stiffness of lateral restraints, there is an apparent tendency for proposed λ_{cr} values in the final column of Table 8.1 to exceed theoretical elastic λ_{cr} values by an amount which varies with increasing R^2 and also with increasing level of load application relative to the shear centre. However, considerably more experimental data than that presented in Table 8.1 would be required before the maximum proposed value of $\lambda_{cr}=11$ could safely be regarded as being the design criterion for all restraints to centrally loaded beams. As the observed tendency is for λ_{cr} to increase with R^2, it is conceivable that values of λ_{cr} well in excess of eleven might be required for initially imperfect, more slender beams than those considered in the present study.

Comparison of FINAS λ_{cr} predictions with those derived from experimental results and from elastic bifurcation theory is complicated by the inability of the FINAS analysis always to reveal the nature of the failure mode. As noted in the previous Chapter, this is frequently due to non-convergence of the numerical solution and the resulting termination of analysis before "structural collapse" of the mathematical model. This condition is indicated by the entry "indeterminate" in the penultimate column of Table 8.2 which shows the failure modes of beams predicted by FINAS. Comparison of the final columns of Tables 8.1 and 8.2 shows good agreement, although for Set 2 no upper bound estimate for λ_{cr} based on FINAS results is possible. In Set 1, the value of

Table 8.2: Failure Modes of Test Beams Predicted by FINAS

Test set	Test	FINAS analysis performed	λ used in analysis	Predicted failure mode	Suggested FINAS λ_{cr} for set
1	1	x	-	-	< 2
	2	√	2	plastic hinge	
	3	√	3	plastic hinge	
2	4	x	-	-	unknown
	5	x	-	-	
	6	√	4	indeterminate	
	7	√	5	indeterminate	
3	8	√	4	indeterminate	< 5
	9	x	-	-	
	10	√	5	second mode	
4	11	x	-	-	< 6
	12	x	-	-	
	13	√	5	indeterminate	
	14	√	6	plastic hinge	
5	15	√	6	indeterminate	< 8
	16	√	8	second mode	
6	17	x	-	-	< 12
	18	x	-	-	
	19	√	10	indeterminate	
	20	√	12	second mode	

$\lambda_{cr} \doteq 2.5$ proposed in Tables 6.3 and 8.1 violates the range indicated in Table 8.2; however, proposed λ_{cr} values for Sets 3 to 6 in Table 8.1 fall neatly within the ranges suggested in Table 8.2 .

The relationship between λ_{cr} values predicted by FINAS and those derived from the analyses of Chapter 2 is similar to that between the experimental and Chapter 2 results due to the previously noted similarity between FINAS and experimentally derived λ_{cr} values.

8.3 Comparison of Experimental and Finite Element Results of Chapter 6 with Previously Published Bracing Requirements and those Currently Specified in Codes of Practice

Examination of Figs. 2.19, 2.21 and 2.22 reveals that λ_{cr} values required for second mode elastic buckling of a beam under central point loading applied at either compression flange or shear centre level are greater than for beams of identical R^2 values under uniform moment. In this Section, attention is generally restricted to the case of central point loading, the condition employed in the experimental programme. However, Table 8.3, summarising the most important lateral restraint requirements proposed in the literature, necessarily includes several studies concerned with uniform moment loading: much of the previous work concerned with bracing requirements was based on the uniform moment condition.

Comparison of the experimental and finite element results of the present study (Tables 6.3 and 8.2) with the recommendations of Table 8.3 is limited to cases of compression flange restraint. Considering first the stiffness criteria, Flint's[59] λ_{cr}=10 for compression flange loading and restraint agrees well with the largest proposed λ_{cr} value of 11 in Table 6.3 . This proposed value is also considerably less onerous than Nethercot's[77] λ_{cr}=25 design requirement, although even Nethercot's stiffness criterion is easily satisfied by all practical bracing members, as the comparative designs considered later in this Chapter demonstrate.

With regard to bracing forces, in all cases of fully effective restraint in Table 6.3 (viz. Tests 3, 7, 9, 10, 14, 16, 20), measured bracing forces at attainment of experimental ultimate loads were consistently less than 0.01P_{cy}. In comparison, Zuk's[45] 0.02P_{cy} and Morris's[75,79] 0.04P_{cy} minima are more demanding whilst Winter's[46] 5% rule applies only to continuous restraints and Nethercot's[77] proposals, supporting the BS 449[33] 2½% rule, can prove more or less demanding, depending on the number of restraints and the efficiency of the primary member in bending.

Direct comparison between the various bracing strength criteria

Table 8.3: Summary of Lateral Restraint Requirements Proposed in the Literature

Investigator	Ref.	Year	Lateral Restraint Requirements	Remarks
Flint	59	1951	$\lambda_{cr}=10$ for compression flange loading & restraint $\lambda_{cr}=15$ for compression flange loading & shear centre restraint	(i) Values shown refer to C.P.L. (ii) Warping effects neglected (iii) Buckling solution hence no strength criterion for design
Zuk	45	1956	$P_{br} > 0.02P_{cy}$ for compression flange restraint $P_{br} > 0.024P_{cy}$ for shear centre restraint	(i) Uniform Moment Loading (ii) Bracing forces for $\frac{u_o}{L} = 0.001$ beam
Winter	46	1958	Continuous lateral restraint to provide approx. 5% of force in fully-yielded flange	(i) based on isolated compression flange model
Massey	47	1962	Inconclusive due to method of testing & Massey's interpretation of results	
Schmidt	62	1965	$\lambda_{cr} \simeq 9.5$ for shear centre loading & restraint	(i) also prescribes torsional restraint criteria for supports
Lay & Galambos	71	1966	Axial strength and stiffness requirements satisfying eqns.(1.9) to (1.11) Flexural stiffness requirements of eqns. to be disregarded[74]	(i) basis for AISC specification (ii) sample calculation given in Appendix VII(b)

Table 8.3: Summary of Lateral Restraint Requirements Proposed in the Literature (contd)

Investigator	Ref.	Year	Lateral Restraint Requirements	Remarks
Hartmann	12	1971	$\lambda_{cr} \simeq 11$ for inelastic beams under C.P.L. loaded and restrained at shear centre	(i) warping effects neglected (ii) rectangular section
Fukumoto & Kubo	76	1972	$P_{br} > 0.02 \times$ maximum compression flange force	(i) uniform moment loading
Nethercot & Rockey	63	1972	$\lambda_{cr} \doteqdot 10$ for $R^2=32$ beam with reduced λ_{cr} values for greater R^2	(i) uniform moment loading (ii) shear centre restraint
Mutton & Trahair	64	1973	λ_{cr} curves shown in Fig. 8.6	(i) only C.P.L. values shown in Fig. 8.6
Morris & Randall	79	1979	Cross-sectional area of brace $\geqslant 0.04A_f$	(i) acknowledges that maximum allowable slenderness ratio requirements usually govern
Morris	75	1981	Cross-sectional area of brace $\geqslant 0.04A_f$ and maximum slenderness ratio of brace = 100	
Nethercot	77	1984	2½% strength rule for braces as in BS 449 and $\lambda_{cr} \simeq 25$	

proposed in the literature and in contemporary design codes is hindered by the expression of bracing forces and required brace strengths in terms of quantities which vary from one text to the next. For example, the maximum compression flange force has traditionally been used in the United Kingdom as the basis for bracing design; however, the magnitudes of this force permitted by the three contemporary British steelwork codes[33,55,56] are different. Recourse to a series of comparative designs is necessary for a quantitative assessment of the various restraint requirements. Such a series of designs was performed, the results described later in this Section.

Of the numerous results of previous investigations presented graphically in Chapter 1, only Fig. 1.18 can be used as a basis for comparison with experimental and finite element results of the present study: the required combination of central point loading, variable R, translational restraint and variable load/restraint geometry is found only in that Figure. Fig. 8.6 is derived from Fig. 1.18 and additionally shows the proposed λ_{cr} values based on the experimental results of Table 6.3 . Tentative curves have been fitted through the experimental data and it is clear that the inelastic relationships between λ_{cr} and R differ considerably from the elastic curves originally presented by Mutton and Trahair[64]. Continuing the trend observed in Section 8.2, inelastic λ_{cr} values proposed in the present study generally exceed those predicted by elastic buckling theory.

Although the range of R values covered by the proposed inelastic curves is small relative to the domain of R shown in Fig. 8.6, that portion of the Figure concerned with R values in excess of about ten is more of academic interest than of practical value. Table 8.4 shows R values for a typical range of span-to-depth ratios for four British rolled sections: the largest R value, of just over ten, corresponds to a span-to-depth ratio of thirty. Consequently, the greater proportion of beams used in practice have R values in the range 2 to 8.

Much of the technical material on which contemporary British steel codes are based is to be found in the literature[77,109]. In published work concerned with the proposed methods for the design of steel beams in BS 5400[55] and BS 5950[56], the modified beam slenderness parameters $\sqrt{M_p/M_E}$ and λ_{LT} are introduced.

Table 8.4: R Values for Typical Span: Depth Ratios

Section	R for span: depth ratio of		
	10	20	30
533 x 210 x 101 UB	2.645	5.291	7.936
305 x 102 x 33 UB	3.276	6.551	9.827
203 x 133 x 25 UB	1.979	3.958	5.938
127 x 76 x 13.4 RSJ	3.370	6.741	10.111

Graphical presentation of the experimental results of the present study in terms of the $\sqrt{M_p/M_E}$ parameter was attempted in Fig. 8.7, M_E being taken as the moment corresponding to the critical load $P_{cr\lambda}$ described in Section 8.2 . Little is revealed by this form of presentation due to the presence of only partial restraint in the majority of tests; no discernible trends in the experimental data are present. Fig. 8.8 shows the results of only those tests in which fully effective restraint was achieved. Like Fig. 8.7, Fig. 8.8 is inconclusive although the tendency for the experimental results of Sets 4 to 6 (compression flange loading) to fall below those of Sets 1 to 3 (shear centre loading) is noticeable.

To enable comparison of the bracing criteria specified in contemporary British steelwork codes[33,55,56], a series of comparative designs was undertaken in which a simply-supported beam under central point loading was braced at midspan by a single lateral restraint. As the selection of a bracing section was dependent on the cross-sectional dimensions of the primary, restrained element, in each design rolled sections for both the beam and its restraint were chosen in accordance with the provisions of the appropriate code. The design calculations are contained in Appendix VII(a) and the results summarised in Table 8.5 .

Several general points arise from the designs. Firstly, beam sections have been chosen for maximum efficiency in bending although the selected sections also satisfy the relevant shear requirements. The efficiencies of the beams in bending are shown in Table 8.5 . R^2 values for these beams varied from 7.89 (BS 5950 design) to 10.0 (BS 449 design), indicating that sections of relatively greater warping rigidity were required to satisfy the provisions of the more recent, limit state codes. All bracing members were designed as single angle struts.

In complying with the requirements of BS 5950 for beams in bending, two checks were required at the ultimate limit state: the first for strength and the other for the lateral-torsional stability of the section. The stability check was performed on the basis of an equivalent applied uniform bending moment, derived by means of specified uniform moment factors based on those of Nethercot et al[25-27].

Table 8.5: Summary of Comparative Bracing Designs in Appendix VII(a)

	Design Complying with Requirements of		
	BS 449 Part 2: 1969	BS 5400 Part 3: 1982	BS 5950 Part 1: 1985
design philosophy	permissible stress	limit state	limit state
selected beam section for M = 90kNm	305 x 102 x 33 UB	305 x 127 x 37 UB	305 x 102 x 28 UB
efficiency of beam in flexure only	$\frac{90}{95.45} = 0.94$	$\frac{135}{145.4} = 0.93$	$\frac{144}{144.6} = 1.0$
R^2 for selected beam section	10.0	8.08	7.89
required bracing element section	25 x 25 x 4 L	30 x 30 x 4 L	25 x 25 x 4 L
efficiency of brace in axial compression	0.98	0.81	0.32
ratio of actual to permissible slenderness	0.98	no permiss. specified	0.98
non-dimensional stiffness (λ) of resulting bracing member	54.95	38.61	67.55

However, restraint design was based on the maximum factored flange force consistent with the actual factored bending moment. This is clearly correct as the actual bending moment gives the higher flange force.

In BS 5400, the two independent checks were not required. The slenderness of the primary element determined the limiting ultimate stress which in turn determined the capacity of the member in bending. A similar approach was adopted in the design of the angle strut where maximum allowable slenderness values were not given. Instead, the actual slenderness of the member determined the limiting compressive stress, which, in BS 5400, drops rapidly with increasing slenderness, falling to less than 10% of the yield stress for slenderness values in excess of 220. Consequently BS 5400 imposes a slenderness limit indirectly by means of very low values of limiting compressive stress.

In the calculations shown in Appendix VII(a), the notation employed is that of the appropriate design document. Hence the parameter λ is used both for the slenderness parameters in BS 5400 and BS 5950 and in its original sense in the present study as the non-dimensional translational restraint stiffness parameter (eqn. (1.2)). This duplicate use of a single parameter is not ideal but should not cause confusion given the context of use.

A major criticism of the current British Steelwork codes[33,55,56] in relation to lateral restraint is that none gives quantitative stiffness criteria for the design of beam bracing. Restraint stiffness is mentioned neither in BS 449 nor in BS 5400. BS 5950 (Part 1, Clause 4.3.2) states:

> "Lateral restraints have to be of adequate stiffness and strength. Restraints may be deemed to provide adequate strength if they are capable of resisting a lateral force of not less than 1% of the maximum factored force in the compression flange."

Ironically, no stiffness criterion is given.

In designing the lateral bracing elements in Appendix VII(a), sections were selected for maximum efficiency in axial compression under the stipulated minimum bracing strengths. In the BS 449 design, both the 2½% strength requirement and the maximum permissible slenderness ratio of 180 for struts were just satisfied by the 25 x 4mm equal angle section. The 2½% rule applied to the factored compression flange force in the BS 5400 design demanded the use of the slightly larger 30 x 4mm equal angle section. Although the efficiency of this section in axial compression was only 81%, no smaller equal angle section satisfying the strength criterion was available. As previously noted, there was no slenderness requirement to be met by the bracing member under the provisions of BS 5400.

Not only did the BS 5950 limit state requirements permit the use of the lightest of the three beam sections; the 1% bracing force requirement was also easily satisfied by the 25 x 4mm equal angle which had previously met the elastic design requirements of BS 449. The selection of a lighter, more efficient bracing section was not permitted by the slenderness limit of 180 for struts imposed by BS 5950.

In all three cases, only very light sections were needed to satisfy the lateral restraint requirements. The non-dimensional restraint stiffness λ for each of the bracing members selected is shown in Table 8.5 . The minimum λ value of 38.6 obtained from the comparative designs is considerably greater than even Nethercot's[77] apparently conservative requirement of $\lambda=25$ in Table 8.3. In relation to the maximum proposed value of $\lambda_{cr}=11$ resulting from the work of the present study, current code requirements are more onerous, although it is apparent that contemporary codes rely on lateral bracing strength requirements and in some cases maximum slenderness ratios to achieve both adequate strength and axial stiffness of restraints.

Although the apparent conservatism of current British steel design codes has been demonstrated for one particular example of a simply-supported, short span beam braced and loaded at midspan, the concession in both BS 449 and BS 5950 that the total bracing force can be divided equally between the points of restraint initially arouses both suspicion and anxiety. However, as was the case in the BS 5950 design previously described, it is likely that the maximum slenderness values permitted in these codes would serve to maintain adequate axial stiffness in each of the bracing members. In such a situation, the result would be an array of bracing members, each of adequate stiffness but of very low efficiency in axial compression. The same dilemma does not occur in BS 5400 where the requirement is for bracing capable of withstanding the equivalent of a full "2½%" force at each point of restraint.

In addition to the comparative designs presented in Appendix VII(a), a short calculation based on the inelastic bracing requirements of Lay and Galambos[71] is presented in Appendix VII(b). In this calculation, the flexural stiffness requirements of Ref. 71 (eqns. (1.12) and (1.13)) were not applied, in accordance with the recommendations of Salmon and Johnson[74]. As illustrated in Appendix VII(b), knowledge of the strain hardening properties of the chosen grade of structural steel in addition to its elastic properties and yield stress is required for application of the criteria of Ref. 71.

The universal beam section selected in the BS 449 design in Appendix VII(a) was assumed as the starting point for the assessment of the axial strength and stiffness requirements of eqns. (1.9) to (1.11). Neither the cross-sectional area nor stiffness criteria were difficult to meet in practice. Indeed, consideration of such factors as permissible slenderness, minimum available sizes of rolled sections and the minimum size of section required to accommodate bolted or welded end connections would have resulted in sections of proportions significantly larger than those demanded by eqns. (1.9) to (1.11). The cross-sectional area of brace satisfying eqn. (1.9) was equivalent to approximately 3.5% of the area of the compression flange of the braced member: this agrees well with the 4% value advocated by Morris and Randall[79].

In conclusion, based on the results of the present study it can be stated that the contemporary British steel design codes BS 449, BS 5400 and BS 5950 are likely to provide both adequate strength and stiffness of lateral restraint by virtue of their minimum bracing strength and maximum slenderness criteria. The extension of this hypothesis to conditions of other than central point loading and compression flange restraint would require to be justified by further study; however, it is likely that the central point loading condition would prove as demanding as any other for the purposes of restraint design as this produces a greater instantaneous compression flange force at midspan than is permitted under uniform moment loading due to considerations of lateral-torsional stability.

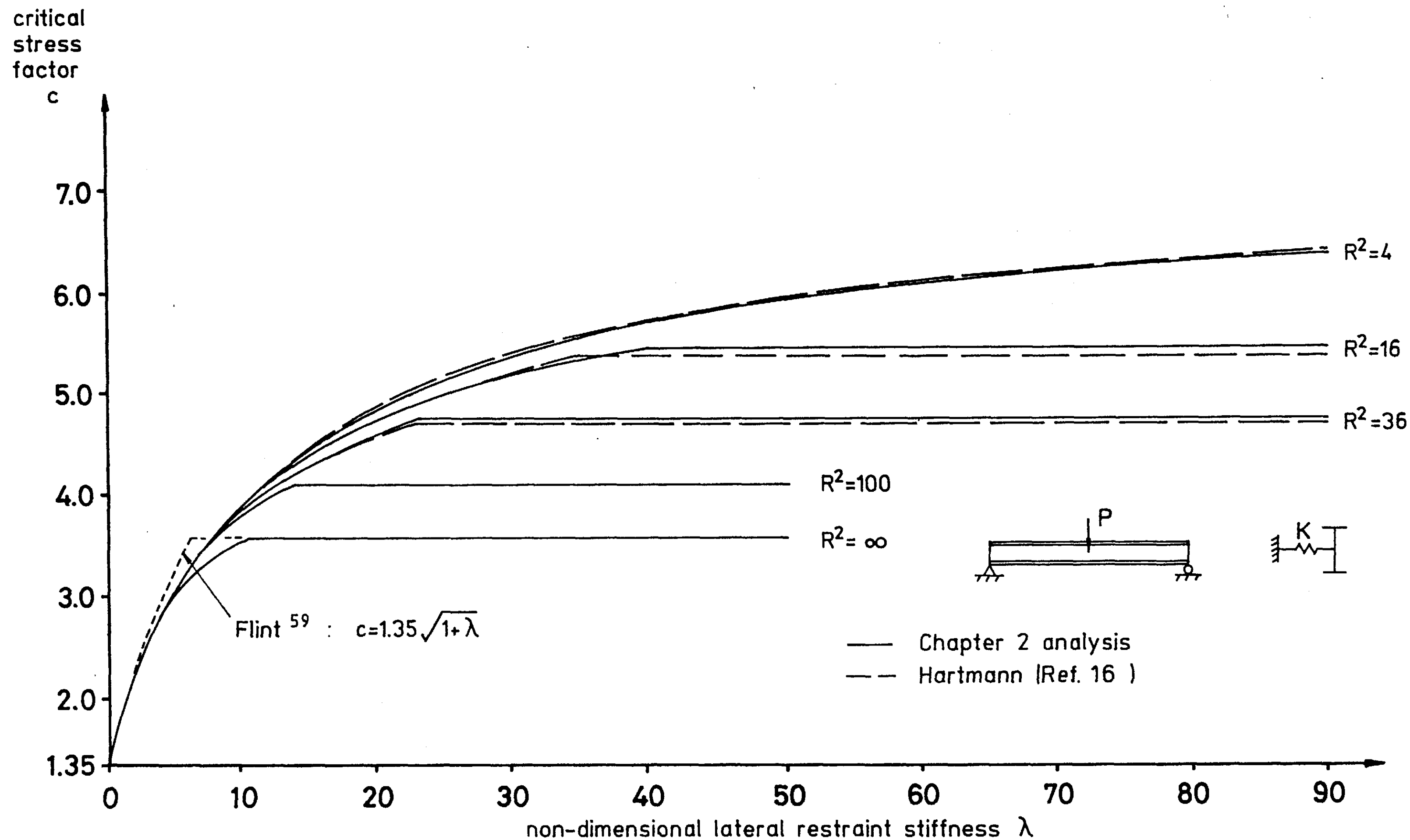

Fig. 8.1 : Comparison of results of AUTOBRAC with those of Hartmann[16] for beams under central point loading, restrained at shear centre level at midspan.

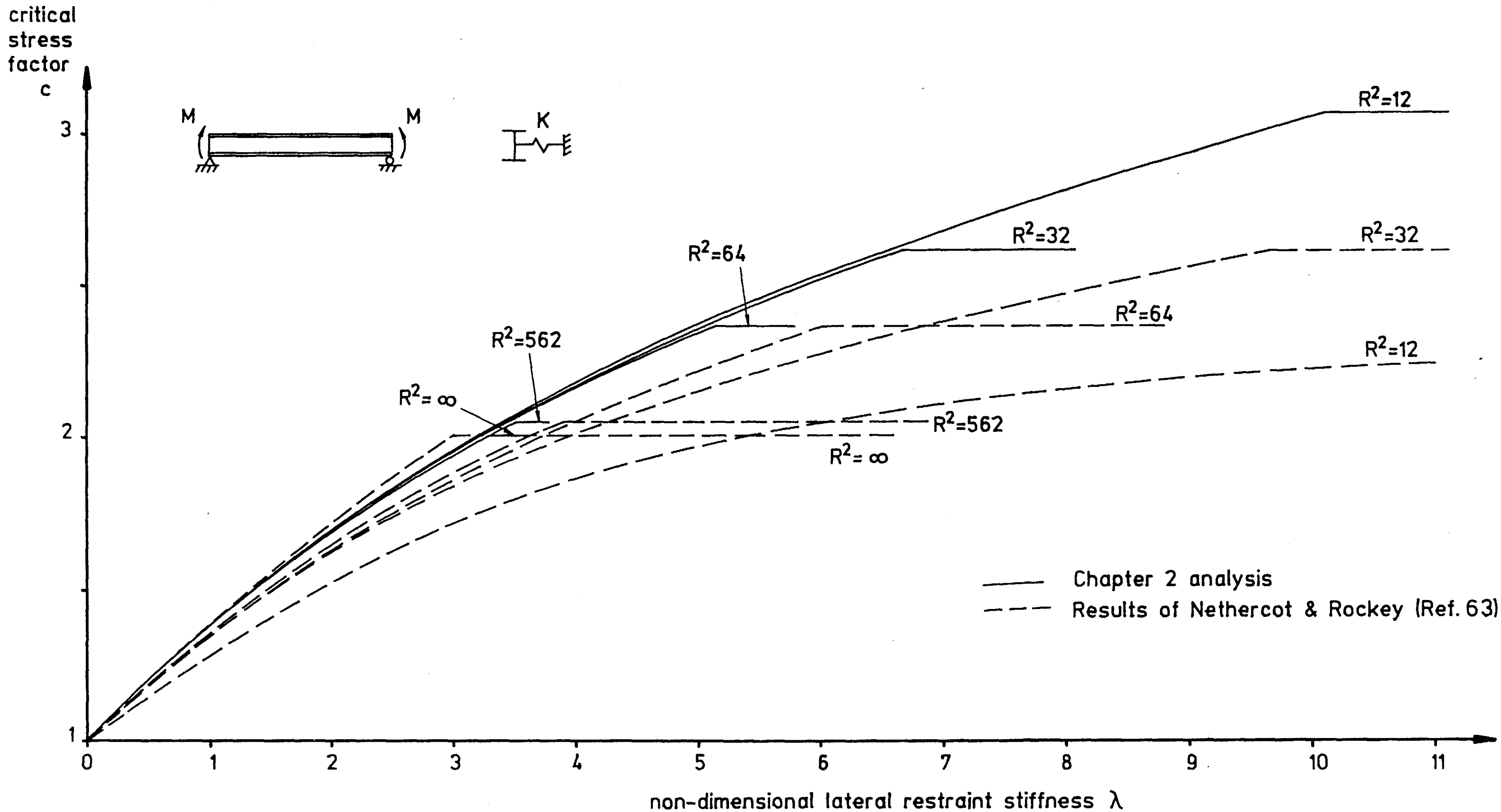

Fig. 8.2 : Comparison of Chapter 2 results with those of Nethercot & Rockey (Ref. 63) for the case of a beam under uniform moment, laterally restrained at midspan.

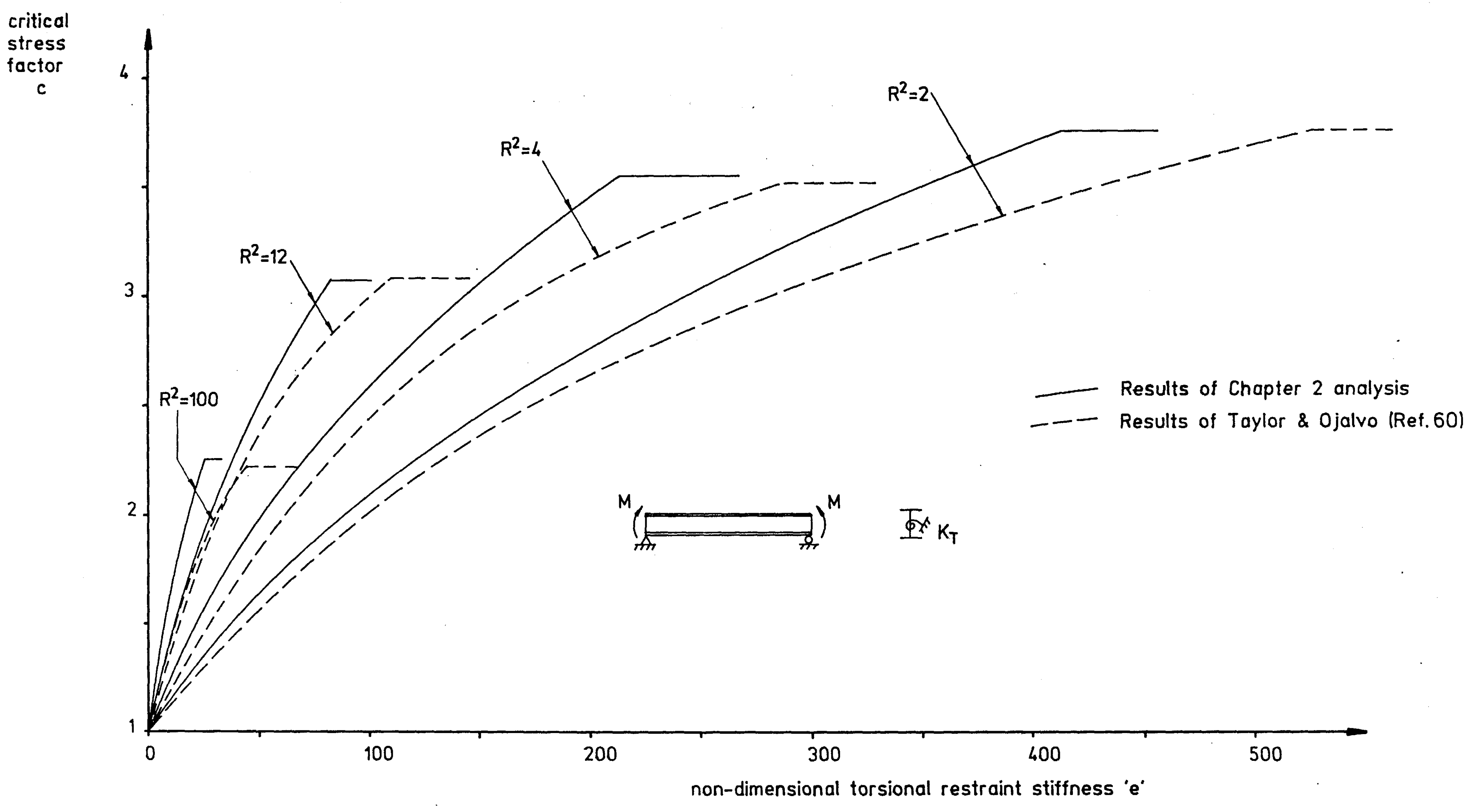

Fig. 8.3 : Comparison of Chapter 2 results with those of Taylor & Ojalvo [60] for the case of a beam under uniform moment, torsionally restrained at midspan.

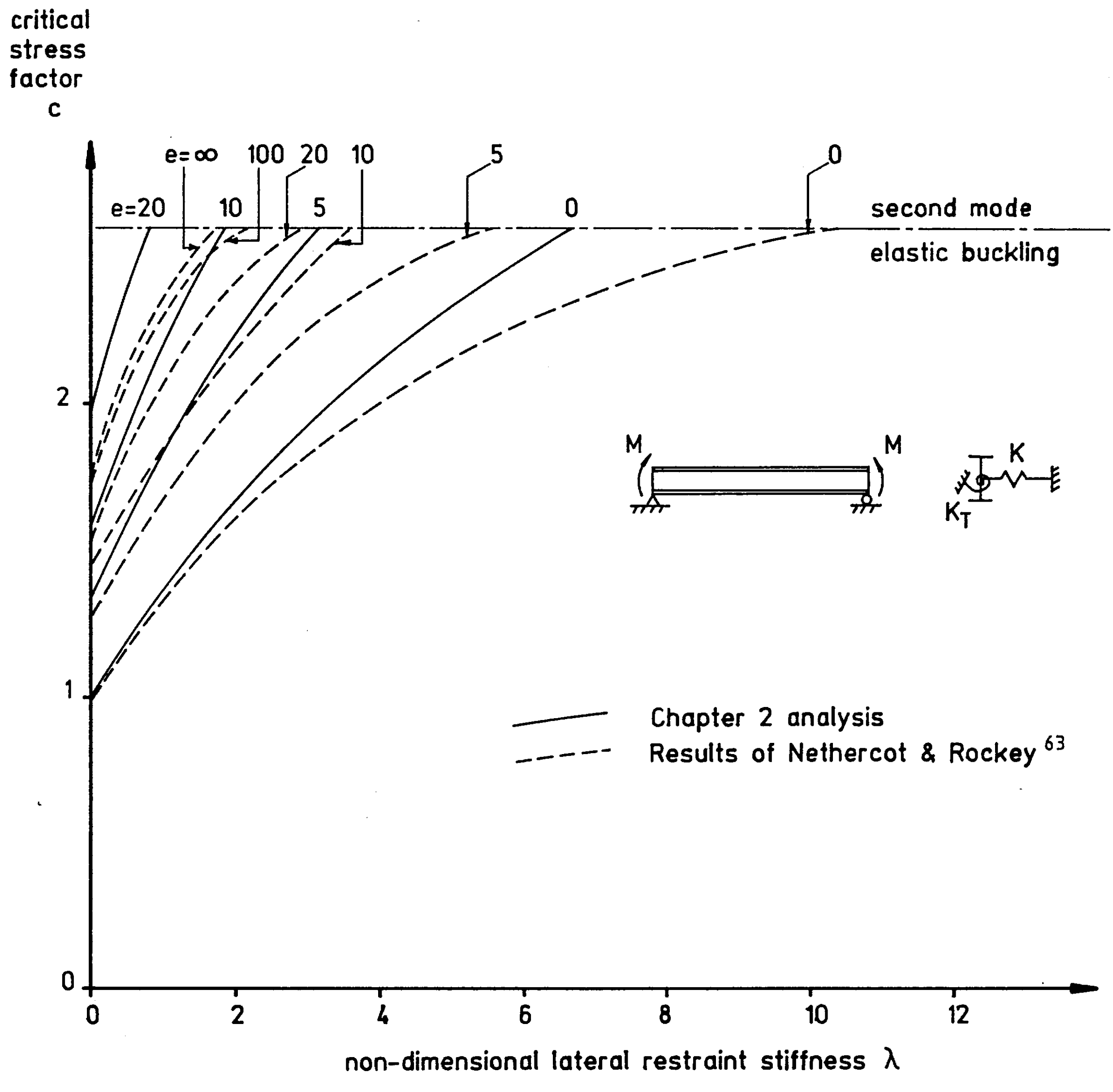

Fig. 8.4 : Comparison of Chapter 2 results with those of Nethercot & Rockey[63] for a beam of R^2=32 subjected to uniform moment loading and with combined midspan restraint.

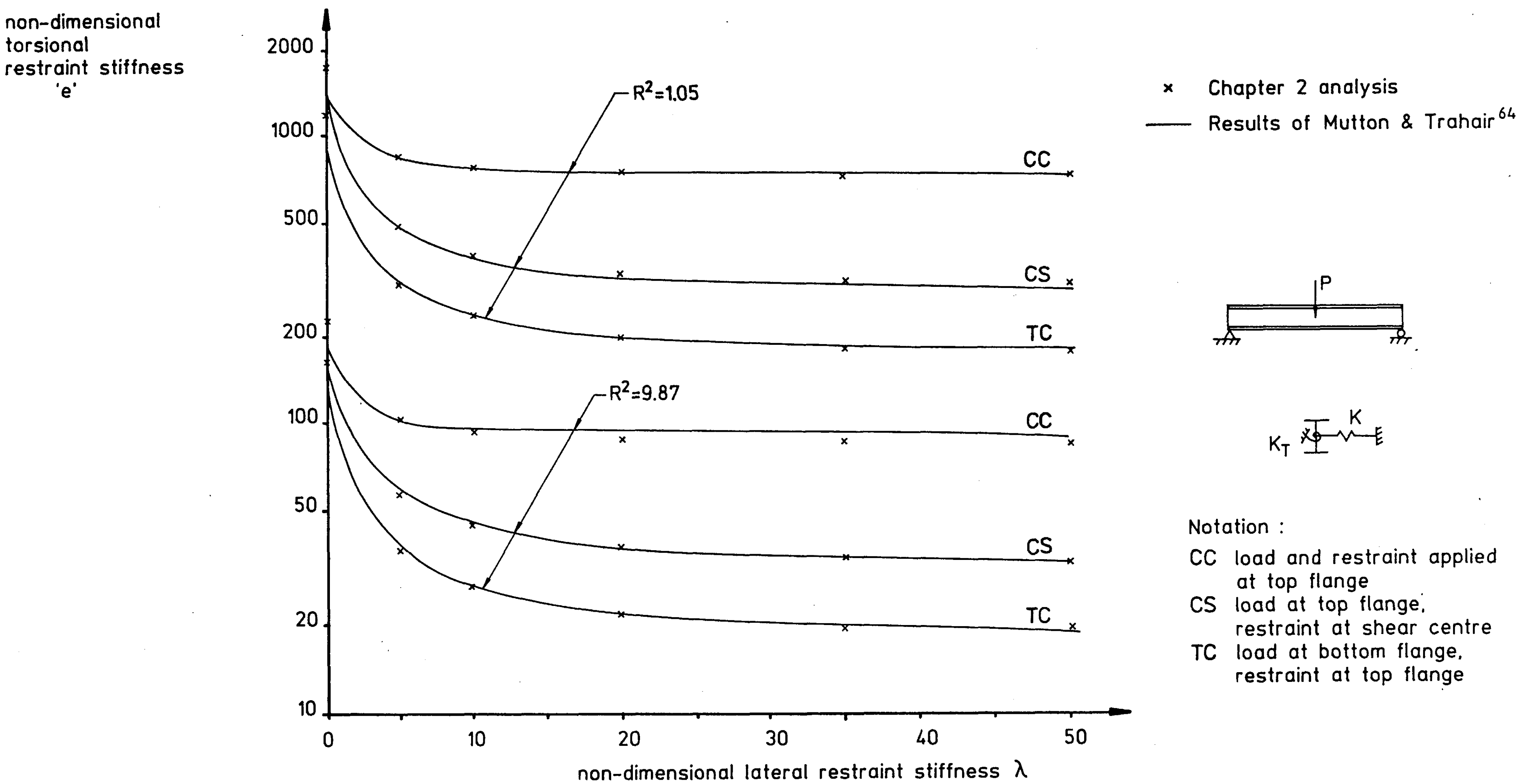

Fig. 8.5 : Comparison of Chapter 2 results with those of Mutton & Trahair[64] for combined midspan restraint of a beam under central point loading.

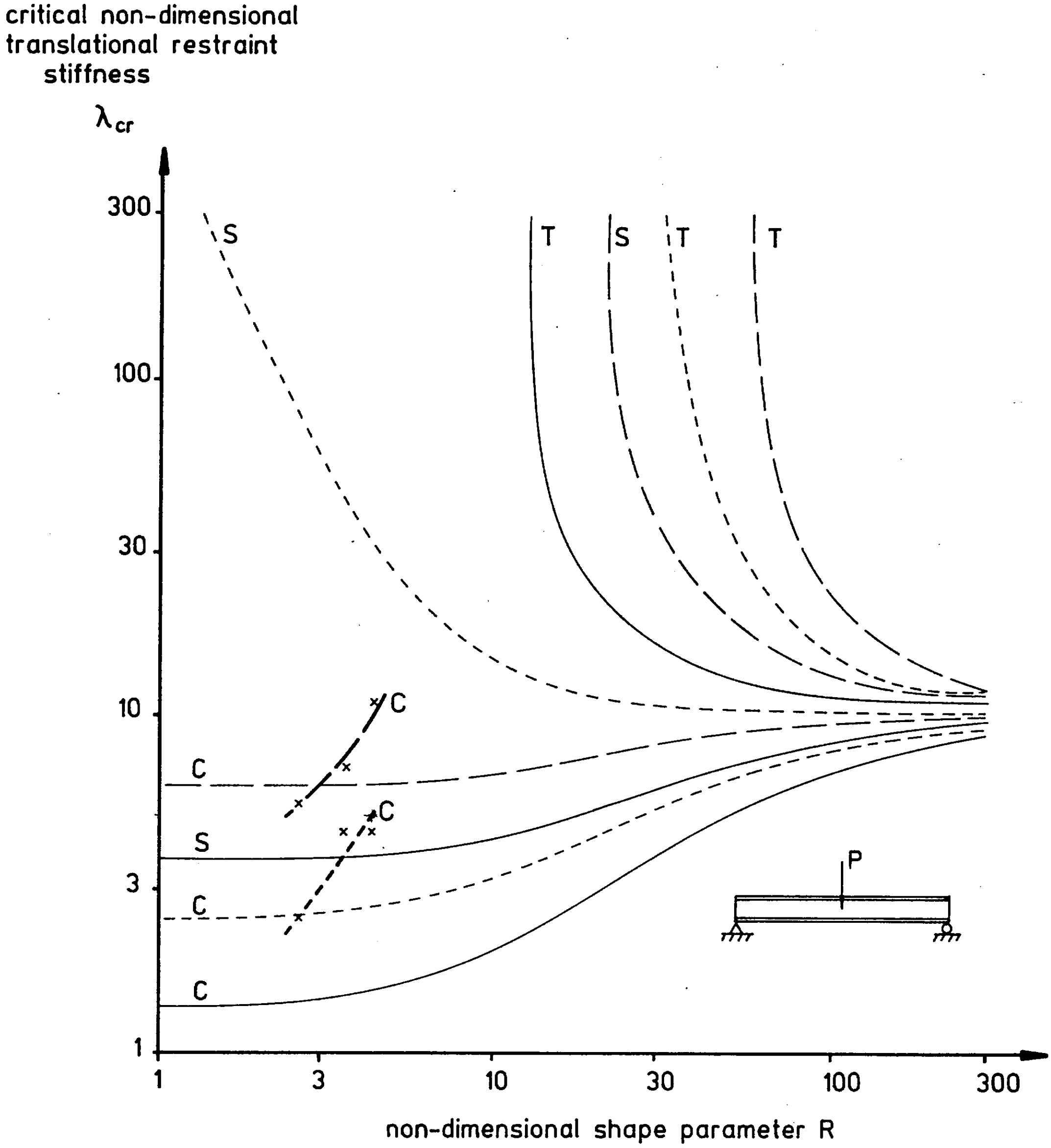

Loading :

- tension flange
- shear centre
- compression flange

Lateral restraint :

T tension flange
S shear centre
C compression flange

- experimental results for compression flange loading
- experimental results for shear centre loading

Fig. 8.6 : Comparison of experimental results with the elastic curves proposed by Mutton & Trahair [64]

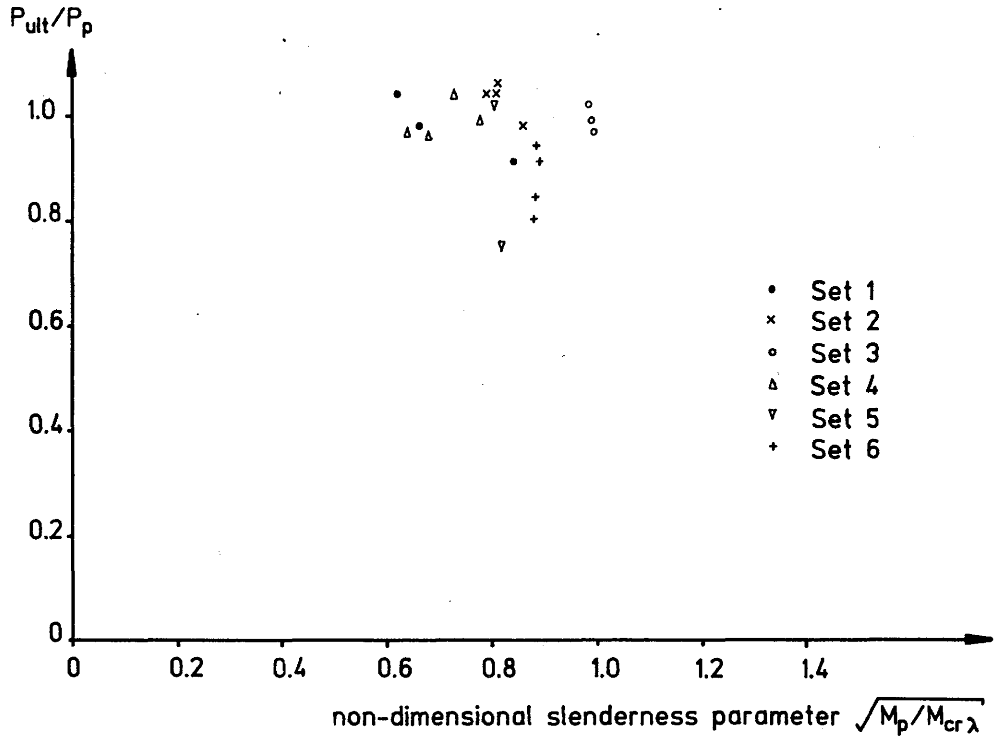

Fig. 8.7 : Presentation of experimental results in terms of the modified slenderness parameter $\sqrt{M_p/M_{cr\lambda}}$

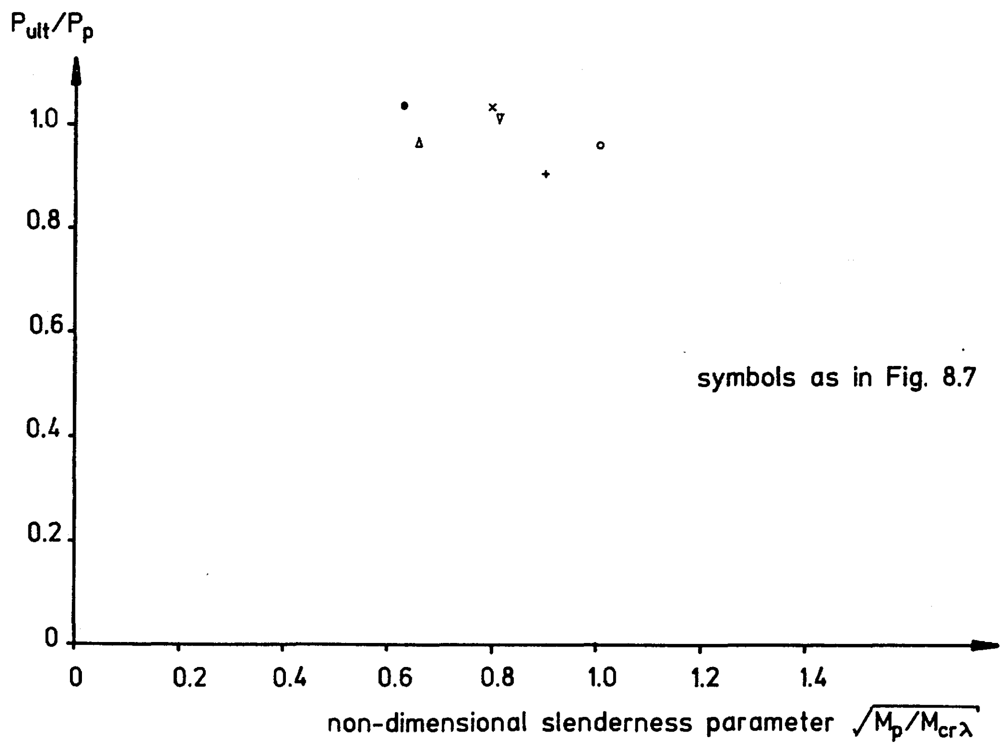

Fig. 8.8 : Experimental results for fully restrained beams in terms of the modified slenderness parameter $\sqrt{M_p/M_{cr\lambda}}$

CHAPTER 9

CONCLUSIONS AND RECOMMENDATIONS FOR FURTHER STUDY

CHAPTER 9

CONCLUSIONS AND RECOMMENDATIONS FOR FURTHER STUDY

9.1 Conclusions

A review of published literature revealed little information concerned with the bracing requirements of steel beams of intermediate slenderness which fail by inelastic lateral-torsional instability, though much has been written about the inelastic strength of such beams under assumed conditions of intermediate and end restraint. In these latter studies the importance of initial geometrical and material imperfections in relation to inelastic beam behaviour was demonstrated, emphasising the need for a theoretical model capable of predicting true collapse behaviour rather than the mathematical phenomenon of buckling.

Consequently, non-linear finite element analyses were performed in an attempt to verify the results of a series of twenty tests on model steel beams with translational restraint to the compression flange at midspan. Throughout the study only the effects of primary or overall instability of the restrained member have been considered. In addition, it has been assumed that adequate lateral and torsional restraint is provided at end supports.

Small scale, steel model I-beams were employed in the experimental investigations. It was considered that the disadvantages of scale effects and the problems associated with the fabrication of model beams were more than offset by the benefits of substantially reduced cost and ease of testing. The need to discard yielded beams after testing meant that a corresponding programme of twenty full-size tests on universal beam sections could not have been contemplated for financial reasons.

The successfulness of the model test programme was highly dependent on the accurate setting-up of tests, careful measurement of deflections, strains and applied loads and the application of increments of enforced vertical displacement of a size sympathetic to the apparent residual stiffness of the restrained beam. The use of displacement rather than load control in tests permitted collapse loads to be clearly ascertained and post-collapse behaviour to be followed with ease.

A novel, though simple method for the provision of lateral restraint to beams was developed: this was necessitated by the very small lateral flexural stiffness of test beams and the frequent need to provide lateral restraint of similar magnitude. The bracing fork device successfully employed in all tests utilised the low flexural stiffness afforded by the cantilever action of a small diameter steel rod anchored in a rigid transverse plate. Constant stiffness of lateral restraint was maintained by a procedure allowing the bracing fork to be lowered vertically, thus minimising relative vertical displacement between the bracing fork and beam. Forces developed in the midspan bracing as a result of lateral motion of the primary member were deduced from recorded strains in strain gauges attached to the prongs of the bracing fork.

FINAS non-linear finite element solutions used to provide theoretical verification of experimental results were largely successful although earlier NASTRAN analyses employing first shell and then beam elements had proved unsatisfactory due to the occurrence of numerical instability in all BEAM element analyses and the excessive computing time and storage demands of QUAD4 shell element analyses. However, neither programme proved capable of predicting the behaviour of an initially imperfect beam under uniform moment loading. Although numerical instability of the solution had been regarded as being indicative of physical collapse in an earlier study, this was not adopted as the collapse criterion in the present study.

As the FINAS analysis was sensitive to the magnitude and distribution of initial imperfections, accurate measurement and numerical modelling of the imperfections present in test beams was required. In several cases the coupled non-linear facility in FINAS proved capable of predicting the post-collapse behaviour of test beams although it was necessary to counter the tendency towards numerical instability of solutions (due to vanishing structural stiffness) by the specification of very small increments of enforced displacement. In general, however, agreement between experimental and FINAS results was satisfactory.

The primary aim of the study, namely the provision of strength and stiffness criteria for inelastic beam bracing, was fulfilled for the case of simply-supported beams under central point loading and with midspan, compression flange restraint. The study was undertaken because it had been anticipated that bracing requirements would be more onerous for inelastic than for more slender, elastic beams.

As expected, both finite element and experimental results revealed that bracing criteria were highly dependent on the magnitude and distribution of initial imperfections and the relative positions of load and restraint application on the cross-section. Greater restraint stiffnesses were required for compression flange than for shear centre loading and for beams of intermediate than of low slenderness. However, on the assumption that the bracing requirements of initially imperfect, slender elastic beams are even approximately predicted by classical buckling analysis, it would appear that bracing stiffness criteria expressed in terms of the parameter λ are most critical for intermediate than for either very low or very high slenderness values.

Comparison of bracing requirements derived from experimental and finite element results with those obtained from elastic bifurcation analyses revealed that bracing proportioned to be adequate for fully effective restraint on the basis of an elastic lateral-torsional buckling analysis was generally insufficient for the prevention of inelastic buckling.

For compression flange loading λ=11 was suggested to provide adequate stiffness of restraint whilst a reduced value of λ=5 was considered adequate for shear centre loading. With regard to strength requirements, in no case of fully effective restraint did the bracing force corresponding to the collapse condition exceed 1% of the ultimate compression flange force. However, substantially larger bracing forces were developed during post-collapse unloading of the beam.

A series of comparative designs complying with the three current British steelwork codes (BS 449, BS 5950 and BS 5400) demonstrated that, in the cases examined, present code requirements provide both adequate stiffness and strength of midspan restraints. In all cases, bracing members were designed as struts and compliance with both strength and limiting slenderness criteria ensured adequate axial stiffness.

9.2 Recommendations for Future Research

It is possible to identify several areas of interest within the present study worthy of further investigation. Although these topics are described below under the apparently rigidly defined headings of theory and experimentation, the present study has clearly demonstrated the need for a coordinated programme of experimental and theoretical work. The highly non-linear behaviour characteristic of inelastic lateral-torsional collapse makes simple prediction of structural behaviour impossible. Satisfactory correlation between experimental and theoretical results therefore assumes greater importance, as the significance of two sets of results in agreement far outweighs the total significance of the two sets in isolation. In addition, although only model tests were employed in the study, it is considered unwise to accept model test results alone as a basis for or validation of design criteria.

The need for extension of the present work to conditions of loading other than central point loading is immediately obvious. Although the case of uniform moment loading is uncommon in practice, it has become almost a standard feature of lateral-torsional buckling investigations and should therefore receive attention in future extensions of this work. The appropriateness of such an investigation has recently (1985) been heightened by the publication of BS 5950 in which equivalent uniform moments form the basis of design. Other loading conditions are clearly also possible.

In the present study attention has been restricted to purely translational restraint at compression flange level. It is recommended that this be carried forward to a subsequent study as compression flange restraint is provided in most situations in practice. Moreover, although substantial benefits accrue from the provision of torsional in addition to translational restraint, moment connections between beams and their restraints cannot generally be relied upon to translate the flexural stiffness of bracing members into torsional restraints on the primary member.

As all beams examined were simply-supported on a single span, the possibility exists for an investigation of the influence on bracing requirements of the restraint afforded by continuity at supports in a continuous beam.

Powerful though the numerical techniques adopted in FINAS have been shown to be, a need exists for yet more advanced numerical algorithms capable of dealing with the non-positive definite matrices associated with the collapse analysis of structural systems. Until these become available, the finite element analysis of inelastic collapse behaviour must be supported by experimental evidence. The development and testing of such algorithms, and their subsequent calibration in relation to the results of an experimental investigation is considered to be beyond the scope of a short-term investigation. Nevertheless, the development of such programmes rather than the adoption of commercially available programmes is to be encouraged as the inability to access source programmes in the latter case proves frustrating and generally unsatisfactory.

REFERENCES

The following abbreviations are used throughout:

J.Str.Div.	Journal of the Structural Division, ASCE
J.Eng.Mech.Div.	Journal of the Engineering Mechanics Division, ASCE
Str.Engr.	The Structural Engineer
Proc.ICE	Proceedings of the Institution of Civil Engineers
BSI	British Standards Institution

1. Horne, M.R. and Merchant, W.: "The stability of frames", 1st edition, Pergamon, Oxford, 1965.

2. Timoshenko, S.P.: "Theory of bending, torsion and buckling of thin-walled members of open cross-section", Journal of the Franklin Institute, Vol 239, Nos. 3 - 5, March - May 1945.

3. Trahair, N.S.: "Elastic stability of continuous beams", J.Str.Div., ASCE, Vol 95, No. ST6, June 1969, pp 1295 - 1312.

4. Dux, P.F. and Kitipornchai, S.: "Inelastic beam buckling experiments", University of Queensland, Dept. of Civil Engineering Research Report Series, Research Report No. CE24, May 1981.

5. Kitipornchai, S. and Trahair, N.S.: "Inelastic buckling of simply-supported steel I-beams", J.Str.Div., ASCE, Vol 101, No. ST7, July 1975, pp 1333 - 1347.

6. Hartmann, A.J.: "Experimental study of flexural-torsional buckling", J.Str.Div., ASCE, Vol 96, No. ST7, July 1970, pp 1481 - 1493.

7. Sawyer, H.A.: "Post-elastic behaviour of wide-flange steel beams", J.Str.Div., ASCE, Vol 87, No. ST8, December 1961, pp 43 - 71.

8. Timoshenko, S.P. and Gere, J.M.: "Theory of elastic stability", 2nd edition, McGraw-Hill, Tokyo, 1961.

9. Allen, H.G. and Bulson, P.S.: "Background to buckling", McGraw-Hill, Maidenhead, 1980.

10. Chen, W.F. and Atsuta, T.: "Theory of beam-columns": Vol 1. "In-plane behaviour and design" (1976) and Vol 2. "Space behaviour and design" (1977), McGraw-Hill, New York.

11. Massey, P.C.: "The torsional rigidity of steel I-beams", Civil Engineering and Public Works Review, Vol 58, March 1963, pp 367 - 371 and April 1963, pp 488 - 492.

12. Hartmann, A.J.: "Inelastic flexural-torsional buckling", J.Eng.Mech.Div., ASCE, Vol 97, No. EM4, August 1971, pp 1103-1119.

13. Galambos, T.V.: "Inelastic lateral buckling of beams", J.Str.Div., ASCE, Vol 89, No. ST5, October 1963, pp 217 - 242.

14. Trahair, N.S. and Kitipornchai, S.: "Buckling of inelastic I-beams under uniform moment", J.Str.Div., ASCE, Vol 98, No. ST11, November 1972, pp 2551 - 2566.

15. Kitipornchai, S. and Trahair, N.S.: "Buckling of inelastic I-beams under moment gradient", J.Str.Div., ASCE, Vol 101, No. ST5, May 1975, pp 991 - 1004.

16. Hartmann, A.J.: "Elastic lateral buckling of continuous beams", J.Str.Div., ASCE, Vol 93, No. ST4, August 1967, pp 11 - 26.

17. Lay, M.G. and Galambos, T.V.: "Inelastic beams under moment gradient", J.Str.Div., ASCE, Vol 93, No. ST1, February 1967, pp 381 - 399.

18. Massey, P.C. and Pitman, F.S.: "Inelastic lateral stability under a moment gradient", J.Eng.Mech.Div., ASCE, Vol 92, No. EM2, April 1966, pp 101 - 111.

19. Richter, N.J.: "Application of the finite integral method to lateral buckling of beams", M.Eng.Sc. Thesis, University of Queensland, Dept. of Civil Engineering, 1979.

20. Vacharajittiphan, P. and Trahair, N.S.: "Analysis of lateral buckling in plane frames", J.Str.Div., ASCE, Vol 101, No. ST7, July 1975, pp 1497 - 1516.

21. Powell, G. and Klingner, R.: "Elastic lateral buckling of steel beams",J.Str.Div., ASCE, Vol 96, No. ST9, September 1970, pp 1919 - 1932.

22. Nethercot, D.A. and Rockey, K.C.: "Finite element solutions for the buckling of columns and beams", International Journal of Mechanical Sciences, Vol 13, 1971, pp 945 - 949.

23. Barsoum, R.S. and Gallagher, R.H.: "Finite element analysis of torsional and torsional-flexural stability problems", International Journal for Numerical Methods in Engineering, Vol 2, 1970, pp 335 - 352.

24. Nethercot, D.A. and Trahair, N.S.: "Inelastic lateral buckling of determinate beams", J.Str.Div., ASCE, Vol 102, No. ST4, April 1976, pp 701 - 717.

25. Nethercot, D.A. and Trahair, N.S.: "Lateral buckling approximations for elastic beams", Str.Engr., Vol 54, No. 6, June 1976, pp 197 - 204.

26. Nethercot, D.A. and Rockey, K.C.: "Lateral buckling of beams with mixed end conditions", Str.Engr., Vol 51, No. 4, April 1973, pp 133 - 138.

27. Nethercot, D.A. and Rockey, K.C.: "A unified approach to the elastic lateral buckling of beams", Str.Engr., Vol 49, No. 7, July 1971, pp 321 - 330.

28. Southwell, R.V.: "On the analysis of experimental observations in problems of elastic stability", Proceedings of the Royal

Society, Series A, Vol 135, London, 1932, pp 601 - 616.

29. Massey, P.C.: "Southwell plot applied to lateral instability of beams", The Engineer, Vol 218, August 1964, p 320.

30. Trahair, N.S.: "Deformations of geometrically imperfect beams", J.Str.Div., ASCE, Vol 95, No. ST7, July 1969, pp 1475 - 1496.

31. Meck, H.R.: "Experimental evaluation of lateral buckling loads", J.Eng.Mech.Div., ASCE, Vol 103, No. EM2, April 1977, pp 331 - 337.

32. Attard, M.M.: "Determining experimental lateral buckling loads by extrapolation techniques", Uniciv Report No. R-202, University of New South Wales, School of Civil Engineering, March 1982.

33. BS 449: "Specification for the use of structural steel in building", BSI, London, 1969.

34. AS 1250 - 1975: "S.A.A. Steel structures code", Standards Association of Australia, Sydney, 1975.

35. Kerensky, O.A., Flint, A.R. and Brown, W.C.: "The basis for design of beams and plate girders in the revised British Standard 153", Proc.ICE, Vol 5, August 1956, pp 396 - 461.

36. BS 153: "Specification for steel girder bridges. Part 3B: Stresses" and "Part 4: Design and Construction", BSI, London, 1958.

37. BS 449: "Specification for the use of structural steel in building", BSI, London, 1959.

38. Dibley, J.E.: "Lateral-torsional buckling of I-sections in Grade 55 steel", Proc.ICE, Vol 43, August 1969, pp 599 - 627.

39. Nethercot, D.A.: "Imperfections and the design of steel beams", Proc.ICE, Vol 57, June 1974, pp 291 - 306.

40. Nethercot, D.A.: "Residual stresses and their influence upon the lateral buckling of rolled steel beams", Str.Engr., Vol 52, No.3, March 1974, pp 89 - 96.

41. Nethercot, D.A.: "Factors affecting the buckling stability of partially plastic beams", Proc.ICE, Vol 53, September 1972, pp 285 - 304.

42. BS 4: "Structural steel sections. Part 1: Hot rolled sections", BSI, London, 1980.

43. Trahair, N.S. and Woolcock, S.T.: "Effect of major axis curvature on I-beam stability", J.Eng.Mech.Div., ASCE, Vol 99, No. EM1, February 1973, pp 85 - 98.

44. Nethercot, D.A.: "Lateral-torsional buckling of beams", lecture 5 of the conference "The background to the new British Standard for structural steelwork" organised jointly by Imperial College and Constrado. Held Imperial College, London, 4th - 6th July 1978.

45. Zuk, W.: "Lateral bracing forces on beams and columns", J.Eng.Mech. Div., ASCE, Vol 82, No. EM3, July 1956, pp 1032.1 - 1032.16.

46. Winter, G.: "Lateral bracing of columns and beams", J.Str.Div. ASCE, Vol 84, No. ST2, March 1958, pp 1561.1 - 1561.22

47. Massey, P.C.: "Lateral bracing forces of steel I-beams", J.Eng.Mech.Div., ASCE, Vol 88, No. EM6, December 1962, pp 89 - 113.

48. Massey, P.C.: "Elastic and inelastic lateral instability of I-beams", The Engineer, Vol 216, October 1963, pp 672 - 674.

49. Medland, I.C.: "A basis for the design of column bracing", Str.Engr., Vol 55, No. 7, July 1977, pp 301 - 307.

50. Fukumoto, Y., Itoh, Y. and Kubo, M.: "Strength variation of laterally unsupported beams", J.Str.Div., ASCE, Vol 106, No. ST1, January 1980, pp 165 - 181.

51. Fukumoto, Y. and Itoh, Y.: "Statistical study of experiments on welded beams", J.Str.Div., ASCE, Vol 107, No. ST1, January 1981, pp 89 - 103.

52. Fukumoto, Y., Itoh, Y. and Hattori, R.: "Lateral buckling tests on welded continuous beams", J.Str.Div., ASCE, Vol 108, No. ST10, October 1982, pp 2245 - 2262.

53. Lui, E.M. and Chen, W.F.: "Strength of H-columns with small end restraints", Str.Engr., Vol 61B, No. 1, March 1983, pp 17 - 26.

54. Nethercot, D.A.: "Design of beams and plate girders - treatment of overall and local flange buckling", paper 13 of the conference "The design of steel bridges" held University College, Cardiff, March 1980. Conference proceedings ed. Rockey, K.C. and Evans, H.R., Granada, London, 1981.

55. BS 5400: "Steel, concrete and composite bridges. Part 3: Code of practice for design of steel bridges" (1982) and "Part 6: Specification for materials and workmanship, steel" (1980), BSI, London.

56. BS 5950: "Structural use of steelwork in building. Part 1: Code of practice for design in simple and continuous construction: hot rolled sections", BSI, London, 1985.

57. "Specifications for the design, fabrication and erection of structural steel for buildings", American Institute for Steel Construction, New York, 1978.

58. DoE Technical Memorandum BE 3/76: "Interim rules for design and construction of plate girders and rolled section beams in bridges", Dept. of the Environment, London, 1976. Also Amendment No. 1 to this document, DoE, London, May 1977.

59. Flint, A.R.: "The influence of restraints on the stability of beams", Str.Engr., Vol 29, September 1951, pp 235 - 246.

60. Taylor, A.C. and Ojalvo, M.: "Torsional restraint of lateral buckling", J.Str.Div., ASCE, Vol 92, No. ST2, April 1966, pp 115 - 129.

61. Nishida, S., Yoshida, H. and Fukumoto, Y.: "Lateral buckling strength and bracing effect of cross beams", Transactions of the Japan Society of Civil Engineers, Vol 9, 1977, pp 100 - 101.

62. Schmidt, L.C.: "Restraints against elastic lateral buckling", J.Eng.Mech.Div., ASCE, Vol 91, No. EM6, December 1965, pp 1 - 10.

63. Nethercot, D.A. and Rockey, K.C.: "The lateral buckling of beams having discrete intermediate restraints", Str.Engr., Vol 50, No. 10, October 1972, pp 391 - 403.

64. Mutton, B.R. and Trahair, N.S.: "Stiffness requirements for lateral bracing", J.Str.Div., ASCE, Vol 99, No. ST10, October 1973, pp 2167 - 2182.

65. Roeder, C.W. and Assadi, M.: "Lateral stability of I-beams with partial support", J.Str.Div., ASCE, Vol 108, NO. ST8, August 1982, pp 1768 - 1780.

66. O'Connor, C.: "Combined stiffnesses for beam and column braces", University of Queensland, Dept. of Civil Engineering Research Report Series, Research Report No. CE13, May 1980.

67. Trahair, N.S.: "Elastic lateral buckling of continuously restrained beam-columns", paper contained in "The profession of a civil engineer", edited Campbell, Allen and Davis, Sydney University Press, 1979.

68. Trahair, N.S. and Nethercot, D.A.: "Bracing requirements in thin-walled structures", Chapter 3 of "Developments in thin-walled structures, Vol 2", edited Rhodes, J. and Walker, A.C., Elsevier Applied Science Publishers, 1984.

69. Lay, M.G., Galambos, T.V. and Schmidt, L.C.: discussion of "Lateral bracing forces of steel I-beams" by Massey, P.C., J.Eng.Mech.Div., ASCE, Vol 89, No. EM3, June 1963, pp 217 - 224.

70. "Specifications for the design, fabrication and erection of structural steel for buildings", American Institute for Steel Construction, New York, 1963.

71. Lay, M.G. and Galambos, T.V.: "Bracing requirements for inelastic steel beams", J.Str.Div., ASCE, Vol 92, No. ST2, April 1966, pp 207 - 228.

72. Lay, M.G.: "Flange local buckling in wide flange shapes", J.Str.Div., ASCE, Vol 91, No. ST6, December 1965, pp 95 - 116.

73. Lay, M.G. and Galambos, T.V.: "Inelastic steel beams under uniform moment", J.Str.Div., ASCE, Vol 91, No. ST6, December 1965, pp 67 - 93.

74. Salmon, C.G. and Johnson, J.E.: "Steel structures - design and behaviour", 2nd edition, Harper and Row, New York, 1980, pp 511 - 514.

75. Morris, L.J.: "A commentary on portal frame design", Str.Engr., Vol 59A, No. 12, December 1981, pp 394 - 404.

76. Fukumoto, Y. and Kubo, M.: "Lateral buckling strength of girders with bracing systems", Preliminary Report, 9th Congress IABSE, Amsterdam, May 1972, pp 299 - 307.

77. Nethercot, D.A.: "Beam buckling and the design of beams", lecture 16 of the course "Structural steelwork design" organised jointly by University of Glasgow and Constrado. Held University of Glasgow, 19th - 23rd March 1984.

78. AS 1250 - 1981: "S.A.A. Steel structures code", Standards Association of Australia, Sydney, 1981.

79. Morris, L.J. and Randall, A.L.: "Plastic design", Constrado, London, 1975.

80. Briggs, M.H.: "Report on criteria for the design of eaves members in plastically designed portal frames", report prepared for Constrado, May 1978.

81. Correspondence on "A commentary on portal frame design" by L.J. Morris. Str.Engr., Vol 61A, No. 7, July 1983, pp 212 - 221.

82. Tauchert, T.R.: "Energy principles in structural mechanics", McGraw-Hill, New York, 1974.

83. Roberts, T.M. and Jhita, P.S.: "Lateral, local and distortional buckling of I-beams", Thin-walled structures, Vol 1, Applied Science Publishers, 1983, pp 289 - 308.

84. Zienkiewicz, O.C.: "The finite element method in engineering science", McGraw-Hill, London, 1971.

85. Cook, R.D.: "Concepts and applications of finite element analysis", John Wiley & Sons, New York, 1974.

86. Desai, C.S. and Abel, J.F.: "Introduction to the finite element method", Van Nostrand Reinhold, New York, 1972.

87. Nadai, A.: "Theory of flow and fracture of solids", 2nd edition, McGraw-Hill, New York, 1950.

88. Bathe, K.J.: "Finite element procedures in engineering analysis", Prentice-Hall, Englewood Cliffs, New Jersey, 1982.

89. Owen, D.R.J. and Hinton, E.: "Finite elements in plasticity: theory and practice", Pineridge Press, Swansea, 1980.

90. Nayak, G.C.: "Plasticity and large deformation problems by the finite element method", doctoral thesis, University of Wales, Swansea, 1971.

91. Cheung, Y.K. and Yeo, M.F.: "A practical introduction to finite element analysis", Pitman, London, 1979.

92. Hinton, E. and Owen, D.R.J.: "Finite element programming", Academic Press, London, 1977.

93. MacNeal, R.H.: "A simple quadrilateral shell element", Computers and Structures, Vol 8, 1978, pp 175 - 183.

94. Bates, D.: "Nonlinear finite element analysis of curved beams and shells", Ph.D. Thesis, University of London, 1985.

95. Dowling, P.J., Harding, J.E. and Agelidis, N.: "Collapse of box girder stiffened webs", paper contained in "Instability and plastic collapse of steel structures", edited Morris, L.J., Granada, 1983.

96. Litle, W.A., Falcone, P. and Reimer, R.B.: "Structural behaviour of small-scale steel models", Bulletin No. 10, American Iron & Steel Institute, April 1968.

97. Harris, H.G.: "Use of structural models as an alternative to full-scale testing", contained in "Full-scale load testing of structures", ASTM STP 702, edited Schriever, W.R., American Society for Testing and Materials, 1980, pp 25 - 44.

98. Mills, R.S.: "Small-scale modelling of the nonlinear response of steel framed buildings to earthquakes", paper 17 of the conference "Dynamic modelling of structures" held Building Research Station, Garston, Watford, England, 1981.

99. Baker, J.F., Horne, M.R. and Heyman, J.: "The steel skeleton. Vol 2: Plastic behaviour and design", Cambridge University Press, 1956.

100. Owens, G.W. and Dowling, P.J.: discussion of "An elementary study of nonlinear buckling phenomena in stiffened plates" by Walker, A.C. and Davies, P., proceedings of symposium "Structural analysis nonlinear behaviour and techniques", TRRL Supplementary Report 164UC, Transport and Road Research Laboratory, Crowthorne, 1975.

101. Neal, B.G.: "The lateral instability of yielded mild steel beams of rectangular cross-section", Philosophical Transactions of the Royal Society, Vol 242, Series A, January 1950, pp 197 - 242.

102. DoE: "Buckling Research", article in "Offshore research focus", No. 26, August 1981.

103. Lindner, J.: "Developments on lateral-torsional buckling", extract from the proceedings of the international colloquium "Stability of structures under static and dynamic loads", held Washington D.C., 17th - 19th May, 1977. Published ASCE, 1977.

104. "Recommended standard practices for structural testing of steel models", TRRL Supplementary Report 254, Transport and Road Research Laboratory, Crowthorne, 1977.

105. Needham, F.H. and Weller, A.D.: "Steels for structures", lecture 1 of the BCSA course "Fabrication and erection of structural steelwork", held Wolverhampton, 9th - 10th July 1985.

106. Nethercot, D.A.: "Buckling of columns", lecture 13 of the course

"Structural steelwork design", organised jointly by University of Glasgow and Constrado. Held University of Glasgow, 19th - 23rd March 1984.

107. BS 18: "Methods of tensile testing of metals. Part 2: Steel (general)" and "Part 3: Steel sheet and strip (less than 3mm and not less than 0.5mm thick)", BSI, London, 1971.

108. McClintock, F.A. and Argon, A.S.: "Mechanical behaviour of materials", Addison-Wesley, 1966.

109. Rockey, K.C. and Evans, H.R. (eds): "The design of steel bridges", proceedings of the conference held University College, Cardiff, March 1980. Published Granada, London, 1981.

APPENDIX I

Computer Programmes MODBRACE AND AUTOBRAC

Appendix I(a) - Listing of Programme MODBRACE

```
      PROGRAM MODBRACE
C
C   ******************************************************************
C   ** PROGRAM USED INTERACTIVELY TO DETERMINE THE ELASTIC
C   ** CRITICAL LOAD OF A SIMPLY-SUPPORTED I-BEAM WITH MIDSPAN
C   ** LATERAL RESTRAINT OF NON-DIMENSIONAL STIFFNESS  λ AND
C   ** TORSIONAL RESTRAINT OF NON-DIMENSIONAL STIFFNESS  e UNDER
C   ** THE ACTION OF A CENTRAL POINT LOAD OR UNIFORM MOMENT.
C   **    LEVEL OF LOAD APPLICATION AND LEVEL OF LATERAL RESTRAINT
C   ** ATTACHMENT ARE VARIABLE FOR CPL ANALYSIS WHEREAS VARIABLE
C   ** LEVEL OF LOAD APPLICATION IS NOT RELEVANT IN THE CASE OF
C   ** UNIFORM MOMENT.
C   **   THE END CONDITIONS ARE  U = PHI = (PHI)'' = 0 AT EACH END.
C   **   GAUSSIAN ELIMINATION IS PERFORMED, THE DETERMINANT EVALUATED
C   ** AND THE STURM SEQUENCE FORMED. THE USER SHOULD SUPPLY
C   ** AN INITIAL ESTIMATE FOR P AND TERMINATES THE RUN
C   ** WHEN THE DETERMINANT OBTAINED BY SUCCESSIVE BISECTION
C   ** IN THE PROGRAM IS CONSIDERED SUFFICIENTLY CLOSE TO ZERO.
C
C      VARIABLES IN USE
C      ----------------
C      K                NON-DIMENSIONAL AXIAL STIFFNESS OF BRACE (λ)
C      L                SPAN
C      P                GENERALISED APPLIED LOAD
C      E                ELASTIC MODULUS
C      EI               MINOR AXIS FLEXURAL RIGIDITY
C      H                LEVEL OF RESTRAINT ATTACHMENT
C      A                LEVEL OF LOAD APPLICATION
C      D                DISTANCE BETWEEN FLANGE CENTROIDS
C      B                FLANGE BREADTH
C      TF,TW            FLANGE AND WEB THICKNESSES RESPECTIVELY
C      G                SHEAR MODULUS
C      J                ST. VENANT TORSION CONSTANT
C      C                =GJ, TORSIONAL RIGIDITY
C      C1               =EΓ , WARPING RIGIDITY
C      DETG             DETERMINANT OF THE COEFFICIENT MATRIX
C      KT               NON-DIMENSIONAL TORSIONAL STIFFNESS OF BRACE (e)
C
C   ******************************************************************
C
      DOUBLE PRECISION K,L,P,E,EI,H,D,B,TF,TW,G,J,C,C1,PI,
     .     DETG,A,ABOVE(2),BELOW(2),KT
C
C  ** DETERMINE WHICH TYPE OF ANALYSIS
C
      WRITE(4,1003)
 1003 FORMAT(' ENTER 1 = UNIF. MOM., ELASTIC CENTRAL RESTRAINT',/,
     .'       2 = CPL, ELASTIC CENTRAL RESTRAINT',/,
     .'       3 = CPL, RIGID CENTRAL RESTRAINT')
      READ(3,*) KODE
  300 CONTINUE
C
C  ** ENTER DATA INPUT ROUTINE
C
      CALL INPUT(KODE,K,H,A,L,D,B,TF,TW,E,KT)
C
C  ** CALC AND PRINT OUT SECTION PROPS
C
      EI=E*((TF*B**3)/6.0+((D-TF)*TW**3)/12.0)
      G=E/2.6
      J=(2*B*TF**3+D*TW**3)/3.0
      C=G*J
      C1=(E*TF*D**2*B**3)/24.0
      PI=3.141592653578793
```

```
      WRITE(4,1005) K,KT,L,E,EI,J,C,C1,A,H
 1005 FORMAT(' ***** STRUCTURAL PROPERTIES ******',//,
     .' NON-DIM AXIAL BRACE STIFFNESS LAMBDA =',D12.6,/,
     .' NON-DIM TORS BRACE STIFFNESS E =',D12.6,/,
     .' BEAM LENGTH =',D12.6,/,
     .' YOUNGS MODULUS =',D12.6,/,
     .' MINOR AXIS BENDING RIGIDITY =',D12.6,/,
     .' J =',D12.6,/,
     .' C =',D12.6,/,
     .' C1 = ',D12.6,/,
     .' LEVEL OF LOAD APPLICATION = ',F7.3,/,
     .' LEVEL OF RESTRAINT ATTACHMENT = ',F7.3)
C
C  ** PROMPT FOR AND READ INITIAL TRIAL VALUE OF LOAD OR MOMENT
C
      WRITE(4,1010)
 1010 FORMAT(//,' GIVE INITIAL TRIAL VALUE OF P')
      READ(3,*) P
      DETG=0.0
      NSINAG=0
C
C  ** EVALUATE DETERMINANT FOR CURRENT LOAD
C
      CALL DETERM(P,L,PI,EI,C,C1,DETG,NSINAG,KODE,H,A,K,KT)
      IF(NSINAG.GT.0) GOTO 302
C
C  ** TRIAL P LESS THAN PCR SO STORE THIS VALUE AND SEARCH
C  ** FOR A VALUE OF P GREATER THAN P(CRIT)
C
      BELOW(1)=DETG
      BELOW(2)=P
      DO 305 KLOOP1=1,20
      P=1.2*P
      CALL DETERM(P,L,PI,EI,C,C1,DETG,NSINAG,KODE,H,A,K,KT)
      IF(NSINAG.GT.0) GOTO 315
  305 CONTINUE
  315 CONTINUE
      ABOVE(1)=DETG
      ABOVE(2)=P
      GOTO 325
  302 CONTINUE
C
C  ** TRIAL P GREATER THAN PCR SO STORE THIS VALUE AND SEARCH
C  ** FOR A VALUE OF P LESS THAN P(CRIT)
C
      ABOVE(1)=DETG
      ABOVE(2)=P
      DO 310 KLOOP2=1,20
      P=0.8*P
      CALL DETERM(P,L,PI,EI,C,C1,DETG,NSINAG,KODE,H,A,K,KT)
      IF(NSINAG.LT.1) GOTO 320
  310 CONTINUE
  320 CONTINUE
      BELOW(1)=DETG
      BELOW(2)=P
  325 CONTINUE
C
C  ** ENTER LOOP TO SUCCESSIVELY BISECT PREVIOUS BEST VALUES
C  ** AND EVALUATE DETERMINANT FOR THIS BISECTED VALUE. THEN
C  ** OUTPUT RESULTS FOR TWENTY SUCCESSIVE EVALUATIONS.
C
      DO 330 LOOP5=1,20
      P=0.5*(ABOVE(2)+BELOW(2))
      CALL DETERM(P,L,PI,EI,C,C1,DETG,NSINAG,KODE,H,A,K,KT)
      IF(NSINAG.GT.0) GOTO 335
```

```
      KMARK=0
      IF(DETG.LT.BELOW(1)) KMARK=1
      IF(KMARK.EQ.1) BELOW(1)=DETG
      IF(KMARK.EQ.1) BELOW(2)=P
      GOTO 340
  335 CONTINUE
      KMARK=0
      IF(DETG.GT.ABOVE(1)) KMARK=1
      IF(KMARK.EQ.1) ABOVE(1)=DETG
      IF(KMARK.EQ.1) ABOVE(2)=P
  340 CONTINUE
      WRITE(4,1001) P,DETG,NSINAG
 1001 FORMAT(' LOAD = ',F11.3,'  DETERMINANT = ',D14.6,
     .'  NO OF SIGN AGREEMENTS =',I3)
  330 CONTINUE
C
C  ** ENQUIRE IF THIS DETERMINANT IS SUFFICIENTLY CLOSE TO
C  ** ZERO OR IF FURTHER ITERATION IS REQUIRED
C
      WRITE(4,1002)
 1002 FORMAT(' ENTER -1 = STOP RUN, 0 = NEW PROBLEM, 1 = ITERATIONS')
      READ(3,*) KONTIN
      IF(KONTIN.GT.0) GOTO 325
C
C  ** IF USER'S CONVERGENCE CRITERIA SATISFIED OUTPUT FINAL
C  ** RESULTS.
C
      CALL OUTPUT(C1,PI,C,L,EI,KODE,P,DETG,NSINAG,K,KT)
      IF(KONTIN.EQ.0) GOTO 300
      STOP
      END
C
C     -----------------
      SUBROUTINE DETERM(P,L,PI,EI,C,C1,DETG,NSINAG,KODE,H,A,K,KT)
C     -----------------
      DOUBLE PRECISION P,L,PI,EI,C,C1,DETG,H,A,K,KT,
     .G11,G12,G21,G22,FACT,STURMO,STURM1,STURM2,
     .F1,F2,F3,F4,F5,F6,F7,F8,F9,D1,D2,D3
C
C  ** THIS SUBROUTINE EVALUATES THE CURRENT DETERMINANT AND
C  ** THE NUMBER OF SIGN AGREEMENTS IN THE STURM SEQUENCE WHICH
C  ** IS CONSTRUCTED AFTER GAUSSIAN ELIMINATION.
C
      IF(KODE.EQ.2) GOTO 10
      IF(KODE.EQ.3) GOTO 20
C
C  ** KODE=1 , UNIF MOM WITH CENTRAL EL BRACE
C  ** FOR P READ M AND FOR K READ LAMBDA, FOR KT READ EKT
C
      F1=-(P**2*L)/(4.0*EI)
      F2=(24.0*P**2*L*K)/(PI**4*EI)/(1.0+K)
      F3=(24.0*EI*H**2*K)/L**3/(1.0+K)
      F4=(48.0*P*H*K)/(PI**2*L)/(1.0+K)+KT*C/2.0/L
      F5=C*PI**2/4.0/L
      F6=C1*PI**4/4.0/L**3
      G11=2.0*(F1+F2+F3+F4+F5+F6)
      G12=(2.0*F2/9.0)+(2.0*F3)+(10.0*F4/9.0)
      G21=G12
      G22=2.0*(F1+F2/81.0+F3+F4/9.0+9.0*F5+81.0*F6)
      GOTO 30
   10 CONTINUE
C
C  ** KODE=2 , CPL WITH ELASTIC CENTRAL RESTRAINT
C
      D1=(P**2*L**6)*(1.0+4.0/PI**2-4.0/PI)/PI**4
```

```
     .   +(4.0*P*L**3*EI*H)*(1.0-2.0/PI)/PI**2
     .   +(4.0*EI**2*H**2)
      D2=(P**2*L**6)*(1.0+4.0/9.0/PI**2+4.0/3.0/PI)/(9.0*PI**4)
     .   +(4.0*P*L**3*EI*H)*(1.0+2.0/3.0/PI)/PI**2
     .   +(36.0*EI**2*H**2)
      D3=(P**2*L**6)*(1.0-4.0/3.0/PI-4.0/3.0/PI**2)/(3.0*PI**4)
     .   +(6.0*P*L**3*EI*H)*(1.0-2.0/PI)/PI**2
      F1=0.5*(KT*C/L-P*A)
      F2=-(P**2*L**3)*(1.0+6.0/PI**2)/(192.0*EI)
      F3=-(5.0*P**2*L**3)/(64.0*PI**2*EI)
      F4=-(P**2*L**3)*(3.0+2.0/PI**2)/(576.0*EI)
      F5=C*PI**2/4.0/L
      F6=C1*PI**4/4.0/L**3
      F7=(6.0*D1*K)/(EI*L**3)/(1.0+K)
      F8=(2.0*D2*K)/(3.0*EI*L**3)/(1.0+K)
      F9=(4.0*D3*K)/(EI*L**3)/(1.0+K)
      G11=2.0*(F1+F2+F5+F6+F7)
      G12=2.0*F1+F3+F9
      G21=G12
      G22=2.0*(F1+F4+9.0*F5+81.0*F6+F8)
      GOTO 30
   20 CONTINUE
C
C  ** KODE=3 , CPL WITH RIGID CENTRAL RESTRAINT
C  ** K,KT,H,A IGNORED HERE
C
      F1=(-P**2*L**3)*(1.0/3.0-1.0/2.0/PI**2)/(64.0*EI)
      F2=(C*PI**2/L)+(4.0*C1*PI**4/L**3)
      G11=F1+F2
      G12=(-P**2*L**3)/(36.0*EI*PI**2)
      G21=G12
      F3=(-P**2*L**3)*(1.0/3.0-1.0/8.0/PI**2)/(64.0*EI)
      F4=(4.0*C*PI**2/L)+(64.0*C1*PI**4/L**3)
      G22=F3+F4
   30 CONTINUE
      FACT=G21/G11
      G22=G22-FACT*G12
      G21=0.0
      DETG=G11*G22
      STURM0=1.0
      STURM1=-G11
      STURM2=G11*G22
      NSINAG=0
      IF(STURM0.GT.0.0.AND.STURM1.GT.0.0) NSINAG=NSINAG+1
      IF(STURM1.GT.0.0.AND.STURM2.GT.0.0) NSINAG=NSINAG+1
      IF(STURM1.LT.0.0.AND.STURM2.LT.0.0) NSINAG=NSINAG+1
      RETURN
      END
C
C     ----------------
      SUBROUTINE INPUT(KODE,K,H,A,L,D,B,TF,TW,E,KT)
C     ----------------
      DOUBLE PRECISION K,H,A,L,D,B,TF,TW,E,KT
C
C  ** THIS SUBROUTINE PROMPTS FOR AND READS DATA APPROPRIATE TO
C  ** THE TYPE OF ANALYSIS BEING PERFORMED.
C
      IF(KODE.EQ.2) GOTO 50
      IF(KODE.EQ.3) GOTO 60
C
C  ** KODE 1 - UNIFORM MOMENT
C
      WRITE(4,10)
   10 FORMAT(' INPUT REAL FF VALUES FOR LAMBDA,EKT,H,L,D,B,TF,TW,E')
      READ(3,*) K,KT,H,L,D,B,TF,TW,E
```

```
      A=0.0
      GOTO 70
   50 CONTINUE
C
C  ** KODE 2 - CPL WITH ELASTIC RESTRAINT
C
      WRITE(4,20)
   20 FORMAT(' INPUT REAL FF VALUES FOR LAMBDA,EKT,H,A,L,D,B,TF,TW,E')
      READ(3,*) K,KT,H,A,L,D,B,TF,TW,E
      GOTO 70
   60 CONTINUE
C
C  ** KODE 3 - CPL WITH RIGID CENTRAL RESTRAINT
C
      WRITE(4,30)
   30 FORMAT(' INPUT REAL FF VALUES FOR L,D,B,TF,TW,E')
      READ(3,*) L,D,B,TF,TW,E
      K=0.0
      KT=0.0
      H=0.0
      A=0.0
   70 CONTINUE
      RETURN
      END
C
C     -----------------
      SUBROUTINE OUTPUT(C1,PI,C,L,EI,KODE,P,DETG,NSINAG,K,KT)
C     -----------------
      DOUBLE PRECISION MCRUM,C1,PI,C,L,EI,RATIO2,P,DETG,K,M,PNOK,
     .RATIO1,KT
      EXTERNAL DSQRT
C
C  ** THIS SUBROUTINE PRINTS OUT THE FINAL RESULTS OF THE
C  ** CONVERGED SOLUTION. THE NATURE OF THE OUTPUT IS
C  ** DEPENDENT ON THE TYPE OF ANALYSIS BEING PERFORMED.
C
      WRITE(4,1015)
      WRITE(4,1016)
      WRITE(4,1015)
      MCRUM=(1.0+C1*PI**2/C/L**2)*EI*C
      MCRUM=DSQRT(MCRUM)
      MCRUM=PI*MCRUM/L
      IF(KODE.NE.1) GOTO 10
C
C  ** OUTPUT FINAL RESULTS FOR UNIF MOM CASE
C
      RATIO2=P/MCRUM
      WRITE(4,1017) P
      WRITE(4,1018) RATIO2
      WRITE(4,1019) DETG
      WRITE(4,1020) NSINAG
      WRITE(4,1021) K
      WRITE(4,1024) KT
      GOTO 20
   10 CONTINUE
C
C  ** CPL CASES
C
      M=P*L/4.0
      RATIO2=M/MCRUM
      PNOK=(16.94/L**2)*DSQRT(EI*C)*DSQRT(1.0+C1*PI**2/C/L**2)
      RATIO1=P/PNOK
      WRITE(4,1022) P
      WRITE(4,1017) M
      WRITE(4,1018) RATIO2
```

```
      WRITE(4,1023) RATIO1
      WRITE(4,1021) K
      WRITE(4,1024) KT
      WRITE(4,1019) DETG
      WRITE(4,1020) NSINAG
   20 CONTINUE
 1015 FORMAT(//,1X,40('*'))
 1016 FORMAT(/,10X,'FINAL RESULTS')
 1017 FORMAT(' CRITICAL MOMENT FOR THIS SYSTEM = ',E12.6)
 1018 FORMAT(' RATIO OF MCR/MCRUM = ',F6.3)
 1019 FORMAT(' FINAL DETERMINANT = ',E12.6)
 1020 FORMAT(' NO. OF SIGN AGREEMENTS IN STURM TERMS = ',I3)
 1021 FORMAT(' LAMBDA = ',F7.3)
 1022 FORMAT(' CRITICAL LOAD FOR THIS SYSTEM = ',F10.3)
 1023 FORMAT(' RATIO OF PCR/PNOK = ',F6.3)
 1024 FORMAT(' E (NON-DIM KT) = ',F7.3)
      RETURN
      END
```

Appendix I(b) - Details of Typical MODBRACE Run

Example showing the use of MODBRACE in calculating the elastic critical load of a restrained beam.

The critical load of the following beam/restraint system is to be determined:

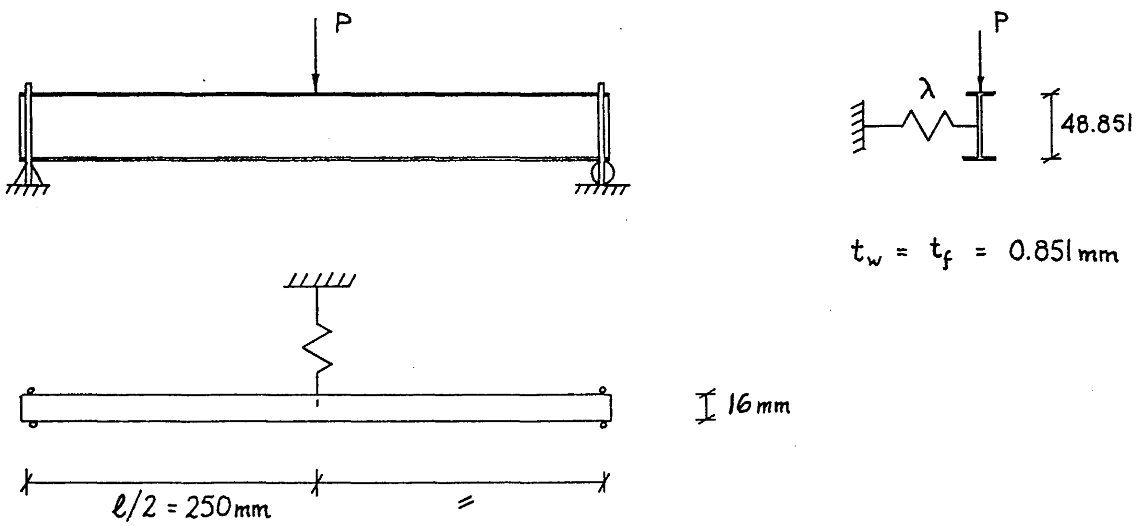

Load is applied at the level of the compression flange (a=24.4255mm) whilst the translational restraint (λ=13.664) is attached at the shear centre of the section (h=0) and no torsional restraint is applied (e=0). In the example, the following notation is employed as only upper case variables were available:

LAMBDA	=	λ	= 13.664
EKT	=	e	= 0.0
H	=	h	= 0.0
A	=	a	= 24.4255mm
L	=	l	= 500mm
D	=	distance between flange centroids = 48.851mm	
B	=	b_f	= 16mm
TF, TW	=	flange & web thicknesses, respectively = 0.851mm	
E	=	Young's modulus = 196000N/mm^2	

```
RUN ZB
 ENTER 1 = UNIF. MOM., ELASTIC CENTRAL RESTRAINT
       2 = CPL, ELASTIC CENTRAL RESTRAINT
       3 = CPL, RIGID CENTRAL RESTRAINT


2


 INPUT REAL FF VALUES FOR LAMBDA,EKT,H,A,L,D,B,TF,TW,E


13.664,0.0,0.0,24.4255,500.,48.851,16.,.851,.851,196000.


 ***** STRUCTURAL PROPERTIES ******

 NON-DIM AXIAL BRACE STIFFNESS LAMBDA =0.136640D+02
 NON-DIM TORS BRACE STIFFNESS E =0.000000D+01
 BEAM LENGTH =0.500000D+03
 YOUNGS MODULUS =0.196000D+06
 MINOR AXIS BENDING RIGIDITY =0.114349D+09
 J =0.166094D+02
 C =0.125209D+07
 C1 = 0.679331D+11
 LEVEL OF LOAD APPLICATION =  24.426
 LEVEL OF RESTRAINT ATTACHMENT =   0.000


 GIVE INITIAL TRIAL VALUE OF P
1350.0

 LOAD =    1485.000  DETERMINANT =  -0.456478D+10  NO OF SIGN AGREEMENTS =  1
 LOAD =    1417.500  DETERMINANT =  -0.163388D+08  NO OF SIGN AGREEMENTS =  1
 LOAD =    1383.750  DETERMINANT =   0.224598D+10  NO OF SIGN AGREEMENTS =  0
 LOAD =    1400.625  DETERMINANT =   0.111582D+10  NO OF SIGN AGREEMENTS =  0
 LOAD =    1409.062  DETERMINANT =   0.549988D+09  NO OF SIGN AGREEMENTS =  0
 LOAD =    1413.281  DETERMINANT =   0.266887D+09  NO OF SIGN AGREEMENTS =  0
 LOAD =    1415.391  DETERMINANT =   0.125290D+09  NO OF SIGN AGREEMENTS =  0
 LOAD =    1416.445  DETERMINANT =   0.544793D+08  NO OF SIGN AGREEMENTS =  0
 LOAD =    1416.973  DETERMINANT =   0.190712D+08  NO OF SIGN AGREEMENTS =  0
 LOAD =    1417.236  DETERMINANT =   0.136646D+07  NO OF SIGN AGREEMENTS =  0
 LOAD =    1417.368  DETERMINANT =  -0.748610D+07  NO OF SIGN AGREEMENTS =  1
 LOAD =    1417.302  DETERMINANT =  -0.305981D+07  NO OF SIGN AGREEMENTS =  1
 LOAD =    1417.269  DETERMINANT =  -0.846669D+06  NO OF SIGN AGREEMENTS =  1
 LOAD =    1417.253  DETERMINANT =   0.259896D+06  NO OF SIGN AGREEMENTS =  0
 LOAD =    1417.261  DETERMINANT =  -0.293386D+06  NO OF SIGN AGREEMENTS =  1
 LOAD =    1417.257  DETERMINANT =  -0.167448D+05  NO OF SIGN AGREEMENTS =  1
 LOAD =    1417.255  DETERMINANT =   0.121576D+06  NO OF SIGN AGREEMENTS =  0
 LOAD =    1417.256  DETERMINANT =   0.524155D+05  NO OF SIGN AGREEMENTS =  0
 LOAD =    1417.256  DETERMINANT =   0.178353D+05  NO OF SIGN AGREEMENTS =  0
 LOAD =    1417.257  DETERMINANT =   0.545252D+03  NO OF SIGN AGREEMENTS =  0
 ENTER -1 = STOP RUN, 0 = NEW PROBLEM, 1 = ITERATIONS
```

```
1
 LOAD =     1417.257  DETERMINANT =  -0.809979D+04  NO OF SIGN AGREEMENTS =  1
 LOAD =     1417.257  DETERMINANT =  -0.377727D+04  NO OF SIGN AGREEMENTS =  1
 LOAD =     1417.257  DETERMINANT =  -0.161601D+04  NO OF SIGN AGREEMENTS =  1
 LOAD =     1417.257  DETERMINANT =  -0.535378D+03  NO OF SIGN AGREEMENTS =  1
 LOAD =     1417.257  DETERMINANT =   0.493721D+01  NO OF SIGN AGREEMENTS =  0
 LOAD =     1417.257  DETERMINANT =  -0.265220D+03  NO OF SIGN AGREEMENTS =  1
 LOAD =     1417.257  DETERMINANT =  -0.130142D+03  NO OF SIGN AGREEMENTS =  1
 LOAD =     1417.257  DETERMINANT =  -0.626022D+02  NO OF SIGN AGREEMENTS =  1
 LOAD =     1417.257  DETERMINANT =  -0.288325D+02  NO OF SIGN AGREEMENTS =  1
 LOAD =     1417.257  DETERMINANT =  -0.119476D+02  NO OF SIGN AGREEMENTS =  1
 LOAD =     1417.257  DETERMINANT =  -0.350520D+01  NO OF SIGN AGREEMENTS =  1
 LOAD =     1417.257  DETERMINANT =   0.716003D+00  NO OF SIGN AGREEMENTS =  0
 LOAD =     1417.257  DETERMINANT =  -0.139460D+01  NO OF SIGN AGREEMENTS =  1
 LOAD =     1417.257  DETERMINANT =  -0.339303D+00  NO OF SIGN AGREEMENTS =  1
 LOAD =     1417.257  DETERMINANT =   0.188358D+00  NO OF SIGN AGREEMENTS =  0
 LOAD =     1417.257  DETERMINANT =  -0.754768D-01  NO OF SIGN AGREEMENTS =  1
 LOAD =     1417.257  DETERMINANT =   0.564485D-01  NO OF SIGN AGREEMENTS =  0
 LOAD =     1417.257  DETERMINANT =  -0.951234D-02  NO OF SIGN AGREEMENTS =  1
 LOAD =     1417.257  DETERMINANT =   0.234643D-01  NO OF SIGN AGREEMENTS =  0
 LOAD =     1417.257  DETERMINANT =   0.697590D-02  NO OF SIGN AGREEMENTS =  0
 ENTER -1 = STOP RUN, 0 = NEW PROBLEM, 1 = ITERATIONS

-1

 ****************************************

        FINAL RESULTS

 ****************************************
 CRITICAL LOAD FOR THIS SYSTEM =    1417.257
 CRITICAL MOMENT FOR THIS SYSTEM = 0.177157E+06
 RATIO OF MCR/MCRUM =  1.329
 RATIO OF PCR/PNOK =  0.986
 LAMBDA =  13.664
 E (NON-DIM KT) =    0.000
 FINAL DETERMINANT = 0.697590E-02
 NO. OF SIGN AGREEMENTS IN STURM TERMS =   0
Ready
```

Appendix I(c) - Flowchart & Listing of Programme AUTOBRAC

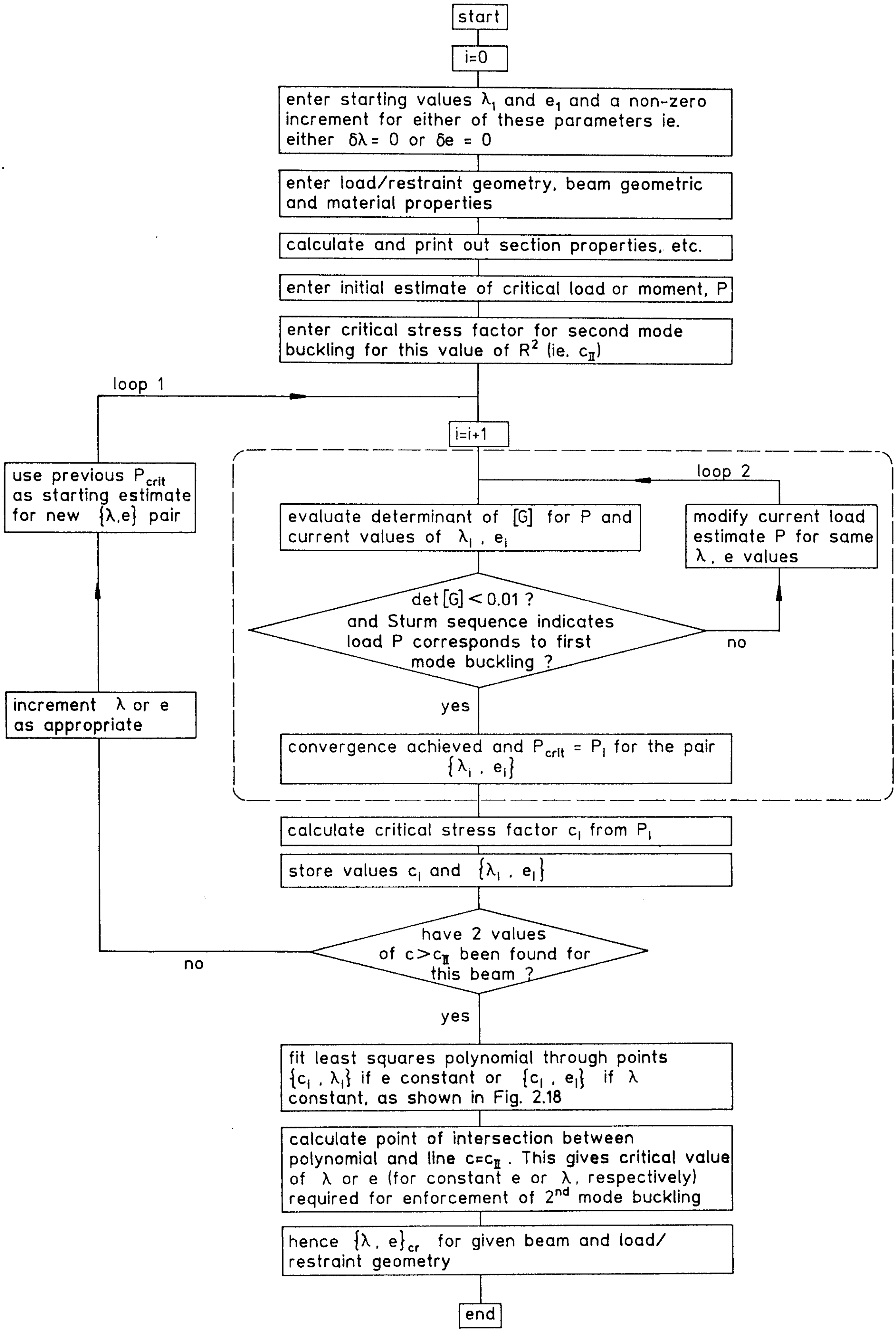
start
i=0
enter starting values λ1 and e1 and a non-zero increment for either of these parameters ie. either δλ = 0 or δe = 0
enter load/restraint geometry, beam geometric and material properties
calculate and print out section properties, etc.
enter initial estimate of critical load or moment, P
enter critical stress factor for second mode buckling for this value of R2 (ie. cII)
loop 1
i=i+1
use previous Pcrit as starting estimate for new {λ,e} pair
loop 2
evaluate determinant of [G] for P and current values of λi , ei
modify current load estimate P for same λ , e values
det [G] < 0.01 ? and Sturm sequence indicates load P corresponds to first mode buckling ?
no
increment λ or e as appropriate
yes
convergence achieved and Pcrit = Pi for the pair {λi , ei}
calculate critical stress factor ci from Pi
store values ci and {λi , ei}
have 2 values of c>cII been found for this beam ?
no
yes
fit least squares polynomial through points {ci , λi} if e constant or {ci , ei} if λ constant, as shown in Fig. 2.18
calculate point of intersection between polynomial and line c=cII . This gives critical value of λ or e (for constant e or λ, respectively) required for enforcement of 2nd mode buckling
hence {λ, e}cr for given beam and load/restraint geometry
end

```
      PROGRAM AUTOBRAC
C
C    ****************************************************************
C    ** PROGRAM USED INTERACTIVELY TO DETERMINE THE CRITICAL
C    ** COMBINATION OF LATERAL RESTRAINT STIFFNESS ( λ ) AND
C    ** TORSIONAL RESTRAINT STIFFNESS ( e ) REQUIRED FOR THE FULLY
C    ** EFFECTIVE MIDSPAN RESTRAINT OF A SIMPLY SUPPORTED I-BEAM
C    ** UNDER CENTRAL POINT OR UNIFORM MOMENT LOADING.
C    **    LEVEL OF LOAD APPLICATION AND LEVEL OF LATERAL RESTRAINT
C    ** ATTACHMENT ARE VARIABLE FOR CPL ANALYSIS WHEREAS VARIABLE
C    ** LEVEL OF LOAD APPLICATION IS NOT RELEVANT IN THE CASE OF
C    ** UNIFORM MOMENT.
C    **   THE END CONDITIONS ARE  U = PHI = (PHI)'' = 0 AT EACH END.
C    **   GAUSSIAN ELIMINATION IS PERFORMED, THE DETERMINANT EVALUATED
C    ** AND THE STURM SEQUENCE FORMED. THE USER SHOULD SUPPLY
C    ** AN INITIAL ESTIMATE FOR P AND THE CRITICAL STRESS FACTOR
C    ** APPROPRIATE TO SECOND MODE BUCKLING.
C    **   AUTOBRAC INCREMENTS THE LATERAL OR TORSIONAL STIFFNESS
C    ** VALUES UNTIL CALCULATED CRITICAL LOADS EXCEED THE SECOND MODE
C    ** BUCKLING LOAD. A POLYNOMIAL IS THEN FITTED TO THE BRACE
C    ** STIFFNESSES AND THE CRITICAL {λ, e} COMBINATION DETERMINED
C    ** BY INTERPOLATION.
C
C       VARIABLES IN USE
C       ----------------
C       K                NON-DIMENSIONAL AXIAL STIFFNESS OF BRACE ( λ )
C       L                SPAN
C       P                GENERALISED APPLIED LOAD
C       E                ELASTIC MODULUS
C       EI               MINOR AXIS FLEXURAL RIGIDITY
C       H                LEVEL OF RESTRAINT ATTACHMENT
C       A                LEVEL OF LOAD APPLICATION
C       D                DISTANCE BETWEEN FLANGE CENTROIDS
C       B                FLANGE BREADTH
C       TF,TW            FLANGE AND WEB THICKNESSES RESPECTIVELY
C       G                SHEAR MODULUS
C       J                ST. VENANT TORSION CONSTANT
C       C                =GJ, TORSIONAL RIGIDITY
C       C1               =EΓ , WARPING RIGIDITY
C       DETG             DETERMINANT OF THE COEFFICIENT MATRIX
C       KT               NON-DIMENSIONAL TORSIONAL STIFFNESS OF BRACE ( e )
C
C    ****************************************************************
C
      INTEGER MM,KPLUS1,NROWS,IFAIL,NDEGRE,NPLUS1
      DOUBLE PRECISION K,L,P,E,EI,H,D,B,TF,TW,G,J,C,C1,PI,RATIO2,
     .     DETG,A,ABOVE(2),BELOW(2),KT,KTINC,CLIMIT,ARALAM(100),
     .     ARAEKT(100),ARAPCR(100),ARAC(100),ARADET(100),X(8),Y(8),
     .     W(8),WORK1(3,8),WORK2(2,8),AA(8,8),S(8),COEFFT(8),XBAR,
     .     KTCRIT,KINC
C
C  ** DETERMINE WHICH TYPE OF ANALYSIS
C
      WRITE(4,1003)
 1003 FORMAT(' ENTER 1 = UNIF. MOM., ELASTIC CENTRAL RESTRAINT',/,
     .'        2 = CPL, ELASTIC CENTRAL RESTRAINT',/,
     .'        3 = CPL, RIGID CENTRAL RESTRAINT')
      READ(3,*) KODE
  300 CONTINUE
C
C  ** ENTER DATA INPUT ROUTINE
C
      CALL INPUT(KODE,K,H,A,L,D,B,TF,TW,E,KT,KTINC,KINC)
C
```

```
C  ** CALC AND PRINT OUT SECTION PROPS
C
      EI=E*((TF*B**3)/6.0+((D-TF)*TW**3)/12.0)
      G=E/2.6
      J=(2*B*TF**3+D*TW**3)/3.0
      C=G*J
      C1=(E*TF*D**2*B**3)/24.0
      PI=3.141592653578793
      WRITE(4,1005) K,KT,L,E,EI,J,C,C1,A,H
 1005 FORMAT(' ***** STRUCTURAL PROPERTIES ******',//,
     .' NON-DIM AXIAL BRACE STIFFNESS LAMBDA =',D12.6,/,
     .' NON-DIM TORS BRACE STIFFNESS E =',D12.6,/,
     .' BEAM LENGTH =',D12.6,/,
     .' YOUNGS MODULUS =',D12.6,/,
     .' MINOR AXIS BENDING RIGIDITY =',D12.6,/,
     .' J =',D12.6,/,
     .' C =',D12.6,/,
     .' C1 = ',D12.6,/,
     .' LEVEL OF LOAD APPLICATION = ',F7.3,/,
     .' LEVEL OF RESTRAINT ATTACHMENT = ',F7.3)
C
C  ** PROMPT FOR AND READ INITIAL TRIAL VALUE OF LOAD OR MOMENT
C
      WRITE(4,1010)
 1010 FORMAT(//,' GIVE INITIAL TRIAL VALUE OF P')
      READ(3,*) P
      WRITE(4,1011)
 1011 FORMAT(//,' GIVE 2ND MODE VALUE OF CRIT STRESS FACTOR C')
      READ(3,*) CLIMIT
      KPAIR=0
      KEXIT=0
  301 CONTINUE
      KPAIR=KPAIR+1
      IF(KPAIR.LE.100) GOTO 415
      WRITE(4,1019)
 1019 FORMAT(//,' KPAIR HAS EXCEEDED 100 SO MODIFY INCREMENT')
      GOTO 300
  415 CONTINUE
      DETG=0.0
      NSINAG=0
C
C  ** EVALUATE DETERMINANT FOR CURRENT LOAD
C
      CALL DETERM(P,L,PI,EI,C,C1,DETG,NSINAG,KODE,H,A,K,KT)
      IF(NSINAG.GT.0) GOTO 302
C
C  ** TRIAL P LESS THAN PCR SO STORE THIS VALUE AND SEARCH
C  ** FOR A VALUE OF P GREATER THAN P(CRIT)
C
      BELOW(1)=DETG
      BELOW(2)=P
      DO 305 KLOOP1=1,20
      P=1.2*P
      CALL DETERM(P,L,PI,EI,C,C1,DETG,NSINAG,KODE,H,A,K,KT)
      IF(NSINAG.GT.0) GOTO 315
  305 CONTINUE
  315 CONTINUE
      ABOVE(1)=DETG
      ABOVE(2)=P
      GOTO 325
  302 CONTINUE
C
C  ** TRIAL P GREATER THAN PCR SO STORE THIS VALUE AND SEARCH
C  ** FOR A VALUE OF P LESS THAN P(CRIT)
C
```

```
      ABOVE(1)=DETG
      ABOVE(2)=P
      DO 310 KLOOP2=1,20
      P=0.8*P
      CALL DETERM(P,L,PI,EI,C,C1,DETG,NSINAG,KODE,H,A,K,KT)
      IF(NSINAG.LT.1) GOTO 320
  310 CONTINUE
  320 CONTINUE
      BELOW(1)=DETG
      BELOW(2)=P
  325 CONTINUE
C
C  ** ENTER LOOP TO SUCCESSIVELY BISECT PREVIOUS BEST VALUES
C  ** AND EVALUATE DETERMINANT FOR THIS BISECTED VALUE. THEN
C  ** OUTPUT RESULTS FOR TWENTY SUCCESSIVE EVALUATIONS.
C
      DO 330 LOOP5=1,100
      P=0.5*(ABOVE(2)+BELOW(2))
      CALL DETERM(P,L,PI,EI,C,C1,DETG,NSINAG,KODE,H,A,K,KT)
      IF(NSINAG.GT.0) GOTO 335
      KMARK=0
      IF(DETG.LT.BELOW(1)) KMARK=1
      IF(KMARK.EQ.1) BELOW(1)=DETG
      IF(KMARK.EQ.1) BELOW(2)=P
      GOTO 340
  335 CONTINUE
      KMARK=0
      IF(DETG.GT.ABOVE(1)) KMARK=1
      IF(KMARK.EQ.1) ABOVE(1)=DETG
      IF(KMARK.EQ.1) ABOVE(2)=P
  340 CONTINUE
C
C  ** CONVERGENCE CRITERION IS ABS(DETG) < 0.01
C
      IF(DABS(DETG).LT.0.01) GOTO 331
  330 CONTINUE
  331 CONTINUE
C
C  ** CALL ROUTINE TO EVALUATE CRIT STRESS FACTOR C=RATIO2
C
      CALL CALRA2(C1,PI,C,L,EI,KODE,P,RATIO2)
      ARALAM(KPAIR)=K
      ARAEKT(KPAIR)=KT
      ARAPCR(KPAIR)=P
      ARAC(KPAIR)=RATIO2
      ARADET(KPAIR)=DETG
C
C  ** EXIT THIS LOOP IF 2 VALUES OF C GREATER THAN CLIMIT HAVE BEEN
C  ** FOUND OR IF A KODE=3 ANALYSIS IS BEING PERFORMED.
C
      IF(KEXIT.EQ.1) GOTO 350
      IF(KODE.EQ.3) GOTO 350
      IF(RATIO2.GT.CLIMIT) KEXIT=1
C
C  ** INCREMENT LAMBDA AND EKT
C
      K=K+KINC
      KT=KT+KTINC
      GOTO 301
  350 CONTINUE
C
C  ** PRINT OUT TABLE OF RESULTS
C
      WRITE(4,1012)
      WRITE(6,1012)
```

```
 1012 FORMAT(//,' LAMBDA         PCRIT          DETG          C',
     .'               EKT')
      DO 355 I=1,KPAIR
      WRITE(4,1013) ARALAM(I),ARAPCR(I),ARADET(I),ARAC(I),ARAEKT(I)
      WRITE(6,1013) ARALAM(I),ARAPCR(I),ARADET(I),ARAC(I),ARAEKT(I)
  355 CONTINUE
C
C  ** IF KPAIR < 8 A CURVE WILL NOT BE FITTED AND A NAG ERROR WILL
C  ** OCCUR, THEREFOR CHECK KPAIR, OUTPUT A SUITABLE MESSAGE AND
C  ** RETURN TO DATA INPUT IF <8
C
      IF(KPAIR.GE.8) GOTO 399
      WRITE(4,1018)
 1018 FORMAT(//,' NO OF DATA PTS FOR CURVE <8 SO ENTER DATA',//)
      GOTO 300
  399 CONTINUE
C
C  ** USE THE LAST 8 POINTS IN ARRAYS ARAC AND ARAEKT TO FIT A
C  ** LEAST SQUARES POLYNOMIAL OF MAX DEGREE 7
C
      JO=KPAIR-7
      I=0
      DO 400 J=JO,KPAIR
      I=I+1
      X(I)=ARAC(J)
      Y(I)=ARAEKT(J)
      IF(KINC.GT.0.0000001) Y(I)=ARALAM(J)
      W(I)=1.0
  400 CONTINUE
      MM=8
      KPLUS1=8
      NROWS=8
      IFAIL=0
      CALL E02ADF(MM,KPLUS1,NROWS,X,Y,W,WORK1,WORK2,AA,S,IFAIL)
      WRITE(4,1014)
 1014 FORMAT(//,' POLYNOM DEGREE     LEAST SQUARES RESIDUAL')
      DO 405 I=1,8
      WRITE(4,1015) I-1,S(I)
  405 CONTINUE
 1015 FORMAT(1X,I6,7X,D12.6)
C
C  ** DETERMINE FROM ABOVE LIST THE DEGREE OF POLYNOMIAL REQD.
C
      WRITE(4,1016)
 1016 FORMAT(///,' EXAMINE ABOVE RESIDUALS & ENTER REQD DEGREE')
      READ(3,*) NDEGRE
      NPLUS1=NDEGRE+1
C
C  ** EVALUATE THE CRIT NON-DIM. STIFFNESS KTCRIT USING NAG
C
      DO 410 I=1,NPLUS1
      COEFFT(I)=AA(NPLUS1,I)
  410 CONTINUE
      XBAR=((CLIMIT-X(1))-(X(8)-CLIMIT))/(X(8)-X(1))
      IFAIL=0
      CALL E02AEF(NPLUS1,COEFFT,XBAR,KTCRIT,IFAIL)
      IF(KTINC.GT.0.0000001) WRITE(4,1017) K,KTCRIT
      IF(KINC.GT.0.0000001) WRITE(4,1017) KTCRIT,KT
 1017 FORMAT(//,' CRITICAL COMBINATION : LAMBDA=',F8.3,'  EKT= ',F8.3)
 1013 FORMAT(1X,5(D12.6,2X))
      WRITE(4,1002)
 1002 FORMAT(' ENTER -1 = STOP RUN,  O = NEW PROBLEM')
      READ(3,*) KONTIN
      IF(KONTIN.EQ.0) GOTO 300
      STOP
```

```
      END
C
C     -----------------
      SUBROUTINE DETERM(P,L,PI,EI,C,C1,DETG,NSINAG,KODE,H,A,K,KT)
C     -----------------
      DOUBLE PRECISION P,L,PI,EI,C,C1,DETG,H,A,K,KT,
     .G11,G12,G21,G22,FACT,STURMO,STURM1,STURM2,
     .F1,F2,F3,F4,F5,F6,F7,F8,F9,D1,D2,D3
C
C  ** THIS SUBROUTINE EVALUATES THE CURRENT DETERMINANT AND
C  ** THE NUMBER OF SIGN AGREEMENTS IN THE STURM SEQUENCE WHICH
C  ** IS CONSTRUCTED AFTER GAUSSIAN ELIMINATION.
C
      IF(KODE.EQ.2) GOTO 10
      IF(KODE.EQ.3) GOTO 20
C
C  ** KODE=1 , UNIF MOM WITH CENTRAL EL BRACE
C  ** FOR P READ M AND FOR K READ LAMBDA, FOR KT READ EKT
C
      F1=-(P**2*L)/(4.0*EI)
      F2=(24.0*P**2*L*K)/(PI**4*EI)/(1.0+K)
      F3=(24.0*EI*H**2*K)/L**3/(1.0+K)
      F4=(48.0*P*H*K)/(PI**2*L)/(1.0+K)+KT*C/2.0/L
      F5=C*PI**2/4.0/L
      F6=C1*PI**4/4.0/L**3
      G11=2.0*(F1+F2+F3+F4+F5+F6)
      G12=(2.0*F2/9.0)+(2.0*F3)+(10.0*F4/9.0)
      G21=G12
      G22=2.0*(F1+F2/81.0+F3+F4/9.0+9.0*F5+81.0*F6)
      GOTO 30
   10 CONTINUE
C
C  ** KODE=2 , CPL WITH ELASTIC CENTRAL RESTRAINT
C
      D1=(P**2*L**6)*(1.0+4.0/PI**2-4.0/PI)/PI**4
     .   +(4.0*P*L**3*EI*H)*(1.0-2.0/PI)/PI**2
     .   +(4.0*EI**2*H**2)
      D2=(P**2*L**6)*(1.0+4.0/9.0/PI**2+4.0/3.0/PI)/(9.0*PI**4)
     .   +(4.0*P*L**3*EI*H)*(1.0+2.0/3.0/PI)/PI**2
     .   +(36.0*EI**2*H**2)
      D3=(P**2*L**6)*(1.0-4.0/3.0/PI-4.0/3.0/PI**2)/(3.0*PI**4)
     .   +(6.0*P*L**3*EI*H)*(1.0-2.0/PI)/PI**2
      F1=0.5*(KT*C/L-P*A)
      F2=-(P**2*L**3)*(1.0+6.0/PI**2)/(192.0*EI)
      F3=-(5.0*P**2*L**3)/(64.0*PI**2*EI)
      F4=-(P**2*L**3)*(3.0+2.0/PI**2)/(576.0*EI)
      F5=C*PI**2/4.0/L
      F6=C1*PI**4/4.0/L**3
      F7=(6.0*D1*K)/(EI*L**3)/(1.0+K)
      F8=(2.0*D2*K)/(3.0*EI*L**3)/(1.0+K)
      F9=(4.0*D3*K)/(EI*L**3)/(1.0+K)
      G11=2.0*(F1+F2+F5+F6+F7)
      G12=2.0*F1+F3+F9
      G21=G12
      G22=2.0*(F1+F4+9.0*F5+81.0*F6+F8)
      GOTO 30
   20 CONTINUE
C
C  ** KODE=3 , CPL WITH RIGID CENTRAL RESTRAINT
C  ** K,KT,H,A IGNORED HERE
C
      F1=(-P**2*L**3)*(1.0/3.0-1.0/2.0/PI**2)/(64.0*EI)
      F2=(C*PI**2/L)+(4.0*C1*PI**4/L**3)
      G11=F1+F2
      G12=(-P**2*L**3)/(36.0*EI*PI**2)
```

```
      G21=G12
      F3=(-P**2*L**3)*(1.0/3.0-1.0/8.0/PI**2)/(64.0*EI)
      F4=(4.0*C*PI**2/L)+(64.0*C1*PI**4/L**3)
      G22=F3+F4
   30 CONTINUE
      FACT=G21/G11
      G22=G22-FACT*G12
      G21=0.0
      DETG=G11*G22
      STURMO=1.0
      STURM1=-G11
      STURM2=G11*G22
      NSINAG=0
      IF(STURMO.GT.0.0.AND.STURM1.GT.0.0) NSINAG=NSINAG+1
      IF(STURM1.GT.0.0.AND.STURM2.GT.0.0) NSINAG=NSINAG+1
      IF(STURM1.LT.0.0.AND.STURM2.LT.0.0) NSINAG=NSINAG+1
      RETURN
      END
C
C     ----------------
      SUBROUTINE INPUT(KODE,K,H,A,L,D,B,TF,TW,E,KT,KTINC,KINC)
C     ----------------
      DOUBLE PRECISION K,H,A,L,D,B,TF,TW,E,KT,KTINC,KINC
C
C  ** THIS SUBROUTINE PROMPTS FOR AND READS DATA APPROPRIATE TO
C  ** THE TYPE OF ANALYSIS BEING PERFORMED.
C
      IF(KODE.EQ.2) GOTO 50
      IF(KODE.EQ.3) GOTO 60
C
C  ** KODE 1 - UNIFORM MOMENT
C
      WRITE(4,10)
   10 FORMAT(' GIVE  VALUES FOR LAMBDA,DLAMB,EKT,DEKT,H,L,D,B,TF,TW,E')
      READ(3,*) K,KINC,KT,KTINC,H,L,D,B,TF,TW,E
      A=0.0
      GOTO 70
   50 CONTINUE
C
C  ** KODE 2 - CPL WITH ELASTIC RESTRAINT
C
      WRITE(4,20)
   20 FORMAT(' GIVE VALUES OF LAMBDA,DLAMB,EKT,DEKT,H,A,L,D,B,TF,TW,E')
      READ(3,*) K,KINC,KT,KTINC,H,A,L,D,B,TF,TW,E
      GOTO 70
   60 CONTINUE
C
C  ** KODE 3 - CPL WITH RIGID CENTRAL RESTRAINT
C
      WRITE(4,30)
   30 FORMAT(' INPUT REAL FF VALUES FOR L,D,B,TF,TW,E')
      READ(3,*) L,D,B,TF,TW,E
      K=0.0
      KT=0.0
      H=0.0
      A=0.0
      KTINC=0.0
   70 CONTINUE
      RETURN
      END
C
C     -----------------
      SUBROUTINE CALRA2(C1,PI,C,L,EI,KODE,P,RATIO2)
C     -----------------
      DOUBLE PRECISION MCRUM,C1,PI,C,L,EI,P,RATIO2,M
```

```
      EXTERNAL DSQRT
C
C  ** THIS SUBROUTINE CALCULATES THE CRITICAL STRESS FACTOR C (HERE
C  ** CALLED RATIO2) FROM THE ARGUMENT PARAMETER P WHICH HAS JUST
C  ** SATISFIED THE CONVERGENCE CRITERION. RATIO2 IS THEN RETURNED
C  ** TO THE MAIN PROGRAM
C
      MCRUM=(1.0+C1*PI**2/C/L**2)*EI*C
      MCRUM=DSQRT(MCRUM)
      MCRUM=PI*MCRUM/L
      IF(KODE.NE.1) GOTO 10
C
C  ** UNIFORM MOMENT CASE
C
      RATIO2=P/MCRUM
      GOTO 20
   10 CONTINUE
C
C  ** CPL CASES
C
      M=P*L/4.0
      RATIO2=M/MCRUM
   20 CONTINUE
      RETURN
      END
```

Appendix I(d) - Example of Use of AUTOBRAC with $\lambda \neq 0$, $e = 0$

```
RUN ZB
 ENTER 1 = UNIF. MOM., ELASTIC CENTRAL RESTRAINT
       2 = CPL, ELASTIC CENTRAL RESTRAINT
       3 = CPL, RIGID CENTRAL RESTRAINT

2

 GIVE VALUES OF LAMBDA,DLAMB,EKT,DEKT,H,A,L,D,B,TF,TW,E

.1,1.5,0.0,0.0,0.0,24.4255,500.,48.851,16.,.851,.851,196000.

 ***** STRUCTURAL PROPERTIES ******

 NON-DIM AXIAL BRACE STIFFNESS LAMBDA =0.100000D+00
 NON-DIM TORS BRACE STIFFNESS E =0.000000D+01
 BEAM LENGTH =0.500000D+03
 YOUNGS MODULUS =0.196000D+06
 MINOR AXIS BENDING RIGIDITY =0.114349D+09
 J =0.166094D+02
 C =0.125209D+07
 C1 = 0.679331D+11
 LEVEL OF LOAD APPLICATION =  24.426
 LEVEL OF RESTRAINT ATTACHMENT =   0.000

 GIVE INITIAL TRIAL VALUE OF P

1350.0

 GIVE 2ND MODE VALUE OF CRIT STRESS FACTOR C

1.329
```

LAMBDA	PCRIT	DETG	C	EKT
0.100000D+00	0.952432D+03	0.784656D-02	0.893370D+00	0.000000D+01
0.160000D+01	0.116099D+04	0.217232D-02	0.108900D+01	0.000000D+01
0.310000D+01	0.125262D+04	-.930160D-02	0.117494D+01	0.000000D+01
0.460000D+01	0.130534D+04	-.468104D-02	0.122440D+01	0.000000D+01
0.610000D+01	0.133983D+04	-.537760D-02	0.125674D+01	0.000000D+01
0.760000D+01	0.136421D+04	-.498346D-02	0.127962D+01	0.000000D+01
0.910000D+01	0.138239D+04	0.266757D-02	0.129667D+01	0.000000D+01
0.106000D+02	0.139648D+04	-.793222D-02	0.130988D+01	0.000000D+01
0.121000D+02	0.140772D+04	-.565149D-02	0.132043D+01	0.000000D+01
0.136000D+02	0.141690D+04	-.141306D-02	0.132904D+01	0.000000D+01
0.151000D+02	0.142454D+04	-.506147D-02	0.133621D+01	0.000000D+01

POLYNOM DEGREE	LEAST SQUARES RESIDUAL
0	0.367423D+01
1	0.997367D+00
2	0.247585D+00
3	0.556051D-01
4	0.109822D-01
5	0.183725D-02
6	0.244733D-03
7	0.000000D+01

```
 EXAMINE ABOVE RESIDUALS & ENTER REQD DEGREE

6

 CRITICAL COMBINATION : LAMBDA=  13.593  EKT=     0.000
 ENTER -1 = STOP RUN,  0 = NEW PROBLEM

-1
Ready
```

Appendix I(e) - Example of Use of AUTOBRAC with $\lambda \neq 0$, $e = 0.5$

```
RUN ZB
 ENTER 1 = UNIF. MOM., ELASTIC CENTRAL RESTRAINT
       2 = CPL, ELASTIC CENTRAL RESTRAINT
       3 = CPL, RIGID CENTRAL RESTRAINT

2

 GIVE VALUES OF LAMBDA,DLAMB,EKT,DEKT,H,A,L,D,B,TF,TW,E

.1,1.5,.5,0.0,0.0,24.4255,500.,48.851,16.,.851,.851,196000.

 ***** STRUCTURAL PROPERTIES ******

 NON-DIM AXIAL BRACE STIFFNESS LAMBDA =0.100000D+00
 NON-DIM TORS BRACE STIFFNESS E =0.500000D+00
 BEAM LENGTH =0.500000D+03
 YOUNGS MODULUS =0.196000D+06
 MINOR AXIS BENDING RIGIDITY =0.114349D+09
 J =0.166094D+02
 C =0.125209D+07
 C1 = 0.679331D+11
 LEVEL OF LOAD APPLICATION =  24.426
 LEVEL OF RESTRAINT ATTACHMENT =   0.000

 GIVE INITIAL TRIAL VALUE OF P

1350.0

 GIVE 2ND MODE VALUE OF CRIT STRESS FACTOR C

1.329

 LAMBDA         PCRIT          DETG           C              EKT
 0.100000D+00   0.974731D+03   0.157790D-02   0.914287D+00   0.500000D+00
 0.160000D+01   0.119112D+04   0.476403D-02   0.111726D+01   0.500000D+00
 0.310000D+01   0.128675D+04   -.518059D-02   0.120696D+01   0.500000D+00
 0.460000D+01   0.134196D+04   -.577624D-02   0.125875D+01   0.500000D+00
 0.610000D+01   0.137816D+04   -.265489D-02   0.129270D+01   0.500000D+00
 0.760000D+01   0.140379D+04   0.273921D-02   0.131674D+01   0.500000D+00
 0.910000D+01   0.142293D+04   0.694732D-03   0.133469D+01   0.500000D+00
 0.106000D+02   0.143777D+04   0.213263D-03   0.134861D+01   0.500000D+00

 POLYNOM DEGREE     LEAST SQUARES RESIDUAL
       0         0.367423D+01
       1         0.177162D+01
       2         0.693258D+00
       3         0.227363D+00
       4         0.619961D-01
       5         0.137246D-01
       6         0.234064D-02
       7         0.000000D+01

 EXAMINE ABOVE RESIDUALS & ENTER REQD DEGREE

6

 CRITICAL COMBINATION : LAMBDA=    8.579  EKT=     0.500
 ENTER -1 = STOP RUN,  0 = NEW PROBLEM

-1
Ready
```

APPENDIX II

Computer Programme NEWMESH

```
C  ********************************
C  *                              *
C  *   N E W M E S H              *
C  *                              *
C  ********************************
C
C ** PROGRAM TO GENERATE NODAL AND ELEMENT DATA FOR FE MESH
C ** AND OUTPUT TO A FILE IN A FORM COMPATIBLE WITH NASTRAN OR FINAS
C ** INPUT DATA
C **   THE PROGRAM ACCEPTS INITIAL IMPERFECTION DATA AND CONVERTS
C ** IT (VIA NAG CURVE FITTING ROUTINES) TO THE EQUIVALENT GRID
C ** POINT COORDINATES OF THE NASTRAN OR FINAS DATA.
C **   THE PROGRAM FITS A SEPARATE CURVE TO EACH LINE OF NODES
C ** THEREBY MODELLING AS ACCURATELY AS POSSIBLE THE ACTUAL GEOMETRY
C **   ALLOWANCES ARE MADE FOR SELF WEIGHT AND SLANT, THE FINAL
C ** COORDINATES BEING BASED ON THE ASSUMPTION THAT THE FOUR WEB
C ** VERTICES LIE IN THE VERTICAL PLANE AT THE START OF THE TEST.
C
      PROGRAM NEWMESH
      DIMENSION POSRDG(20),T1(20),C1(20),W1(20),W2(20),W3(20),BRT(20),
     .BRC(20),T2(20),C2(20),T3(20),T4(20),W4(20),W5(20),C3(20),C4(20),
     .DELTA(20),CORRW1(20),CORRW2(20),CORRW3(20),COORD(1200,5),
     .LINNOD(30,200),INCR(200),FACTOR(200),LINEL(30,200),REF(13,2),
     .STNDAT(150,7),AZ(61,5),W(1134)
C
C  ALTER FIRST DIMENSION OF AZ ON PREVIOUS LINE FOR EACH PLOTTING RUN
C
C  NUMBER OF POINTS IN PLOT IN X DIRECTN LIMITED TO 50 CURRENTLY
C
      DOUBLE PRECISION ORDT1(20),ORDT2(20),ORDT3(20),ORDT4(20),
     .ORDW1(20),ORDW2(20),ORDW3(20),ORDW4(20),ORDW5(20),ORDC1(20),
     .ORDC2(20),ORDC3(20),ORDC4(20),CURVT1(20),CURVT2(20),CURVT3(20),
     .CURVT4(20),CURVW1(20),CURVW2(20),CURVW3(20),CURVW4(20),
     .CURVW5(20),CURVC1(20),CURVC2(20),CURVC3(20),CURVC4(20),
     .CURV(13,21),A(20),XBAR,P
      EXTERNAL SIN,COS,ATAN
      REAL IMINOR,IMAJOR
      INTEGER NRDGS,IFAIL,NPLUS1
C
C  **********************************************************
C  READ IMPERFECTION DATA FROM FILE, CALCULATE AND PRINT
C  GEOMETRIC PROPERTIES OF SECTION
C  **********************************************************
C
C ** READ IMPERFECTION DATA FROM FILE - FREE FORMAT
      READ(5,*) NRDGS,SELFWT,HBAR,GMT,E,KODE
      READ(5,*) (POSRDG(KK),KK=1,NRDGS)
      READ(5,*) (T1(KK),KK=1,NRDGS)
      READ(5,*) (C1(KK),KK=1,NRDGS)
      READ(5,*) (W1(KK),KK=1,NRDGS)
      READ(5,*) (W2(KK),KK=1,NRDGS)
      READ(5,*) (W3(KK),KK=1,NRDGS)
      READ(5,*) (BRT(KK),KK=1,NRDGS)
      READ(5,*) (BRC(KK),KK=1,NRDGS)
C ** CALCULATE CORRESPONDING SETS OF RDGS ON LOWER FLANGE TIPS
      DO 101 KNT=1,NRDGS
      T2(KNT)=T1(KNT)-BRT(KNT)
      C2(KNT)=C1(KNT)-BRC(KNT)
  101 CONTINUE
C ** CALCULATE AVE BRDTHS OF TENSION AND COMP FLGS
      BRTBAR=0.0
      BRCBAR=0.0
      DO 102 KNT=1,NRDGS
      BRTBAR=BRTBAR+BRT(KNT)
```

```
      BRCBAR=BRCBAR+BRC(KNT)
  102 CONTINUE
      RDGS=FLOAT(NRDGS)
      BRTBAR=BRTBAR/RDGS
      BRCBAR=BRCBAR/RDGS
C ** CALC APPROX 2ND MOMENT OF INERTIA ABOUT MINOR AXIS
C ** THIS IS APPROX DUE TO VARIATIONS IN FLGE BRDTH.
      IMINOR=(BRCBAR**3+BRTBAR**3+GMT**2*(HBAR-2.0*GMT))
     .*GMT/12.0
C ** CALC APPROX 2ND MOMENT OF INERTIA ABOUT MAJOR AXIS
C ** THIS ALLOWS FOR VARIATIONS IN THE POSITION OF THE N.A.
C ** DUE TO UNEQUAL FLANGE BREADTHS. HOWEVER, THE RESULT IS
C ** STILL APPROXIMATE DUE TO THE AVERAGE FLANGE BREADTH BEING USED
C ** IN CALCULATIONS
      ACF=BRCBAR*GMT
      AWP=(HBAR-2.0*GMT)*GMT
      ATF=BRTBAR*GMT
      ATOT=ACF+AWP+ATF
C ** TAKE MOMENTS ABOUT BASE TO FIND POSITN OF N.A.
      FIRSMO=(ATF*GMT/2.0)+(AWP*HBAR/2.0)+(ACF*(HBAR-GMT/2.0))
      PNA=FIRSMO/ATOT
      GCTONA=HBAR-GMT/2.0-PNA
      GWTONA=HBAR/2.0-PNA
      GTTONA=PNA-GMT/2.0
      CFI=(BRCBAR*GMT**3)/12.0+ACF*GCTONA**2
      WPI=(GMT*(HBAR-2.0*GMT)**3)/12.0+AWP*GWTONA**2
      TFI=(BRTBAR*GMT**3)/12.0+ATF*GTTONA**2
      IMAJOR=CFI+WPI+TFI
C ** PRINT TITLE PAGE AND INITIAL IMPERFECTION DATA
      WRITE(6,105)
      WRITE(6,106)
      WRITE(6,107) E
      WRITE(6,108) POSRDG(NRDGS),GMT
      WRITE(6,109) SELFWT
      WRITE(6,110) NRDGS
      WRITE(6,111) HBAR
      WRITE(6,112) IMINOR
      WRITE(6,117) IMAJOR
      WRITE(6,113)
      WRITE(6,114)
      WRITE(6,115)
      DO 120 K=1,NRDGS
      WRITE(6,116) K,POSRDG(K),C1(K),T1(K),W1(K),W2(K),W3(K),BRC(K),
     .BRT(K)
  120 CONTINUE
C ** ALTER RDGS TO ACCOUNT FOR HALF THICKNESS OF WEB
      DO 125 K=1,NRDGS
      W1(K)=W1(K)-0.5*GMT
      W2(K)=W2(K)-0.5*GMT
      W3(K)=W3(K)-0.5*GMT
  125 CONTINUE
C
C ****************************************************************
C CORRECT INITIAL IMPERFECTION READINGS FOR THE EFFECT OF SELF WT.
C DEFLECTION DURING IMPERFECTION MEASUREMENT
C ****************************************************************
C
      IF(SELFWT.LT.1.0E-4) GOTO 195
      GO TO 139
C ** DELTAC IS THE MIDSPAN DEFLECTION ABOUT THE MINOR AXIS. OTHER
C ** DEFLECTIONS ARE OBTAINED FROM PARABOLIC DISTRIBUTION
      DELTAC=(5.0*SELFWT*POSRDG(NRDGS)**4)/(384.0*E*IMINOR)
      DELTA(1)=0.0
      DELTA(NRDGS)=0.0
C ** FOLLOWING LINE RESTRICTS PROGRAM TO NRDGS EVEN
```

C

```
      DO 130 KNT=2,NRDGS/2
      KNT1=NRDGS-KNT+1
      BB=POSRDG(NRDGS)/2.0
      AA=BB-POSRDG(KNT)
      DELTA(KNT)=DELTAC*(1.0-AA**2/BB**2)
      DELTA(KNT1)=DELTA(KNT)
  130 CONTINUE
      DO 180 KNT=2,NRDGS-1
      T1(KNT)=T1(KNT)+DELTA(KNT)
      T2(KNT)=T2(KNT)+DELTA(KNT)
      C1(KNT)=C1(KNT)+DELTA(KNT)
      C2(KNT)=C2(KNT)+DELTA(KNT)
      W1(KNT)=W1(KNT)+DELTA(KNT)
      W2(KNT)=W2(KNT)+DELTA(KNT)
      W3(KNT)=W3(KNT)+DELTA(KNT)
  180 CONTINUE
  139 CONTINUE
C ** ALTER RDGS FOR THE EFFECTS OF SELF WT DEFLECTIONS.
C ** THIS CORRECTN TAKES ACCOUNT OF THE HOGGING EFFECT
C ** INDUCED BY THE CANTILEVER ENDS DURING IMPERFECTION
C ** MEASUREMENT
C **  READ OVERHANG AT EACH END AA, TOTAL LENGTH TOTL
      READ(5,*) AA,TOTL
      DELTA(1)=0.0
      DELTA(NRDGS)=0.0
C ** FOLLOWING LINE RESTRICTS PROGRAM TO NRDGS EVEN
      DO 140 KNT=2,NRDGS/2
      KNT1=NRDGS-KNT+1
      XX=POSRDG(KNT)+AA
      TERM1=XX**4-AA**4
      TERM2=2.0*TOTL*(XX-AA)**3
      TERM3=6.0*TOTL*(XX-AA)*((TOTL/2.0-AA)**2-(TOTL**2)/12.0)
      TERM4=SELFWT/(24.0*E*IMINOR)
      DELTA(KNT)=TERM4*(TERM1-TERM2+TERM3)
      DELTA(KNT1)=DELTA(KNT)
      WRITE(4,142) KNT,TERM1,TERM2,TERM3,TERM4,DELTA(KNT)
  142 FORMAT(1X,I4,5(2X,E12.6))
  140 CONTINUE
      DO 141 KNT=2,NRDGS-1
      DEL=DELTA(KNT)
      T1(KNT)=T1(KNT)+DEL
      T2(KNT)=T2(KNT)+DEL
      C1(KNT)=C1(KNT)+DEL
      C2(KNT)=C2(KNT)+DEL
      W1(KNT)=W1(KNT)+DEL
      W2(KNT)=W2(KNT)+DEL
      W3(KNT)=W3(KNT)+DEL
  141 CONTINUE
      DELTAC=9.9999
C ** RDGS HAVE NOW BEEN CORRECTED FOR S/W
C ** PRINT OUT RDGS ADJUSTED FOR SELF WT
      WRITE(6,190) DELTAC
      WRITE(6,191)
      DO 195 KK=1,NRDGS
      WRITE(6,192) KK,DELTA(KK),C1(KK),T1(KK),W1(KK),W2(KK),W3(KK)
  195 CONTINUE
C
C ****************************************
C ADJUST RDGS SO THAT ALL ARE RELATIVE
C TO WEB VERTICES COPLANAR IN VERTICAL PLANE
C ****************************************
C
C ** CORRECT RDGS W1,T1,T2 FOR SLANT
      CORRW1(NRDGS)=W1(NRDGS)-W1(1)
      CORRW1(1)=0.0
```

D

```
      CALL EO2AFF(NRDGS,ORDC2,CURVC2,IFAIL)
      IFAIL=0
      CALL EO2AFF(NRDGS,ORDC3,CURVC3,IFAIL)
      IFAIL=0
      CALL EO2AFF(NRDGS,ORDC4,CURVC4,IFAIL)
      DO 450 KNT=1,NRDGS
      CURV(1,KNT+1)=CURVT1(KNT)
      CURV(2,KNT+1)=CURVT3(KNT)
      CURV(3,KNT+1)=CURVW1(KNT)
      CURV(4,KNT+1)=CURVT4(KNT)
      CURV(5,KNT+1)=CURVT2(KNT)
      CURV(6,KNT+1)=CURVW4(KNT)
      CURV(7,KNT+1)=CURVW2(KNT)
      CURV(8,KNT+1)=CURVW5(KNT)
      CURV(9,KNT+1)=CURVC1(KNT)
      CURV(10,KNT+1)=CURVC3(KNT)
      CURV(11,KNT+1)=CURVW3(KNT)
      CURV(12,KNT+1)=CURVC4(KNT)
      CURV(13,KNT+1)=CURVC2(KNT)
  450 CONTINUE
      DO 460 KL=1,10,3
      WRITE(4,501)
  501 FORMAT(1X,//,' THE FOLLOWING ARE THE CEBYSHEV POLYNOM. COEFFTS')
      DO 502 KNT=2,NRDGS+1
      WRITE(4,505) CURV(KL,KNT),CURV(KL+1,KNT),CURV(KL+2,KNT)
  502 CONTINUE
  505 FORMAT(1X,3(D21.15,3X))
      WRITE(4,506)
  506 FORMAT(1X,//,' EXAMINE COLS ABOVE. KEEP HOW MANY IN EACH.')
      READ(3,*) CURV(KL,1),CURV(KL+1,1),CURV(KL+2,1)
  460 CONTINUE
      WRITE(4,501)
      DO 507 KNT=2,NRDGS+1
      WRITE(4,505) CURV(13,KNT)
  507 CONTINUE
      WRITE(4,506)
      READ(3,*) CURV(13,1)
C ** PROGRAM NOW HAS NUMBER OF COEFFTS AND COEFFTS STORED IN 'CURV'
C
C ******************************************************************
C CALCULATE COORDS OF ALL NODES REQUIRED FOR A NASTRAN QUAD4 SHELL
C ANALYSIS. STRATEGY BASED ON PRIMARY AND SECONDARY OR CONGRUENT NODE
C LINES. AT THE END OF THIS CALCULATION ALL COORDS RELATE TO AN
C INITIALLY PERFECT BEAM. IMPERFECTIONS ADDED LATER.
C ******************************************************************
C
C ** READ NO. LINES,ELS,NODES, PRIMARY NODE LINES,SUPPORT NODE
      READ(5,*) NLINS,NELS,NNODS,NPRIM,NODSUP
C ** INITIALISE COORD ARRAY
      DO 600 I=1,NNODS
      DO 600 J=1,5
      COORD(I,J)=0.0
  600 CONTINUE
      COORD(NODSUP,5)=1.0
C ** ENTER LOOP OVER PRIMARY LINES IN THE MESH
      DO 605 KPRIM=1,NPRIM
C ** READ LINE NAME, NO. NODES ON LINE, NO. CONGRT LINES, REAL SPC
C ** CODE FOR INTERIOR NODES ON LINE, FIRST NODE, INTEGER INCREMENTS
C ** BETWEEN NODES, X COORD OF FIRST NODE, POSITION ON CROSS SECTION
C ** RELATIVE TO FOLLOWING SKETCH
C
C                13 * 12 * 11 * 10 * 9
C                          *
C                          8
C                          *
```

G

```
      DO 201 KNT=2,NRDGS-1
      CORRW1(KNT)=POSRDG(KNT)/POSRDG(NRDGS)*CORRW1(NRDGS)
  201 CONTINUE
      DO 202 KNT=2,NRDGS
      W1(KNT)=W1(KNT)-CORRW1(KNT)
      T1(KNT)=T1(KNT)-CORRW1(KNT)
      T2(KNT)=T2(KNT)-CORRW1(KNT)
  202 CONTINUE
C ** CORRECT RDGS W3,C1 C2 FOR SLANT
      CORRW3(NRDGS)=W3(NRDGS)-W3(1)
      CORRW3(1)=0.0
      DO 203 KNT=2,NRDGS-1
      CORRW3(KNT)=POSRDG(KNT)/POSRDG(NRDGS)*CORRW3(NRDGS)
  203 CONTINUE
      DO 204 KNT=2,NRDGS
      W3(KNT)=W3(KNT)-CORRW3(KNT)
      C1(KNT)=C1(KNT)-CORRW3(KNT)
      C2(KNT)=C2(KNT)-CORRW3(KNT)
  204 CONTINUE
C ** CORRECT RDGS W2 FOR SLANT
      DO 205 KNT=1,NRDGS
      CORRW2(KNT)=(CORRW1(KNT)+CORRW3(KNT))/2.0
      W2(KNT)=W2(KNT)-CORRW2(KNT)
  205 CONTINUE
C ** ADJUST ALL RDGS REL TO T FLANGE AS DATUM
      DIFF=W3(1)-W1(1)
      DO 206 KNT=1,NRDGS
      W3(KNT)=W3(KNT)-DIFF
      C1(KNT)=C1(KNT)-DIFF
      C2(KNT)=C2(KNT)-DIFF
      W2(KNT)=W2(KNT)-DIFF/2.0
  206 CONTINUE
      WRITE(4,*) T2(1),T2(2),T2(3),T2(4)
C ** PRINT OUT RDGS ADJUSTED REL TO COPLANAR WEB VERTICES
      WRITE(6,207)
      WRITE(6,208)
      DO 210 KK=1,NRDGS
      WRITE(6,192) KK,T1(KK),W1(KK),T2(KK),W2(KK),C1(KK),W3(KK),C2(KK)
  210 CONTINUE
C ** CREATE NEW LINES W4,W5,T3,T4,C3,C4 AS AVERAGES OF EXISTING LINES
      DO 301 KNT=1,NRDGS
      T3(KNT)=(T1(KNT)+W1(KNT))/2.0
      T4(KNT)=(T2(KNT)+W1(KNT))/2.0
      W4(KNT)=(W1(KNT)+W2(KNT))/2.0
      W5(KNT)=(W2(KNT)+W3(KNT))/2.0
      C3(KNT)=(C1(KNT)+W3(KNT))/2.0
      C4(KNT)=(C2(KNT)+W3(KNT))/2.0
  301 CONTINUE
C
C ***************************************************************
C DETERMINE COORDS OF NODES ON BEAM CROSS-SECTION AT END '0'.
C ALL GLOBAL X COORDS HERE ZERO
C ***************************************************************
C
      REF(1,1)=0.002
      REF(5,1)=T1(1)-T2(1)+0.002
      REF(2,1)=T1(1)-T3(1)+0.002
      REF(4,1)=T1(1)-T4(1)+0.002
      REF(3,1)=T1(1)-W1(1)+0.002
      REF(7,1)=T1(1)-W2(1)+0.002
      REF(11,1)=T1(1)-W3(1)+0.002
      REF(6,1)=T1(1)-W4(1)+0.002
      REF(8,1)=T1(1)-W5(1)+0.002
      REF(9,1)=T1(1)-C1(1)+0.002
      REF(13,1)=T1(1)-C2(1)+0.002
```

```
      REF(10,1)=T1(1)-C3(1)+0.002
      REF(12,1)=T1(1)-C4(1)+0.002
      REF(1,2)=0.0
      REF(5,2)=0.0
      REF(2,2)=0.0
      REF(4,2)=0.0
      REF(3,2)=0.0
      REF(7,2)=0.5*(HBAR-GMT)
      REF(11,2)=HBAR-GMT
      REF(6,2)=0.25*(HBAR-GMT)
      REF(8,2)=0.75*(HBAR-GMT)
      REF(9,2)=REF(11,2)
      REF(13,2)=REF(11,2)
      REF(10,2)=REF(11,2)
      REF(12,2)=REF(11,2)
C
C *******************************************************************
C CALCULATE OFFSETS DEFINING INITIAL CROOKEDNESS RELATIVE TO A CHORD
C JOINING WEB VERTICES AT OPPOSITE ENDS OF THE SPAN. NAG CURVE FITTING
C ROUTINE THEN USED TO CALCULATE CHEBYSHEV POLYNOMIAL COEFFTS FOR
C EACH CURVE.
C *******************************************************************
C
C ** CALCULATE OFFSETS RELATIVE TO THE Y VALUE OF THE END 'O' NODE  AND
C ** REVERSE THE ORDER SINCE THE NAG CURVE FITTING ROUTINE ACCEPTS THE
C ** ORDINATES STARTING WITH XBAR= +1.0
      DO 401 KNT=1,NRDGS
      K=NRDGS-KNT+1
      ORDT1(K)=DBLE(T1(1)-T1(KNT))
      ORDT2(K)=DBLE(T2(1)-T2(KNT))
      ORDT3(K)=DBLE(T3(1)-T3(KNT))
      ORDT4(K)=DBLE(T4(1)-T4(KNT))
      ORDW1(K)=DBLE(W1(1)-W1(KNT))
      ORDW2(K)=DBLE(W2(1)-W2(KNT))
      ORDW3(K)=DBLE(W3(1)-W3(KNT))
      ORDW4(K)=DBLE(W4(1)-W4(KNT))
      ORDW5(K)=DBLE(W5(1)-W5(KNT))
      ORDC1(K)=DBLE(C1(1)-C1(KNT))
      ORDC2(K)=DBLE(C2(1)-C2(KNT))
      ORDC3(K)=DBLE(C3(1)-C3(KNT))
      ORDC4(K)=DBLE(C4(1)-C4(KNT))
  401 CONTINUE
C ** USE NAG TO EVALUATE THE CHEBYSHEV POLYNOMIAL COEFFTS FOR EACH OF
C ** THE ABOVE
      IFAIL=0
      CALL EO2AFF(NRDGS,ORDT1,CURVT1,IFAIL)
      IFAIL=0
      CALL EO2AFF(NRDGS,ORDT2,CURVT2,IFAIL)
      IFAIL=0
      CALL EO2AFF(NRDGS,ORDT3,CURVT3,IFAIL)
      IFAIL=0
      CALL EO2AFF(NRDGS,ORDT4,CURVT4,IFAIL)
      IFAIL=0
      CALL EO2AFF(NRDGS,ORDW1,CURVW1,IFAIL)
      IFAIL=0
      CALL EO2AFF(NRDGS,ORDW2,CURVW2,IFAIL)
      IFAIL=0
      CALL EO2AFF(NRDGS,ORDW3,CURVW3,IFAIL)
      IFAIL=0
      CALL EO2AFF(NRDGS,ORDW4,CURVW4,IFAIL)
      IFAIL=0
      CALL EO2AFF(NRDGS,ORDW5,CURVW5,IFAIL)
      IFAIL=0
      CALL EO2AFF(NRDGS,ORDC1,CURVC1,IFAIL)
      IFAIL=0
```

F

```
      CALL EO2AFF(NRDGS,ORDC2,CURVC2,IFAIL)
      IFAIL=0
      CALL EO2AFF(NRDGS,ORDC3,CURVC3,IFAIL)
      IFAIL=0
      CALL EO2AFF(NRDGS,ORDC4,CURVC4,IFAIL)
      DO 450 KNT=1,NRDGS
      CURV(1,KNT+1)=CURVT1(KNT)
      CURV(2,KNT+1)=CURVT3(KNT)
      CURV(3,KNT+1)=CURVW1(KNT)
      CURV(4,KNT+1)=CURVT4(KNT)
      CURV(5,KNT+1)=CURVT2(KNT)
      CURV(6,KNT+1)=CURVW4(KNT)
      CURV(7,KNT+1)=CURVW2(KNT)
      CURV(8,KNT+1)=CURVW5(KNT)
      CURV(9,KNT+1)=CURVC1(KNT)
      CURV(10,KNT+1)=CURVC3(KNT)
      CURV(11,KNT+1)=CURVW3(KNT)
      CURV(12,KNT+1)=CURVC4(KNT)
      CURV(13,KNT+1)=CURVC2(KNT)
  450 CONTINUE
      DO 460 KL=1,10,3
      WRITE(4,501)
  501 FORMAT(1X,//,' THE FOLLOWING ARE THE CEBYSHEV POLYNOM. COEFFTS')
      DO 502 KNT=2,NRDGS+1
      WRITE(4,505) CURV(KL,KNT),CURV(KL+1,KNT),CURV(KL+2,KNT)
  502 CONTINUE
  505 FORMAT(1X,3(D21.15,3X))
      WRITE(4,506)
  506 FORMAT(1X,//,' EXAMINE COLS ABOVE. KEEP HOW MANY IN EACH.')
      READ(3,*) CURV(KL,1),CURV(KL+1,1),CURV(KL+2,1)
  460 CONTINUE
      WRITE(4,501)
      DO 507 KNT=2,NRDGS+1
      WRITE(4,505) CURV(13,KNT)
  507 CONTINUE
      WRITE(4,506)
      READ(3,*) CURV(13,1)
C ** PROGRAM NOW HAS NUMBER OF COEFFTS AND COEFFTS STORED IN 'CURV'
C
C ******************************************************************
C CALCULATE COORDS OF ALL NODES REQUIRED FOR A NASTRAN QUAD4 SHELL
C ANALYSIS. STRATEGY BASED ON PRIMARY AND SECONDARY OR CONGRUENT NODE
C LINES. AT THE END OF THIS CALCULATION ALL COORDS RELATE TO AN
C INITIALLY PERFECT BEAM. IMPERFECTIONS ADDED LATER.
C ******************************************************************
C
C ** READ NO. LINES,ELS,NODES, PRIMARY NODE LINES,SUPPORT NODE
      READ(5,*) NLINS,NELS,NNODS,NPRIM,NODSUP
C ** INITIALISE COORD ARRAY
      DO 600 I=1,NNODS
      DO 600 J=1,5
      COORD(I,J)=0.0
  600 CONTINUE
      COORD(NODSUP,5)=1.0
C ** ENTER LOOP OVER PRIMARY LINES IN THE MESH
      DO 605 KPRIM=1,NPRIM
C ** READ LINE NAME, NO. NODES ON LINE, NO. CONGRT LINES, REAL SPC
C ** CODE FOR INTERIOR NODES ON LINE, FIRST NODE, INTEGER INCREMENTS
C ** BETWEEN NODES, X COORD OF FIRST NODE, POSITION ON CROSS SECTION
C ** RELATIVE TO FOLLOWING SKETCH
C
C               13 * 12 * 11 * 10 * 9
C                         *
C                         8
C                         *
```

G

```
C                          7
C                          *
C                          6
C                          *
C                 5 *  4 *3  *  2 * 1
C
      READ(5,*) LINPRI,NODES,NSAME,SPC,LINNOD(LINPRI,1),
     .(INCR(I),I=1,NODES-1),COORD(LINNOD(LINPRI,1),1),NPOSN
C ** READ BASIC DELTA VECTOR, DELTA FACTORS
      READ(5,*) DELTAX,DELTAY,DELTAZ,(FACTOR(I),I=1,NODES-1)
      XXINCR=DELTAX
C ** GET COORDS OF FIRST NODE FROM REFERENCE CROSS SECTION
      COORD(LINNOD(LINPRI,1),2)=REF(NPOSN,1)
      COORD(LINNOD(LINPRI,1),3)=REF(NPOSN,2)
      COORD(LINNOD(LINPRI,1),5)=FLOAT(NPOSN)
C  ** ENTER LOOP OVER NODES IN PRIMARY LINE TO GENERATE NODE NOS
C  ** AND COORDINATES
      DO 670 KNODE=2,NODES
      LINNOD(LINPRI,KNODE)=LINNOD(LINPRI,KNODE-1)+INCR(KNODE-1)
      NODCUR=LINNOD(LINPRI,KNODE)
      NODLAS=LINNOD(LINPRI,KNODE-1)
      COORD(NODCUR,1)=COORD(NODLAS,1)+DELTAX*FACTOR(KNODE-1)
      COORD(NODCUR,2)=COORD(NODLAS,2)+DELTAY*FACTOR(KNODE-1)
      COORD(NODCUR,3)=COORD(NODLAS,3)+DELTAZ*FACTOR(KNODE-1)
      COORD(NODCUR,5)=FLOAT(NPOSN)
      IF(KNODE.NE.NODES) COORD(NODCUR,4)=SPC
  670 CONTINUE
C  ** IF THERE ARE NO CONGRT LINES SKIP TO NEXT PRIMARY
      IF(NSAME.EQ.0) GO TO 605
C  ** ENTER LOOP OVER CONGRNT LINES
      DO 675 KSAME=1,NSAME
C  ** READ LINE NAME, REAL SPC CODE FOR 2ND TO PENULT NODE,
C  ** INTEGER DIFFERENCE BETWEEN NODES ON THIS LINE AND
C  ** CORRESPONDING NODES ON PRIMARY LINE, X COORD
C  ** DELTA BETWEEN THESE CORRESPONDING NODES,POSITN ON X SECTN
      READ(5,*) LSAME,SPC,NDIFF,DELTAX,NPOSN
C  ** ENTER LOOP OVER NODES IN CONGRNT LINE
      DO 675 KNODE=1,NODES
      LINNOD(LSAME,KNODE)=LINNOD(LINPRI,KNODE)+NDIFF
      NODCUR=LINNOD(LSAME,KNODE)
      NODLAS=LINNOD(LINPRI,KNODE)
      COORD(NODCUR,1)=COORD(NODLAS,1)+DELTAX
      COORD(NODCUR,2)=REF(NPOSN,1)
      COORD(NODCUR,3)=REF(NPOSN,2)
      IF(KNODE.NE.1.AND.KNODE.NE.NODES) COORD(NODCUR,4)=SPC
      COORD(NODCUR,5)=FLOAT(NPOSN)
  675 CONTINUE
  605 CONTINUE
C
C  *****************************************************
C  ALTER PREVIOUSLY CALCULATED GRID COORDINATES TO ALLOW
C  FOR INITIAL GEOMETRIC IMPERFECTIONS IN THE BEAM.
C  PRESENTLY RESTRICTED TO BOW IN ONLY ONE PLANE.
C  NAG ROUTINE EO2AEF USED TO EVALUATE BOW OFFSET AT GRID
C  POINTS.
C  *****************************************************
C
C ** LOOP THRO' ALL GRID POINTS TO ALLOW FOR IMPERFECTIONS
C ** NAG ROUTINE EO2AEF MUST BE CALLED FOR EACH GRID POINT SINCE
C ** EACH HAS AN UNIQUE COMBINATION OF CURVE NUMBER AND XBAR
      XMAX=POSRDG(NRDGS)
      XMIN=POSRDG(1)
      IFAIL=0
      DO 701 KGRID=1,NNODS
      XBAR=((COORD(KGRID,1)-XMIN)-(XMAX-COORD(KGRID,1)))/(XMAX-XMIN)
```

```
      NCURV=INT(COORD(KGRID,5))
      WRITE(4,771) NCURV,KGRID
  771 FORMAT(1X,I4,2X,I4)
      NPLUS1=IDINT(CURV(NCURV,1))
      DO 702 KNT=1,NPLUS1
      A(KNT)=CURV(NCURV,KNT+1)
  702 CONTINUE
      CALL E02AEF(NPLUS1,A,XBAR,P,IFAIL)
      COORD(KGRID,2)=COORD(KGRID,2)+P
  701 CONTINUE
C
C *****************************************************************
C GINO ROUTINE FOR SURFACE PLOT OF INITIALLY IMPERFECT WEB - FLANGES
C OMITTED FOR CLARITY.
C *****************************************************************
C
      WRITE(4,954)
  954 FORMAT('ENTER 1 = WEB SURF PLOT, 0 = NO PLOT')
      READ(3,*) KPLOT
      IF(KPLOT.EQ.0) GOTO 955
C  ** DETERMINE WHICH DEVICE IN USE
      WRITE(4,956)
  956 FORMAT(' SPECIFY DEVICE : 1=T4014 , 2=SIGMA , 3=BENSON , 4=HP')
      READ(3,*) NDEV
      GOTO(0,957,958,959),NDEV
      CALL T4014
      GOTO 960
  957 CALL S5600
      GOTO 960
  958 CALL B1302
      CALL DEVPAP(210.,297.,0)
      GOTO 960
  959 CALL HP747
      CALL CHASWI(1)
      CALL SHIFT2(150.,20.)
      CALL ROTAT2(90.0)
      CALL SCALE(0.5)
  960 CONTINUE
      DO 950 LOOP1=1,5
      SECPOS=3.0
      IF(LOOP1.EQ.2) SECPOS=6.0
      IF(LOOP1.EQ.3) SECPOS=7.0
      IF(LOOP1.EQ.4) SECPOS=8.0
      IF(LOOP1.EQ.5) SECPOS=11.0
      KNTAGR=0
      DO 951 NODLUP=1,NNODS
      IF(COORD(NODLUP,5).NE.SECPOS) GOTO 952
      KNTAGR=KNTAGR+1
      AZ(KNTAGR,LOOP1)=-COORD(NODLUP,2)
  952 CONTINUE
  951 CONTINUE
  950 CONTINUE
      WRITE(4,953)
  953 FORMAT(' TYPE IN VALUE OF FACTOR TO EXAGGERATE CONTOURS')
      READ(3,*) G
      YHIGH=HBAR-GMT
      CALL PICCLE
      CALL CHASIZ(0.01,0.01)
      CALL HEIRAT(G)
      CALL ISOFRA(2)
      CALL ISOPRJ(NODES,XMIN,XMAX,5,0.0,YHIGH,AZ,0,1134,W)
      CALL DEVEND
  955 CONTINUE
C
C *****************************************************************
```

```
C CALCULATE TWIST, COMP. FLANGE BOW, ETC. AT EACH EQUALLY SPACED
C LONGITUDINAL STATION. THE RESULTS ARE MEANINGLESS FOR RUNS OTHER
C THAN A REGULAR MESH THROUGHOUT. SKIP TO 751 IF KODE=0 IE. IF
C THIS IS A RUN FOR NASTRAN MESH GENERATION.
C ******************************************************************
C
      IF(KODE.EQ.0) GO TO 751
      NODE1=6
      NODE2=2
      NNGAPS=INT(POSRDG(NRDGS)/XXINCR)
      WRITE(6,768)
      WRITE(6,769)
C ** ENTER LOOP TO CALCULATE TWIST,COMPRESSION FLGE BOW,
C ** BREADTHS OF THE TENSION AND COMPRESSION FLANGE SEGMENTS
C ** ACCORDING TO THE FOLLOWING SKETCH
C **
C **      NODED ********* NODE1 ********** NODEC
C **              CBRYP      *      CBRYN
C **                         *
C **                         *
C **                         *
C **              TBRYP      *      TBRYN
C **      NODEB ********* NODE2 ********** NODEA
C **
C **                        Z 1
C **                          1
C **                          1
C **                  Y ----- X
      DO 750 KNT=1,NNGAPS+1
      NODEA=NODE2-1
      NODEB=NODE2+1
      NODEC=NODE1-1
      NODED=NODE1+1
      TYN=COORD(NODE2,2)-COORD(NODEA,2)
      TYP=COORD(NODEB,2)-COORD(NODE2,2)
      CYN=COORD(NODE1,2)-COORD(NODEC,2)
      CYP=COORD(NODED,2)-COORD(NODE1,2)
      TWIST=((COORD(NODE1,2)-COORD(NODE2,2))/(HBAR-GMT))*57.296
      TWIST=-TWIST
      OFFSET=COORD(NODE1,2)-COORD(6,2)
      WRITE(6,770) KNT,COORD(NODE1,1),TWIST,OFFSET,TYN,TYP,CYN,CYP
      STNDAT(KNT,1)=COORD(NODE1,1)
      STNDAT(KNT,2)=TWIST
      STNDAT(KNT,3)=OFFSET
      STNDAT(KNT,4)=TYN
      STNDAT(KNT,5)=TYP
      STNDAT(KNT,6)=CYN
      STNDAT(KNT,7)=CYP
      NODE1=NODE1+7
      NODE2=NODE2+7
  750 CONTINUE
  882 CONTINUE
C
C ******************************************************************
C GENERATE AND PRINT OUT DATA FOR FINAS BEAM ELEMENTS WITH REF. AXIS
C EITHER AT WEB/COMP. FLANGE JUNCTION OR AT SHEAR CENTRE.
C ******************************************************************
C
C**     READ NO OF FINAS ELEMENTS TO BE GENERATED, NFINAS
      WRITE(4,886)
      READ(3,*) NFINAS
      WRITE(6,850)
      WRITE(6,106)
      WRITE(4,900)
      READ(3,*) NPOSRF
```

I

J

```
      IF(NPOSRF.EQ.0) GOTO 902
C
C**     REFERENCE AXIS OF FINAS BEAM ELEMENT AT WEB/COMPRESSION
C**     FLANGE JUNCTION
C
      DO 852 KFINAS=1,NFINAS
C**    READ NAMES OF FIRST AND LAST STATS ON THIS ELEMENT
      WRITE(4,853)
      READ(3,*) NFIR,NLAS
      WRITE(6,854) KFINAS
C**    OUTPUT NODES DEFINING THE ELEMENT
      NODD1=KFINAS*2-1
      NODD2=NODD1+1
      NODD3=NODD2+1
      WRITE(6,856) NODD1,NODD2,NODD3
C**    CALCULATE COORDS FOR THE 3 DEFINING NODES - 1ST AND
C       LAST NODES ARE OK BUT IF NLAS-NFIR IS EVEN, THEN COORDS
C       ALREADY EXIST FOR THE MID STATION WHICH WILL FORM THE
C       MIDSIDE NODE. IF THE DIFF IS ODD THEN THE COORDS WILL BE
C       LINEARLY INTERPOLATED FROM ADJACENT NODES
      NGRID1=(NFIR-1)*7+6
      NGRID4=(NLAS-1)*7+6
C**     OUTPUT ELEMENT LENGTH
      FINLL=(COORD(NGRID4,1)-COORD(NGRID1,1))*1000.0
      WRITE(6,858) FINLL
      DO 860 NEVEN=2,50,2
      IF(NEVEN.EQ.(NLAS-NFIR)) GOTO 862
  860 CONTINUE
C**    IF YOU FALL IN HERE THEN (NLAS-NFIR) IS ODD
C**    NOW FIND THE STATIONS ABOVE AND BELOW THE EL MIDPT
      NBELOW=NFIR+(NLAS-NFIR-1)/2
      NABOVE=NBELOW+1
C**    CONVERT THE STATION LABELS NFIR, NBELOW, NABOVE,
C      NLAS INTO GRID POINTS RECOGNISABLE TO THE IMPERFN
C      MESH VIZ. NGRID1, NGRID2, ETC.
      NGRID2=(NBELOW-1)*7+6
      NGRID3=(NABOVE-1)*7+6
      XXMID=(COORD(NGRID1,1)+COORD(NGRID4,1))*500.0
      YYMID=(COORD(NGRID2,2)+COORD(NGRID3,2))*500.0
      ZZMID=(COORD(NGRID2,3))*1000.0
      GOTO 864
  862 CONTINUE
C**     FIND MID STATION AND CONVERT IT TO RECOGNISABLE GRID
      NMID=(NFIR+NLAS)/2
      NGRID2=(NMID-1)*7+6
      XXMID=COORD(NGRID2,1)*1000.0
      YYMID=COORD(NGRID2,2)*1000.0
      ZZMID=COORD(NGRID2,3)*1000.0
  864 CONTINUE
C**   OUTPUT THE GLOBAL X,Y,Z COORDS OF THE 3 NODES DEFINING
C     THIS ELEMENT
      WRITE(6,866) NODD1,(1000.*COORD(NGRID1,1)),
     .(1000.*COORD(NGRID1,2)),(1000.*COORD(NGRID1,3))
      WRITE(6,868) NODD2,XXMID,YYMID,ZZMID
      WRITE(6,868) NODD3,(COORD(NGRID4,1)*1000.),
     .(COORD(NGRID4,2)*1000.),(COORD(NGRID4,3)*1000.)
C
C**   START ANALYSING THE AVERAGE SECTION FOR THIS ELEMENT AND
C     RELATE THE SEGMENT END NODES TO THE LOCAL AXES S,T (S
C     VERTICAL, T +VE IN -VE Y DIRECTION) WITH ORIGIN AT THE
C     WEB/COMPRESION FLANGE JUNCTION
C
      AVTWST=0.0
      AVETYN=0.0
      AVETYP=0.0
```

```
      AVECYN=0.0
      AVECYP=0.0
      DO 870 KONT=NFIR,NLAS
      AVTWST=AVTWST+STNDAT(KONT,2)
      AVETYN=AVETYN+STNDAT(KONT,4)
      AVETYP=AVETYP+STNDAT(KONT,5)
      AVECYN=AVECYN+STNDAT(KONT,6)
      AVECYP=AVECYP+STNDAT(KONT,7)
  870 CONTINUE
      NOGAPS=NLAS-NFIR+1
      RNGAPS=FLOAT(NOGAPS)
      AVTWST=AVTWST/RNGAPS
      AVETYN=AVETYN/RNGAPS
      AVETYP=AVETYP/RNGAPS
      AVECYN=AVECYN/RNGAPS
      AVECYP=AVECYP/RNGAPS
C**   WRITE AVTWST, AVETYN, AVETYP, ETC.
      WRITE(6,872) AVTWST
      WRITE(6,874) (AVECYP*1000.0),(AVECYN*1000.0)
      WRITE(6,876) (AVETYP*1000.0),(AVETYN*1000.0)
C**   THE BASIC EXTERNAL FUNCTIONS SIN AND COS OPERATE ON
C     ARGUMENTS EXPRESSED IN RADIANS RATHER THAN DEGREES
C     SO CONVERT AVTWST TO RAD. THEY MUST BE DECLARED IN
C     AN EXTERNAL STATEMENT.
C
C**   THE S AND T LOCAL COORDS WILL BE DENOTED BY PREFIXING
C     THE SEGMENT NODE NAME (EG. S1) BY EITHER S OR T EG.
C     SS1 IS THE S COORD OF SEGMENT NODE S1
      AVTWST=AVTWST/57.29578
C**   CALCULATE INCREMENTAL COORDS FOR SEGMENT NODES
      DSS4=-(AVECYN*SIN(AVTWST))
      DTS4=AVECYN*COS(AVTWST)
      DSS6=AVECYP*SIN(AVTWST)
      DTS6=-(AVECYP*COS(AVTWST))
      DSS2=-((HBAR-GMT)*COS(AVTWST))
      DTS2=-((HBAR-GMT)*SIN(AVTWST))
      DSS1=-(AVETYN*SIN(AVTWST))
      DTS1=AVETYN*COS(AVTWST)
      DSS3=AVETYP*SIN(AVTWST)
      DTS3=-(AVETYP*COS(AVTWST))
      TS5=0.0
      SS5=0.0
      TS4=(TS5+DTS4)*1000.
      SS4=(SS5+DSS4)*1000.
      TS6=(TS5+DTS6)*1000.
      SS6=(SS5+DSS6)*1000.
      TS2=(TS5+DTS2)*1000.
      SS2=(SS5+DSS2)*1000.
      TS1=TS2+DTS1*1000.
      SS1=SS2+DSS1*1000.
      TS3=TS2+DTS3*1000.
      SS3=SS2+DSS3*1000.
      KKK=1
      WRITE(6,878)
      WRITE(6,880) KKK,SS1,TS1
      KKK=KKK+1
      WRITE(6,880) KKK,SS2,TS2
      KKK=KKK+1
      WRITE(6,880) KKK,SS3,TS3
      KKK=KKK+1
      WRITE(6,880) KKK,SS4,TS4
      KKK=KKK+1
      WRITE(6,880) KKK,SS5,TS5
      KKK =KKK+1
      WRITE(6,880) KKK,SS6,TS6
```

```
  852 CONTINUE
      GOTO 904
C
C**     REF. AXIS OF FINAS BEAM ELEMENT AT SHEAR CENTRE
C
  902 CONTINUE
      DO 906 KFINAS=1,NFINAS
C**    READ NAMES OF FIRST AND LAST STATS ON THIS ELEMENT
      WRITE(4,853)
      READ(3,*) NFIR,NLAS
      WRITE(6,854) KFINAS
C**    OUTPUT NODES DEFINING THE ELEMENT
      NODD1=KFINAS*2-1
      NODD2=NODD1+1
      NODD3=NODD2+1
      WRITE(6,856) NODD1,NODD2,NODD3
C**    CALCULATE COORDS FOR THE 3 DEFINING NODES - 1ST AND
C       LAST NODES ARE OK BUT IF NLAS-NFIR IS EVEN, THEN COORDS
C       ALREADY EXIST FOR THE MID STATION WHICH WILL FORM THE
C       MIDSIDE NODE. IF THE DIFF IS ODD THEN THE COORDS WILL BE
C       LINEARLY INTERPOLATED FROM ADJACENT NODES
      NGRD1A=(NFIR-1)*7+2
      NGRD1B=(NFIR-1)*7+6
      NGRD4A=(NLAS-1)*7+2
      NGRD4B=(NLAS-1)*7+6
C**     OUTPUT ELEMENT LENGTH
      FINLL=(COORD(NGRD4A,1)-COORD(NGRD1A,1))*1000.0
      WRITE(6,858) FINLL
      DO 908 NEVEN=2,50,2
      IF(NEVEN.EQ.(NLAS-NFIR)) GOTO 910
  908 CONTINUE
C**    IF YOU FALL IN HERE THEN (NLAS-NFIR) IS ODD
C**    NOW FIND THE STATIONS ABOVE AND BELOW THE EL MIDPT
      NBELOW=NFIR+(NLAS-NFIR-1)/2
      NABOVE=NBELOW+1
C**    CONVERT THE STATION LABELS NFIR, NBELOW, NABOVE,
C      NLAS INTO GRID POINTS RECOGNISABLE TO THE IMPERFN
C      MESH VIZ. NGRID1, NGRID2, ETC.
      NGRD2A=(NBELOW-1)*7+2
      NGRD2B=(NBELOW-1)*7+6
      NGRD3A=(NABOVE-1)*7+2
      NGRD3B=(NABOVE-1)*7+6
      XXMID=(COORD(NGRD1A,1)+COORD(NGRD4A,1))*500.0
      YYMID=(COORD(NGRD2A,2)+COORD(NGRD2B,2)+COORD(NGRD3A,2)+
     .COORD(NGRD3B,2))*250.0
      ZZMID=(COORD(NGRD2A,3)+COORD(NGRD2B,3))*500.0
      GOTO 912
  910 CONTINUE
C**     FIND MID STATION AND CONVERT IT TO RECOGNISABLE GRID
      NMID=(NFIR+NLAS)/2
      NGRD2A=(NMID-1)*7+2
      NGRD2B=(NMID-1)*7+6
      XXMID=COORD(NGRD2A,1)*1000.0
      YYMID=(COORD(NGRD2A,2)+COORD(NGRD2B,2))*500.0
      ZZMID=(COORD(NGRD2A,3)+COORD(NGRD2B,3))*500.0
  912 CONTINUE
C**   OUTPUT THE GLOBAL X,Y,Z COORDS OF THE 3 NODES DEFINING
C     THIS ELEMENT
      XXEND1=COORD(NGRD1A,1)*1000.0
      YYEND1=(COORD(NGRD1A,2)+COORD(NGRD1B,2))*500.0
      ZZEND1=(COORD(NGRD1A,3)+COORD(NGRD1B,3))*500.0
      XXEND4=COORD(NGRD4A,1)*1000.0
      YYEND4=(COORD(NGRD4A,2)+COORD(NGRD4B,2))*500.0
      ZZEND4=(COORD(NGRD4A,3)+COORD(NGRD4B,3))*500.0
      WRITE(6,866) NODD1,XXEND1,YYEND1,ZZEND1
```

```
      WRITE(6,868) NODD2,XXMID,YYMID,ZZMID
      WRITE(6,868) NODD3,XXEND4,YYEND4,ZZEND4
C
C**   START ANALYSING THE AVERAGE SECTION FOR THIS ELEMENT AND
C     RELATE THE SEGMENT END NODES TO THE LOCAL AXES S,T (S
C     VERTICAL, T +VE IN -VE Y DIRECTION) WITH ORIGIN AT THE
C     SHEAR CENTRE
C
      AVTWST=0.0
      AVETYN=0.0
      AVETYP=0.0
      AVECYN=0.0
      AVECYP=0.0
      DO 914 KONT=NFIR,NLAS
      AVTWST=AVTWST+STNDAT(KONT,2)
      AVETYN=AVETYN+STNDAT(KONT,4)
      AVETYP=AVETYP+STNDAT(KONT,5)
      AVECYN=AVECYN+STNDAT(KONT,6)
      AVECYP=AVECYP+STNDAT(KONT,7)
  914 CONTINUE
      NOGAPS=NLAS-NFIR+1
      RNGAPS=FLOAT(NOGAPS)
      AVTWST=AVTWST/RNGAPS
      AVETYN=AVETYN/RNGAPS
      AVETYP=AVETYP/RNGAPS
      AVECYN=AVECYN/RNGAPS
      AVECYP=AVECYP/RNGAPS
C**   WRITE AVTWST, AVETYN, AVETYP, ETC.
      WRITE(6,872) AVTWST
      WRITE(6,874) (AVECYP*1000.0),(AVECYN*1000.0)
      WRITE(6,876) (AVETYP*1000.0),(AVETYN*1000.0)
C**   THE BASIC EXTERNAL FUNCTIONS SIN AND COS OPERATE ON
C     ARGUMENTS EXPRESSED IN RADIANS RATHER THAN DEGREES
C     SO CONVERT AVTWST TO RAD. THEY MUST BE DECLARED IN
C     AN EXTERNAL STATEMENT.
C
C**   THE S AND T LOCAL COORDS WILL BE DENOTED BY PREFIXING
C     THE SEGMENT NODE NAME (EG. S1) BY EITHER S OR T EG.
C     SS1 IS THE S COORD OF SEGMENT NODE S1
      AVTWST=AVTWST/57.29578
C  ** CALCULATE COMPTS OF VECTOR V FOR NASTRAN RUNS. THIS
C     DEFINES THE ATTITUDE OF THE LOCAL AXES W.R.T. THE GLOBAL
C     AXES X,Y,Z.
      YOFSET=YYEND4-YYEND1
      THETAZ=ATAN(YOFSET/FINLL)
      SINX=SIN(AVTWST)
      COSX=COS(AVTWST)
      SINZ=SIN(THETAZ)
      COSZ=COS(THETAZ)
      XGLOB=20.0*(COSZ-COSX*SINZ)
      YGLOB=20.0*(SINZ+COSX*COSZ)
      ZGLOB=20.0*SINX
C  ** OUTPUT COMPTS OF VECTOR V FOR NASTRAN
      WRITE(6,877) XGLOB,YGLOB,ZGLOB
C**   CALCULATE INCREMENTAL COORDS FOR SEGMENT NODES
      DSS4=-(AVECYN*SIN(AVTWST))
      DTS4=AVECYN*COS(AVTWST)
      DSS6=AVECYP*SIN(AVTWST)
      DTS6=-(AVECYP*COS(AVTWST))
      DSS2=-((HBAR-GMT)*COS(AVTWST))
      DTS2=-((HBAR-GMT)*SIN(AVTWST))
      DSS1=-(AVETYN*SIN(AVTWST))
      DTS1=AVETYN*COS(AVTWST)
      DSS3=AVETYP*SIN(AVTWST)
      DTS3=-(AVETYP*COS(AVTWST))
```

```
      TS5=0.0
      SS5=0.0
      TS4=(TS5+DTS4)*1000.
      SS4=(SS5+DSS4)*1000.
      TS6=(TS5+DTS6)*1000.
      SS6=(SS5+DSS6)*1000.
      TS2=(TS5+DTS2)*1000.
      SS2=(SS5+DSS2)*1000.
      TS1=TS2+DTS1*1000.
      SS1=SS2+DSS1*1000.
      TS3=TS2+DTS3*1000.
      SS3=SS2+DSS3*1000.
      DSS2=-500.0*DSS2
      DTS2=-500.0*DTS2
      SS1=SS1+DSS2
      SS2=SS2+DSS2
      SS3=SS3+DSS2
      SS4=SS4+DSS2
      SS5=SS5+DSS2
      SS6=SS6+DSS2
      TS1=TS1+DTS2
      TS2=TS2+DTS2
      TS3=TS3+DTS2
      TS4=TS4+DTS2
      TS5=TS5+DTS2
      TS6=TS6+DTS2
      KKK=1
      WRITE(6,878)
      WRITE(6,880) KKK,SS1,TS1
      KKK=KKK+1
      WRITE(6,880) KKK,SS2,TS2
      KKK=KKK+1
      WRITE(6,880) KKK,SS3,TS3
      KKK=KKK+1
      WRITE(6,880) KKK,SS4,TS4
      KKK=KKK+1
      WRITE(6,880) KKK,SS5,TS5
      KKK =KKK+1
      WRITE(6,880) KKK,SS6,TS6
  906 CONTINUE
  904 CONTINUE
      WRITE(4,884)
      READ(3,*) KMORE
      IF(KMORE.EQ.1) GOTO 882
  751 CONTINUE
C  **************************************************************
C
C     GENERATE NASTRAN QUAD4 ELEMENT NAMES AND CONNECTIVITY DATA
C
C  **************************************************************
C
C  ** READ NO. OF PRIMARY ELEMENT LINES INTO NPRIM
      READ(5,*) NPRIM
C  ** ENTER LOOP OVER PRIMARY ELEMENT LINES
      DO 801 KPRIM=1,NPRIM
C  ** READ NO. ELS ON LINE, EL LINE NAME, LOWER\RIGHT BOUNDING
C  ** NODE LINE, OTHER BOUNDING NODE LINE, LIST OF ELS ON LINE,
C  ** NO. CONGRNT LINES
      READ(5,*) NOELS,LINPRI,LINE1,LINE2,(LINEL(LINPRI,I),I=1,NOELS),
     .NSAME
      DO 802 KELS=1,NOELS
      NELCUR=LINEL(LINPRI,KELS)
      K2=KELS+1
      WRITE(6,803) NELCUR,LINNOD(LINE1,KELS),LINNOD(LINE1,K2),
     .LINNOD(LINE2,K2),LINNOD(LINE2,KELS)
```

K

```
  802 CONTINUE
      IF(NSAME.EQ.0) GO TO 801
C  ** ENTER LOOP OVER CONGRUENT LINES
      DO 804 KSAME=1,NSAME
C  ** READ INTEGER DIFFERENCE BETWEEN CORRESPONDING ELEMENTS
C  ** ON THIS LINE AND PRIMARY LINE, BOUNDING NODE LINES
      READ(5,*) NDIFF,LINE1,LINE2
C  ** ENTER LOOP OVER CONGRUENT ELEMENTS IN LINE LSAME
      DO 804 KELS=1,NOELS
      NELCUR=LINEL(LINPRI,KELS)+NDIFF
      K2=KELS+1
      WRITE(6,803) NELCUR,LINNOD(LINE1,KELS),LINNOD(LINE1,K2),
     .LINNOD(LINE2,K2),LINNOD(LINE2,KELS)
  804 CONTINUE
  803 FORMAT(' CQUAD4',2X,I4,4X,'20',6X,I4,3(4X,I4))
  801 CONTINUE
C  **  PRINT OUT NODAL DATA IN A FORM ACCEPTABLE TO NASTRAN
      DO 810 KNODE=1,NNODS
      KSPC=INT(COORD(KNODE,4))
      WRITE(6,811) KNODE,(COORD(KNODE,I),I=1,3),KSPC
  810 CONTINUE
C
C     *********************************
C     FORMAT STATEMENTS
C     *********************************
C
  811 FORMAT(1X,'GRID',4X,I4,12X,3(F8.6),8X,I6)
  105 FORMAT(//,35H1I M P E R F E C T I O N   D A T A)
  106 FORMAT(1H0,34('*'))
  107 FORMAT(//////,23H IMPERFECTIONS FOR BEAM,28X,14HYOUNGS MODULUS,
     .6X,3H=  ,E11.5)
  108 FORMAT(11H0SPAN     =,5X,F6.4,29X,3HGMT,17X,3H=  ,F8.6)
  109 FORMAT(15H0OVERALL LENGTH,36X,12HBEAM SELF WT,8X,3H=  ,E11.5)
  110 FORMAT(5H0DATE,46X,18HNO OF SAMPLING PTS,2X,3H=  ,I3)
  111 FORMAT(12H0UNITS : N,M,39X,18HMEAN OVERALL DEPTH,2X,3H=  ,F8.6)
  112 FORMAT(1H0,50X,7HI MINOR,13X,3H=  ,E11.5)
  113 FORMAT(1H1,///,31X,17HORIGINAL READINGS)
  114 FORMAT(1H0,48HRDG NO   DIST FROM    RDG C1    RDG TI    RDG W1,
     .40H    RDG W2    RDG W3    COMP FL    TENS FL)
  115 FORMAT(1X,9X,8HEND  "0",54X,5HBRDTH,6X,5HBRDTH,/)
  116 FORMAT(1X,2X,I2,6X,F9.6,7(2X,F8.5))
  117 FORMAT(1H0,50X,7HI MAJOR,13X,3H=  ,E11.5)
  190 FORMAT(1X,//////,17X,34HREADINGS  CORRECTED  FOR  SELF  WT,
     .15H  :  DELTAC =  ,F9.6)
  191 FORMAT(1H0,6HRDG NO,5X,5HDELTA,6X,28HRDG C1    RDG T1    RDGW1   ,
     .18H  RDG W2    RDG W3,/)
  192 FORMAT(1X,2X,I2,5X,7(1X,F9.6))
  207 FORMAT(1H1,///,17X,42HREADINGS  ADJUSTED  REL  TO  COPLANAR  WEB,
     .10H  VERTICES)
  208 FORMAT(1H0,6HRDG NO,6X,30HRDG T1    RDG W1    RDG T2    ,
     .36HRDG W2    RDG C1    RDG W3    RDG C2,/)
  768 FORMAT(//////,1X,'FOLLOWING RESULTS HOLD ONLY FOR INITIAL RUN')
  769 FORMAT(51H STATION NO     X-COORD     TWIST(DEG)     COMP BOW,
     .45H   T.FL(Y -)  T.FL(Y +)  C.FL(Y -)  C.FL(Y +))
  770 FORMAT(3X,I4,6X,F8.5,5X,F10.6,4X,F9.6,1X,4(2X,F9.6))
  850 FORMAT('1',///,' FINAS ELEMENT DATA')
  853 FORMAT(' TYPE IN FIRST & LAST STATIONS DEFINING ELEMENT')
  854 FORMAT(///,' ***  FINAS ELEMENT',I4,'  ***')
  856 FORMAT(/,' NODES - FIRST, MID, LAST',3I4)
  858 FORMAT(' ELEMENT LENGTH (MM)  ',F7.2)
  866 FORMAT(/,' NODAL COORDS OF ENDS & MID',I4,3(3X,F9.4))
  868 FORMAT(27X,I4,3(3X,F9.4))
  872 FORMAT(/,' TWIST AVERAGED OVER ELEMENT LENGTH  ',F9.6,' DEG')
  874 FORMAT(/,' AVE FLGE SEGMENT BRDTHS: COMP Y+  ',F6.3,4X,
     .'Y-  ',F6.3)
```

```
876 FORMAT(26X,'TENS Y+  ',F6.3,4X,'Y-  ',F6.3)
877 FORMAT(/,' GLOBAL X,Y,Z COMPTS OF NASTRAN VECTOR V',3(2X,F8.4))
878 FORMAT(/,' SEGMENT DATA')
880 FORMAT(5X,' SEGMENT NODE',I4,'  S=',F9.4,'    T=',F9.4)
884 FORMAT(' ANOTHER MESH...  ENTER 1=YES, O=NO')
886 FORMAT(' HOW MANY ELEMENTS')
900 FORMAT(' ENTER O = REF. AXIS AT CENT OR 1 = WEB/C FL JN.')
    STOP
    END
```

APPENDIX III

Error in Measuring "Midspan" Deflections at a Point 10mm from Midspan of Test Beams

Appendix III - The Difference between Elastic Vertical Deflections of a Beam at Midspan and Those at a Point 10mm from Midspan

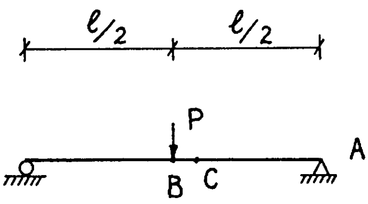

Using the moment area method to calculate the ratio of the deflection of point C to that of point B (both deflections relative to their undeflected positions),

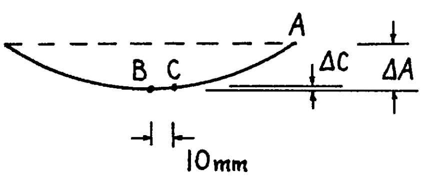

$$\Delta_A = \frac{Pl^3}{48EI}$$

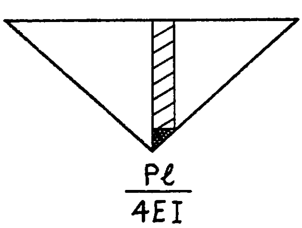

Now,

slope of $\frac{M}{EI}$ line $= \frac{P}{2EI}$

$\therefore$ drop in $\frac{M}{EI}$ value in 10mm $= \frac{5P}{EI}$

where E and I are in mm units

Area of solid shaded triangle in $\frac{M}{EI}$ diagram $= \frac{1}{2} \times \frac{5P}{EI} \times 10 = \frac{25P}{EI}$

and that of hatched rectangle $= 10\left(\frac{Pl}{4EI} - \frac{5P}{EI}\right) = \frac{10P}{EI}\left(\frac{l}{4} - 5\right)$

and hence first moments of these regions about C

$$= \left(\frac{25P}{EI} \times \frac{20}{3}\right) + \frac{10P}{EI}\left(\frac{l}{4} - 5\right) \times 5$$

$$= \frac{500P}{3EI} + \frac{50P}{EI}\left(\frac{l}{4} - 5\right)$$

Hence $\Delta_A - \Delta_C = \frac{Pl^3}{48EI} - \frac{500P}{3EI} - \frac{50P}{EI}\left(\frac{l}{4} - 5\right)$

and thus
$$\frac{\Delta_A - \Delta_C}{\Delta_A} = \frac{\frac{l^3}{48} - \frac{500}{3} - 50\left(\frac{l}{4} - 5\right)}{\frac{l^3}{48}}$$

$$= 1 + \frac{4000}{l^3} - \frac{600}{l^2}$$

for $l = 600$, $\frac{\Delta_A - \Delta_C}{\Delta_A} = 0.9984$

$l = 800$, - do.- $= 0.9991$

$l = 1000$, - do.- $= 0.9994$

APPENDIX IV

Corrections to be Applied to Measured

Vertical Deflection of Test Beams

Appendix IV(a) - A Twist Correction to be Applied to Measured Vertical Deflections of Beams to give True Centroidal Deflections

In this derivation, the following notation is employed:

Δ_{meas} = measured vertical deflection of ball at midspan
Δ_{inc} = vertical deflection of ball due to beam deformation only
Δ_G = vertical deflection of beam centroid
φ = angle of twist (clockwise +ve)
h_G = distance from beam centroid to centroid of ball
τ = required centroidal twist correction

The positions of the beam cross-section after the $(n - 1)^{th}$ and n^{th} load increments are shown in the diagram. The centroid of the steel ball is distant h_G from the section centroid.

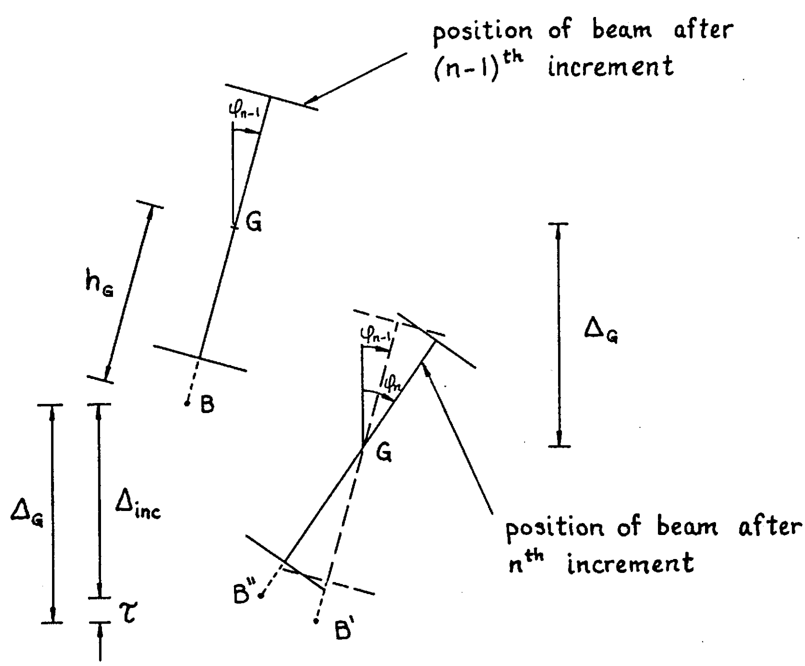

In the following derivation, it is assumed that the value Δ_{inc} is the vertical displacement of the ball corrected for the effects of support movement.

As a result of the n^th^ increment of load the ball moves from position B to position B", the level difference between these two positions being Δ_{inc}. The corresponding change in angle of twist is (φ_n - φ_{n-1}). It can be seen that the vertical movement of the centroid of the section falls vertically by an amount Δ_G, which is also the level difference between points B and B' in the diagram. The deflection Δ_G is greater than Δ_{inc} by an amount τ which is dependent on the change in angle of twist ie. $\Delta_G = \Delta_{inc} + \tau$

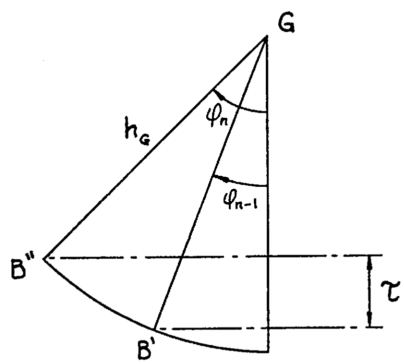

The diagram on the left shows that

$$\tau = h_G \left(\cos \varphi_{n-1} - \cos \varphi_n\right)$$

where φ is considered to be positive measured in a clockwise sense in the diagrams.

Hence the centroidal deflection is

$$\Delta_G = \Delta_{inc} + h_G \left(\cos \varphi_{n-1} - \cos \varphi_n\right)$$

Appendix IV(b) - Vertical Deflection of Beam Compression Flange relative to Bracing Forks

Unlike the two-stage correction derived in Appendix IV(a) for the determination of centroidal deflections of the midspan section of a test beam relative to its end supports, calculation of the vertical deflection of the compression flange relative to the bracing forks does not require the measured beam deflection to be corrected for average support deflection. This is because support deflections increase the movement of the flange relative to the bracing box and hence contribute to the total relative movement between flange and bracing forks. In terms of the notation adopted in Appendix IV(a), the compression flange deflection Δ_{CF} is dependent on Δ_{meas} and not Δ_{inc} .

The twist correction to be added algebraically to the measured increments of deflection Δ_{meas} increases from the value τ in Appendix IV(a) to a value τ_1 defined as

$$\tau_1 = \tau \frac{h_{CF}}{h_G}$$

where h_G is as defined in Appendix IV(a) and h_{CF} is the distance from the centre of the ball to the web/compression flange junction as shown in the diagram.

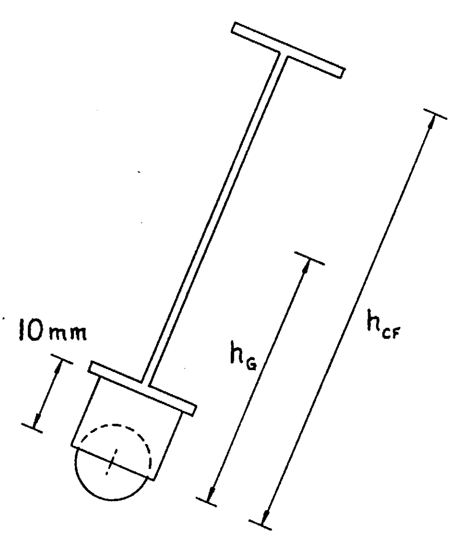

In Appendix IV(a) it was shown that the corrected incremental centroidal deflection Δ_G was

$$\Delta_G = \Delta_{inc} + \tau$$

The corresponding equation for the incremental vertical deflection of the compression flange (Δ_{CF}) relative to the bracing box is

$$\Delta_{CF} = \Delta_{meas} + \tau_1$$

The summation of incremental Δ_{CF} values ($\Sigma\, \Delta_{CF}$) also gives the required total vertical deflection of the bracing forks relative to their initial position in order to maintain constant restraint stiffness during the test.

An example of the use of the equations derived in Appendices IV(a) and IV(b) is presented in Appendix IV(c) where actual test measurements (from model beam test 6 in the main series of tests) have been used to demonstrate the method of calculation. There, the calculation of Δ_{CF} values has been labelled "Correction 3".

Appendix IV(c) - Example Calculation showing Corrections Applied to Results of Model Beam Test 6 to Allow for Support Deflections and the Twist Corrections τ and τ_1 derived in Appendices IV(a) and IV(b)

Test 6

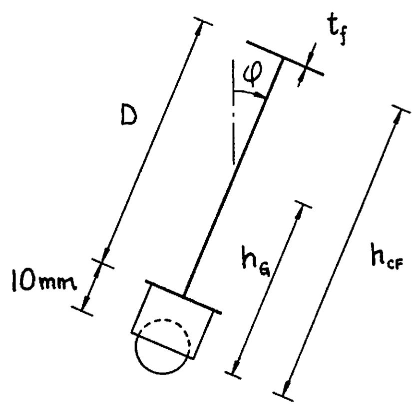

D = mean overall depth of beam section = 49.862mm

t_f = mean flange thickness = 0.9155mm

h_G = ½D + 10mm = 34.931mm

h_{CF} = h_G + ½(D - t_f) = 59.404mm

τ magnification factor = $\dfrac{h_{CF}}{h_G}$ = 1.701

A brief explanation of the corrections shown in the accompanying table follows.

Correction 1 - Correction of Measured Midspan Deflections for Support Deflection

The cumulative midspan deflection $\Sigma\Delta_{meas}$ in col. 3 (as measured by the dial gauge of Fig. 4.10) is reduced by the average total support deflection of col. 6 to yield the cumulative vertical deflection of the midspan ball (Fig. 4.10) relative to the beam supports (col. 7).

Correction 2

Values of ball deflection in col. 7 represent $\Sigma\Delta_{inc}$ with Δ_{inc}

as defined in Appendix IV(a). Col. 8 shows the incremental values Δ_{inc} which compose the col. 7 values previously calculated in correction 1. The centroidal twist correction τ (col. 10) is calculated from angles of twist at midspan (col. 9) according to the expression for τ developed in Appendix IV(a). These values of τ are then added to the Δ_{inc} values to obtain the corresponding increments of centroidal deflection Δ_G in col. 11 and cumulative centroidal deflection $\Sigma\Delta_G$ in col. 12. Comparison of col. 7 and col. 12 values shows the effect of the twist correction. For small angles of twist such as that shown for load increment 17, the effect of the twist correction is seen to be negligible; for larger angles of twist such as that of load increment 19, the correction is more significant. In general, the effect of correction 2 is only appreciable for beams at the onset of instability or in the post-buckling condition when angles of twist become significant. Consequently, for beams with fully effective compression flange restraint at midspan, where angles of twist are typically small, the twist correction is insignificant.

Correction 3

The incremental values Δ_{meas} in col. 13 are derived from the total values in col. 3 and the twist correction τ_1 (col. 14) applied as described in Appendix IV(b). Col. 16 shows the total vertical deflection of the bracing forks required to maintain constant restraint stiffness during the test. In practice, the forks are lowered prior to application of the next load increment, eg. a total fork deflection of 4.60mm (as measured by the dial gauge of Figs. 4.16 - 4.18) would be enforced prior to application of load increment 19. In this way the correct restraint stiffness is achieved at the start of each load increment. Due to the dependence of τ_1 on τ, correction 3 is only of importance for significant angles of twist.

The following table of experimental readings is taken from the post-buckling phase during model beam Test 6. Steps in the correction of apparent vertical deflections for the effects of support deflection and beam twist are illustrated.

1	2	3	4	5	6	7	8	9	10	11	12	13	14	15	16
Load incr. no.	Total applied load P (N)	Total meas. vert. defln. @ midspan $\Sigma \Delta_{meas}$ (mm)	Total vert. defln. of Support A (mm)	Total vert. defln. of Support B (mm)	Ave. total support defln. (mm)	Total vert. defln. of ball due to beam deformation only $\Sigma \Delta_{inc}$ (mm)	Δ_{inc} (mm)	Total angle of twist from the vert. φ (clockwise +ve) * (rad)	Centroidal twist correction τ (mm)	$\Delta_G = \Delta_{inc} + \tau$ (mm)	Corrected vert. defln. of beam centroid $\Sigma \Delta_G$ (mm)	Incr. of meas. vert. defln.@ midspan Δ_{meas} (mm)	Compr. flange twist correction $\tau_1 = 1.701\tau$ (see App. IV(c)) (mm)	Actual vert. defln. of compr. flange, rel. to bracing box on this incr. $\Delta_{CF} = \Delta_{meas} + \tau_1$ (mm)	Reqd. total vert. defln. of bracing forks to maintain constant restraint stiffness $\Sigma \Delta_{CF}$ (mm)
17	1557.3	4.32	0.28	0.26	0.27	4.05	.305	-.03195	0.013	.318	4.0678	.31	.0221	.332	4.35
18	1550.2	4.53	0.29	0.27	0.28	4.25	.20	-.04710	0.0209	.2209	4.2887	.21	.0356	.246	4.60
19	1484.4	4.88	0.29	0.28	0.285	4.595	.345	-.10198	0.1427	.4877	4.7764	.35	.2427	.593	5.19

CORRECTION 1 CORRECTION 2 CORRECTION 3

* Angle of twist is obtained from measured lateral deflections of the flanges.

APPENDIX V

Strain-Bending Moment Relationships

for Bracing Prongs

Appendix V - Determination of Moment-Strain Relationships to be Used in Deriving Brace Forces from Measured Bracing Fork Strains which exceed the Yield Strain of the Prong Steel

The average stress-strain curve for the Stubbs steel rod used for the bracing prongs is shown in Fig. 4.24 . A tri-linear approximation to this curve is also shown, in which the three linear portions can be described by the following equations:

(i) for $\epsilon_{max} \leqslant 0.0026$, $\sigma = 196915\,\epsilon$ (σ in N/mm^2)

(ii) $0.0026 < \epsilon_{max} \leqslant 0.0044$, $\sigma = 84667\,\epsilon + 291.8$ (-do.-)

(iii) $\epsilon_{max} > 0.0044$, $\sigma = 17113\,\epsilon + 589.1$ (-do.-)

Considering separately cases (ii) and (iii), it is possible to derive theoretical expressions which relate measured maximum inelastic bending strains ϵ_{max} (defined in Section 4.4.3) to corresponding bending moments 'M' in the prong at the gauge section.

$0.0026 < \epsilon_{max} \leqslant 0.0044$

In the following derivation, reference will be made to zones ① and ② on the cross-section of the bracing prong as shown in Figs. (a) and (b).

In zone ① , the bending stress is related to bending strain by

$$\sigma = 196915\,\epsilon \quad \text{from above,}$$

whilst in zone ② , the relationship

$$\sigma = 84667\,\epsilon + 291.8 \quad \text{applies.}$$

The parameter y_1 will be used to denote the distance from the neutral axis to the edge of zone ① . 'r' represents the radius of the bracing prong.

If the symbol 'y' is used to represent the perpendicular distance of a point in the cross-section from the neutral axis then it can be seen from Fig. (a) that the strain at $y = y_1$ is $\epsilon_y = 0.0026$ and

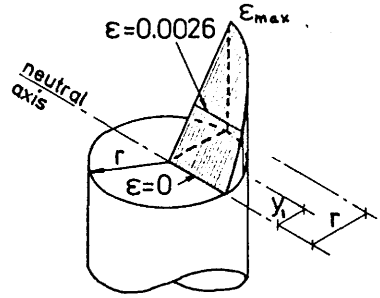

Fig. (a) : distribution of bending strains over one quadrant of the cross-section of the bracing prong

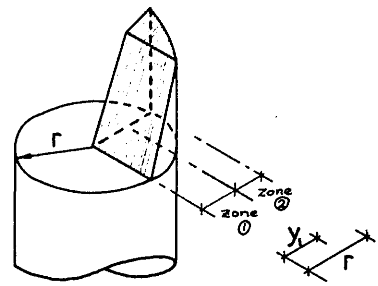

Fig. (b) : corresponding distribution of bending stresses

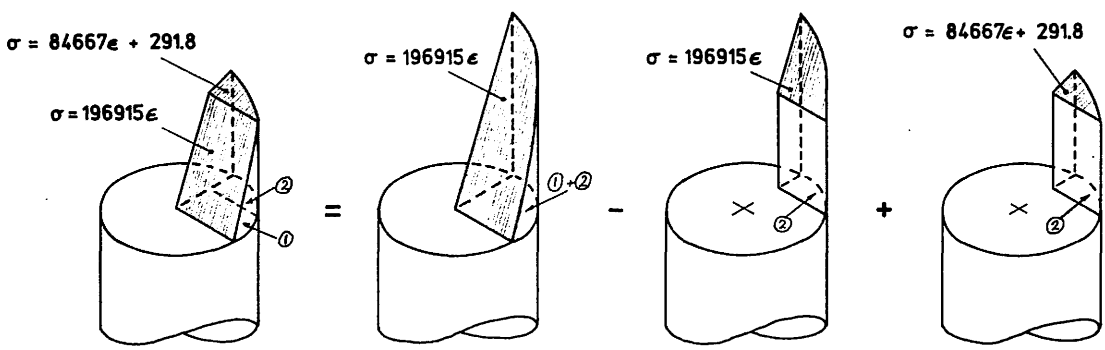

Fig. (c) : stress "equation" for bending stresses on a quadrant of the cross-section

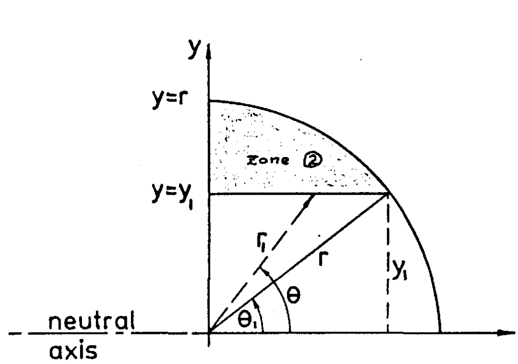

Fig. (d) : geometry of quadrant of cross-section hence, because the distribution of strain is linear,

$$y_1 = \frac{0.0026\ r}{\epsilon_{max}}$$

The bending moment on the cross-section of the prong arises from bending stresses distributed over the cross-section in a manner typified by those for the quadrant in Fig. (b). Consequently bending moment on the section

$$= 4 \left\{ \begin{array}{l} \text{bending moment arising from bending stresses of} \\ \text{Fig. (b)} \end{array} \right\}$$

In calculating the bending moment due to the stresses acting over a quadrant, the stress "equation" of Fig. (c) will be employed and the bending moments associated with each of the three "terms" on the right hand side of this equation evaluated. For the first "term", beam theory predicts:

$$\text{bending moment over full cross-section} = \frac{\pi r^3}{4}(196915\ \epsilon_{max})$$

$$M_{1st\ term} = 154657 r^3 \epsilon_{max}$$

For the second "term", the elastic stress-strain relationship

$$\sigma = 196915\ \epsilon$$

can be expressed in terms of dimensions y and y_1 by noting that

$$\epsilon = \frac{0.0026\ y}{y_1}$$

Hence $$\sigma = \frac{511.98\ y}{y_1}$$

The bending moment over the full cross-section produced by typical bending stresses of "term 2" in Fig. (c) can be deduced from examination of the geometry of the quadrant shown in Fig. (d) and by noting that the bending moment due to the above stresses σ acting over zone 2 can be represented by a polar integral in which θ and r_1 (Fig. (d)) are the integration variables. The limits on θ and r_1 in this integration are clearly

$$\theta_1 \leqslant \theta \leqslant \frac{\pi}{2}$$

$$\frac{y_1}{\sin\theta} \leqslant r_1 \leqslant r$$

where $$\theta_1 = \sin^{-1}\left(\frac{y_1}{r}\right)$$

hence bending moment over full cross-section

$$M_{2^{nd}\ term} = 4\int_{\theta=\theta_1}^{\pi/2}\int_{r_1=\frac{y_1}{\sin\theta}}^{r}\left(\frac{511.98}{y_1}r_1^2\sin^2\theta\right)r_1\,dr_1\,d\theta$$

$$= \frac{4\times 511.98}{y_1}\int_{\theta_1}^{\pi/2}\sin^2\theta\,d\theta\int_{\frac{y_1}{\sin\theta}}^{r}r_1^3\,dr_1$$

which on simplification, yields

$$M_{2^{nd}\ term} = \frac{511.98}{y_1}\left[\frac{r^4}{4}\left(\pi - 2\theta_1 + \sin 2\theta_1\right) - y_1^4\cot\theta_1\right]$$

The bending moment over the full cross-section arising from stresses typified by those of the third "term" of Fig. (c) is obtained by noting that

$$\sigma = 84666\epsilon + 291.8$$

which can be expressed as

$$\sigma = \frac{220.1y}{y_1} + 291.8$$

as $$\epsilon = \frac{0.0026\ y}{y_1}$$ is still valid

Similar reasoning to that previously employed gives the bending moment over the cross-section:

$$M_{3^{rd}\ term} = 4\int_{\theta=\theta_1}^{\pi/2}\int_{r_1=\frac{y_1}{\sin\theta_1}}^{r}\left(\frac{220.1}{y_1}r_1^2\sin^2\theta + 291.8r_1\sin\theta\right)r_1\,dr_1\,d\theta$$

= (after evaluation of the integrals)

$$= \frac{55r^4}{y_1}\left(\pi - 2\theta_1 + \sin 2\theta_1\right) + 389.1r^3\cos\theta_1 - 609.3y_1^3\cot\theta_1$$

The equation of Fig. (c) gives the final moment on the cross-section:

$$M = M_{1^{st}\ term} - M_{2^{nd}\ term} + M_{3^{rd}\ term}$$

$$= 154657\,r^3\epsilon_{max} - 72.96\,\gamma_1\left(\pi - 2\theta_1 + \sin 2\theta_1\right)$$

$$- 97.3\,y_1^3\cot\theta_1 + 389.1\,r^3\cos\theta_1$$

where $\gamma_1 = \dfrac{r^4}{y_1}$

$\epsilon_{max} > 0.0044$

A similar method to that adopted above is employed, except that the quadrant is divided into three zones instead of two, reflecting the increased number of stress-strain relationships to be considered. Polar integration is again employed and the additional parameters

$$y_2 = \frac{0.0044\ r}{\epsilon_{max}}$$

and $$\theta_2 = \sin^{-1}(y_2/r)$$

introduced. The total bending moment on the section corresponding to a maximum strain of ϵ_{max} is:

$$M = 154657\, r^3 \epsilon_{max} + 145.92\, \theta_1 \gamma_1 - 72.96\, \gamma_1 \sin 2\theta_1$$

$$+ 389.13\, r^3 \cos\theta_1 - 97.3\, y_1^3 \cot\theta_1 + 87.82\, \theta_2 \gamma_1$$

$$- 43.91\, \gamma_1 \sin 2\theta_2 + 396.31\, r^3 \cos\theta_2$$

$$- 99.07\, y_2^3 \cot\theta_2 - 116.87\, \pi \gamma_1$$

APPENDIX VI

Programme KURVTURE and Rate of Straining Calculations

Appendix VI - Programme KURVTURE and Rate of Straining Calculations

The rates of load application not to be exceeded in beam tests were based on the cross-sectional dimensions of the beam given at the end of Section 5.5 . With these dimensions and the material properties $E=196000N/mm^2$ and $\sigma_y=234.5N/mm^2$, elastic and plastic bending theories were used to produce limiting values of applied loads on simply-supported beams of span 600, 800 and 1000mm. The results of these analyses are shown in the following table.

beam span (mm)	M_y (Nmm)	M_{ffy}: moment at which flanges fully yielded, web still elastic (Nmm)	M_p (Nmm)	corresponding central point loads		
				P_y (N)	P_{ffy} (N)	P_p (N)
600	244831	250046	291187	1632.2	1666.8	1941.2
800	244831	250046	291187	1224.2	1250.2	1455.9
1000	244831	250046	291187	979.3	1000.2	1164.7

It will be observed that the ratio $M_{ffy}/M_y=1.021$ is considerably smaller than $M_p/M_y=1.189$. In terms of the calculations involved in determining maximum rates of loading, these ratios indicate that solution of the cubic equation (derived in Section 5.6) by means of the computer programme KURVTURE is only necessary for central point loads producing inelastic moments in the section which exceed M_y by not more than 2.1%. In contrast, solution of the quadratic equation of Section 5.6 is necessary for a much wider range of moments: those exceeding M_y by between 2.1% and 18.9%.

The following tables show the data from which Figs. 5.12 to 5.14 were drawn. The results of several of the intermediate calculations described in Section 5.6 are shown in these tables and the nature of the solution (ie. whether from the cubic or quadratic equation) is indicated.

```
      PROGRAM KURVTURE
C
C    ***********************************************************
C
C    THIS PROGRAMME PROVIDES AN APPROXIMATE SOLUTION TO
C    THE CUBIC EQUATION LINKING BEAM CURVATURE AND IN-PLANE
C    BENDING MOMENT WHEN THE YIELDED ZONES ARE CONFINED TO
C    THE FLANGES.
C
C    ***********************************************************
C
      DOUBLE PRECISION H,T,B,AO,C2,A1,R,RHS,RATK,RATLAS,RHSLAS
      H=49.828
      T=0.914
      B=16.0
C    CALC AO, THE VARIABLE USED HERE FOR PARAMETER Q3 IN THE TEXT
      AO=(8.0*T**3)-(12.0*H*T**2)+(6.0*T*H**2)-H**3
      AO=(AO/H**3)*2.0
      C2=H-2.0*T
      C2=(C2**3/H**3)*2.0*T/B
      AO=AO+C2
      WRITE(4,*) AO
C    CALC A1, THE VARIABLE USED HERE FOR PARAMETER Q2 IN THE TEXT
      A1=(T**2/3.0)+(H-T)**2
      A1=(12.0*T*A1)/H**3
      C2=(H-(2.0*T))**3
      C2=(2.0*T*C2)/(B*H**3)
      A1=A1+C2
      WRITE(4,*) A1
  350 CONTINUE
      WRITE(4,100)
  100 FORMAT(' ENTER RATIO P/PY')
      READ(3,*) R
      IF(R.LT.0.01) GOTO 270
      R=R*A1-3.0
      RATK=1.0
      I=1
  250 CONTINUE
      I=I+1
      IF(I.GT.700000) GOTO 270
      RHS=(RATK**3)+(R*RATK)-AO
      IF(RHS.LT.0.0) GOTO 200
      RATLAS=RATK
      RHSLAS=RHS
      RATK=RATK*0.9999999995
      GOTO 250
  200 CONTINUE
      WRITE(4,300) RATLAS,RHSLAS
      WRITE(4,301) RATK,RHS
  300 FORMAT(' LAST KY/K = ',F12.10,'  GAVE RHS = ',D12.6)
  301 FORMAT(' THIS KY/K = ',F12.10,'  GAVE RHS = ',D12.6)
      GOTO 350
  270 CONTINUE
      STOP
      END
```

Rate of Straining: span = 600mm

P	M/M_y	χ/χ_y	$\mu\epsilon = \frac{\chi\sigma_y}{\chi_y E} \times 10^6$	$\Delta(\mu\epsilon)$ for 10N	Δt for 10N	Δt for 20N	Δt for 30N	Δt for 40N	Δt for 50N	cubic or quadratic solution
1632.2	1.0	1.0	1196	8	.027	.057	.097	(.152)	(.235)	-
1642.2	1.006127	1.0065306	1204	9	.03					C
1652.2	1.012253	1.0141214	1213	12	.04					C
1662.2	1.018380	1.0234847	1225	[38	.127]					C
1672.2	1.024507	1.0557716	1263	25	.083	.17	.26	.36	.467	Q
1682.2	1.030634	1.0763057	1288	26	.087					
1692.2	1.036760	1.0980828	1314	27	.09	.19				
1702.2	1.042887	1.1212415	1341	30	.10		.317			
1712.2	1.049014	1.1459301	1371	32	.107	.217		.47		
1722.2	1.055140	1.1723204	1403	33	.11				.663	
1732.2	1.061267	1.200627	1436	37	.123	.253	.396			
1742.2	1.067394	1.2310883	1473	39	.13					
1752.2	1.0735204	1.263989	1512	43	.143	.300		.657		
1762.2	1.0796471	1.299679	1555	47	.157		.514			
1772.2	1.0857738	1.338573	1602	50	.167	.357			1.057	
1782.2	1.09190050	1.381182	1652	57	.19					
1792.2	1.0980272	1.4281373	1709	62	.207	.44	.70	1.0		
1802.2	1.1041539	1.480232	1771	70	.233					
1812.2	1.1102806	1.538478	1841	78	.26	.56				
1822.2	1.1164073	1.6041897	1919	90	.3		1.05		2.123	
1832.2	1.122534	1.6791109	2009	103	.343	.75		1.823		
1842.2	1.1286607	1.765616	2112	122	.407					
1852.2	1.134787	1.867028	2234	145	.483	1.07	1.82			
1862.2	1.1409141	1.988213	2379	177	.59					
1872.2	1.1470408	2.136530	2556	224	.747	1.734		5.288	9.398	
1882.2	1.153168	2.3239285	2780	296	.987		4.541	8.651	22.614	
1892.2	1.159294	2.571183	3076	416	1.387	3.554	7.664	21.627		
1902.2	1.165421	2.9190618	3492	650	2.167		20.24			
1912.2	1.171548	3.4616177	4142	1233	4.11	18.073				
1922.2	1.177674	4.4922488	5375	4189	13.963					
1932.2	1.183801	7.9941046	9564							

Rate of Straining: span = 800m

P	M/M_y	χ/χ_y	$\mu\epsilon$	$\Delta(\mu\epsilon)$	Δt for 10N	Δt for 20N	Δt for 30N	Δt for 40N	Δt for 50N	cubic or quadratic solution
1224.2	1.0	1.0	1196			.08	(.145)	(.255)	(.375)	-
				11	.037					
1234.2	1.008169	1.0089195	1207							C
				13	.043					
1244.2	1.016337	1.0200887	1220							C
				[43	.143]					
1254.2	1.024506	1.055768	1263							
				33	.11	.23	.36	.503	.656	Q
1264.2	1.032674	1.083413	1296							
				36	.12					
1274.2	1.040843	1.113354	1332							
				39	.13	.273				
1284.2	1.0490116	1.145920	1371							
				43	.143		.469			
1294.2	1.057180	1.181522	1414							
				46	.153	.326		.736		
1304.2	1.065349	1.220665	1460							
				52	.173				1.11	
1314.2	1.073517	1.26397	1512							
				58	.193	.410	.657			
1324.2	1.081686	1.312243	1570							
				65	.217					
1334.2	1.089854	1.3665	1635							
				74	.247	.527		1.247		
1344.2	1.0980232	1.428105	1709							
				84	.28		1.0			
1354.2	1.106192	1.498868	1793							
				99	.33	.72			2.543	
1364.2	1.114360	1.581304	1892							
				117	.39					
1374.2	1.122529	1.679045	2009							
				142	.473	1.06	1.823	2.866	4.419	
1384.2	1.130698	1.797485	2151							
				176	.587					
1394.2	1.138866	1.945118	2327							
				229	.763	1.806			12.622	
1404.2	1.147035	2.136374	2556							
				313	1.043		5.279	11.859		
1414.2	1.155203	2.397992	2869							
				466	1.553	4.236	10.816			
1424.2	1.163372	2.787508	3335							
				805	2.683	9.263				
1434.2	1.171540	3.4607	4140							
				1974	6.58					
1444.2	1.179709	5.110287	6114							
1454.2	1.187878	No sol^n.								

Rate of Straining: span = 1000m

P	M/M_y	χ/χ_y	$\mu\epsilon$	$\Delta(\mu\epsilon)$	Δt for 10N	Δt for 20N	Δt for 30N	Δt for 40N	Δt for 50N	cubic or quadratic solution
979.3	1.0	1.0	1196			.11	(.195)	(.342)	(.505)	-
				14	.047					
989.3	1.0102113	1.0114423	1210							C
				19	.063					
999.3	1.0204227	1.0272738	1229							C
				[59	.197]					
1009.3	1.0306341	1.076306	1288							
				44	.147	.31	.493	.703	.94	Q
1019.3	1.0408455	1.113363	1332							
				49	.163					
1029.3	1.0510569	1.154532	1381							
				55	.183	.393				
1039.3	1.0612682	1.200633	1436							
				63	.21		.720			
1049.3	1.0714796	1.252738	1499							
				71	.237	.51		1.223		
1059.3	1.0816910	1.312275	1570							
				82	.273				2.07	
1069.3	1.0919024	1.381196	1652							
				97	.323	.713	1.19			
1079.3	1.102114	1.462259	1749							
				117	.39				3.441	
1089.3	1.1123251	1.559501	1866							
				143	.477	1.084		3.051		
1099.3	1.122536	1.679137	2009							
				182	.607		2.574		8.154	
1109.3	1.132748	1.83136	2191							
				243	.810	1.967			24.597	
1119.3	1.1429592	2.034236	2434							
				347	1.157			23.79		
1129.3	1.153171	2.324033	2781							
				555	1.85	5.58	22.63			
1139.3	1.163382	2.788107	3336							
				1119	3.73	20.78				
1149.3	1.173593	3.723253	4455							
				5116	17.05					
1159.3	1.183805	7.99976	9571							

APPENDIX VII

Comparative Design Calculations

APPENDIX VII(a): Comparative Design Calculations to BS 449, BS 5400, BS 5950

A simply-supported beam of span 3.019m (giving R^2=10 for the 305x102x33 UB chosen in the BS 449 design) is subjected to a central point load producing a bending moment of 90kNm at midspan. The beam is laterally restrained at midspan by a single, equal angle bracing member of length 1m. The beam and its restraint are to be designed in Grade 50 steel to each of the above steelwork codes. The beam self weight can be neglected in calculations.

In applying partial load factors consistent with the limit state requirements of BS 5400 and BS 5950, the appropriate factors for imposed loading should be taken from Part 2 and Part 1 of these codes, respectively.

The "destabilising" load condition of BS 5950 may be neglected as, for midspan restraint of a beam under central point loading, there is no chance of lateral movement.

BS 449 (Part 2): 1969

A 305x102x33 UB is loaded with a central point load and restraint is afforded to the compression flange at midspan. The beam is torsionally restrained at its supports and is simply supported on a single span. Grade 50 steel is to be used for both the primary member and the bracing element. The span is such that $R^2 \simeq 10$.

$J = 12.31\text{cm}^4, \quad \Gamma = 43147.21\text{cm}^6$

Assuming $\nu = 0.3$, $\dfrac{E}{G} = 2.6$

$$R^2 = \frac{L^2 GJ}{E\Gamma} \quad \text{or} \quad L^2 = \frac{R^2 E\Gamma}{GJ}$$

$$L^2 = \frac{10 \times 2.6 \times 43147.21}{12.31} \Rightarrow L = 301.9\text{cm}$$

ie. $L = 3.019\text{m}$

BS 449, Clause 26(b): $l_e = \dfrac{L}{2} = 1.5095\text{m}$

$r_{yy} = 21.5\text{mm}$

$$\therefore \frac{l_e}{r_y} = \frac{1509.5}{21.5} = 70.21$$

$D = 312.7\text{mm}$

$T = 10.8\text{mm}$

$$\frac{D}{T} = \frac{312.7}{10.8} = 28.95$$

Table 3b: $p_{bc} = 230\text{N/mm}^2$

$z_e = 415 \times 10^3\text{mm}^3$

$\therefore$ Moment capacity of section to BS 449 $= p_{bc}z_e$

$$= 230 \times 415 \times 10^3 \text{Nmm}$$

$$= 95.45\text{kNm}$$

Assume applied bending moment on section = 90kNm

Combined bending and shear stresses in web:

Central point load giving rise to b. moment of 90kNm $= \dfrac{4 \times 90}{3.019}$

$$= 119.24\text{kN}$$

$\therefore$ Max. shear $= \dfrac{119.24}{2} = 59.62\text{kN}$

Clause 23(b): Ave. shear stress $= \dfrac{59.62 \times 10^3}{312.7 \times 6.6}$

$$= 28.89\text{N/mm}^2 = f_q'$$

Table 11: $p_q' = 140\text{N/mm}^2$

$\dfrac{f_q'}{p_q'} < 1.0$ $\therefore$ OK in web shear

Elastic modulus for outer fibre of web

$$= 415000 \times \frac{312.7/2}{(312.7 - 21.6)/2}$$

$$= 445790\text{mm}^3$$

$\therefore$ bending stress at this point $= \dfrac{90 \times 10^6}{445790} = 201.89\text{N/mm}^2$

Clause 14(c): Due to the quadratic distribution of shear stress over the web, f_q' will be smaller than the max. shear stress f_q at the neutral axis, but greater than the shear stress at the extremities of the web panel. Hence f_q' can be used as a conservative estimate for f_q at the extremities.

$$f_e = (201.89^2 + 3 \times 28.89^2)^{\frac{1}{2}} = 208.0\text{N/mm}^2$$

Table 1: $p_e = 320\text{N/mm}^2$

$\therefore \dfrac{f_e}{p_e} < 1.0$ $\therefore$ section OK in combined bending & shear.

<u>BS 449, Clause 26e(i)</u>: lateral restraint member to be capable of carrying 2½% of max. flange force

distance from N.A. to flange centroid $= \dfrac{D - T}{2} = \dfrac{312.7 - 10.8}{2}$

$= 151.0\text{mm}$

$\therefore$ stress at centroid compression flange

$$= \frac{90 \times 10^6 \times 151}{64870000} = 209.5\text{N/mm}^2$$

$\therefore$ max. flange force $= 102.4 \times 10.8 \times 209.5 = 231.7 \times 10^3\text{N}$

$\therefore$ strength of restraint $\geqslant 0.025 \times 231.7 = 5.79\text{kN}$

Assume a single restraint is to be provided. Its length is 1.0m . Restraint "held in position at each end and in direction at one end"; then its effective length

$$l_e = 0.85 \times 1000 = 850\text{mm}$$

Clause 33: $\dfrac{l_e}{r_{min}} \not> 180$

$$\therefore (r_{min}) \not< \frac{850}{180} = 4.72\text{mm}$$

Try 25 x 25 x 4L giving $r_{min} = 4.8\text{mm}$

$$\therefore \frac{l_e}{r_{min}} = \frac{850}{4.8} = 177.1$$

Table 17(b) (Grade 50 steel) $\Rightarrow$ $p_c = 32\text{N/mm}^2$

Now $f_c = \dfrac{5790}{185} = 31.30\text{N/mm}^2$

$\therefore \dfrac{f_c}{p_c} < 1.0$

$K = \text{axial stiffness} = \dfrac{AE}{L} = \dfrac{185 \times 210000}{1000} = 38850\text{N/mm}$

$\lambda = \dfrac{KL^3}{48EI_\eta} = \dfrac{38850 \times 3019^3}{48 \times 210000 \times 1930000} = 54.95$

BS 5400: Part 3 (1982)

Nominal Applied Moment = 90kNm as before.
This is caused by a point load at midspan. From Part 2 of BS 5400, an ULS load factor of 1.50 will be applied to the above. This is the factor used for HA vehicle loading and is therefore the γ_{fL} factor most appropriate to an imposed point load.

$\therefore$ ULS bending moment on section = 1.5 x 90
= 135kNm

Here it is not sufficient to assume that the previously used 305x102x33 UB is adequate, as the section size determines the compn. flange force and thus a section needs to be selected.

The beam section, whatever its size, will be a hot rolled section and therefore will satisfy the "compact" requirements of Part 3:

3/9.9.1.2: σ_{lc} is reqd.

3/9.8.2: for compact sectn., $\sigma_{lc} = \sigma_{li}$ from 3/9.8.1

3/Fig. 5: a = 3109mm

b = (102.4 - 6.6)/2 = 47.9

$\therefore \dfrac{a}{b} = 64.9$

as $\dfrac{a}{b} > 0.5$, curve 2 for unrestrained plate panels is appropriate $\therefore$

$$\lambda = \frac{b}{t}\sqrt{\frac{\sigma_y}{355}} = \frac{47.9}{10.8} \times 1.0 = 4.44$$

$\therefore$ from Fig. 5, $K_c = 1.0$

3/9.8.1: $\sigma_{yc} = K_c\,\sigma_y = 355\text{N/mm}^2$

$$\left.\begin{array}{ll} \text{3/9.6.2:} & l_e = \dfrac{L}{2} = 1509.5\text{mm} \\ & \\ \text{3/9.7.2} & r_y = 21.5\text{mm} \end{array}\right\}\ \text{as BS 449 design}$$

$k_4 = 0.9$ for rolled I-section to BS 4848

Applied loading is not concentrated within the middle fifth of the length between points of lateral restraint hence 3/Fig. 9 is appropriate

3/Fig. 9: hogging moments +ve

$M_B = 0$ at support, $M_M = 0$, M_A -ve as sagging

$\therefore \frac{M_B}{M_A} = 0$ and $\frac{M_A}{M_M} = -\infty$

hence $\eta \simeq 0.76$

3/9.7.2: $\lambda_f = \frac{l_e}{r_y}\left(\frac{t_f}{D}\right) = 70.21 \times \frac{1}{28.95} = 2.425$

$i = 0.5$ as section is doubly symmetric

3/Table 9: $\therefore v = 0.912 + 0.575(0.956 - 0.912)$

$= 0.937$

3/9.7.2: $\lambda_{LT} = \frac{l_e}{r_y} k_4 \eta v$

$= 70.21 \times 0.9 \times 0.76 \times 0.937 = 45.0$

3/9.8.1: $\lambda_{LT}\sqrt{\frac{\sigma_{yc}}{355}} = \lambda_{LT} = 45$

3/Fig. 10: $\Rightarrow \frac{\sigma_{li}}{\sigma_{yc}} = 1.0$ ie. $\sigma_{li} = 355\text{N/mm}^2$

$\sigma_{lc} = \sigma_{li} = 355\text{N/mm}^2$

3/9.9.1.2: $z_{pe} = 479900\text{mm}^3$

3/4.3.3: $\gamma_{f3} = 1.1$

3/Table 2: $\gamma_m = 1.2$

3/9.9.1.2: $M_D = \dfrac{z_{pe}\,\sigma_{1c}}{\gamma_m\,\gamma_{f3}} = \dfrac{479900 \times 355}{1.2 \times 1.1} = 129.06 \times 10^6$Nmm

$\therefore$ section fails

Assuming σ_{1c} can be maintained at 355N/mm^2, reqd. z_{pe} $\geqslant \dfrac{135}{129.06} \times 479900 = 502220$mm^3

<u>Try 305 x 127 x 57 UB</u> (z_{pe} = 540500mm^3)

3/Fig. 5: As a/b again >> 0.5 curve 2 is appropriate

$= \dfrac{b}{t}\sqrt{\dfrac{\sigma_y}{355}}$

$b = (123.5 - 7.2)/2 = 58.15$mm

$\lambda = \dfrac{58.15}{10.7} = 5.43$

$\therefore K_c = 1.0$

3/9.6.2: $l_e = 1509.5$mm as before

3/9.7.2: $r_y = 26.7$mm

$k_4 = 0.9,\ \eta = 0.76$

$\lambda_f = \dfrac{1509.5}{26.7} \times \dfrac{10.7}{303.8} = 1.99$

$i = 0.5$ as before

3/Table 9: $v = 0.956$

3/9.7.2: $\lambda_{LT} = \dfrac{1509.5}{26.7} \times 0.9 \times 0.76 \times 0.956 = 36.97$

3/Fig. 10 &
3/9.8.2: $\sigma_{1c} = \sigma_{1i} = 355$Nmm^2

3/9.9.1.2: $M_D = \dfrac{540500 \times 355}{1.2 \times 1.1} = 145.36 \times 10^6$Nmm

$\therefore M_D > M_{applied}$ $\therefore$ section OK in bending for above section,

$$R^2 = \frac{L^2GJ}{E\Gamma} = \frac{301.9^2 \times 15.63}{2.6 \times 67802.3} = 8.08$$

Check section in combined bending and shear

3/9.9.2.2: $d_{we} = 264.6\text{mm}$; $D = 303.8\text{mm}$; $t_w = 7.2\text{mm}$

$$\lambda = \frac{d_{we}}{t_w} \quad (\text{as } \sigma_{yw} = 355\text{N/mm}^2)$$

$$= \frac{264.6}{7.2} = 36.75$$

$$\tau_y = \frac{\sigma_{yw}}{\sqrt{3}} = \frac{355}{\sqrt{3}} = 204.96\text{N/mm}^2$$

3/Figs.
11 - 17: for $\lambda = 36.8$, τ_1 independent of ϕ and m_{fw}

hence $\tau_1 = \tau_y = 204.96\text{N/mm}^2$

3/9.9.2.2: $$V_D = \frac{7.2 \times 303.8 \times 204.96}{1.05 \times 1.1} = 388.2 \times 10^3\text{N}$$

3/9.9.3.1: $V = 1.5 \times 59.62 = 89.4\text{kN}$

(Note 1) As the calculation of V_D was independent of m_{fw},

$V_D = V_R$ and hence

$0.5V_R = 0.5 \times 388.2 = 194.1\text{kN}$

$\therefore\ V < 0.5V_R$

Previously shown that $M < M_D$

Hence section OK in combined bending and shear.

Restraint Design

Evaluate b. moment on section when flanges are fully yielded and web forms elastic core.

$$\text{force in fully yielded flange} = \frac{355}{1.2 \times 1.1} \times 123.5 \times 10.7$$

$$= 355.39 \times 10^3\text{N}$$

distance between flange centroids = $D - t_f$ = 293.1mm

$\therefore$ couple produced by flange forces = 355.39 x 0.2931
= 104.16kNm

elastic section modulus of web = $\dfrac{I_{web}}{y} = \dfrac{t_w(D-2t_f)^2}{6}$

$$z_{e\ web} = \frac{7.2 \times (303.8-21.4)^2}{6}$$
$$= 95699.7\text{mm}^3$$

$\therefore$ elastic moment in web = $z_{e\ web} \times \dfrac{355}{1.2 \times 1.1}$
= 95699.7 x 268.94
= 25.737 x 10^6Nmm

$\therefore$ b. moment on section when flanges fully yielded
= 104.16 + 25.74 = 129.9kNm

As this is less than the applied ULS b. moment of 135kNm, the yielded zone extends into the flange under the applied b. moment.

Therefore the force in the flange under the 135kNm b. moment is 355.39kN.

3/9.12.1: Only one restraint is used and there is only one beam
$\therefore$ ΣP_f in this clause will be taken to be 355.39kN

Restraint force = F = $\dfrac{\Sigma P_f}{40} = \dfrac{355.39}{40}$ = 8.885kN

3/10.4.2.1: for a single angle member l_e = L = 1000mm

<u>Try 30 x 30 x 4 L</u>

3/10.3.1: b_o = 30 - 4 - 5 = 21mm
t_o = 4mm
$\therefore$ $\dfrac{b_o}{t_o} = 5.25 \ll 12\sqrt{\dfrac{355}{\sigma_y'}}$ $\therefore$ OK

3/10.5.2.1: $k_h = 1.0$ and $K_c = 1.0$ as 3/10.3.1 satisfied

$\therefore A_e = A = 227mm^2$

3/10.6.1.2: The 0.8 factor is not applied as the end conditions of this restraint match those used in the BS 449 design.

3/10.6.1.1: $l_e = 1000mm$

$r_{vv} = 5.8mm$

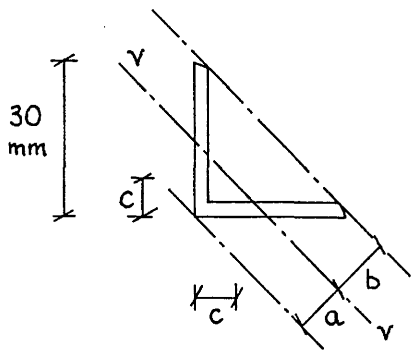

$$a + b \simeq \frac{30}{\sqrt{2}} = 21.21mm$$

$$a = \sqrt{2}c = \sqrt{2} \times 8.8 = 12.44mm$$

$$\therefore \; a > b \text{ and } y = a = 12.44mm$$

$$\frac{r_{vv}}{y} = \frac{5.8}{12.44} = 0.466$$

$$\frac{l_e}{r}\sqrt{\frac{\sigma_y}{355}} = \frac{1000}{5.8} = 172.41$$

3/Fig. 37: $\frac{\sigma_c}{\sigma_y} \simeq 0.158 \Rightarrow \sigma_c = 0.158 \times 355 = 56.09N/mm^2$

3/10.6.1.1: $\Rightarrow P_D = \frac{227 \times 56.09}{1.05 \times 1.1} = 11025N$

$\therefore P_D > F = 8885N \qquad \therefore OK$

$$K = \frac{AE}{L} = \frac{227 \times 205000}{1000} = 46535N/mm$$

$$\lambda = \frac{46535 \times 3019^3}{48 \times 205000 \times 3370000} = 38.61$$

BS 5950, Part 1 (1985)

Nominal applied bending moment = 90kNm
Table 2 of BS 5950 gives an ULS load factor of γ_f=1.6 for an imposed point load on the beam.

∴ ULS bending moment on section = 1.6 x 90
= 144kNm

The 305x102x33 UB which satisfied the requirements of BS 449 is unlikely to satisfy the requirements of this higher bending moment. Consequently, the 305x127x37 UB selected by BS 5400 design methods will be checked to BS 5950. If the section is inefficient in bending, then the ligher section will be checked.

Table 6: $p_y = 355\text{N/mm}^2$ for Grade 50 rolled section of maximum thickness $\leqslant$ 16mm

Table 7: $\epsilon = \left(\frac{275}{355}\right)^{\frac{1}{2}} = 0.880$

outstand of compression flange: $b = \frac{123.5}{2} = 61.75\text{mm}$

$T = 10.7\text{mm}$

$\frac{b}{T} = \frac{61.75}{10.7} = 5.771$

$8.5\epsilon = 7.48 > \frac{b}{T}$ ∴"plastic"

web, neutral axis at mid-depth: $d = 264.6\text{mm}$

$t = 7.2\text{mm}$

$\therefore \frac{d}{t} = 36.75$

$79\epsilon = 69.5 > \frac{d}{t}$ ∴"plastic"

3.5.2: Section is therefore plastic (ie. "section 1")

4.2.3: Shear: $P_v = 0.6p_ytD = 0.6 \times 355 \times 7.2 \times 303.8$
$= 465.9 \times 10^3\text{N}$

for point load applied to beam at midspan the ULS factored load causing a b. moment of 144kNm is

$$W = \frac{4 \times 144}{3.019} = 190.79\text{kN}$$

$$\therefore \text{max. ULS shear} = \frac{W}{2} = 95.4\text{kN} = F_v$$

$0.6P_v = 279.5$kN

4.2.5: as $F_v < 0.6P_v$, $M_c = p_yS$ but $\leqslant 1.2p_yz$
$S = 540500\text{mm}^3$
$\therefore p_yS = 540500 \times 355 = 191.88 \times 10^6$Nmm
$1.2p_yz = 1.2 \times 355 \times 471500 = 200.86 \times 10^6$Nmm
$\therefore M_c = 191.88$kNm

This is $\gg$ ULS applied moment of 144kNm $\therefore$ OK

4.3.4: It is assumed that the load is applied at the shear centre and so the "destabilising load condition" does not apply.

4.3.5: $L_E = \frac{L}{2} = 1509.5$mm

4.3.7.1: The conservative approach for equal flanged rolled sections will not be applied. The more rigorous approach will be adopted.

4.3.7.2: $M_A = 144$kNm

4.3.7.6: for a member of uniform cross-section $n = 1.0$

Table 18: $\beta = 0 \quad \therefore m = 0.57$

4.3.7.2: $\therefore \bar{M} = mM_A = 0.57 \times 144 = 82.08$kNm

4.3.7.5: $\lambda = \frac{L_E}{r_y} = \frac{1509.5}{26.7} = 56.54$

Appendix B

2.5.1: $u = \left(\dfrac{4S_x{}^2\gamma}{A^2h_s{}^2}\right)^{\frac{1}{4}}$

$I_x = 71620000\text{mm}^4$, $I_y = 3370000\text{mm}^4$,
$A = 4750\text{mm}^2$, $h_s = D - T = 303.8 - 10.7 = 293.1\text{mm}$

$$\gamma = 1 - \frac{I_y}{I_x} = 1 - \frac{337}{7162} = 0.953$$

$$u = \left(\frac{4 \times 540500^2 \times 0.953}{4750^2 \times 293.1^2}\right)^{\frac{1}{4}} = 0.8706$$

4.3.7.5: $N = 0.5$

$$x = 0.566h_s(A/J)^{\frac{1}{2}} = 0.566 \times 293.1\left(\frac{4750}{156300}\right)^{\frac{1}{2}}$$

$$= 28.92$$

$$\frac{\lambda}{x} = \frac{56.54}{28.92} = 1.955$$

Table 14: $v = 0.96$

4.3.7.5: $\lambda_{LT} = nuv\lambda = 1.0 \times 0.8706 \times 0.96 \times 56.54 = 47.25$

Table 11: $p_b = 292 + \dfrac{2.75}{5}(309 - 292) = 301.4\text{N/mm}^2$

4.3.7.3: $M_b = S_xp_b = 540500 \times 301.4 = 162.91 \times 10^6\text{Nmm}$

$\overline{M} = 82.08\text{kNm} << M_b = 162.91\text{kNm}$

∴ Lateral instability does not occur

The 305x127x37 UB has a maximum efficiency of $\dfrac{144}{191.88} = 0.75$

which is low. The 305x102x33 UB will therefore be checked.

<u>Try 305 x 102 x 33 UB</u>

ULS bending moment on section = 144kNm

Table 6: $p_y = 355\text{N/mm}^2$

Table 7: outstand of compn. flange: $b = \frac{102.4}{2} = 51.2mm$

$T = 10.8mm$

$\therefore \frac{b}{T} < 8.5\epsilon$

web, neutral axis at mid-depth: $d = 275.8mm$

$t = 6.6mm$

$\therefore \frac{d}{t} = 41.79 < 79\epsilon$

3.5.2: Hence section is plastic

4.2.3: $P_v = 0.6 \times 355 \times 6.6 \times 312.7 = 439.6 \times 10^3N$

$F_v = 95.4kN < 0.6P_v$

4.2.5: $S = 479900mm^3$

$\therefore p_yS = 479900 \times 355 = 170.36 \times 10^6Nmm >> 144kNm$

<u>Try 305 x 102 x 28 UB</u>

ULS bending moment on section = 144kNm

Table 6: $p_y = 355N/mm^2$

Table 7: outstand of compn. flange: $b = \frac{101.9}{2} = 50.95mm$

$T = 8.9mm$

$\therefore \frac{b}{T} = 5.72 < 7.48$ ∴"plastic"

web, neutral axis at mid-depth: $d = 275.8mm$

$t = 6.1mm$

$\therefore \frac{d}{t} = 45.21 < 69.5$ ∴"plastic"

3.5.2: Hence section is plastic.

4.2.3: $P_v = 0.6 \times 355 \times 6.1 \times 308.9 = 401.4 \times 10^3N$

$Fv = 95.4kN < 0.6Pv$

4.2.5: $S = 407200\text{mm}^3$

$\therefore\ p_yS = 355 \times 407200 = 144.6 \times 10^6\text{Nmm}$

$1.2p_yz = 1.2 \times 355 \times 351000 = 149.5 \times 10^6\text{Nmm}$

$\therefore\ M_c = 144.6\text{kNm} > 144\text{kNm applied} \therefore \text{OK}$

As before, $L_E = 1509.5\text{mm}$, $M_A = 144\text{kNm}$, $n = 1.0$, $m = 0.57$, $\bar{M} = 82.08\text{kNm}$

4.3.7.5: $\lambda = \dfrac{L_E}{r_y} = \dfrac{1509.5}{20.8} = 72.57$

Appendix B

2.5.1 : $I_x = 54210000\text{mm}^4$, $I_y = 1570000\text{mm}^4$,

$A = 3630\text{mm}^2$, $h_s = 308.9 - 8.9 = 300\text{mm}$

$\gamma = 1 - \dfrac{157}{5421} = 0.971$

$$u = \left(\frac{4 \times 407200^2 \times 0.971}{3630^2 \times 300^2}\right)^{\frac{1}{4}} = 0.858$$

4.3.7.5: $N = 0.5$

$$x = 0.566 \times 300\left(\frac{3630}{77400}\right)^{\frac{1}{2}} = 36.77$$

$$\frac{\lambda}{x} = \frac{72.57}{36.77} = 1.974$$

Table 14: $v = 0.96$

4.3.7.5: $\lambda_{LT} = 1.0 \times 0.858 \times 0.96 \times 72.57 = 59.77$

Table 11: $p_b \doteqdot 257\text{N/mm}^2$

4.3.7.3: $M_b = S_xp_b = 407200 \times 257 = 104.65 \times 10^6\text{Nmm}$

$\therefore\ \bar{M} = 82.08\text{kNm} < M_b = 104.65\text{kNm}$

for above section, $R^2 = \dfrac{L^2GJ}{E\Gamma} = \dfrac{301.9^2 \times 7.74}{2.6 \times 34386.4} = 7.89$

Design of Lateral Restraint

4.3.2: Lateral restraint member to be capable of carrying 1% of the factored force in the compression flange of the beam.
As M_A is almost equal to M_C, the flanges will be fully yielded under the action of M_A and thus

max. factored force in compn. flange

$$= 355 \times 101.9 \times 8.9$$

$$= 321.95 \times 10^3 N$$

$\therefore$ 1% of factored force $\doteqdot$ 3.22kN

Try 25 x 25 x 4 L

4.7.10.2: $0.85L/r_{vv} = \frac{0.85 \times 1000}{4.8} = 177.1$

$0.7L/r_{aa} + 30 = \frac{0.7 \times 1000}{7.4} + 30 = 124.6$

$\therefore \lambda = 177.1$

4.7.3.2: $\lambda < 180 \quad \therefore$ OK

Table 7: from previous calculation, $8.5\epsilon = 7.48$
for single rolled angle section, $\frac{b}{t} = \frac{d}{t} = \frac{25}{4} = 6.25 < 8.5\epsilon$

$\therefore$ angle is "plastic" section

4.7.4: for plastic section, $P_c = A_g p_c$
$A_g = 185\text{mm}^2$

Table 25: indicates Table 27(c) is appropriate

Table 27(c): $p_c \doteqdot 54\text{N/mm}^2$

$\therefore P_c = 185 \times 54 = 9.99 \times 10^3 N >>$ required restraint force of 3.22kN

However, the permissible slenderness λ of 180 has almost been attained $\therefore$ 25 x 25 x 4 L must be used

$$K = \frac{AE}{L} = \frac{185 \times 205000}{1000} = 37925\text{N/mm}$$

$$\lambda = \frac{KL^3}{48EI_\eta} = \frac{37925 \times 3019^3}{48 \times 205000 \times 1570000} = 67.55$$

Appendix VII(b): The Bracing Requirements of Lay & Galambos[71]

For the purposes of determining approximate bracing member proportions which satisfy the strength and stiffness criteria of Ref. 71, the 305x102x33 UB selected in accordance with BS 449 and BS 5950 will be assumed adequate.

Brace Stiffness

In calculating $A_b{}^*$ from eqn. (1.9), the following quantities are required.

$$A_f = 102.8 \times 10.8 = 1110.2\text{mm}^2$$

$$l_L = l_R = 3019/2 = 1509.5\text{mm}$$

$$\frac{1}{l_{av}} = 0.5\left(2 \times \frac{1}{1509.5}\right) = \frac{1}{1509.5}\ \text{mm}^{-1}$$

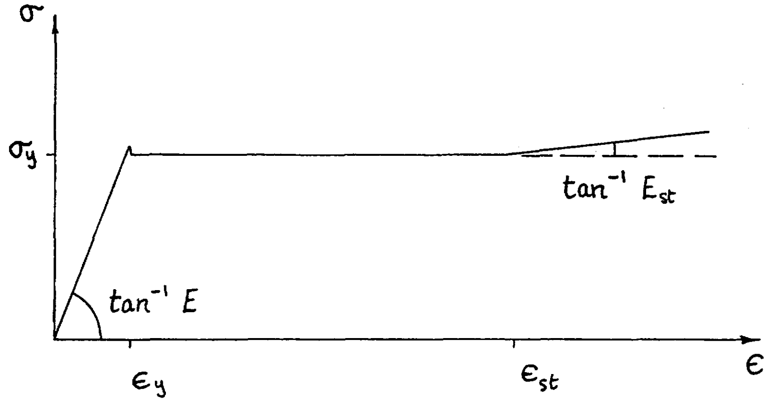

The above stress-strain diagram will be assumed typical of the behaviour of most low carbon structural steels. Examination of typical mechanical properties reveals the following values:-

$$\frac{\epsilon_{st}}{\epsilon_y} \simeq 13, \qquad \frac{E}{E_{st}} \simeq 20$$

Although some variation in the above values with strength is known to occur, they will be regarded as sufficiently accurate for the purposes of this bracing check.

Eqn. (1.9): $A_b^* = \frac{2}{3}\left(\frac{13 - 1}{20 - \sqrt{20}}\right)\frac{1110.2 \times 102.8}{1509.5}$

ie. $A_b^* = \frac{2}{3} \times 0.773 \times 75.61$

$= 38.96\text{mm}^2$

As a proportion of the area of the compn. flange the above represents

$\frac{A_b^*}{A_f} = 0.0351$ ie. $\sim 3.5\%$ of A_f

Adopting a 25 x 25 x 3 L section, the actual brace area supplied is

$A_b = 142\text{mm}^2$

The brace stiffness is controlled by eqn. (1.11) which yields

$$l_b < 0.86\, l_{av}\left(\frac{A_b}{A_f}\right)\left(\frac{l_a}{b_f}\right)^2$$

or

$$l_b < 0.86 \times 1509.5\left(\frac{142}{1110.2}\right)\left(\frac{1509.5}{102.8}\right)^2$$

$$= 35801\text{mm}$$

Clearly the l_b requirement above imposes little restriction on the design of restraint systems in practice as it represents a bracing member slenderness of

$$\frac{l_b}{r_{vv}} = \frac{35801}{4.8} = 7458$$

ie. considerably higher than that generally permitted for either tension or compression elements (eg. BS 449 Clauses 33 and 44a). In accordance with the recommendations of Salmon & Johnson[74] the flexural stiffness requirements of Ref. 71 will not be considered.

Brace Strength

The assumption of full yielding in the bracing member at the onset of local flange buckling in the primary member means that $(P_{br})_{max}$ and P_{cy} in eqn. (1.10) are in the same ratio as $A_b{}^*$ and A_f in eqn. (1.9). Hence

$$\frac{(P_{br})_{max}}{P_{cy}} = \frac{A_b{}^*}{A_f} = 0.0351$$